

**The design, synthesis and optimisation of  
calcium release-activated calcium (CRAC)  
channel inhibitors and mitochondrial  
permeability transition pore (mPTP)  
modulators,  
using phenotypic screening**

Thesis submitted to the University of Strathclyde for the degree  
of Doctor of Philosophy

**Yannick Lacroix**

**August 2015**

University of Strathclyde, Department of Pure and Applied  
Chemistry, and GlaxoSmithKline



## **Declaration of Authenticity and Author's Rights**

This thesis is the result of the author's original research. It has been composed by the author and has not been previously submitted for examination which has led to the award of a degree.

The copyright of this thesis belongs to GlaxoSmithKline in accordance with the author's contract of engagement with GlaxoSmithKline under the terms of the United Kingdom Copyright Acts. Due acknowledgement must always be made of the use of any material contained in, or derived from, this thesis.

Signed:

Date: August 2015

## Acknowledgements

I would firstly like to thank my academic supervisor, Dr Craig Jamieson, for his continuous support during the past four years. His enthusiasm and his advice were not only pivotal for the writing of this thesis, but also acted as true motivators for me in order to focus on delivering the best I could.

I also wish to express my gratitude to Professor Colin Suckling, my internal examiner, for analysing my work so carefully. I have truly benefited from his vast experience and his attention to detail.

My thanks go to my two industrial supervisors, Dr Richard Hatley in the UK and Dr Mahmood Ahmed in Singapore, for their continuous encouragement since the beginning of this project. Richard has generated several insightful discussions about my  $I_{CRAC}$  results, triggering my willingness to always look for stronger scientific explanations. Even during those exceptional work circumstances, Mahmood has found the time and the dedication to challenge my thinking on my mPTP results. I have been fortunate to be supervised by such an inspirational scientist for the last two years.

My past supervisor in the UK, Dr David House, has been instrumental in providing help and support towards the construction of this thesis. His deep scientific knowledge combined with his dedication to provide valuable feedback have been crucial in improving the quality of my thinking. Probably the best mentor anyone can have.

I would also like to thank the  $I_{CRAC}$  team members, Matthew Moriarty, Emily Wix, Elvis Maduli, and Dr Paul Gore, whose work and inputs were essential for several of the discussions enclosed in this thesis. Additionally, the lead  $I_{CRAC}$  programme biologist, Dr Malcolm Begg, has always been keen to answer the many naive biological questions I had around CRAC and other ion channels.

Similarly, my thanks go to the mPTP chemistry team in Singapore, Sarah Duncan, Dr Emma Rivers, Dr Kiew Ching Lee, Abel Chiew, Evelyn Tan, Scott Graham and David Chan, for creating an amazing work environment and also for welcoming me as a new starter in the mPTP group. I would like to express my gratitude to Dr Richard Rutter for reviewing the mPTP biology section present in this report.

I am highly grateful to both Professor Harry Kelly and Professor Billy Kerr, who initiated this PhD programme between the University of Strathclyde and GSK. They gave me the opportunity to embark upon a fantastic journey of personal development and they provided me with continuous support while I have been living in three different continents within the last four years.

I would also like to thank David Allen and Dr Ceri Davies for providing the financial support enabling this PhD to happen.

Of course, a huge *remerciement* goes to my family and especially to my parents. They have always encouraged me in every choice or decision I made and, perhaps most importantly, they taught me the willingness to learn continuously. A large part of this work is for them.

Last but not least, my thoughts goes to my fiancée, Nora Pataut, who has always been supportive, even during the difficult times that come with writing such a thesis. I truly thank her for having stood by my side, even when I was spending more time behind a computer screen than with her. “Nearly there!...” was probably the main thing I have told her for a long time now, but trust me Nora, I am nearly there!

## Abstract

Several previous studies have shown that the current low success of new drug molecules reaching the market can be attributed to safety-related drug attrition. Additionally, the link between the physicochemical properties of small molecule drugs and their toxicity profile has been demonstrated. Moreover, the type of pharmacological assay used to measure the biological activity of compounds when carrying out a drug discovery effort is critical to ensure the efficacy of compounds towards modulating specific signalling pathways. Recent studies have suggested that phenotypic screening, for which a target-agnostic measure of a biological response is used to develop an assay, can be more appropriate than target-based screening when developing first-in-class small molecules in the context of under-defined biological targets. This thesis describes the efforts in improving the physicochemical properties of small molecules, using phenotypic screening, towards the identification of therapeutic agents modulating two biological targets, respectively: the calcium release-activated calcium channel and the mitochondrial permeability transition pore.

### *CRAC channel*

The allergen stimulation of immune cells such as T cells and mast cells triggers the depletion of the calcium stores located in the endoplasmic reticulum, which in turn leads to an influx of calcium ions across the plasma membrane through calcium release-activated calcium (CRAC) channels. This process of store-operated calcium entry through CRAC channels is the main pathway of increasing the intracellular calcium concentration in T cells and mast cells, which controls a wide range of downstream cellular functions, such as the release of pro-inflammatory cytokines and mediators like histamine and prostaglandins. Inhibiting the ion current passing through the CRAC channel ( $I_{\text{CRAC}}$ ) could help to modulate immune inflammatory responses, and thus development of an  $I_{\text{CRAC}}$  blocker would be of considerable clinical interest to treat conditions such as asthma. The aim of the first medicinal chemistry programme described in this thesis is to identify selective small molecule

oral  $I_{CRAC}$  inhibitors as novel agents for the treatment of asthma and other inflammatory diseases. This report describes the design, chemical synthesis and application of modern medicinal chemistry principles for the identification of novel  $I_{CRAC}$  blockers, starting from hit molecules originating from a high throughput screen.

### ***mPTP***

The mitochondrial permeability transition pore (mPTP) is a voltage sensitive protein channel present in the inner membrane of mitochondria and it plays a key role in cellular apoptosis and necrosis. The exact composition of the pore is not fully elucidated, however, it is thought to be a combination of several molecular constituents. Under conditions of cellular stress, the channel transitions to a state of high conductance and becomes non-selectively permeable to a wide range of solutes which freely diffuse into the mitochondria. Additionally, proteins contained in the mitochondria, such as pro-apoptotic messengers, are released into the cytosol, which leads to cell death. The sustained opening of the mPTP is believed to be a key triggering event in the pathology of several diseases. The second part of this thesis describes the design and synthesis of small molecule modulators of the mPTP as novel agents for the treatment of diseases mediated by the opening of the mPTP.

# Contents

|   |            |
|---|------------|
| <b>Acknowledgements.....</b>  | <b>ii</b>  |
| <b>Abstract.....</b>  | <b>iv</b>  |
| <b>Abbreviations .....</b>  | <b>xii</b> |
| <br>  |            |
| <b>1. CHAPTER 1: Opportunities and challenges to increase chance of success during drug development.....</b>            | <b>1</b>   |
| 1.1. The drug discovery crisis .....  | 1          |
| 1.2. Importance of the physicochemical parameters of small molecules and introduction to modern drug design tools ..... | 2          |
| 1.2.1. Ligand efficiency and ligand-lipophilicity efficiency .....  | 4          |
| 1.2.2. Aqueous solubility and Property Forecast Index .....   | 6          |
| 1.2.3. Protein binding.....   | 10         |
| 1.2.4. <i>In vitro</i> microsomal clearance.....  | 11         |
| 1.2.5. Inhibition of the hERG channel .....   | 12         |
| 1.3. Phenotypic screening .....   | 14         |
| <br>  |            |
| <b>2. CHAPTER 2: Design, synthesis and optimisation of <math>I_{CRAC}</math> inhibitors.....</b>                        | <b>18</b>  |
| 2.1. $I_{CRAC}$ as a biological target of therapeutic relevance .....   | 18         |
| 2.1.1. Introduction to ion channels .....   | 18         |
| 2.1.1.1. Basic features of ion channels .....   | 18         |
| 2.1.1.2. Ion channels as therapeutic targets .....  | 22         |
| 2.1.2. Introduction to $Ca^{2+}$ channels .....   | 24         |
| 2.1.2.1. Role of $Ca^{2+}$ in the immune response .....   | 24         |

|          |  |    |
|----------|--|----|
| 2.1.2.2. | Nomenclature of Ca <sup>2+</sup> channels .....  | 25 |
| 2.1.3.   | Overview of the CRAC system .....  | 29 |
| 2.1.4.   | Molecular components of the CRAC channel .....   | 31 |
| 2.1.5.   | Communication between STIM1 and ORAI1 .....  | 33 |
| 2.1.6.   | Crystal structure of ORAI1 .....   | 35 |
| 2.1.7.   | Physiological implications of CRAC channels deficiencies and<br>therapeutic potential.....       | 39 |
| 2.1.8.   | <i>In vitro</i> assays supporting the identification of <i>I</i> <sub>CRAC</sub> inhibitors..... | 40 |
| 2.1.8.1. | Jurkat cell assay .....  | 40 |
| 2.1.8.2. | LAD2 mast cell assay .....   | 44 |
| 2.1.8.3. | PBMCs assays: CytoStim-stimulated IFN $\gamma$ and LPS-stimulated TNF $\alpha$<br>.....          | 45 |
| 2.1.8.4. | Electrophysiology assay .....  | 49 |
| 2.2.     | Medicinal chemistry approaches to <i>I</i> <sub>CRAC</sub> inhibitors .....                      | 53 |
| 2.2.1.   | Background and chemical landscape of CRAC blockers .....   | 53 |
| 2.2.2.   | First generation of inhaled <i>I</i> <sub>CRAC</sub> inhibitors from our laboratories .....      | 56 |
| 2.2.3.   | Overall objective of the second generation of oral <i>I</i> <sub>CRAC</sub> inhibitors ...       | 58 |
| 2.3.     | Results and discussion: Second <i>I</i> <sub>CRAC</sub> HTS .....                                | 60 |
| 2.3.1.   | An HTS triage focused on physicochemical properties.....   | 60 |
| 2.3.2.   | Introduction to the oxadiazole amine series and definition of the<br>optimisation goals .....    | 66 |
| 2.3.3.   | Introduction to the indole series and definition of the optimisation goals<br>.....              | 68 |
| 2.4.     | Results and discussion: The indole series.....   | 72 |
| 2.4.1.   | Resynthesis of the hit indole <b>2.18</b> .....  | 72 |
| 2.4.2.   | Strategy devised in order to achieve the optimisations goals .....                               | 77 |
| 2.4.3.   | The benzyl group of the tetrazolyindole template .....   | 78 |



|           |  |            |
|-----------|--|------------|
| 2.4.4.    | The indole ring.....   | 84         |
| 2.4.5.    | The tetrazole linker .....   | 86         |
| 2.4.6.    | Conclusion of the indole series.....   | 96         |
| 2.5.      | Results and discussion: The oxadiazole amine series.....   | 99         |
| 2.5.1.    | Validation of the HTS hit.....   | 99         |
| 2.5.2.    | Improvement of the physicochemical properties.....   | 108        |
| 2.5.3.    | Wider profile of the isoxazole amine series.....   | 113        |
| 2.5.3.1.  | Identification of potential developability issues and strategies devised to overcome them.....   | 113        |
| 2.5.3.2.  | Attempt to reduce rat microsomal <i>in vitro</i> clearance.....                                  | 115        |
| 2.5.3.3.  | Modulation of p <i>K</i> <sub>a</sub> in an attempt to improve the chemical series profile ..... | 121        |
| 2.5.4.    | Conclusion of the oxadiazole series.....   | 131        |
| 2.6.      | Overall conclusions of the <i>I</i> <sub>CRAC</sub> programme .....                              | 134        |
| <b>3.</b> | <b>CHAPTER 3: Design, synthesis and optimisation of mPTP modulators.....</b>                     | <b>137</b> |
| 3.1.      | mPTP as a biological target of therapeutic relevance.....  | 137        |
| 3.1.1.    | Description of the mitochondria .....  | 137        |
| 3.1.2.    | Mitochondrial permeability transition and mitochondrial permeability transition pore .....       | 139        |
| 3.1.3.    | Diseases associated with sustained opening of the mPTP and therapeutic opportunities.....        | 142        |
| 3.1.4.    | Published mPTP modulators.....   | 145        |
| 3.1.4.1.  | Cyclic peptides as mPTP modulators .....   | 145        |
| 3.1.4.2.  | Small molecules as mPTP modulators.....  | 147        |

|          |   |     |
|----------|---|-----|
| 3.1.5.   | <i>In vitro</i> assay supporting the identification of mPTP modulators: CRC assay.....                | 150 |
| 3.2.     | Introduction to the mPTP medicinal chemistry programme and setting of the optimisation goals.....     | 152 |
| 3.2.1.   | Overall aim of the research programme and introduction to the cinnamide and the isoxazole series..... | 152 |
| 3.2.1.1. | Objectives for the isoxazole series.....  | 154 |
| 3.2.1.2. | Objectives for the cinnamide series.....  | 156 |
| 3.2.2.   | Screening approaches and pre-candidate profile criteria.....  | 159 |
| 3.3.     | Results and discussion: Synthetic chemistry work on the isoxazole series.....                         | 161 |
| 3.3.1.   | Optimisation of the synthetic route to isoxazole <b>3.17b</b> .....                                   | 161 |
| 3.3.1.1. | Strategy devised in order to optimise the synthesis of <b>3.17b</b> .....                             | 161 |
| 3.3.1.2. | Exploration of the synthetic option 2.....  | 168 |
| 3.3.1.3. | Exploration of the synthetic option 3.....  | 173 |
| 3.3.1.4. | Comparison of the synthetic option 2 vs. option 3 and conclusion of compound <b>3.17b</b> .....       | 183 |
| 3.3.2.   | Optimisation of the synthetic route to isoxazole <b>3.16a</b> .....                                   | 186 |
| 3.3.2.1. | Limitations of the current synthetic route to compound <b>3.16a</b> .....                             | 186 |
| 3.3.2.2. | Improvement of the Mitsunobu step.....  | 188 |
| 3.3.3.   | Conclusion on the improvements to the synthesis of compound <b>3.16a</b> .....                        | 196 |
| 3.4.     | Medicinal chemistry work on the cinnamide series: Previous results....                                | 199 |
| 3.4.1.   | Previously established SAR of the cinnamide series.....   | 199 |
| 3.4.2.   | Previous attempts to increase the solubility of the cinnamide series.....                             | 201 |
| 3.5.     | Results and discussion: Optimisation of the cinnamide series.....                                     | 206 |

|           |  |            |
|-----------|--|------------|
| 3.5.1.    | Strategy to improve the profile of the cinnamide series .....  | 206        |
| 3.5.2.    | Introduction of a basic group in the cinnamide series .....  | 206        |
| 3.5.3.    | Attempts to optimise the DMPK profile of the basic group-containing cinnamides .....                   | 223        |
| 3.5.3.1.  | Investigation of the 1 <sup>st</sup> metabolic site: the toluene methyl group .....                    | 227        |
| 3.5.3.2.  | Investigation of the 2 <sup>nd</sup> metabolic site: the <i>para</i> -position to the amide bond ..... | 229        |
| 3.5.3.3.  | Investigation of the 3 <sup>rd</sup> metabolic site: <i>N</i> -demethylation of the piperazine .....   | 235        |
| 3.5.3.4.  | Investigation of the 4 <sup>th</sup> metabolic site: the piperazinyl ring .....                        | 236        |
| 3.5.4.    | Conclusion of the work on the basic group-containing cinnamides .....                                  | 241        |
| 3.5.5.    | The pyridyl cinnamide series .....   | 243        |
| 3.5.5.1.  | Previous work done on the pyridyl cinnamide series .....   | 243        |
| 3.5.5.2.  | Introduction of a di- <i>ortho</i> -substitution pattern to the amide bond on the pyridine .....       | 247        |
| 3.5.6.    | Conclusion on the work carried out on the cinnamide series .....                                       | 255        |
| 3.6.      | Overall conclusions of the mPTP programme and future work .....  | 257        |
| <b>4.</b> | <b>Experimental section .....</b>  | <b>260</b> |
| 4.1.      | General Methods .....  | 260        |
| 4.2.      | Experimental preparation of the indole analogues for the <i>I</i> <sub>CRAC</sub> programme .....      | 266        |
| 4.3.      | Experimental preparation of the oxadiazole analogues for the <i>I</i> <sub>CRAC</sub> programme .....  | 291        |
| 4.4.      | Experimental preparation of the isoxazole analogues for the mPTP programme .....                       | 313        |
| 4.5.      | Experimental preparation of the cinnamide analogues for the mPTP programme .....                       | 335        |

|           |  |            |
|-----------|--|------------|
| <b>5.</b> | <b>Appendices.....</b>   | <b>364</b> |
| 5.1.      | Appendix 1: Single crystal X-ray diffraction crystallography of<br>compound <b>2.18</b> .....  | 364        |
| 5.2.      | Appendix 2: VCD analysis of compounds <b>3.17a</b> and <b>3.17b</b> .....                      | 372        |
| 5.3.      | Appendix 3: Single crystal X-ray diffraction crystallography of<br>compound <b>3.16a</b> ..... | 376        |
| <b>6.</b> | <b>References.....</b>   | <b>390</b> |

## Abbreviations

|                                   |   |
|-----------------------------------|---|
| A $\beta$                         | : Amyloid $\beta$   |
| Ac                                | : Acetyl  |
| AD                                | : Alzheimer's disease   |
| ADMET                             | : Absorption, distribution, metabolism, excretion, toxicity   |
| ALS                               | : Amyotrophic lateral sclerosis   |
| ANT                               | : Adenine nucleotide translocase  |
| ATP                               | : Adenosine triphosphate  |
| AUC                               | : Area under the curve (for compound exposure in a PK study)  |
| B cell                            | : Bone-marrow derived cell  |
| BINAP                             | : 2,2'-bis(Diphenylphosphino)-1,1'-binaphthyl   |
| Boc                               | : <i>tert</i> -Butoxycarbonyl   |
| °C                                | : Degree celsius  |
| [Ca <sup>2+</sup> ] <sub>0</sub>  | : Extracellular calcium concentration   |
| [Ca <sup>2+</sup> ] <sub>ER</sub> | : Calcium concentration in the endoplasmic reticulum  |
| [Ca <sup>2+</sup> ] <sub>i</sub>  | : Intracellular calcium concentration   |
| Ca <sub>v</sub>                   | : Voltage-gated calcium channel   |
| CBS                               | : Corey-Bakshi-Shibata  |
| CDI                               | : 1,1'-Carbonyldiimidazole  |
| Chrom logD <sub>7.4</sub>         | : Chromatographic measurement of the logarithm of the <i>n</i> -octanol : water partition at pH 7.4 |
| CLND                              | : Chemi-luminescence nitrogen detection   |
| clogP                             | : Daylight calculated logarithm of the <i>n</i> -octanol : water partition coefficient              |
| C <sub>max</sub>                  | : Maximal concentration (achieved by a compound in a PK study)                                      |
| C <sub>mpd</sub>                  | : Compound  |
| CNS                               | : Central nervous system  |
| <i>m</i> -CPBA                    | : <i>meta</i> -Chloroperbenzoic acid  |
| CRAC                              | : Calcium release-activated calcium   |
| CRACM1                            | : Calcium release-activated calcium modulator 1   |
| CRC                               | : Calcium retention capacity  |
| CsA                               | : Cyclosporin A   |
| CV                                | : Column volume   |

|                  |  |
|------------------|--|
| Cyp A            | : Cyclophilin A  |
| Cyp D            | : Cyclophilin D  |
| CYPs             | : Cytochrome P450 enzymes  |
| $\delta$         | : Chemical shift (in NMR spectroscopy)   |
| DCC              | : <i>N,N'</i> -Dicyclohexylcarbodiimide  |
| DCM              | : Dichloromethane  |
| d.e.             | : Diastereomeric excess  |
| DIAD             | : Diisopropyl azodicarboxylate   |
| DIPEA            | : <i>N,N</i> -Diisopropylethylamine  |
| DMAP             | : 4-Dimethylaminopyridine  |
| DMF              | : <i>N,N</i> -Dimethylformamide  |
| DMPK             | : Drug metabolism and pharmacokinetics   |
| DMS              | : Dimethylsulfide  |
| DMSO             | : Dimethylsulfoxide  |
| $\Delta\Psi_m$   | : Mitochondrial membrane potential   |
| EDTA             | : Ethylenediaminetetraacetic acid  |
| e.e.             | : Enantiomeric excess  |
| eq               | : Equivalent   |
| ER               | : Endoplasmic reticulum  |
| ES               | : Electrospray   |
| Et               | : Ethyl  |
| EtOAc            | : Ethyl acetate  |
| FaSSIF           | : Fasted state simulated intestinal fluid  |
| Fc $\epsilon$ RI | : High-affinity immunoglobulin E receptor  |
| FP               | : Fluorescence polarisation  |
| FRET             | : Förster resonance energy transfer  |
| fS               | : Femtosiemen (= $10^{-15}$ Siemen)  |
| Fu,bl            | : Fraction unbound in rat blood  |
| Glu              | : Glutamic acid  |
| Gly              | : Glycine  |
| GSK              | : GlaxoSmithKline  |
| HAC              | : Heavy atom count   |
| HATU             | : 1-[Bis(dimethylamino)methylene]-1 <i>H</i> -1,2,3-triazolo[4,5-<br>b]pyridinium 3-oxid hexafluorophosphate |
| hERG             | : Human ether-à-go-go-related gene   |

|   |  |
|---|--|
| HMBC                                    | : Heteronuclear multiple bond correlation                    |
| HPLC                                    | : High-performance liquid chromatography                     |
| HRMS                                    | : High-resolution mass spectroscopy                          |
| HSA                                     | : Human serum albumin  |
| HTS                                     | : High throughput screening                                  |
| $I_{CRAC}$                              | : Calcium release-activated calcium channel current          |
| IFN $\gamma$                            | : Interferon-gamma   |
| IgE                                     | : Immunoglobulin E   |
| IMM                                     | : Inner mitochondrial membrane                               |
| InsP <sub>3</sub> (or IP <sub>3</sub> ) | : Inositol-1,4,5-trisphosphate                               |
| InsP <sub>3</sub> R                     | : Inositol-1,4,5-trisphosphate receptor                      |
| IR                                      | : Infrared   |
| IV                                      | : Intravenous  |
| (h / r / m) IVC                         | : (human / rat / mouse microsomes) <i>in vitro</i> clearance |
| $J$                                     | : Coupling constant (in NMR spectroscopy)                    |
| KcsA                                    | : Potassium crystallographically-sited activation channel    |
| LCMS                                    | : Liquid chromatography-mass spectrometry                    |
| LDA                                     | : Lithium diisopropylamide                                   |
| LE                                      | : Ligand efficiency  |
| LLE                                     | : Ligand-lipophilicity efficiency                            |
| LPS                                     | : Lipopolysaccharide   |
| MDAP                                    | : Mass directed auto-preparative HPLC                        |
| Me                                      | : Methyl   |
| Met                                     | : Metal  |
| MOE®                                    | : Molecular operating environment®                           |
| mp                                      | : Melting point  |
| mPT                                     | : Mitochondrial permeability transition                      |
| mPTP                                    | : Mitochondrial permeability transition pore                 |
| MW                                      | : Molecular weight   |
| $m/z$                                   | : Mass-to-charge ratio                                       |
| NA                                      | : Not applicable   |
| nAr                                     | : Number of aromatic rings                                   |
| ND                                      | : Not determined   |
| NFAT                                    | : Nuclear factor of activated T cells                        |
| NF- $\kappa$ B                          | : Nuclear factor- $\kappa$ B                                 |

|                                    |   |
|------------------------------------|---|
| NK cell                            | : Natural killer cell   |
| NMR                                | : Nuclear magnetic resonance  |
| OMM                                | : Outer mitochondrial membrane  |
| OXPHOS                             | : Oxidative phosphorylation   |
| PBMCs                              | : Peripheral blood mononuclear cells                                      |
| PD                                 | : Pharmacodynamic   |
| Pd <sub>2</sub> (dba) <sub>3</sub> | : Tris(dibenzylideneacetone)dipalladium(0)                                |
| Pd(OAc) <sub>2</sub>               | : Palladium(II) acetate   |
| PFI and cPFI                       | : Measured property forecast index and calculated property forecast index |
| PG                                 | : Protecting group  |
| Ph                                 | : Phenyl  |
| pIC <sub>50</sub>                  | : Negative logarithm of the 50% inhibitory concentration                  |
| PIP <sub>2</sub>                   | : Phosphatidylinositol-4,5-bisphosphate                                   |
| PK                                 | : Pharmacokinetic   |
| PLC $\gamma$                       | : Phospholipase C $\gamma$  |
| PMCA                               | : Plasma membrane calcium ATPase  |
| +ve                                | : Positive  |
| ppm                                | : Parts per million   |
| PyBOP                              | : (Benzotriazol-1-yloxy)tripyrrolidinophosphonium hexafluorophosphate     |
| QTOF                               | : Quadrupole time-of-flight   |
| R&D                                | : Research and development  |
| ROS                                | : Reactive oxygen species   |
| rt                                 | : Room temperature  |
| Rt                                 | : Retention time  |
| RuPhos                             | : Dicyclohexyl(2',6'-diisopropoxy-[1,1'-biphenyl]-2-yl)phosphine          |
| RyR                                | : Ryanodine receptor  |
| SAR                                | : Structure-activity relationship   |
| SCID                               | : Severe-combined immunodeficiency  |
| SCX                                | : Strong cation exchange  |
| Ser                                | : Serine  |
| SERCA                              | : Sarcoplasmic/endoplasmic reticulum calcium ATPase                       |
| siRNA                              | : Small interfering ribonucleic acid                                      |
| SOA                                | : Short oral absorption PK <i>in vivo</i> model                           |

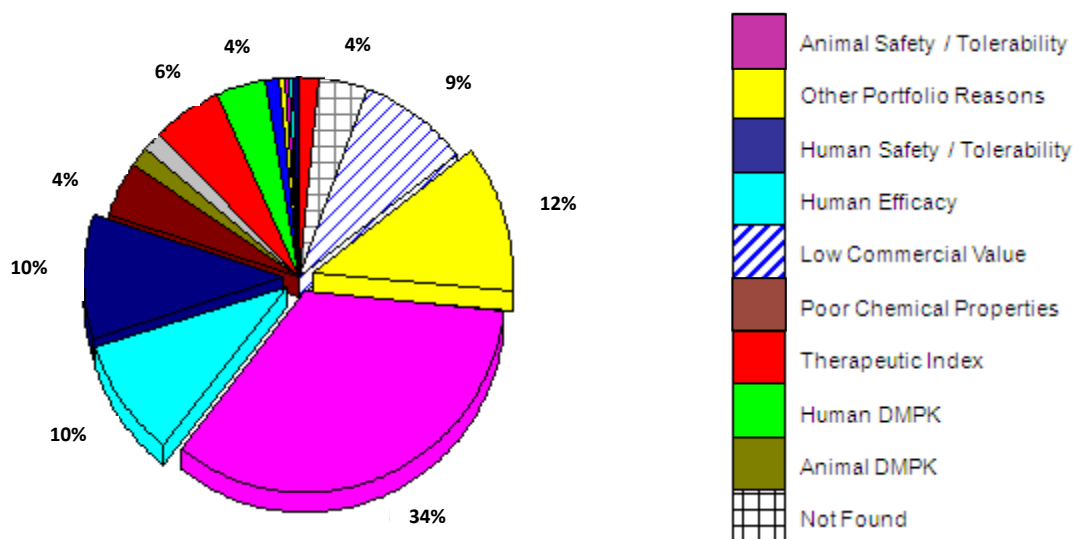


|                  |   |
|------------------|---|
| SOCE             | : Store-operated calcium entry  |
| SOD1             | : Superoxide dismutase-1  |
| STIM1            | : Stromal interaction molecule 1  |
| TBAF             | : Tetrabutylammonium fluoride   |
| TBME             | : <i>tert</i> -Butyl methyl ether   |
| <i>t</i> Bu      | : <i>tert</i> -Butyl  |
| T cell           | : Thymus cell   |
| TFA              | : Trifluoroacetic acid  |
| THF              | : Tetrahydrofuran   |
| THP              | : Tetrahydropyranyl   |
| Thr              | : Threonine   |
| TM               | : Transmembrane   |
| T <sub>max</sub> | : Time at which the maximal concentration of an investigated compound is achieved in a PK study |
| TNF $\alpha$     | : Tumor necrosis factor-alpha   |
| TSPO             | : The mitochondrial translocator protein  |
| UV               | : Ultraviolet   |
| VCD              | : Vibrational circular dichroism  |
| VDAC             | : Voltage-dependent anion channel   |
| v/v              | : By volume   |
| XantPhos         | : (9,9-Dimethyl-9 <i>H</i> -xanthene-4,5-diyl)bis(diphenylphosphine)                            |
| XPhos            | : Dicyclohexyl(2',4',6'-triisopropyl-[1,1'-biphenyl]-2-yl)phosphine                             |

# 1. CHAPTER 1: Opportunities and challenges to increase chance of success during drug development

## 1.1. The drug discovery crisis

The number of new drugs approved, especially small molecules, has not been proportional to the increase in research and development (R&D) spending both in the public and private sectors. Hence, the number of new drugs approved per billion US dollars spent on R&D has halved every nine years since 1950.<sup>1</sup> Studies have shown that this productivity decline was associated with an increasing concentration of R&D investments in areas of unmet therapeutic needs, which are characterised by a high risk of failure.<sup>2</sup> The recent low success rate of new drug molecules reaching the market can mostly be attributed to drug attrition. Indeed, it has been estimated that 93% to 96% of candidate drugs (that is when a molecule is considered for human clinical trial) fail at some stage during drug development.<sup>3</sup> Consequently, understanding the causes underlying drug attrition is a sensible approach in order to devise strategies to tackle it. A recent study of the reasons for terminating drug discovery programmes (after candidate selection) within our laboratories<sup>4</sup> determined that safety was the main factor for compounds failing to progress through the development process (**Figure 1**). This finding was similar to the observations made when analysing the principal causes for candidate failures of ten pharmaceutical companies<sup>3</sup> and for AstraZeneca only.<sup>5</sup>



**Figure 1: Reasons associated with termination of GlaxoSmithKline (GSK) drug candidates<sup>4</sup>**

Even if several causes associated with drug attrition are independent to the quality of the compound (*e.g.* choice of the biological target, biological target-based toxicity and choice of patients population in clinical trials), most of them are directly linked with the chemical structure of the molecule. Indeed, it is now widely accepted that the physicochemical properties of small molecules not only impact their binding affinity to the target, but also their pharmacokinetic properties (permeability, absorption, exposure) and non target-related toxicological effects.<sup>6</sup> Therefore, it is the medicinal chemist's responsibility to ensure that the physicochemical properties of the compounds synthesised are carefully considered.

## **1.2. Importance of the physicochemical parameters of small molecules and introduction to modern drug design tools**

Several studies examining the profile of marketed drugs introduced the proposal that specific value ranges for a number of physicochemical properties would help molecules to optimally exert their biological effect while improving ADMET (absorption, distribution, metabolism, excretion and toxicity) properties. Probably the first main contribution to the field was the paper from Lipinski and co-workers<sup>7</sup>

introducing the “rule of five” physicochemical property guidelines. Analysing a database of clinical candidates reaching Phase II trials or further, it was noticed that poor absorption or permeability was more likely when clogP (the calculated logarithm of the *n*-octanol : water partition coefficient) is  $> 5$ ; molecular mass is  $> 500$  daltons; the number of hydrogen-bond donors (OH plus NH count) is  $> 5$ ; and the number of hydrogen-bond acceptors (O plus N atoms) is  $> 10$ . Almost 20 years after these first guidelines, the definitions of the “drug-like space” have been revised further and the concept of “drug-likeness” of oral small molecules has been introduced.<sup>6,8,9</sup>

Among all the physicochemical parameters, lipophilicity, which is defined as the affinity of a molecule for a lipophilic environment, is the most important drug-like physical property. The intrinsic lipophilicity (logP) describes the partition of the unionised form of a compound between *n*-octanol and water and is constant for a given compound. The effective lipophilicity (logD<sub>pH</sub>) represents the partition of all forms of the compounds (ionised or not) between the phases for a given pH. Consequently, at physiological pH (pH = 7.4), some compounds may be ionised and thus display a different apparent lipophilicity to their corresponding non-ionised form. The associated clogP (calculated logP) measure is of particular relevance since it was determined that high lipophilicity has a negative impact on numerous development criteria, such as aqueous solubility, metabolism, hepatic clearance and bioavailability.<sup>10</sup>

However, a retrospective analysis of medicinal chemistry practices reviewed by Leeson and Springthorpe<sup>11</sup> underlined that the chemical space occupied the recent medicinal chemistry efforts was different compared to the one of the historical drugs. More specifically, it was realised that the recent reduction in the number of drugs launched correlated with an increase in molecular weight (MW) and in clogP. Thus, the mean clogP and MW of the oral drugs marketed between 1983 and 2007 was 2.7 and 358, respectively, whereas the mean clogP and MW of patented compounds from four large pharmaceutical companies in the period of 2003 to 2007 was 4.1 and 450, respectively.<sup>11</sup> A similar trend was observed when focusing on lead compounds (which is the stage prior to candidate drugs), for which it was shown that historical

lead compounds had smaller MW and clogP compared to the most recent ones.<sup>12</sup> Moreover, the analysis from Leeson and Springthorpe showed that an increase in clogP and in MW was linked to a greater level of off-target activity and consequently, to potential for toxicity.<sup>11</sup> This trend is explained by the fact that protein binding sites are lipophilic in nature, implying that the more lipophilic compounds have a greater probability of binding to multiple targets. These observations were critical in highlighting the need to keep several physicochemical parameters under control during drug discovery optimisation efforts.

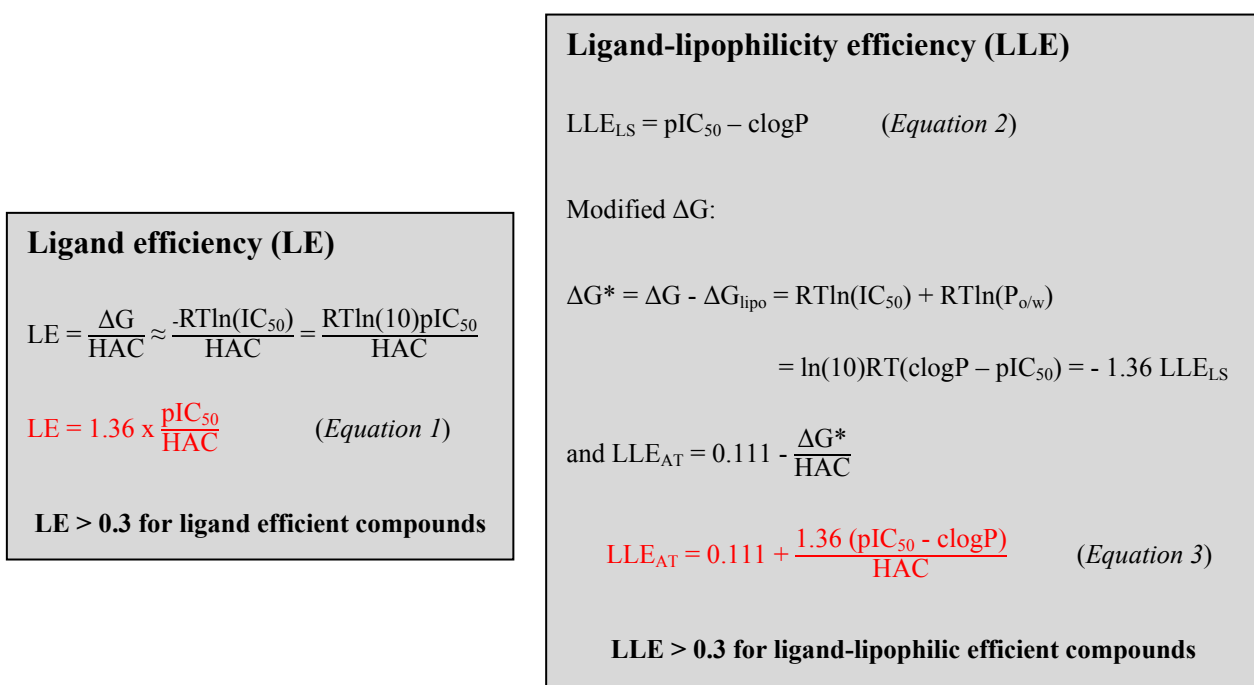
Following on from these critical studies, more recent analyses have been conducted and their relevance to drug optimisation efforts is outlined below.

### 1.2.1. Ligand efficiency and ligand-lipophilicity efficiency

Within a chemical series, potency is often strongly correlated with MW and lipophilicity. However, an increase in MW and in lipophilicity is generally associated with an increased risk of toxicity, and thus with an increased risk of drug attrition. Therefore, new concepts taking into account drug potency per unit of mass and per unit of lipophilicity were introduced in order to keep control of both MW and lipophilicity while choosing an initial lead compound, and also while carrying out lead optimisation. Hopkins and co-workers<sup>13</sup> proposed a new concept of ligand efficiency (LE, *equation 1*, **Figure 2**), based on the binding energy per heavy atom. Ligand efficiency is formally defined as the ratio of the free energy of binding ( $\Delta G$ ) to the number of heavy atoms (heavy atom count = HAC). To determine the lowest acceptable limit for LE, a hypothetical compound having a potency of 10 nM and a MW of 500, which after analysis of the Pfizer corporate screening data corresponds to a HAC of 38,<sup>13</sup> is chosen. With this value in hand, a lower limit for LE of 0.3 is defined. Thus, when undertaking lead optimisation, efforts should be made to keep the LE constant, or at least to ensure that LE is higher than 0.3.

In order to incorporate lipophilicity in the LE measure, Leeson and Springthorpe initially introduced a simple new concept, ligand-lipophilicity efficiency (LLE<sub>LS</sub>, *equation 2*, **Figure 2**).<sup>11</sup> Nevertheless, to harmonise the lower limits of LE and LLE,

a more appropriate definition of LLE has been introduced by the Astex Company (LLE<sub>AT</sub>, equation 3, **Figure 2**).<sup>14</sup> In the Astex definition of the ligand-lipophilicity efficiency, the binding process of a drug molecule is represented as a two step process: first transfer from the aqueous to a generic hydrophobic environment (with free energy change  $\Delta G_{\text{lipo}}$ ) and second the specific binding of the ligand to the protein ( $\Delta G^*$ ). A constant term of 0.111 is introduced so that when calculating the LLE of a target compound with a potency of 10 nM and a HAC of 36 (slight variation from the Pfizer definition), then the LLE<sub>AT</sub> is 0.3. Thus, when carrying out lead optimisation, it is recommended to keep LLE<sub>AT</sub> above the same lower limit than the one set up for LE, which is 0.3.



**Figure 2: Definitions of ligand efficiency (LE) and ligand-lipophilicity efficiency (LLE)**

In an attempt to summarise the various guidelines suggested in the literature,<sup>15</sup> **Table 1** defines the current definitions of what constitutes the preferred oral drug-like space. It is worth noting that a lower limit of lipophilicity is important for efficient membrane permeability (hence oral absorption).<sup>16</sup>

| Drug properties  | Desired target area |
|------------------|---------------------|
| Molecular weight | < 400 daltons       |
| logP             | [0 – 3]             |
| logD             | [1 – 3]             |
| LE               | > 0.3               |
| LLE              | > 0.3               |

**Table 1: Recommended physicochemical properties values for oral drugs**

### 1.2.2. Aqueous solubility and Property Forecast Index

A drug molecule has to be dissolved in an aqueous environment prior to engagement with its target and, additionally, aqueous solubility is a prerequisite for oral absorption. In our laboratories, aqueous solubility was primarily measured using chemi-luminescence nitrogen detection (CLND), which is a high-throughput method for kinetic solubility assessment from compounds dissolved in DMSO. Practically, 5  $\mu$ L of a 10 mM DMSO stock solution was diluted to 100  $\mu$ L with pH 7.4 phosphate buffered saline and the concentration of the compound was measured after filtration. The aqueous solubility was referred as low when CLND solubility < 30  $\mu$ g/mL, medium when CLND solubility was between 30 and 100  $\mu$ g/mL and high when CLND solubility > 100  $\mu$ g/mL.

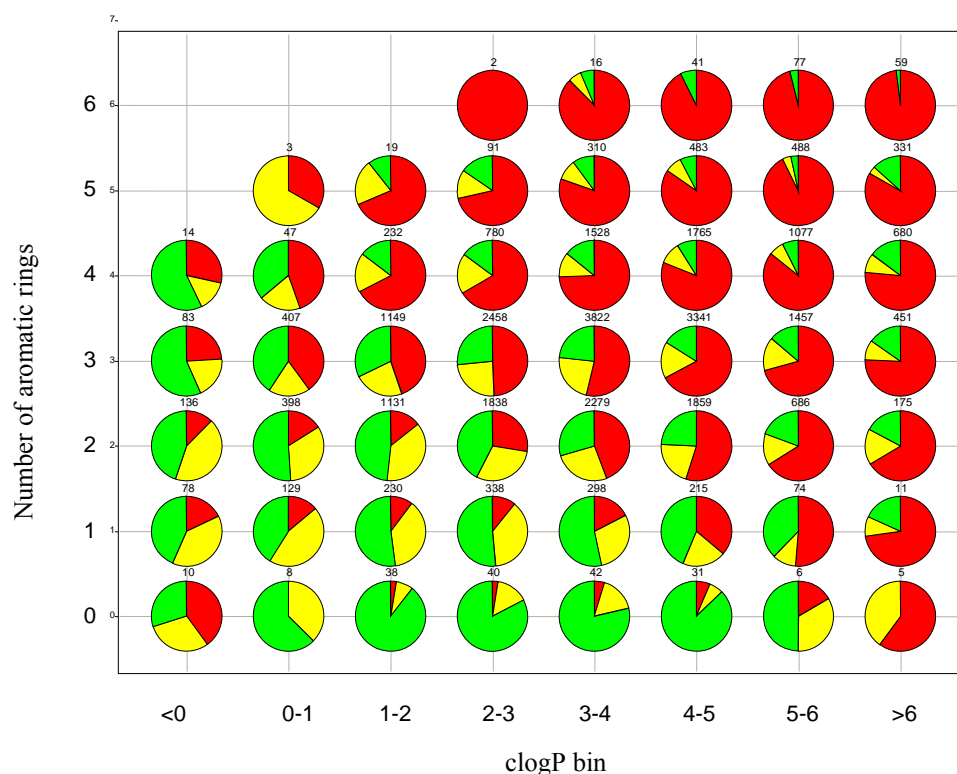
It seems reasonably obvious that there is a correlation between lipophilicity and aqueous solubility and indeed, an analysis of more than 40,000 GSK compounds by Gleeson showed that the chances of achieving high aqueous solubility are increased significantly for molecules that exhibit a logP < 3.<sup>17</sup> However, the impact of aromatic ring count on various drug developability measures, such as aqueous solubility, lipophilicity and serum albumin binding is probably less foreseeable (**Table 2**).<sup>18</sup> Nevertheless, it was highlighted in the literature that increasing the number of aromatic rings in small molecules increases their lipophilicity (*e.g.* the addition of a phenyl ring increases the molecular weight by 76 and the clogP by 2.14 units), with concomitant reduction of aqueous solubility, increase in the level of plasma protein binding and increase in the likelihood of off-target activity.<sup>18</sup>

| <b>Number of aromatic rings</b>               | <b>1</b> | <b>2</b> | <b>3</b> | <b>4</b> | <b>5</b> |
|---|----------|----------|----------|----------|----------|
| <b>clogP</b>                                  | 1.9      | 2.9      | 3.7      | 4.4      | 5.1      |
| <b>LogD<sub>7.4</sub></b>                     | 1.3      | 2.1      | 2.4      | 2.7      | 2.9      |
| <b>Serum albumin binding (%)</b>              | 78       | 88       | 93       | 96       | 96       |
| <b>Aqueous solubility (µg/mL)</b>             | 100      | 79       | 57       | 36       | 28       |
| <b>P450 3A4 inhibition (pIC<sub>50</sub>)</b> | 4.7      | 4.9      | 5.2      | 5.4      | 5.6      |
| <b>hERG inhibition (pIC<sub>50</sub>)</b>     | 5.2      | 5.6      | 5.7      | 5.7      | 5.5      |

**Table 2: Mean values of a set of physicochemical parameters vs. number of aromatic rings for a set of GSK compounds<sup>18</sup>**

It is worth noting that the average number of aromatic rings in marketed oral drugs is 1.6 and that it was observed that more than three aromatic rings in a molecule correlates with poorer compound developability profile and, therefore, with an increased risk of compound attrition.<sup>18</sup> To exemplify further the detrimental impact of increasing the aromatic ring count, a plot of the number of aromatic rings in clogP bins and its effect on the aqueous solubility was generated (**Figure 3**).<sup>18</sup> Hence, in the same clogP bin, a greater number of aromatic rings was correlated with a reduction in solubility of the compound.



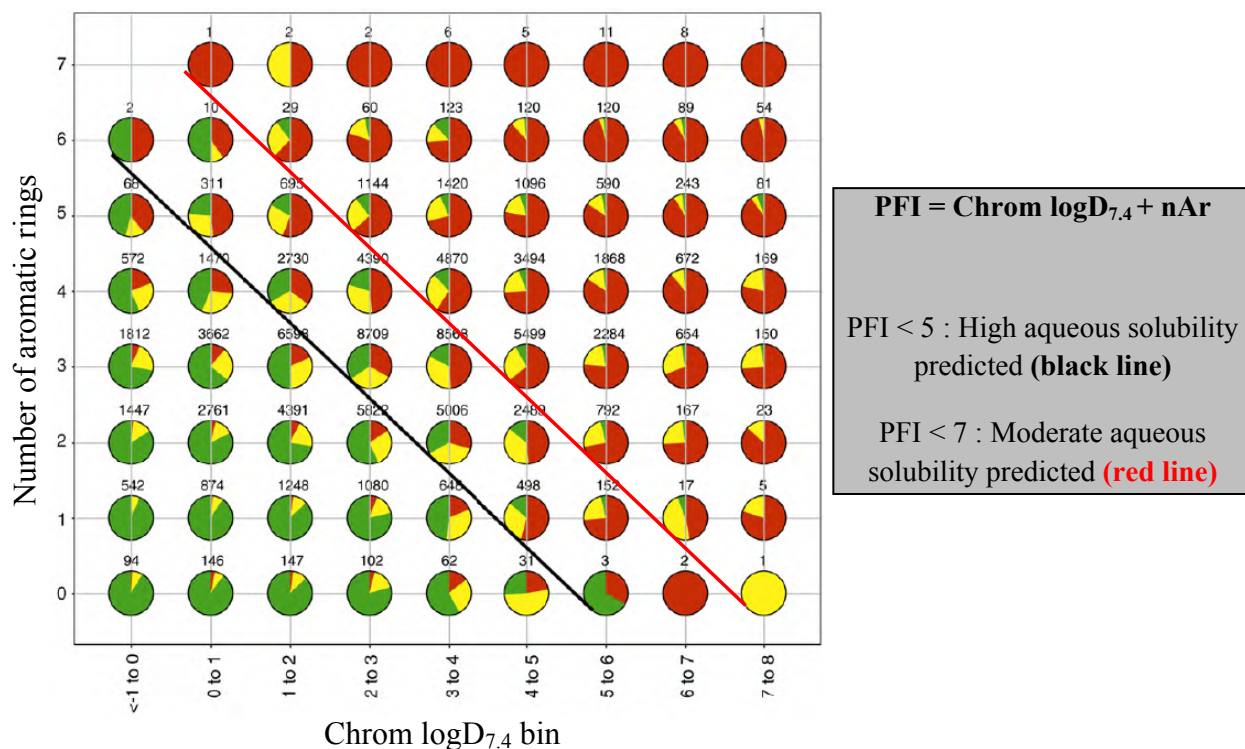


Pie charts are divided into three aqueous solubility segments: < 50 µg/mL in red, 50-100 µg/mL in yellow and >100 µg/mL in green. The number above the pie charts is the number of compounds in the sample set.

**Figure 3: Effect of number of aromatic rings on solubility<sup>18</sup>**

Following on these observations, Young and co-workers<sup>19,20</sup> introduced a new metric named Property Forecast Index (PFI), defined as the sum of the chromatographic  $\log D_{7.4}$  and the number of aromatic rings. Initially, it was identified as a simplistic but powerful guide for predicting likelihood of aqueous solubility. The associated parameter Chrom  $\log D_{7.4}$  is defined as the logarithm of the *n*-octanol : water partition at pH 7.4 and is measured by the retention of compounds on a lipophilic chromatographic column (the longer the retention time, the more lipophilic). Chrom  $\log D_{7.4}$  was recently established in our laboratories as the principal measurement of lipophilicity, because of its relevance and reproducibility at physiological pH. Furthermore, software developed in our laboratories to calculate Chrom  $\log D_{7.4}$  has proven to be particularly accurate in predicting the experimentally determined Chrom  $\log D_{7.4}$  value. When PFI was calculated for a large dataset of molecules from

GSK, Hill and Young realised that a PFI less than 5 was predictive of a high aqueous solubility, a PFI between 5 and 7 was predictive of a moderate aqueous solubility and that a PFI greater than 7 was predictive of a low aqueous solubility (**Figure 4**).<sup>19</sup>



Pie charts are divided into three aqueous solubility segments: < 50 µg/mL in red, 50-100 µg/mL in yellow and >100 µg/mL in green. The numbers above the pie charts are the number of compounds in the sample set.

**Figure 4: Pie chart matrix representation of solubility category as a function of Chrom logD<sub>7.4</sub> and number of aromatic rings**<sup>19</sup>

Furthermore, the PFI concept was also predictive of additional drug developability parameters. Thus, the profile of compounds with PFI < 7 was more consistent with a profile of an oral drug candidate, with regard to values of human serum albumin binding, cytochrome P450s binding, microsomal *in vitro* clearance, and binding to important biological targets known to cause side-effects, such as human ether-à-go-go-related gene (hERG).<sup>20</sup> The relevance of these parameters in an oral lead optimisation setting is expanded upon in the following sections.

### 1.2.3. Protein binding

The extent to which drug molecules bind to plasma protein is an important parameter to monitor during drug discovery, as high plasma protein binding of a drug is precluded to reduce the free drug fraction in the blood able to circulate and to move across barriers in order to reach the biological target and exert efficacy.<sup>21</sup> The “free drug principle” is the theory that the unbound drug concentration at the site of action, as opposed to the total drug concentration, is the key parameter leading to pharmacological efficacy.<sup>22</sup> This parameter is again largely influenced by lipophilicity of the molecules, that is to say the more lipophilic the compound is, the greater the extent to which it binds to plasma protein.<sup>23</sup> This is largely explained by the fact that the binding sites of the plasma protein are lipophilic in nature. However, the significance of plasma protein binding on drug efficacy and therefore its clinical relevance has been controversially debated in the literature.<sup>24,25,26</sup> If plasma protein binding seems to be a crucial parameter from a pharmacokinetic (PK) standpoint, as it directly drives the amount of free unbound drug, its impact on the pharmacodynamic (PD) properties of a drug is more complex to rationalise. Indeed, many other factors are now to be taken into account, such as tissue binding, drug affinity for its target, location of the biological target (extracellular or intracellular) and blood clearance. Nevertheless, it is important to avoid highly to very highly plasma protein bound compound by reducing the overall lipophilicity of compounds. Since human serum albumin (HSA) is the most abundant protein in human plasma, it is commonly used to assess ability of compounds to bind plasma protein. Typically, highly protein bound molecules are compounds with a HSA binding greater than 95%, and very highly protein bound molecules are compounds displaying a HSA binding greater than 99%.

#### 1.2.4. *In vitro* microsomal clearance

Absorption, distribution, metabolism, and excretion of a pharmaceutical molecule are all crucial parameters to control during the development of an oral drug. Indeed, poor bioavailability, resulting either from low intestinal absorption or from high metabolic instability (or both), leads to a low concentration of the drug in systemic circulation and consequently, reduces pharmacological efficacy. Of all these factors, drug metabolism, which is the biotransformation of a molecule by enzymes to make it more easily eliminated by the body, is perhaps the feature that is the most straightforward to measure in a pre-clinical setting.<sup>27</sup> In an attempt to reduce drug attrition during later stages of development, several *in vitro* metabolic stability assays are now commonly used by medicinal chemists. The data generated at the early stage of the programme are also useful when later predicting the drug metabolism in humans.<sup>28</sup> In most cases, the drug metabolism pathway involves the oxidation of the parent drug (phase I metabolism), predominantly by the cytochrome P450 enzymes (CYPs), followed by conjugation of the oxidised metabolite with for example glucuronic acid (phase II metabolism). CYPs are a family of heme-containing enzymes and they represent the main enzymes involved in drug metabolism and bioactivation, accounting for the metabolism of approximately two-thirds of marketed drugs.<sup>29</sup> Their function is to catalyse the oxidation of exogenous and endogenous organic substances to favour their excretion. The biotransformation of their substrate into a more polar product makes it easier to be subsequently excreted by the body.

A study of about 47,000 compounds by scientists from Pfizer showed that microsomal clearance, using human liver microsomes, increased when lipophilicity increased.<sup>30</sup> Additionally, high PFI values were also shown to correlate with high values of human liver microsomal clearance for a set of 8700 GSK compounds, and a PFI values > 7 led to more than 50% of compounds having high clearance.<sup>20</sup>

In our laboratories, in order to investigate early in a research programme the metabolic stability of a compound in a relatively high throughput manner, *in vitro* clearance (IVC) assays, using liver microsomes from a range of different species (rat, mouse and human), are used. This approach is often employed to eliminate high

clearance compounds *in vitro* during the initial stages of drug discovery. Microsomes are a subcellular fraction obtained *via* differential centrifugation of liver homogenates and they contain a range of enzymes involved in drug metabolism. The microsomes isolated from liver are used, since liver is the primary site of drug metabolism, explaining why hepatic clearance is of critical interest. The IVC measurement was not quantitative but qualitative only and it primarily enabled classification of compounds as having either a low (IVC < 2 mL/min/g), moderate (between 2 and 10 mL/min/g) or high clearance (IVC > 10 mL/min/g).

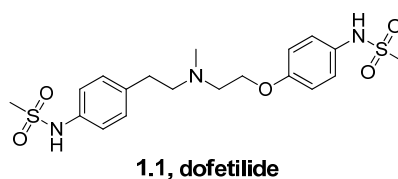
### 1.2.5. Inhibition of the hERG channel

The human ether-à-go-go-related gene (hERG) channel is a potassium channel expressed on the cardiac myocytes that plays a key role in the normal repolarisation of action potential of the heart. Its blockade has been associated with a delay in this repolarisation, causing prolongation of the time between Q and T waves on an electrocardiogram. Additionally, long QT syndrome can lead to the development of severe arrhythmias (*i.e.* an abnormal electrical activity in the heart) and to the risk of sudden cardiac death. As a result of this important side-effect, a number of drugs have been withdrawn from the market in recent years due to cardiovascular toxicity associated with undesirable blockade of the hERG potassium channel.<sup>31</sup>

Alongside its pharmacological importance, the hERG ion channel is characterised by a unique ability to bind a wide range of chemical structures. Consequently, the importance of mitigating the risk of inhibiting the hERG channel early in the drug discovery process has now been recognised and novel technologies are available to facilitate hERG screening.<sup>32,33</sup> A crystal structure of the hERG channel is not yet available, however, several homology models (based on other potassium channels) have been generated, enabling the generation of a pharmacophore of hERG blockers.<sup>34,35,36</sup> These studies have highlighted two aromatic residues of the hERG channel, the tyrosine at position 652 and the phenylalanine at position 656, as being pivotal for the binding of channel blockers. The Y652 participates in  $\pi$ -cation type interactions with basic amines and the hydrophobic surface of F656 participates in

hydrophobic interaction (especially with aromatic rings) with hERG blockers. Thus, a common pharmacophore for potent hERG blockers consists of a hydrophobic aromatic part combined with a basic motif, usually a nitrogen that would be protonated at physiological pH. Consistently with the above observations, an analysis of 7685 AstraZeneca compounds showed that basic compounds were markedly more likely to have hERG activity than neutral and acidic compounds.<sup>37</sup> In this study, increased hERG liability was also correlated with higher lipophilicity.<sup>37</sup>

In our laboratories, the compound ability to inhibit the hERG channel was tested using two biological assays. Firstly, a fluorescence polarisation (FP) hERG binding assay, where the ability of the test compound to compete against a potent hERG blocker (dofetilide **1.1**, **Figure 5**) labelled with a fluorescent tag was measured. Secondly, a direct measure of the compound effect to block the hERG channel using an automated patch clamp electrophysiological method (IonWorks Barracuda®) was employed.



**Figure 5: Structure of dofetilide**

To summarise this discussion, a common historical assumption in medicinal chemistry efforts was that compounds with higher *in vitro* potency at their target(s) would have a greater likelihood to translate into successful therapeutics.<sup>38</sup> This was sometimes achieved while neglecting other developability parameters, such as lipophilicity, aqueous solubility and aromatic ring count. In the programmes of work described here, a considerable emphasis was placed on the physicochemical properties of the molecules designed and synthesised. Additionally, the two different screening strategies used in each of the two medicinal chemistry programmes investigated here (see **Figure 31**, p. 59 and **Figure 57**, p. 160) focused with equal importance on the primary *in vitro* activity against the biological target and on several physicochemical parameters. By doing so, we were accepting the challenge

represented by concomitantly optimising potency and ADMET properties, since they often have diametrically opposed relationship.<sup>38</sup>

Also relevant to drug attrition is the pharmacological measurement of compound biological activity, which is discussed in the next section.

### **1.3. Phenotypic screening**

The pharmacological assays used to identify new medicines can be classified into two major types: target-based assays and phenotypic assays. In the first approach, the aim is to manipulate a biological system by pharmacologically modulating a specific component or target, which for instance could be an enzyme, an ion channel or a receptor. In relation to phenotypic assays, a characteristic associated with a disease is exploited to develop an assay which relies on a target-agnostic measure of a biological response. Additionally, a phenotypic assay typically measures the activity of a compound in a more physiologically relevant media, such as cells, tissues or whole organisms.

The two approaches both have their advantages and disadvantages.<sup>39</sup> A target-based assay is often high throughput and allows the testing of a large number of compounds in a short period of time. Furthermore, the knowledge of the molecular target identity can help guide toxicology studies during preclinical development, since potential target-associated safety liabilities and toxicity can be predicted.<sup>39</sup> Of particular relevance for medicinal chemists, the target-based approach can facilitate the lead optimisation process by offering a structure-activity relationship (SAR) that is easier to rationalise. A specific advantage of knowing the biological target is that this can enable the use of structure-based drug discovery tools such as X-ray crystallography and computational homology modelling, which assist the molecular design process.

A disadvantage of the target-based approach is that there is a risk that the specific molecular hypothesis may not be relevant to the disease pathogenesis. Indeed, the success of the target-based screening approach relies on the hypothesis that the biological target investigated is strongly linked to a disease and that the mode of

action at the target in question is one that is capable of achieving the desired biological response in a more complex environment. However, several analyses have revealed that high drug attrition rates in Phase II and III are in a large proportion due to lack of efficacy and this could be partially driven by a poor correlation between a single biological target modulation and a phenotypic outcome.<sup>5,40</sup>

The phenotype-based approach provides an unbiased way to find active compounds in the context of complex biological systems.<sup>41</sup> This strategy does not require prior understanding of the molecular mechanism of action and this is therefore an attractive option when little is known about the exact signalling pathway involved or for understudied diseases. For instance, phenotypic screening has been widely investigated in neurodegenerative diseases, which are complex diseases involving multiple genes and proteins as well as multiple pathways rather than converging on a single gene, protein or target.<sup>42,43</sup> There has also been a major emphasis on phenotypic approaches to drug discovery for neglected diseases, particularly in the areas of malaria and human African trypanosomiasis.<sup>44</sup> An additional benefit of a phenotypic screening approach is that it has not only the potential to identify molecules that modify a disease phenotype by acting on a target previously not described, but it also can detect agents acting simultaneously on more than one target. This is referred to as polypharmacology and it is now recognised that the synergistic effects of multiple modes of action can sometimes lead to a better therapeutic outcome.<sup>45,46</sup> Finally, a major advantage of the phenotypic approach is that activity in such assays might be translated into therapeutic impact in a given disease state more effectively than target-based assays. Indeed, a phenotypic assay uses a more native biological system and is less artificial than a target-based assay.<sup>41</sup>

A drawback of phenotypic assays is that they usually have a considerably lower throughput than target-based assays. Additionally, another challenge faced by the phenotypic approach is the impossibility of performing structure-based drug discovery, which renders the molecular design of drugs more complicated. Nevertheless, even when the biological target is known, the binding site is often not fully characterised and in this case, it remains difficult to rationalise the specific interactions occurring between the pharmacological molecule and the receptor.



Consequently, medicinal chemists will generate SAR by performing systematic structural changes to the hit molecule, as this would also be the case for a phenotypic approach. Finally, the preclinical and clinical development can be more challenging with an unknown target, particularly because it is more difficult to predict mechanism-based toxicities.<sup>47</sup> For this reason, in a medicinal discovery programme initiated with a phenotypic screening, efforts are often made to subsequently identify the biological target(s). Several methods are now available to carry out the deconvolution of biological targets and this usually relies on a combination of genetics and chemical proteomics.<sup>48,49</sup> Nevertheless, it is worth mentioning that the knowledge of the identity of the biological target is not mandatory for the launch of a new medicine and that regulatory agencies will approve a drug without requiring the precise mechanism of action or the molecular target(s), as long as the drug is efficacious and safe for patients.<sup>39</sup>

Historically, the phenotypic-based strategy constituted the main approach used in drug discovery.<sup>50</sup> Indeed, before the introduction of the target-based approach, drug discovery was driven primarily by phenotypic assays, often with limited knowledge of the molecular mechanisms of disease. For instance, aspirin was discovered after phenotypic observations and it took more than 70 years to determine its mechanism of action and molecular target.<sup>51</sup> Nevertheless, the pharmaceutical industry was successful in the discovery and development of new innovative medicines. With the advent of gene cloning and sophisticated molecular biology techniques in the mid-1980s, it became possible to rationalise the mode of action of therapeutic agents and therefore to work in a more hypothesis-based and rational manner on defined protein targets. Several pharmaceutical companies adopted the target-based drug discovery approach allowing rapid screens of large chemical libraries using purified recombinant proteins or engineered cell-lines.

In an attempt to assess whether this switch in focus has been successful, Swinney and co-workers<sup>52</sup> analysed the discovery strategies and the molecular mechanisms of action of the 259 new molecular entities and new biologics that were approved by the US Food and Drug Administration between 1999 and 2008. When focusing solely on the first-in-class drugs, that is therapeutics that modulate an as-yet unprecedented

drug target or biological pathway, and on small molecules, which means ignoring biologics and synthetic versions of natural substances, there were 45 first-in-class small molecules approved during this period. Out of these 45 drugs, 28 (62% of the 45 drugs) were discovered by phenotypic screening and 17 (38% of the 45 drugs) by target-based screening. This observation led to the conclusion that a target-centric approach for first-in-class drugs, without consideration of an optimal molecular mode of action, can partially explain the current high pharmaceutical attrition rates.<sup>52</sup>

However, a possible contributing factor to this trend could be the lag time between the introduction of new technologies and their impact in terms of number of approved first-in-class drugs derived from target-based screening. Indeed, given the relatively recent introduction of target-based approaches in the context of the long time frames of drug development, their full impact might not yet have become apparent. Consequently, another group carried out a similar analysis,<sup>53</sup> but on the extended period between 1999 to 2013. With these additional 5 years, 78 first-in-class small molecules were approved, out of which 33 (42% of the 78 drugs) were discovered by phenotypic screening and 45 (58% of the 78 drugs) by target-based screening. Therefore, in the last 5 years of the analysis, a significant increase in the approval of first-in-class small molecules were discovered in a target-based fashion.

In the two medicinal chemistry projects studied in this thesis, the exact biological signalling pathways were not fully defined and therefore, a phenotypic approach was favoured. Additionally, this strategy offered the opportunity to identify biologically active compounds regardless of their mode of action. Finally, the combination of a phenotypic approach with a strong focus on physicochemical properties was anticipated to lead to better quality compounds with increased chance of success during drug development. However, this was accepting the challenge to generate consistent SAR without having access to robust structure-based design methods.

## **2. CHAPTER 2: Design, synthesis and optimisation of $I_{CRAC}$ inhibitors**

### **2.1. $I_{CRAC}$ as a biological target of therapeutic relevance**

#### **2.1.1. Introduction to ion channels**

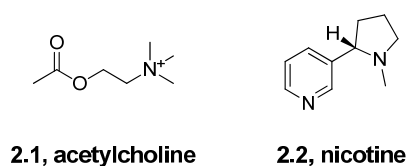
##### **2.1.1.1. Basic features of ion channels**

In order to respond to changes in their immediate environment, cells must be able to receive and process signals that originate outside their borders.<sup>54</sup> In multicellular organisms, growth factors, hormones and neurotransmitters are some of the many types of chemicals that cells use. For instance, neurotransmitters are a class of short-range signalling molecules that travel across the tiny spaces between adjacent neurons or between neurons and muscle cells. Cells have proteins called receptors that bind these signalling molecules and initiate a physiological response. Receptors are generally transmembrane proteins, which bind to signalling molecules outside the cell and subsequently transmit the signal through a sequence of molecular switches to internal signalling pathways. Different receptors are specific for different molecules or biological signals. Consequently, membrane receptors fall into three major classes: G-protein-coupled receptors, enzyme-linked receptors and ion channel receptors. The names of these receptor classes refer to the mechanism by which the receptors transform external signals into internal ones: *via* protein action, *via* enzyme activation or *via* ion channel opening and closing, respectively.<sup>54</sup>

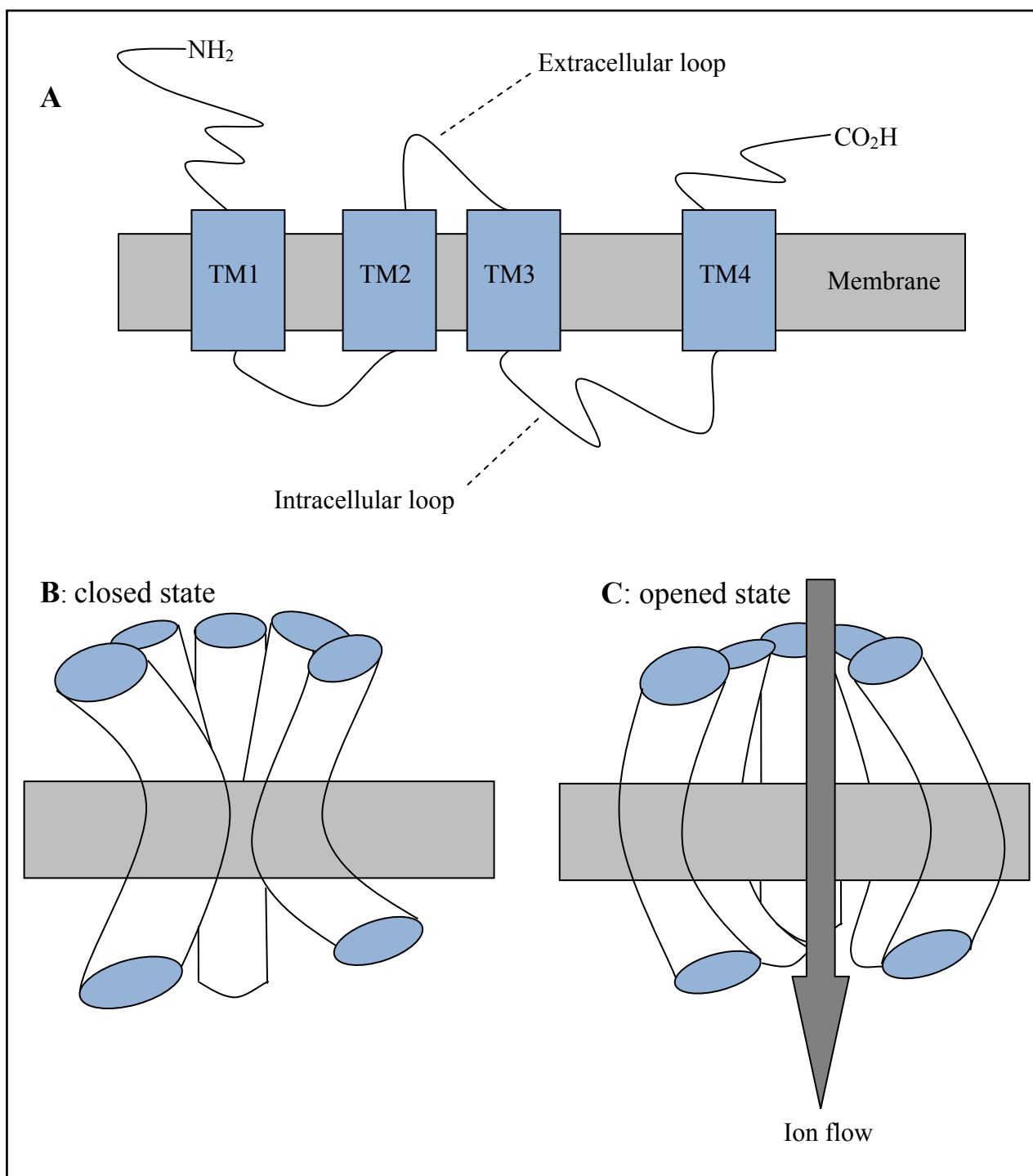
Ion channels are pore-forming membrane proteins whose functions include establishing a resting membrane potential, controlling electrical signals and regulating the concentrations of ions within cells.<sup>55</sup> They achieve these roles by gating and controlling the flow of ions across the cell or organelle membrane. The two main features that differentiate ion channels from other types of ion transporter proteins is the very high rate at which the ions are transported ( $10^6$  ions per second and higher) and the fact that ions move through the channel because of an electrochemical gradient, which results from ion concentration and membrane potential. Ion channels are narrow tunnels that allow only ions of a certain size and charge to pass through, as a result of the specific arrangement of the side chains of

the amino acids lining the pore region. Typically, the narrowest point of the pore region of ion channels is only one or two atoms wide, contributing to the high degree of selectivity of these proteins. The transport of ions through the pore is controlled by a “gate”, which opens and closes in response to chemical signals, electrical signals, temperature or mechanical forces. Ion channels are classified by the way their opening and closing are regulated, referred to as gating. The two main classes of ion channels are the voltage-gated channels, which are regulated by changes in the membrane potential of the cell, and the ligand-gated channels, opening of which is triggered by the binding of a specific endogenous ligand or an ion.<sup>56</sup>

Ion channel proteins are also classified by the number of times they span the membrane.<sup>57</sup> The majority of ion channels are 4-transmembrane (4-TM), like the nicotinic acetylcholine receptor for instance, or 6-TM, however, 2-TM and 3-TM channels also exist. Additionally, ion channels are typically formed as assemblies of several individual proteins, usually into a circular arrangement of homologous proteins closely packed around the pore through the plane of the membrane. As an example, the nicotinic acetylcholine receptor, a non-selective cation channel expressed on the membrane of neurons, is constituted from five subunits, arranged around a central ion pore. Each subunit comprises four transmembrane domains with both the *N*- and *C*-terminus located extracellularly (**Figure 7**). The opening of the nicotinic acetylcholine receptor is triggered by the binding of acetylcholine **2.1** and nicotine **2.2** (**Figure 6**).



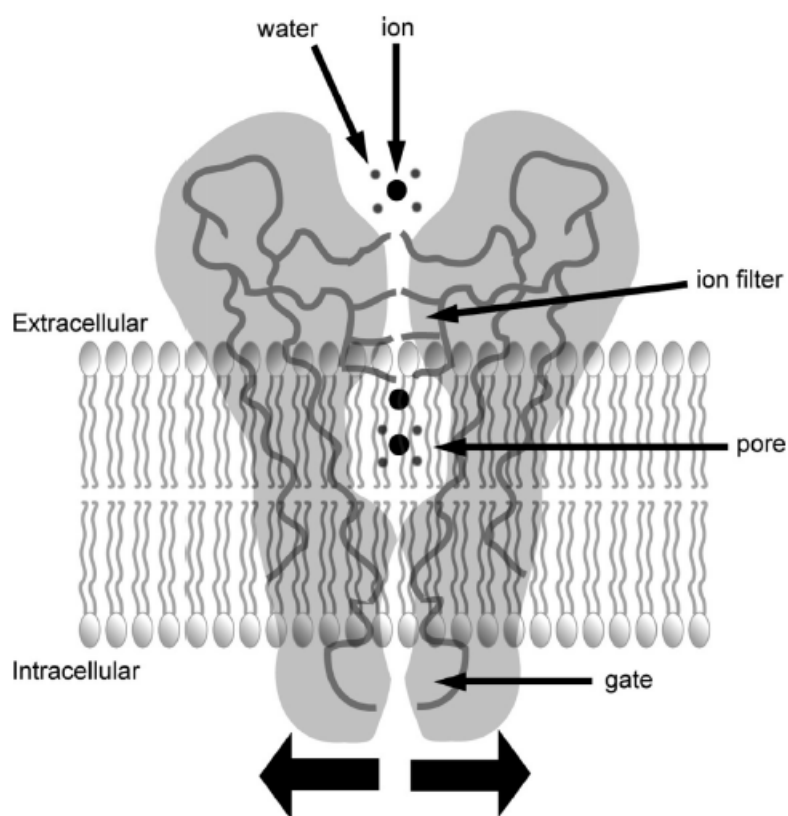
**Figure 6: Structures of acetylcholine and nicotine**



- (A) Representation of a nicotinic acetylcholine receptor monomeric subunit, embedded in a lipid bilayer. The four transmembrane helices are represented by blue rectangles.
- (B) Five subunits of nicotinic acetylcholine receptor symmetrically arranged form the cation conduction pore, represented here in the closed state.
- (C) Representation of the opened state.

**Figure 7: Structure of the nicotinic acetylcholine receptor, a 4-TM ion channel**

The first structural determination of an ion channel was achieved in 1998 by Roderick MacKinnon and co-workers,<sup>58</sup> which provided access to the crystal structure of the potassium crystallographically-sited activation channel (KcsA) from the soil bacteria *Streptomyces lividans*. In recent years, a variety of ion channels have been crystallised<sup>59</sup> giving additional insight into the location of the binding sites regulating the function of ion channels. It was discovered that most ion channels possess a pore-loop region called the selectivity filter that regulates which ions are permitted through the pore (**Figure 8**). Hence, when ions pass through the narrow selectivity filter, they lose some of the water molecules bound to them, which is not energetically favourable. Therefore, an ion is only able to pass through the channel if the binding energy of interaction with the key amino residues of the selectivity filter compensates for the energy loss on dehydration. This compensation can only occur if the hydrated ion fits and binds optimally to the binding site. Hence, this process is not only based on ionic diameter, but also on the thermodynamics of desolvation.



**Figure 8: Schematic representation of the basic structural component of an ion channel<sup>60</sup>**

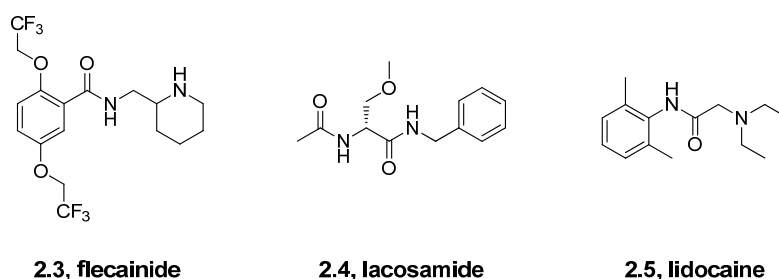
### 2.1.1.2. Ion channels as therapeutic targets

Ions are fundamental in physiological events and their role as second messengers is central to the process of cell signalling. Ions are small, water soluble and they readily diffuse extracellularly and intracellularly. Their concentration inside cells changes rapidly upon receptor activation, and they act as mediators to regulate the activity of other target signalling molecules. Indeed, ions have the ability to bind proteins and to cause conformational changes, hence acting as biological messengers. For instance,  $\text{Ca}^{2+}$  is attracted to the negatively charged oxygen atoms of the side chains of aspartic and glutamic acids, and to the uncharged oxygen of the side chains of asparagine and glutamine. Since it can form ligands with up to eight oxygen atoms,  $\text{Ca}^{2+}$  is able to cause large conformational changes in proteins. As an illustration, the protein calmodulin, which mediates crucial processes such as inflammation, metabolism and apoptosis, is activated after conformational changes resulting from calcium binding.<sup>61</sup> Additionally, oscillation in intracellular concentration of ions is critical in the functioning of muscles, nerves and cardiac cells.

The widespread tissue distribution of ion channels, combined with the many physiological consequences of their opening and closing, makes ion channel-targeted drug discovery highly attractive.<sup>60</sup> The most compelling evidence for the role of ion channels in diseases has come from studies of the inheritance of genetic diseases caused by mutations that affect the function of specific ion channels.<sup>62</sup> For instance, mutations of *KCNQ2* and *KCNQ3*, genes encoding for  $\text{K}^+$  channels that are broadly expressed in the central nervous system (CNS), cause a form of epilepsy in newborns. Similarly, mutations in *SCN5A*, a gene encoding for a voltage-gated  $\text{Na}^+$  channel mediating depolarisation of cardiac myocytes, lead to the long QT syndrome, which is a severe cardiac arrhythmia.

In a recent comprehensive survey<sup>63</sup> looking at the biological target classes of the FDA approved drugs, it was shown that drugs targeting ion channels represented 13.4% of the total number of approved drugs. Hence, ion channels were among the most represented biological target classes in drug discovery, along with nuclear receptors (13% of approved drugs), and behind G-protein-coupled receptors (26.8% of approved drugs). The most common applications for ion channel drugs are for

cardiac, neurophysiological and local anaesthetic indications. For instance, the mode of action of flecainide **2.3** (**Figure 9**), an agent used to prevent and treat tachyarrhythmia, is believed to be centred around the blockade of both Na<sup>+</sup> and Ca<sup>2+</sup> cardiac ion channels.<sup>64</sup> As an example of neurophysiological drugs, lacosamide **2.4** (**Figure 9**) has been recently developed as an antiepileptic drug acting through modulation of voltage-gated Na<sup>+</sup> channels in neurons.<sup>65</sup> Finally, lidocaine **2.5** (**Figure 9**), which has been used since 1949 as a local anaesthetic, exerts its effect through inhibition of voltage-gated Na<sup>+</sup> channels.<sup>66</sup>



**Figure 9: Structures of a set of marketed ion channel inhibitors**

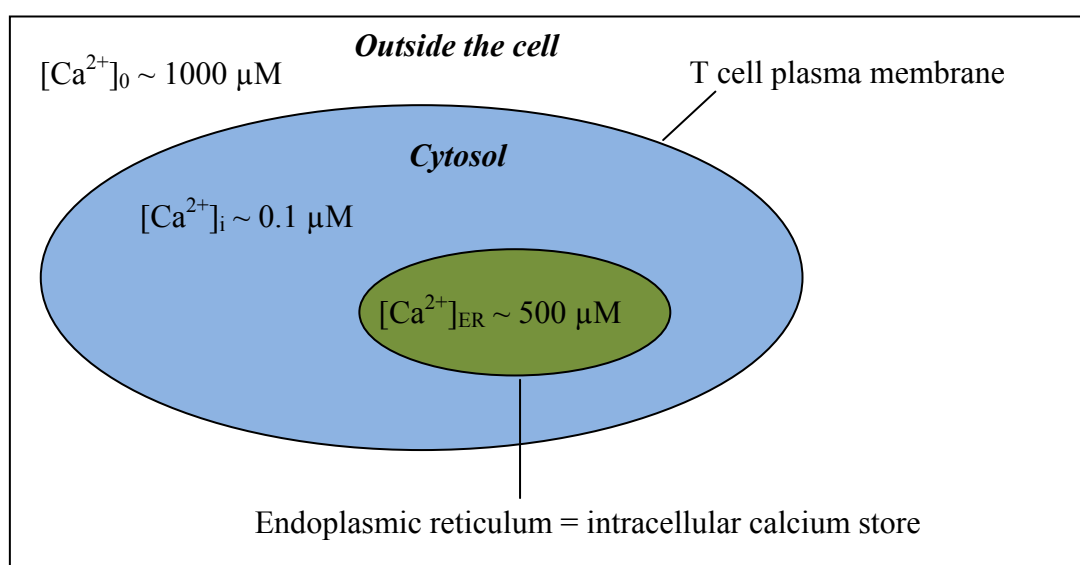
Having briefly discussed the therapeutic potential of ion channel inhibitors, it is also notable how few drugs from this biological target class have gained approval in the past decade. This is suggested to be a likely consequence of clinical failures due to efficacy and safety, and of the apparent difficulty in identifying clinical candidate quality molecules across the ion channel family.<sup>60</sup> The most challenging aspect of ion channel drug discovery may be the identification of an appropriate small molecule drug lead with desirable physicochemical properties that make it suitable for further progression.<sup>67</sup>



## 2.1.2. Introduction to $\text{Ca}^{2+}$ channels

### 2.1.2.1. Role of $\text{Ca}^{2+}$ in the immune response

Thymus cells (T cells, also called T lymphocytes) belong to a group of white blood cells known as lymphocytes, and play a pivotal role in cell-mediated immunity. The calcium concentration in the cytoplasm of T cells in a resting state (denoted  $[\text{Ca}^{2+}]_i$ , **Figure 10**) is much lower ( $\sim 0.1 \mu\text{M}$ ) than the extracellular calcium concentration (denoted  $[\text{Ca}^{2+}]_0 \sim 1000 \mu\text{M}$ ) or than the calcium concentration in the endoplasmic reticulum (denoted  $[\text{Ca}^{2+}]_{\text{ER}} \sim 500 \mu\text{M}$ , where ER stands for endoplasmic reticulum).



**Figure 10: Calcium concentration in T cells**

The intracellular  $\text{Ca}^{2+}$  concentration is tightly regulated *via* calcium exchange with the extracellular environment and the ER compartment through  $\text{Ca}^{2+}$  channels located either on the cell membrane or on the ER membrane. Since  $\text{Ca}^{2+}$  interacts with other signalling pathways, changes in the  $[\text{Ca}^{2+}]_i$  can have an impact on the immune response.<sup>68</sup> Hence, an increase in cytosolic concentration of  $\text{Ca}^{2+}$  stimulates the  $\text{Ca}^{2+}$ -sensitive protein phosphatase calcineurin which activates the transcription factors located in the cytoplasm, such as nuclear factor of activated T cells (NFAT) and nuclear factor- $\kappa\text{B}$  (NF- $\kappa\text{B}$ ).<sup>69</sup> When these transcription factors are activated, they enter the nucleus of T cells and trigger gene transcription and cell proliferation. The

resulting release of several interleukins instigates an inflammatory response. Moreover, activated T cells recruit other cells of the immune system, such as macrophages and neutrophils.<sup>70</sup> Based on this, T cells are thought to play a prominent role in various allergic and inflammatory disorders.

In addition to the signalling role of  $\text{Ca}^{2+}$  in T cells, an increase in cytosolic concentration of  $\text{Ca}^{2+}$  initiates several cellular mechanisms in other cell types of the immune system. For instance, under these conditions bone-marrow derived cells (B cells) produce cytokines and mast cells degranulate to release different biological pro-inflammatory mediators, such as histamine and prostaglandins.

From consideration of all of the above, being able to control the cytosolic calcium concentration by modulating  $\text{Ca}^{2+}$  channels could have a therapeutic potential in the management of chronic inflammatory disorders.

#### **2.1.2.2. Nomenclature of $\text{Ca}^{2+}$ channels**

There are a wide range of ion channels which exhibit selective permeability to calcium ions, enabling the control of the calcium concentration within the cytoplasm. They are divided in two categories, the voltage-gated and the ligand-gated  $\text{Ca}^{2+}$  channels.

The voltage-gated calcium channels are located in the membrane of most excitable cells and their nomenclature is based upon the membrane potential required to activate the channel and their sensitivity to certain classes of heterogeneous inhibitors (**Table 3**):<sup>71</sup>

- (i) L-type calcium channels (denoted  $\text{Ca}_v1.x$ ) are moderate to high voltage-activated calcium channels that are typically blocked by dihydropyridines, phenylalkylamines and benzothiazepines.
- (ii) P-, Q-, N- and R-type calcium channels (denoted  $\text{Ca}_v2.x$ ) are moderate to high voltage-activated calcium channels which are unaffected by dihydropyridines, phenylalkylamines and benzothiazepines. However, they are blocked by polypeptide toxins from snail and spider venoms.

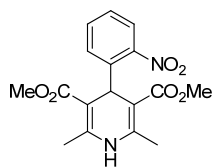
(iii) T-type calcium channels (denoted  $Ca_v3.x$ ) are low voltage-activated calcium channels, for which no selective blockers have yet been discovered.<sup>72</sup>

| Type      | Membrane potential required for activation | Nomenclature | Location                       | Inhibitor information                                 |
|-----------|--|--------------|--------------------------------|---|
| L-type    | high                                       | $Ca_v1.1$    | skeletal muscle                | dihydropyridines, phenylalkylamines, benzothiazepines |
|           | high                                       | $Ca_v1.2$    | heart, smooth muscle, brain    |   |
|           | moderate                                   | $Ca_v1.3$    | brain, pancreas, kidney, ovary |   |
|           | moderate                                   | $Ca_v1.4$    | retina                         |   |
| P-/Q-type | moderate                                   | $Ca_v2.1$    | brain                          | polypeptide toxins from snail and spider venoms       |
| N-type    | high                                       | $Ca_v2.2$    | brain, nervous system          |   |
| R-type    | moderate                                   | $Ca_v2.3$    | heart, brain, retina           |   |
| T-type    | low  | $Ca_v3.1$    | brain, nervous system          | only non-selective blockers have been identified      |
|           | low  | $Ca_v3.2$    | brain, heart, kidney, liver    |   |
|           | low  | $Ca_v3.3$    | brain                          |   |

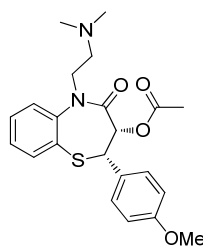
**Table 3: Nomenclature of the voltage-gated  $Ca^{2+}$  channels**

**Figure 11** shows a set of molecules that are or have been marketed and that represent an overview of the main classes of voltage-gated  $Ca^{2+}$  channels blockers.

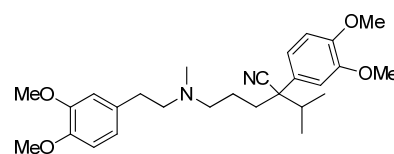
### L-type Ca<sup>2+</sup> channel blockers:



**2.6, nifedipine**  
dihydropyridine class,  
hypertension and chronic angina

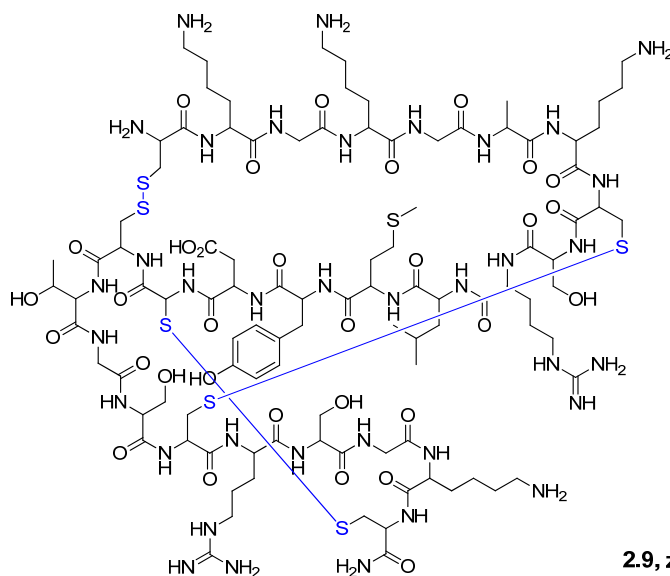


**2.7, diltiazem**  
benzothiazepine class, hypertension,  
angina and arrhythmia



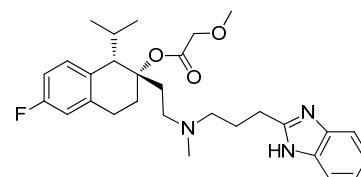
**2.8, verapamil**  
phenylalkylamine class, hypertension,  
angina and arrhythmia

### N-type Ca<sup>2+</sup> channel blocker:



**2.9, ziconotide**  
derived from the  $\omega$ -conotoxin of cone snail,  
polypeptide class,  
analgesic  
(disulfide bridges are drawn in blue for clarity)

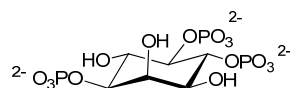
### T-type Ca<sup>2+</sup> channel blocker:



**2.10, mibefradil**  
non-selective, also blocking L-type,  
hypertension and chronic angina

**Figure 11: Examples of voltage-gated Ca<sup>2+</sup> channel blockers, with their therapeutic applications**

The second main category of Ca<sup>2+</sup> channels, the ligand-gated calcium channels, are located either on the cell membrane or on the ER membrane. The ryanodine receptor (RyR) and the inositol-1,4,5-trisphosphate receptor (InsP<sub>3</sub>R), respectively, are gated by calcium itself and by inositol-1,4,5-trisphosphate **2.11** (InsP<sub>3</sub>, also noted IP<sub>3</sub>, **Figure 12**). These receptors are found on the ER membrane and are responsible for the initial elevation in cytoplasmic calcium that occurs after cell stimulation.

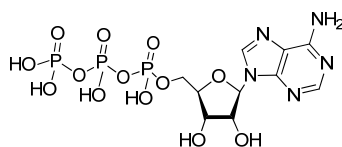


**2.11, inositol-1,4,5-trisphosphate**

**Figure 12: Structure of inositol-1,4,5-trisphosphate (IP<sub>3</sub>)**

Calcium release-activated calcium (CRAC) channels are ligand-gated calcium channels located on the cell membrane which are activated after calcium is released from the ER. These channels are discussed in more detail in the following sections. Their role is to maintain prolonged elevations in intracellular calcium and to refill the endoplasmic reticulum. RyR, InsP<sub>3</sub>R and CRAC channels are ubiquitously expressed and participate in a wide variety of important calcium phenomena, especially in immune cells.

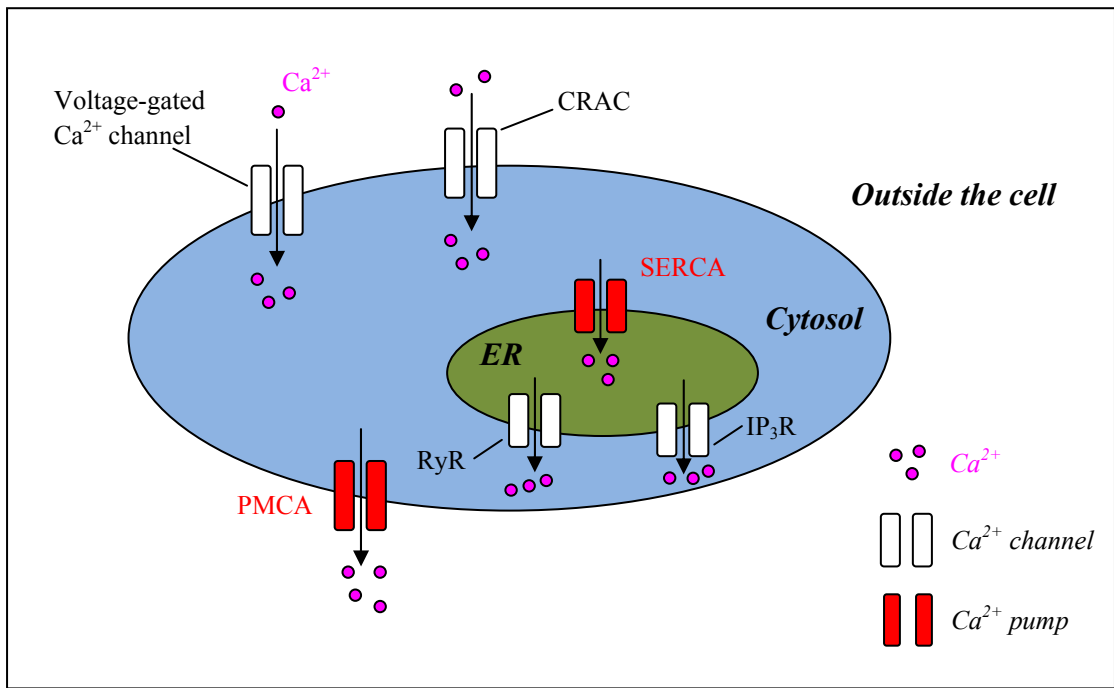
To balance the role of these voltage-gated and ligand-gated calcium channels and to help maintain cytosolic calcium homeostasis, cells are also equipped with calcium pumps. In contrast to the previously described calcium channels, these pumps function through the hydrolysis of adenosine triphosphate **2.12** (ATP, **Figure 13**), with a stoichiometry of one Ca<sup>2+</sup> ion removed for each molecule of ATP hydrolysed. There are two types of calcium pumps, one located on the plasma membrane (PMCA, plasma membrane calcium ATPase), which pumps calcium out of cells, and one positioned on the ER membrane (SERCA, sarcoplasmic/endoplasmic reticulum calcium ATPase), which pumps calcium into the ER.



**2.12, adenosine triphosphate**

**Figure 13: Structure of adenosine triphosphate (ATP)**

**Figure 14** is a schematic representation of the different Ca<sup>2+</sup> channels and Ca<sup>2+</sup> pumps that ensure calcium homeostasis within cells.



**Figure 14: Schematic model for calcium homeostasis in a generic cell**

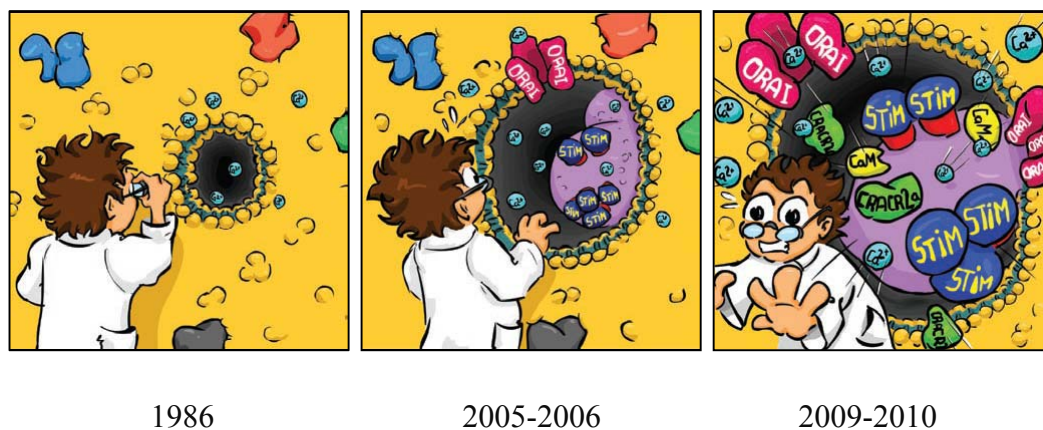
### 2.1.3. Overview of the CRAC system

Putney<sup>73</sup> was first to suggest that the depletion of ER calcium levels could in turn trigger the opening of membrane calcium channels. These store-operated calcium entry (SOCE) channels ensure a relatively constant concentration of calcium in the ER. The main actor of this class of channels is the CRAC channel,<sup>74,75</sup> responsible for the  $I_{\text{CRAC}}$  current. Pharmacological, electrophysiological and genetic evidence supports the notion that CRAC channels are the principal route for calcium ions to enter the cytoplasm of T cells.<sup>76</sup> Due to the major role of  $I_{\text{CRAC}}$  on the concentration of calcium within the immune cells and thus on the lymphatic functions, CRAC channels represent a promising drug target for inflammation and allergic disorders.<sup>77,78,79</sup>

CRAC channels have an extraordinarily high selectivity for  $\text{Ca}^{2+}$  over other ions (e.g. permeability  $\text{Ca}^{2+}$  / permeability  $\text{Na}^{+}$  = 1000),<sup>80</sup> which appears to be the result of a highly selective calcium binding site within the channel pore. CRAC channels are also characterised by a relatively narrow pore size of 4 to 6 Å and an extremely small

apparent, but not undetectable, unitary conductance of 10 to 30 femtosiemens (fS), approximately 1000-fold lower than that of other ion channels.<sup>75</sup>

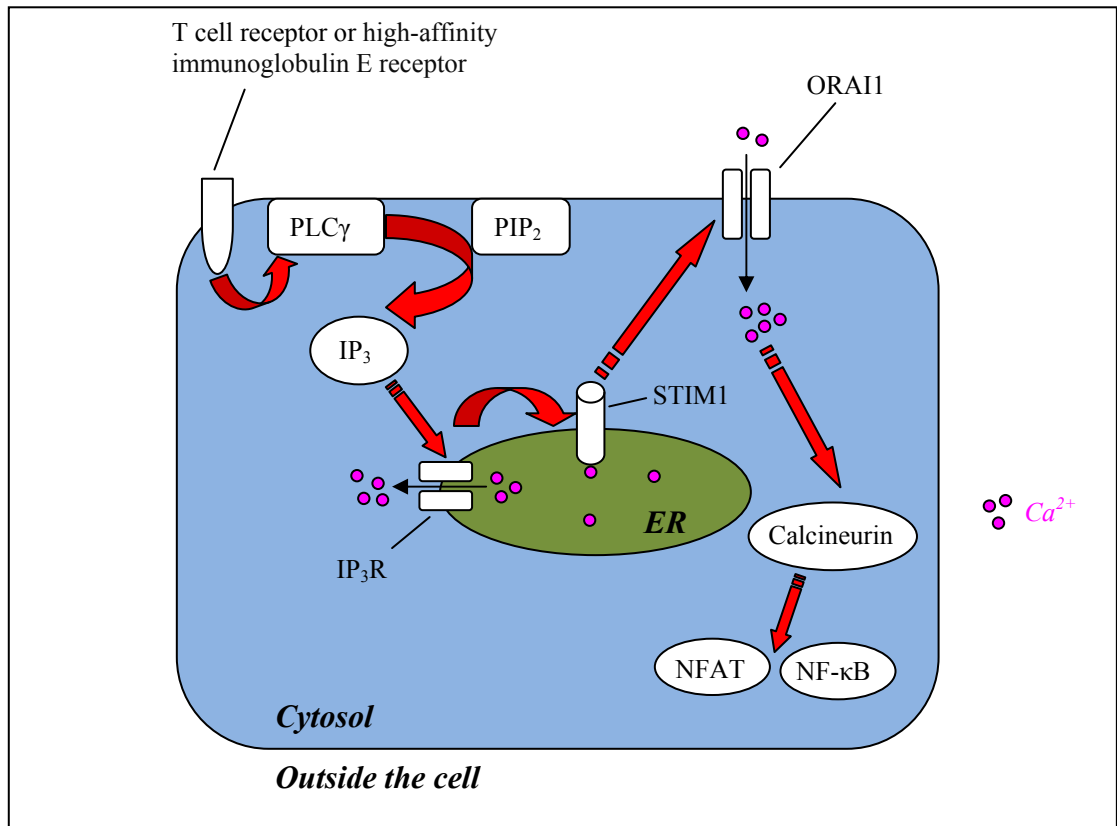
The molecular basis of the CRAC channel has long been subject to debate, however, the recent identification of two key proteins, STIM1 (stromal interaction molecule 1) and ORAI1 (calcium release-activated calcium channel protein 1; also known as CRAC Modulator 1, CRACM1) has yielded greater insight into the mechanism of the channel and also initiated a vast increase in interest around CRAC (**Figure 15**).<sup>81</sup>



**Figure 15: Milestones in the identification of the molecular components of the CRAC channel<sup>82</sup>**

**Figure 16** outlines the proposed mechanism of the SOCE channels in T cells and mast cells. Activation of the enzyme phospholipase C $\gamma$  (PLC $\gamma$ ), by an antigen in lymphocytes or through high-affinity immunoglobulin E receptors in mast cells, leads to a dual increase in the cytosolic Ca<sup>2+</sup> concentration. Firstly, the hydrolysis of the membrane phospholipid phosphatidylinositol-4,5-bisphosphate (PIP<sub>2</sub>), mediated by PLC $\gamma$ , generates IP<sub>3</sub> which binds to InsP<sub>3</sub>R on the membrane of the ER, resulting in calcium ions being released from the ER into the cytoplasm. Secondly, STIM1, which resides across the ER membrane, senses this decrease in the Ca<sup>2+</sup> concentration in the ER and migrates along the ER membrane in order to come closer to the cell membrane. STIM1 then recruits ORAI1, the pore forming subunit of the CRAC channel located on the cell plasma membrane, resulting in channel opening, allowing calcium into the cell. As discussed in **Section 2.1.2.1 (p. 24)**,

sustained increase in  $[Ca^{2+}]_i$  activates  $Ca^{2+}$ -sensitive enzymes, such as the cytosolic  $Ca^{2+}$ -sensor calcineurin, and thereby transcription factors, such as nuclear factor of activated T cells (NFAT) and nuclear factor- $\kappa$ B (NF- $\kappa$ B), leading to an inflammatory response. Based on this, inhibition of one or more aspects of this pathway could lead to a reduced inflammatory response.



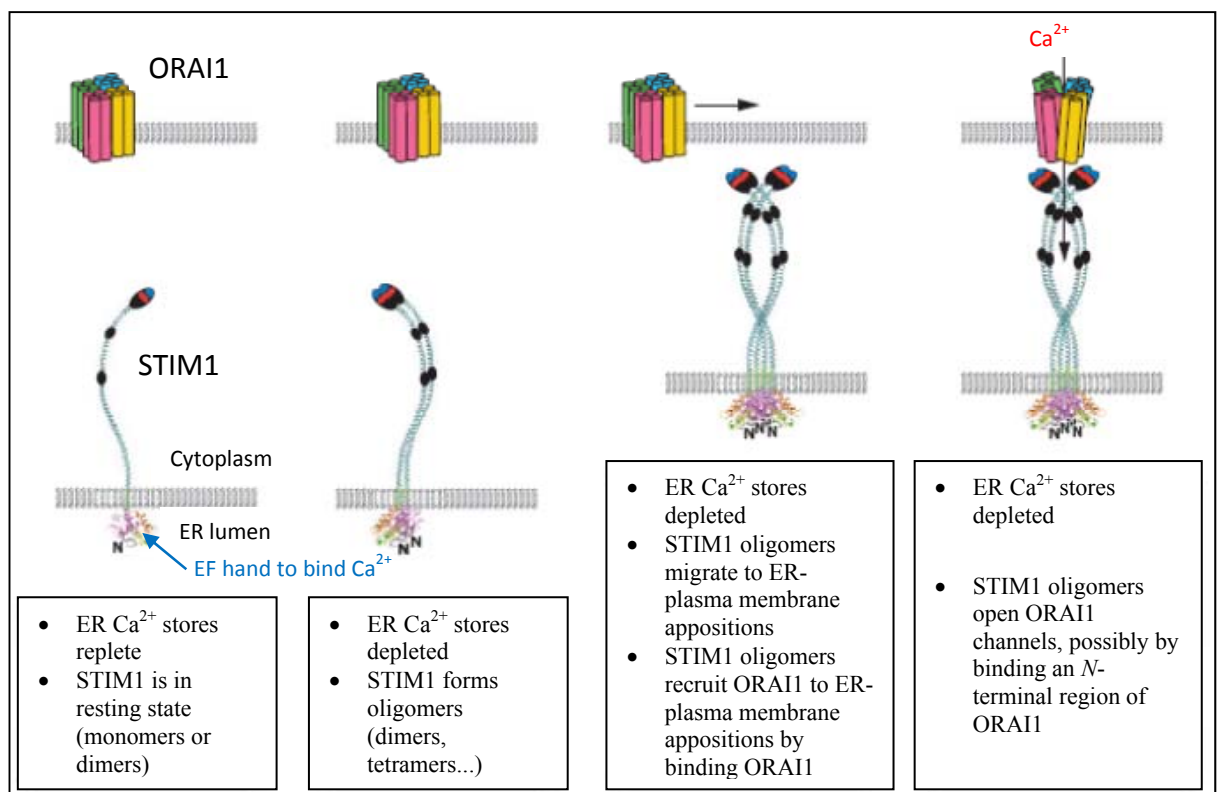
**Figure 16: Store-operated calcium entry in T cell and mast cell**

#### 2.1.4. Molecular components of the CRAC channel

Despite the fact that the CRAC channel was described more than 20 years ago,<sup>83</sup> it is only recently that its key molecular components have been elucidated and reviewed in the literature.<sup>75</sup> The first advance was the identification of STIM1 as playing an essential role in the mechanism of the CRAC channel, by two different groups in 2005, using short interfering RNA (siRNA) studies in *Drosophila* cells<sup>84</sup> and in human cells.<sup>85</sup>



STIM1 is a 77 kDa protein<sup>86</sup> that spans the ER membrane once and is characterised by an EF hand in the ER lumen, which is a calcium-binding motif composed of two helices (E and F) joined by a loop. Thus, by binding  $\text{Ca}^{2+}$  in the internal part of the ER, STIM1 acts as a sensor of the calcium concentration in the ER. STIM1 is homogeneously distributed through the the ER membrane in its resting state, however, upon calcium store depletion and dissociation of  $\text{Ca}^{2+}$  from its EF-hand, STIM1 oligomerises into discrete puncta, which can be observed by confocal microscopy and which give clusters of STIM1 proteins.<sup>85</sup> Following an as yet unclear mechanism, these oligomers migrate along the ER membrane up to a location where they are close enough to the cell membrane for them to interact with the pore subunit of the CRAC channel, ORAI1 (**Figure 17**).



**Figure 17: Sequence of steps in store-operated calcium entry<sup>75</sup>**

One year later, in 2006, siRNA studies carried out concurrently in *Drosophila* by three different groups,<sup>87,88,89</sup> led to the identification of ORAI1 as a key component of the SOCE mechanism. ORAI1 is a 33 kDa four-transmembrane protein expressed in the plasma membrane, with the *N* and *C* termini located inside the cytoplasm. Several ORAI1 site-directed mutagenesis experiments,<sup>80,90</sup> such as the mutation of two conserved acidic residues in the transmembrane segments (E106D and E190Q),<sup>91</sup> demonstrated ORAI1 to be a pore-forming subunit of the channel. The functional stoichiometry of the unitary CRAC channel has been controversial for several years. Indeed, evidence suggested that ORAI1 was a dimer in its resting state and a tetramer after STIM1 activation,<sup>92,93</sup> however, the recent solution of the crystal structure of *Drosophila* ORAI1 revealed that the calcium channel is composed of a hexameric assembly of ORAI1 subunits.<sup>94</sup>

### **2.1.5. Communication between STIM1 and ORAI1**

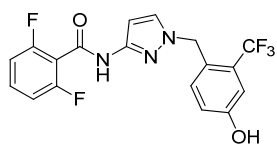
The way STIM1 and ORAI1 communicate with each other is undoubtedly the area which is the least understood and is currently under significant investigation.<sup>95</sup> It remains unknown whether STIM1 interacts directly with ORAI1 or whether an intermediate messenger is involved.<sup>82</sup> Nevertheless, activation of the CRAC channel following an interaction with activators/sensors across membrane compartments is an unprecedented mechanism. In some sub-regions, the distance separating the ER and the plasma membrane is estimated around 10-25 nm, which is small enough to envisage direct protein-protein interactions.<sup>96</sup>

Both STIM1 and ORAI1 are required for the activation of the CRAC channels, since their individual over-expression in proteins does not amplify  $I_{CRAC}$ . However, over-expression of the two proteins together greatly enhances the current of the CRAC channels. This result,<sup>97</sup> along with others,<sup>98,99</sup> suggests that STIM1 and ORAI1 are both necessary and sufficient to mediate the mechanism of SOCE through the CRAC channels.

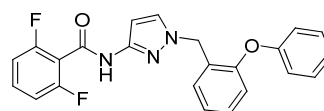
In order to further understand the interaction between STIM1 and ORAI1, Romanin and co-workers used Förster Resonance Energy Transfer (FRET) spectroscopy and revealed a dynamic coupling of STIM1 and ORAI1. Additionally, they underlined a key role of the C-terminal coiled-coil motif of ORAI1,<sup>100</sup> as well as a modulatory domain within STIM1 C-terminus.<sup>101</sup>

The complexity of the CRAC channel activation still remains to be fully understood and in particular, how ORAI1 is gated by STIM1. However, the recent solution of the crystal structure of ORAI1<sup>94</sup> (discussed further in the subsequent section) paved the way for a greater understanding of the interactions between STIM1 and ORAI1.

From the perspective of developing CRAC inhibitors, questions also remain around the exact biological target. Small molecule blockers could in theory interfere with STIM1 only, with ORAI1 only, with the protein-protein interaction between STIM1 and ORAI1, or could simply function as an ORAI1 pore blocker. Having stated this, several experiments were carried by Christoph Romanin and co-workers<sup>102</sup> in an attempt to characterise the site of action on the CRAC channels of a first generation of inhaled  $I_{\text{CRAC}}$  inhibitors previously developed in our laboratories (see **Section 2.2.2, p. 56**, for more discussions about our first generation of inhaled  $I_{\text{CRAC}}$  inhibitors). In these studies, FRET microscopy analyses with two selective CRAC channel blockers, 3-aminopyrazole GSK-7975A and GSK-5503A (**2.13** and **2.14**, respectively, **Figure 18**), showed that these compounds exerted their action downstream of the STIM1-ORAI1 coupling machinery, since they left STIM1 oligomerisation and STIM1/ORAI1 interaction unaffected. Additionally, when mutating some residues located in the pore region of ORAI1, 3-aminopyrazole GSK-7975A still inhibited  $I_{\text{CRAC}}$ , suggesting that the compound was not blocking the pore, but rather acting *via* an allosteric effect. Lastly, compounds GSK-7975A and GSK-5503A had a noticeably slower onset of action compared to a classical CRAC pore blocker such as  $\text{La}^{3+}$ , indicating that the 3-aminopyrazole analogues had restricted access to their site of action. Given their moderate lipophilicity (clogP = 3.4 for GSK-7975A) and high artificial membrane permeability (360 nm/s for GSK-7975A), the possibility that these compounds reached their site of action by diffusion through the cell membrane cannot be excluded.



2.13, GSK-7975A

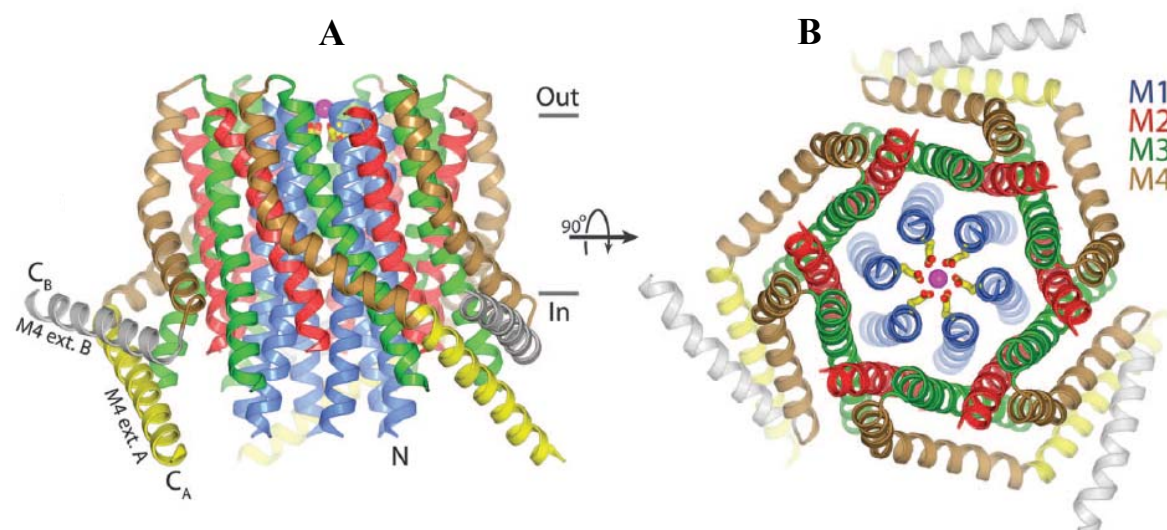


2.14, GSK-5503A

**Figure 18: Structures of 3-aminopyrazoles GSK-7975A and GSK-5503A, from the first generation of inhaled  $I_{CRAC}$  inhibitors developed in our laboratories**

### 2.1.6. Crystal structure of ORAI1

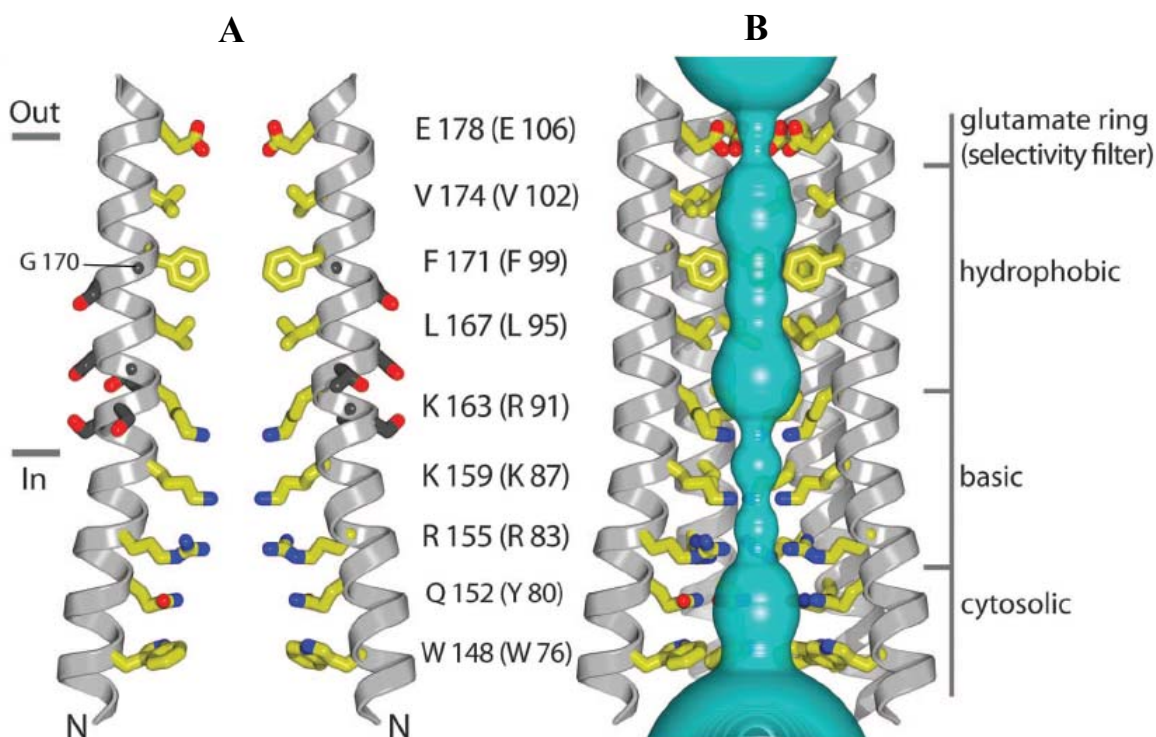
A major advance in the  $I_{CRAC}$  field was achieved in 2012 when Hou and co-workers solved the crystal structure of *Drosophila* ORAI1 in its closed state, at a 3.35 Å resolution.<sup>94</sup> A key finding of this work was the revelation that the CRAC channel assembles as a hexamer of ORAI1 subunits arranged around a central axis (**Figure 19**). Each ORAI1 subunit contains four transmembrane helices (M1 to M4, **Figure 19**) and a helix following M4 that extends into the cytosol. The ion pore is located at the centre of the channel along the sixfold axis and the transmembrane helices are arranged in three concentric rings. Six M1 helices, one from each subunit, make up an inner ring of helices, forming the ion pore. The M2 and M3 helices constitute a middle ring, surrounding the transmembrane portion of the M1 helices. The M4 helices, which are arranged in an outer ring, are located at the periphery of the channel (**Figure 19**).<sup>94</sup>



- (A) Ribbon representation showing the tertiary structure of the CRAC channel from the side. The helices are coloured: M1 (blue), M2 (red), M3 (green), M4 (brown), M4 extension (yellow in subunit A and gray in subunit B). Also shown are a  $\text{Ca}^{2+}$  ion (magenta sphere) and the nearby  $\text{Glu}^{178}$  residues (yellow sticks). The “Out” and “In” horizontal lines represent the boundaries of the cell membrane.
- (B) Orthogonal view of the channel from the extracellular side.

**Figure 19: Crystal structure of the ORAI1 protein<sup>94</sup>**

A large amount of information was gained by investigating the chemical environment along the ion pore, which is determined by the side chains of the amino acids of M1 that line the pore. The pore of ORAI1 has four distinct sections (**Figure 20**): a ring of glutamate residues at its extracellular end composed of six  $\text{Glu}^{178}$  side chains, a hydrophobic section spanning three helical turns of M1 within the transmembrane region, a basic section spanning three helical turns near the intracellular side, and a wider section that extends into the cytosol. From this configuration, it was hypothesised that CRAC channels may achieve their exquisite  $\text{Ca}^{2+}$  selectivity by high-affinity binding of  $\text{Ca}^{2+}$  to the glutamate residues that probably constitutes the ion selectivity filter.<sup>94</sup> For instance, the ionic radii of  $\text{Ca}^{2+}$  and  $\text{Na}^{+}$  are nearly identical (0.99 and 0.95 Å, respectively), however, the higher selectivity of the CRAC channel for  $\text{Ca}^{2+}$  could be the result of its greater positive charge over  $\text{Na}^{+}$ .

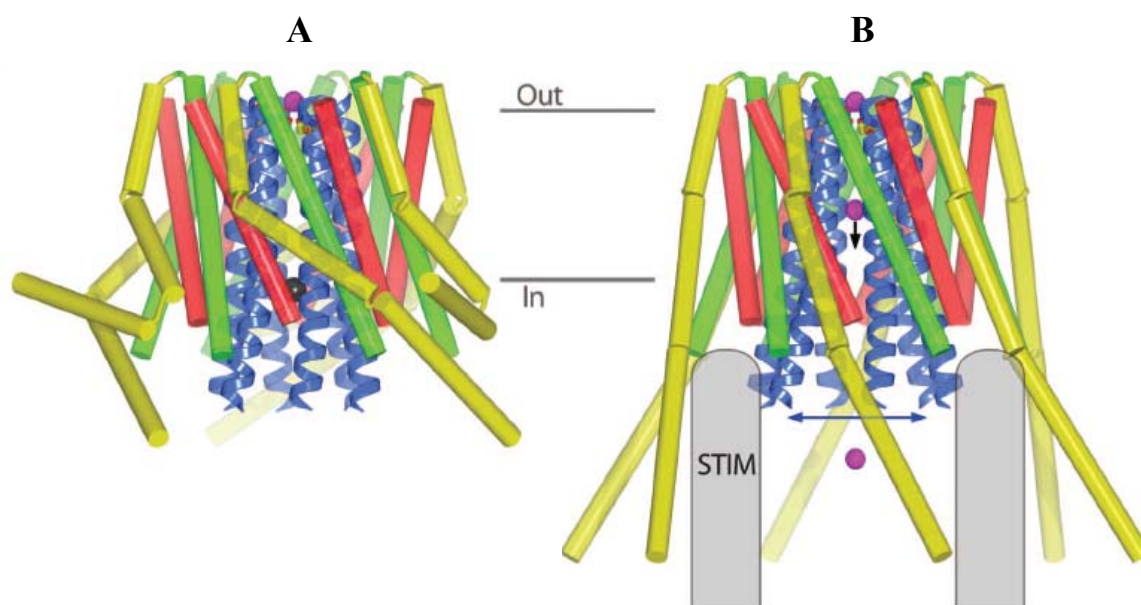


- (A) Two M1 helices are drawn (four are omitted for clarity), showing the amino acids lining the pore in yellow. The “Out” and “In” horizontal lines represent the boundaries of the cell membrane. The corresponding amino acids in human ORAI1 are shown in parentheses. Ser<sup>161</sup>, Ser<sup>162</sup>, Thr<sup>164</sup>, Ser<sup>165</sup>, and Gly<sup>170</sup> are drawn in grey sticks.
- (B) Four M1 helices are drawn (two are omitted for clarity), showing the minimal radial distance from the centre of the pore to the nearest van der Waals protein contact.

**Figure 20: Chemical environment of the ion pore of ORAI1, determined by the side chains of the amino acids of M1 that line the pore<sup>94</sup>**

The ion flux assays conducted with this crystallised structure of ORAI1 indicated that the pore was in its closed conformation.<sup>94</sup> The authors of this study hypothesised that the narrow width of the basic region of the pore combined with its high positive charge may not be permeable to Ca<sup>2+</sup> in this configuration, hence forming a closed gate.<sup>94</sup> Moreover, additional experiments soaking the ORAI1 in the anion iridium hexachloride (IrCl<sub>6</sub>)<sup>3-</sup> led to the conclusion that the basic region of ORAI1 can bind anion(s).<sup>94</sup> Hence, an hypothesis is that the pore binds available intracellular anion(s) blocking access to Ca<sup>2+</sup> (**Figure 21, A**). Combining the information obtained from

this crystal structure and previous observations made when carrying out site-directed mutations of the ORAI1 protein, the authors of this paper proposed a working model for the open conformation of the CRAC channel (**Figure 21, B**).<sup>94</sup> In this model, the M4 extension helices project into the cytosol and interact with a cytosolic portion of STIM1. Additionally, an interaction between the *N*-terminal regions of the M1 helices with STIM1 would widen the basic section of the pore. Consequently, the affinity of the basic region for anion(s) would be reduced, allowing them to be displaced.



- (A) *Observed structure of ORAI1 in a closed state.* The view is from the side with the M1 helices drawn as blue ribbons and the other helices shown as cylinders (M2 in red, M3 in green, M4 and M4 extension in yellow). A Ca<sup>2+</sup> ion in the external site is drawn as a magenta sphere and an anion in the basic region of the pore is drawn as a black sphere. The “Out” and “In” horizontal lines represent the boundaries of the cell membrane.
- (B) *Hypothetical model of a CRAC channel open state.* The pore is widened by the outward dilation of the M1 helices (left-right arrow). A downward-pointing arrow indicates that Ca<sup>2+</sup> is able to move through the pore unobstructed. The intracellular ends of the M1 helices are hypothesised to interact with a cytosolic portion of STIM1, as are the M4 extensions, which are modelled to protrude into the cytosol.

**Figure 21: Observed ORAI1 in a closed state and the hypothetical open state of the CRAC channel<sup>94</sup>**

The determination of the crystal structure of ORAI1 provided a crucial new perspective on the architecture and function of the CRAC channel. However, the exact molecular coupling mechanisms between ORAI1 and STIM1 can only be hypothesised at present. Solution of the structure of the two proteins co-crystallised would potentially increase the understanding of this complex intermolecular signalling process.

### **2.1.7. Physiological implications of CRAC channels deficiencies and therapeutic potential**

The effects of dysfunction of the CRAC channel have been examined both in *in vitro* studies and directly in human patients who lack functional ORAI1 or STIM1. The strongest evidence that calcium influx through CRAC channels is essential for lymphocyte activation and immune responses comes from the study of rare inherited immunodeficiency syndromes involving defects in SOCE. In 1994, patch clamp and calcium imaging experiments to record fluxes of calcium into cells from either healthy donors or patients suffering from a primary immunodeficiency showed that the defect of T cell proliferation in the disease was linked to an absence of  $\text{Ca}^{2+}$  conductance through the cell membrane.<sup>103</sup> These data, along with others,<sup>104</sup> were among the first to reveal the key role of the SOCE in immune function. Later, the principal defect in T cell activation and gene expression in two severe-combined immunodeficiency (SCID) patients, initially thought to be driven by NFAT dysfunctions, was attributed to aberrant transmembrane calcium influx,<sup>105</sup> actually resulting from defective CRAC channels.<sup>76</sup> Furthermore, the malfunction of the CRAC channel in these SCID patients was revealed to be inherited by a mutation in ORAI1.<sup>88</sup> Likewise, severe defects in the SOCE of three other patients with a SCID clinical phenotype was directly linked to a STIM1 deficiency.<sup>106</sup>

In addition, parents of the SCID patients with non-functional ORAI1 were shown to be heterozygous carriers of the causal gene mutation for SCID.<sup>88</sup> After treatment with thapsigargin, the concentration of  $\text{Ca}^{2+}$  in T cells isolated from these parents was shown to be about 50% compared to the  $\text{Ca}^{2+}$  concentration in wild-type control



T cells. Despite this partial functioning of the CRAC channels, the parents of the SCID patients displayed a healthy phenotype and a regular immune response.<sup>88</sup> These findings, consistent with a “gene-dosage” effect, underline the clinical opportunity of delivering safe, selective CRAC inhibitors to treat relevant T cell-driven conditions and diseases.

Additionally, Ca<sup>2+</sup> influx mediated by CRAC in mast cells is known to regulate the secretion of pro-inflammatory lipid mediators. Abnormal mast cell activation has been linked to a range of allergic disorders including asthma, rhinitis and eczema. Indeed, mast cells from both STIM1-deficient<sup>107</sup> and ORAI1-deficient<sup>108</sup> mice showed a reduced degranulation and cytokine release. These results build confidence that a drug based on a CRAC inhibitor could help to control diseases caused by allergen-evoked degranulation of mast cells.

Taken together, these observations suggest that selective  $I_{CRAC}$  inhibitors have a therapeutic potential for the treatment of inflammatory diseases, including asthma, allergic rhinitis, chronic obstructive pulmonary disease (COPD) and rheumatoid arthritis. The following sections will describe efforts towards the identification of  $I_{CRAC}$  inhibitors with a balanced physicochemical profile, using a phenotypic screening approach.

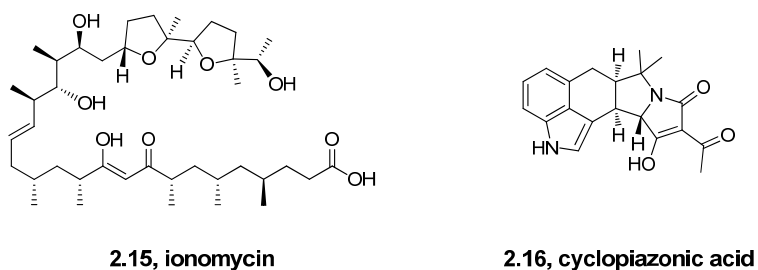
## **2.1.8. *In vitro* assays supporting the identification of $I_{CRAC}$ inhibitors**

### **2.1.8.1. Jurkat cell assay<sup>109</sup>**

A functional cell-based assay was used as a primary assay to measure the ability of the molecules developed in our laboratories to reduce the Ca<sup>2+</sup> influx through CRAC channels. This assay relied on the measurement of Ca<sup>2+</sup> concentration within Jurkat cells after the activation of  $I_{CRAC}$ . Since it was a biological target-agnostic assay, the Jurkat cell assay can be regarded as a phenotypic assay, which offered the ability to detect multiple modes of action blocking  $I_{CRAC}$ . Jurkat cells are an immortalised

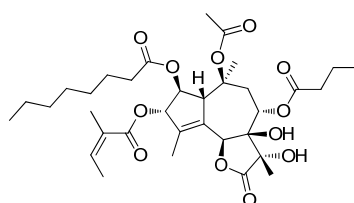
cancer line of human T lymphocyte cells, which have previously been shown to express a functional  $I_{CRAC}$  current.

There exist several ways to trigger the depletion of the ER calcium stores in cells, thereby activating  $I_{CRAC}$ . The calcium ionophore (lipid-soluble molecule that transports ions across membranes) ionomycin **2.15** (**Figure 22**), which accumulates in ER membranes and transports ER calcium into the cytosol, is one example. Other alternatives, such as the use of cyclopiazonic acid **2.16** (**Figure 22**), rely on the inhibition of SERCA pumps, whose role is to pump calcium into the lumen of the ER from the cytosol.



**Figure 22: Structures of molecules which trigger the depletion of the ER calcium store, ionomycin and cyclopiazonic acid**

Thapsigargin **2.17** (**Figure 23**) is a highly selective and effectively irreversible inhibitor of SERCA pumps,<sup>110</sup> allowing the depletion of the  $Ca^{2+}$  stores and the activation of the SOCE, while bypassing receptor activation and the production of  $IP_3$  in Jurkat cells. This agent was chosen for the Jurkat assay used in our laboratories.

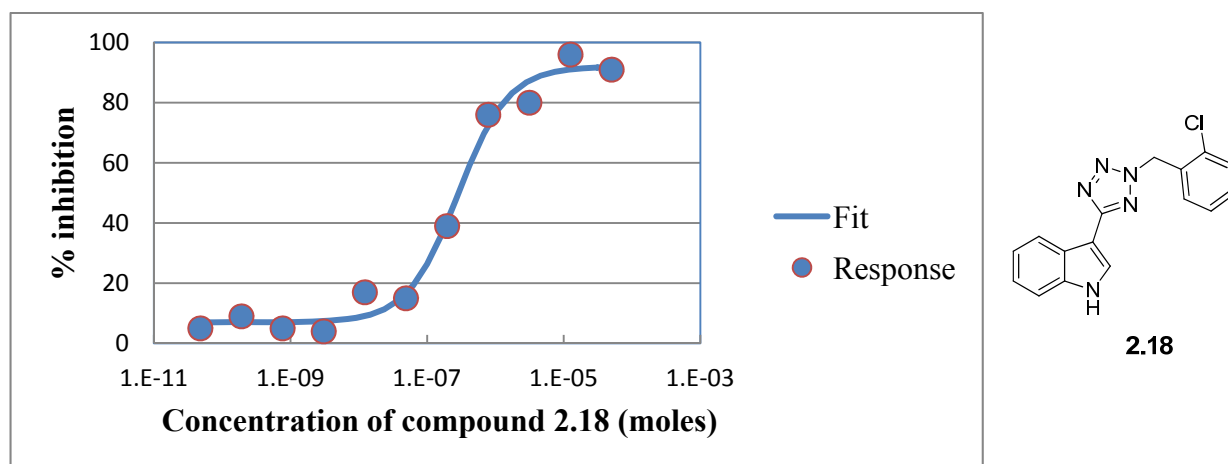


**2.17, thapsigargin**

**Figure 23: Structure of thapsigargin**

Changes in intracellular calcium concentration were measured by the inclusion of the calcium sensitive fluorescent dye Fluo-4 and the use of a fluorometric imaging detection system. Fluo-4 is one of the most commonly used intracellular  $\text{Ca}^{2+}$  indicators and, when excited at a wavelength of 480 nm, it gives an emission at 525 nm, with an increase in fluorescence upon binding to  $\text{Ca}^{2+}$ .<sup>111</sup>

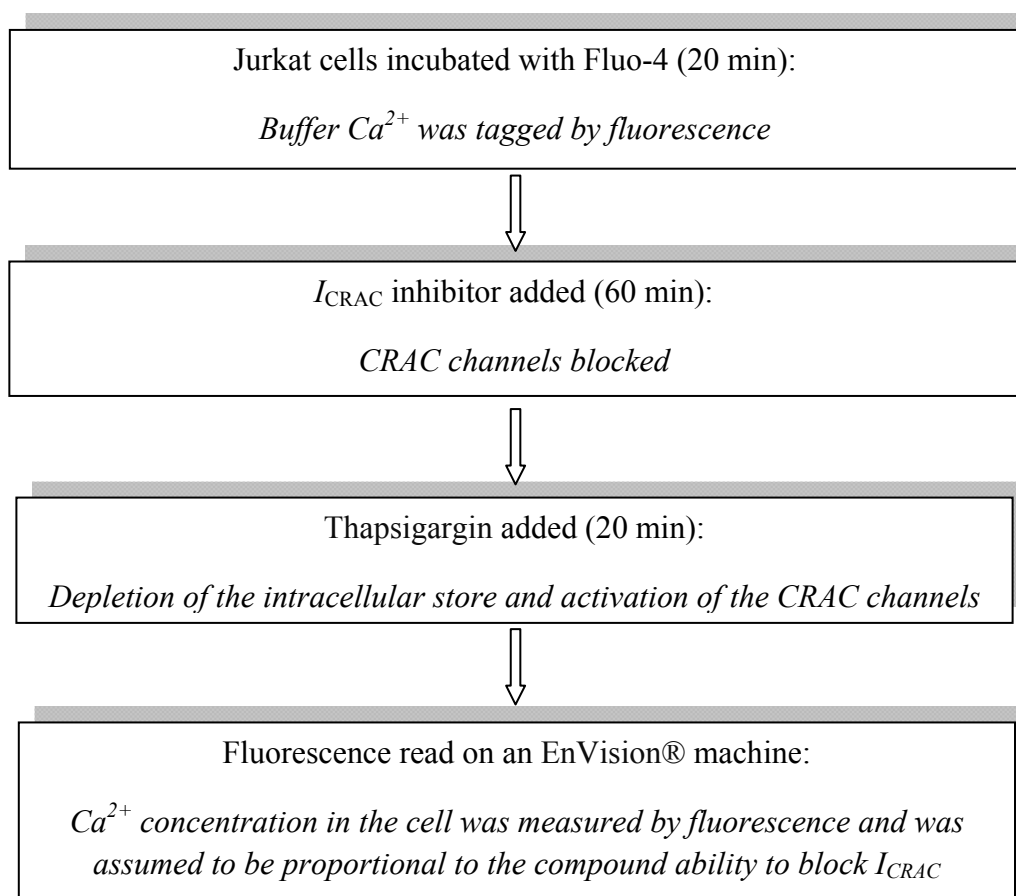
Hence, in this phenotypic assay set-up, inhibitors of  $I_{\text{CRAC}}$  would be expected to decrease the calcium influx following thapsigargin activated store depletion, therefore reducing the fluorescent signal. The potency of the tested compounds were then expressed as the negative logarithm of the compound concentration to achieve 50% inhibition ( $\text{pIC}_{50} = -\log\text{IC}_{50}$ ). The dose-response curve of tetrazolyindole **2.18** (Jurkat  $\text{pIC}_{50} = 6.0$ , compound discussed subsequently, **Table 9, p. 70**) is shown in **Figure 24** as an illustration.



**Figure 24: Calcium influx inhibition vs. tetrazolyindole 2.18 concentration**<sup>109</sup>

In practice, the Jurkat cells were pre-incubated with Fluo-4 for 20 minutes. The compound of interest was then added and the cells were left to stand for one hour. A solution of thapsigargin was added and the plate was incubated for an additional hour. To assess the ability of the compound to block the  $\text{Ca}^{2+}$  influx through the CRAC channel, the calcium concentration within the Jurkat cells was indirectly

measured as a fluorescent signal on an EnVision® fluorescence reader<sup>112</sup> (**Figure 25**). This assay could be routinely run in 384-well plates to provide sufficient throughput for screening up to 100 compounds in each assay.



**Figure 25: Protocol of the Jurkat cell assay<sup>109</sup>**

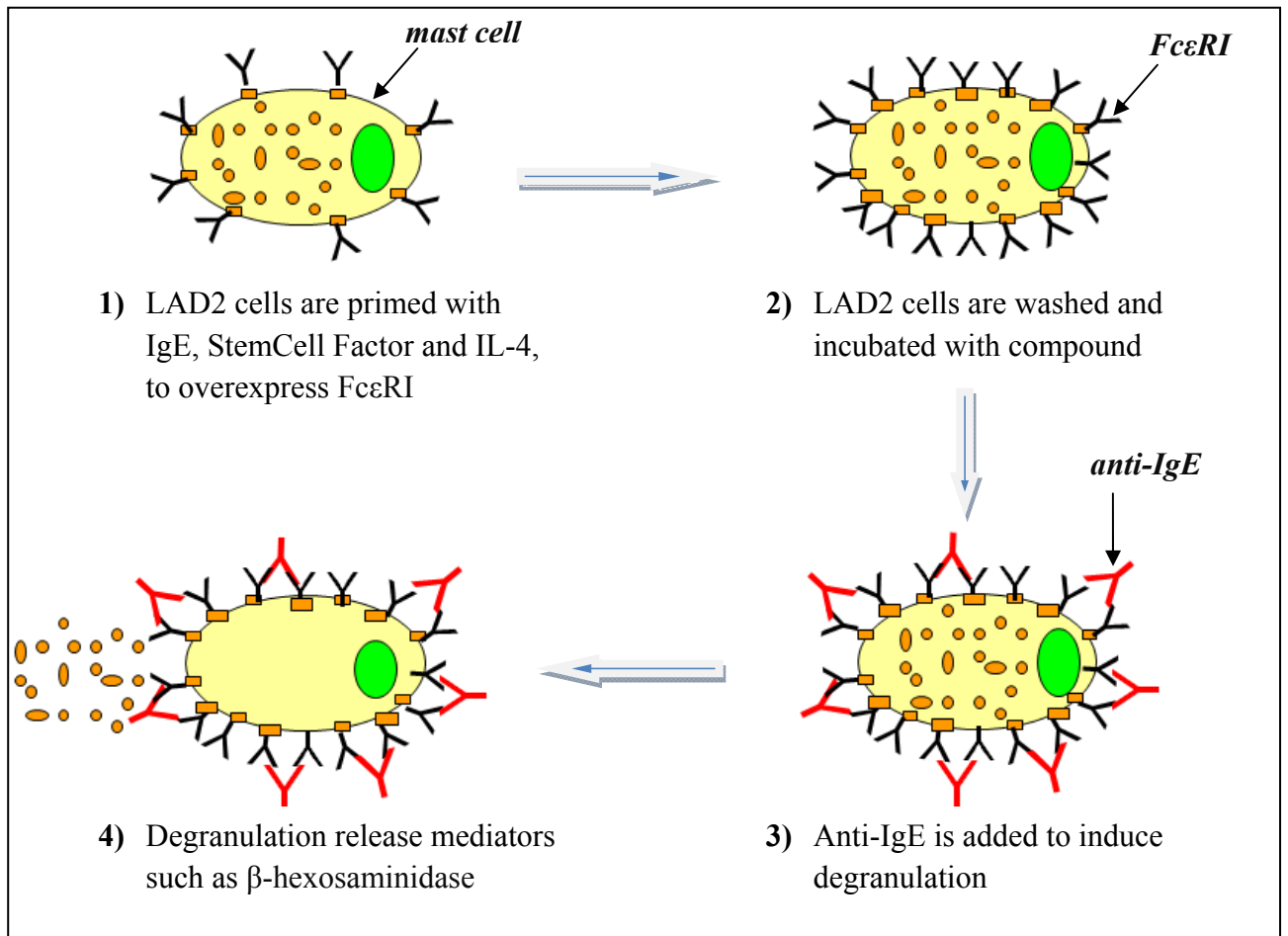
However, it should be noted that the signal observed in this assay cannot exclusively be ascribed to *I*<sub>CRAC</sub> inhibition alone, a potential drawback of the phenotypic approach. Having stated this, a combination of downstream assays can be used to determine the specificity of putative *I*<sub>CRAC</sub> inhibitors. These assays are described in the following sections.

### 2.1.8.2. LAD2 mast cell assay<sup>113</sup>

On their membrane surface, mast cells express high-affinity immunoglobulin E (IgE) receptors (noted FcεRI). The binding of the antibody anti-IgE to FcεRI, after downstream activation of several protein kinases, triggers the release of Ca<sup>2+</sup> from the ER Ca<sup>2+</sup> stores. Consequently, the CRAC channels are activated. The resulting rise in the free calcium concentration within the cytoplasm causes mast cell degranulation, leading to the release of several mediators, such as histamine, prostaglandins, cytokines and β-hexosaminidase. *I*<sub>CRAC</sub> inhibitors block this process of mast cell degranulation and the compound potency can therefore be evaluated by measuring the amount of inflammatory mediators released during this process.

The LAD2 cells used in our laboratories were a human mast cell line which were obtained from the National Institute of Health from patients with mast cell leukaemia.<sup>114</sup> The LAD2 cells were primed for five days with IgE, stemcell factor and interleukin-4. Under these conditions, LAD2 cells over-expressed FcεRI. LAD2 cells were then washed and incubated with the compound for one hour. The degranulation of mast cells was induced by the addition of anti-IgE which cross-links FcεRI. This causes the release of the granule contents, and of particular interest to our assay, the release of β-hexosaminidase. The last step of the assay consisted of removing the supernatant, lysing the cells and removing the lysate. The amount of β-hexosaminidase was measured by a fluorescence assay and was proportional to the amount of cell degranulation, which in turn depended on the ability of the compound to inhibit *I*<sub>CRAC</sub> (**Figure 26**).

Because of the technical complexity of the assay, the LAD2 assay was not run on all the *I*<sub>CRAC</sub> inhibitors identified, but only on selected compounds which were previously shown to be active in the Jurkat assay (usually when Jurkat pIC<sub>50</sub> > 5.5).



**Figure 26: Protocol of the LAD2 cell assay<sup>113</sup>**

### **2.1.8.3. PBMCs assays: CytoStim-stimulated IFN $\gamma$ and LPS-stimulated TNF $\alpha$ <sup>115</sup>**

Peripheral blood mononuclear cells (PBMCs) are white blood cells that have a round nucleus, as opposed to neutrophils, eosinophils and basophils, which have a lobed nucleus. They are attractive as a model for *in vitro* assays for two main reasons: firstly, they are particularly suitable for the development of screens measuring cytokine production and secondly, they are a primary cell type phenotypically relevant to human physiology. Cytokines are proteins secreted by immune cells and their function is to act as signalling molecules within the cellular communication

process. Commonly, the inhibition of an immune-related biological target leads to the inhibition of certain cytokine production.

PBMCs are constituted of around 75% of lymphocytes (*i.e.* T cells, B cells and natural killer cells (NK cells)) and approximately 25% of monocytes (macrophages and dendritic cells, **Figure 27**). Depending on the stimulus used to activate a mixed population of PBMCs, a specific biological target pathway can be selectively invoked. For instance, a PBMCs mixture can be stimulated either with a lymphocyte-specific or with a monocyte-specific stimulus. Within the PBMCs population, the CRAC target is known to be functional in T cells but not in monocytes. Thus, an  $I_{CRAC}$  inhibitor would inhibit a response when PBMCs are stimulated with a T cell-specific stimulus, however, no effect would be expected when using a monocyte-specific stimulus.

Of relevance for the  $I_{CRAC}$  PBMCs assays, two stimuli were used in our laboratories to activate PBMCs purified from blood samples obtained by donation:<sup>114</sup> CytoStim,<sup>116</sup> specific to T cells, and lipopolysaccharide (LPS),<sup>117</sup> specific to monocytes. CytoStim, an antibody-based reagent, caused activation of T cells through binding to the T cell receptor. Hence, upon stimulation with CytoStim,  $I_{CRAC}$  was activated and T cell-secreted cytokines, such as interferon-gamma ( $IFN\gamma$ ), were evoked.<sup>118</sup> Independently, when PBMCs were stimulated with LPS, which consists of a lipid and a polysaccharide linked together with a covalent bond, monocytes were activated through the binding of LPS to the cluster of differentiation 14 receptor. The result was the secretion of pro-inflammatory cytokines, such as tumor necrosis factor-alpha ( $TNF\alpha$ ). Importantly, these signalling pathways do not require CRAC channels for their function.

From the perspective of assays relevant to the identification of selective  $I_{CRAC}$  blockers, CytoStim-stimulated PBMCs led to the release of  $IFN\gamma$ , and were antagonised by an  $I_{CRAC}$  inhibitor. Conversely, LPS-stimulated PBMCs led to the production of  $TNF\alpha$  by macrophages, and were not affected by an  $I_{CRAC}$  inhibitor. Therefore, the CytoStim-stimulated  $IFN\gamma$  assay was a phenotypically relevant *in vitro* assay to assess the potency of  $I_{CRAC}$  inhibitors and the LPS-stimulated  $TNF\alpha$  assay was used to identify non-selective  $I_{CRAC}$  inhibitors that were previously active

in the Jurkat assay, by highlighting off-target activity. This bifurcated pathway is illustrated in **Figure 27**.

In summary, through the combined use of phenotypic assays, the medicinal chemistry programme could ensure the optimisation of compounds with on-target pharmacology.



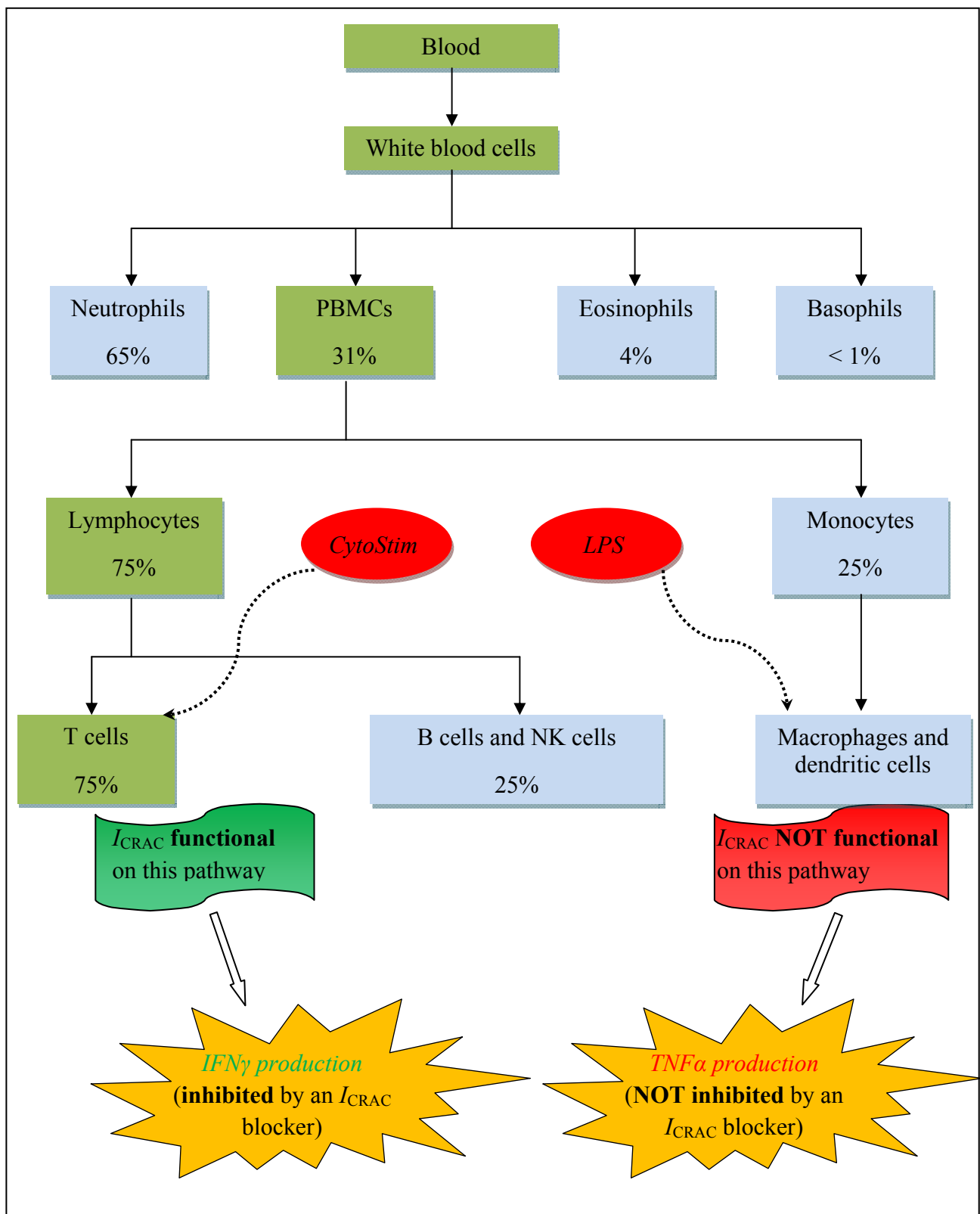


Figure 27: Difference between CytoStim- and LPS-stimulated PBMCs assays

#### 2.1.8.4. Electrophysiology assay

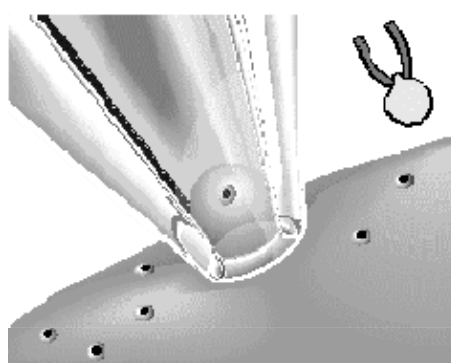
##### General description of electrophysiology:

Electrophysiology<sup>119</sup> is the study of the electrical properties of biological cells and tissues and it involves the measurement of voltage changes or electric currents. In biological systems, electric currents are carried by ions in solution and electrophysiology experiments study the transport of charged solutes across membranes and the proteins that carry out this transport. There are two main methods of electrophysiological measurements, the intracellular and the extracellular recordings. In the intracellular recording, the electrode used to measure the change in voltage or currents is either inserted into the cell or tightly adheres to the cell membrane. In the extracellular recording, the electrode is located in the extracellular space and the electrical properties of one or several cells can be measured.

The intracellular recording is the most relevant method to measure the electrical properties of ion channels and there exists three different techniques of intracellular recordings: the voltage clamp, the current clamp and the patch clamp techniques. The voltage clamp technique measures the ion currents through the membranes while holding the membrane voltage at a set level. Therefore, this method is useful in order to observe how cells react to changes in membrane potential and this is relevant to the study of voltage-gated ion channels. Conversely, the current clamp technique records the membrane potential while a varying current is applied *via* the electrode. This approach permits to assess how cells respond when an electric current passes through their membrane. Contrary to the two techniques described previously, in the patch clamp method,<sup>120</sup> the electrode is not inserted inside the cell, however, a physical interaction between the extremely small exterior of a glass pipette and a single cell is achieved. The pipette is then used to both apply a command potential and to measure the current response from the cell, in a similar way to the voltage clamp technique. The patch clamp method is the most sophisticated electrophysiological technique available and there are two common patch clamp techniques (**Figure 28**):

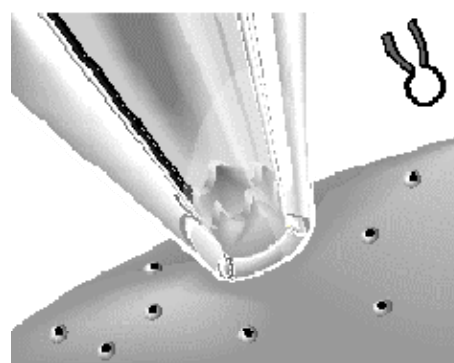
i) First, the **single channel recording** consists of placing the end of the pipette onto the cell membrane without breaking the integrity of the cell membrane. The connection achieved between the pipette and the cell membrane results in a tight seal (the “patch”) and this connection is so small that opening or closing of a single ion channel causes a significant alteration in the overall conductance of the “patch”. This method is therefore used to study the activity of just one or the few ion channels that are present in the “patch” of the membrane. This configuration leaves the cell intact and, in that regard, is the most physiologically representative. However, this method comes with its disadvantages, such as the difficulty in manipulating the media on either side of the membrane and the impossibility to directly modify intracellular pathways.

ii) The second patch clamp technique is **the whole cell recording**, in which after obtaining a high resistance contact between the pipette and the cell membrane, a short pulse of negative pressure is applied in order to break the cell membrane and to create a direct connection between the pipette and the inside of the cell. Hence, this technique allows the measurement of the current that results from ion movements across the membrane of the whole cell and this can be useful when investigating low conductance ion channels. Additionally, this approach enables the control of the inside of the cell. However, the main drawback of this method is that the interior of the cell is slowly replaced by the content of the electrode, therefore leaving a limited time window during which the cell behaves naturally.



**Single channel recording:**

A single ion channel conductance is measured



**Whole cell recording:**

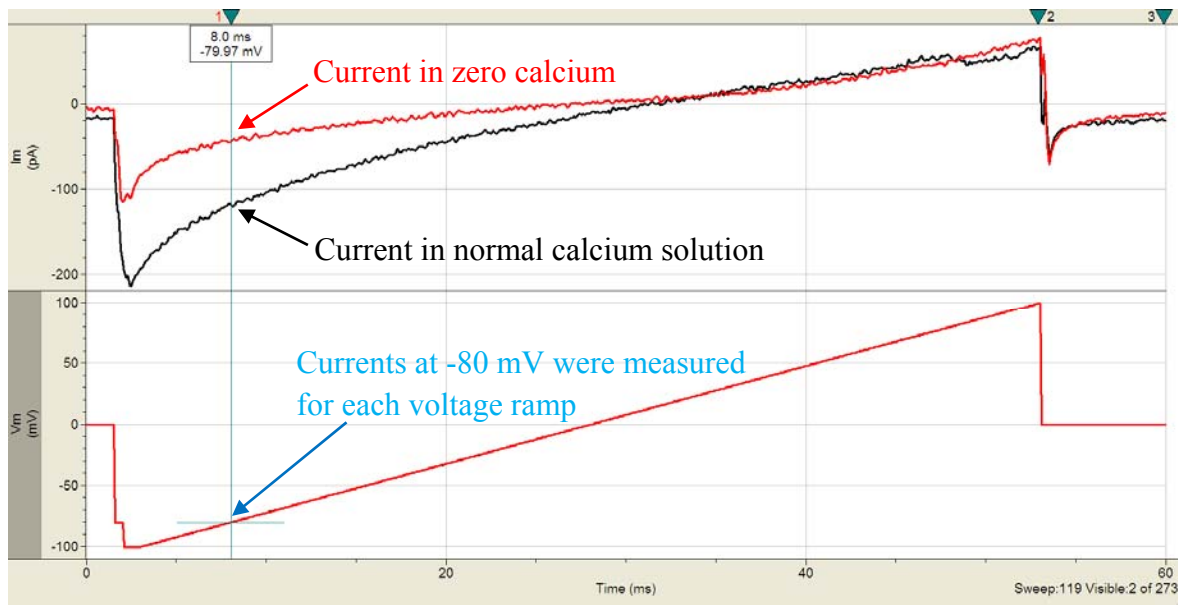
Current that results from ion movements across the membrane of the whole cell is measured.

**Figure 28: The two patch clamp techniques**<sup>121</sup>

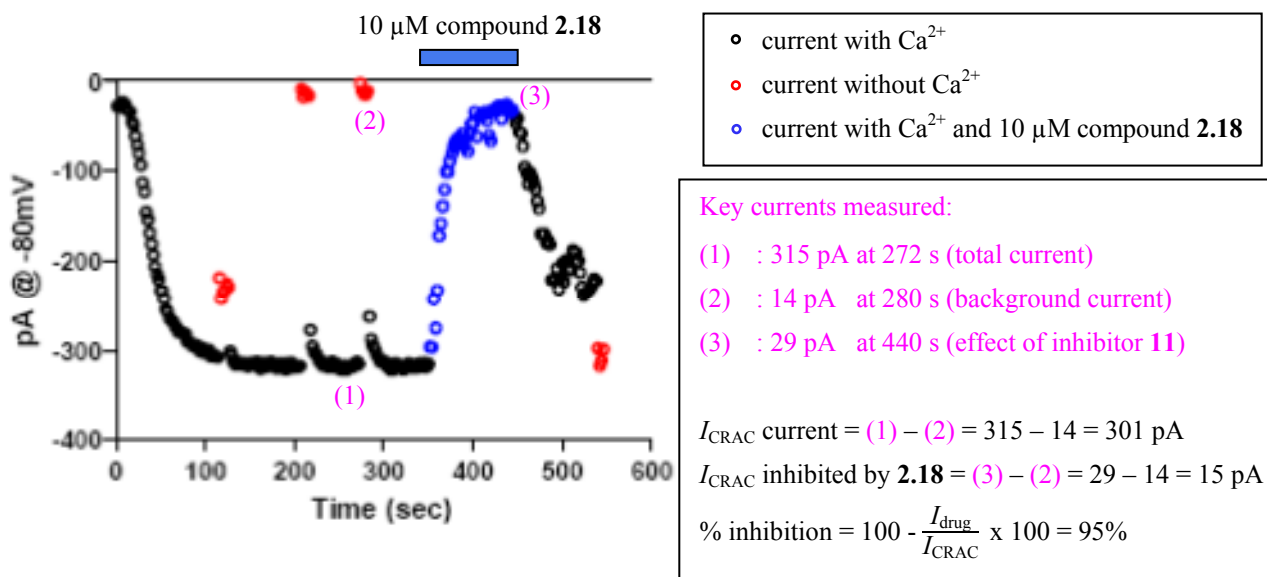
## Description of the electrophysiology assay used in our laboratories to study

$I_{\text{CRAC}}$ :<sup>122</sup>

Given the small magnitude of the  $I_{\text{CRAC}}$  current (see **Section 2.1.3, p. 29**), the whole cell recording technique was chosen for the electrophysiological study of  $I_{\text{CRAC}}$ . The electrophysiology assays were performed using human embryonic kidney cells expressing human STIM1 and ORAI1. In addition to make physical contact with the cell and to rupture the cell membrane, the pipette employed in the experiment also contained a solution of  $\text{IP}_3$  and  $\text{Cs}^+$ . The aim of  $\text{IP}_3$  was to deplete the ER  $\text{Ca}^{2+}$  stores and hence to activate  $I_{\text{CRAC}}$ , whereas the function of  $\text{Cs}^+$  was to block inward rectifying potassium channels. Following successful connection with the cell, a voltage ramp from -100 mV to +100 mV over 50 ms was delivered every 2 seconds using the electrode. As a response to this stimulation, the cell conducted  $\text{Ca}^{2+}$  ions (contained in the extracellular medium) using the CRAC channels to rectify the membrane potential leading to the  $I_{\text{CRAC}}$  current. The inward current at -80 mV was measured for every voltage ramp and once the magnitude of the current stabilised, an extracellular solution containing nominal zero calcium was applied in order to determine the current obtained when the CRAC channel were not used (*i.e.* the background current, see **Figure 29** for an example of a single voltage ramp). This step was repeated several times in order to obtain a consistent measure of the background current. Once the background current was determined and that  $I_{\text{CRAC}}$  current stabilised again after returning to control extracellular solution containing  $\text{Ca}^{2+}$ , the test compound was applied and current was measured until the level of blockade reached a plateau. The level of reduction of the current after treatment with compound (generally dosed at 10  $\mu\text{M}$ ) indicated its ability to block  $I_{\text{CRAC}}$ , where the amplitude of  $I_{\text{CRAC}}$  current was defined as the difference between current in normal calcium solution and current obtained in nominal zero calcium. As an example of this assay, an electrophysiology experiment using 10  $\mu\text{M}$  of the  $I_{\text{CRAC}}$  blocker tetrazolyindole **2.18** (compound discussed subsequently, **Table 9, p. 70**) is shown on **Figure 30**.



**Figure 29: Currents measured in nominal zero calcium solution and in normal calcium solution for a voltage ramp from -100 mV to +100 mV over 50 ms**



**Figure 30: 95% inhibition of  $I_{CRAC}$  was obtained with tetrazolylindole 2.18 at 10  $\mu$ M in an electrophysiology experiment<sup>122</sup>**

## 2.2. Medicinal chemistry approaches to $I_{CRAC}$ inhibitors

### 2.2.1. Background and chemical landscape of CRAC blockers

As discussed in **Section 2.1.7 (p. 39)**, molecules inhibiting the CRAC current are thought to have the potential to beneficially modulate the immune response and are therefore relevant to the drug discovery community. In recent years, the number of patents describing small molecule inhibitors of  $I_{CRAC}$  has increased dramatically, underlining the interest this biological target represents. A review published in 2009 elegantly summarised the  $I_{CRAC}$  chemical landscape up to that date.<sup>78</sup> The major pharmaceutical companies which contributed to the field are Abbott Labs,<sup>123</sup> Astellas Pharma (previously Yamanouchi Pharmaceuticals),<sup>124</sup> Boehringer Ingelheim,<sup>125</sup> Synta Pharmaceuticals,<sup>126</sup> and CalciMedica.<sup>127</sup> The molecules in **Table 4** provide an overview of the chemotypes described in these patents, alongside with their potency measured in the Jurkat assay available in our laboratories, and their physicochemical properties.

| Company name          | Cmpd | Structure | Jurkat pIC <sub>50</sub> | MW  | clogP | CLND (µg/mL) <sup>i</sup> |
|-----------------------|------|-----------|--------------------------|-----|-------|---------------------------|
| Abbott Labs           | 2.19 |           | 6.9                      | 416 | 3.4   | 8                         |
| Astellas Pharma       | 2.20 |           | 7                        | 421 | 3.3   | 6                         |
| Boehringer Ingelheim  | 2.21 |           | ND <sup>a</sup>          | 380 | 4.9   | ND                        |
| Synta Pharmaceuticals | 2.22 |           | 6.7 <sup>b</sup>         | 352 | 3     | 6                         |
| CalciMedica           | 2.23 |           | 5.7                      | 416 | 5.6   | 30                        |

<sup>a</sup>ND = not determined; <sup>b</sup>Compound failed to fit a curve in 4 out of 293 test occasions.

**Table 4: Published *I*<sub>CRAC</sub> inhibitors**

Despite this activity in the medicinal chemistry community, the development of molecules targeting CRAC channels is still in its relative infancy. Indeed, to the best of our knowledge, all *I*<sub>CRAC</sub> drug discovery programmes are at the pre-clinical stage, except compound CM2489 (structure unknown) from CalciMedica, which is studied as a once-daily oral therapeutic for patients with moderate to severe plaque psoriasis.<sup>128</sup> There is very little information about this compound and no public communication was made around its *in vitro* and *in vivo* efficacy. A clinical trial was initiated in 2011, involving 48 healthy volunteers, in order to determine safety, tolerability and pharmacokinetic profile of CM2489 in humans.<sup>128</sup> The results of this study have not been communicated.

<sup>i</sup>In all the compounds profile tables of this thesis, CLND refers to CLND solubility.

The molecules typifying the  $I_{\text{CRAC}}$  chemical landscape (**Table 4**) display a common pharmacophore, since they contain a similar lipophilic motif: aryl ring-aryl ring-amide bond-aryl ring. Despite being relatively small with regard to their molecular weight, none of the molecules presented above exhibits polar functionality, except for CalciMedica compound **2.23**, which contains a carboxylic acid. This lack of polar functionality translates into a rather high clogP for these molecules (clogP  $\geq 3$ , outside the recommended physicochemical properties values for oral drugs discussed in **Table 1, p. 6**). Additionally, these flat and largely aromatic structures are missing the rotational freedom which would help to achieve good aqueous solubility. Thus, the measured aqueous solubility of these compounds is very low as five out of the six compounds have an aqueous solubility of less than 10  $\mu\text{g/mL}$ , and only CalciMedica compound **2.23** exhibits a modest aqueous solubility of 30  $\mu\text{g/mL}$ .

Hence, the developability parameters of the current generation of published  $I_{\text{CRAC}}$  inhibitors are not ideal for an oral drug molecule. The combination of high lipophilicity with poor solubility is anticipated to lead to a low probability of achieving good pharmacokinetics, based on the modern concepts of property control discussed previously (see **Section 1.2, p. 2**). More generally, the compounds from the published chemical landscape underline the difficulty in developing inhibitors of  $I_{\text{CRAC}}$  with physicochemical properties consistent with oral dosing.

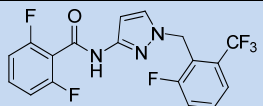


### 2.2.2. First generation of inhaled $I_{CRAC}$ inhibitors from our laboratories

Prior to the author commencing work on this area, efforts were made in our laboratories to develop inhaled  $I_{CRAC}$  inhibitors for the treatment of asthma and the *in vitro*  $I_{CRAC}$  potency of several compounds from this first generation of inhibitors was discussed in the literature. Firstly, compounds were shown to completely inhibit calcium influx through CRAC channels using patch clamp electrophysiology.<sup>102</sup> Secondly, several analogues were demonstrated to inhibit mediator release from mast cells and pro-inflammatory cytokine release from T cells in a variety of species.<sup>129,130</sup>

Given the contrasting requirements between oral and inhaled therapeutics, the physicochemical properties of the associated molecules are different. Firstly, in order to increase the therapeutic window and because a large fraction of an inhaled drug is swallowed during the inhalation process, an inhaled molecule is designed to have low oral bioavailability, often by having a high hepatic clearance.<sup>131</sup> Secondly, in order for inhaled drugs to have a long duration of action, they are often designed to have low aqueous solubility, since this has proven to prolong the retention of the compound in the lung.<sup>132</sup> Interestingly, it is now recognised that this strategy for inhaled compounds design can promote lung pathology findings related to an excess of undissolved drug.<sup>133</sup> Indeed, the presence of undissolved material within the alveolar air spaces leads to changes in the morphology and the function of the alveolar macrophages.<sup>134</sup>

As an example of the first generation of inhaled  $I_{CRAC}$  inhibitors developed by our group,<sup>135,136</sup> 3-aminopyrazole **2.24** (Table 5) displayed physicochemical parameters which are expected to be different to those anticipated for an oral profile.

| Structure                            |  |
|--------------------------------------|--|
| Compound                             | <b>2.24</b>  |
| Jurkat pIC <sub>50</sub>             | 6.3  |
| LAD2 pIC <sub>50</sub>               | 6.3  |
| PBMCs IFN $\gamma$ pIC <sub>50</sub> | 6.1  |
| PBMCs TNF $\alpha$ pIC <sub>50</sub> | 4.7 <sup>a</sup>   |
| ePhys (at 10 $\mu$ M)                | 78% <i>I</i> <sub>CRAC</sub> inhibition with a half-life <sup>ii</sup> of 55 s     |
| LE / LLE <sup>iii</sup>              | 0.31 / 0.24  |
| MW                                   | 399  |
| clogP                                | 3.7  |
| PFI                                  | 8.4  |
| CLND ( $\mu$ g/mL)                   | 34 <sup>b</sup>  |

<sup>a</sup>Compound reported inactive<sup>iv</sup> in 9 out of 16 test occasions; <sup>b</sup>Compound reported with a CLND  $\geq$  75  $\mu$ g/mL in 1 out of 15 test occasions.

**Table 5: Profile of 3-aminopyrazole 2.24, key exemplar of the first generation of inhaled *I*<sub>CRAC</sub> blockers developed in our laboratories<sup>135,136</sup>**

Pyrazole **2.24** exhibits a similar pharmacophore to the one displayed by the published *I*<sub>CRAC</sub> inhibitors (Table 4, p. 54), with the motif aryl ring-aryl ring-amide bond-aryl ring. The average lipophilicity (clogP = 3.7) and high PFI (PFI = 8.4) resulted in a relatively low aqueous solubility of 34  $\mu$ g/mL. Analogue **2.24** displayed micromolar potency across the series of *I*<sub>CRAC</sub> biological assays (Jurkat, LAD2 and IFN $\gamma$ ), which was an appropriate level of activity for target engagement *in vivo*. Indeed, key analogues of this aminopyrazole series with similar *in vitro* *I*<sub>CRAC</sub> potency showed efficacy in *in vivo* animal models of asthma.<sup>137</sup>

<sup>ii</sup> In the context of electrophysiology, half-life is defined as the time required for the tested compound to effect 50% of the maximal inhibition.

<sup>iii</sup>In all the compounds profile tables of this chapter (for the *I*<sub>CRAC</sub> programme), LE and LLE are calculated with the Jurkat cell assay pIC<sub>50</sub> values, which was the primary assay of the *I*<sub>CRAC</sub> programme.

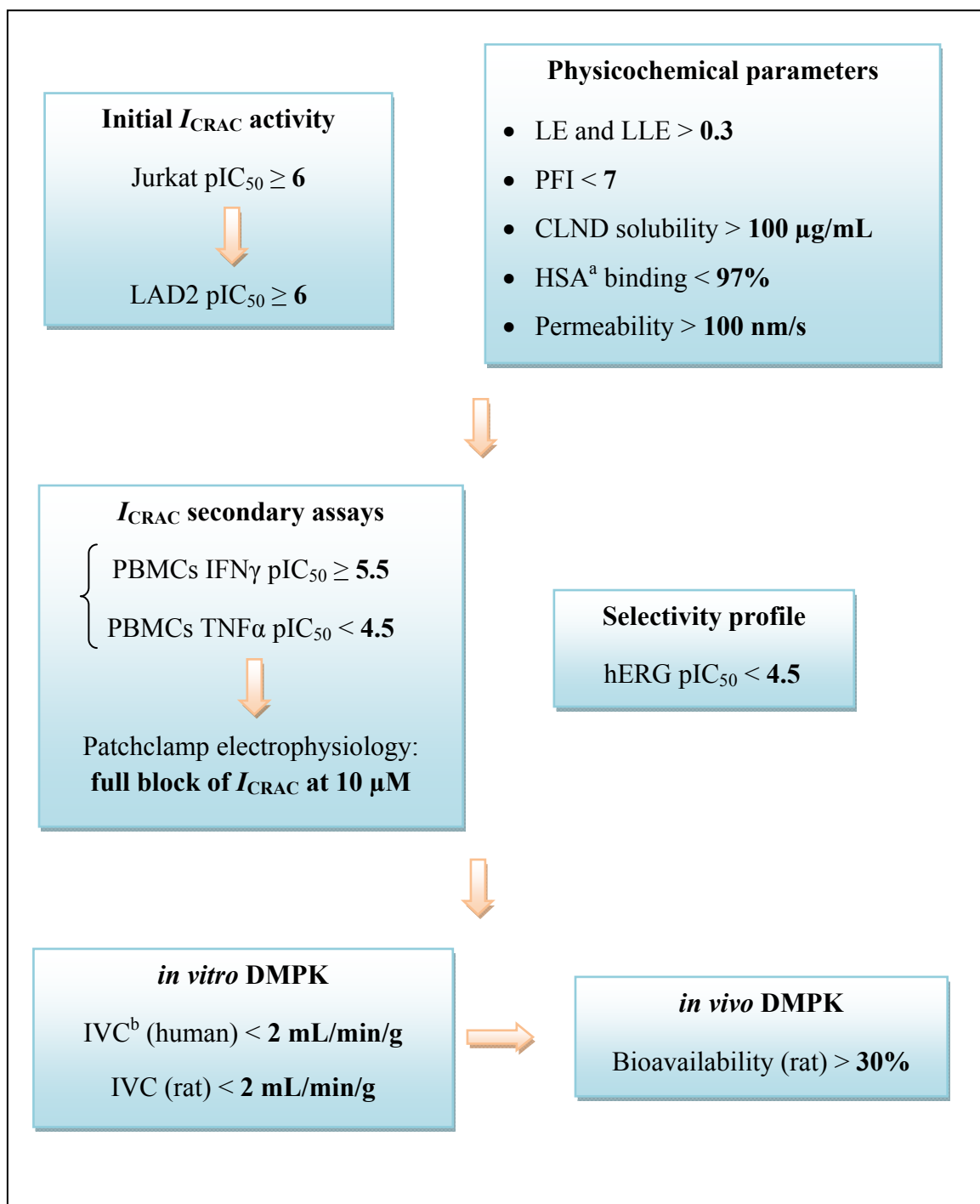
<sup>iv</sup> In this thesis, compounds are referred as “inactive” when their activity is below the threshold of activity of the biological assay they are measured in, at the concentration they are measured at.

### 2.2.3. Overall objective of the second generation of oral $I_{CRAC}$ inhibitors

Subsequently to the first generation of inhaled  $I_{CRAC}$  inhibitors discussed previously, attention focused on the development of oral  $I_{CRAC}$  inhibitors. In addition to its suitability for a wider range of indications, the advantages of an oral approach included improved patient compliance and stronger competitive position. As discussed in the next section, a high throughput screening (HTS) campaign was used to identify hit compounds for the second generation of oral  $I_{CRAC}$  inhibitors. The overall objective of the current study was to optimise a selection of hit compounds identified from the HTS into lead compounds displaying an overall profile that enables the initiation of a lead optimisation programme. The profile targeted for an ideal lead oral  $I_{CRAC}$  inhibitor is defined below and the optimisation guidelines with regard to profile of compounds are more explicitly described in **Figure 31**.

- Equivalent or greater potency than the previous first generation  $I_{CRAC}$  inhibitors (Jurkat and LAD2  $pIC_{50} \geq 6$ );
- Less than 0.5 log unit activity drop in primary human cells (PBMCs  $IFN\gamma \geq 5.5$ );
- High LE and LLE (LE > 0.3 and LLE > 0.3);
- High aqueous solubility (CLND solubility > 100  $\mu\text{g/mL}$ );
- Drug metabolism and pharmacokinetics (DMPK) profile predictive of a low human dose.

When comparing the above target profile with the one from the published  $I_{CRAC}$  inhibitors (**Table 4, p. 54**), it was expected that lipophilicity and aqueous solubility would potentially be difficult parameters to control, since the CRAC target seems to selectively bind flat lipophilic structures, a challenge often encountered in medicinal chemistry programmes.



<sup>a</sup>HSA = human serum albumin; <sup>b</sup>IVC = (microsomal) *in vitro* clearance.

**Figure 31: Screening approaches for selection of  $I_{CRAC}$  lead molecules**

## 2.3. Results and discussion: Second $I_{CRAC}$ HTS<sup>138</sup>

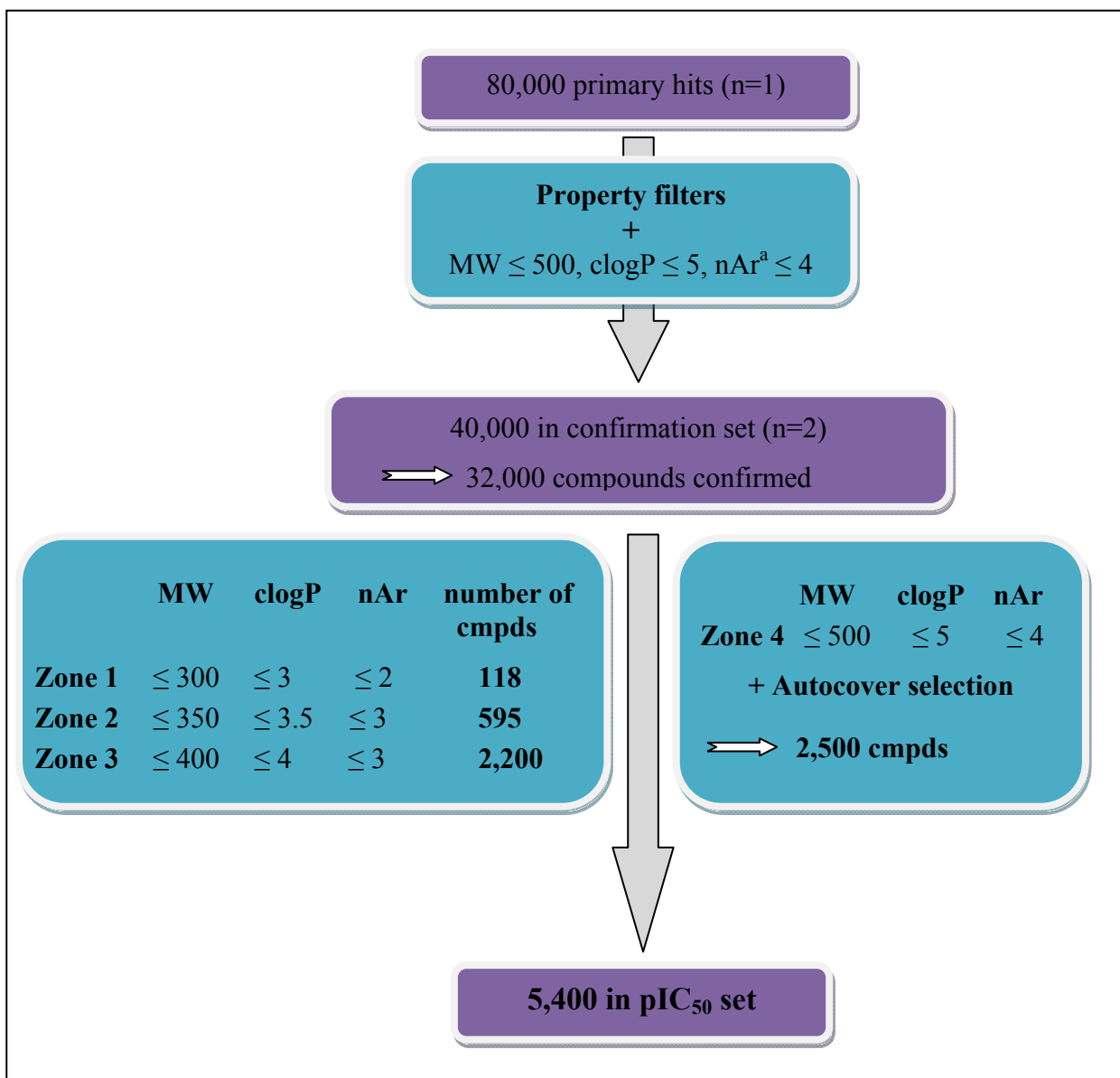
### 2.3.1. An HTS triage focused on physicochemical properties

The first generation of inhaled  $I_{CRAC}$  inhibitors developed in our laboratories originated from an HTS ran against  $I_{CRAC}$  using our internal compound library.<sup>137</sup> This campaign did not identify a suitable starting point for an oral therapy, however, it did furnish the pyrazole chemotype, suitable for an inhaled delivery approach (**Table 5, p. 57**). For the current oral  $I_{CRAC}$  programme, other methods to discover new chemical hits,<sup>139</sup> such as fragment-based drug discovery, analogue design and virtual screening, were considered. A fragment-based screening approach constitutes probably the most efficient strategy to identify small fragment inhibitors, with improved binding efficiency (both LE and LLE) and with better physicochemical parameters.<sup>140</sup> These fragments are usually weakly active to start with and require high-concentration biochemical or biophysical assays to be put in place. Our experience with typical  $I_{CRAC}$  inhibitors has shown that these molecules are relatively weakly potent (approximately 1  $\mu$ M) and this would potentially render such a fragment-based screening difficult. Additionally, co-crystallising the CRAC channel with a bound inhibitor had never been achieved, rendering structure-based design impossible. Since novel chemotypes, with a differentiated pharmacophore compared to the one described in the literature and to our first generation of  $I_{CRAC}$  blockers, were sought, analogue design and virtual screening were also disregarded.

In order to access a differentiated variety of chemotypes, a second HTS was considered to be the most attractive hit identification strategy. Indeed, the size of the compound collection available in our laboratories had increased since the first HTS campaign (especially with more oral drug-like compounds), and a new assay was available which was designed to detect alternative modes of action. Hence, in the assay used for the first  $I_{CRAC}$  HTS campaign, compounds were added concomitantly with thapsigargin whereas in the current assay available, compounds were pre-incubated with the Jurkat cells for 60 min prior to triggering the opening of the CRAC channels by addition of thapsigargin (see **Figure 25, p. 43**).

Taking the above points into consideration, an HTS was run using our internal compound library in order to identify a second generation of oral  $I_{CRAC}$  inhibitors. With the new assay set up, the primary hit rate of the second HTS (4%) was significantly greater than the initial  $I_{CRAC}$  HTS (1.6%). Moreover, it is worth mentioning that HTS is now a well established hit generation technique and can often furnish novel chemotypes through random screening of a large compounds collection. In this instance, the approach taken differed somewhat from the more usual target-based strategy, as the phenotypic Jurkat assay described previously was used as a primary screen. Thus, we have effectively combined two important paradigms to enable the identification of novel  $I_{CRAC}$  blockers.

As the current focus was to identify novel templates with properties suited to oral administration and good aqueous solubility, an innovative HTS triage strategy was designed and implemented by the author, in collaboration with other members of our laboratories,<sup>138</sup> based on physicochemical properties. The HTS hits were ranked and divided into four different “zones” according to three different parameters: molecular weight, clogP and number of aromatic rings. Zone 1 contained molecules with the most attractive physicochemical parameters and zone 4 defined the least favoured compounds (**Figure 32**).



<sup>a</sup>nAr = number of aromatic rings.

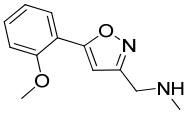
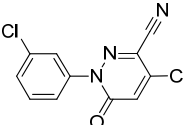
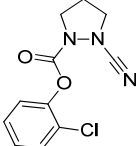
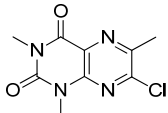
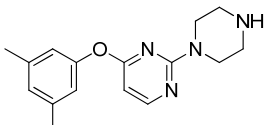
**Figure 32: The HTS triage strategy based on physicochemical parameters**

As shown in **Figure 32**, the output from the primary screen yielded 80,000 hits. These compounds were first subjected to property filters and to initial limits for MW, clogP and number of aromatic rings. The property filters applied were a set of substructure and machine-based filters developed in our laboratories<sup>137</sup> in order to remove compounds considered to be inappropriate for further screening. For example, molecules with more than 60 heavy atoms or with more than 4 halogens are excluded by these filters. In addition to these property filters, all the molecules

displaying a MW greater than 500, a clogP greater than 5 or a number of aromatic rings greater than 4 were excluded. Interestingly, this relatively straightforward set of filters halved the number of hits, from 80,000 to 40,000. The resulting 40,000 compounds were tested again at a single concentration in the Jurkat assay and inactive compounds were excluded to give a set of 32,000 compounds. This set was then divided into the four different zones 1 to 4, according to the MW, clogP and number of aromatic rings cut-offs described in **Figure 32**. Zone 4 was further reduced using a technique developed in our laboratories named Autocover Selection,<sup>137</sup> a computational program used to identify a diverse subset of compounds, which is representative of the chemical space, based on Daylight similarity. Application of this strategy enabled the expedient identification of a set of 5,400 compounds out of the initial list of 80,000 hits. These 5,400 compounds were submitted to the  $I_{\text{CRAC}}$  Jurkat assay in order to generate a concentration-response curve, providing a  $\text{pIC}_{50}$  for each of the compounds. In addition, this prioritisation based on three key physicochemical parameters enabled us to focus on compounds with a desired oral drug-like profile from the outset of the research programme.

Compounds from zone 1, which have the most attractive physicochemical properties, were clustered in priority using computational means according to their structural similarity. An illustrative selection of the main clusters resulting from this analysis is displayed in **Table 6**. Each cluster was then further investigated by searching the database of available compounds within our laboratories for structurally related analogues in order to expand available SAR.



| Cmpd number | Structure  | Jurkat pIC <sub>50</sub> | PBMCs IFN $\gamma$ pIC <sub>50</sub> | PBMCs TNF $\alpha$ pIC <sub>50</sub> | MW PFI CLND ( $\mu\text{g/mL}$ ) |
|-------------|--|--------------------------|--------------------------------------|--------------------------------------|----------------------------------|
| 2.25        |   | 5.1                      | < 4.7                                | 4.4 <sup>a</sup>                     | 218<br>4.3<br>61 <sup>b</sup>    |
| 2.26        |   | 5.7                      | 6.6                                  | 6.9                                  | 266<br>7.4<br>24                 |
| 2.27        |   | 5.4                      | 6.4                                  | 6.4 <sup>c</sup>                     | 252<br>ND<br>140                 |
| 2.28        |   | 5.6                      | 6.1                                  | 6.3 <sup>d</sup>                     | 241<br>4.7<br>105 <sup>e</sup>   |
| 2.29        |  | 5.5                      | < 4.7 <sup>f</sup>                   | 4.2 <sup>a</sup>                     | 284<br>5.3<br>$\geq 239$         |

<sup>a</sup>Compound reported inactive in 1 out of 2 test occasions; <sup>b</sup>Compound reported with a CLND  $\geq 79$   $\mu\text{g/mL}$  in 1 out of 2 test occasions; <sup>c</sup>Compound reported inactive in 2 out of 8 test occasions; <sup>d</sup>Compound reported inactive in 1 out of 14 test occasions; <sup>e</sup>Compound reported with a CLND  $\geq 104$ ,  $\geq 113$ ,  $\geq 117$  and  $\geq 130$   $\mu\text{g/mL}$  out of the 5 test occasions; <sup>f</sup>Compound reported active in 1 out of 6 test occasions.

**Table 6: Exemplars of chemotypes from the HTS zone 1**

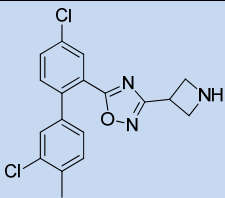
The chemotypes illustrated in **Table 6** were differentiated from the previously established  $I_{\text{CRAC}}$  pharmacophore, since none of them exhibited the motif aryl ring-aryl ring-amide bond-aryl ring described in the literature and in our first generation of  $I_{\text{CRAC}}$  blockers (see **Table 4**, p. 54 and **Table 5**, p. 57, respectively). Subsequently to the physicochemical properties values defining zone 1 ( $\text{MW} \leq 300$ ,  $\text{clogP} \leq 3$  and  $n_{\text{Ar}} \leq 2$ ), the PFI values of the compounds in **Table 6** were reduced compared to our first generation of  $I_{\text{CRAC}}$  inhibitors (PFI = 8.4 for compound **2.24**, **Table 5**, p. 57). More importantly, the aqueous solubility of these starting points was higher

compared to those previously described for  $I_{CRAC}$  blockers, as exemplified by the aqueous solubility of the piperazinyl-pyrimidine analogue **2.29** of  $\geq 239$   $\mu\text{g/mL}$ . Despite these encouraging features, a large number of the compounds from zone 1 were characterised by unexpectedly high PBMCs  $\text{pIC}_{50}$  values, such as compounds **2.26**, **2.27** and **2.28**, which displayed a greater PBMCs potency (in both  $\text{IFN}\gamma$  and  $\text{TNF}\alpha$  assays) than their Jurkat  $I_{CRAC}$  activity. This observation prompted concerns regarding the potential cellular toxicity of these compounds. Therefore, a biological assay was carried out by other members of our laboratories<sup>115</sup> on several exemplars from zone 1 in order to identify the likely cause of any potential toxicity. This assay was a human PBMCs-based screen designed to measure the mitochondrial activity of the cells after incubation with test compound. Cytotoxic compounds were identified when no more mitochondrial activity was measured after compound incubation, indicative of cell death. Unfortunately, a very large proportion of compounds from zone 1 were positive in this PBMCs-based cytotoxicity assay. Accordingly, no chemical series from this HTS category was progressed further.

Progressive analysis of zones 2, 3 and 4 by the author and other members of our laboratories<sup>138</sup> was achieved by clustering the HTS hits based on structural similarity, in order to efficiently map the chemical space defined by the hits. The level of confidence in the activity of each chemotype was further increased by submitting to the  $I_{CRAC}$  Jurkat biological screen additional related analogues present in our compounds database. Additionally, the PBMCs-based cytotoxicity assay was used on several key exemplars of each cluster to verify that each chemical series was not cytotoxic in nature. This work led to the identification of two novel chemical series that are studied in more detail: the oxadiazole amine series and the indole series.

### 2.3.2. Introduction to the oxadiazole amine series and definition of the optimisation goals

From the analysis of the second  $I_{CRAC}$  HTS described above, the oxadiazole amine series was identified, and is exemplified by the hit compound **2.30** (Table 7). This chemotype was clearly differentiated from the usual  $I_{CRAC}$  pharmacophore of the type aryl ring-aryl ring-amide bond-aryl ring (see published  $I_{CRAC}$  inhibitors, Table 4, p. 54) and contained a basic amine, which to the best of our knowledge, was an unprecedented feature in the  $I_{CRAC}$  inhibitor literature. The introduction of this basic group had the potential to profoundly improve the aqueous solubility compared to the previously described  $I_{CRAC}$  blockers, meaning that this significant hurdle would potentially be addressed from the outset of the optimisation efforts.

| Structure                            |  |
|--------------------------------------|--|
| Compound                             | <b>2.30</b>  |
| Jurkat pIC <sub>50</sub>             | 5.8 <sup>a</sup>   |
| LAD2 pIC <sub>50</sub>               | 5.4 <sup>b</sup>   |
| PBMCs IFN $\gamma$ pIC <sub>50</sub> | 5.1 <sup>c</sup>   |
| PBMCs TNF $\alpha$ pIC <sub>50</sub> | 4.7  |
| LE / LLE                             | 0.33 / 0.22  |
| MW                                   | 360  |
| clogP                                | 3.8  |
| PFI                                  | 7.6  |
| CLND ( $\mu\text{g/mL}$ )            | 31   |
| Permeability (nm/s) <sup>v</sup>     | 400  |
| HSA binding                          | 97%  |

<sup>a</sup>Compound reported inactive in 1 out of 6 test occasions; <sup>b</sup>Compound reported inactive in 1 occasion and failed to fit a curve in 5 occasions out of 8 test occasions; <sup>c</sup>Compound reported inactive in 2 occasions and failed to fit a curve in 1 occasion out of 10 test occasions.

**Table 7: Profile of oxadiazole amine 2.30, identified as a hit from the HTS**

Oxadiazole azetidine **2.30** (Table 7) was characterised by a molecular weight of 360 and a clogP of 3.8. Ligand efficiency (LE = 0.33) was attractive as a starting point, however, the HAC and the clogP of the series would have to be reduced in order to improve LLE (LLE = 0.22). The  $I_{\text{CRAC}}$  Jurkat potency (pIC<sub>50</sub> = 5.8) placed this hit compound in the high range of the usual  $I_{\text{CRAC}}$  activity spectrum, yet a noticeable drop in potency in the LAD2 assay (pIC<sub>50</sub> = 5.4) and in the IFN $\gamma$  assay (pIC<sub>50</sub> = 5.1) was observed. Additionally, compound **2.30** displayed a high permeability (400 nm/s) and a high plasma protein binding (HSA binding = 97%). The aqueous

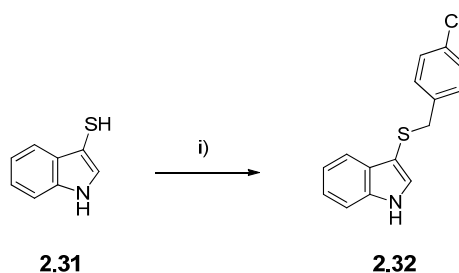
<sup>v</sup>In all the compounds profile tables of this thesis, permeability refers to artificial membrane permeability.

solubility of the hit compound **2.30**, measured at 31  $\mu\text{g/mL}$ , was below our optimisation goals (CLND solubility  $> 100 \mu\text{g/mL}$ ).

The first objective for the oxadiazole amine series was to confirm the  $I_{\text{CRAC}}$  activity by progressing an analogue to the electrophysiology experiments, since no more material of **2.30** was available. The second objective was to optimise the hit compound **2.30** in order to deliver lead oral  $I_{\text{CRAC}}$  inhibitors having the profile defined in **Figure 31** (p. 59). The efforts are described in later sections of this thesis.

### 2.3.3. Introduction to the indole series and definition of the optimisation goals

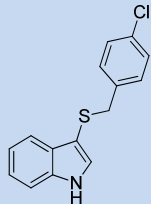
Concomitantly to the second HTS being analysed, a data-mining exercise of the existing potent  $I_{\text{CRAC}}$  inhibitors available in our laboratories was carried out by the author, in collaboration with another member of our laboratories<sup>141</sup> focusing on ligand efficiency. The aim was to identify compounds that had a high ligand efficiency value ( $\text{LE} > 0.45$ ), even if they were lipophilic or with sub-optimal aqueous solubility, since their low HAC would give the opportunity to investigate the incorporation of polar functionalities in their structure. This analysis identified 3-thioindole **2.32**, as having one of the highest LE scores ( $\text{LE} = 0.46$ ). In order to obtain confirmation on the structure tested from our internal compound collection, compound **2.32** was resynthesised by alkylating 1*H*-indole-3-thiol **2.31** with 1-(bromomethyl)-4-chlorobenzene, using sodium hydride as a base (**Scheme 1**).



i) 60% by weight NaH (1.2 eq), then 1-(bromomethyl)-4-chlorobenzene (1.2 eq), DMF, rt, 77%.

**Scheme 1: Synthesis of 3-thioindole 2.32**

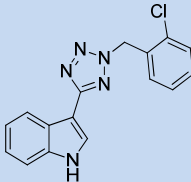
The high ligand efficiency of 3-thioindole **2.32** resulted from the combination of its low HAC and its  $I_{CRAC}$  Jurkat activity of  $pIC_{50}$  6.1 (**Table 8**). However, this compound suffered from high lipophilicity ( $clogP = 5$  and  $PFI = 10.1$ ), resulting in a low ligand-lipophilicity efficiency of 0.2 and a low aqueous solubility of 2  $\mu\text{g/mL}$ . Despite displaying good potency in both the Jurkat and the LAD2 assays, compound **2.32** exhibited a one log unit drop in activity in the PBMCs  $\text{IFN}\gamma$  assay. This drop was hypothesised to be driven by the high lipophilicity of the compound, making it prone to non-specific binding to exogenous proteins present in the PBMCs assay (*e.g.* the CytoStim-stimulated  $\text{IFN}\gamma$  assay contains 10% of foetal bovine serum). Nevertheless, the activity of **2.32** in the electrophysiology assay gave unequivocal evidence of its  $I_{CRAC}$  inhibition. The presence of a sulfur atom was anticipated to make this molecule prone to metabolism, as sulfides tend to be readily oxidised to sulfoxides.<sup>142</sup> These two negative properties of metabolic liability and high lipophilicity led us to predict that compound **2.32** would display high clearance leading to poor ADMET properties, not consistent with acceptable oral bioavailability.

| Structure                           |  |
|-------------------------------------|--|
| Compound                            | <b>2.32</b>  |
| Jurkat $pIC_{50}$                   | 6.1  |
| LAD2 $pIC_{50}$                     | 6  |
| PBMCs $\text{IFN}\gamma$ $pIC_{50}$ | 5.1  |
| PBMCs $\text{TNF}\alpha$ $pIC_{50}$ | 4.5 <sup>a</sup>   |
| ePhys (at 10 $\mu\text{M}$ )        | complete $I_{CRAC}$ inhibition   |
| LE / LLE                            | 0.46 / 0.2   |
| MW                                  | 274  |
| $clogP$                             | 5  |
| PFI                                 | 10.1   |
| CLND ( $\mu\text{g/mL}$ )           | 2  |

<sup>a</sup>Compound reported inactive in 1 out of 6 test occasions.

**Table 8: Profile of 3-thioindole 2.32**

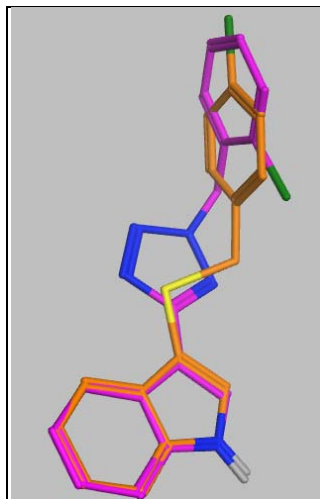
Despite the limitations of 3-thioindole **2.32**, its high LE value prompted us to analyse the HTS output to search for similar chemical structures retaining an attractive ligand efficiency, however, with better physicochemical properties and reduced metabolic liability. This investigation enabled the identification of the related 3-tetrazolyindole analogue **2.18** (Table 9), with an  $I_{CRAC}$  Jurkat  $pIC_{50}$  of 6. The  $clogP$  of 3-tetrazolyindole **2.18** was still high ( $clogP = 4.2$ ), but lower than the corresponding 3-thioindole **2.32** ( $clogP = 5$ ). In addition, incorporation of the tetrazole alleviated the sulfur metabolism liabilities, offering an improvement compared to compound **2.32**. However, 3-tetrazolyindole **2.18** contained an additional aromatic ring, hence the PFI remained very high (PFI = 10).

| Structure                     |  |
|-------------------------------|--|
| Compound                      | <b>2.18</b>  |
| Jurkat $pIC_{50}$             | 6  |
| LAD2 $pIC_{50}$               | 5.9  |
| PBMCs IFN $\gamma$ $pIC_{50}$ | 5.2 <sup>a</sup>   |
| PBMCs TNF $\alpha$ $pIC_{50}$ | 4.4 <sup>b</sup>   |
| ePhys (at 10 $\mu$ M)         | 95% $I_{CRAC}$ inhibition with a half-life of 23 s                                 |
| LE / LLE                      | 0.37 / 0.23  |
| MW                            | 310  |
| $clogP$                       | 4.2  |
| PFI                           | 10   |
| CLND ( $\mu$ g/mL)            | 5 <sup>c</sup>   |
| HSA binding                   | 97.9%  |

<sup>a</sup>Compound reported inactive in 3 occasions and failed to fit a curve in 2 occasions out of 17 test occasions; <sup>b</sup>Compound reported inactive in 5 out of 12 test occasions; <sup>c</sup>Compound reported with a CLND < 1  $\mu$ g/mL in 1 occasion and assay failed to generate a value in 1 occasion out of 6 test occasions.

**Table 9: Profile of 3-tetrazolyindole 2.18, identified from the recent HTS**

An overlay between the minimised energy conformation of the indoles **2.32** and **2.18** (**Figure 33**), calculated using Molecular Operating Environment® (MOE®) software,<sup>143</sup> confirmed the level of conformational similarity between the compounds **2.32** and **2.18**.



**Figure 33: Overlay of the low energy conformation of 3-thioindole 2.32 (orange) and 3-tetrazolyindole 2.18 (pink)**

When comparing the profile of 3-thioindole **2.32** (**Table 8, p. 69**) with that of 3-tetrazolyindole **2.18** (**Table 9**), it was recognised that these two compounds were equipotent across the range of  $I_{CRAC}$  relevant biological assays. Compound **2.18** had a slightly higher HAC compared to compound **2.32** (22 vs. 18) which translated into a smaller LE (0.37 vs. 0.46). This increase in HAC was however balanced by a lower lipophilicity (clogP of 4.2 vs. 5), which resulted in a slight increase in LLE (0.23 vs. 0.20). Similarly to compound **2.32**, the physicochemical properties of 3-tetrazolyindole **2.18** translated into negligible aqueous solubility, underlining the need to improve the physicochemical properties of this indole series.

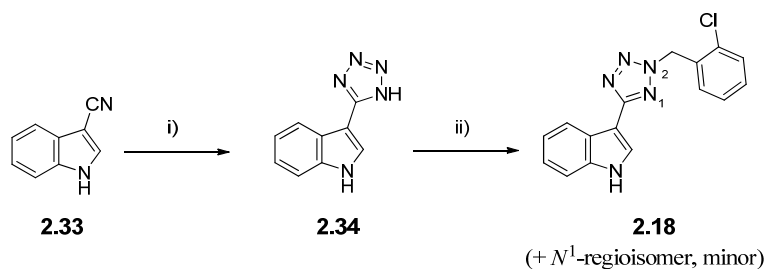
To summarise, the hit compound **2.18**, identified through crossover of the HTS readout and a data-mining investigation centred on ligand efficiency, was a consistently potent  $I_{CRAC}$  inhibitor in the Jurkat and LAD2 assays. In order to optimise this chemical series to deliver a lead  $I_{CRAC}$  molecule, the primary objective was to increase the polarity and the aqueous solubility of the compounds, while retaining the  $I_{CRAC}$  potency.



## 2.4. Results and discussion: The indole series

### 2.4.1. Resynthesis of the hit indole 2.18

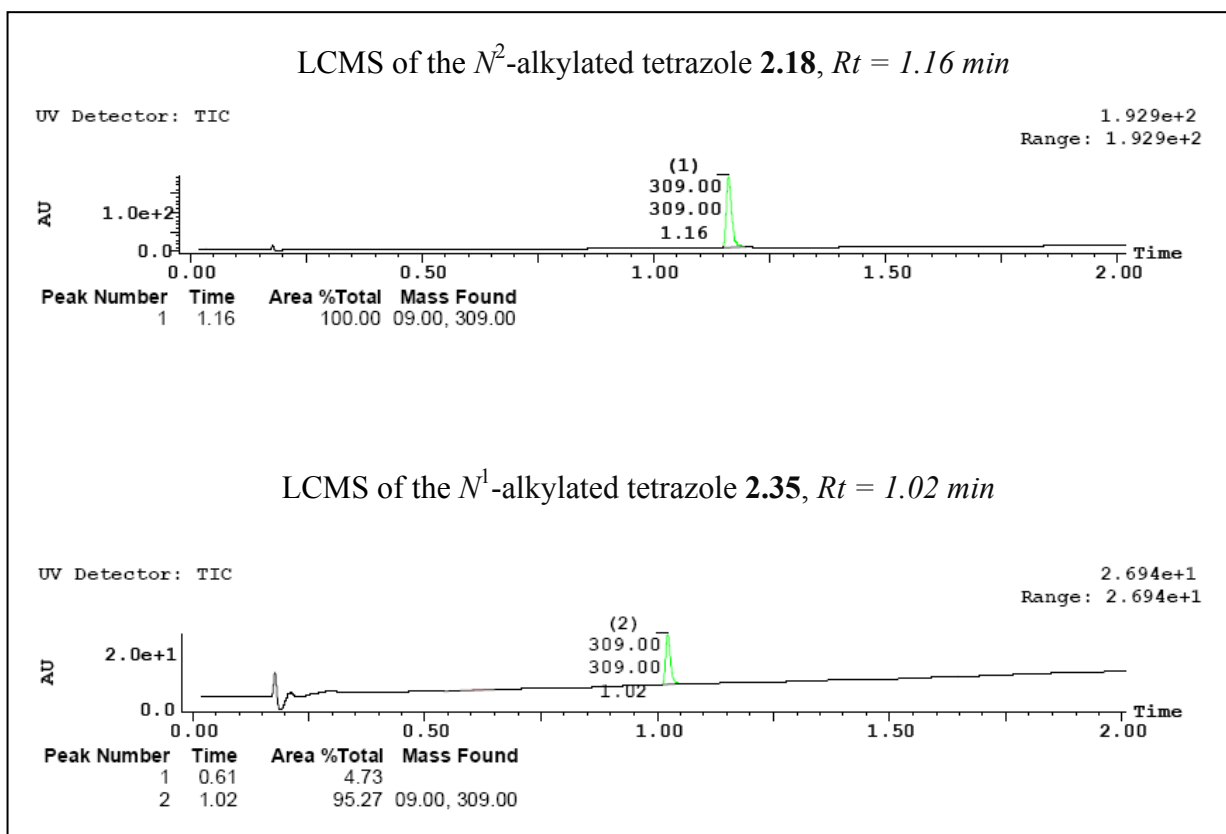
In the first instance, to confirm its activity and to generate some of the enabler data displayed in **Table 9 (p. 70)**, the nascent hit tetrazolyindole **2.18** was resynthesised. The compound was prepared in two steps from the commercially available 1*H*-indole-3-carbonitrile **2.33**, first by forming the tetrazole and then by alkylating the *N*<sup>2</sup>-position of the tetrazole (**Scheme 2**).



i) NaN<sub>3</sub> (2 eq), NEt<sub>3</sub>.HCl (3 eq), toluene, reflux, **71%**; ii) 1-(bromomethyl)-2-chlorobenzene (1.1 eq), K<sub>2</sub>CO<sub>3</sub> (1.5 eq), DMF, rt, **60%**.

#### Scheme 2: Synthesis of *N*<sup>2</sup>-alkylated-3-tetrazolyindole 2.18

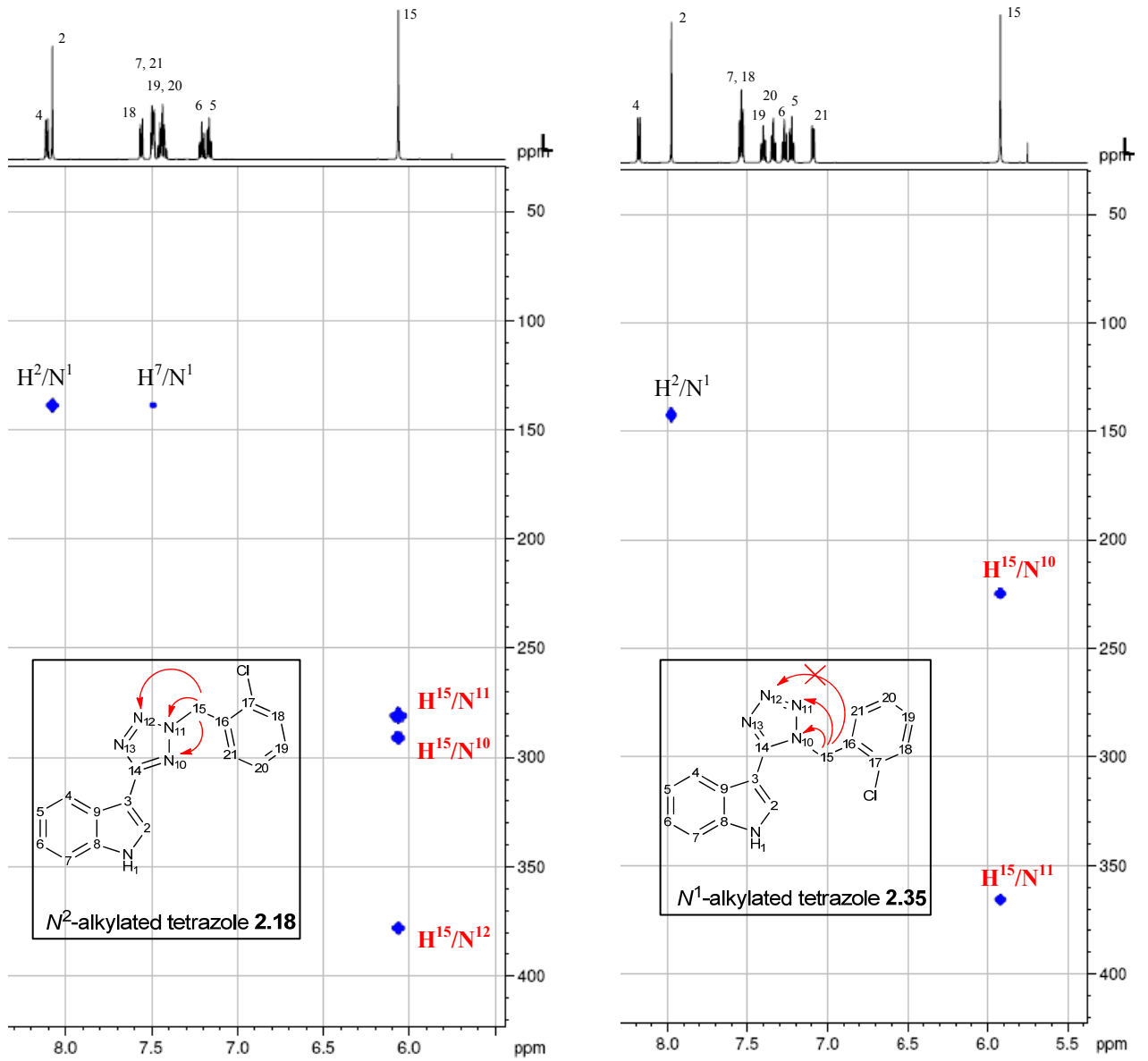
The mechanism of the tetrazole formation reaction was thought to occur *via* a concerted 1,3-dipolar cycloaddition, in which the nitrile acted as the dipolarophile towards the azide. As an alternative to the direct use of the toxic and extremely explosive hydrazoic acid, a combination of sodium azide and triethylamine hydrochloride was used to generate hydrazoic acid *in situ*.<sup>144</sup> The tetrazole alkylation step yielded a mixture of *N*<sup>1</sup>- and *N*<sup>2</sup>-alkylated tetrazoles (**2.35** and **2.18**, respectively), in a ratio of 93:7 in favour of the *N*<sup>2</sup>-alkylated tetrazole analogue in this specific example using 1-(bromomethyl)-2-chlorobenzene. In this case, it is likely that the *N*<sup>2</sup>-alkylated system is favoured because of steric hindrance. Similarly, when generating other analogues, this ratio varied depending on the alkylating agent used and an average ratio obtained across alkylations was 85:15 in favour of the *N*<sup>2</sup>-alkylated tetrazole analogue. This mixture was readily separated by chromatography and was easily discernible by liquid chromatography-mass spectrometry (LCMS) (**Figure 34**).



**Figure 34: LCMS chromatograms of the two tetrazole regioisomers 2.18 and 2.35 resulting from the alkylation step**

Heteronuclear multiple bond correlation (HMBC) NMR was used in order to assign the  $N^1$ - and  $N^2$ -alkylated tetrazole regioisomeric mixture with confidence. For the  $N^2$ -alkylated regioisomer **2.18**, key HMBC correlations were observed from  $H^{15}$  to  $N^{10}$  (291 ppm), to  $N^{11}$  (281 ppm) and to  $N^{12}$  (378 ppm); whereas for the  $N^1$ -alkylated regioisomer **2.35**, key HMBC correlations were observed from  $H^{15}$  to  $C^{14}$  (150.6 ppm),  $N^{10}$  (225 ppm) and  $N^{11}$  (366 ppm) (**Figure 35**).

## HBMC NMR between $^1\text{H}$ and $^{15}\text{N}$



## HBMC NMR between $^1H$ and $^{13}C$

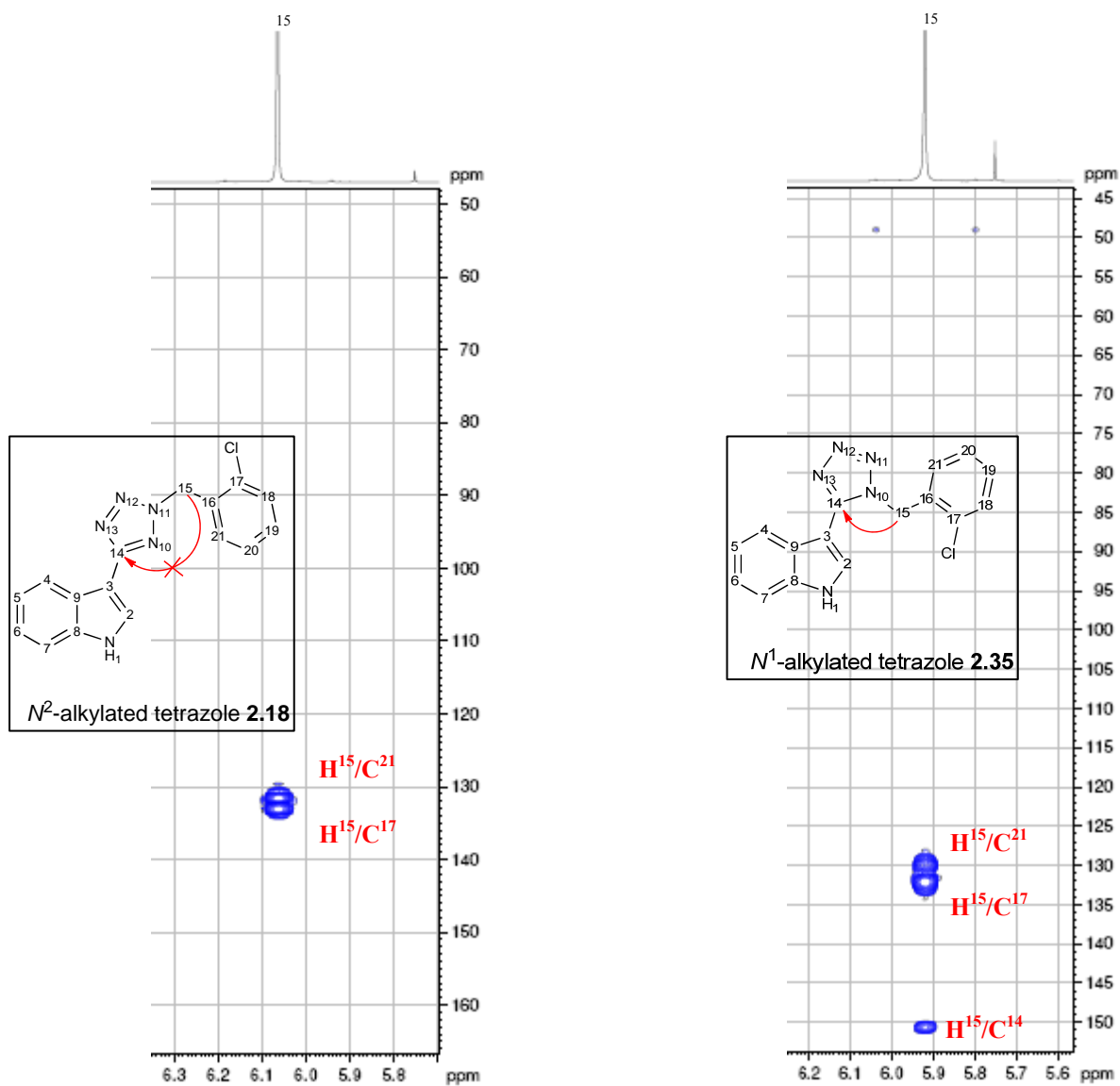
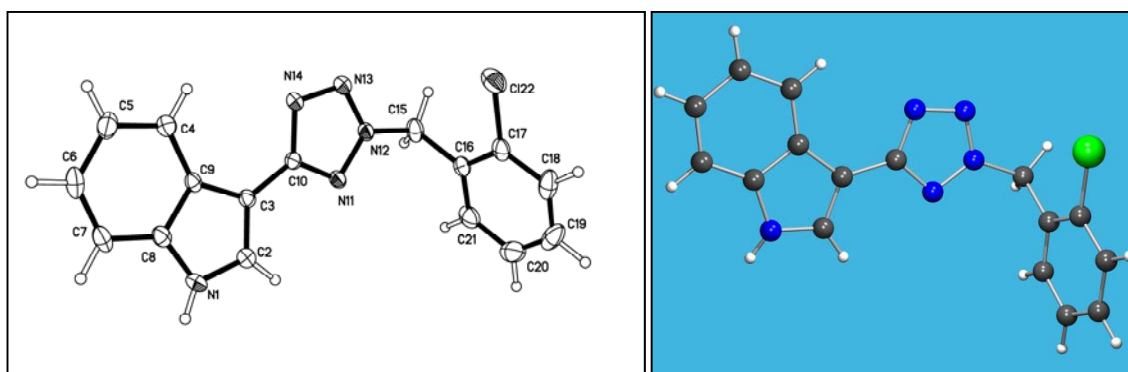


Figure 35: Key HBMC correlations in  $N^2$ - and  $N^1$ -alkylated tetrazole regioisomers 2.18 and 2.35, respectively

In order to unequivocally assign the regiochemistry of compound **2.18**, its crystal structure was obtained from a single crystal X-ray diffraction experiment by another member of our laboratories<sup>145</sup> (**Figure 36**). The crystallisation of compound **2.18** occurred spontaneously from a mixture of acetonitrile (+ 0.1% formic acid) and water (+0.1% formic acid) after purification. The conformation of indole **2.18** generated *in silico* by MOE® calculations (**Figure 33, p. 71**) was highly similar to the conformation in solid state obtained by the X-ray diffraction analysis, particularly with regard to the co-planarity of the indole and the tetrazole rings. The generation of this single crystal X-ray data therefore gave confidence in the accuracy of the minimised energy conformation provided previously by the MOE® calculations.



**Figure 36: Single crystal X-ray structure of compound 2.18**<sup>145</sup>

It is worth noting that the corresponding *N*<sup>1</sup>-benzyl-tetrazolyindole **2.35** was tested against *I*<sub>CRAC</sub> in the Jurkat assay and found to be inactive, indicating that substitution at the *N*<sup>2</sup>-position of the tetrazole was a requirement for *I*<sub>CRAC</sub> activity.

### 2.4.2. Strategy devised in order to achieve the optimisations goals

As discussed in the introduction section of the indole series (p. 68), the primary objective was to assess whether the aqueous solubility of the template can be increased while retaining (or ideally increasing) its  $I_{CRAC}$  potency. It was recognised that the high lipophilicity and the aromatic ring count ( $nAr = 4$ ) were probably the two main contributors to the low aqueous solubility of compound **2.18**, hence these two parameters constituted the main areas of focus. In order to delineate our optimisation strategy, the tetrazolyindole template was divided into three different areas of work: the indole ring, the tetrazole linker and the benzyl group (Figure 37). The initial aim was to investigate the SAR of these three areas separately, with a view to subsequently combining improved features.

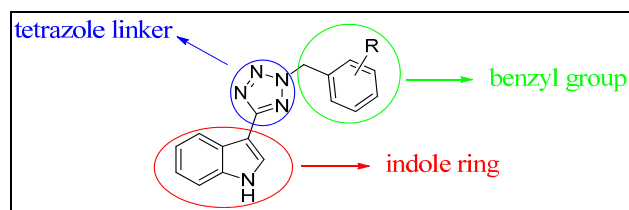
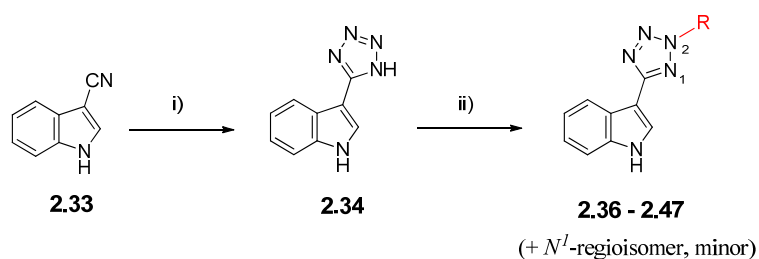


Figure 37: The tetrazolyindole template divided into three distinct areas of work

### 2.4.3. The benzyl group of the tetrazolylindole template

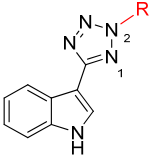

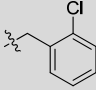
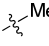
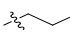
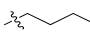
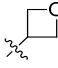
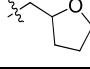
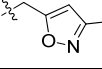
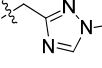
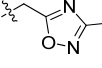
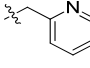
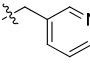
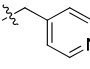
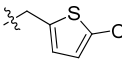
The first approach was to investigate replacements of the benzyl group linked to the  $N^2$ -position of the tetrazole (**Figure 37**). It was identified that this position could be easily amenable to synthetic diversification, since the tetrazole alkylation was the last step of the synthesis. An array chemistry effort was therefore designed and a large batch of the 3-tetrazolylindole intermediate **2.34** was prepared, allowing a number of tetrazole alkylations to be carried out subsequently (**Scheme 3**). The tetrazole alkylation was successfully enabled by the author with a varied set of alkylating agents (compounds **2.18**, **2.43**, **2.44** and **2.47**, **Table 10**). The remaining analogues were designed by the author and synthesised by another member of our laboratories.<sup>148</sup>



i)  $\text{NaN}_3$  (2 eq),  $\text{NEt}_3 \cdot \text{HCl}$  (3 eq), toluene, reflux, **71%**; ii) alkylating agent R-X (1.2 eq),  $\text{K}_2\text{CO}_3$  (1.5 to 4.5 eq), DMF, rt to 110 °C, thermally or microwave, **3-54%**.

#### Scheme 3: Synthetic route investigating replacements of the benzyl group

To improve the physicochemical properties of the series, the first set of monomers chosen were replacing the benzyl group with a range of small aliphatic alkyls (**2.36-2.38**, **Table 10**) and heteroaliphatic rings (**2.39-2.40**). In addition to reducing the clogP, this strategy offered the advantage of reducing the aromatic ring count of the hit compound from four to three. Furthermore, the benzene of the 3-tetrazolylindole **2.18** was replaced by five-membered (**2.41-2.43**) and six-membered heteroaromatic rings (**2.44-2.46**). Indeed, it was recently highlighted in the literature<sup>146,147</sup> that replacing phenyl rings by heteroaromatic or aliphatic rings offers the potential to reduce lipophilicity and to increase aqueous solubility. Finally, in order to further explore the SAR of the benzylic position, the 5-chlorothiophene derivative **2.47** was prepared as an isosteric replacement of the progenitor compound **2.18**, even if this replacement was not predicted to dramatically reduce the lipophilicity.

|  |   |     |       |                  |                          |
|---|---|-----|-------|------------------|--------------------------|
| Compound  |    | MW  | clogP | CLND (µg/mL)     | Jurkat pIC <sub>50</sub> |
| <b>2.18</b> <sup>vi</sup>   |    | 310 | 4.2   | 5 <sup>a</sup>   | 6                        |
| <b>2.36</b> <sup>148</sup>  |    | 199 | 1.7   | 107              | < 4.8                    |
| <b>2.37</b> <sup>148</sup>  |    | 227 | 2.7   | 128 <sup>b</sup> | ≤ 4.8 <sup>c</sup>       |
| <b>2.38</b> <sup>148</sup>  |    | 241 | 3.3   | 27               | 5.1                      |
| <b>2.39</b> <sup>148</sup>  |    | 241 | 1.2   | ≥ 99             | < 4.8                    |
| <b>2.40</b> <sup>148</sup>  |    | 269 | 2     | 37 <sup>d</sup>  | < 4.8                    |
| <b>2.41</b> <sup>148</sup>  |   | 280 | 1.7   | 73 <sup>e</sup>  | < 4.8                    |
| <b>2.42</b> <sup>148</sup>  |  | 280 | 0.6   | ≥ 73             | < 4.8                    |
| <b>2.43</b>   |  | 281 | 1.1   | 86               | < 4.8                    |
| <b>2.44</b>   |  | 276 | 1.9   | 82               | < 4.8                    |
| <b>2.45</b> <sup>148</sup>  |  | 276 | 1.9   | 99               | < 4.8                    |
| <b>2.46</b> <sup>148</sup>  |  | 276 | 1.9   | 76               | < 4.8                    |
| <b>2.47</b>   |  | 316 | 3.8   | 11               | 5.4 <sup>f</sup>         |

<sup>a</sup>Compound reported with a CLND < 1 µg/mL in 1 occasion and assay failed to generate a value in 1 occasion out of 6 test occasions; <sup>b</sup>Compound reported with a CLND ≥ 223 µg/mL in 1 out of 3 test occasions; <sup>c</sup>Compound reported active (pIC<sub>50</sub> = 4.8) in 1 occasion out of 3 test occasions; <sup>d</sup>Compound reported with a CLND ≥ 96 µg/mL in 1 out of 3 test occasions; <sup>e</sup>Compound reported with a CLND ≥ 93 µg/mL in 1 out of 2 test occasions; <sup>f</sup>Compound reported inactive in 1 out of 4 test occasions.

**Table 10: N<sup>2</sup>-alkylated tetrazole array investigating the SAR of the benzylic position**

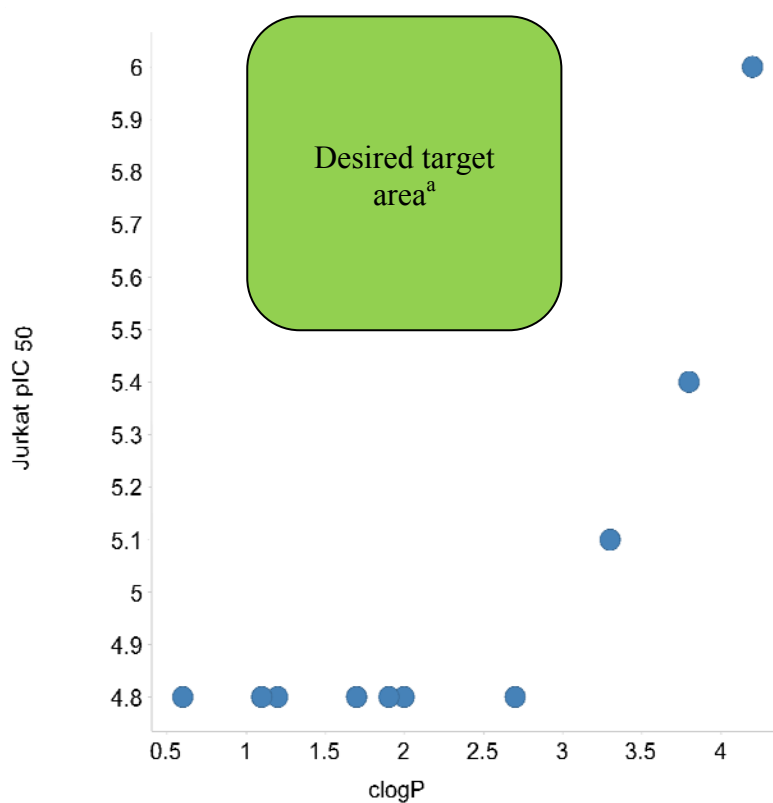
<sup>vi</sup>Compounds shaded in grey in compounds profile tables are the “reference” compounds for the current discussion.



As illustrated in **Table 10**, the replacement of the 2-chlorobenzyl group of compound **2.18** with aliphatic or heteroaromatic groups led to a dramatic reduction of the lipophilicity. For instance, the clogP of the triazole analogue **2.42** (clogP = 0.6) and the oxetane analogue **2.39** (clogP = 1.2) were noticeably lower than the progenitor chlorobenzene **2.18** (clogP = 4.2). Consequently, the aqueous solubility of these replacement compounds increased markedly, with two analogues displaying a solubility meeting our optimisation goals (> 100 µg/mL) and with a maximum solubility of 128 µg/mL achieved by the propyltetrazole analogue **2.37**.

However, the benzyl group replacement analogues were in majority below the threshold of detection of the Jurkat assay. When compared to the initial hit **2.18**, these results suggested that the corresponding receptor binding pocket was predominantly lipophilic at that specific position and that the introduction of polarity in this region of the molecule was detrimental to  $I_{CRAC}$  activity. The other argument supporting the lipophilicity requirement at this position was the fact that the activity of the small alkyl analogues was only detected by our assay when the number of carbon atoms was greater than three (compound **2.38**). Only the 5-chlorothiophene **2.47**, a lipophilic mimic of the initial 2-chlorobenzene **2.18**, displayed appreciable potency in the  $I_{CRAC}$  Jurkat assay ( $pIC_{50} = 5.4$ ).

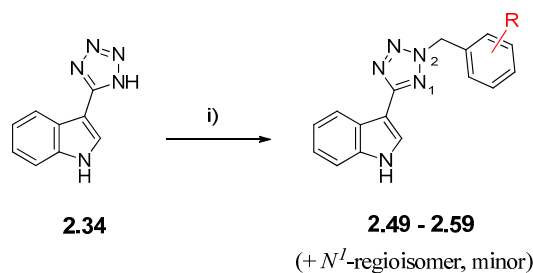
In a more concise manner, when plotting the Jurkat  $pIC_{50}$  vs. clogP for the tetrazolylindole derivatives synthesised so far, it became apparent that only compounds with a clogP greater than 3 were active in our primary assay (**Figure 38**). When comparing this result with the current  $I_{CRAC}$  chemical landscape (**Table 4, p. 54**), this observation confirmed the requirement for  $I_{CRAC}$  blockers to exhibit a reasonable degree of lipophilicity.



<sup>a</sup>The desired target area (green box) was defined for compounds with a clogP between 1 and 3, and a Jurkat pIC<sub>50</sub> > 5.5

**Figure 38: Relationship between Jurkat activity and lipophilicity for the tetrazolyindole analogues**

Following these initial findings, the SAR in this region of the tetrazolyindole series suggested that a benzyl group was the most appropriate moiety in order to achieve  $I_{CRAC}$  activity and hence would have to remain in future compounds, despite the fact that these derivatives may be less attractive from a developability perspective. Based on this, it was assessed whether a more polar substituted benzyl group compared to the 2-chlorobenzene could be identified. Thus, analogues with a fluorine, methyl group and methoxy group at the *ortho*-, *meta*- and *para*-positions of the benzene were synthesised in an array fashion, according to **Scheme 4**. Indeed, replacement of the chlorine with fluorine, methyl group and methoxy group reduced clogP. The corresponding isomeric 3- and 4-chlorobenzyl derivatives were prepared as reference compounds.

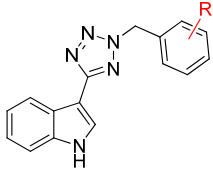


i) R-benzyl-X (1.2 eq), K<sub>2</sub>CO<sub>3</sub> (1.5 eq), DMF, rt, **31-59%**.

#### Scheme 4: Synthetic route investigating substitution of the benzene

As expected, when the 2-position of the tetrazole ring was substituted with a benzyl group (**Table 11**), the indole compounds displayed reasonable *I*<sub>CRAC</sub> activity in the Jurkat assay. However, the SAR of the phenyl ring was somewhat flat and none of the new substituted benzyl derivatives was as potent as the progenitor compound **2.18**. Nevertheless, on a more qualitative level, the *ortho*-substituted benzyl analogues consistently gave higher potency, as suggested by the activities of compounds **2.18**, **2.54** and **2.57** (Jurkat pIC<sub>50</sub> = 6, 5.9 and 5.7, respectively) in comparison to their respective *meta*- and *para*-substituted benzyl analogues. Most likely as a result of the decrease in lipophilicity, the replacement of chlorine with fluorine, methyl group and methoxy group offered a noticeable increase in aqueous solubility over the progenitor chlorobenzyl system. Despite this encouraging improvement, the aqueous solubility of the majority of the newly synthesised compounds remained below our optimisation goals (CLND solubility > 100 µg/mL).

It should also be noted that the majority of the corresponding *N*<sup>1</sup>-alkylated tetrazole analogues from **Table 11** were separated and isolated, and all were found to be inactive against *I*<sub>CRAC</sub>. This result confirmed the previous observation that *N*<sup>2</sup>-substitution of the tetrazole was critical for *I*<sub>CRAC</sub> activity.

|  |       |     |       |                           |                          |
|---|-------|-----|-------|---------------------------|--------------------------|
| Compound  | R     | MW  | clogP | CLND (µg/mL) <sup>a</sup> | Jurkat pIC <sub>50</sub> |
| 2.18  | 2-Cl  | 310 | 4.2   | 5                         | 6                        |
| 2.48 <sup>149</sup>   | H     | 275 | 3.4   | 11                        | 5.3                      |
| 2.49  | 2-F   | 293 | 3.6   | 104                       | 5.4                      |
| 2.50  | 3-F   | 293 | 3.6   | 61                        | 5.4                      |
| 2.51  | 4-F   | 293 | 3.6   | 42                        | 5.3                      |
| 2.52  | 3-Cl  | 310 | 4.2   | 3                         | 5.5                      |
| 2.53  | 4-Cl  | 310 | 4.2   | 3                         | 5.6                      |
| 2.54  | 2-Me  | 289 | 3.9   | 45                        | 5.9 <sup>b</sup>         |
| 2.55  | 3-Me  | 289 | 3.9   | 59                        | 5.5 <sup>c</sup>         |
| 2.56  | 4-Me  | 289 | 3.9   | 36                        | 5.4                      |
| 2.57  | 2-OMe | 305 | 3.4   | 2                         | 5.7                      |
| 2.58  | 3-OMe | 305 | 3.4   | 87                        | 5.4 <sup>d</sup>         |
| 2.59  | 4-OMe | 305 | 3.4   | 61                        | 5.4                      |

<sup>a</sup>In this table, CLND solubilities were reported as an average of the individual measurements, including values with a < or a ≥; <sup>b</sup>Compound was reported with a pIC<sub>50</sub> < 5.5 in 1 out of 7 test occasions; <sup>c</sup>Compound was reported with a pIC<sub>50</sub> < 5.5 in 1 out of 4 test occasions; <sup>d</sup>Compound failed to fit a curve in 1 out of 3 test occasions.

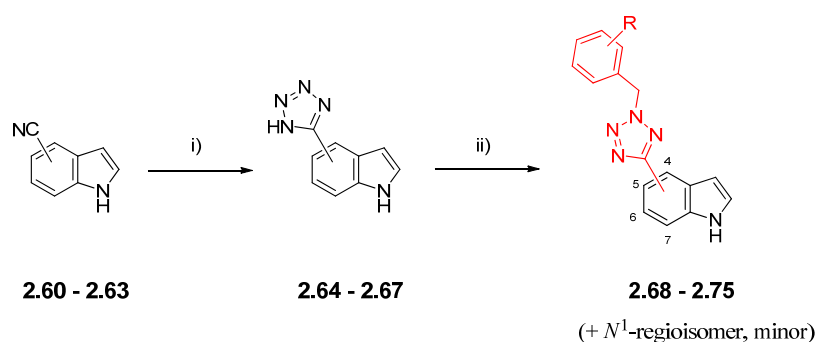
**Table 11: N<sup>2</sup>-benzyl-tetrazole derivatives**

To summarise the investigation carried out on the SAR of the position occupied by the benzyl group of the tetrazolyindole series, it appeared that this region offered limited opportunity to increase the aqueous solubility of the template while retaining activity against *I*<sub>CRAC</sub>. Hence, no additional efforts were made on this position and study of the indole ring was initiated. Nevertheless, a small number of analogues, such as thiophene 2.47 (Table 10, p. 79), 2-fluorobenzene 2.49 (Table 11) and 2-

methylbenzene **2.54** (Table 11), with respective Jurkat pIC<sub>50</sub> of 5.4, 5.4 and 5.9, were identified as potential interesting replacements for the initial 2-chlorobenzene **2.18** offering a marginal increased aqueous solubility.

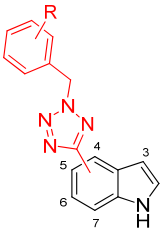

#### 2.4.4. The indole ring

In the initial HTS hit compound **2.18**, the indole ring was substituted with a tetrazole at the 3-position. One of the first priority considerations, before investigating if the tetrazole linker can be replaced by a more polar group, was to assess whether this position was the ideal vector for substitution from the indole. In an attempt to address this, some of the most potent analogues in the 3-substituted indole series, the *ortho*- and *para*-chlorobenzyl derivatives, were selected in order to probe the indole vector. Hence, the *ortho*- and *para*-chlorobenzyl analogues were prepared with the tetrazole moiety attached to the 4-, 5-, 6- and 7-position of the indole, respectively (Scheme 5). A two-step process of tetrazole formation followed by alkylation was used, starting from the commercially available 1*H*-indole-4-, 5-, 6- or 7-carbonitrile **2.60-2.63** in order to deliver the targeted tetrazolyindoles **2.68-2.75**, respectively. Following synthesis of the requisite intermediates **2.64-2.67**, the alkylation chemistry was enabled to prepare the 4-tetrazolyindoles **2.68** and **2.69**, before being further exemplified by another member of our laboratories.<sup>148</sup>



i) NaN<sub>3</sub> (1.2 eq), NEt<sub>3</sub>.HCl (2 eq), toluene, reflux, **20%-quantitative**; ii) 1-(bromomethyl)-2-chlorobenzene or 1-(bromomethyl)-4-chlorobenzene (1.2 eq), K<sub>2</sub>CO<sub>3</sub> (1.5 to 3 eq), DMF, rt, **8-59%**.

**Scheme 5: Synthesis of the 4-, 5-, 6- and 7-tetrazolyindoles 2.68-2.75**

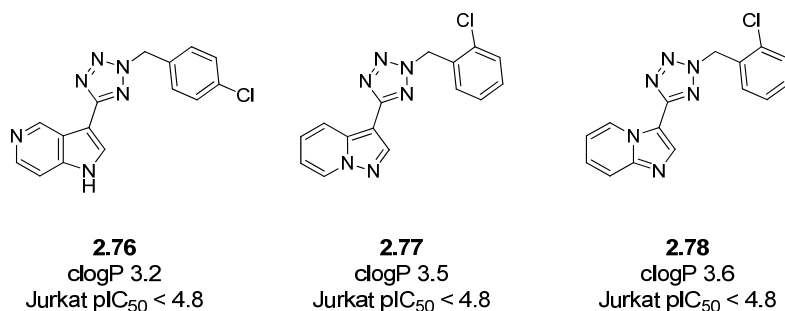
|  |   |      |                          |
|---|---|------|--------------------------|
| Compound  |  |      | Jurkat pIC <sub>50</sub> |
| <b>2.18</b>   | 3-indole  | 2-Cl | 6                        |
| <b>2.53</b>   |   | 4-Cl | 5.6                      |
| <b>2.68</b>   | 4-indole  | 2-Cl | < 4.8                    |
| <b>2.69</b>   |   | 4-Cl | 5.3 <sup>a</sup>         |
| <b>2.70</b> <sup>148</sup>  | 5-indole  | 2-Cl | < 4.8 <sup>b</sup>       |
| <b>2.71</b> <sup>148</sup>  |   | 4-Cl | 5.5 <sup>a</sup>         |
| <b>2.72</b> <sup>148</sup>  | 6-indole  | 2-Cl | < 4.8                    |
| <b>2.73</b> <sup>148</sup>  |   | 4-Cl | < 4.8 <sup>c</sup>       |
| <b>2.74</b> <sup>148</sup>  | 7-indole  | 2-Cl | < 4.8 <sup>c</sup>       |
| <b>2.75</b> <sup>148</sup>  |   | 4-Cl | < 4.8 <sup>d</sup>       |

<sup>a</sup>Compound reported inactive (pIC<sub>50</sub> < 4.8) in 2 out of 5 test occasions; <sup>b</sup>Compound reported active in 2 out of 6 test occasions; <sup>c</sup>Compound reported active in 1 out of 5 test occasions; <sup>d</sup>Compound reported active in 2 out of 5 test occasions.

**Table 12: Exploration of the tetrazole regiochemistry**

The data displayed in **Table 12** indicated that when the tetrazole was attached to the 4-, 5-, 6- or 7-position of the indole, compounds were either inactive or only partially active against *I*<sub>CRAC</sub>. Based on this observation, it was hypothesised that a specific geometry for the indole was required for optimal binding with the receptor, with substitution at the 3-position of the indole ring.

In an attempt to introduce polarity in the indole ring, several azaindole derivatives (compounds **2.76-2.78**, **Figure 39**) were designed by the author and prepared elsewhere in our laboratories,<sup>150</sup> however, all of these analogues were inactive in the Jurkat assay. It was therefore hypothesised that the *I*<sub>CRAC</sub> activity of the indole moiety was driven by a combination of the appropriate degree of electronic density and lipophilicity.



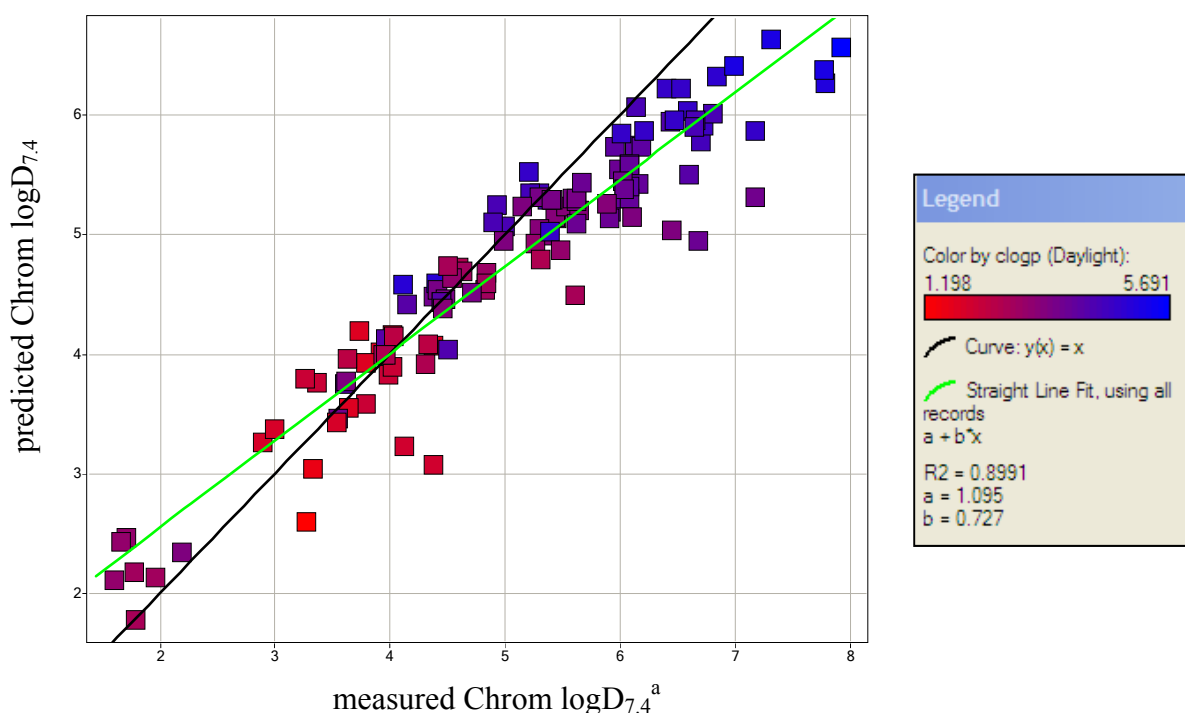
**Figure 39: Structure of azaindole analogues of the hit indole 2.18<sup>150</sup>**

Despite being only a small dataset, the results shown in **Figure 39** highlighted the difficulty in replacing the indole while retaining biological activity. Therefore, this aromatic ring was retained in future compounds.

#### 2.4.5. The tetrazole linker

Having explored the benzylic substituents of the tetrazole and the associated isomeric compounds, another area of focus was the replacement of the tetrazole with an alternative 5-membered heteroaromatic ring. This strategy could offer the potential to introduce additional polarity within the linker, thereby improving the aqueous solubility of the series. The number of 5-membered heteroaromatic rings containing a permutation of carbon, oxygen and nitrogen atoms was too large for each discrete analogue to be synthesised. Accordingly, in order to prioritise the synthesis of different heteroaromatic linkers, some design criteria were devised and implemented. The PFI metric ( $PFI = nAr + Chrom \log D_{7.4}$ ), discussed in **Section 1.2.2 (p. 6)**, has been shown to be a powerful tool to design compounds with increased aqueous solubility<sup>19,20</sup> and was therefore considered for the current study. According to the PFI concept, compounds are predicted to have acceptable aqueous solubility when their PFI is less than 7. The initial indole lead compound **2.18** had four aromatic rings (two for indole, one for tetrazole and one for benzene) and the SAR established thus far necessitated having these four aromatic rings in order to obtain reasonable potency at  $I_{CRAC}$ . Consequently, in order for the indole series to exhibit acceptable predicted aqueous solubility, the  $Chrom \log D_{7.4}$  of the analogues should be kept

below 3. To assess whether the tool to predict Chrom  $\log D_{7.4}$  was applicable to the indole series, it was pertinent to compare the measured Chrom  $\log D_{7.4}$  of all the previously synthesised indoles vs. their predicted Chrom  $\log D_{7.4}$  (**Figure 40**).



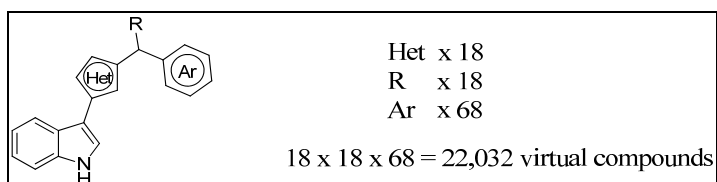
<sup>a</sup>This plot contains indole analogues synthesised by other members of our laboratories<sup>137</sup>

**Figure 40: Predicted vs. measured Chrom  $\log D_{7.4}$  for indoles synthesised in our laboratories**

The plot of predicted vs. measured Chrom  $\log D_{7.4}$  for the previously synthesised indoles underlined the fact that the model to predict Chrom  $\log D_{7.4}$  could be applied with confidence to the indole series. Indeed, the  $y = x$  (black line) and the best fit curve (green line,  $y = 1.1 + 0.73x$ , coefficient of determination  $R^2 = 0.90$ ) gave a good correlation, and was mainly shifted for the highly lipophilic compounds (measured Chrom  $\log D_{7.4} > 5$ ), region where it is known that the model becomes less accurate.

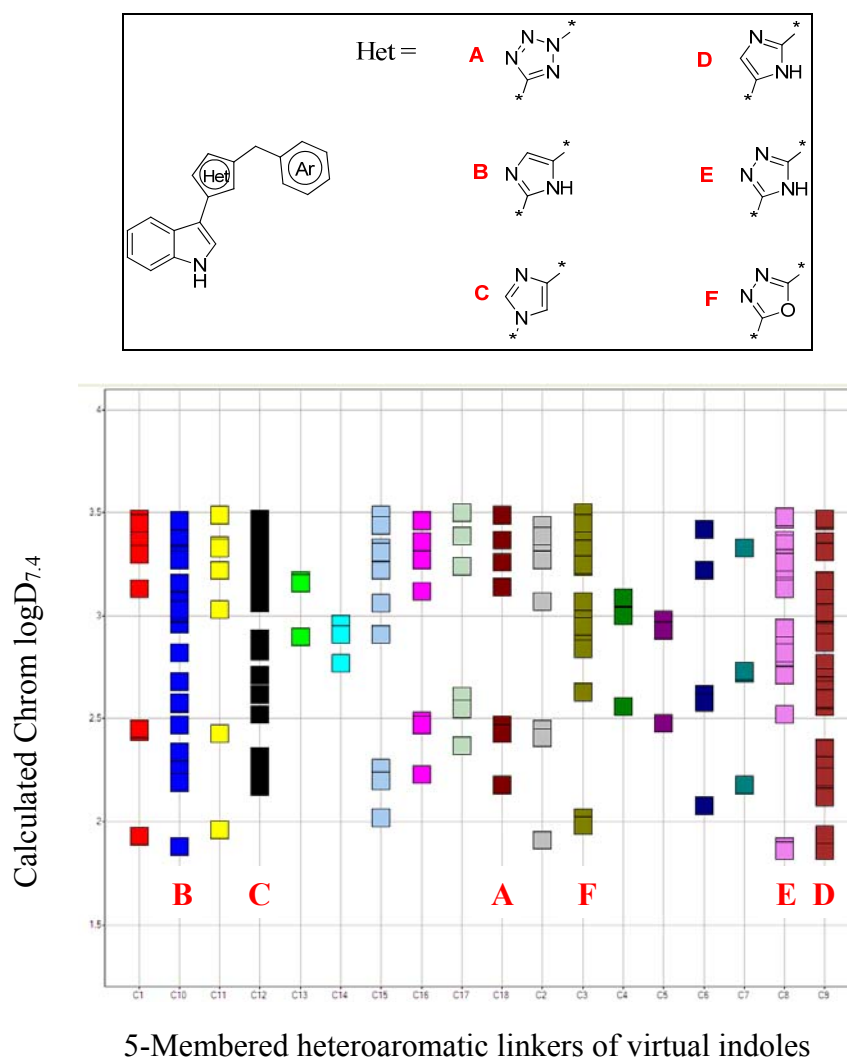


Hence, a set of over 22,000 virtual compounds, comprising 18 different 5-membered heteroaromatic linkers, 18 different benzyl substituents and 68 different aromatic rings in place of the most potent 2-chlorobenzene, was enumerated by the author using ADEPT, a Daylight Enumeration and Profiling Tool,<sup>151</sup> and their Chrom  $\log D_{7.4}$  was calculated (**Figure 41**).



**Figure 41: Virtual indoles to guide prioritisation in the synthesis**

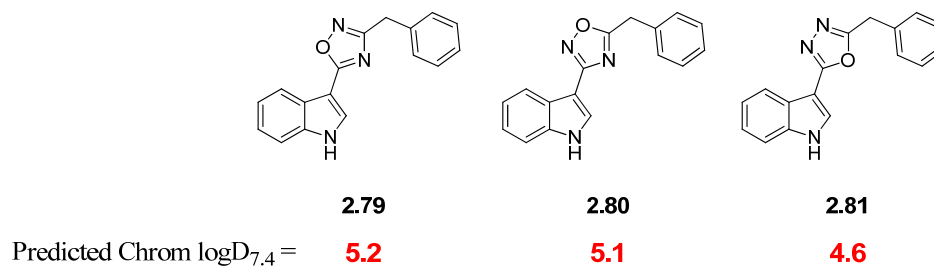
In the first instance, in order to prioritise which 5-membered heteroaromatic linkers to synthesise, virtual compounds without substitution at the benzylic position ( $R = H$  in **Figure 41**) were filtered to retain only those compounds with a predicted Chrom  $\log D_{7.4}$  located in the range of 1.5 – 3.5, thus displaying an attractive PFI without being too polar to avoid potential  $I_{CRAC}$  potency and permeability issues (**Figure 42**). Substitution at the benzylic position could then be later revisited to further tune the physicochemical parameters once a viable replacement for the tetrazole had been identified. The 5-membered heteroaromatic linkers which enabled the most extensive variation of the phenyl group (Ar in **Figure 41**), whilst maintaining Chrom  $\log D_{7.4}$  in the targeted range, were then prioritised.



**Figure 42: Calculated Chrom logD<sub>7.4</sub> in the targeted range 1.5 – 3.5 for virtual indoles with various 5-membered heteroaromatic linkers and aromatic groups. A subset of 5-membered heterocyclic linkers (A to F) is represented for illustration (top frame)**

As a first observation, it was interesting to note that tetrazole linker (labelled **A**-■ in **Figure 42**) did not allow a wide range of compounds to be synthesised in the requisite Chrom logD<sub>7.4</sub> range, reflecting the relatively high lipophilicity of this heteroaromatic system. On the other hand, imidazole linkers (labelled **B**-■, **C**-■, **D**-■ in **Figure 42**) and triazole linkers (labelled **E**-■ in **Figure 42**) allowed more freedom in the number of analogues within the defined Chrom logD<sub>7.4</sub> range. The

last observation, and perhaps the least intuitive, was that the 1,3,4-oxadiazole compounds, such as compound **2.81**, (labelled **F-■**) was predicted to have a Chrom  $\log D_{7.4}$  half a log unit lower than the corresponding 1,2,4-oxadiazole regioisomers **2.79** and **2.80**, as illustrated by the set of compounds shown in **Figure 43**.



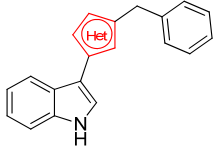
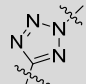
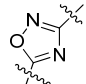
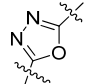
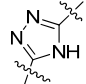
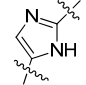
**Figure 43: Calculated Chrom  $\log D_{7.4}$  for a set of oxadiazole compounds**

The greater polarity of the symmetrical oxadiazole **2.81** over its unsymmetrical partners **2.79** and **2.80** could be explained by a larger permanent dipole moment. The permanent dipole moment  $\mu$  (Debye) of a large set of 5-membered heteroaromatic systems containing nitrogen are known,<sup>152</sup> and  $\mu(1,3,4\text{-oxadiazole}) = 3.28$  Debye compared with  $\mu(1,2,4\text{-oxadiazole}) = 1.15$  Debye. Interestingly, a recent observation made by scientists at AstraZeneca,<sup>153</sup> where a systematic comparison of 1,2,4- and 1,3,4-oxadiazole matched pairs of compounds (n=148 matched pairs) was carried out. Not only did the 1,3,4-oxadiazole isomers show a statistical reduction of lipophilicity (measured by  $\log D$ ) over their 1,2,4-oxadiazole counterparts, but a significant improvement in terms of metabolic stability, hERG inhibition and aqueous solubility was also observed.

The outcome of this analysis was that three different linkers were chosen as candidates to be synthesised because of their low predicted Chrom  $\log D_{7.4}$  (**Table 13**): 1,3,4-oxadiazole **2.81** (cPFI<sup>vii</sup> = 8.6), triazole **2.82** (cPFI = 7.8) and imidazole **2.83** (cPFI = 7.6). As a point of reference, a compound with a cPFI similar compared to the one of the active progenitor tetrazole **2.48** (cPFI = 9.1), 1,2,4-oxadiazole **2.79** (cPFI = 9.2) was also included. Furthermore,  $\text{clog} P$  is also displayed in **Table 13** and

<sup>vii</sup>cPFI refers to **calculated** PFI, whereas PFI refers to **measured** PFI.

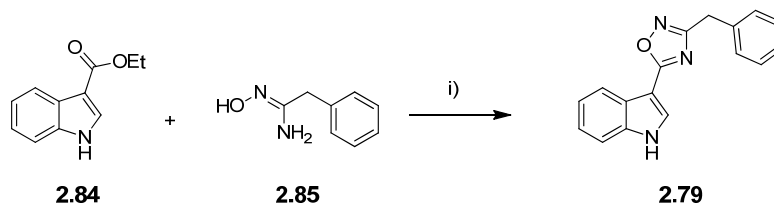
this underlined the fact that the clogP descriptor would have not been helpful in discriminating the polarity variation between these different 5-membered rings, since it was broadly similar across all the compounds examined.

|  |   |                |       |
|---|---|----------------|-------|
| Compound  | Structure   | Calculated PFI | clogP |
| 2.48  |    | 9.1            | 3.4   |
| 2.79  |    | 9.2            | 3.6   |
| 2.81  |    | 8.6            | 3.6   |
| 2.82  |  | 7.8            | 3.6   |
| 2.83  |  | 7.6            | 4.2   |

**Table 13: Calculated PFI and clogP for the novel 5-membered ring linkers, chosen for synthesis**

Although none of the analogues proposed in **Table 13** formally met the target PFI < 7, they were considered useful in assessing the tolerance of introducing polarity in place of the 5-membered heteroaromatic ring. If any of these replacements proved to increase aqueous solubility while retaining  $I_{CRAC}$  activity, the benzylic position (R group in **Figure 41, p. 88**) could subsequently be modified to introduce further polarity in the indole series in order to achieve the targeted PFI.

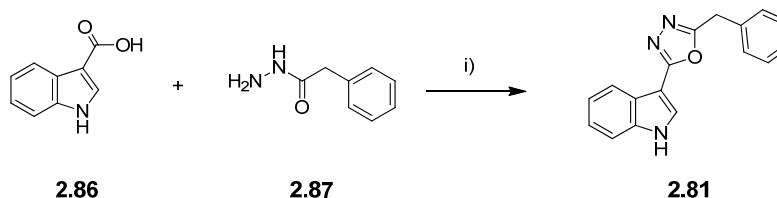
Turning our attention to the synthesis of the selected compounds, 1,2,4-oxadiazole **2.79** was synthesised from two commercially available starting materials: ethyl indole-3-carboxylate **2.84** and *N*-hydroxy-2-phenylacetimidamide **2.85** (Scheme 6).



i) indole-3-carboxylate **2.84** (1 eq), *N*-hydroxy-2-phenylacetimidamide **2.85** (1.2 eq), NaOMe (1.5 eq), THF, microwave, 150 °C, 74%.

#### Scheme 6: Synthesis of 1,2,4-oxadiazole indole **2.79**

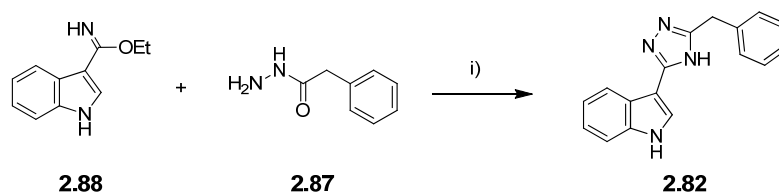
The 1,3,4-oxadiazole indole analogue **2.81** was prepared by condensation of indole-3-carboxylic acid **2.86** with phenylacetohydrazide **2.87** in presence of an excess of phosphorous oxychloride (Scheme 7). POCl<sub>3</sub> was used as both a chlorinating agent for the formation of the intermediate acid chloride derivative and as a dehydrating agent for the ring formation.



i) phenylacetohydrazide **2.87** (1 eq), indole-3-carboxylic acid **2.86** (1.2 eq), POCl<sub>3</sub> (excess), microwave, 140 °C, 16%.

#### Scheme 7: Synthesis of 1,3,4-oxadiazole indole **2.81**

The triazole indole analogue **2.82** was synthesised in a similar fashion, by condensation of ethyl indole-3-carbimide **2.88** with phenylacetohydrazide **2.87** in the presence of base (Scheme 8).



i) ethyl indole-3-carbimidate **2.88** (1 eq), phenylacetohydrazide **2.87** (1.1 eq), NEt<sub>3</sub> (3 eq), DMF, microwave, 120 °C to 160 °C, 6%.

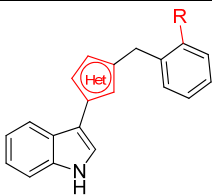


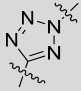
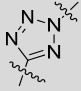
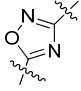
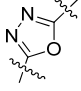
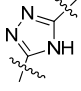
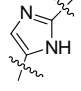
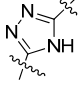
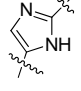
### Scheme 8: Synthesis of triazole indole **2.82**

It is worth noting that the syntheses of analogues **2.81** and **2.82** were typified by poor yields (16% and 6%, respectively). However, the objective at this stage was to deliver these targets in a timely manner to promptly assess the *I*<sub>CRAC</sub> activity in response to modifications made to the heterocyclic linker, and therefore the reactions were not optimised. It was our intention that the synthetic chemistry would subsequently be optimised if these classes of compounds met the selection criteria discussed above.

With regard to the imidazole indole **2.83**, the compound and its synthetic route was designed by the author and the synthesis was carried out by an external collaborator.<sup>viii,154</sup>

After synthesising compounds **2.79**, **2.81**, **2.82** and **2.83**, the analogues were submitted to the Jurkat assay and Chrom logD<sub>7.4</sub> was measured (**Table 14**).

<sup>viii</sup>The experimental conditions used to synthesise compounds made by external collaborators are not described in the experimental section, however, the LCMS and <sup>1</sup>H NMR of the final compounds made by external collaborators are presented in the experimental section.

|  |   |   |              |                           |                          |
|---|---|---|--------------|---------------------------|--------------------------|
| Compound  |    |  | Measured PFI | CLND ( $\mu\text{g/mL}$ ) | Jurkat $\text{pIC}_{50}$ |
| 2.18  |    | Cl  | 10           | 5 <sup>a</sup>            | 6                        |
| 2.48  |    | H   | 9.4          | 11                        | 5.3                      |
| 2.79  |    | H   | 9.9          | 2 <sup>b</sup>            | < 4.8 <sup>c</sup>       |
| 2.81  |    | H   | 8.6          | 4                         | < 4.3                    |
| 2.82  |   | H   | 7.6          | 73                        | 4.8                      |
| 2.83 <sup>154</sup>   |  | H   | 7.6          | 62                        | 4.6 <sup>d</sup>         |
| 2.89 <sup>155</sup>   |  | Cl  | 8.2          | 12                        | 5.3 <sup>e</sup>         |
| 2.90 <sup>155</sup>   |  | Cl  | 8.2          | 27 <sup>f</sup>           | 4.9 <sup>g</sup>         |

<sup>a</sup>Compound reported with a CLND < 1  $\mu\text{g/mL}$  in 1 occasion and assay failed to generate a value in 1 occasion out of 6 test occasions; <sup>b</sup>Compound reported with a CLND < 1  $\mu\text{g/mL}$  in 1 out of 3 test occasions; <sup>c</sup>Compound reported active in 3 out of 8 test occasions; <sup>d</sup>Compound reported inactive in 3 out of 6 test occasions; <sup>e</sup>Compound reported inactive in 1 out of 8 test occasions; <sup>f</sup>Assay failed to generate a CLND value in 1 out of 2 test occasions; <sup>g</sup>Compound reported inactive in 2 out of 8 test occasions.

**Table 14: Profile of the 5-membered ring linker replacement analogues**

The data of compounds in **Table 14** revealed that the PFI strategy based on predicted Chrom logD<sub>7.4</sub> was successful in improving aqueous solubility within the indole series. Indeed, the two compounds with the highest PFI, the initial tetrazole analogue **2.48** and 1,2,4-oxadiazole **2.79** (PFI of 9.4 and 9.9, respectively), displayed low aqueous solubility (11 µg/mL and 2 µg/mL, respectively). By contrast, triazole **2.82** and imidazole **2.83**, both with a reduced PFI of 7.6, displayed a significantly increased aqueous solubility of 73 µg/mL and 62 µg/mL, respectively, coming closer to our optimisation goal of 100 µg/mL. Interestingly, triazole **2.82** and imidazole **2.83** had a PFI value almost 2 units lower than the progenitor tetrazole **2.48**, which was a remarkable improvement considering the small structural change involved. Although the improvement of the physicochemical profile was encouraging, these changes were accompanied with a noticeable reduction in primary *I*<sub>CRAC</sub> activity in comparison to tetrazole **2.48**. Triazole **2.82** and imidazole **2.83** displayed weak activity in the Jurkat assay, with pIC<sub>50</sub> less than 5, and 1,2,4-oxadiazole **2.81** was below the threshold of detection of the assay. Even 1,2,4-oxadiazole **2.79**, which was prepared as an isostere of tetrazole with similar lipophilicity, was also inactive.

In an attempt to increase the biological potency of the two most soluble linkers identified from this study (triazole and imidazole), the corresponding 2-chlorobenzyl analogues were synthesised by other members of our laboratories<sup>155</sup> (compounds **2.89** and **2.90**, **Table 14**). However, the weak level of *I*<sub>CRAC</sub> activity achieved by compounds **2.89** and **2.90** underlined the necessity of retaining a hydrophobic heterocyclic linker in this region of the molecule for potency. Nevertheless, one compound which emerged from the dataset, the triazole analogue **2.89**, combined a Jurkat pIC<sub>50</sub> of 5.3, with a reduced PFI of 8.2 and a marginally improved solubility of 12 µg/mL.

This exercise demonstrated that acceptable levels of solubility could be achieved through judicious control of physicochemical properties and careful drug design, although in this instance, target potency was somewhat compromised.

Based on all of the above, it became apparent that balancing physicochemical properties with acceptable levels of potency was difficult to achieve for the indole series, which ultimately prompted a reassessment of the viability of this chemotype in meeting our optimisation goals.



#### 2.4.6. Conclusion of the indole series

A combined data mining and scaffold hopping strategy was used to expedite progression of an indole-based series from a recently completed  $I_{CRAC}$  HTS, using a phenotypic screen. The tetrazolyindole series emerged from this as a successful replacement of the initial 3-thioindole series, where the presence of the sulfur atom was predicted to be a serious metabolic liability. The tetrazolyindole series was initially attractive because of its low HAC and high  $I_{CRAC}$  potency, rendering this series both ligand efficient and chemically tractable. The main issue, identified from the outset, centred on its poor physicochemical properties, resulting in aqueous solubility of this series being barely measurable. Therefore, the hit to lead strategy to enhance the tetrazolyindole series was focused on increasing polarity and reducing the aromatic ring count, while attempting to retain activity against  $I_{CRAC}$ .

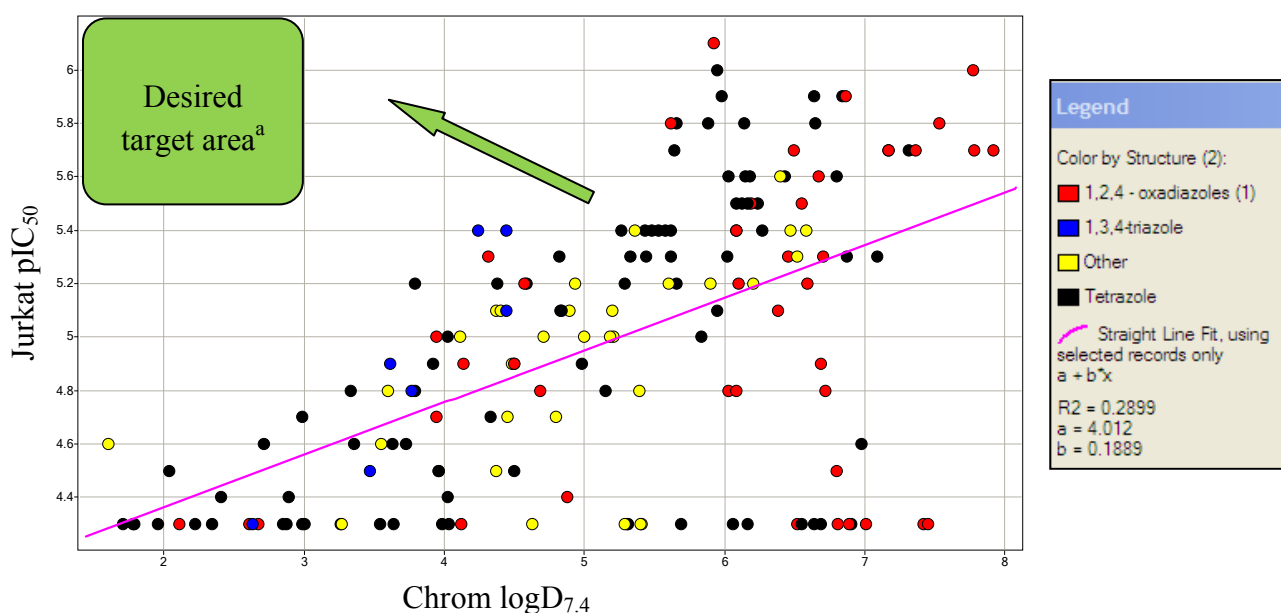
The early efforts to introduce polarity in place of the initial 2-chlorobenzene centred on removing the phenyl ring and on replacing the substituted benzene with either a saturated or a heteroaromatic ring. This approach, based on sound medicinal chemistry principles and on literature precedent, was made possible by enabling synthetic chemistry that could be carried out in an array fashion, therefore facilitating rapid SAR exploration. This first strategy had modest success as physicochemical parameters could be optimised, however, striking a balance with  $I_{CRAC}$  activity proved challenging. In this regard, 2-methylbenzene **2.54** (Table 11, p. 83) had the best overall profile with an improved aqueous solubility of 45  $\mu\text{g/mL}$  and a Jurkat  $\text{pIC}_{50}$  of 5.9.

A thorough evaluation of the optimal vector around the indole led to the conclusion that the 3-substitution of the indole ring was optimal. Furthermore, the indole ring was demonstrated as having the ideal electronic and lipophilicity requirements to achieve the optimal potency against  $I_{CRAC}$ .

Following on from these initial efforts, a pragmatic strategy utilising the recently developed PFI metric was adopted in order to prioritise the synthesis of different 5-membered ring linkers as replacement for the initial tetrazole. This work successfully delivered molecules with reduced lipophilicity and, most of all, with improved

aqueous solubility, highlighting the value of this approach. However, these improvements were obtained at the expense of the  $I_{CRAC}$  activity. Consideration of the PFI approach and comparison to initial findings in relation to physicochemical parameters suggested that high lipophilicity was necessary to achieve potent  $I_{CRAC}$  activity.

Based on the above, an analysis of the relationship between  $I_{CRAC}$  Jurkat activity and the measured Chrom  $\log D_{7.4}$  of all the indole analogues synthesised by both the author and other members of our laboratories<sup>156</sup> was carried out and is displayed in **Figure 44**. From consideration of this data, it was apparent that no indole-containing compound successfully managed to break the correlation between  $I_{CRAC}$  potency and lipophilicity. Consequently, compounds with the required levels of potency and lipophilicity were not identified, despite extensive experimentation.



<sup>a</sup>The desired target area (green box) was defined for compounds with a Chrom  $\log D_{7.4}$  between 1.5 and 3, and a Jurkat  $pIC_{50} > 5.5$

**Figure 44: Relationship between  $I_{CRAC}$  potency and Chrom  $\log D_{7.4}$  of indoles<sup>156</sup>**

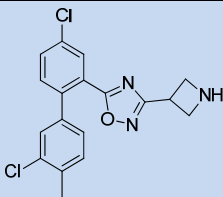
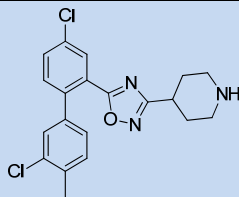
To summarise, a thorough SAR exploration of the indole series was undertaken by examining optimal vectors, modifying the indole ring and by exploring the benzyl side chain and the tetrazole linker. The phenotypic screening approach adopted proved to be viable in delineating SAR within the indole series. Extensive use of design tools allowed the improvement of the physicochemical properties and solubility of the indole series, and analogues of potential interest were identified. In accordance with published  $I_{CRAC}$  inhibitors (**Table 4, p. 54**), the indole series displayed a strong correlation between lipophilicity and  $I_{CRAC}$  activity, which could not be uncoupled. For this chemical series, the window in which potency could be balanced with lipophilicity was too narrow to successfully deliver a compound meeting our overall targeted profile. Against this background, efforts on this series were halted in favour of the promising oxadiazole amine class, which is described in the following section.

## 2.5. Results and discussion: The oxadiazole amine series

### 2.5.1. Validation of the HTS hit

As discussed in the introduction of the oxadiazole amine series (p. 66), the HTS hit compound **2.30** (Table 15) displayed a distinct chemotype from the typical  $I_{CRAC}$  pharmacophore typified by an aryl ring-aryl ring-amide bond-aryl ring connectivity (see published  $I_{CRAC}$  inhibitors, Table 4, p. 54), and contained a basic amine. Hence, the first objective for this chemical series was to confirm  $I_{CRAC}$  activity by electrophysiology. Since no solid sample of oxadiazole **2.30** was available, a close analogue was studied instead. The piperidine analogue **2.91** (Table 15) was identified as being available in the compound collection of our laboratories in multi-milligram scale and after chromatographic re-purification and subsequent characterisation, piperidine **2.91** was subjected to further profiling.

Oxadiazole piperidine **2.91** displayed slightly lower potency in the Jurkat assay ( $pIC_{50} = 5.3$ ) compared to the azetidine analogue **2.30** ( $pIC_{50} = 5.8$ ), however, the decision was still taken to progress it in the electrophysiology assay in order to validate this HTS derived chemical series as an  $I_{CRAC}$  blocker. In the patch clamp technique experiment, oxadiazole **2.91** displayed 51% inhibition of the CRAC current and was characterised by very slow on rate kinetics, as the inhibition was still occurring at the end of the 5 min experiment (compared with the half-life of 23 s of 3-tetrazolyindole **2.18**, Table 9, p. 70). This difference in kinetics in the electrophysiology assay of the oxadiazole series was not fully understood at this stage, however, it could be attributed to a difference in mode of action or in binding site of the compound. Nevertheless, the partial inhibition of the CRAC current with oxadiazole **2.91** by electrophysiology gave compelling evidence of the  $I_{CRAC}$  activity associated with this novel HTS derived series.

| Structure  |  |                  |
|--|---|---|
| <b>Compound</b>                                      | <b>2.30</b>   | <b>2.91</b>   |
| <b>Jurkat pIC<sub>50</sub></b>                       | 5.8 <sup>a</sup>  | 5.3   |
| <b>LAD2 pIC<sub>50</sub></b>                         | 5.4 <sup>b</sup>  | 5.1   |
| <b>PBMCs IFN<math>\gamma</math> pIC<sub>50</sub></b> | 5.1 <sup>c</sup>  | 5.6 <sup>d</sup>  |
| <b>PBMCs TNF<math>\alpha</math> pIC<sub>50</sub></b> | 4.7   | 5.7   |
| <b>ePhys (at 10 <math>\mu</math>M)</b>               | ND  | 51% <i>I</i> <sub>CRAC</sub> inhibition with very slow on rate kinetics, in 3 out of 4 cells tested |
| <b>LE / LLE</b>                                      | 0.33 / 0.22   | 0.28 / 0.14   |
| <b>MW</b>  | 360   | 388   |
| <b>clogP</b>   | 3.8   | 4.8   |
| <b>PFI</b>   | 7.6   | 7.9   |
| <b>CLND (<math>\mu</math>g/mL)</b>                   | 31  | 61  |
| <b>Permeability (nm/s)</b>                           | 400   | 380   |
| <b>HSA binding</b>                                   | 97%   | 96.9%   |

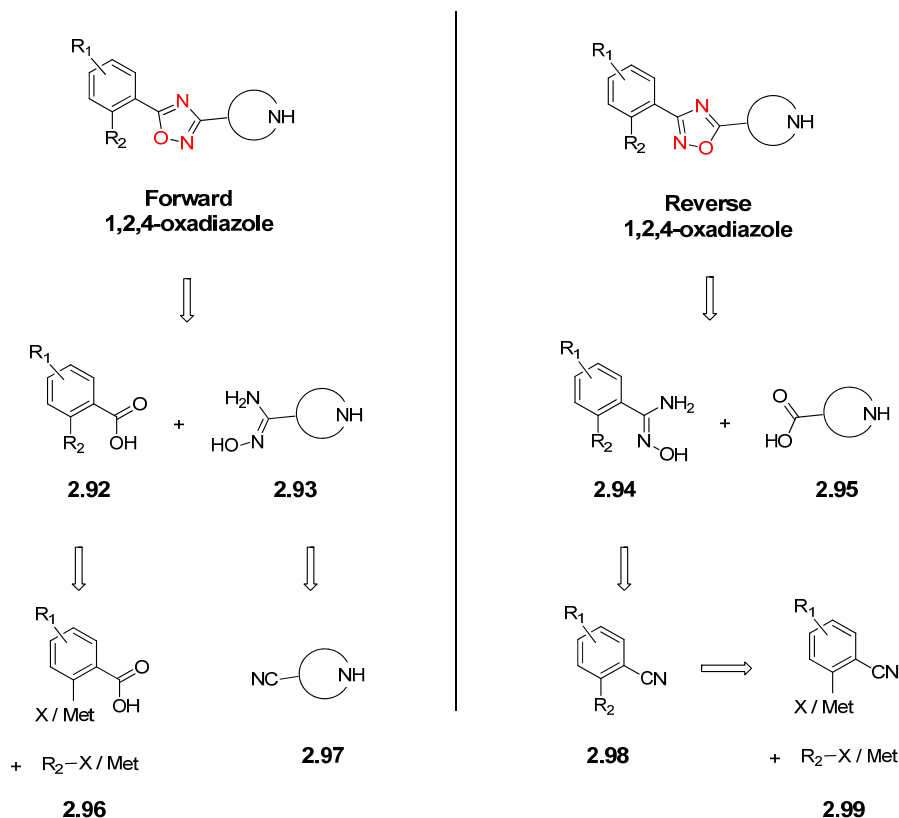
<sup>a</sup>Compound reported inactive in 1 out of 6 test occasions; <sup>b</sup>Compound reported inactive in 1 occasion and failed to fit a curve in 5 occasions out of 8 test occasions; <sup>c</sup>Compound reported inactive in 2 occasions and failed to fit a curve in 1 occasion out of 10 test occasions. <sup>d</sup>Compound failed to fit a curve in 6 out of 14 test occasions.

**Table 15: Profile of the HTS hit 2.30 and its oxadiazole piperidine analogue 2.91**

In contrast to the previous indole series, oxadiazole amines **2.30** and **2.91** displayed encouraging aqueous solubilities of 31  $\mu$ g/mL and 61  $\mu$ g/mL, respectively, which is likely attributable to the presence of the basic amine. Based on this, the oxadiazole amine series was better positioned from a physicochemical perspective compared to the indole series. However, the high clogP of compound **2.91** led to a low LLE of 0.14. Most importantly, the level of activity in the off-target PBMCs TNF $\alpha$  assay (pIC<sub>50</sub> = 5.7) represented a serious concern, which would need to be addressed. Compound **2.91** was not active in the PBMCs-based cytotoxicity assay, thus the off-

target activity could be explained by general promiscuity resulting from a combination of high lipophilicity and a basic amine, which is aligned with the observations from Leeson and Springthorpe.<sup>11</sup> Finally, oxadiazoles **2.30** and **2.91** were characterised by high plasma protein binding and high artificial membrane permeability.

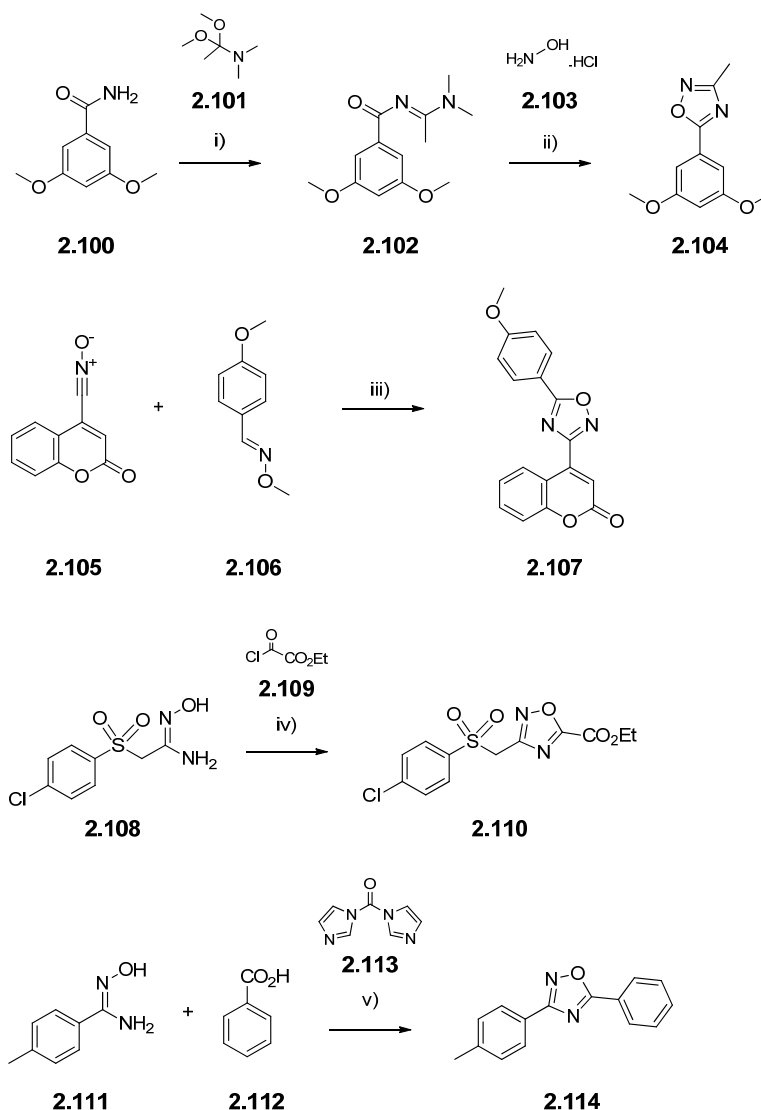
In order to investigate the synthetic chemistry required to access the oxadiazole amines and to give more flexibility in terms of availability of the starting reagents, a pair of isomeric 1,2,4-oxadiazole analogues was considered. The denomination “forward” and “reverse” oxadiazole was arbitrarily chosen, classifying the first oxadiazole compound identified **2.30** as “forward” (**Figure 45**). A retrosynthetic analysis of these two generic structures involved the formation of the 1,2,4-oxadiazole as a last step from the corresponding amidoxime (**2.93** and **2.94**, respectively) and carboxylic acid derivatives (**2.92** and **2.95**, respectively), accompanied with the use of a coupling agent. The amidoxime intermediates (**2.93** and **2.94**, respectively) would be formed from the corresponding nitrile derivatives (**2.97** and **2.98**, respectively). Finally, the *ortho*-substituent R<sub>2</sub> of the phenyl ring would be introduced using a palladium-catalysed approach from the corresponding halogen- and metal-containing coupling partners (**2.96** and **2.99**, respectively) (**Figure 45**).



**Figure 45: Definition of the “forward” and “reverse” 1,2,4-oxadiazole designations and their corresponding retrosynthetic approach**

The formation of the 1,2,4-oxadiazole represented the key step of this retrosynthetic approach and was therefore investigated in more detail. Literature precedent suggests that there are several methods to access 1,2,4-oxadiazoles (**Scheme 9**). They can be prepared from amides *via* the formation of acylacetamidine, as exemplified with the formation of the acylacetamidine **2.102** from the reaction of the corresponding amide **2.100** with *N,N*-dimethylacetamide dimethyl acetal **2.101**. Subsequent treatment of **2.102** with hydroxylamine hydrochloride **2.103** furnished the required 1,2,4-oxadiazole **2.104**.<sup>157</sup> The cycloaddition of nitrile *N*-oxides with *N*-methoxy-imines has also been described, an example of which is the formation of the 1,2,4-oxadiazole coumarin **2.107** by reaction of the nitrile *N*-oxide coumarin **2.105** with the aryl *N*-methoxy-imine **2.106**.<sup>158</sup> Furthermore, 1,2,4-oxadiazoles can be synthesised *via* acylation of acetamide oximes, as exemplified by the successful reaction of the arylsulfonylacetamide oxime **2.108** with ethyl oxalyl chloride **2.109** to form the corresponding arylsulfonylmethyl-1,2,4-oxadiazole **2.110** (**Scheme 9**).<sup>159</sup>

The method employed in our laboratories was developed through variation of the last process, which is a one-pot synthesis from an amidoxime derivative, a carboxylic acid derivative and a peptide coupling agent. Indeed, this combination offered the mildest experimental conditions and the widest substrate scope. As an example, the formation of the biaryl 1,2,4-oxadiazole **2.114** was previously prepared by reacting *p*-toluene amidoxime **2.111** with benzoic acid **2.112** in presence of 1,1'-carbonyldiimidazole (CDI) **2.113** as a coupling agent (Scheme 9).<sup>160</sup>



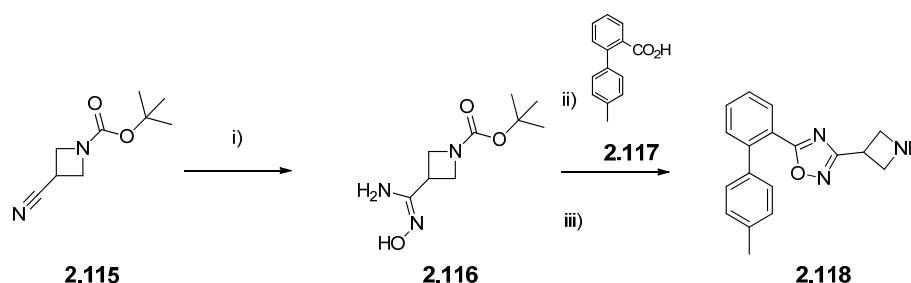
i) 120 °C, **90%**; ii) 5 N sodium hydroxide, 70% aqueous acetic acid, rt, **95%**; iii) CHCl<sub>3</sub>, rt, **25%**; iv) THF, reflux, **75%**; v) diglyme, rt to 100 °C, **57%**.

**Scheme 9: Literature examples of the formation of 1,2,4-oxadiazole derivatives**<sup>157,158,159,160</sup>



The pair of isomeric 1,2,4-oxdiazoles considered for the current study was also aimed to reduce lipophilicity by removing two chlorine atoms compared to the initial hit compound **2.30**: 1,2,4-oxdiazole **2.118** (Scheme 10) and **2.122** (Scheme 11).

The required amidoxime azetidine **2.116** was synthesised in good yield upon treatment of the corresponding nitrile azetidine derivative **2.115** with hydroxylamine hydrochloride. The formation of the oxadiazole ring was achieved in a one-pot process, whereby biphenyl carboxylic acid **2.117** was first activated at room temperature with CDI, followed by reaction with amidoxime **2.116** at 140 °C under microwave irradiation. Finally, removal of the *tert*-butoxycarbonyl (Boc) protecting group under acidic conditions afforded the forward 1,2,4-oxadiazole **2.118** (Scheme 10).

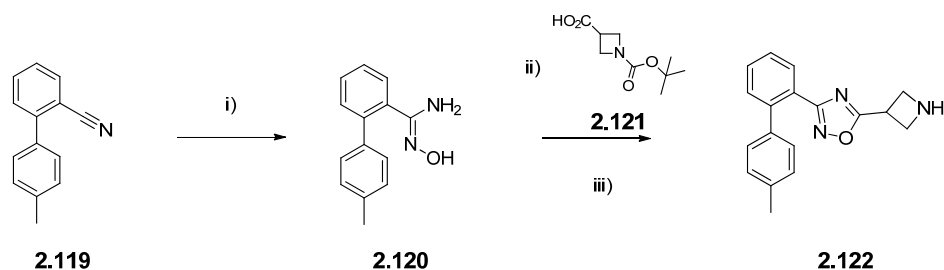


i) hydroxylamine hydrochloride (2 eq), NaOMe (2 eq), MeOH, reflux, **95%**; ii) 4'-methyl-[1,1'-biphenyl]-2-carboxylic acid **2.117** (1.1 eq), CDI (1.1 eq), K<sub>2</sub>CO<sub>3</sub> (1.1 eq), DMF, rt and then microwave, 140 °C; iii) TFA (excess), DCM, rt, **52% over 2 steps**.

#### Scheme 10: Synthetic route to access the “forward” oxadiazole **2.118**

The reverse 1,2,4-oxadiazoles were synthesised similarly by reversing the functionality of the starting materials (Scheme 11). In this case, the first step consisted of forming biphenyl amidoxime **2.120** from the corresponding biphenyl nitrile **2.119** in presence of hydroxylamine hydrochloride. In this specific example, the low yield of 17% for this step was explained by poor recovery from chromatographic purification, as the silica cartridge was overloaded with crude material. Again, the formation of the oxadiazole ring was achieved by pre-activating the azetidine carboxylic acid **2.121** at ambient temperature with CDI, and then stirring the activated acid with amidoxime **2.120** at 140 °C under microwave

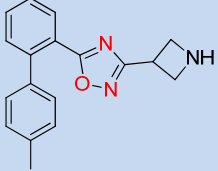
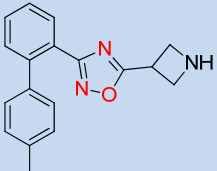
irradiation. The removal of the Boc protecting group allowed isolation of the reverse 1,2,4-oxadiazole **2.122** in low yields (7% over 2 steps, **Scheme 11**). Subsequent profiling of the reaction using LCMS revealed that the microwave condensation step was initiated before achieving full conversion of the activated acid, therefore explaining the overall poor yield of the oxadiazole formation step.



i) hydroxylamine hydrochloride (2 eq), NaOMe (2 eq), MeOH, reflux, **17%**; ii) 1-(*tert*-butoxycarbonyl)azetidine-3-carboxylic acid **2.121** (1.1 eq), CDI (1.1 eq), K<sub>2</sub>CO<sub>3</sub> (1.1 eq), DMF, rt and then microwave, 140 °C to 160 °C; iii) TFA (excess), DCM, rt, **7% over 2 steps**.

#### **Scheme 11: Synthetic route to access the “reverse” oxadiazole 2.122**

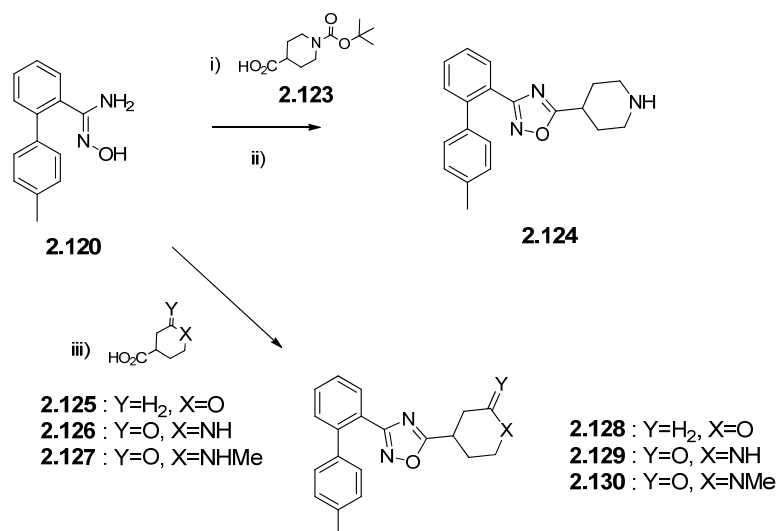
Turning our attention to the profile of the newly prepared analogues (**Table 16**), oxadiazole azetidines **2.118** and **2.122** displayed reduced potency against *I*<sub>CRAC</sub> in comparison to the azetidine HTS hit **2.30** (Jurkat pIC<sub>50</sub> = 5.8, **Table 15, p. 100**). However, the reduced HAC and lipophilicity afforded by the less functionalised biphenyl group resulted in analogues **2.118** and **2.122** exhibiting higher LLE. Additionally, with a reduced PFI of less than 7, oxadiazoles **2.118** and **2.122** had an aqueous solubility meeting our optimisation goals of greater than 100 µg/mL. More importantly, the fact that this isomeric pair of 1,2,4-oxadiazoles **2.118** and **2.122** had equivalent potency suggested that changes to this region of the molecule could be tolerated without affecting the *I*<sub>CRAC</sub> potency. This feature could be exploited in the future, through taking advantage of the modular synthesis of this template using carboxylic acid and amidoxime derivatives as starting materials.

| Structure                |  |  |
|--------------------------|--|---|
| Compound number          | 2.118  | 2.122   |
| 1,2,4-oxadiazole class   | forward  | reverse   |
| Jurkat pIC <sub>50</sub> | 5.1  | 5.2   |
| LE / LLE                 | 0.31 / 0.28  | 0.32 / 0.29   |
| MW                       | 291  | 291   |
| clogP                    | 2.4  | 2.4   |
| PFI                      | 6.3  | 6.5   |
| HSA binding              | 88.6%  | 85.1%   |
| CLND (μg/mL)             | 125 <sup>a</sup>   | 105   |

<sup>a</sup>Compound reported with a CLND  $\geq$  137 μg/mL in 1 out of 3 test occasions.

**Table 16: Profile of the 1,2,4-oxadiazole regioisomers 2.118 and 2.122**

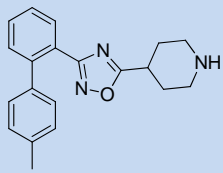
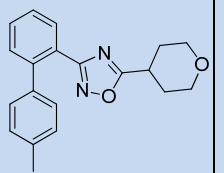
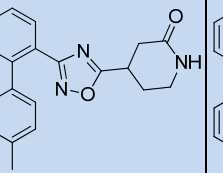
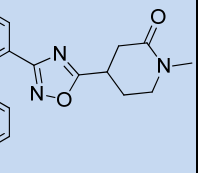
The last feature which remained to be investigated in order to validate further this new  $I_{CRAC}$  chemical series was to understand the importance of the basic moiety (*i.e.* the azetidine or the piperidine NH) for the pharmacophore, especially as it represented a hitherto unprecedented functional group in an  $I_{CRAC}$  inhibitor. Hence, a set of 6-membered heteroaliphatic rings analogues **2.128-2.130** were synthesised as non-basic replacement compounds of a comparator piperidine analogue **2.124** (Scheme 12). In light of the above result showing that reverse oxadiazoles were equipotent to forward oxadiazoles, the set of non-basic analogues **2.128-2.130** were synthesised in the reverse oxadiazole class, due to the ready availability of the requisite carboxylic acid starting materials **2.125-2.127**.



i) 1-(*tert*-butoxycarbonyl)piperidine-4-carboxylic acid **2.123** (1 eq), CDI (1.1 eq), K<sub>2</sub>CO<sub>3</sub> (1.1 eq), DMF, rt and then microwave, 140 °C; ii) TFA (excess), DCM, rt, **89% over 2 steps**; iii) acid carboxylic derivative **2.125-2.127** (1.1 eq), CDI (1.1 eq), K<sub>2</sub>CO<sub>3</sub> (1.1 eq), DMF, rt and then microwave, 140 °C, **78-86%**.

### Scheme 12: Synthesis of piperidine **2.124** and its non-basic oxadiazole analogues **2.128-2.130**

The oxadiazole piperidine analogue **2.124** was slightly less active (Jurkat pIC<sub>50</sub> = 4.9, **Table 17**) than its azetidine counterpart **2.122** (Jurkat pIC<sub>50</sub> = 5.2, **Table 16, p. 106**). This result suggested that, when also considering the matched pair of azetidine/piperidine compounds **2.30/2.91** (Jurkat pIC<sub>50</sub> = 5.8 and 5.3, respectively, **Table 15, p. 100**), the azetidine motif was preferred for inhibition of the CRAC channel over piperidine. When removing the basic centre of piperidine **2.124**, as exemplified by tetrahydropyran **2.128**, 2-pyridone **2.129** and methyl-2-pyridone **2.130**, compounds were inactive in the Jurkat assay (pIC<sub>50</sub> < 4.3), indicating that the basic centre was critical for binding affinity of the oxadiazole amine series.

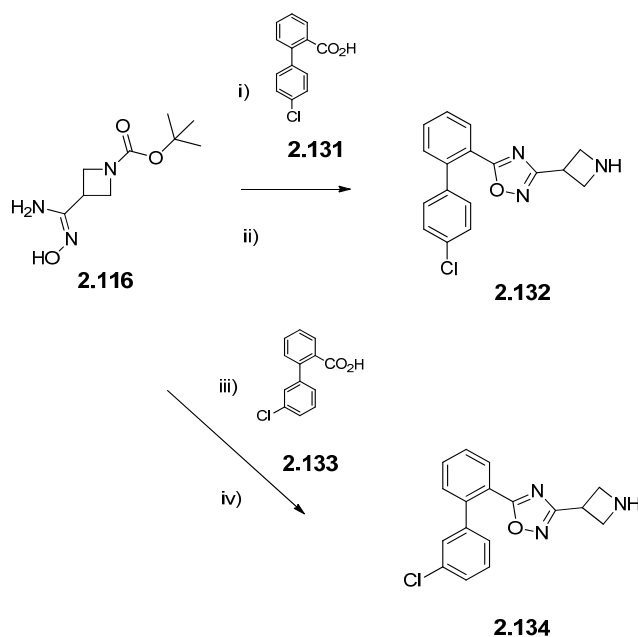
| Structure                |  |  |  |  |
|--------------------------|---|---|---|---|
| Compound                 | <b>2.124</b>  | <b>2.128</b>  | <b>2.129</b>  | <b>2.130</b>  |
| Jurkat pIC <sub>50</sub> | 4.9   | < 4.3   | < 4.3   | < 4.3   |

**Table 17: Jurkat assay activity of the non-basic replacements of the piperidine**

To summarise this section, the activity of one exemplar of the oxadiazole amine series in the electrophysiology experiments combined with the early SAR observations discussed above validated the oxadiazole amine series as being a genuine novel  $I_{CRAC}$  inhibitor pharmacophore. These results therefore completed our first objective for this chemical series. Consequently, additional optimisation efforts were initiated with a view to increasing potency of the CRAC current inhibition and improving the physicochemical properties of the oxadiazole amines.

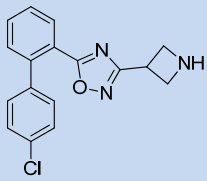
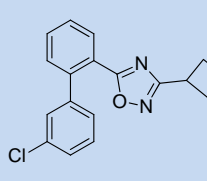
### 2.5.2. Improvement of the physicochemical properties

In the initial HTS hit compound **2.30** (Table 15, p. 100), the biphenyl group was substituted with two chlorine atoms and a methyl group. The corresponding methylbiphenyl analogue **2.118** (Table 16, p. 106), despite being less potent than its functionalised precursor **2.30** (Jurkat pIC<sub>50</sub> of 5.1 vs. 5.8, respectively), offered a reduced HAC and clogP, which translated into similar LE and improved LLE (LLE of 0.28 and 0.22 for compounds **2.118** and **2.30**, respectively). This promising early result highlighted the opportunity in reducing the lipophilic component of the biphenyl group and therefore the overall lipophilicity of the final compounds. In order to confirm this finding, two chlorobiphenyl analogues **2.132** and **2.134** were prepared (Scheme 13), using the amidoxime azetidine **2.116** synthesised previously (Scheme 10, p. 104) and either CDI or (benzotriazol-1-yloxy)tripyrrolidinophosphonium hexafluorophosphate (PyBOP) as a coupling agent to activate the carboxylic acid intermediate.



i) 4'-chloro-[1,1'-biphenyl]-2-carboxylic acid **2.131** (1.2 eq), PyBOP (1.2 eq), DIPEA (3 eq), pyridine (5 eq), DMF, rt and then microwave, 110 °C; ii) TFA (excess), DCM, rt, **18% over 2 steps**; iii) 3'-chloro-[1,1'-biphenyl]-2-carboxylic acid **2.133** (1.1 eq), CDI (1.1 eq), K<sub>2</sub>CO<sub>3</sub> (1.1 eq), DMF, rt and then microwave, 140 °C; iv) TFA (excess), DCM, rt, **34% over 2 steps**.

**Scheme 13: Synthesis of the chlorobiphenyl oxadiazoles 2.132 and 2.134**

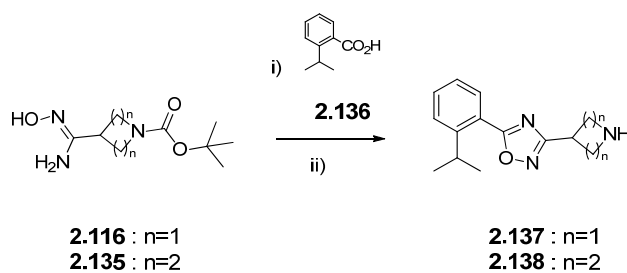
| Structure                      |  |  |
|--------------------------------|---|--|
| <b>Compound</b>                | <b>2.132</b>  | <b>2.134</b>   |
| <b>Jurkat pIC<sub>50</sub></b> | 5.5   | 5.3 <sup>a</sup>   |
| <b>LE / LLE</b>                | 0.34 / 0.29   | 0.33 / 0.28  |
| <b>MW</b>                      | 312   | 312  |
| <b>clogP</b>                   | 2.6   | 2.6  |
| <b>PFI</b>                     | 6.6   | 6.5  |
| <b>HSA binding</b>             | 91.9%   | 91.4%  |
| <b>CLND (µg/mL)</b>            | 186   | 122  |

<sup>a</sup>Compound failed to fit a curve in 1 out of 9 test occasions.

**Table 18: Profile of the chlorobiphenyl oxadiazoles 2.132 and 2.134**

In keeping with the results obtained with the methylbiphenyl compound **2.118**, the two chlorobiphenyl analogues **2.132** and **2.134** exhibited reasonable Jurkat activity, with a  $pIC_{50}$  of 5.5 and 5.3, respectively (**Table 18**). Moreover, the reduction in lipophilicity translated into LLE values approaching the required target profile (LLE > 0.3). Similarly to compounds **2.118** and **2.122** (**Table 16, p. 106**), the aqueous solubility of the two chlorobiphenyl analogues **2.132** and **2.134** was greater than 100  $\mu\text{g/mL}$ . This result was particularly significant as for the first time, high levels of aqueous solubility were consistently achieved without significant detriment to  $I_{CRAC}$  activity. Finally, the protein binding of **2.132** and **2.134**, 91.9% and 91.4%, respectively, was largely reduced compared with the protein binding of the starting HTS hit **2.30**, which displayed a protein binding of 97%.

Having established that reducing lipophilicity of the biphenyl ring could be achieved while retaining reasonable levels of  $I_{CRAC}$  activity, our attention turned to establishing the minimum active pharmacophore of the oxadiazole amine series. Accordingly, a strategy of reducing the aromatic ring count was adopted as a means of reducing PFI. The HTS hit oxadiazole **2.30** contained three aromatic rings and had a measured Chrom  $\log D_{7.4}$  of 4.6, which therefore led to a PFI of 7.6. This PFI value was just above the limit of a predicted acceptable aqueous solubility (PFI < 7) and indeed, the aqueous solubility of compound **2.30** (31  $\mu\text{g/mL}$ ), despite being generally superior compared to the indole series, was still below our optimisation goals. With a reduced lipophilicity and an associated PFI of 6.6 and 6.5, respectively, analogues **2.132** and **2.134** displayed an increased solubility of 186  $\mu\text{g/mL}$  and 122  $\mu\text{g/mL}$ , respectively. Encouraged by these findings, the terminal phenyl ring of the biphenyl system was replaced with an isopropyl group in compounds **2.137** and **2.138** (**Scheme 14**). These derivatives were prepared from 2-isopropylbenzoic acid **2.136**.

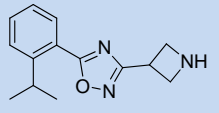
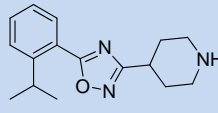


i) 2-isopropylbenzoic acid **2.136** (1.2 eq), PyBOP (1.2 eq), DIPEA (3 eq), pyridine (5 eq) DMF, rt and then microwave, 110 °C; ii) TFA (excess), DCM, rt, **12-18% over 2 steps**.

**Scheme 14: Synthesis of the isopropylbenzyl 1,2,4-oxadiazole analogues **2.137** and **2.138****

The data in **Table 19** show that the isopropyl group replacement of the terminal phenyl ring of the progenitor compound **2.30** led to molecules which retained  $I_{CRAC}$  potency. The improvement in physicochemical properties of the oxadiazole amine series was noticeable as exemplified by the azetidine **2.137**, which was characterised by a low molecular weight of 243, a reduced lipophilicity ( $clogP = 1.7$ ) and a ligand-lipophilicity efficiency of 0.38. Overall, this replacement defined unprecedented physicochemical space for an  $I_{CRAC}$  inhibitor. With one less aromatic ring, the PFI of analogues **2.137** and **2.138** was low (PFI = 4.8 and 5.1, respectively). As predicted when designing these compounds, they displayed good levels of aqueous solubility, with a CLND solubility of  $\geq 157 \mu\text{g/mL}$  and  $182 \mu\text{g/mL}$  for **2.137** and **2.138**, respectively. Additionally, the plasma protein binding was dramatically reduced (HSA binding = 63% and 74.8% for **2.137** and **2.138**, respectively) in comparison to the HTS hit **2.30** (HSA binding = 97%), and these values were predictive of a larger fraction of available unbound drug.



| Structure                      |  |  |
|--------------------------------|---|---|
| <b>Compound</b>                | <b>2.137</b>  | <b>2.138</b>  |
| <b>Jurkat pIC<sub>50</sub></b> | 5.3 <sup>a</sup>  | 5.1   |
| <b>LE / LLE</b>                | 0.4 / 0.38  | 0.35 / 0.27   |
| <b>MW</b>                      | 243   | 271   |
| <b>clogP</b>                   | 1.7   | 2.7   |
| <b>PFI</b>                     | 4.8   | 5.1   |
| <b>HSA binding</b>             | 63%   | 74.8%   |
| <b>CLND (µg/mL)</b>            | ≥ 157   | 182   |

<sup>a</sup>Compound failed to fit a curve in 1 out of 7 test occasions.

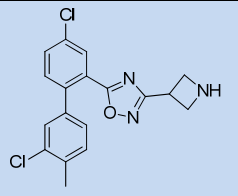
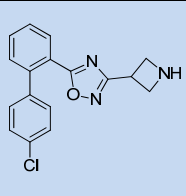
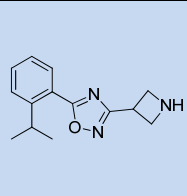
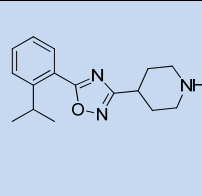
**Table 19: Profile of the isopropylbenzyl 1,2,4-oxadiazole analogues 2.137 and 2.138**

To summarise this section, the objective of the isoxazole amine series to reduce polarity and to increase aqueous solubility while retaining  $I_{CRAC}$  activity was achieved. However, the fundamental goal was to deliver a  $I_{CRAC}$  lead molecule from the HTS, hence, the wider pharmacological profile of several of the newly identified analogues was investigated.

### 2.5.3. Wider profile of the isoxazole amine series

#### 2.5.3.1. Identification of potential developability issues and strategies devised to overcome them

Having demonstrated the ability to combine Jurkat potency with aqueous solubility, several isoxazole amine derivatives were investigated in the PBMCs assays in order to assess their wider biological profile (**Table 20**). Additionally, in an attempt to investigate early pharmacokinetic parameters, their *in vitro* metabolic clearance was measured in human and rat microsomes. Finally, since it was stated previously that a common pharmacophore for potent hERG blockers consists of compounds containing a basic nitrogen in conjunction with an aromatic ring (see **Section 1.2.5, p. 12**), this liability was also considered.

| Structure  |  |  |  |  |
|--|--|---|--|--|
| <b>Compound</b>                                      | <b>2.30</b>  | <b>2.132</b>  | <b>2.137</b>   | <b>2.138</b>   |
| <b>Jurkat pIC<sub>50</sub></b>                       | 5.8 <sup>a</sup>   | 5.5   | 5.3 <sup>b</sup>   | 5.1  |
| <b>PBMCs IFN<math>\gamma</math> pIC<sub>50</sub></b> | 5.1 <sup>c</sup>   | 5.2 <sup>d</sup>  | < 4.8  | < 4.8 <sup>e</sup>   |
| <b>PBMCs TNF<math>\alpha</math> pIC<sub>50</sub></b> | 4.7  | 4.9   | 4.5  | 5.3  |
| <b>h IVC (mL/min/g)<sup>ix</sup></b>                 | 0.9  | ND  | 1.6  | < 0.5  |
| <b>r IVC (mL/min/g)<sup>ix</sup></b>                 | 16.1   | ND  | 15.1   | 24.6   |
| <b>FP hERG pIC<sub>50</sub></b>                      | 5.3  | 5.2   | 4.6  | 4.7  |
| <b>clogP</b>   | 3.8  | 2.6   | 1.7  | 2.7  |
| <b>PFI</b>   | 7.6  | 6.6   | 4.8  | 5.1  |

<sup>a</sup>Compound reported inactive in 1 out of 6 test occasions; <sup>b</sup>Compound failed to fit a curve in 1 out of 7 test occasions; <sup>c</sup>Compound reported inactive in 2 occasions and failed to fit a curve in 1 occasion out of 10 test occasions; <sup>d</sup>Compound reported inactive in 4 occasions and failed to fit a curve in 3 occasions out of 11 test occasions; <sup>e</sup>Compound reported active in 2 out of 6 test occasions.

**Table 20: Wider profile of a selected set of isoxazole amine compounds**

<sup>ix</sup> In all the compounds profile tables of this thesis, h IVC refers to human microsomes *in vitro* clearance and r IVC refers to rat microsomes *in vitro* clearance.

According to the data from **Table 20**, it became apparent that the drop in potency between the Jurkat assay and the PBMCs IFN $\gamma$  assay initially observed with the HTS hit **2.30** was also noted for the recently synthesised oxadiazole compounds. More importantly, compounds from **Table 20** also inhibited the production of TNF $\alpha$  from PBMCs upon stimulation with LPS. Hence, no discernible selectivity was achieved between the PBMCs IFN $\gamma$  and the PBMCs TNF $\alpha$  pIC<sub>50</sub>, suggesting that the compounds described so far were not fully selective for *I*<sub>CRAC</sub> and potentially promiscuous. According to the analysis from Leeson and Springthorpe<sup>11</sup> and others,<sup>161</sup> the risk of unwanted pharmacology increases with lipophilicity and is dependent on the ionisation class; basic compounds being notably more promiscuous than acids, neutral compounds and zwitterions. Since the lipophilicity of the isoxazole amine series had already been reduced markedly, focusing on reducing the basicity of the molecules seemed a sensible strategy to address the potential promiscuity observed. It is worth noting that removing the basic centre was not envisaged since it was shown previously that this structural motif was critical for binding affinity (**Table 17, p. 108**).

The second important piece of data from **Table 20** was that the 1,2,4-oxadiazole amine chemotype displayed noticeable activity against the hERG channel, as expected with a combination of aromaticity and a basic amine. Hence, the starting hit compound **2.30** had a hERG pIC<sub>50</sub> of 5.3. Nevertheless, when the biphenyl group of **2.30** was truncated to an isopropylbenzyl group in compound **2.137**, the pIC<sub>50</sub> in the hERG binding assay was reduced from 5.3 to 4.6. As described previously (see **Section 1.2.5, p. 12**), the hERG binding site facilitates hydrophobic aromatic interactions and thus the reduction of the aromatic ring count could explain this improvement in the hERG profile. Of particular relevance for the current study, Jamieson and co-workers<sup>162</sup> have identified four distinct strategies to reduce hERG inhibition: discrete structural modification, zwitterion formation, control of molecule lipophilicity and reduction of the p*K*<sub>a</sub>. Although these strategies were found to be equally effective at reducing hERG affinity, reducing lipophilicity in the first instance was advocated where clogP is greater than 3, as this would also be beneficial for other drug developability parameters. The lipophilicity of the isopropylbenzyl derivatives **2.137** and **2.138** was already low and therefore,

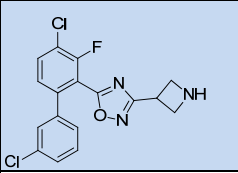
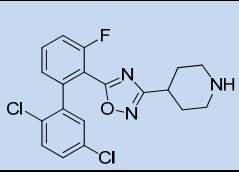
according to the strategic decision tree suggested by Jamieson and co-workers to reduce hERG activity,<sup>162</sup> reducing the clogP further would not be the best option in this instance. However, reducing basicity was an alternative strategy worth considering. This investigation is discussed subsequently in **Section 2.5.3.3 (p. 121)**.

Regarding *in vitro* pharmacokinetic profile, the oxadiazole analogues from **Table 20** displayed low human microsomal IVC meeting our optimisation goals (IVC < 2 mL/min/g), but very high rat microsomal IVC. This discordant behaviour could be attributed to interspecies differences in metabolising enzymes. It is indeed precedented that pharmacokinetic parameters are dependent on the species investigated.<sup>163</sup> From a metabolism perspective, the main family of metabolising enzymes, the cytochrome P450 enzymes, display different metabolising profiles depending on species.<sup>164</sup> Not only do the levels of expression of CYPs differ across animal species and humans, but also their functions vary.<sup>165</sup>

A general strategy to reduce *in vitro* metabolism is to decrease the lipophilicity of compounds,<sup>10</sup> however, in the current study, reducing lipophilicity did not appear to lower rat microsomal IVC, as indicated by the very high rat microsomal IVC of compounds **2.137** and **2.138** (rat IVC = 15.1 and 24.6 mL/min/g, respectively). Therefore, the strategy considered was to investigate the internal database available in our laboratories in order to identify structural features that could potentially reduce rat IVC for our specific template.

### **2.5.3.2. Attempt to reduce rat microsomal *in vitro* clearance**

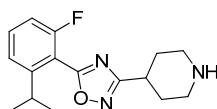
The interrogation of the compound collection available in our laboratories for oxadiazole amine analogues with already measured *in vitro* clearance allowed us identify the compounds **2.139** and **2.140**, which had been prepared prior to the  $I_{CRAC}$  programme and which had demonstrated moderate to low clearance in rat (**Table 21**).<sup>137</sup>

| Structure                |  |  |
|--------------------------|---|--|
| Compound                 | <b>2.139</b>  | <b>2.140</b>   |
| Jurkat pIC <sub>50</sub> | 5.5   | 5.5  |
| MW                       | 364   | 392  |
| clogP                    | 3.5   | 4.2  |
| PFI                      | ND  | 6.7  |
| h IVC (mL/min/g)         | < 0.5   | 0.9  |
| r IVC (mL/min/g)         | 1.1   | 3.2  |

**Table 21: Profile of the previously prepared oxadiazoles 2.139 and 2.140<sup>137</sup>**

In the biphenyl oxadiazole compounds **2.139** and **2.140** (Table 21), the rat microsomal clearance was noticeably reduced compared to compounds **2.30**, **2.137** and **2.138** discussed in Table 20 (p. 113). In an attempt to link the reduction in the rat clearance of compounds **2.139** and **2.140** with their chemical structure, two main structural differences between these compounds and those previously described could potentially explain this observation. First, the *ortho*-position of the aromatic ring attached to the oxadiazole was substituted with a fluorine atom in compounds **2.139** and **2.140**, as opposed to being unfunctionalised in 1,2,4-oxadiazoles **2.30**, **2.137** and **2.138**. Based on this, it was hypothesised that the fluorine could be blocking a site of oxidative metabolism in the aromatic ring, which is preceded in the literature.<sup>166</sup> Additionally, compounds **2.139** and **2.140** did not have a benzylic hydrogen, compared to compounds **2.30**, **2.137** and **2.138**. Given that the benzylic position is a potential site for metabolism,<sup>166</sup> this feature could also account for the improvement in metabolic stability observed.

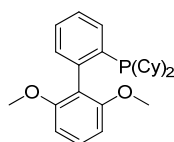
In order to investigate the role of fluorine *ortho* to the oxadiazole, this structural feature was introduced in the isopropylbenzyl compound **2.138** to furnish the fluorobenzyl analogue **2.141** (Figure 46).



2.141

**Figure 46: Fluorobenzyl isoxazole 2.141, designed to reduce rat microsomal clearance**

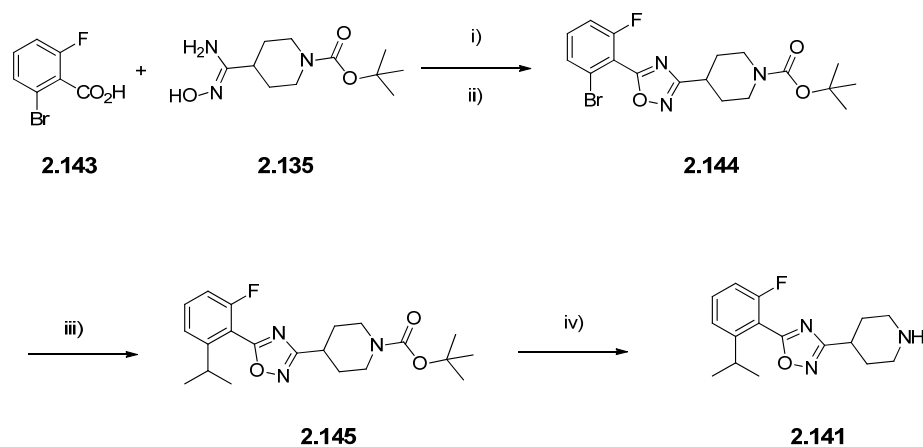
The required starting benzoic acid needed for the formation of the oxadiazole ring was not commercially available with both the *ortho*-isopropyl and the *ortho*-fluoro substitution pattern and thus required synthesis. Introducing a fluorine atom on a benzene that already contains an isopropyl substituent was deemed more challenging than carrying this out in the opposite manner. Accordingly, the construction of a secondary alkyl-aryl C-C bond using metal-mediated chemistry was envisaged in order to introduce the isopropyl group. The transition metal-catalysed cross-coupling reactions of  $sp^2$  hybridised carbon nucleophile with  $sp^2$  hybridised carbon bearing a halide has been extensively described in the literature. However, the cross-coupling between a  $sp^2$  and a  $sp^3$  carbon is less exemplified, probably due to the synthetic issues resulting from the unfavourable  $\beta$ -hydride elimination and the slow reductive elimination step. The  $sp^2$ - $sp^3$  cross-coupling can be achieved *via* Negishi reaction, which involves coupling an organozinc reagent with an aryl halide under catalysis by a transition metal. Coupling reactions catalysed by nickel<sup>167,168</sup> or by palladium<sup>169</sup> have been reported. For the synthesis of compound **2.141**, a coupling involving isopropylzinc was considered, however, the potential  $\beta$ -hydride elimination pathway could lead to the unwanted *n*-propyl version of the product. Nevertheless, a recent publication from Buchwald<sup>170</sup> compared the ratio of isopropyl *vs.* *n*-propyl cross-coupled products from a palladium-catalysed Negishi reaction when different ligands are employed. Based on these observations, the commercially available ligand that offered a superior ratio of isopropylbenzyl product, dicyclohexyl(2',6'-dimethoxy-[1,1'-biphenyl]-2-yl)phosphine **2.142** (Figure 47),<sup>170</sup> was selected for the current study.



**2.142**

**Figure 47: Dicyclohexyl(2',6'-dimethoxy-[1,1'-biphenyl]-2-yl)phosphine ligand 2.142 selected for the  $sp^2$ - $sp^3$  Negishi cross-coupling**

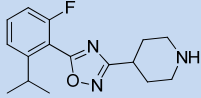
The first step in accessing the required compound **2.141** consisted of the oxadiazole formation from the commercially available benzoic acid derivative **2.143** and the piperidine amidoxime **2.135** using 1-[bis(dimethylamino)methylene]-1*H*-1,2,3-triazolo[4,5-*b*]pyridinium 3-oxid hexafluorophosphate (HATU) as a coupling agents (**Scheme 15**). The introduction of the isopropyl group *via* a Negishi cross-coupling using **2.142** as a ligand (**Figure 47**) yielded the required isopropylbenzyl intermediate **2.145** in 14% yield, alongside its corresponding *n*-propyl isomeric analogue in 19% yield. The subsequent removal of the Boc protecting group using trifluoroacetic acid led to the isolation of the desired target **2.141**.



i) *tert*-butyl 4-(*N*-hydroxycarbamimidoyl)piperidine-1-carboxylate **2.135** (1 eq), 2-bromo-6-fluorobenzoic acid **2.143** (1.1 eq), HATU (1.2 eq), DIPEA (2.5 eq), DMF, rt; ii)  $K_2CO_3$  (1 eq), DMF, microwave, 140 °C, **20% over 2 steps**; iii) isopropylzinc bromide 0.5 M in THF (1.1 eq), dicyclohexyl(2',6'-dimethoxy-[1,1'-biphenyl]-2-yl)phosphine **2.142** (0.07 eq),  $Pd(OAc)_2$  (0.1 eq), THF, rt, **14%**; iv) TFA (excess), DCM, rt, **94%**.

**Scheme 15: Synthesis of *ortho*-fluorobenzyl 1,2,4-oxadiazole 2.141, using a Negishi reaction as a key step**

The *ortho*-fluorobenzyl 1,2,4-oxadiazole **2.141** (Table 22) displayed similar Jurkat potency to its des-fluoro counterpart **2.138**. The low HAC of this molecule, combined with its low lipophilicity, translated into high LE, LLE and aqueous solubility. Additionally, human IVC was very low, in accordance with the data observed for the progenitor compound **2.138**. However, compound **2.141** displayed very high *in vitro* clearance in rat. Thus, it was hypothesised that the clearance in rat was a combination of multiple factors and could not be addressed by the addition of a fluorine *ortho* to the oxadiazole alone.

| Structure                |  |
|--------------------------|--|
| Compound                 | <b>2.141</b>   |
| Jurkat pIC <sub>50</sub> | 5 <sup>a</sup>   |
| LE / LLE                 | 0.32 / 0.25  |
| MW                       | 289  |
| clogP                    | 2.8  |
| PFI                      | 5  |
| CLND (µg/mL)             | ≥ 187  |
| Permeability (nm/s)      | 520  |
| h IVC (mL/min/g)         | < 0.5  |
| r IVC (mL/min/g)         | 41.2   |

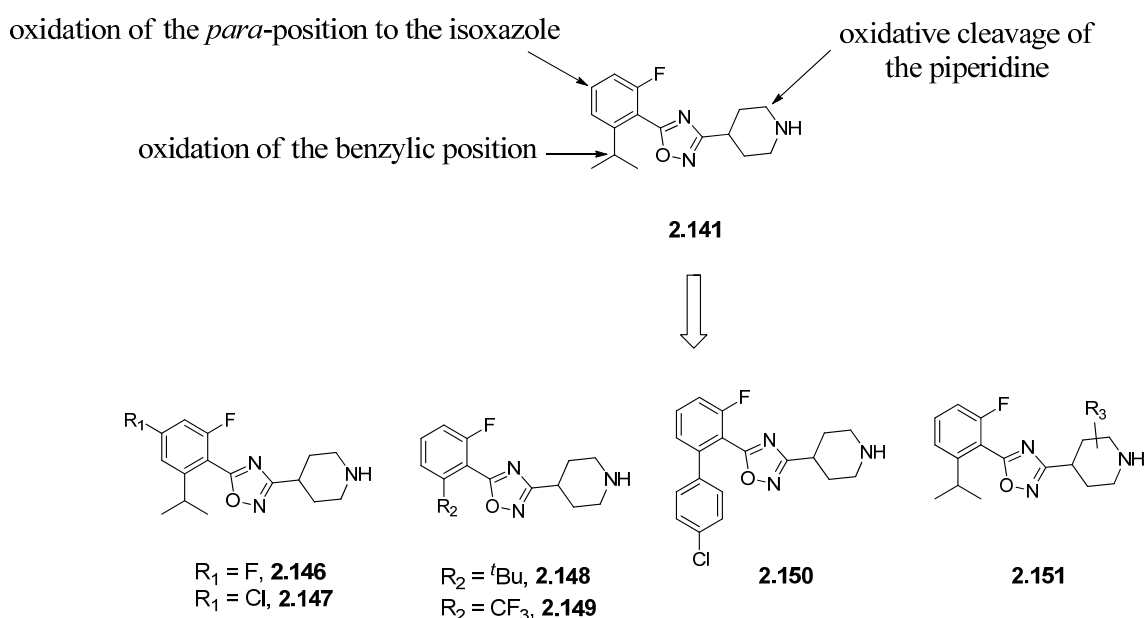
<sup>a</sup>Compound reported inactive in 1 out of 4 test occasions.

**Table 22: Profile of *ortho*-fluorobenzyl 1,2,4-oxadiazole **2.141****

In an attempt to understand further the potential metabolic liability of compound **2.141**, an *in silico* metabolite identification study was carried out by another member of our laboratories<sup>171</sup> using MetaSite® software.<sup>172</sup> This analysis suggested that the major sites of metabolism of compound **2.141** were the *para*-position to the isoxazole ring, the benzylic position of the isopropyl group and the piperidine ring (Figure 48). Several compounds were suggested by the author to potentially block these metabolically liable positions (Figure 48). Hence, compounds **2.146** and **2.147**



block the *para*-position to the isoxazole with a fluorine and a chlorine, respectively; compounds **2.148**, **2.149** and **2.150** no longer exhibit a benzylic hydrogen; and, in the general structure **2.151**, functionalisation of the piperidine was envisaged in order to increase the steric hindrance of this position to potentially hamper the binding to the metabolising enzymes. However, none of the suggested structures from **Figure 48** were prepared as our attention shifted to reduce the basicity of the oxadiazole amine series. Indeed, the investigation of tuning the series  $pK_a$  would involve modifying the piperidine, which according to the *in silico* metabolite identification, could also impact microsomal clearance, as well as potentially being of benefit to selectivity against the hERG channel.



**Figure 48: Major metabolic soft spots of compound 2.141, observed after an *in silico* metabolite identifications study.<sup>171</sup> Compounds 2.146 to 2.151 were suggested to potentially block these metabolic liabilities.**

### 2.5.3.3. Modulation of $pK_a$ in an attempt to improve the chemical series profile

As discussed in **Section 2.5.3.1 (p. 113)**, reducing the basicity of the isoxazole amine series was identified as being an attractive strategy to potentially reduce unwanted pharmacology, and therefore reducing activity of the series in the PBMCs TNF $\alpha$  and in the hERG assays. The results obtained when removing the basic group (compounds **2.128-2.130**, **Table 17, p. 108**) underlined the necessity of having a basic nitrogen at this position of the molecule in order to maintain inhibitory activity at  $I_{CRAC}$ . Perhaps more importantly, the lack of activity of the lactam **2.129** (**Table 17, p. 108**) suggested that the efficiency of the binding could be the result of an ionic interaction rather than a hydrogen bond donating effect, although intolerance of the carbonyl group of **2.129** in the binding site cannot be excluded. Taken together, these findings highlighted that modulation of the  $pK_a$  would have to be carried out in a controlled manner, as excessive reduction of the  $pK_a$  could be detrimental for potency against  $I_{CRAC}$ .

In order to prioritise the large number of possible compounds with reduced basicity which could be synthesised, prediction of the  $pK_a$  of a series of hypothetical 1,2,4-oxadiazole amines was considered. To assess the validity of this software in appropriately predicting the  $pK_a$  of this class of analogues, the  $pK_a$  of the oxadiazoles piperidines **2.138** and **2.141** were experimentally determined by another member of our laboratories<sup>173</sup> using a spectroscopic ultraviolet (UV) detection method. The  $pK_a$  of compound **2.138** was predicted to be 9.5 and was measured at 9.3 and the  $pK_a$  of compound **2.141** was predicted at 9.4 and was measured at 9.4. This good correlation between measured and predicted  $pK_a$  values gave us confidence in using the ACD  $pK_a$  predictor tools to help prioritise our synthetic strategy.

Focusing on potential approaches for  $pK_a$  modulation, a recent review from Morgenthaler and co-workers<sup>174</sup> demonstrated how the basicity of an amine can be tuned within a context of lead optimisation. This study highlighted the impact of incorporating an electron withdrawing group on the  $pK_a$  of a cyclic amine. Considering the 1,2,4-oxadiazole amine series, it was reasoned that variation of the size of the cyclic amine (from piperidine, to pyrrolidine and to azetidine), in order to

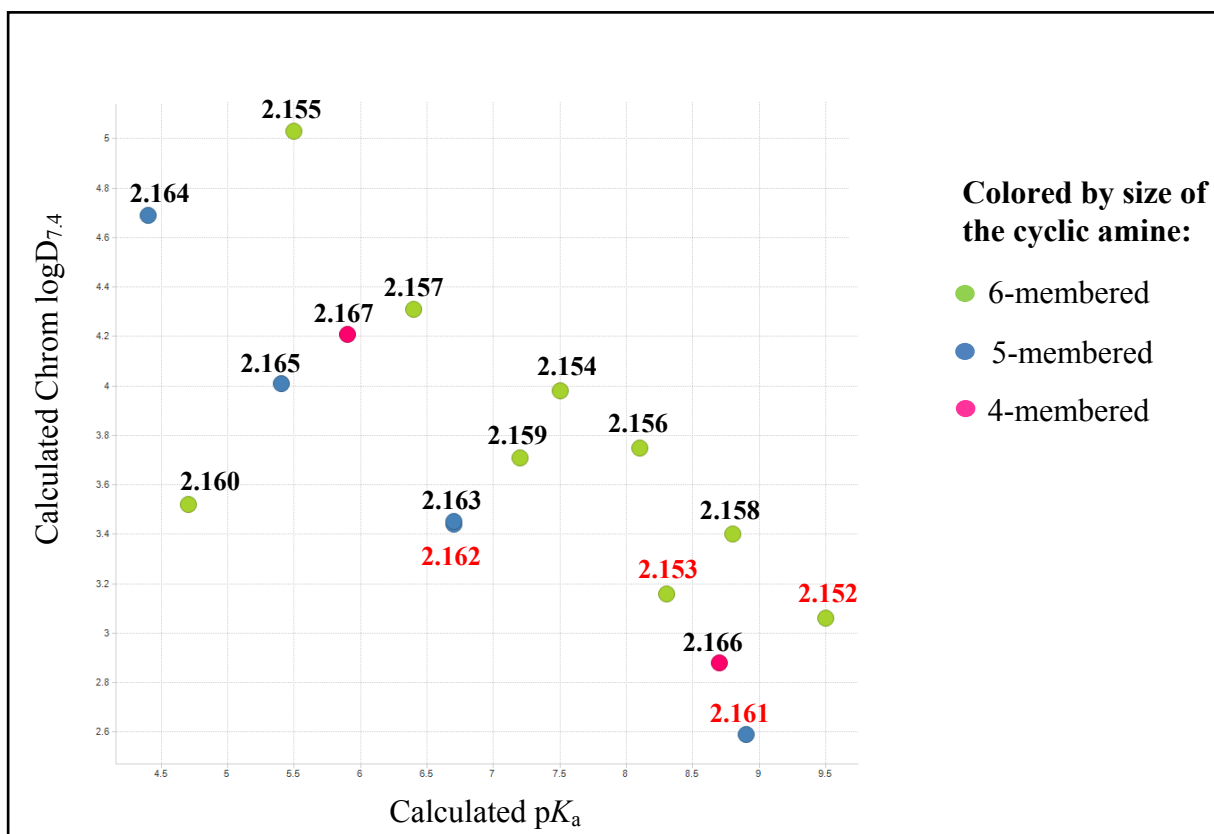
bring the basic amine closer to the electron-withdrawing oxadiazole ring, and substitution of the cyclic amine with fluorine, ketone and sulfone motifs would assist in reducing the  $pK_a$  of the molecule. **Table 23** displays the structures considered for synthesis with their calculated  $pK_a$  and calculated Chrom  $\log D_{7.4}$ . The investigation was conducted on the reverse oxadiazole class of compounds, since varying the cyclic amine part of the molecule would be more readily achieved, given the availability of the necessary carboxylic acid starting materials.

|  |              |              |              |              |
|--|--------------|--------------|--------------|--------------|
| <b>Structure</b>                       |              |              |              |              |
| <b>Cmpd</b>                            | <b>2.152</b> | <b>2.153</b> | <b>2.154</b> | <b>2.155</b> |
| <b><math>pK_a</math></b>               | 9.5          | 8.3          | 7.5          | 5.5          |
| <b>Chrom <math>\log D_{7.4}</math></b> | 3.1          | 3.2          | 4            | 5            |
| <b>Structure</b>                       |              |              |              |              |
| <b>Cmpd</b>                            | <b>2.156</b> | <b>2.157</b> | <b>2.158</b> | <b>2.159</b> |
| <b><math>pK_a</math></b>               | 8.1          | 6.4          | 8.8          | 7.2          |
| <b>Chrom <math>\log D_{7.4}</math></b> | 3.8          | 4.3          | 3.4          | 3.7          |
| <b>Structure</b>                       |              |              |              |              |
| <b>Cmpd</b>                            | <b>2.160</b> | <b>2.161</b> | <b>2.162</b> | <b>2.163</b> |
| <b><math>pK_a</math></b>               | 4.7          | 8.9          | 6.7          | 6.7          |
| <b>Chrom <math>\log D_{7.4}</math></b> | 3.5          | 2.6          | 3.4          | 3.5          |
| <b>Structure</b>                       |              |              |              |              |
| <b>Cmpd</b>                            | <b>2.164</b> | <b>2.165</b> | <b>2.166</b> | <b>2.167</b> |
| <b><math>pK_a</math></b>               | 4.4          | 5.4          | 8.7          | 5.9          |
| <b>Chrom <math>\log D_{7.4}</math></b> | 4.7          | 4            | 2.9          | 4.2          |

**Table 23: Calculated  $pK_a$  and calculated Chrom  $\log D_{7.4}$  of hypothetical 1,2,4-oxadiazoles**

According to  $pK_a$  predictions, the set of structures from **Table 23** offered the possibility of tuning the cyclic amine basicity anywhere from  $pK_a$  of 9.5 for piperidine **2.152**, up to  $pK_a$  of 4.4 for difluoropyrrolidine **2.164**. The proximity of the basic *NH* to the oxadiazole had a modest impact on  $pK_a$ , as exemplified by the size reduction of the cyclic amine, going from 4-piperidine **2.152** (calcd  $pK_a = 9.5$ ), to pyrrolidine **2.161** (calcd  $pK_a = 8.9$ ) and to azetidine **2.166** (calcd  $pK_a = 8.7$ ). A significant reduction in the predicted  $pK_a$  was achieved by introducing electron-withdrawing groups at the  $\beta$ -position of the basic centre. Thus, introduction of a fluorine atom at the  $\beta$ -position of the nitrogen reduced  $pK_a$  by two log units and this effect was additive, as illustrated by the  $pK_a$  modulation from unsubstituted piperidine **2.152** (calcd  $pK_a = 9.5$ ), to fluoropiperidine **2.154** (calcd  $pK_a = 7.5$ ) and to difluoropiperidine **2.155** (calcd  $pK_a = 5.5$ ). However, the addition of fluorine atoms also gradually increased the lipophilicity of one log unit per fluorine atom. Perhaps the most dramatic effect on the  $pK_a$  reduction was observed when introducing a  $\beta$ -sulfone, which allowed a reduction of four log units, as exemplified by the difference between unsubstituted 3-piperidine **2.158** (calcd  $pK_a = 8.8$ ) and its corresponding  $\beta$ -sulfone analogue **2.160** (calcd  $pK_a = 4.7$ ). This significant observation was supported by measured data available from the literature,<sup>175</sup> giving further confidence in our predictive model.

In order to more clearly visualise the distribution of the predicted  $pK_a$  and Chrom  $\log D_{7.4}$  values that are covered by the set of structures from **Table 23**, the data are displayed as a scatter plot in **Figure 49**.



**Figure 49: Plot of calculated Chrom  $\log D_{7.4}$  vs. calculated  $pK_a$  of the set of hypothetical 1,2,4-oxadiazoles. Compounds in red were chosen for synthesis**

From this set of hypothetical structures, the decision was taken, as a first iteration, to synthesise:

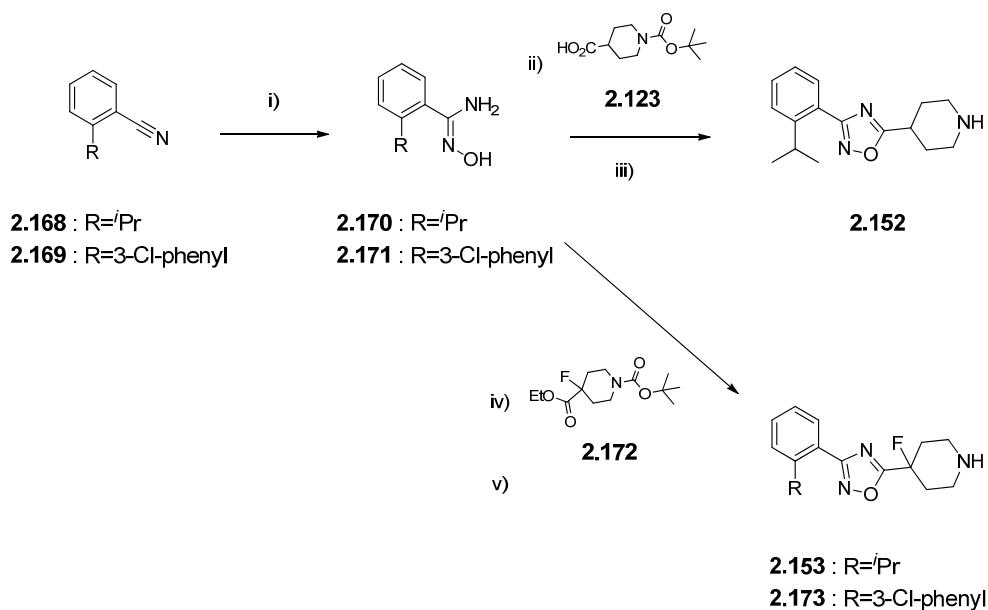
- Piperidine **2.152** as a reference compound, as this would allow pair wise comparisons to be made in order to assess the impact of attenuating the basicity within the series.
- Fluoropiperidine **2.153**, as this compound had a particularly low predicted Chrom  $\log D_{7.4}$  despite the introduction of the additional fluorine.
- Pyrrolidine **2.161** and fluoropyrrolidine **2.162**, as the pyrrolidine ring offered a lower lipophilicity. The additional feature of interest of these pyrrolidine-based structures was the fact they introduced a stereogenic centre at the ring junction between the 1,2,4-oxadiazole and the cyclic amine. In addition to lowering the  $pK_a$  of the basic nitrogen, the additional molecular complexity and the presence of a

stereogenic centre could potentially benefit binding specificity and other physicochemical parameters. According to a recent report in the literature,<sup>176</sup> the increase in molecular complexity (measured by the fraction of sp<sup>3</sup> hybridised atoms, defined as the ratio of the number of sp<sup>3</sup> hybridised carbons to the total carbon count) and the addition of stereogenic centres enhance the likelihood of success for biological molecules progressing beyond the drug discovery stage.

In order to interpret with further confidence the impact of these structural changes on the profile of compounds, two previously identified potent phenyl groups at the left-hand side position of the molecule would be investigated: 2-isopropylbenzyl and 3-chlorobiphenyl groups.

Turning our attention to the synthesis of the reference piperidine **2.152** and of the piperidine analogues with a fluorine atom attached at the aliphatic ring junction **2.153** and **2.173**, the first step consisted of forming the benzyl amidoximes **2.170** and **2.171** from the corresponding benzonitrile analogues **2.168** and **2.169**, respectively (**Scheme 16**). The oxadiazole piperidine **2.152** was then obtained by starting from isopropylbenzyl amidoxime **2.170** and using CDI as a coupling agent.

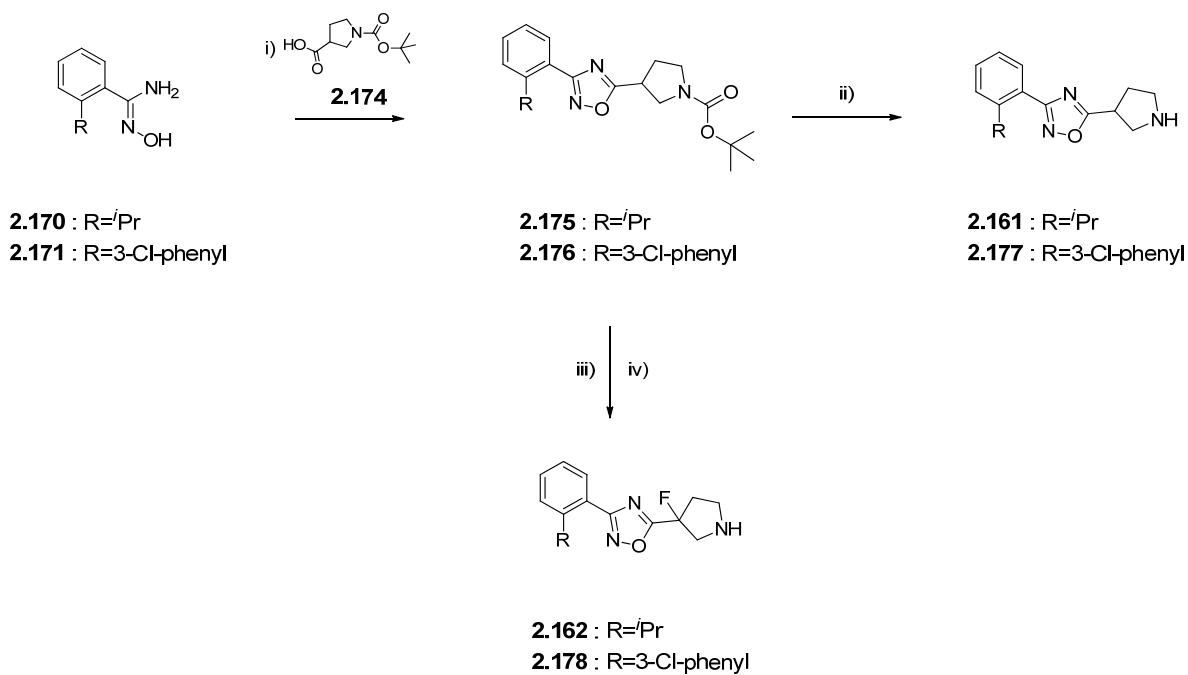
Regarding the compounds with a fluorine at the ring junction of the cyclic amine, the requisite 4-fluoropiperidine was commercially available in the form of the ethyl ester **2.172** (**Scheme 16**). Hence, the oxadiazole formation was attempted without recourse to pre-activation of the carboxylic acid moiety, as described previously. The oxadiazole ring construction and subsequent deprotection of the Boc group afforded the required piperidine analogues **2.153** and **2.173** in 36% and 17%, respectively, over two steps.



i) hydroxylamine hydrochloride (2 to 4 eq), NaOMe (2 to 4 eq), MeOH, reflux or microwave 150 °C, **21-42%**; ii) (reaction with **2.170** only), 1-(*tert*-butoxycarbonyl)piperidine-4-carboxylic acid (1 eq), CDI (1.1 eq), K<sub>2</sub>CO<sub>3</sub> (1.1 eq), DMF, rt and then microwave, 140 °C; iii) TFA (excess), DCM, rt, **39% over 2 steps**; iv) 1-*tert*-butyl 4-ethyl 4-fluoropiperidine-1,4-dicarboxylate **2.172** (2.4 eq), NaOMe (3 eq), THF, microwave, 150 °C; v) TFA (excess), DCM, rt, **17-36% over 2 steps**.

#### Scheme 16: Synthesis of piperidine **2.152** and fluoropiperidines **2.153** and **2.173**

To achieve the synthesis of the pyrrolidine-based targets, the previously prepared amidoximes **2.170** and **2.171** were utilised in the oxadiazole formation step, by reacting them with β-proline **2.174** to furnish the key oxadiazole intermediates **2.175** and **2.176**, respectively (**Scheme 17**). These derivatives afforded pyrrolidines **2.161** and **2.177**, respectively, after amine deprotection. Additionally, fluorination of **2.175** and **2.176** using *N*-fluoro-*N*-(phenylsulfonyl)benzenesulfonamide and subsequent removal of the Boc group afforded fluoropyrrolidines **2.162** and **2.178**, respectively.

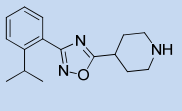
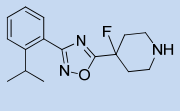
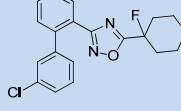
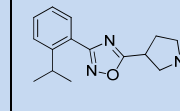
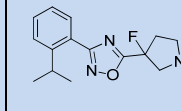
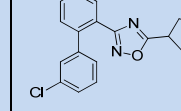
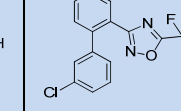


i) 1-(*tert*-butoxycarbonyl)pyrrolidine-3-carboxylic acid **2.174** (1.2 eq), CDI (1.2 eq), K<sub>2</sub>CO<sub>3</sub> (1.2 eq), DMF, rt and then microwave, 140 °C, **92-99%**; ii) TFA (excess), DCM, rt, **99-100%**; iii) LDA (2 M in THF, 1.2 eq), *N*-fluoro-*N*-(phenylsulfonyl)benzenesulfonamide (1.2 eq), THF, -78 °C to rt; iv) TFA (excess), DCM, rt, **17-21% over 2 steps**.

### Scheme 17: Synthesis of pyrrolidines **2.161**, **2.177**, **2.162** and **2.178**

All of the novel compounds prepared above to assess the impact of reducing the basicity of the series were screened across various assays discussed previously (**Table 24**).



| Structure  |  |  |  |  |  |  |  |
|--|---|---|---|---|---|---|---|
| <b>Compound</b>                                      | <b>2.152</b>  | <b>2.153</b>  | <b>2.173</b>  | <b>2.161</b>  | <b>2.162</b>  | <b>2.177</b>  | <b>2.178</b>  |
| <b>Jurkat pIC<sub>50</sub></b>                       | 4.8 <sup>a</sup>  | 5.3   | 6.1   | 5.1   | 5.5   | 5.4   | 6   |
| <b>LE / LLE</b>                                      | 0.33 / 0.25   | 0.34 / 0.26   | 0.33 / 0.23   | 0.37 / 0.31   | 0.37 / 0.29   | 0.32 / 0.24   | 0.34 / 0.24   |
| <b>PBMCs IFN<math>\gamma</math> pIC<sub>50</sub></b> | < 4.7   | ND  | < 4.7 <sup>b</sup>  | < 4.7   | < 4.7   | 5.2 <sup>c</sup>  | 5.2 <sup>d</sup>  |
| <b>PBMCs TNF<math>\alpha</math> pIC<sub>50</sub></b> | 5.1   | 4.6   | 4.6   | 4.4 <sup>e</sup>  | 4.7   | 4.8   | 4.7   |
| <b>clogP</b>   | 2.7   | 3   | 3.8   | 2.3   | 2.9   | 3.2   | 3.7   |
| <b>PFI</b>   | 4.9   | 6.4   | 8.1   | 5.2   | 7.3   | 7   | 8.9   |
| <b>CLND (<math>\mu\text{g/mL}</math>)</b>            | 71 <sup>f</sup>   | 149 <sup>g</sup>  | 157 <sup>g</sup>  | 142 <sup>h</sup>  | $\geq 152$  | 134   | 149   |
| <b>Calculated pK<sub>a</sub></b>                     | 9.5   | 8.3   | 8.3   | 8.9   | 6.7   | 8.9   | 6.7   |
| <b>Measured pK<sub>a</sub></b>                       | 9.4   | 8.4   | 8.4   | 8.7   | ND  | 8.6   | ND  |
| <b>ePhys hERG pIC<sub>50</sub></b>                   | 4.8 <sup>i</sup>  | < 4.3   | ND  | < 4.2   | ND  | 4.7   | ND  |
| <b>h IVC (mL/min/g)</b>                              | < 0.5   | 0.6   | ND  | < 0.5   | ND  | 1.1   | ND  |
| <b>r IVC (mL/min/g)</b>                              | 26.8  | 28.7  | ND  | 32.8  | ND  | 13.4  | ND  |
| <b>HSA binding</b>                                   | 68.2%   | 86.3%   | 95.1%   | 68.1%   | ND  | 91.5%   | 96.4%   |

<sup>a</sup>Compound failed to fit a curve in 1 out of 6 test occasions; <sup>b</sup>Compound reported active in 2 out of 6 test occasions; <sup>c</sup>Compound reported inactive in 2 occasions and failed to fit a curve in 1 occasion out of 6 test occasions; <sup>d</sup>Compound reported inactive in 2 out of 4 test occasions; <sup>e</sup>Compound reported inactive in 1 out of 4 test occasions; <sup>f</sup>Compound reported with a CLND  $\geq 179$   $\mu\text{g/mL}$  in 1 out of 2 test occasions; <sup>g</sup>Assay failed to generate a CLND value in 1 out of 2 test occasions; <sup>h</sup>Compound reported with a CLND  $\geq 150$   $\mu\text{g/mL}$  in 1 out of 2 test occasions; <sup>i</sup>Compound reported inactive in 1 out of 4 test occasions.

**Table 24: Profile of the reduced pK<sub>a</sub> oxadiazole amine analogues**

First, it should be noted that  $pK_a$  values were experimentally measured on a range of analogues (compounds **2.152**, **2.153**, **2.173**, **2.161** and **2.177**) and that they were in good agreement with the predicted values, providing further confidence in the software used to predict  $pK_a$ . Based on the data shown in **Table 24**, the introduction of the fluorine at the linking point between the oxadiazole and the cyclic amine ring offered a noticeable increase in activity in the Jurkat assay. Indeed, when focusing on the set of corresponding des-fluoro/fluoro matched pairs **2.152/2.153**, **2.161/2.162**, **2.177/2.178**, the introduction of the fluorine atom led to an average increase in the Jurkat  $pIC_{50}$  of 0.5 log unit. Consequently, compounds such as fluoropiperidine **2.173** and fluoropyrrolidine **2.178** displayed a Jurkat  $pIC_{50}$  greater than 6, which was our optimisation goal for this biological assay.

However, this relatively high potency in the primary assay did not translate into the functional PBMCs  $IFN\gamma$  assay. Indeed, none of the analogues from **Table 24** had a PBMCs  $IFN\gamma$  greater than 5.2 and the activity of most of the compounds was below the threshold of detection of the assay. This drop in activity between the Jurkat functional and the PBMCs functional assays was difficult to rationalise. One suggestion is that the difference in cell lines used in these two respective assays could result in the oxadiazole amine series having variable ability to block the CRAC channels. As opposed to the PBMCs assays that use primary cells, the Jurkat assay relied on a cancer cell line. These different cell lines may have varying level of transporter proteins and consequently, the efflux and influx profile may differ according to the precise cell line used. Hence, if the oxadiazole amine series targets an intracellular binding site, then a difference in efficiency could be observed. Additionally, a difference in the nature and level of expression of metabolising enzymes could be anticipated between Jurkat cells and PBMCs. Therefore, the oxadiazole amine series could have a different tendency to be metabolised between these two cell lines and, for instance, could be converted to an inactive metabolite to a greater extent in PBMCs.

All the compounds from **Table 24** weakly inhibited the production of TNF $\alpha$  from PBMCs upon stimulation with LPS. Therefore, the strategy to reduce the pK<sub>a</sub> of the analogues in order to avoid unwanted pharmacology was ultimately not completely successful. It was apparent that the oxadiazole amine series had a propensity to be active in the TNF $\alpha$  assay and that no discernible selectivity was obtained for the two PBMCs assays, as necessitated by our optimisation goals (PBMCs IFN $\gamma$  pIC<sub>50</sub>  $\geq$  5.5 and PBMCs TNF $\alpha$  pIC<sub>50</sub>  $<$  4.5).

In relation to inhibition of the hERG channel, the activity of compounds **2.153** and **2.161** was below the threshold of detection of the electrophysiology assay, while compound **2.177** had a pIC<sub>50</sub> of 4.7. Not all the compounds were able to be tested in the hERG assay, hence it was difficult to fully appreciate the impact on reducing the pK<sub>a</sub> on the hERG inhibition. Nevertheless, the fact that several oxadiazole amine compounds were identified as being inactive in the hERG assay gave confidence that a level of selectivity between blocking the CRAC and the hERG channels could be achieved for this particular chemotype.

Finally, almost all the compounds from this last study had an aqueous solubility greater than 100  $\mu$ g/mL. In addition to this, the compounds screened in the *in vitro* DMPK assays displayed a low human IVC of less than 2 mL/min/g, however, the rat clearance remained high.

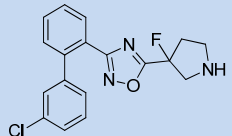
#### 2.5.4. Conclusion of the oxadiazole series

The recently run  $I_{CRAC}$  HTS, using a phenotypic approach, identified the oxadiazole amine series, which is structurally differentiated from other  $I_{CRAC}$  chemotypes described in the literature. After confirming the  $I_{CRAC}$  activity associated with this series through electrophysiology experiments, efforts were made to develop early SAR. The phenotypic approach gave some confidence that the oxadiazole series was engaging with a well defined molecular target, based on the Jurkat data obtained. It was shown that the high level of lipophilicity of the initial substituted biphenyl ring was not a key requirement for  $I_{CRAC}$  potency, and that the terminal ring of the biphenyl motif could be replaced with an isopropyl group. The isoxazole moiety proved tolerant of regioisomerism, and both “forward” and “reverse” classes of 1,2,4-oxadiazoles displayed similar levels of Jurkat activity. Regarding the aliphatic cyclic amine, it was demonstrated that the size of the ring could be increased from 4- to 5- and to 6-membered ring. Although a basic nitrogen was required for binding activity, its basicity could be attenuated without decreasing Jurkat activity.

Subsequently to a reduction in the lipophilicity of the biphenyl ring, several compounds were synthesised with high LLE and low PFI. Additionally, the aqueous solubility of the oxadiazole amine series was noticeably increased and several active molecules were identified with high aqueous solubility. This was believed to be an unprecedented discovery for compounds with activity at the  $I_{CRAC}$  biological target.

In an attempt to reduce off-target activity and to increase the window between the PBMCs IFN $\gamma$  and TNF $\alpha$  assays, decreasing the basicity of the series was investigated. This was conducted by using  $pK_a$  predictions and by searching the literature on ways to efficiently modulate basicity of cyclic amines. As a result, it was shown that the introduction of a fluorine atom on the cyclic amine increased Jurkat potency and that activity against hERG could be reduced. Regarding the objective of delivering a lead compound with the target profile defined in **Figure 31 (p. 59)**, several parameters robustly achieved our optimisation goals, such as Jurkat  $pIC_{50}$ , PFI, LE and LLE, CLND solubility, HSA binding and hERG  $pIC_{50}$ .

Having underlined the progress made on the oxadiazole amine series, there were, however, two pivotal developability parameters that could not be addressed with the current set of compounds. Firstly, the drop in potency from the Jurkat assay to the PBMCs IFN $\gamma$  assay and secondly, the rat *in vitro* clearance. Investigation of data available in our laboratories suggested that introducing a fluorine atom *ortho* to the oxadiazole ring could decrease rat *in vitro* clearance, however, it was shown that the high rat IVC could not be reduced to acceptable levels by relying on this structural modification alone. An interesting *in silico* metabolite identification study prompted us to suggest potential avenues to investigate in order to reduce the rat *in vitro* clearance and this is a proposal for future work on this series (**Figure 48, p. 120**). Regarding the drop in potency going from primary to secondary assays, this was considered a serious issue for the progression of this chemical series. In an attempt to understand further the pharmacology of the isoxazole series across the different  $I_{CRAC}$  assays, one of the most potent compounds in the Jurkat assay identified from this study, fluoropyrrolidine **2.178** (**Table 24, p. 128**), was studied in the LAD2 degranulation assay and by electrophysiology (**Table 25**).

|  |  |
|--|--|
| <b>Structure</b>                                     |  |
| <b>Compound</b>                                      | <b>2.178</b>   |
| <b>Jurkat pIC<sub>50</sub></b>                       | 6  |
| <b>LAD2 pIC<sub>50</sub></b>                         | 5.3 <sup>a</sup>   |
| <b>PBMCs IFN<math>\gamma</math> pIC<sub>50</sub></b> | 5.2 <sup>b</sup>   |
| <b>PBMCs TNF<math>\alpha</math> pIC<sub>50</sub></b> | 4.7  |
| <b>ePhys (at 10 <math>\mu</math>M)</b>               | 81% $I_{CRAC}$ inhibition with a half-life of 72 s                                   |
| <b>LE / LLE</b>                                      | 0.34 / 0.24  |

<sup>a</sup>Compound reported inactive in 1 out of 3 test occasions;

<sup>b</sup>Compound reported inactive in 2 out of 4 test occasions

**Table 25: Pharmacological profile of fluoropyrrolidine 2.178**

Whereas the most advanced compounds from the first generation of inhaled  $I_{CRAC}$  inhibitors developed in our laboratories were generally equipotent in the Jurkat, LAD2 and PBMCs  $IFN\gamma$  assays (see 3-aminopyrazole **2.24**, **Table 5**, **p. 57** for an example), the most active isoxazole amine compounds consistently displayed a drop in potency from Jurkat to the LAD2 and PBMCs  $IFN\gamma$  assays. Having stated this, the high level of activity obtained with **2.178** in the electrophysiology assay gave compelling evidence of the ability of the isoxazole amine series to inhibit  $I_{CRAC}$  allied with highly encouraging physicochemical properties. Despite this, however, the inconsistent pharmacology remained an unresolved hurdle to the successful development of this chemical series.

Observing a reduction in activity in more phenotypically relevant assays using primary cells isprecedented,<sup>177</sup> however, fully understanding the underlying reasons is complex. Indeed, there could be several explanations accounting for the observed drop in potency across the assays, such as the difference in cell type used, the variation in the level of expression in membrane transporters, the difference in the level of expression of metabolising enzymes and the non-specific binding to other proteins contained in the assay. It would have been highly interesting to investigate all these areas if sufficient time was available for a more extensive investigation into these potential issues.

## 2.6. Overall conclusions of the $I_{CRAC}$ programme

The currently published  $I_{CRAC}$  small molecule inhibitors are typified by a common lipophilic pharmacophore. A first generation of inhaled  $I_{CRAC}$  blockers developed in our laboratories shared this common pharmacophore and were characterised by low aqueous solubility. As a consequence, there are to date no potent  $I_{CRAC}$  inhibitors displaying high aqueous solubility and a physicochemical profile consistent with oral dosing.

In order to identify high quality starting points for an oral approach, an HTS was conducted using a phenotypic assay and an innovative triage strategy based on physicochemical properties was adopted. The cellular assay used for this HTS had a longer compound incubation time compared to the previous HTS run in our laboratories, to facilitate the detection of more varied modes of action, however, this tended to increase the susceptibility to cytotoxic agents. Nevertheless, several non-cytotoxic chemical series emerged from this HTS as promising templates for hit to lead chemistry. The work discussed in this chapter has focused on the optimisation of two HTS hit compounds towards lead  $I_{CRAC}$  inhibitors with a profile consistent with oral dosing.

The first chemical series contained an indole template and was characterised by high  $I_{CRAC}$  potency across the four assays used in our laboratories to assess  $I_{CRAC}$  activity (Jurkat, LAD2, PBMCs IFN $\gamma$  and electrophysiology). The hit compound had low molecular weight and high ligand efficiency, leaving lipophilicity and aqueous solubility as the key parameters to optimise. An extensive SAR exploration of the series focused on reducing lipophilicity and aromatic ring count, however, the strong correlation between lipophilicity and  $I_{CRAC}$  potency could not be uncoupled. Consequently, the efforts on this chemical series were stopped. In this specific case, the two initial hurdles identified at the outset of this study (optimising concomitantly biological potency and physicochemical properties, and the absence of structure-based design methods when using a phenotypic assay) proved difficult to overcome.

The second chemical series, the oxadiazoles, was particularly attractive since it represented a novel and differentiated  $I_{CRAC}$  pharmacophore. It was demonstrated that the lipophilicity and the aromatic ring count could be reduced while successfully retaining micromolar potency in the Jurkat assay. Consequently, several potent  $I_{CRAC}$  inhibitors were identified with high aqueous solubility, which was a notable achievement in this field. Additionally, it was shown that the basicity of the series could be attenuated while increasing the Jurkat activity, which was an attractive SAR finding. However, the high rat *in vitro* microsomal clearance could not be reduced and the drop in potency between the Jurkat assay and the PBMCs IFN $\gamma$  assay could not be improved upon. Despite these challenges, several potential avenues have been postulated which would be worthy of future exploration.

In summary, these hit optimisation studies have underlined the difficulty in identifying oral  $I_{CRAC}$  small molecule blockers with acceptable developability properties, although significant progress was made towards this goal, particularly in the case of the oxadiazole chemical series. The absence of structural information was a further challenge to rational design, however, the recently solved crystal structure of ORAI1, discussed in **Section 2.1.6 (p. 35)**, may open up new possibilities for the structure-based design of agents specifically targeted against ORAI1.

The fact that only one group has successfully managed to progress an  $I_{CRAC}$  inhibitor into the clinic, despite the involvement of numerous companies in this area, emphasises the difficulty in developing oral inhibitors for this biological target. It will be extremely interesting to witness additional breakthroughs in this field, potentially assisted by recent advances in our structural understanding of this ion channel.

Furthermore, the use of a phenotypic approach has been proven effective in identifying hit compounds from an HTS and for SAR generation using the Jurkat assay, however, retaining potency across a set of phenotypic assays has proven challenging depending on the chemical series investigated. Additionally, optimising compound potency against a



backdrop of “flat” SAR represented a major barrier to improvement as the impact of structural changes was often subtle and difficult to rationalise. Nevertheless, the results obtained in this chapter demonstrated the rationale in combining a phenotypic screening approach with strong emphasis on physicochemical parameters. This strategy could be relevant in other research programmes, and was in fact applied to the medicinal chemistry project described in the following chapter.

### 3. CHAPTER 3: Design, synthesis and optimisation of mPTP modulators

#### 3.1. mPTP as a biological target of therapeutic relevance

##### 3.1.1. Description of the mitochondria

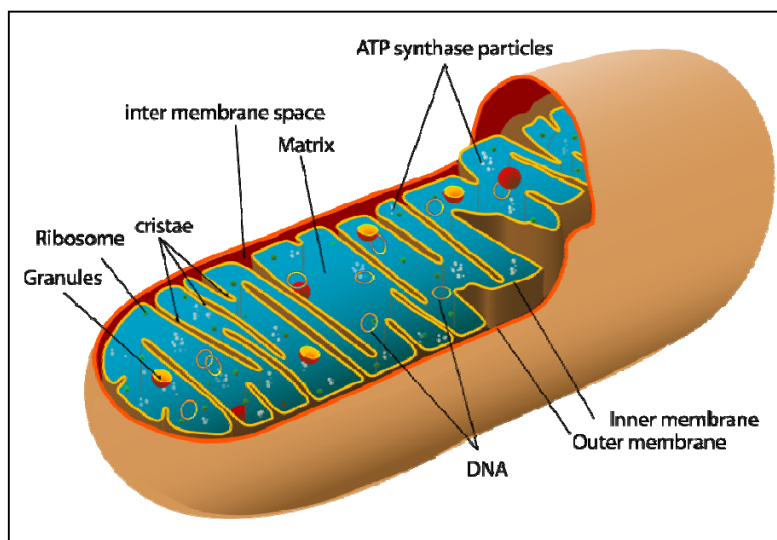
Mitochondria are multifunctional organelles which reside in the cytosol of most eukaryotic cells and they are renowned as being the main site of production of the nucleotide ATP.<sup>178</sup> In addition to this pivotal role, these organelles help in maintaining intracellular  $\text{Ca}^{2+}$  homeostasis through their particular ability to absorb and retain  $\text{Ca}^{2+}$  within their own organelle membrane.<sup>178</sup> Mitochondria are also involved in programmed cell death and generate endogenous reactive oxygen species (ROS) as a by-product of the oxidative phosphorylation.<sup>179</sup> Mitochondria display a particular structural feature as they are organised into a double-membrane system (**Figure 50**).<sup>179</sup> They present five different compartments: the outer mitochondrial membrane (OMM), the intermembrane space (which is the space between the outer and the inner membranes), the inner mitochondrial membrane (IMM), the cristae space (which is formed by infoldings of the inner membrane), and the matrix (which is the region contained within the inner membrane). Each of the two mitochondrial membranes has different permeability characteristics. The OMM is permeable towards metabolites and solutes up to 5 kDa in molecular weight, whereas the IMM is impermeable towards the majority of ions and water.<sup>180</sup>

Mitochondria produce energy through a process called oxidative phosphorylation (OXPHOS), which involves five different protein complexes (complex I to V) located on the IMM.<sup>179</sup> This system extrudes protons out of the matrix into the intermembrane space, therefore generating an electrochemical gradient across the IMM. The mitochondrial membrane potential, denoted  $\Delta\Psi_m$ , is normally in the range of 80 to 140 mV, however, in certain compromised disease states,  $\Delta\Psi_m$  can reach values greater than 140 mV and this leads to increased ROS production at the expense of ATP generation.<sup>179</sup>

It is worth noting that in humans, approximately 90% of ATP is produced by mitochondria.<sup>179</sup>

As stated above, mitochondria are also a site of formation of ROS, including superoxide anion ( $O_2^{\bullet-}$ ), the highly reactive hydroxyl radical ( $\bullet OH$ ) and reactive nitrogen species such as nitric oxide ( $\bullet NO$ ).<sup>181</sup>

Finally, mitochondria have a major role in the mechanism of cell death that can be apoptotic or necrotic.<sup>180,181</sup> These two methods of cell death were initially classified according to microscopic observations. While apoptosis consists of a naturally occurring programmed and targeted dismantling of cells, necrosis leads to the loss of cell membrane integrity and to an uncontrolled release of dead tissue near the site of cell death.<sup>179</sup>



**Figure 50: Structure of a mitochondrion**

In light of their pivotal regulatory role in all the above mentioned signalling pathways, mitochondria are a critical component of a healthy cellular phenotype. Conversely, mitochondrial dysfunction is associated with the pathogenesis of various human disease states<sup>179</sup> and this will be discussed in more detail in **Section 3.1.3 (p. 142)**.

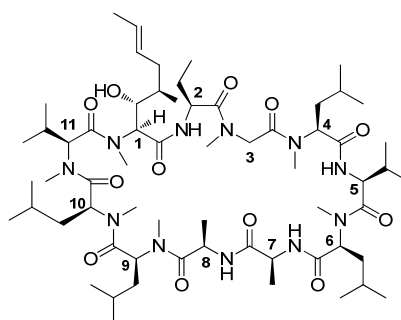
### **3.1.2. Mitochondrial permeability transition and mitochondrial permeability transition pore**

The term mitochondrial permeability transition (mPT) refers to an abrupt increase in the permeability of the inner mitochondrial membrane to low molecular weight solutes.<sup>182</sup> This phenomenon occurs when the mitochondria are under cellular stress, such as excessive intracellular calcium, ROS accumulation, or mitochondrial membrane depolarisation. This increased permeability of the IMM is the result of the opening of a non-specific channel that is permeable to molecules less than 1.5 kDa in size. This channel, which spans across the IMM and the OMM, is called the mitochondrial permeability transition pore (mPTP).<sup>183</sup> There are multiple consequences of the sustained opening of the mPTP, both at the mitochondrial and at the cellular level.<sup>182</sup> Firstly, the mPTP allows free movement of small molecules across the IMM whilst retaining proteins (which are generally larger than 1.5 kDa in molecular weight) in their compartment. As the protein concentration in the matrix is much greater than in the cytosol or in the intermembrane space, an osmotic pressure is created and low molecular weight osmolytes flow into the matrix space, leading to swelling of the matrix compartment.<sup>182</sup> This matrix enlargement is compensated by the unfolding of the cristae and, as the matrix expands, it exerts pressure on the OMM which eventually ruptures. This loss of integrity of the mitochondrial membrane generates the release of the sequestered calcium as well as certain pro-apoptotic proteins such as cytochrome *c*, which were contained in the intermembrane space.<sup>183</sup> The cytosolic release of pro-apoptotic material can initiate apoptotic cell death. Secondly, when mPTP is opened, the IMM is no longer able to act as a barrier for the protons in the OXPHOS process of synthesis of ATP.<sup>182</sup> Consequently, mitochondria cannot synthesise ATP which results in cellular metabolic failure and necrotic cell death.<sup>184</sup>

The conditions required for the formation of the mPTP, its properties and the consequences of its opening are well understood and described,<sup>182,183</sup> however, the exact molecular identity of the mPTP remains unclear. There is a body of evidence suggesting that the mPTP is composed of several proteins, but the role of a number of these proteins

is controversial. Indeed, some proteins have been shown to influence mPTP functioning, however, it has not been firmly established whether they were part of the pore's constitution or not.

Nevertheless, from this conflicting landscape, there is consensus that the mitochondrial matrix protein cyclophilin D (Cyp D) is a critical component of the mPTP.<sup>185,186</sup> Indeed, early in the discovery of mPTP, it was shown that cyclosporin A (**3.1**, CsA, **Figure 51**), a potent immunosuppressant originally isolated from the fungus *Tolypocladium inflatum*, inhibited the formation of the mPTP.<sup>187</sup> Additionally, protein purification studies demonstrated that the inhibitory role of CsA was mediated by direct inhibition of Cyp D.<sup>188</sup> When tested in the calcium retention capacity assay available in our laboratories (CRC, see **Section 3.1.5**, **p. 150**, for more detail of this mPTP-relevant assay), the pIC<sub>50</sub> of CsA was 7.2.



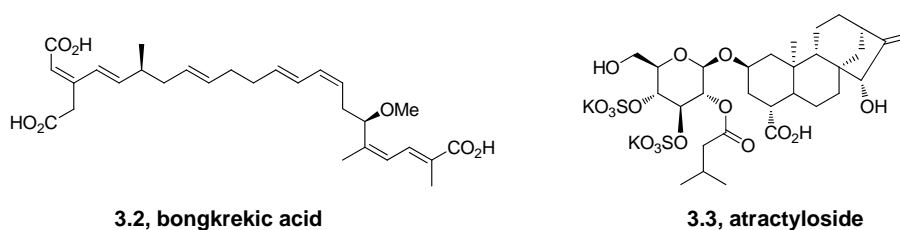
**3.1, cyclosporin A**  
Liver CRC pIC<sub>50</sub> = 7.2<sup>a,b</sup>

<sup>a</sup>This compound was only reported with a measured pIC<sub>50</sub> value in 544 out of the 551 test occasions: for the other 5 test occasions pIC<sub>50</sub> was greater than 9 and for the other 2 test occasions the assay failed to return a value.

**Figure 51: Structure of cyclosporin A (CsA)**

Perhaps the strongest evidence of the involvement of Cyp D in the formation of the mPTP comes from genetic studies, where it was shown that mice lacking the gene encoding for Cyp D were protected from ischemia/reperfusion-induced cell death *in vivo*, a condition mediated by the mPTP.<sup>189</sup> Additionally, mitochondria isolated from livers, hearts and brains of these genetically modified mice were resistant to mitochondrial swelling and permeability transition *in vitro*.<sup>189</sup>

In addition to Cyp D, it was proposed until recently that the other main structural components of mPTP were the voltage-dependent anion channel (VDAC), spanning across the OMM, and the adenine nucleotide translocase (ANT), a protein spanning across the IMM. The contributing role of ANT to the normal function of the mPTP was suggested after finding that ANT inhibitors, such as bongkreikic acid (**3.2, Figure 52**), delay the opening of the mPTP.<sup>190</sup> Conversely, ANT activators, such as atractyloside (**3.3, Figure 52**), sensitise the response of the mPTP to  $\text{Ca}^{2+}$ .<sup>190</sup> However, mitochondria of mice lacking the genes encoding for ANT were shown to still undergo mPT, resulting in the release of cytochrome *c*.<sup>191</sup> These mixed results concerning the involvement of ANT in mPT underline a probable indirect link between ANT and formation of the mPTP.



**Figure 52: Structure of bongkreikic acid, a ANT inhibitor and atractyloside, a ANT sensitiser**

Similarly, despite earlier results suggesting that VDAC was the outer membrane component of the mPTP,<sup>192</sup> it was demonstrated that mitochondria of mice lacking the genes encoding for VDAC exhibited an oxidative stress- and  $\text{Ca}^{2+}$ -induced mPT similar to mitochondria from wild-type mice.<sup>193</sup>

The quest to determine the exact molecular composition of the mPTP is still actively engaging the scientific community, and several alternative proteins are considered to play a role in the functioning of the mPTP.<sup>194</sup> Novel components of the mPTP have actually emerged from the literature during the course of writing this thesis. Firstly, a transgenic mouse study demonstrated that the mitochondrial phosphate carrier, which is the main protein responsible for phosphate import across the mitochondrial membrane, is not a direct component of the mPTP, but that it participates in the regulation of the pore opening.<sup>195</sup> Subsequently, two different groups presented strong evidence for F<sub>0</sub>F<sub>1</sub> ATP synthase, an enzyme that participates in the production of ATP, to be the pore constituent of the mPTP.<sup>196,197</sup> F<sub>0</sub>F<sub>1</sub> ATP synthase has therefore been added to the most recent models describing the core components of the mPTP,<sup>198,199</sup> however, additional experiments are still needed to unambiguously reveal the exact structural composition of the mPTP.

### **3.1.3. Diseases associated with sustained opening of the mPTP and therapeutic opportunities**

Ischemic heart diseases are the leading cause of death in Western countries.<sup>200</sup> Indeed, each year 17 million people worldwide suffer from myocardial infarctions and several of those result from the injury the heart suffers during reperfusion after a prolonged period of ischemia.<sup>200</sup> As described in the previous section, the key factor responsible for mPTP opening is calcium overload, especially when this is accompanied by oxidative stress and mitochondrial depolarisation; and these are actually the same conditions the heart experiences during post-ischemic reperfusion.<sup>201</sup> Hence, it has been established that the mPTP opens after reperfusion of the heart, and its role in the development of myocardial necrosis has been widely reviewed in the literature.<sup>202,203</sup> The importance of mPTP opening in mediating ischemia reperfusion injury was first demonstrated in isolated perfused rat hearts where CsA was shown to have a protective effect.<sup>204</sup> These observed benefits have since been transferred into clinical studies targeting the mPTP in order to reduce ischemia-reperfusion injury. Indeed, in a group of 58 patients undergoing

percutaneous coronary intervention, the cardioprotective effect of CsA was demonstrated and results showed a significantly reduced overall infarcted area in the group treated with CsA compared with the control group.<sup>205</sup> Furthermore, in a group of 78 adult patients undergoing coronary artery bypass graft surgery, a single intravenous bolus of CsA at 2.5 mg/kg, administered prior to the surgery, has proved to significantly reduce the extent of peri-operative myocardial injury.<sup>206</sup> Additionally, the cardioprotective effect of CsA was also demonstrated in a clinical trial with 61 patients, where CsA was administered at the time of reperfusion during aortic valve surgery.<sup>207</sup> This body of evidence provides a strong clinical proof-of-concept that modulation of the mPTP is a validated strategy to reduce myocardial damage at the time of reperfusion in humans.

Several acute and chronic CNS disorders have common pathogenic factors, including oxidative stress, disruption of calcium homeostasis and mitochondrial dysfunction, yet all these symptoms induce mPT.<sup>208</sup> A common factor to neurodegenerative diseases is aging, which is a process associated with impairment of mitochondrial bioenergetic function and increased oxidative stress.<sup>209,181</sup> It is thought that several degenerative diseases can trigger the mPTP opening and, the concomitant cell death induced compromises further the biological system.<sup>208,209,210</sup> The first neurological disorder in which the mPTP has been shown to be involved is Alzheimer's disease (AD). Indeed, amyloid  $\beta$  (A $\beta$ ), a neurotoxic peptide recognised to be a major component in AD pathogenesis, can negatively affect mitochondrial functions such as increasing ROS production and altering mitochondrial membrane potential.<sup>211</sup> Probably the strongest experimental evidence relies on imaging studies which showed that A $\beta$  accumulates in brain mitochondria obtained from AD patients and from transgenic AD mice, and that A $\beta$  binds to Cyp D.<sup>212</sup> This interaction caused the formation of the mPTP, as evidenced by compromised respiration function, promotion of ROS and release of cytochrome *c*. Conversely, the mitochondria from transgenic Cyp D deficient mice were resistant to A $\beta$ - and Ca<sup>2+</sup>-induced mitochondrial swelling and mPT.<sup>212</sup> These results, along with other experiments,<sup>211</sup> suggest that the mPTP is a potential target for AD therapy.



Amyotrophic lateral sclerosis (ALS) is a neurodegenerative disease characterised by upper and lower motor neuron death causing paralysis and usually leading to death within 1 to 5 years from diagnosis. The pathological characteristics of ALS are associated with pronounced and progressive changes in mitochondrial morphology, bioenergetics and Ca<sup>2+</sup> homeostasis.<sup>213</sup> Several *in vitro* and *in vivo* experiments suggest that addressing mitochondrial dysfunction is a valid target for ALS.<sup>213</sup> Firstly, using a transgenic mouse model of ALS, G93A-mutated superoxide dismutase-1 (SOD1) mice, it was demonstrated that intrathecal administration of CsA prolonged mice survival as compared to vehicle-treated controls.<sup>214</sup> Additionally, the genetic deletion of Cyp D in G93A-SOD1 mice had significant effects on the ALS disease onset and on the survival extension.<sup>215</sup> These results demonstrated that mitochondrial dysfunction may have a causal role in the disease mechanism of ALS.

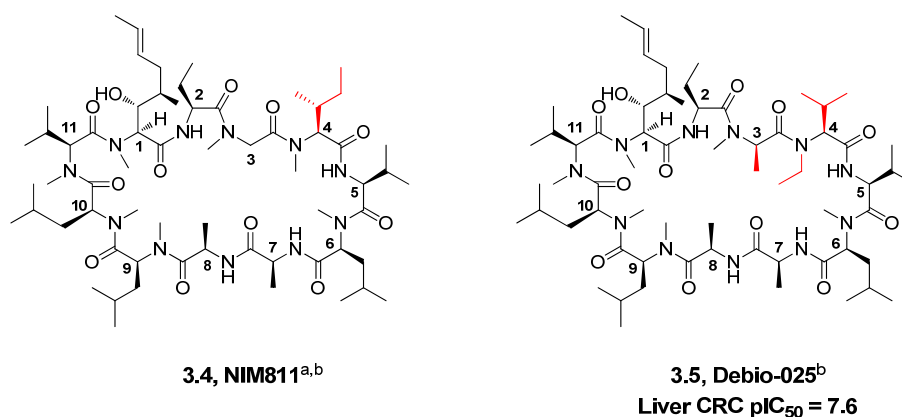
Several other disorders have also been linked to the mPTP. Firstly, treatment with CsA of mice lacking the gene coding for the extracellular matrix protein collagen VI, which have therefore a myopathic phenotype, rescued myofiber alterations.<sup>216</sup> Moreover, inactivation of the gene encoding for Cyp D also rescued the disease phenotype of collagen VI deficiency, validating further the mPTP as a potential pharmacological target for muscular dystrophy.<sup>217</sup> Finally, modulation of the mPTP has also been implicated in traumatic brain injury<sup>218</sup> and in stroke.<sup>219</sup>

Taken as a whole, there now exists a strong body of evidence to support the role of the mPTP in a variety of disease states. Accordingly, significant efforts have now been invested in identifying modulators of the mPTP.

### 3.1.4. Published mPTP modulators

#### 3.1.4.1. Cyclic peptides as mPTP modulators

As outlined in the previous sections, most of the biological understanding of the effect of inhibiting the formation of the mPTP has been generated using CsA. Indeed, most *in vitro* and *in vivo* studies designed to understand the biological and pharmacological implications of blocking the mPTP were carried out with CsA. However, several factors could hamper the medical benefit of CsA as a mPTP modulator. Firstly, CsA is not selective for Cyp D over the rest of the cyclophilin family, and it has the potential to exert unwanted side-effects through its interaction with other cyclophilins.<sup>220</sup> Secondly, through its ability to form a complex with cyclophilin A (Cyp A), CsA inhibits calcineurin, a calcium dependent protein phosphate.<sup>220,201</sup> This inhibition of calcineurin confers to CsA an immunosuppressive effect. Nevertheless, it was later realised that small structural changes to this class of peptidic macrocycles (highlighted in red in **Figure 53**) could reduce its immunosuppressive activity. Thus, the antiviral agents NIM811 and Debio-025 (**3.4** and **3.5**, respectively, **Figure 53**) retain Cyp D inhibitory activity but display a reduced affinity with calcineurin, therefore having a lower immunosuppressive potency.<sup>220</sup> NIM811 was demonstrated to efficiently block the mPTP and, as a consequence, to prevent apoptotic cell death and mitochondrial depolarisation.<sup>221</sup> Similarly, Debio-025 was found to have mPTP inhibitory activity and to not interact with calcineurin, therefore being non-immunosuppressive.<sup>222</sup> Moreover, the ability of Debio-025 to modulate mPTP was demonstrated to lead to *in vitro* protective effect on cell death and *in vivo* improvement of the structure and function of dystrophic mouse muscles.<sup>223</sup>



<sup>a</sup>From this set of compounds, only Debio-025 was tested in the liver CRC assay available in our laboratories; <sup>b</sup>Structural differences from CsA (Figure 51, p. 140) are highlighted in red.

### Figure 53: Structures of cyclic peptides mPTP modulators

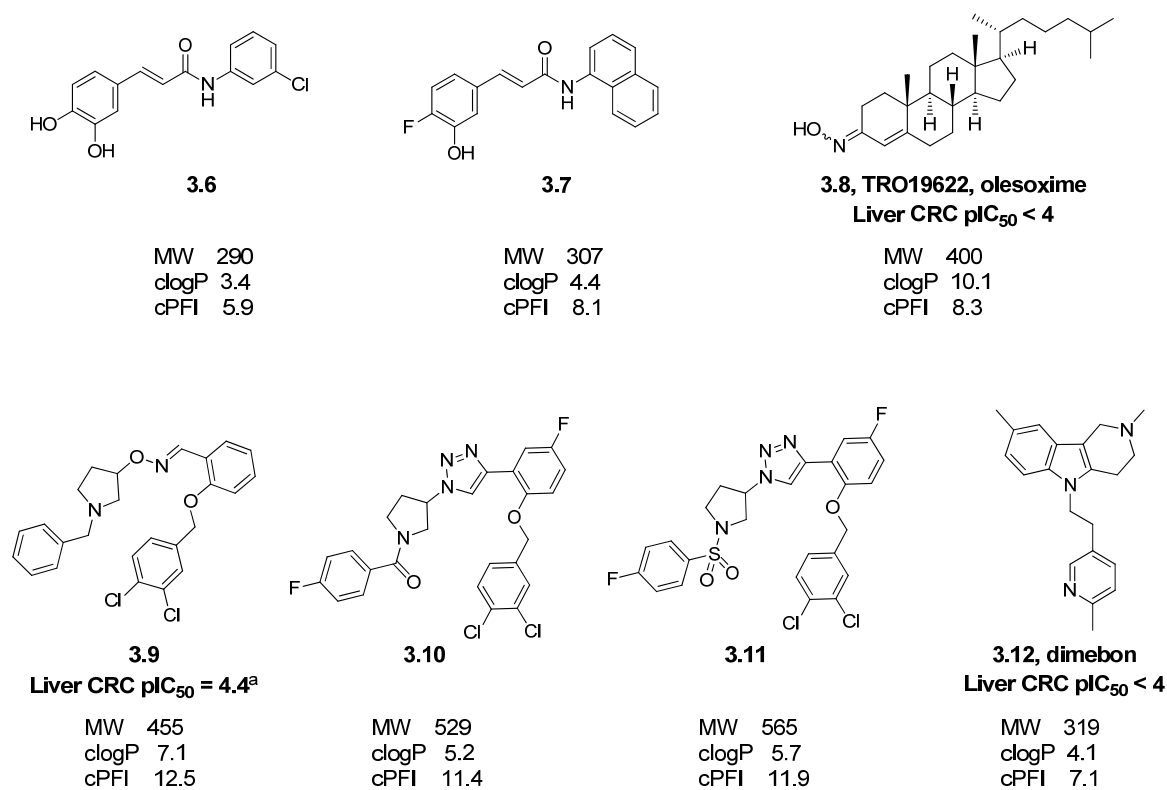
Despite being potent mPTP inhibitors, all the peptidic macrocycles described so far in the literature have several limitations as therapeutic agents. Firstly, not only do they prevent mPTP opening, but they have other biological potencies. For instance they have anti-viral activity, such as anti-human immunodeficiency and anti-hepatitis C virus.<sup>220</sup> Secondly, because of their physicochemical properties, they are peripherally restricted, which would prevent their development as a CNS penetrant neuroprotective agent.<sup>214</sup> Thirdly, most CsA derivatives have severe side effects, including nephrotoxicity, neurotoxicity and hepatotoxicity, which obviously limit their development and use as a medicine.<sup>224</sup> Nevertheless, in a recently published patent,<sup>225</sup> scientists from Debiopharm claimed cyclic undecapeptide (*i.e.* CsA analogues) mPTP inhibitors, which displayed an enhanced anti-cell death activity with reduced cytotoxicity. Moreover, a research group from Novartis disclosed a patent in 2014, describing novel non-immunosuppressive cyclic peptides, with a reduced potential for causing adverse events.<sup>226</sup>

### 3.1.4.2. Small molecules as mPTP modulators

In light of the potential issues in developing a medicine based on cyclic peptides, efforts have also been made to identify small molecules as mPTP modulators. As such, scientists from Congenia reported in 2014<sup>227</sup> the structure-activity relationship of a series of substituted cinnamic anilides that represent a novel class of mPTP inhibitors. This description constituted a more detailed analysis of a set of cinnamic anilides that they patented in 2010.<sup>228</sup> In this communication, the 3-chloroanilide **3.6 (Figure 54)**, originating from a high-throughput screen, was optimised to deliver the more potent naphthyl derivative **3.7 (Figure 54)**. These cinnamic anilides inhibited mPTP opening in response to several stimuli, including calcium overload and oxidative stress. The optimised analogue **3.7** was more potent than CsA in a mitochondrial calcium retention capacity assay (CRC, see **Section 3.1.5, p. 150**, for more detail of this assay), which is a common method to measure mPTP opening. Additionally, the mPTP inhibitory effect of compound **3.7** was additive with that of CsA, suggesting that the molecular target of the cinnamic anilides was different from Cyp D.<sup>227</sup> Moreover, compound **3.7** was tested in an *in vivo* rabbit model of acute myocardial infarction and it showed to significantly limit reperfusion injury.<sup>227</sup>

However, a major limitation of the phenol derivative **3.7** was a sub-optimal pharmacokinetic profile, since after intravenous (IV) dosing in rabbit, compound was cleared very rapidly ( $t_{1/2} \sim 30$  min).<sup>227</sup> Nevertheless, a molecule from this chemical series, GNX-5086 (structure unknown), reportedly entered in 2013 a Phase I clinical trial to evaluate the safety, tolerability and pharmacokinetics of the compound in 33 healthy volunteers.<sup>229</sup> GNX-5086 is under development for the treatment of ischemic/reperfusion injury, and it also has potential in neurodegenerative disorders, including Alzheimer's disease.<sup>229</sup> Another analogue from this chemical series, which was demonstrated to be CNS penetrant, GNX-4728 (structure unknown), was shown to be therapeutic in a mouse model of ALS.<sup>230</sup> In this study, chronic treatment of G37R-human SOD1 transgenic mice with GNX-4728 displayed strong protection against several ALS symptoms. As such, mice survival was significantly extended, the number

of motor neurons were preserved and the integrity of neuromuscular junction was conserved. To further link these *in vivo* observations to mPTP inhibition, GNX-4728 was shown to increase mitochondrial CRC both *in vitro* and *in vivo*.<sup>230</sup>



<sup>a</sup>Compound **3.9** was only reported active in 1 out of 6 test occasions.

**Figure 54: Published small molecules claimed to be mPTP modulators, along with their liver CRC activity (when tested in our laboratories), MW, clogP and calculated PFI**

Using a phenotypic cell-based screening approach, the cholesterol-oxime TRO19622 (**3.8**, also called olesoxime, **Figure 54**) was shown to potently enhance motor neuron survival and growth in culture.<sup>231</sup> Additionally, TRO19622 was active *in vivo* in three animal models of motor neuron degeneration and was therefore considered as a potential treatment for ALS. In an attempt to identify its potential molecular target and

mechanism of action, TRO19622 was screened in several pharmacological experiments and was shown to bind two proteins of the outer mitochondrial membrane: VDAC and the mitochondrial translocator protein (TSPO). TSPO, formerly known as the peripheral benzodiazepine receptor, is believed to have a regulatory role in the mPTP, despite a limited amount of published data.<sup>232</sup> These findings raised the possibility that the neuroprotective effects might be exerted through inhibition of the mPTP opening. However, it was later found that TRO19622 was inactive in the CRC assay, and that it only modulated the mPTP when mPT was triggered by oxidative stress.<sup>233</sup> Therefore, TRO19622 appears not to be a direct mPTP inhibitor.<sup>234</sup> Regardless of its unclear mode of action, TRO19622 entered the clinic for the treatment of ALS, however, it failed to show a significant beneficial effect during a phase III trial conducted on 512 ALS patients.<sup>235</sup>

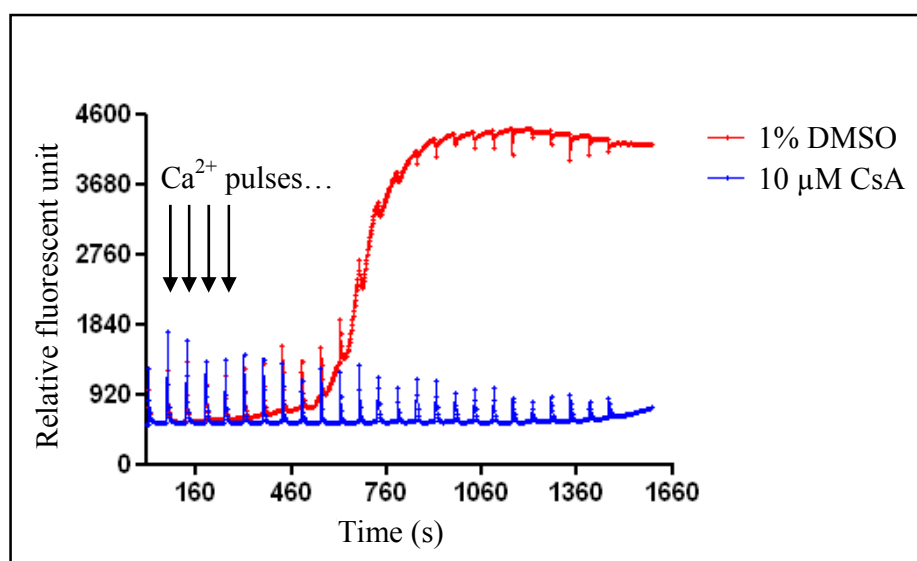
Furthermore, a set of oxime derivatives has been reported to block mPTP opening induced by amyloid- $\beta$ , using a cell-based assay measuring the change of mitochondrial membrane potential.<sup>236</sup> The compound optimisation culminated with the identification of compound **3.9 (Figure 54)**, which was also determined to have a good oral rat PK profile and the ability to enter the CNS.<sup>236</sup> However, when tested in the CRC assay available in our laboratories, compound **3.9** was only weakly active, suggesting that this compound is not a potent direct mPTP modulator. Additionally, its CLND solubility was measured in our laboratories to be less than 1  $\mu\text{g/mL}$ , which could be explained by its high lipophilicity and its subsequent high calculated Property Forecast Index (cPFI = 12.5, **Figure 54**). A subsequent communication disclosed, within the same chemical series, the modification of the oxime moiety into a triazole in order to improve compounds cytochrome P450 enzymes stability.<sup>237</sup> This SAR exercise concluded with the more potent and more metabolically stable triazole derivatives **3.10** and **3.11 (Figure 54)**.

Dimebon (**3.12**, also called latrepirdine, **Figure 54**) is a molecule which has been investigated in a Phase III clinical trial as a potential therapeutic for Alzheimer's disease, and it is believed that a component of its neuroprotective effect could be driven

by its ability to stabilise mitochondrial functions.<sup>238</sup> In an attempt to evaluate its capacity to modulate the mPTP, Dimebon was tested in several different mitochondrial CRC assays and in an amyloid- $\beta$ -induced mitochondrial toxicity assay.<sup>238</sup> From this investigation, the mode of action of Dimebon was ambiguous, since its influence on CRC was dependent on the mode of addition of  $\text{Ca}^{2+}$ . In the mitochondrial CRC assay available in our laboratories, Dimebon was inactive (liver CRC  $\text{pIC}_{50} < 4$ ).

### **3.1.5. *In vitro* assay supporting the identification of mPTP modulators: CRC assay<sup>239</sup>**

In order to measure their ability to modulate mPTP opening, the compounds synthesised in our laboratories were tested in a fluorescence-based assay using mitochondria freshly isolated from rat liver, in which mPTP opening was induced by repetitive addition of  $\text{Ca}^{2+}$ .<sup>240</sup> This assay relied on the role the mitochondria have in calcium homeostasis and in sequestering excess cytosolic  $\text{Ca}^{2+}$ . When the calcium retention capacity (CRC) of mitochondria is reached, opening of the mPTP occurs and the  $\text{Ca}^{2+}$  sequestered in the organelle is released, causing a large increase of the concentration of extra-mitochondrial  $\text{Ca}^{2+}$ . The CRC assay is a measure of a compound ability to protect mitochondrial function to sequester  $\text{Ca}^{2+}$  and to delay or prevent the mPTP opening. A mitochondrial-impermeant calcium fluorophore was used to detect extra-mitochondrial  $\text{Ca}^{2+}$  and was measured using a fluorescent imaging plate reader. The maximum inhibition of mPTP opening was defined with the use of 10  $\mu\text{M}$  CsA (**Figure 55**).



**Figure 55: Comparison of the effect of CsA (10  $\mu$ M) vs. vehicle (DMSO) in a calcium retention capacity (CRC) assay, using rat liver mitochondria**

The compounds of interest were tested at 11 different concentrations (from 0.1 mM to 1 nM, 11 points half-log serially diluted), and for each concentration, the area under the curve was measured and expressed as a percentage of the area under the curve when using 10  $\mu$ M CsA. Compounds  $pIC_{50}$  were then deduced from the plot of percentage of the maximum inhibition vs. concentration. The compounds active in the liver CRC assay were then progressed in a similar CRC assay, but now using mitochondria freshly isolated from rat brain. For the isoxazole and the cinnamide series discussed in this thesis, the liver and brain CRC  $pIC_{50}$  values were generally observed to be in good agreement.

It is worth highlighting that the liver CRC assay used to generate compounds SAR is a biological target-agnostic assay and that activity was measured by monitoring mitochondria function. Therefore, the liver CRC can again be regarded as a phenotypic assay, even if it is an organelle-based assay and not a cell-based assay. Previous efforts in our laboratories, prior to the author joining the research programme, had demonstrated that the phenotypic CRC assay was able to provide meaningful SAR for



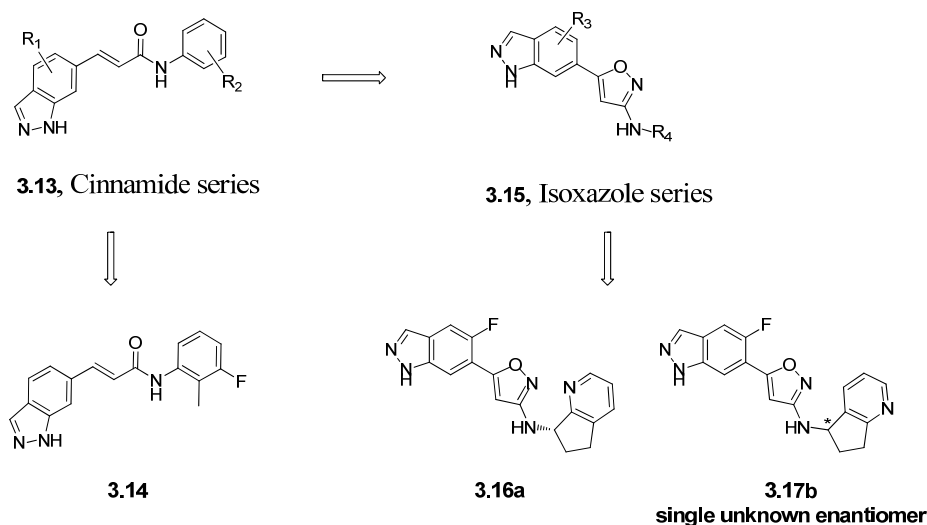
the chemical series investigated.<sup>241</sup> Thus, despite the precise molecular composition of the mPTP being unknown, the target is believed to be tractable using this phenotypic approach. Finally, the CRC assay could be routinely run in 384-well plates to provide sufficient throughput for screening up to 100 compounds in each assay.

### **3.2. Introduction to the mPTP medicinal chemistry programme and setting of the optimisation goals**

#### **3.2.1. Overall aim of the research programme and introduction to the cinnamide and the isoxazole series**

As previously discussed in **Section 3.1 (p. 137)**, there is now a robust body of evidence suggesting that modulating the mPTP has high therapeutic potential. Although CsA and other macrocyclic peptides have shown the benefit of modulating the mPTP, they have limitations as therapeutic agents, particularly in light of their selectivity profile. Regarding small molecule mPTP modulators, only a limited number of them has been demonstrated to be direct pore inhibitors. Additionally, considering the calculated PFI values shown in **Figure 54 (p. 148)**, most of the claimed mPTP small molecule modulators are highly lipophilic which could be a hurdle to their development as a medicine. Taking all these observations together, there is a pressing need to identify novel, selective, small molecule modulators of the mPTP, with physicochemical properties enabling their development as potential drug candidates.

Prior to the author commencing work on this area, a ligand-based design effort in our laboratories, based on previously described mPTP modulators, identified an indazole cinnamide template **3.13** as a hit series of mPTP modulators (**Figure 56**).<sup>241</sup>



**Figure 56: The cinnamide and the isoxazole series, along with their key exemplars**

The indazole ring of the cinnamide series was shown to be an important constituent of the pharmacophore and the right-hand side phenyl ring was demonstrated to tolerate substitution. Initial optimisation of the benzene delivered the 3-fluoro-2-methylbenzyl cinnamide **3.14** (Figure 56).<sup>241</sup>

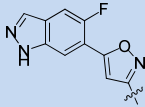
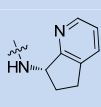
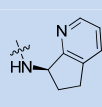
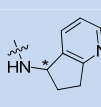
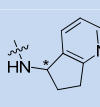
During the course of the optimisation of the cinnamide series, the  $\alpha,\beta$ -unsaturated amide was replaced with various 5-membered heteroaromatic rings and the isoxazole series **3.15** was identified as being one of the only potent isosteres. Further work to optimise the profile of the isoxazole series culminated in the identification of the cyclopentapyridyl analogues **3.16a** and **3.17b**<sup>x</sup> (Figure 56).<sup>241</sup>

<sup>x</sup>In this thesis, pairs of enantiomers will be named **a** and **b**, respectively, according to their order of elution on the chiral HPLC they have been analysed with, compound **a** being the first eluting enantiomer and compound **b** being the second eluting enantiomer.

### 3.2.1.1. Objectives for the isoxazole series

As stated above, isoxazole **3.16a** (Table 26) was identified before the author commencing work on this area as a lead molecule mPTP modulator.<sup>241</sup> It was a highly potent mPTP modulator (liver CRC pIC<sub>50</sub> = 7.7) and this compound was efficient from both a ligand and a ligand-lipophilicity perspective (0.42 and 0.38, respectively). However, compound **3.16a** contained four aromatic rings and displayed a measured PFI greater than 7 (PFI = 7.6), which were likely contributing to its low fasted state simulated intestinal fluid (FaSSIF) solubility of 6 µg/mL. The absolute stereochemistry of this compound was determined using the vibrational circular dichroism (VCD) spectroscopic technique and isoxazole **3.16a** was characterised as the (*S*)-enantiomer.<sup>242</sup> Its respective (*R*)-enantiomer **3.16b** (Table 26) was slightly less potent against mPTP (liver CRC pIC<sub>50</sub> = 6.6) and, accordingly, the progression of this enantiomer was paused.

The close isoxazole analogues **3.17a** and **3.17b** (Table 26), identified subsequently,<sup>241</sup> differed from isoxazole **3.16** by the position of the nitrogen in the cyclopentapyridyl ring. Compounds **3.17a** and **3.17b** were isolated using chiral preparative high-performance liquid chromatography (HPLC), however, their absolute stereochemistry was not determined. With a liver CRC pIC<sub>50</sub> of 7.3, isoxazole **3.17b** displayed relatively similar biological activity compared to **3.16a**, (pIC<sub>50</sub> = 7.7 for **3.16a**). Isoxazole **3.17b** was an attractive compound since it had a greater rat blood free fraction than compound **3.16a** (2.6% compared with 0.7%), and this could potentially imply that more compound would be available to interact with the biological target *in vivo*. The enantiomer **3.17b** was more potent than its counterpart **3.17a** (Table 26) in the liver CRC assay (liver CRC pIC<sub>50</sub> = 7.3 compared with 6.5) and as a result, the progression of compound **3.17a** was paused.

|  |  |  |  |  |
|---|---|---|---|---|
| <b>Compound</b>   | <b>3.16a</b>  | <b>3.16b</b>  | <b>3.17a</b>  | <b>3.17b</b>  |
| <b>Enantiomer identity</b>  | ( <i>S</i> )  | ( <i>R</i> )  | unknown,<br>first eluting   | unknown,<br>second eluting  |
| <b>Liver CRC pIC<sub>50</sub></b>   | 7.7 <sup>a</sup>  | 6.6   | 6.5   | 7.3   |
| <b>Brain CRC pIC<sub>50</sub></b>   | 7.3 <sup>b</sup>  | 6.5   | 6.6   | 7   |
| <b>LE / LLE<sup>xi</sup></b>  | 0.42 / 0.38   | 0.36 / 0.32   | 0.35 / 0.31   | 0.40 / 0.35   |
| <b>MW</b>   | 335   | 335   | 335   | 335   |
| <b>clogP</b>  | 2.8   | 2.8   | 2.8   | 2.8   |
| <b>Chrom logD<sup>xii</sup> / PFI</b>   | 3.6 / 7.6   | 3.7 / 7.7   | 3.1 / 7.1   | 3.2 / 7.2   |
| <b>CLND (µg/mL)</b>   | 5 <sup>c</sup>  | 6   | 1   | 5   |
| <b>FaSSIF (µg/mL)<sup>xii</sup></b>   | 6   | 17  | 4   | 5 <sup>d</sup>  |
| <b>h IVC (mL/min/g)<sup>xii</sup></b>   | 1.2   | 1.2   | 1.5   | 1.6   |
| <b>r IVC (mL/min/g)<sup>xii</sup></b>   | 1.6   | 5.5   | 3.2   | 7.2   |
| <b>m IVC (mL/min/g)<sup>xii</sup></b>   | 4.3   | 8.6   | 4.7   | 3.6   |
| <b>Fu,bl<sup>xii</sup></b>  | 0.7%  | < 0.5%  | 2.7%  | 2.6%  |

<sup>a</sup>Compound was only reported with a measured pIC<sub>50</sub> value in 43 out of 49 test occasions and for the other 6 test occasions, pIC<sub>50</sub> was greater than 9; <sup>b</sup>Compound was only reported with a measured pIC<sub>50</sub> value in 31 out of 32 test occasions and for the other 1 test occasion, pIC<sub>50</sub> was greater than 9; <sup>c</sup>Compound was only reported with a measured CLND value in 5 out of 6 test occasions and for the other 1 test occasion, CLND was less than 1 µg/mL; <sup>d</sup>Compound was only reported with a measured FaSSIF value in 1 out of the 2 test occasions and for the other 1 test occasion, FaSSIF was less than 1 µg/mL.

**Table 26: Profile of isoxazoles 3.16a, 3.16b, 3.17a and 3.17b<sup>241</sup>**

<sup>xi</sup>In all the compounds profile tables of this chapter (for the mPTP programme), LE and LLE are calculated with the liver CRC pIC<sub>50</sub> values, which was the primary assay of the mPTP programme.

<sup>xii</sup>In all the compounds profile tables of this thesis, Chrom logD refers to Chrom logD<sub>7.4</sub>; FaSSIF refers to FaSSIF solubility; h IVC refers to human microsomes *in vitro* clearance; r IVC refers to rat microsomes *in vitro* clearance; m IVC refers to mouse microsomes *in vitro* clearance; Fu,bl refers to fraction unbound in rat blood.

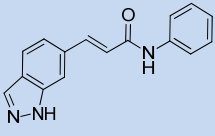
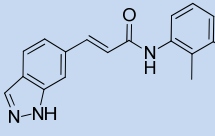
Overall, the profiles of isoxazoles **3.16a** and **3.17b** made them potential candidates for *in vivo* PK/PD animal experiments. These data would indeed help understanding the level of mPTP target engagement required to see *in vivo* efficacy. However, accounting for the significant efforts these assays involved, only one compound could be submitted for this animal work, and it remained to be determined which one of these two isoxazoles presented the most optimal profile. Mouse *in vivo* PK data had already been generated for isoxazole **3.16a** and it displayed a desirable blood exposure after oral administration<sup>241</sup> (these data are described later in **Section 3.3.1.4, p. 183**). However, no *in vivo* PK data were available for compound **3.17b** and consequently, the profile of the two compounds could not be suitably compared. Moreover, the absolute configuration of **3.17b** was unknown and was required to be determined, as this structural information would be necessary in case the compound was to be progressed further within our medicinal chemistry programme.

Therefore, the first objective of the present work (**Section 3.3, p. 161**) was to investigate the synthetic route to compound **3.17b** in order to deliver enough material for the *in vivo* PK enabling studies and to determine its absolute configuration. This information would help determining which molecule from the isoxazole series, between **3.16a** and **3.17b**, would be progressed into *in vivo* PK/PD studies. Then, 100 g of material of the chosen molecule for the animal studies would be required and the objective was to provide the synthetic support to efficiently facilitate this large scale synthesis.

### 3.2.1.2. Objectives for the cinnamide series

The cinnamide series was less advanced than the isoxazole series at the time the author commenced work on the programme, and the initial hit molecule **3.18** (**Table 27**) was identified prior to the author commencing work on this area.<sup>241</sup> This compound was characterised by moderate potency in the liver CRC assay ( $pIC_{50} = 6.5$ ), low molecular weight (MW = 263), attractive ligand efficiency measures (LE and LLE > 0.3) and sub-optimal aqueous solubility (CLND solubility = 37  $\mu\text{g/mL}$ ). These features rendered this

compound an ideal starting point for a lead optimisation effort. The microsomal clearance of compound **3.18** displayed large species differences, with a moderate microsomal clearance in human of 2.3 mL/min/g and a high microsomal clearance in mouse of 42.8 mL/min/g. The fraction unbound of compound **3.18** in rat blood was moderate ( $F_{u,bl} = 1.3\%$ ).

| Structure                         |  |  |
|-----------------------------------|---|---|
| <b>Compound</b>                   | <b>3.18</b>   | <b>3.14</b>   |
| <b>Liver CRC pIC<sub>50</sub></b> | 6.5   | 8.1 <sup>a</sup>  |
| <b>Brain CRC pIC<sub>50</sub></b> | 6 <sup>b</sup>  | 7.9   |
| <b>LE / LLE</b>                   | 0.44 / 0.34   | 0.50 / 0.40   |
| <b>MW</b>                         | 263   | 295   |
| <b>clogP</b>                      | 3.1   | 3.4   |
| <b>Chrom logD / PFI</b>           | 3.6 / 6.6   | 4.1 / 7.1   |
| <b>CLND (µg/mL)</b>               | 37  | 4   |
| <b>FaSSIF (µg/mL)</b>             | ND  | 5   |
| <b>h IVC (mL/min/g)</b>           | 2.3   | 1.7   |
| <b>r IVC (mL/min/g)</b>           | 9.2   | 4.4   |
| <b>m IVC (mL/min/g)</b>           | 42.8  | 5.9   |
| <b>Fu,bl</b>                      | 1.3%  | 2.6%  |

<sup>a</sup>Compound was only reported with a measured pIC<sub>50</sub> value in 8 out of 13 test occasions and for the other 5 test occasions, pIC<sub>50</sub> was greater than 9; <sup>b</sup>Compound was only reported with a measured pIC<sub>50</sub> value in 5 out of 6 test occasions and for the other 1 test occasion, the assay failed to generate a pIC<sub>50</sub> value.

**Table 27: Profile of the initial cinnamide hit compound **3.18** and the more potent 3-fluoro-2-methylbenzyl analogue **3.14**<sup>241</sup>**

In an attempt to develop a structure-activity relationship, several substituents on the benzene were investigated, which resulted in the identification of the 3-fluoro-2-methylbenzyl cinnamide **3.14**,<sup>241</sup> displaying higher CRC pIC<sub>50</sub> in both liver and brain CRC assays (pIC<sub>50</sub> = 8.1 and 7.9, respectively, **Table 27**). However, this increase in mPTP activity was achieved while also increasing the compound lipophilicity, which was reflected by a higher PFI for compound **3.14** compared with the hit cinnamide **3.18** (PFI = 7.1 compared with PFI = 6.6). As a result, the aqueous solubility of compound **3.14** was lower than the solubility of compound **3.18** (CLND solubility = 4 µg/mL compared with CLND solubility = 37 µg/mL). Furthermore, the introduction of the methyl group and the fluorine on the benzene led to a decrease in microsomal clearance, especially in mouse where the clearance was reduced from 42.8 mL/min/g for cinnamide **3.18** to 5.9 mL/min/g for compound **3.14** (**Table 27**). This observation could be explained by the fact these substituents potentially blocked some metabolic soft spots of the phenyl ring.<sup>243,244</sup>

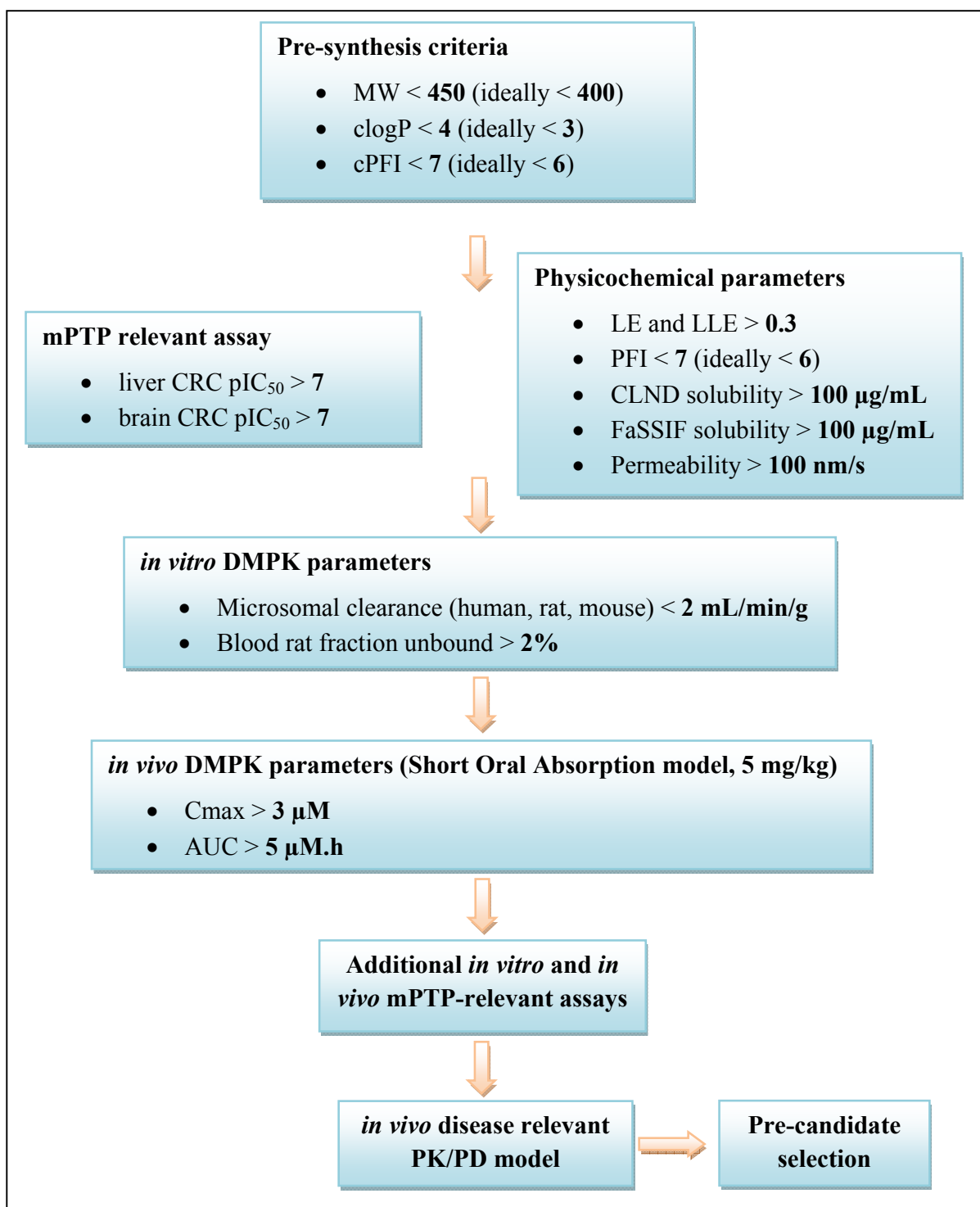
The objective for the cinnamide series in this thesis was to deliver potential candidate molecules for PK/PD animal experiments, however, these compounds needed to have a superior profile compared with the isoxazole molecules. In particular, it was required for this second generation of compounds to have an increased aqueous solubility over the isoxazole series. To satisfy the requirements of an animal PK/PD study, the new cinnamide analogues also needed to have good level of systemic exposure *in vivo*. Therefore, the second objective of this study (**Section 3.4, p. 199**) was to develop the medicinal chemistry of the cinnamide series towards the identification of mPTP modulators, with a differentiated profile compared with the lead isoxazoles. The targeted profile for the novel cinnamide analogues is described in the next section.

### 3.2.2. Screening approaches and pre-candidate profile criteria

In order to design mPTP modulators with the best chance of displaying the required profile to be considered as a drug candidate, the guidelines described in **Figure 57** were generated for compound progression. It is important to mention that the values shown in **Figure 57** were not considered as hard cut-offs for our programme (*i.e.* automatically preventing compounds to be progressed to the downstream assays), however, they were guidelines to help the design and optimisation process.

Prior to compound synthesis, several physicochemical properties were calculated, especially to maintain control of compound lipophilicity. In the current understanding of the pharmacology of the mPTP, a pIC<sub>50</sub> of 7 or above in the rat liver CRC assay was preferred as a potency objective. With regard to physicochemical parameters, a PFI less than 7 and a solubility greater than 100 µg/mL in both the chemi-luminescence nitrogen detection (CLND) and in the fasted state simulated intestinal fluid (FaSSIF) assays were targeted. It is worth mentioning that the CLND assay is a kinetic solubility measurement from compound dissolved in DMSO and that the FaSSIF solubility is a thermodynamic solubility measurement from compound as solids. The *in vitro* microsomal clearance was tested in both human, rat and mouse. The propensity of the compounds to bind to other proteins and lipids in plasma was assessed by determining the fraction unbound in rat blood. Before progressing compounds to additional *in vitro* and *in vivo* mPTP-relevant assays, they were screened in a mouse PK experiment to assess their level of exposure in blood after oral administration. The *in vivo* PK experiments routinely used in our laboratories is further described on **p. 184**.





**Figure 57: Screening approaches for selection of mPTP modulators**

### 3.3. Results and discussion: Synthetic chemistry work on the isoxazole series

#### 3.3.1. Optimisation of the synthetic route to isoxazole 3.17b

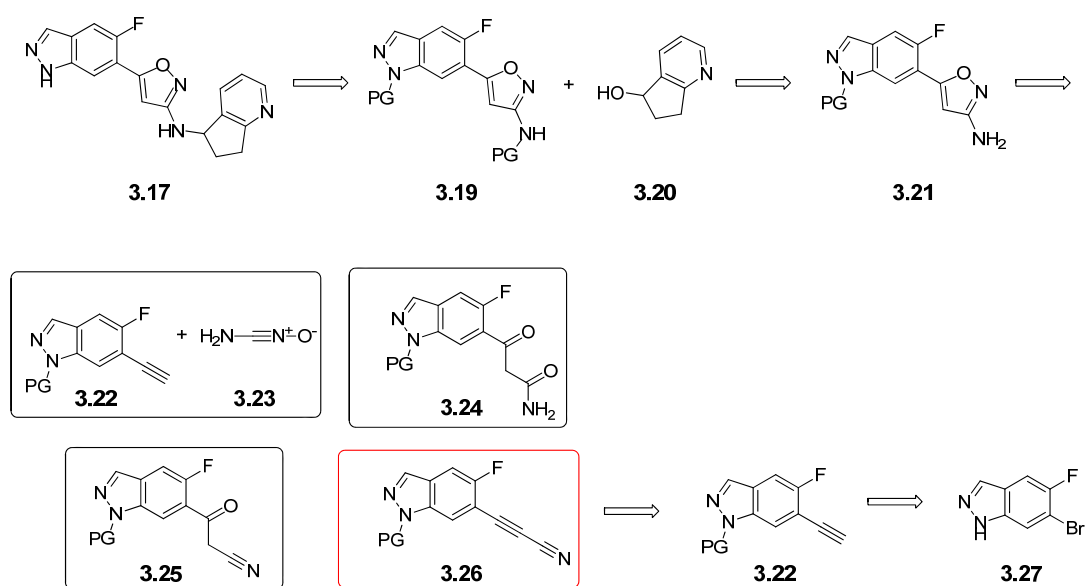
##### 3.3.1.1. Strategy devised in order to optimise the synthesis of 3.17b

As intimated previously, the initial objectives which were needed to be fulfilled for the isoxazole series were to:

- Remake 100 mg of compound **3.17b** (Table 26, p. 155), with an enantiomeric excess greater than 99%, for progression in an oral *in vivo* PK study. The data from this study will then be compared with the already available *in vivo* PK profile from **3.16a**.
- Determine the absolute stereochemistry of **3.17b**.
- Identify an enantiospecific route to access **3.17b**, which would be more desirable in the event of an increased interest in compound **3.17b**, since a significantly larger scale synthesis would then be required in order to meet the needs of downstream biological profiling.

Despite the fact that the design of the synthetic route to access isoxazole **3.17** had been achieved prior to the author commencing work on this area,<sup>241</sup> it was deemed necessary to review the retrosynthetic approach to isoxazole **3.17**, to potentially improve the efficiency of the synthesis in order to access the quantity of compound needed. Thus, the first step of the retrosynthetic analysis of compound **3.17** (Figure 58) involved the disconnection of the bond linking the aminoisoxazole moiety to the cyclopentapyridyl ring. Since cyclopenta[*b*]pyridin-5-ol **3.20** was commercially available, a nucleophilic displacement involving the aminoisoxazole intermediate **3.19** as a nucleophile was envisaged. For the second step of the retrosynthetic analysis, several transformations were considered in order to form the aminoisoxazole analogue **3.21**. Firstly, the aminoisoxazole ring could be formed by a dipolar cycloaddition of the cyanamide oxide

**3.23** with the alkyne-indazole **3.22**. However, synthesising the cyanamide oxide **3.23** appeared to be unprecedented, hence this approach was discarded. Secondly, a reaction between the keto-amide analogue **3.24** and hydroxylamine could lead to the targeted isoxazole **3.21**, but again literature analysis revealed this route to be poorly preceded and therefore this option was abandoned. Finally, the last two possibilities involved the reaction of hydroxylamine with either the keto-propanamide intermediate **3.25** or with the propiolonitrile derivative **3.26**. However, a group from Amgen attempted these two synthetic routes on an isoquinoline template<sup>245</sup> and the overall yield of the isoxazole formation using the propiolonitrile route was higher. This last option to form the aminoisoxazole moiety was therefore prioritised over the alternative possibilities.

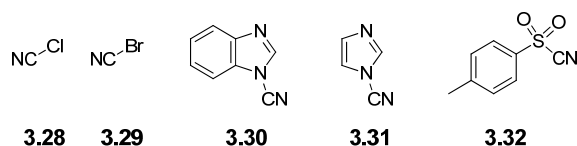


**Figure 58: Retrosynthetic analysis of compound 3.17**

In order to form the propiolonitrile indazole derivative **3.26**, a nucleophilic attack of the alkyne-indazole **3.22** on an electrophilic cyanating agent was considered (**Figure 58**). It is worth mentioning that several electrophilic cyanating agents were envisaged, such as cyanogen chloride **3.28**, cyanogen bromide **3.29**, 1-cyanobenzimidazole **3.30**, 1-cyanoimidazole<sup>246</sup> **3.31** and *p*-toluenesulfonyl cyanide **3.32** (**Figure 59**). However,

cyanogen chloride **3.28**, cyanogen bromide **3.29** and 1-cyanobenzimidazole **3.30** are highly toxic, whereas 1-cyanoimidazole **3.31** and *p*-toluenesulfonyl cyanide **3.32** are less hazardous. Furthermore, *p*-toluenesulfonyl cyanide **3.32** appears to be more widely used, since for instance it has been described for the  $\alpha$ -cyanation of 1,3-dicarbonyl compounds,<sup>247</sup> the preparation of aryl nitriles<sup>248</sup> and the synthesis of polyfunctional nitriles from functionalised organozinc halides.<sup>249</sup> For that reason, *p*-toluenesulfonyl cyanide **3.32** was prioritised as an electrophilic cyanating agent.

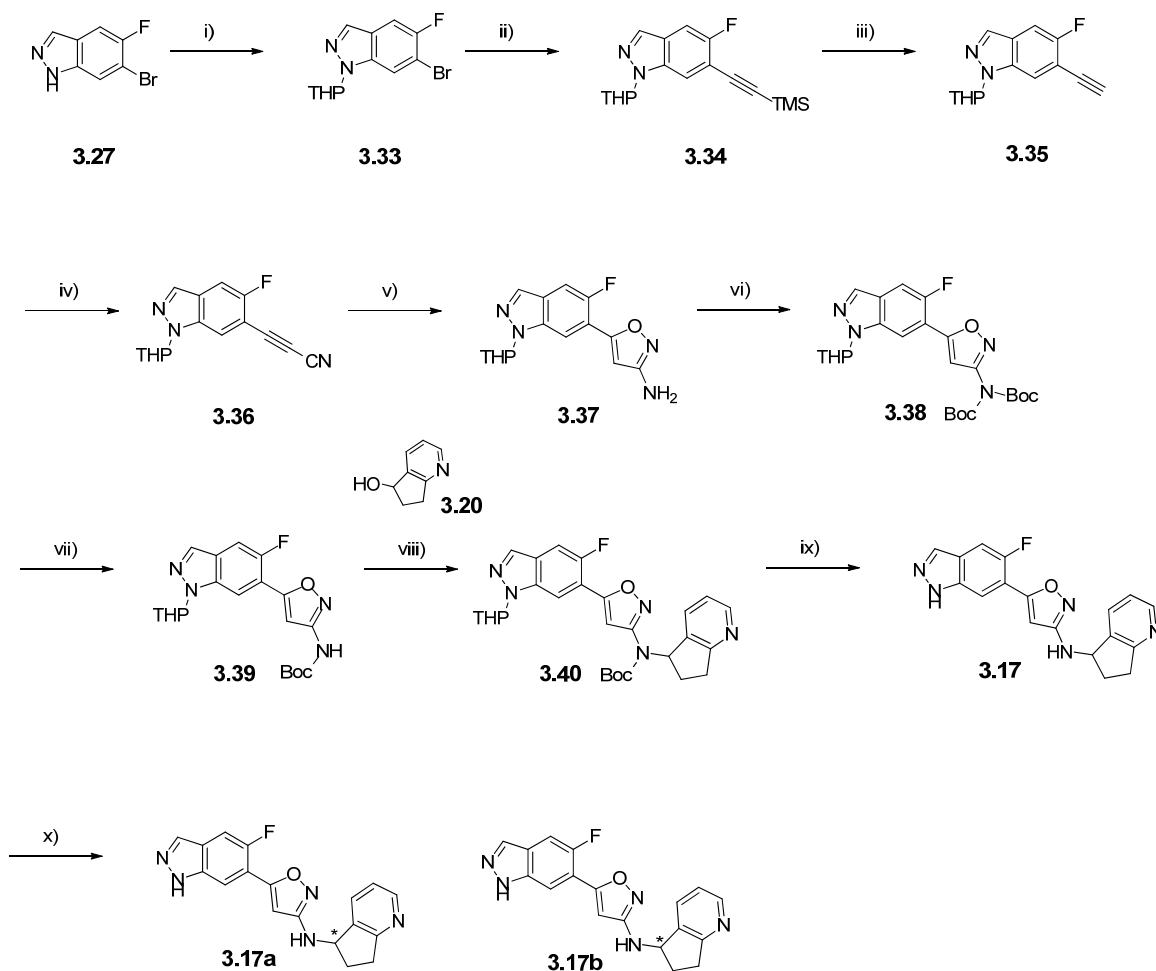
Finally, the alkyne moiety would be introduced onto the indazole ring *via* a Sonogashira coupling from the commercially available 6-bromo-5-fluoro-1*H*-indazole **3.27** (**Figure 58**).



**Figure 59: Various electrophilic cyanating agents**

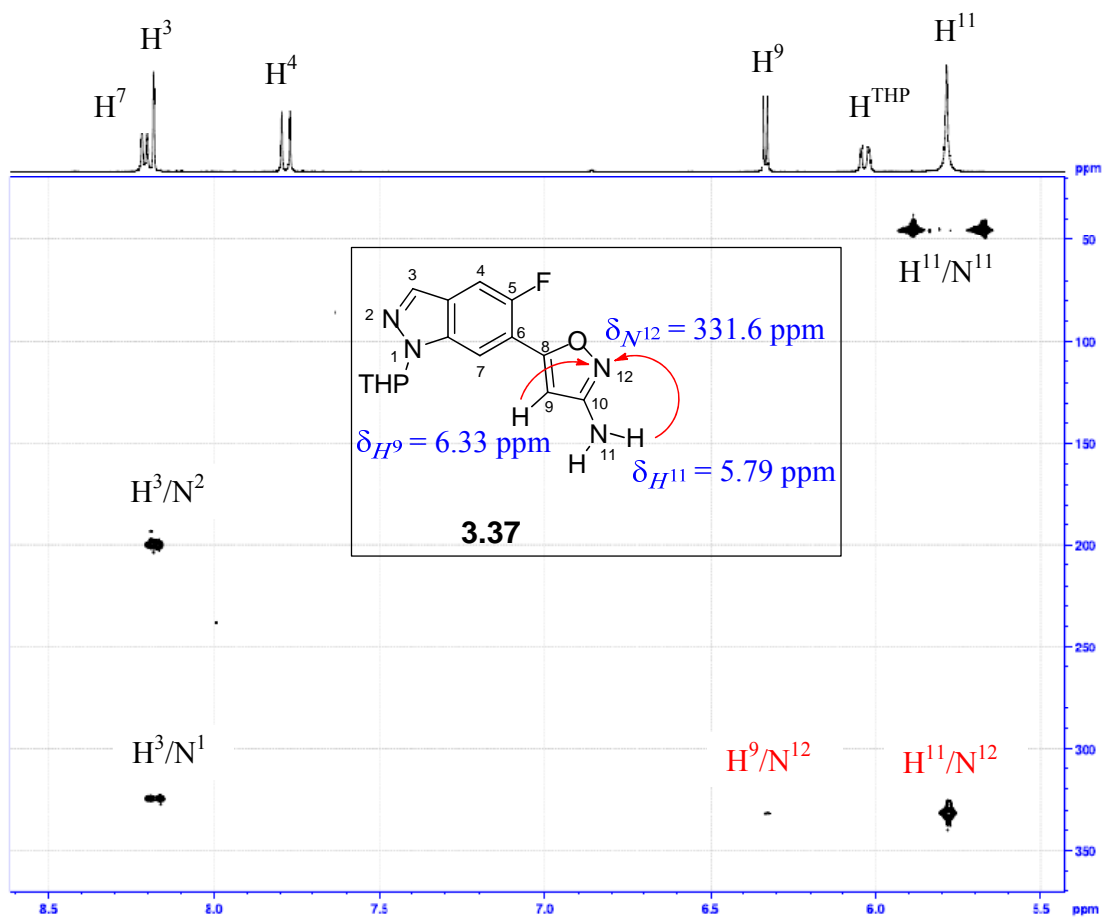
Thus, the racemic synthetic route to access the two isoxazole enantiomer analogues **3.17a** and **3.17b** (**Scheme 18**) started from the commercially available 6-bromo-5-fluoro-1*H*-indazole **3.27** which was firstly protected using a tetrahydropyranyl (THP) group. A Sonogashira coupling then provided the trimethylsilane protected alkyne analogue **3.34**, which was followed by a selective deprotection using tetrabutylammonium fluoride to afford the free alkyne **3.35**. A cyanation reaction using *p*-toluenesulfonyl cyanide **3.32** yielded the propiolonitrile analogue **3.36**, which upon treatment with hydroxylamine hydrochloride allowed the formation of the aminoisoxazole analogue **3.37**. The regiochemistry of the isoxazole ring formation was confirmed by  $^1H/^{15}N$  HMBC NMR experiments (**Figure 60**): a correlation between the isoxazole proton ( $\delta_{H^9} = 6.33$  ppm) and the isoxazole nitrogen ( $\delta_{N^{12}} = 331.6$  ppm) was observed, and a correlation between this same isoxazole nitrogen and the  $NH_2$  protons ( $\delta_{H^{11}} = 5.79$  ppm) was also observed.

The rest of the synthetic route was carried out elsewhere in our laboratories<sup>250,251,252</sup> and a two step process enabled to access the mono Boc-protected aminoisoxazole **3.39**. A Mitsunobu reaction using the racemic 6,7-dihydro-5*H*-cyclopenta[*b*]pyridin-5-ol **3.20** yielded the intermediate **3.40**, which was followed by concomitant deprotection of the THP and the Boc protecting groups under acidic conditions in order to afford the racemic targeted isoxazole **3.17**. A final preparative chiral HPLC separation delivered the single isoxazole enantiomers **3.17a** and **3.17b**, with an undetermined absolute stereochemistry. It is worth mentioning that due to issues with solubility in the loading solvent (EtOH) for the HPLC separation, the recovery after the chiral preparative HPLC was low (21%). As a result, only a small amount of **3.17b** was isolated and was fully consumed in order to generate its initial biological profile.



i) 3,4-dihydro-2H-pyran (2.5 eq), pyridinium *p*-toluenesulfonate (0.1 eq), 2-MeTHF, 85 °C, **93%**; ii) ethynyltrimethylsilane (2 eq), copper(I) iodide (0.15 eq), bis(triphenylphosphine)palladium(II) chloride (0.15 eq), triethylamine (20 eq), 75 °C, **98%**; iii) 1 M tetrabutylammonium fluoride in THF (1.05 eq), THF, 0 °C, **89%**; iv) 1.6 M *n*-butyllithium in hexane (1.4 eq), *p*-toluenesulfonyl cyanide **3.32** (1.1 eq), THF, -78 °C, **70%**; v) hydroxylamine hydrochloride (1.5 eq), 1 M aqueous NaOH (2.5 eq), THF:EtOH = 4:1, rt, **71%**; vi) di-*tert*-butyl dicarbonate (2 eq), triethylamine (1.5 eq), *N,N*-dimethylpyridin-4-amine (0.1 eq), 2-MeTHF, rt, **77%**;<sup>250</sup> vii) 1 M aqueous NaOH (1 eq), MeOH, rt, **99%**;<sup>250</sup> viii) racemic 6,7-dihydro-5H-cyclopenta[*b*]pyridin-5-ol (2 eq), triphenylphosphine (3 eq), diisopropyl azodicarboxylate (DIAD, 3 eq), THF, rt, **80%**;<sup>251</sup> ix) 3 M HCl in MeOH (6 eq), EtOH, 50 °C to 70 °C, **82%**;<sup>251</sup> x) Preparative chiral HPLC, **8%** and **13%**, respectively, for **3.17a** and **3.17b**, overall recovery of the preparative chiral HPLC = **21%**.<sup>252</sup>

**Scheme 18: Initial racemic synthetic route to access isoxazoles 3.17a and 3.17b**



**Figure 60:**  $^1\text{H}/^{15}\text{N}$  HMBC NMR correlations confirming the regiochemistry of the isoxazole formation of compound 3.37

In order to fulfil the objectives discussed in p. 161, several options were considered:

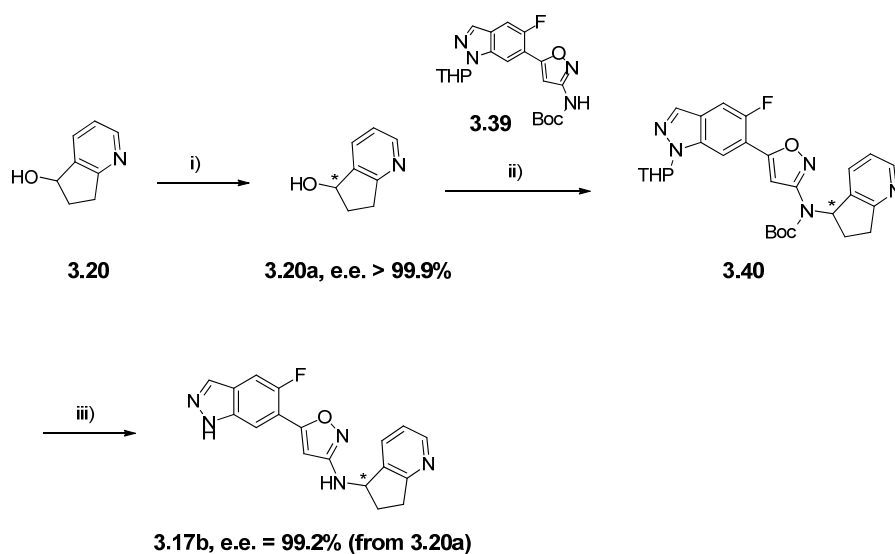
- **Option 1:** Repeat the same synthetic route shown in **Scheme 18**, *i.e.* racemic route with a chiral HPLC separation of the two enantiomers at the end of the synthesis. This option was not attractive since the practical aspect of the separation was limited by the low solubility of the racemic mixture **3.17** in the loading solvent (EtOH) of the HPLC, thus restricting the quantity of compound that can be applied to the chiral column. For the quantity required to be prepared, that would necessitate a very large number of HPLC runs. Hence, this option was discarded at the outset of this study.
- **Option 2:** Investigate the solubility of the commercially available racemic alcohol **3.20** and envisage carrying out a chiral preparative HPLC on this racemic mixture. This would deliver the two pure enantiomers cyclopentapyridyl alcohol **3.20a** and **3.20b** for use in the following Mitsunobu step. Assuming that the Mitsunobu reaction, which would occur with inversion of configuration at the position of the alcohol, and that the last deprotection step would retain the enantiomeric purity of the system, then compounds **3.17a** and **3.17b** would be obtained with high enantiomeric excess (e.e.).
- **Option 3:** Identify an enantioselective route, in order to deliver **3.17b** with an enantiomeric excess greater than 99%. This last option was deemed to be the most efficient and the most attractive, but also probably the most challenging.

Considering all the information discussed above, options 2 and option 3 were investigated concomitantly.



### 3.3.1.2. Exploration of the synthetic option 2

It was quickly noticed that the solubility of 6,7-dihydro-5*H*-cyclopenta[*b*]pyridin-5-ol **3.20** in the chiral preparative HPLC loading solvent (EtOH) was much higher than that of the final isoxazole **3.17**, and therefore separating the mixture of enantiomers **3.20** on a larger scale was considered to be more practical. Thus, the chiral preparative HPLC separation of the racemic mixture of alcohols **3.20** delivered the first eluting enantiomer **3.20a** with an enantiomeric excess greater than 99.9% and the second eluting enantiomer **3.20b** with an enantiomeric excess of 99.8%. The single enantiomer **3.20a** was chosen arbitrarily to proceed with the synthesis (**Scheme 19**). From **3.20a**, a Mitsunobu reaction using the mono Boc-protected aminoisoxazole **3.39** (synthesised according to **Scheme 18, p. 165**) afforded isoxazole **3.40** in 67% yield. Acidic treatment of intermediate **3.40** cleaved concomitantly the Boc and the THP protecting groups, yielding the single enantiomer **3.17b**. The enantiomeric purity of the isoxazole obtained above was confirmed by chiral HPLC and an enantiomeric excess of 99.2% was obtained. In the chiral HPLC, the final compound obtained in **Scheme 19** was the second running enantiomer, which was in fact the enantiomer **3.17b** which was required to be synthesised.

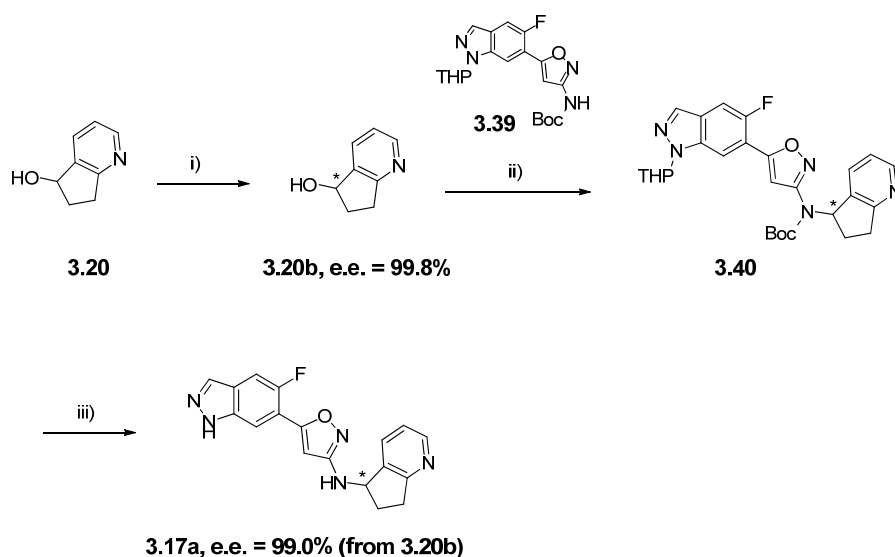


i) Preparative chiral HPLC, **31%**, overall recovery of the preparative chiral HPLC = **51%**,<sup>252</sup> ii) *tert*-butyl (5-(5-fluoro-1-(tetrahydro-2*H*-pyran-2-yl)-1*H*-indazol-6-yl)isoxazol-3-yl)carbamate **3.39** (1 eq), 6,7-dihydro-5*H*-cyclopenta[*b*]pyridin-5-ol **3.20a** (1.2 eq), triphenylphosphine (2 eq), DIAD (2 eq), THF, rt, **67%**; iii) 3 M HCl in MeOH (15 eq), EtOH, 50 °C to 60 °C, **75%**.

#### Scheme 19: Synthetic route to compound **3.17b** via chiral separation of alcohol **3.20a**

An important observation from this synthetic route was that the chiral purity of the system was essentially retained during the Mitsunobu and the final deprotection steps. Indeed, the erosion in enantiomeric excess between the starting alcohol and the final product was negligible, going from an enantiomeric excess greater than 99.9% for **3.20a** to an enantiomeric excess of 99.2% for **3.17b**.

A sufficient quantity of compound **3.17b** (123 mg) for the *in vivo* PK studies with an enantiomeric excess greater than 99% was obtained with the above route, which completed our first resynthesis objective. However, in order to determine the absolute configuration of **3.17b**, it was required to synthesise the other enantiomer **3.17a**. Hence, a similar synthetic route, but now commencing with the other chiral alcohol **3.20b**, delivered the single enantiomer **3.17a** with an enantiomeric excess of 99% (**Scheme 20**).



i) Preparative chiral HPLC, **20%**, overall recovery of the preparative chiral HPLC = **51%**,<sup>252</sup> ii) *tert*-butyl (5-(5-fluoro-1-(tetrahydro-2*H*-pyran-2-yl)-1*H*-indazol-6-yl)isoxazol-3-yl)carbamate **3.39** (1 eq); 6,7-dihydro-5*H*-cyclopenta[*b*]pyridin-5-ol **3.20b** (1.2 eq); triphenylphosphine (2 eq), DIAD (2 eq), THF, rt, **55%**; iii) 3 M HCl in MeOH (20 eq), EtOH, 50 °C to 70 °C, **78%**.

**Scheme 20: Synthetic route to compound 3.17a via chiral separation of alcohol 3.20b**

Several methods are available in order to determine the absolute configuration of chiral molecules, such as X-ray crystallography and the NMR Mosher's method. However, the recently developed VCD technique offers the advantage of not needing to grow single crystals, nor the requirement of molecular derivatisation. VCD is a spectroscopic measure, and is defined as the difference in the absorbance of a chiral molecule for left circularly polarised *vs.* right circularly polarised infrared (IR) radiation during vibrational excitation.<sup>253</sup> The IR spectrum of a pair of enantiomers is identical, however, their VCD spectra are equal in intensity but opposite in sign (mirror images of each other). Additionally, the VCD spectrum of a molecule can be calculated using an *ab initio* density functional theory method. Hence, the absolute configuration of a chiral molecule can be unambiguously determined by comparing its measured VCD spectrum with its calculated spectrum. Recently, the use of the VCD technique has increased dramatically and its basic principles and its application in order to determine the

absolute stereochemistry of small organic molecules, pharmaceutical molecules and natural products have been reviewed in the literature.<sup>253</sup>

Considering its simplicity of use, the VCD technique was employed by another member of our laboratories<sup>242</sup> to determine the absolute configuration of the two enantiomers **3.17a** and **3.17b** (full results are described in the **Appendices section 5.2, p. 372**). Firstly, the theoretical IR and VCD spectra of the (*S*)-enantiomer of isoxazole **3.17** were calculated. Secondly, the IR and VCD spectra of compounds **3.17a** and **3.17b** were experimentally measured and the frequency range 2400 - 800 cm<sup>-1</sup> was compared with the calculated spectrum of the (*S*)-enantiomer of isoxazole **3.17**. The VCD spectrum of isoxazole **3.17b** was largely coincident with the model VCD spectrum of the (*S*)-enantiomer of isoxazole **3.17** (**Figure 61**, top frame), whereas the VCD spectrum of **3.17a** was largely its mirror image (**Figure 62**, top frame). These results were consistent with compound **3.17b** having the same absolute configuration as the model and **3.17a** having the opposite configuration to the model. Consequently, the enantiomer **3.17b** was assigned with (*S*)-configuration and the enantiomer **3.17a** was assigned with (*R*)-configuration (both with a confidence limit greater than 97%).

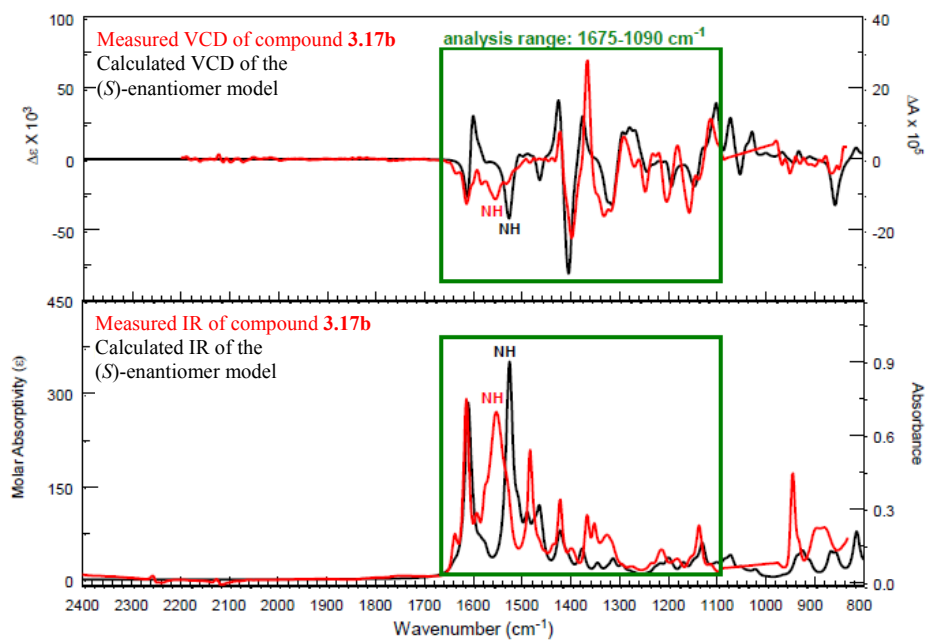


Figure 61: VCD spectra of compound 3.17b and (*S*)-enantiomer model (top frame); IR spectra of compound 3.17b and (*S*)-enantiomer model (bottom frame)<sup>242</sup>

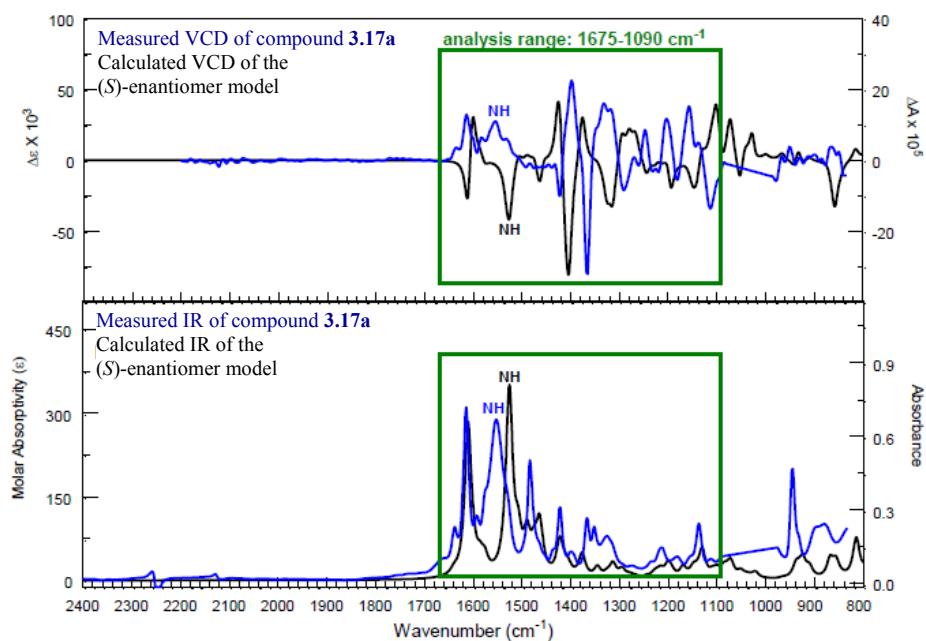
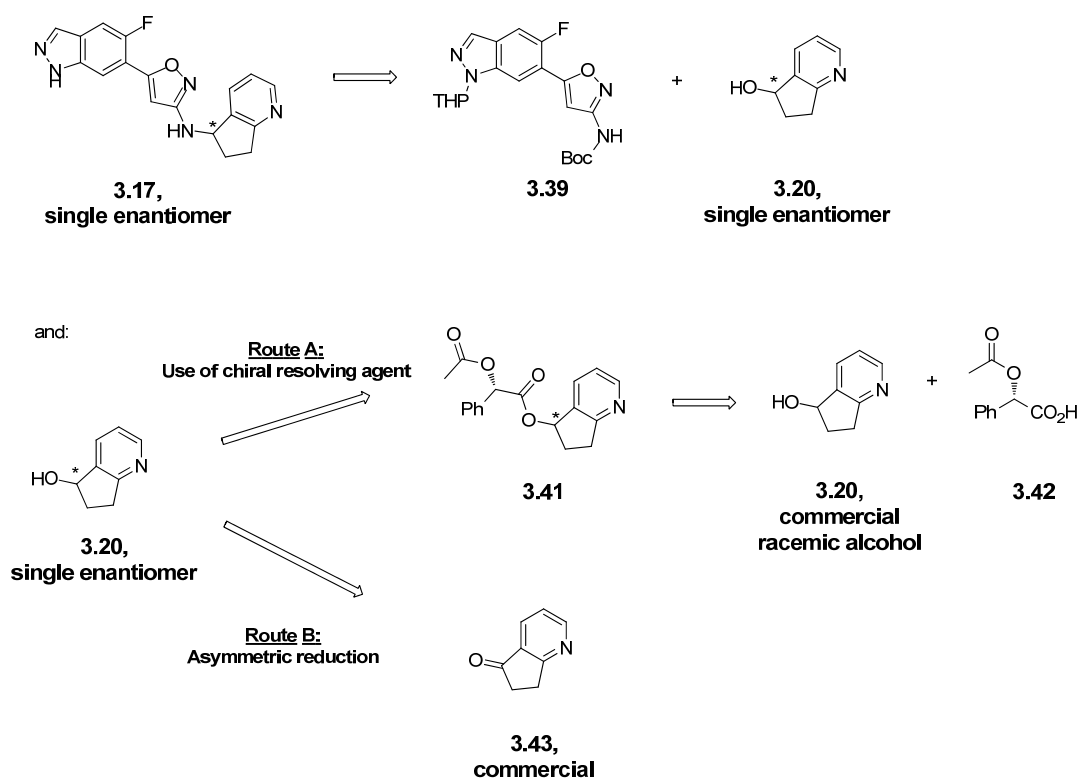


Figure 62: VCD spectra of compound 3.17a and (*S*)-enantiomer model (top frame); IR spectra of compound 3.17a and (*S*)-enantiomer model (bottom frame)<sup>242</sup>

### 3.3.1.3. Exploration of the synthetic option 3

Concomitantly to the work described in the previous section, efforts were made to identify an enantioselective route to deliver **3.17b**. In order to achieve this objective, two separate strategies were considered (**Figure 63**).

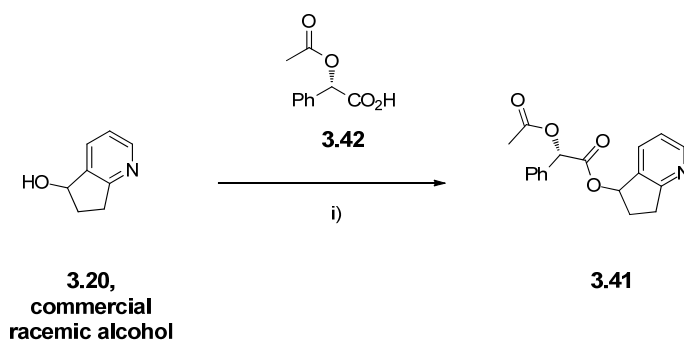


**Figure 63: Strategies envisaged in order to access the single enantiomer versions of compound 3.17**

In this enantioselective synthetic approach, a single enantiomer of **3.17** would be formed by Mitsunobu reaction of the aminoisoxazole **3.39** with the enantiomerically pure cyclopentapyridyl alcohol **3.20** and subsequent deprotection of the Boc and THP protecting groups. This strategy relied on the Mitsunobu and deprotection steps to retain the enantiomeric purity of the system, which had been demonstrated in the previous section. The pivotal factor of this synthetic route was to form the alcohol **3.20** in its

enantiomerically pure form. Two different approaches were considered to achieve this objective. Firstly, an indirect method described in route A (**Figure 63**) would rely on the resolution of the pair of enantiomers **3.20** by reacting them with an optically pure chiral reagent in order to form two diastereoisomers. The physicochemical properties difference of the two diastereoisomers could allow their separation either by chromatography utilising conventional achiral stationary phase columns or by crystallisation. As an example here, the commercial racemic alcohol **3.20** could be reacted with the chiral (*S*)-(+)-*O*-acetylmandelic acid **3.42** in order to form a mixture of two diastereomeric esters **3.41**. The subsequent ester hydrolysis of the separated diastereoisomers will give single enantiomers of the alcohol **3.20**. Secondly, a direct method illustrated in route B (**Figure 63**) would rely on an enantioselective reduction of the cyclopentapyridin-5-one **3.43** in order to afford a single enantiomer of the alcohol **3.20**. Both routes A and B were investigated.

The indirect method of using chiral derivatising agents in order to separate the enantiomers from a racemic mixture<sup>254</sup> has been mainly described for the optical resolution of amino acids.<sup>255,256</sup> There is a wide choice of potential chiral derivatising agents, however, since it was necessary to derivatise an alcohol, it was thought that using a chiral carboxylic acid in order to form an ester was a pragmatic approach. Hence, the diastereoisomeric mixture **3.41** was prepared by reacting the commercially available racemic alcohol **3.20** with (*S*)-(+)-*O*-acetylmandelic acid **3.42** in the presence of *N,N'*-dicyclohexylcarbodiimide (DCC) and 4-dimethylaminopyridine (DMAP) in 89% yield (**Scheme 21**). The chiral identity of the mandelic acid derivative was chosen arbitrarily, as the main aim of this reaction was to assess whether the diastereoisomeric mixture **3.41** would be separable.



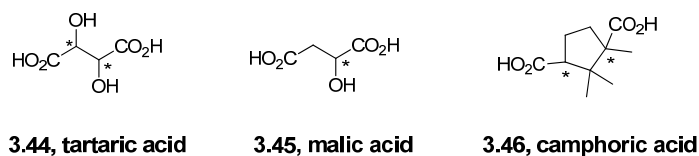
i) (*S*)-(+)-*O*-acetylmandelic acid **3.42** (1.2 eq), DCC (2 eq), DMAP (0.1 eq), DCM, rt, **89%**.

### Scheme 21: Formation of the diastereoisomeric mixture **3.41**

In order to investigate if the diastereoisomeric mixture **3.41** would be separable by achiral chromatography, a set of solvent systems to separate the mixture by thin layer chromatography was explored: cyclohexane:EtOAc, cyclohexane:TBME, cyclohexane:*i*-PrOH and diethylether:EtOAc. None of these systems offered an appreciable separation of the two diastereoisomers **3.41**, however, the cyclohexane:TBME system gave the best results. Therefore, the diastereoisomeric mixture **3.41** was attempted to be purified by normal phase chromatography using a gradient 0 to 100% TBME in cyclohexane. However, a single component was isolated from this preparative step and a separate <sup>1</sup>H NMR analysis of the first and of the last eluting fractions displayed the same 1:1 mixture of the two diastereoisomers **3.41**. After this unsuccessful chromatographic separation, it was considered whether a potential difference in the solubilities of two diastereoisomers could be used in order to separate the diastereoisomers. Based on this principle, recrystallisation of the diastereoisomeric mixture **3.41** was attempted by dissolving the mixture in a minimal amount of refluxing methanol and slowly cooling the mixture to room temperature. However, this recrystallisation trial was also unsuccessful.



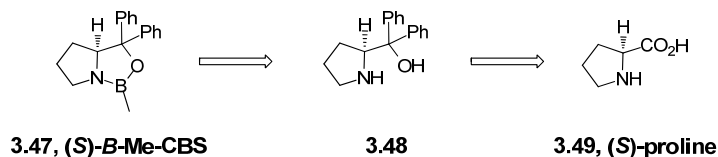
The above results suggested that the lack of noticeable difference in the physicochemical properties of the two diastereoisomers **3.41** rendered the mixture difficult to separate by achiral chromatography and recrystallisation. It would have been interesting to explore additional chiral carboxylic derivatising agents, such as those described in **Figure 64**, and to investigate a screen of recrystallisation solvents, however, it was judged more pertinent to focus on route B (**Figure 63**, p. 173) at this stage.



**Figure 64: Chiral carboxylic acids which could be used as derivatising agents**

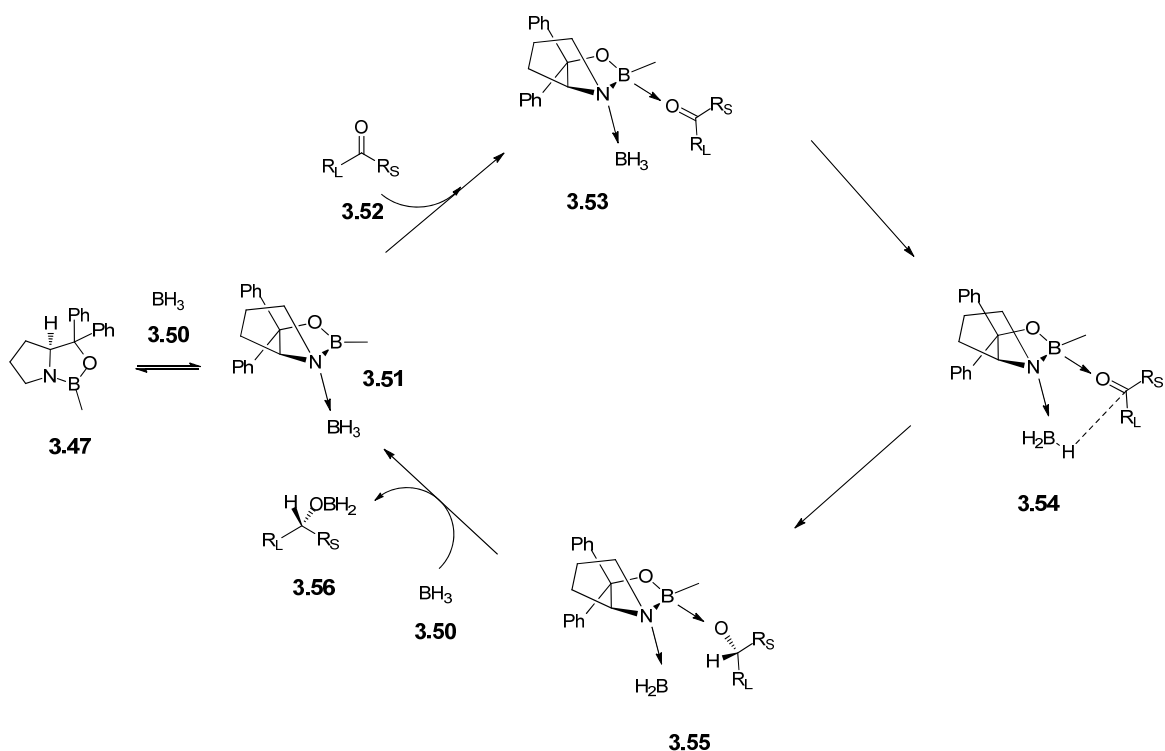
The enantioselective reduction of a prochiral ketone to its corresponding chiral alcohol is now a well established method, and mostly involves the use of metal hydrides. Several asymmetric reducing agents have been reported to this purpose, especially those based on a chirally modified aluminium or boron hydride species.<sup>257</sup> The Corey-Bakshi-Shibata (CBS) reduction,<sup>258</sup> which involves the use of borane in conjunction with a chiral oxazaborolidine catalyst, is probably the most exemplified method to conduct enantioselective reductions of ketone.<sup>259</sup> This method has a number of advantages that include wide scope, predictable absolute stereochemistry, ready availability of the chiral catalyst in both enantiomeric forms, high yields and experimental ease. The most significant advances recently achieved for enhancing the enantioselectivity and practicability of the CBS-mediated reduction have been reviewed in the literature, especially in the context of the catalytic use of the chiral oxazaborolidine agent.<sup>260</sup> Furthermore, oxazaborolidine-mediated asymmetric reduction of prochiral ketones has been widely used to access chiral natural products, intermediates, ligands and building blocks.<sup>261</sup>

The most commonly used chiral oxazaborolidine in the CBS-reduction is (*S*)-*B*-Me-CBS (1-methyl-3,3-diphenylhexahydropyrrolo[1,2-*c*][1,3,2]oxazaborole), **3.47** which is derived from (*S*)-diphenylprolinol **3.48**, the latter being obtained from (*S*)-proline **3.49** (**Figure 65**).



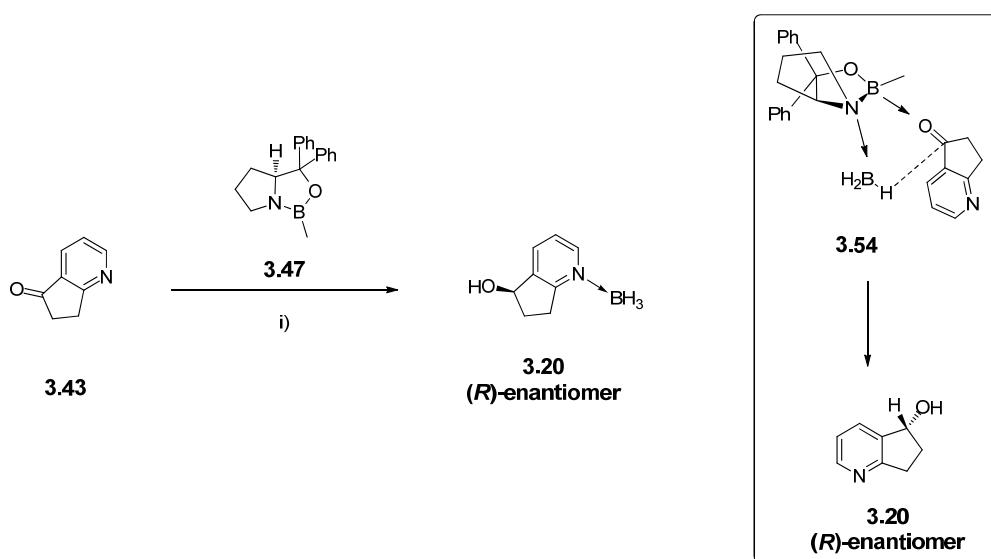
**Figure 65: Retrosynthetic approach of (*S*)-*B*-Me-CBS **3.47****

The mechanism of the CBS-mediated reduction of a prochiral ketone **3.52** is shown on **Scheme 22**. The first step involves the complexation of borane **3.50** to the heterocyclic nitrogen on the  $\alpha$ -face due to the steric interactions present on the  $\beta$ -face, leading to the complex **3.51**. The formation of this complex **3.51** between the precatalyst **3.47** and borane **3.50** activates the ability of borane **3.50** to act as a hydride donor while increasing the Lewis acidity of the endocyclic boron atom. In the following step, the oxygen atom of the ketone **3.52** coordinates to the endocyclic boron, with its small substituent ( $R_S$ ) pointing towards the  $\beta$ -face in order to minimise the steric interactions with the methyl group attached to the endocyclic boron. These interactions lock the complex **3.53** in an ideal conformation for the borane hydride to be delivered *via* a six-membered transition state **3.54**. In the last step, the catalyst species **3.51** is regenerated and the chiral alcohol **3.56** is released by decomposition of the complex **3.55** with an excess of borane **3.50**. It is worth mentioning that oxazaborolidines themselves do not reduce ketones, but only act as reducing agents after addition of a second equivalent of borane. Furthermore, in this CBS-mediated reduction mechanism, oxazaborolidines act both as Lewis acid, by activating the ketone oxygen, and as Lewis base, by coordinating to the borane, which renders the reduction more rapid than the use of borane alone.



**Scheme 22: Mechanism of the CBS-mediated reduction**

Since the absolute configuration of the final isoxazole **3.17b** had now been confirmed to be the (*S*)-enantiomer and because the Mitsunobu step prior to form **3.17b** occurred with inversion of configuration, the (*R*)-enantiomer of the alcohol **3.20** was required, which would be obtained by using the (*S*)-version of the oxazaborolidine reagent, (*S*)-*B*-Me-CBS **3.47**. Indeed, in the transition state of the reaction, the large pyridyl moiety of the ketone **3.43** would be anticipated to sit on the  $\alpha$ -face of the complex **3.54**, due to the steric interactions with the methyl group attached to the endocyclic boron atom (**Scheme 23**). Thus, the cyclopentapyridin-5-one **3.43** was reduced in presence of *N,N*-diethylaniline-borane and (*S*)-*B*-Me-CBS **3.47** (**Scheme 23**).



i) *N,N*-diethylaniline-borane (Table 28), (*S*)-*B*-Me-CBS 3.47 (Table 28), toluene, rt, 31-66%, e.e. 74-96.4%.

### Scheme 23: CBS-mediated reduction of cyclopentapyridin-5-one 3.43

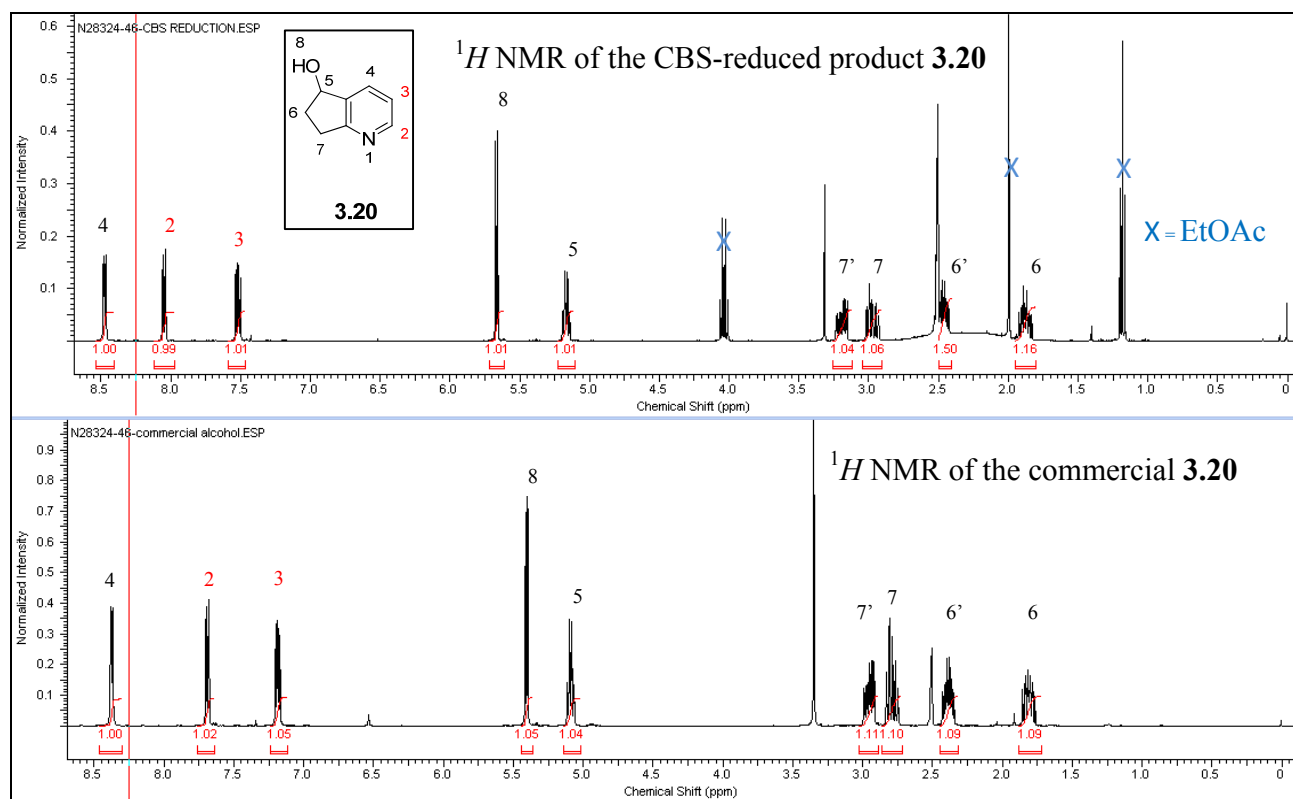
Different reaction conditions were examined in order to assess their impact on the yield and, most importantly, on the enantiomeric excess of the product obtained (Table 28).

| Entry | Eq <i>N,N</i> -diethylaniline-borane | Eq of ( <i>S</i> )- <i>B</i> -Me-CBS 3.47 | Yield (%) | e.e. (%) |
|-------|--------------------------------------|---|-----------|----------|
| 1     | 2                                    | 0.06                                      | 64        | 74       |
| 2     | 1.1                                  | 1.1                                       | 31        | 96.4     |
| 3     | 2                                    | 2   | 66        | 96.4     |

Table 28: Experimental conditions for the CBS-mediated reduction

Firstly, *N,N*-diethylaniline-borane (2 eq) was used as a source of borane in presence of 6 mol% of (*S*)-*B*-Me-CBS **3.47** (Table 28, entry 1). The alcohol **3.20** was obtained in 64% yield, with an encouraging enantiomeric excess of 74%. In an attempt to increase the enantioselectivity of the reaction, the ratio of (*S*)-*B*-Me-CBS **3.47** was increased to 1.1 eq and the amount of *N,N*-diethylaniline-borane was decreased to 1.1 eq, which afforded the alcohol **3.20** in an enantiomeric excess of 96.4%, but with a reduced yield of 31% (Table 28, entry 2). When trying to increase the yield to the previously observed levels, both the amount of *N,N*-diethylaniline-borane and (*S*)-*B*-Me-CBS **3.47** were increased to 2 eq and this resulted in an increased yield of 66%, still with the same enantiomeric excess of 96.4% (Table 28, entry 3). The latter results suggested that an enantiomeric excess of 96.4% was probably the maximal level of enantiocontrol that the CBS-mediated reaction would offer on our system.

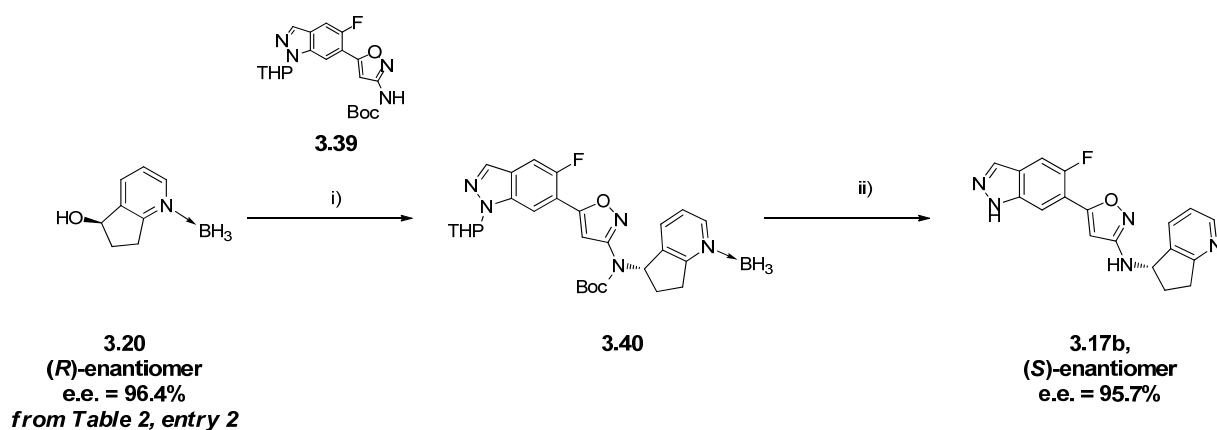
When comparing the LCMS and the <sup>1</sup>H NMR of **3.20** obtained by the CBS-mediated reduction of Scheme 23 with the analytical data from the commercially available racemic **3.20**, several discrepancies were observed. Firstly, the retention time of the CBS-synthesised **3.20** in our reverse phase LCMS system was greater (Rt = 0.70 min) than its corresponding commercial racemic analogue **3.20** (Rt = 0.26 min), suggesting that the CBS-synthesised **3.20** was more lipophilic than the commercial version of **3.20**. Secondly, noticeable variations in the chemical shift of the two pyridyl protons adjacent to the nitrogen atom between the CBS-synthesised **3.20** and the commercial version of **3.20** were observed by <sup>1</sup>H NMR (Figure 66). Finally, a broad peak was observed in the <sup>1</sup>H NMR at 2.3 ppm.



**Figure 66: <sup>1</sup>H NMR differences between the CBS-synthesised alcohol 3.20 and the commercially available racemic alcohol 3.20**

From this set of analytical data, it was concluded that the alcohol **3.20** formed by the CBS-mediated reaction was obtained as a borane adduct complexed on the pyridyl nitrogen. The formation of a borane adduct complexed on a pyridyl nitrogen after an oxazaborolidine-catalysed borane reduction is preceded in the literature<sup>262</sup> and, in fact, borane has previously been employed as a protecting group for pyridine.<sup>263</sup> Additionally, the competitive coordination of borane with the pyridyl nitrogen, instead of coordination with the catalyst, could explain why respectable yields were only obtained when using an excess of *N,N*-diethylaniline-borane.<sup>264</sup>

Different approaches, inspired from the literature, were followed in order to hydrolyse this borane adduct, and the CBS-synthesised **3.20** was heated in refluxing methanol<sup>265</sup> and also heated at 60 °C in methanol with an excess of 1 M HCl.<sup>266,267</sup> Despite repeated attempts, none of the experimental conditions examined were able to hydrolyse the borane adduct. Consequently, the subsequent steps of the synthetic route were carried out, hoping that this adduct could be dissociated later in the synthesis. A Mitsunobu reaction with the chiral alcohol **3.20** complexed with borane and the Boc-protected isoxazole **3.39** synthesised previously, occurring with inversion of configuration, delivered the isoxazole analogue **3.40** (based on retention time in the LCMS, the borane-complex was still present at that stage), where the stereogenic carbon of the cyclopentapyridyl ring was in the (*S*)-configuration (**Scheme 24**). The last deprotection step delivered the (*S*)-enantiomer isoxazole **3.17b**.



i) *tert*-butyl (5-(5-fluoro-1-(tetrahydro-2*H*-pyran-2-yl)-1*H*-indazol-6-yl)isoxazol-3-yl)carbamate **3.39** (1.2 eq), triphenylphosphine (2.2 eq), DIAD (2.2 eq), THF, rt; ii) 3 M HCl in MeOH (10.3 eq), EtOH, 50 °C to 70 °C, 14% over 2 steps.

**Scheme 24: Synthesis of the (*S*)-enantiomer analogue **3.17b****

The first observation was that the NMR and the LCMS of isoxazole **3.17b** obtained in **Scheme 24** were now comparable to those of the initial batch of compound **3.17b** (obtained in **Scheme 19**, p. 169), thus suggesting that the borane complex had been hydrolysed in the final deprotection step. Additionally, the chiral HPLC analysis of **3.17b** obtained *via* the CBS-mediated route was consistent with that of **3.17b** synthesised in **Scheme 19** (p. 169), further confirming that compound **3.17b** was the (*S*)-enantiomer. The enantiomeric excess of isoxazole **3.17b** obtained with this route was 95.7%, verifying once more that no racemisation had occurred during the last two steps of Mitsunobu and deprotection. However, the combined yield of the last two steps of Mitsunobu reaction and removal of the protecting groups under acidic conditions was much lower (14%) compared with the corresponding reactions from the synthetic option 2 (50%).

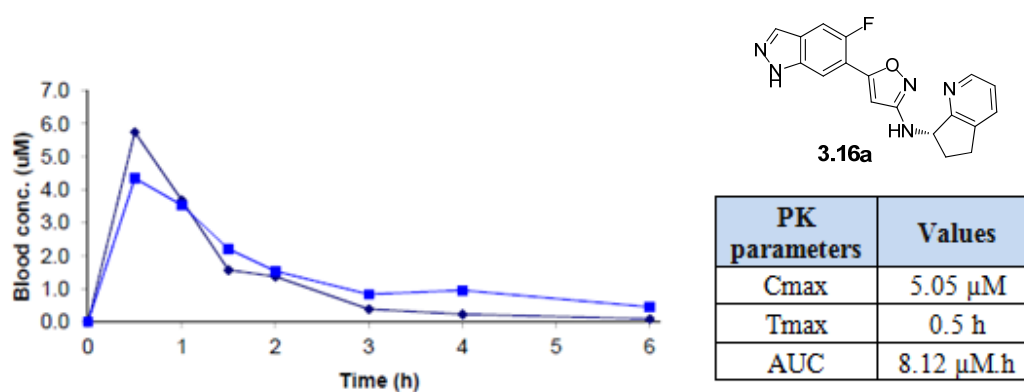
#### **3.3.1.4. Comparison of the synthetic option 2 vs. option 3 and conclusion of compound 3.17b**

The synthetic option 2 (**Section 3.3.1.2**, p. 168), which allowed us to determine the absolute configuration of **3.17b** as being the (*S*)-enantiomer, delivered isoxazole **3.17b** from the commercially available 6,7-dihydro-5*H*-cyclopenta[*b*]pyridin-5-ol **3.20** in an overall yield of 16% and with an e.e. of 99.2%. This route consisted of three synthetic steps: preparative chiral HPLC, Mitsunobu reaction and removal of the protecting groups. The synthetic option 3 (**Section 3.3.1.3**, p. 173) afforded the final analogue **3.17b** from the commercially available 6,7-dihydro-5*H*-cyclopenta[*b*]pyridin-5-one **3.43** in an overall yield of 9% and with an e.e. of 95.7%. This approach also involved three synthetic steps: CBS-mediated reduction, Mitsunobu reaction and final deprotection. Consequently, option 2 was demonstrated to be more efficient than the CBS-mediated route, especially since it afforded the final enantiomer with an enantiomeric excess greater than 99%, which is a purity requirement in our laboratories to submit compounds to downstream biological assays. However, the encouraging enantiomeric excess of



95.7% obtained in the CBS route established the fact that an enantioselective approach could be successfully used to access analogue **3.17b**, which was a key finding.

The initial rationale to develop the synthetic chemistry work described above was motivated by the promising *in vitro* DMPK profile of compound **3.17b** compared with the initial lead isoxazole **3.16a** (Table 26, p. 155). The synthetic approach from option 2 allowed the delivery of the quantity and the purity required to study the mouse PK of isoxazole **3.17b** *in vivo*. The aim was to determine the level of blood concentration over time following oral administration of **3.17b** in mouse and to compare it with that of **3.16a**. Hence, compound **3.16a** was administered, by other members of our laboratories,<sup>xiii,268</sup> orally to two mice at a dose of 5 mg/kg and the blood concentration of compound **3.16a** was accessed by sampling blood from the tail vein at several time points (Figure 67).

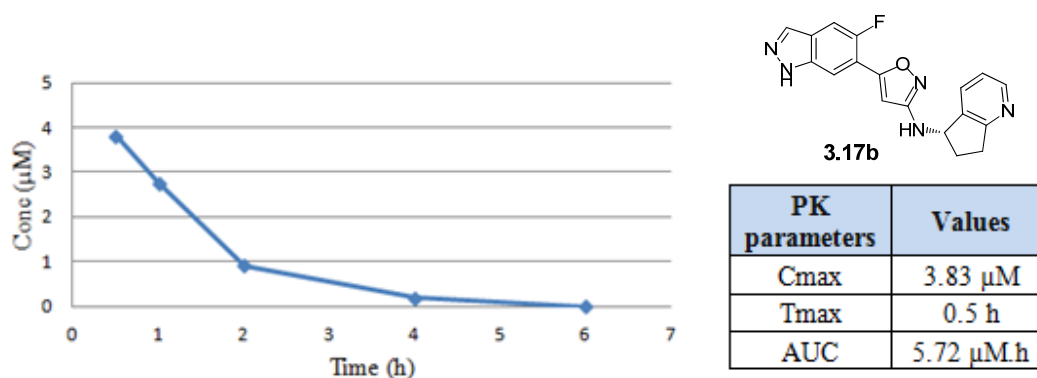


**Figure 67: PK profile of the mouse oral administration of compound 3.16a at 5 mg/kg (values in the table are the average from the two experiments)**

A different *in vivo* PK model, named short oral absorption (SOA), was used to determine the systemic concentration of isoxazole **3.17b** after oral administration in mouse.<sup>268</sup> In this PK experiment, the aim was not only to determine the systemic exposure of the compound over time, but also to assess the compound concentration in

<sup>xiii</sup>All the *in vivo* PK work discussed in this thesis was performed by members of the GSK DMPK group.

different tissues (*e.g.* brain, muscle, *etc.*), which is valuable information when envisaging to progress a compound for different animal PK/PD studies. Thus, several mice were dosed orally with the same concentration of compound and at each time point of interest, a mouse was euthanised and the relevant tissues were collected in order to assess the compound concentration in different tissue matrix. The compound exposure in a specific body compartment *vs.* time curve was then obtained by linking the tissue concentration of each time point, obtained from different mice. The benefit of this *in vivo* assay was that a large body of information (concentration in different tissues) was obtained while using a relatively small number of animals. Its drawback, however, was that the compound exposure curve for a specific tissue was obtained from a combination of exposures in different animals, which could potentially introduce a certain level of discrepancy. However, the level of confidence in this *in vivo* PK model is considered high enough for it to be used for comparison with the previous oral PK experiment of **3.16a**.<sup>268</sup> Thus, **Figure 68** displays the blood exposure in mouse *vs.* time of isoxazole **3.17b** after a 5 mg/kg SOA study.



**Figure 68: PK profile of the mouse SOA model of compound 3.17b at 5 mg/kg**

The two isoxazoles **3.16a** and **3.17b** exhibited an attractive blood exposure with a maximal compound concentration (C<sub>max</sub>) of 5.05 µM for **3.16a** and 3.83 µM for **3.17b**, both of them at a time (T<sub>max</sub>) of 30 min. The areas under the curve for both **3.16a** and

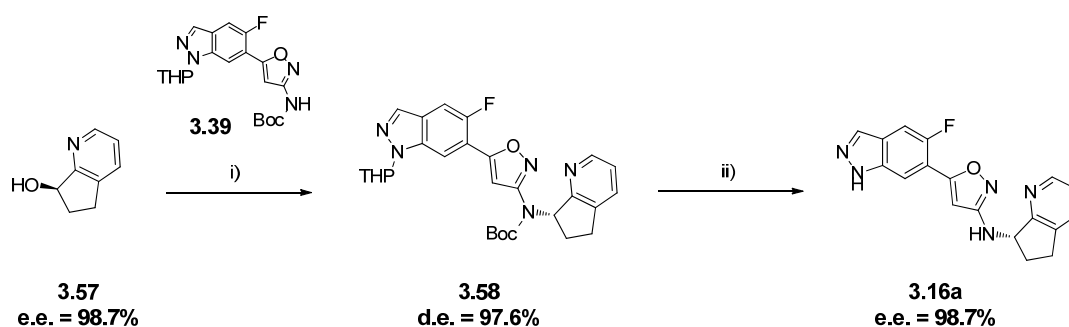
**3.17b**, with a value of 8.12  $\mu\text{M}\cdot\text{h}$  and 5.72  $\mu\text{M}\cdot\text{h}$ , respectively, were meeting our optimisation goal for progression to animal PK/PD work (the targeted AUC in a 5 mg/kg DMPK study for our medicinal chemistry programme was  $> 5 \mu\text{M}\cdot\text{h}$ , see **Figure 57, p. 160**). However, the higher mouse systemic exposure of **3.16a** after oral absorption led us to prioritise **3.16a** for the *in vivo* PK/PD experiments over **3.17b**. This decision to progress isoxazole **3.16a** over **3.16b** for animal efficacy studies completed our first objective for the isoxazole series.

In the next section, the synthetic chemistry effort provided to enable the preparation of the required amount of **3.16a** for the proposed *in vivo* PK/PD work is discussed.

### **3.3.2. Optimisation of the synthetic route to isoxazole 3.16a**

#### **3.3.2.1. Limitations of the current synthetic route to compound 3.16a**

For the *in vivo* PK/PD studies, 100 g of isoxazole **3.16a** with an enantiomeric excess greater than 99% were required to be synthesised and, taking into consideration the scale of the synthesis, the recommendation was made to outsource this work to an external collaborator. Nonetheless, the current route to access **3.16a** needed to be optimised prior to outsourcing. Previously, compound **3.16a** was made employing the route and conditions displayed in **Scheme 25**,<sup>250</sup> where the key isoxazole intermediate **3.39** was synthesised following the route shown in **Scheme 18 (p. 165)** and the chiral alcohol **3.57** was accessed by chiral HPLC separation of the corresponding commercially available racemic mixture.



i) *tert*-butyl (5-(5-fluoro-1-(tetrahydro-2*H*-pyran-2-yl)-1*H*-indazol-6-yl)isoxazol-3-yl)carbamate **3.39** (1.1 eq), triphenylphosphine (3 eq), DIAD (3 eq), THF, 0 °C to rt, 16%; ii) 3 M HCl in MeOH (10 eq), EtOH, 75 °C, 85%.

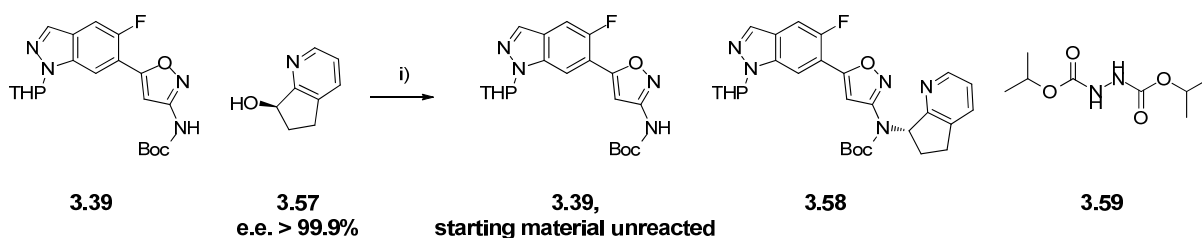
### Scheme 25: Initial synthesis of isoxazole **3.16a**<sup>250</sup>

Interestingly, the Mitsunobu reaction to form the alkylated product **3.58** (yield = 16%) was much less efficient than the corresponding reaction generating the previously studied cyclopentapyridyl isomer **3.40** (yield = 67%, **Scheme 19**, p. 169). The poor yield of 16% obtained for the Mitsunobu step was explained by two main factors. Firstly, the reaction did not go to completion and a large amount of unreacted aminoisoxazole analogue **3.39** was observed by LCMS, even after extended reaction times. Secondly, it was challenging to separate the targeted analogue **3.58** from the by-product diisopropyl hydrazine-1,2-dicarboxylate resulting from the use of diisopropyl azodicarboxylate (DIAD) and only a combination of chromatographic purification and several recrystallisations afforded the pure product **3.58**.<sup>250</sup> The Mitsunobu reaction was therefore the critical step in explaining the overall poor yield of the synthesis of the required final isoxazole analogue **3.16a**. Moreover, the work discussed in **Section 3.3.1.2 (p. 168)** demonstrated the feasibility of carrying out a preparative chiral HPLC on a dihydrocyclopenta[*b*]pyridinol analogue on a gram scale, and our external collaborator had the capability to carry out large scale chiral chromatography purification. Additionally, the time constraint for the required delivery of 100 g of compound **3.16a** did not allow us to considerably modify the current synthetic route to **3.16a**.

Considering all the information discussed above, the decision was taken to solely focus on improving the yield of the Mitsunobu step. Furthermore, the fact that the Mitsunobu reaction was the penultimate step of a nine steps synthesis gave an additional incentive in optimising specifically this reaction.

### 3.3.2.2. Improvement of the Mitsunobu step

The effect of the temperature on the Mitsunobu reaction had previously been investigated in our laboratories,<sup>250</sup> and it was demonstrated that increasing the reaction temperature did not affect the yield of this transformation. Therefore, the impact of the amounts of DIAD and triphenylphosphine used in the reaction was investigated (Scheme 26 and Table 29). For this study, the starting chiral alcohol **3.57** used was obtained by chiral HPLC of the corresponding starting commercial racemic alcohol,<sup>252</sup> and the enantiomeric excess of this batch of chiral alcohol was greater than 99.9%.



i) *tert*-butyl (5-(5-fluoro-1-(tetrahydro-2*H*-pyran-2-yl)-1*H*-indazol-6-yl)isoxazol-3-yl)carbamate **3.39** (1 eq), (*R*)-6,7-dihydro-5*H*-cyclopenta[*b*]pyridin-7-ol **3.57** (1 eq), triphenylphosphine (Table 29), DIAD (Table 29), THF, rt.

**Scheme 26: Mitsunobu reaction to synthesise isoxazole 3.58 using DIAD**

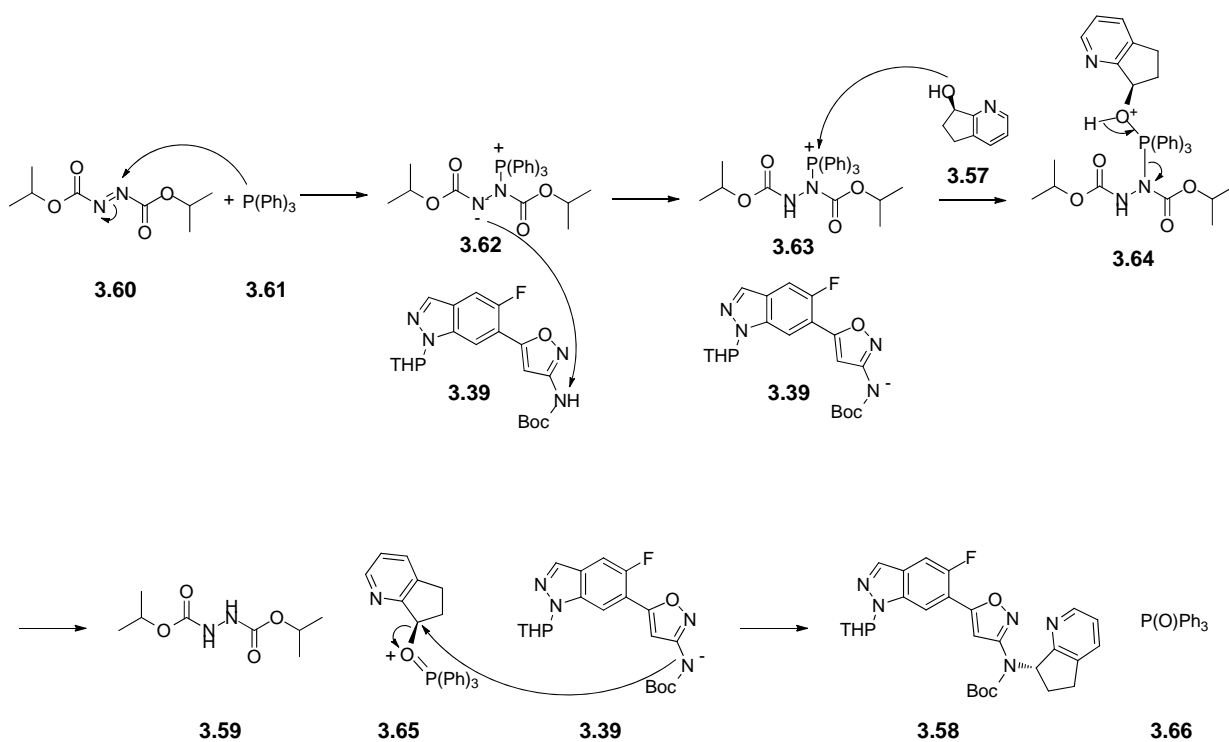
The crude product obtained in these reactions showed four main components: the unreacted starting material **3.39**, the targeted analogue **3.58**, triphenylphosphine oxide and diisopropyl hydrazine-1,2-dicarboxylate **3.59**. The crude mixture was purified by normal phase chromatography, which removed triphenylphosphine oxide and the unreacted starting material **3.39**, however, the expected product **3.58** could not entirely be separated from the by-product diisopropyl hydrazine-1,2-dicarboxylate **3.59**. Hence, the yield of **3.58** obtained was estimated from the  $^1\text{H}$  NMR molar ratio of the product **3.58** to the by-product **3.59** (Table 29).

| Entry | PPh <sub>3</sub> eq used | DIAD eq used | Yield of 3.39 recovered | Molar ratio of product 3.58:by-product 3.59 (determined by $^1\text{H}$ NMR) | Estimated yield of 3.58 obtained by $^1\text{H}$ NMR ratio |
|-------|--------------------------|--------------|-------------------------|--|--|
| 1     | 2                        | 2            | 56%                     | 1:4  | 28%  |
| 2     | 3                        | 3            | 50%                     | 1:7  | 32%  |
| 3     | 10                       | 10           | 56%                     | 1:31   | 28%  |

**Table 29: Investigation of the number of equivalents of DIAD and triphenylphosphine in the Mitsunobu reaction to synthesise the isoxazole analogue 3.58**

The results from **Table 29** suggested that increasing the amount of PPh<sub>3</sub> and DIAD used did not increase the rate of conversion to the product **3.58**, since no difference was observed between using 2 or 10 equivalents of PPh<sub>3</sub>/DIAD. It was interesting to notice that in all cases, more than half of the amount of the starting aminoisoxazole derivative **3.39** was recovered unreacted, highlighting the low reactivity of the system. Furthermore, the increased use of DIAD pinpointed the issue of the contamination of the product with the reduced hydrazide version of the DIAD generated during the reaction. Even if it would have been appropriate to investigate different ways to simplify the work up of the reaction, for instance by looking into using polymer-supported reagents,<sup>269</sup> the low conversion observed triggered the investigation of alternative starting materials.

The mechanism of the Mitsunobu reaction (**Figure 69**)<sup>270</sup> involves an initial nucleophilic addition of triphenylphosphine **3.61** to DIAD **3.60** to generate the reactive betaine intermediate **3.62**. In the presence of an acidic pronucleophile **3.39**, the betaine intermediate **3.62** is protonated to afford the positively charged species **3.63**. The subsequent nucleophilic attack by the alcohol derivative **3.57** and concomitant loss of diisopropyl hydrazine-1,2-dicarboxylate **3.59** lead to the alkoxyphosphonium intermediate **3.65**. A final S<sub>N</sub>2 displacement of the triphenylphosphine oxide **3.66** by the conjugate base form of the pronucleophile **3.39** with complete Walden inversion of stereochemistry delivers the alkylated amine **3.58** in its (*S*)-configuration.

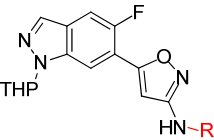

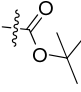
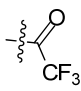
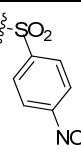
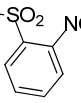


**Figure 69: Mechanism of the Mitsunobu reaction**

As illustrated in **Figure 69**, a key step in this mechanism is the deprotonation of the intermediate **3.39** by the betaine **3.62**. In fact, a well preceded limitation of the Mitsunobu reaction is that the  $pK_a$  of the pronucleophile **3.39** has to be less than 11 for the reaction to be high yielding and that when  $pK_a$  is greater than 13, the reaction does not occur.<sup>270</sup> In the current study, the  $pK_a$  of the Boc-protected aminoisoxazole **3.39** was calculated to be 12.4 (**Table 30**), potentially explaining the low conversion observed during our initial attempts to improve reaction yield by increasing the amount of PPh<sub>3</sub> and DIAD. In order to enhance the reactivity of our system, two avenues were considered: lowering the  $pK_a$  of the protected intermediate **3.39** and increasing the basicity of the betaine intermediate **3.62**. For the first suggestion, the three alternative protecting groups shown in **Table 30** were envisaged after considering their impact on lowering the calculated acidity of the aminoisoxazole NH. In comparison to the initial

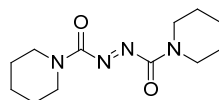


Boc-protected analogue **3.39** ( $pK_a = 12.4$ ), the trifluoroacetamide-protected **3.67** displayed a reduced  $pK_a$  of 10 and, more dramatically, the two nitrophenylsulfonamide-protected **3.68** and **3.69** lowered the  $pK_a$  even further to 5.7 and 5.3, respectively (**Table 30**). Given the potential improvement the compounds **3.67**, **3.68** and **3.69** could bring to the Mitsunobu step, they were attempted to be synthesised. Unfortunately, trying to access these compounds by reacting aminoisoxazole **3.37** (see **Scheme 18**, p. 165) with trifluoroacetic anhydride, 4-nitrobenzene-1-sulfonyl chloride and 2-nitrobenzene-1-sulfonyl chloride, respectively, under various conditions, was ultimately unsuccessful, and that the starting aminoisoxazole **3.37** remained unreacted. Therefore, the decision was made to focus on the second option consisting of increasing the basicity of the betaine intermediate **3.62**.

|  |   |                   |
|--|---|-------------------|
| Compound number  |  | Calculated $pK_a$ |
| <b>3.39</b>  |  | 12.4              |
| <b>3.67</b>  |  | 10                |
| <b>3.68</b>  |  | 5.7               |
| <b>3.69</b>  |  | 5.3               |

**Table 30: Variation of the calculated  $pK_a$  of some aminoisoxazole intermediates, depending on the protecting group used**

Tsunoda and co-workers<sup>271,272</sup> broadened the range of nucleophiles used in the Mitsunobu reaction to less acidic species, by tuning the basicity of the azodicarboxamide reducing agents. Thus, the replacement of the alkoxy group of the DIAD by a secondary amine such as in azodicarboxylic dipiperidide (ADDP, **3.70**, **Figure 70**) increases the basicity of the betaine intermediate **3.62**. Indeed, the piperidine ring helps to localise the negative charge on the azo-nitrogen of the betaine intermediate **3.62**.



**3.70, ADDP**

**Figure 70: Structure of azodicarboxylic dipiperidide (ADDP)**

The Mitsunobu reaction conditions to give isoxazole **3.58** described in **Scheme 26** (p. **188**) were investigated while replacing DIAD with ADDP. Firstly, an investigation on the amount of ADDP-triphenylphosphine used was carried out (**Table 31**).

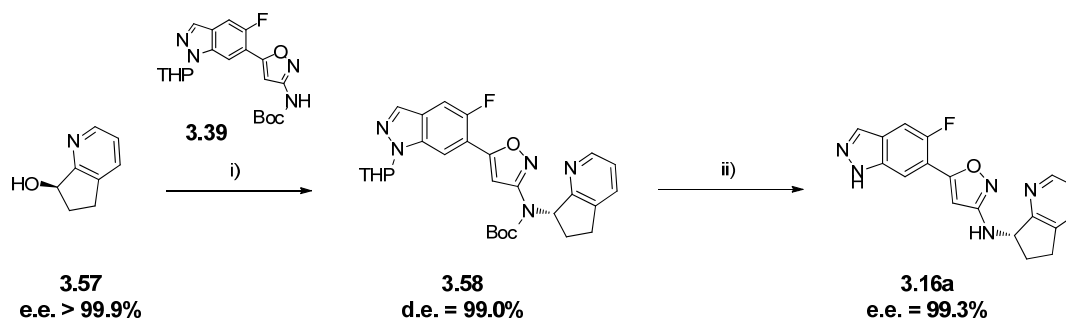
| Entry    | PPh <sub>3</sub><br>eq used | ADDP<br>eq used | Yield of<br>3.58 | d.e. of 3.58    |
|----------|-----------------------------|-----------------|------------------|-----------------|
| <b>1</b> | 2                           | 2               | 0%               | NA <sup>a</sup> |
| <b>2</b> | 3                           | 3               | 29%              | 98.9%           |
| <b>3</b> | 10                          | 10              | 57%              | 98.6%           |

<sup>a</sup>NA = not applicable

**Table 31: Investigation of the number of equivalents of ADDP and triphenylphosphine in the Mitsunobu reaction to synthesise the isoxazole analogue 3.58**

The first experimental observation from using ADDP was that the reduced hydrazide by-product derived from ADDP was easily removed by chromatography, as opposed to the previous observations when using DIAD. Therefore, the targeted product **3.58** was easily obtained as a single component after a single normal phase chromatography. In addition, the use of 10 equivalents of ADDP-triphenylphosphine (**Table 31**, entry **3**) afforded an acceptable 57% yield. Finally, these reaction conditions were also proven to retain the chirality of the product since the d.e. (*cf.* the THP group has a stereogenic centre) obtained were above 98% while starting with a chiral alcohol of an enantiomeric excess greater than 99.9%.

Encouraged by the above observations, the optimised Mitsunobu conditions were tried on a larger scale (5 g of starting isoxazole **3.39**) with ADDP, in order to validate the newly identified reaction conditions and to ultimately synthesise the final isoxazole **3.16a** (**Scheme 27**). For this example, 6 equivalents of ADDP and triphenylphosphine were used, which seemed to be a reasonable compromise in light of the findings from **Table 31**. The 58% yield obtained for the Mitsunobu transformation demonstrated that the yield improvement obtained on the milligram scale during the optimisation process was successfully transferred to a gram scale.



i) *tert*-butyl (5-(5-fluoro-1-(tetrahydro-2*H*-pyran-2-yl)-1*H*-indazol-6-yl)isoxazol-3-yl)carbamate **3.39** (1 eq), triphenylphosphine (6 eq), azodicarboxylic dipiperidide (6 eq), THF, 0 °C to rt, **58%**; ii) 3 M HCl in MeOH (10 eq), EtOH, 75 °C, **88%**.

**Scheme 27: Synthesis of isoxazole 3.16a using the optimised Mitsunobu conditions and starting from 5 g of isoxazole 3.39**

To complete the analysis, the influence of the solvent used in the reaction was investigated, as it has been noted in the literature that solvent can impact the outcome of the Mitsunobu reaction.<sup>270</sup>

| Entry | PPh <sub>3</sub> eq used | ADDP eq used | Solvent used | Yield of 3.58 | d.e. of 3.58 |
|-------|--------------------------|--------------|--------------|---------------|--------------|
| 1     | 6                        | 6            | 2-MeTHF      | 59%           | 98.9%        |
| 2     | 6                        | 6            | toluene      | 70%           | 99.1%        |
| 3     | 6                        | 6            | DCM          | 0%            | NA           |

**Table 32: Investigation of the solvent used in the Mitsunobu reaction to synthesise isoxazole 3.58**

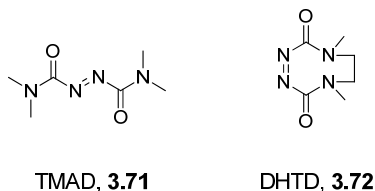
This solvent screen showed that DCM was completely ineffective (yield = 0%, **Table 32**, entry 3) and that 2-MeTHF was offering similar yields compared to the use of THF (59%, **Table 32**, entry 1). Toluene was the most efficient solvent to use for the Mitsunobu reaction (70%, **Table 32**, entry 2).

### 3.3.3. Conclusion on the improvements to the synthesis of compound 3.16a

The mechanistic considerations of the Mitsunobu reaction prompted us to investigate the alternative reducing agent ADDP instead of DIAD in order to successfully increase the yield of this step and also to greatly simplify the work up procedure. Optimisation of the number of equivalents of ADDP and PPh<sub>3</sub> and the reaction solvent suggested that using 6 equivalents of ADDP/PPh<sub>3</sub> in toluene achieved the best results. Consequently, the yield of the Mitsunobu step was improved from 16% with the initial conditions (**Scheme 25, p. 187**) to 70% (**Table 32, p. 195**), which translated into a remarkable increase in the overall yield of the synthetic route to access compound **3.16a** from 4% to 18%, over 9 steps. These optimised conditions were transferred to our external collaborator which repeated the Mitsunobu step several times on a 40 g scale of the starting Boc-protected isoxazole **3.39** and observed an average yield of 68%.<sup>154</sup> After acidic deprotection, the external collaborator delivered the requested 100 g of compound **3.16a**, with an enantiomeric excess greater than 99%, and most importantly ahead of our requested schedule for *in vivo* PK/PD studies.<sup>154</sup>

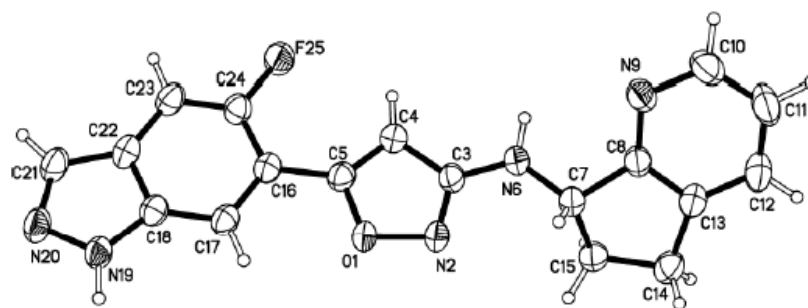
It was recognised that several additional factors could have been investigated further in order to complete the optimisation of the synthetic route to **3.16a**. Firstly, when ADDP is used in the literature, it is often combined with a more nucleophilic phosphine than triphenylphosphine, because of the lower reactivity of ADDP as a Michael acceptor compared to DIAD. Consequently, ADDP is generally used in combination with tributylphosphine,<sup>271,272</sup> however, this chemical could not be accessed in our laboratories due to freight restrictions (tributylphosphine is a flammable and pyrophoric liquid which is spontaneously flammable in air). Even if it would have been interesting to study the effect of using tributylphosphine in the Mitsunobu reaction, the risk associated with handling it on a large scale makes this reagent less attractive than using triphenylphosphine.<sup>273</sup> Secondly, a suggestion for future work could include additional *N,N,N',N'*-tetrasubstituted azodicarboxamide reducing agents, such as *N,N,N',N'*-tetramethylazodicarboxamide (TMAD, **3.71, Figure 71**)<sup>272</sup> or 4,7-dimethyl-3,5,7-

hexahydro-1,2,4,7-tetrazocin-3,8-dione (DHTD, **3.72**, **Figure 71**),<sup>274</sup> which are also reported in the literature to be more efficient than DIAD.

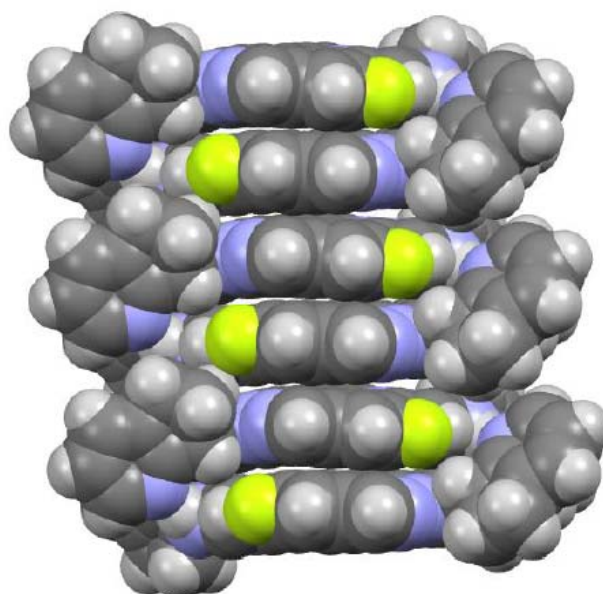


**Figure 71: Alternative reducing agents reported for the Mitsunobu reaction**

In order to fully characterise and validate the stereochemistry of compound **3.16a** obtained in our internal scale-up route of **Scheme 27** (p. **194**), its crystal structure was obtained, by another member of our laboratories, from a single crystal X-ray diffraction experiment (**Figure 72**).<sup>145</sup> The compound crystallisation was carried out in methanol and toluene, after slow evaporation. This analysis enabled us to unambiguously confirm the (*S*)-configuration of compound **3.16a**, validating the results previously obtained using VCD.<sup>241</sup> Additionally, it was shown that the isoxazole ring was approximately coplanar with the indazole ring. The asymmetric unit consisted of four independent molecules of **3.16a** which differed slightly by the orientation of the cyclopentapyridyl ring relative to the mean plane of the rest of the molecule (see **Appendices section 5.3**, p. **376**, for more detail). The four independent molecules formed a discrete tetrameric cluster held together by eight hydrogen bonds. It was observed that the tetrameric units were tightly stacked on top of each other and that the ring-stacking interactions occurred mainly between planes constituted by the indazole-isoxazole units (**Figure 73**). The planarity of the molecule **3.16a** and its propensity to intermolecularly stack was therefore hypothesised to be a key contributor to its apparent low aqueous solubility. This finding will later be considered when attempting to increase the solubility of the cinnamide series (**Section 3.5.2**, p. **206**).



**Figure 72: Crystal structure of compound 3.16a obtained by single crystal X-ray diffraction<sup>145</sup>**



**Figure 73: Space-filling model of three tetramer units of compound 3.16a, showing the ring-stacking interactions within and between tetramers<sup>145</sup>**

### 3.4. Medicinal chemistry work on the cinnamide series: Previous results

The following sections describe the medicinal chemistry effort developed towards the identification of cinnamide mPTP modulators, with an improved developability profile and with an increased aqueous solubility compared with the lead isoxazole **3.16a**. The objective was to identify cinnamide molecules with a profile matching the optimisation guidelines shown in **Figure 57 (p. 160)**, for them to be considered for *in vivo* PK/PD experiments. This study would rely on the use of the phenotypic CRC assay, outlined above, in order to drive SAR within the template.

#### 3.4.1. Previously established SAR of the cinnamide series

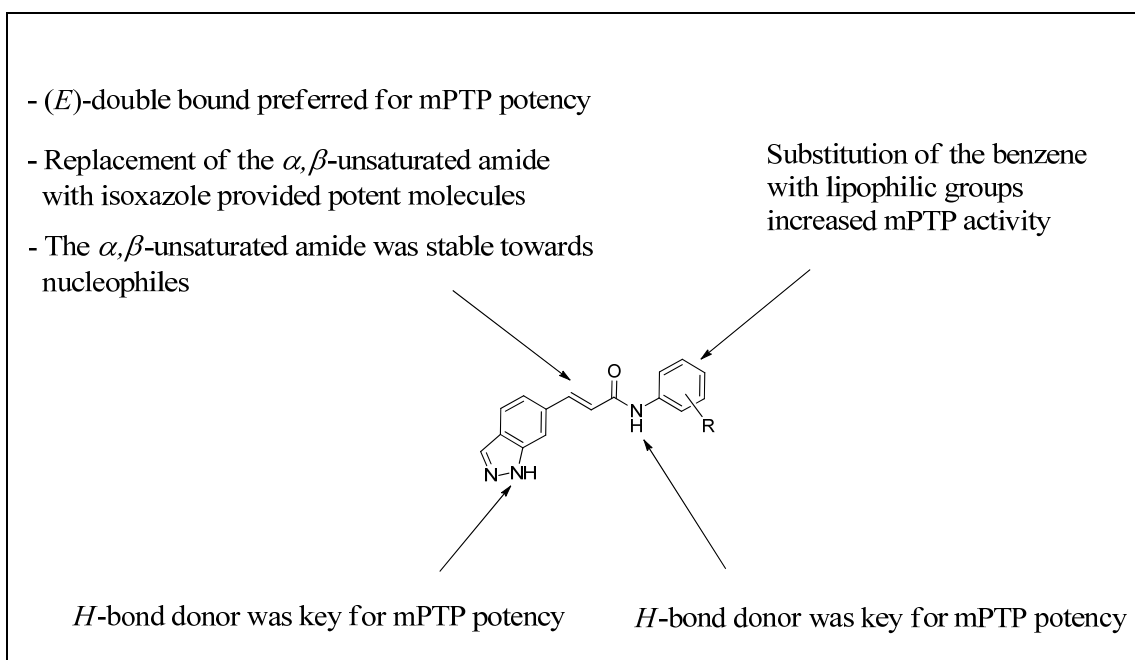
Cinnamide-containing molecules have been reported in the literature with a wide range of pharmacological activities. Indeed, cinnamide derivatives have been described as potent inhibitors of cholinesterases,<sup>275</sup> as modulators of a cellular model of breast cancer stem cells,<sup>276</sup> as antituberculosis agents,<sup>277</sup> as vanilloid receptor-1 antagonists<sup>278</sup> and as potassium channel openers.<sup>279</sup> However, the cinnamide lead compound **3.14 (Table 27, p. 157)**, identified prior to the author commencing work on this area,<sup>241</sup> displayed a good selectivity profile when submitted to our internal selectivity profiling panel. Indeed, **3.14** was tested against 53 biological targets which are known to potentially cause side-effects and the pIC<sub>50</sub> values measured were all below the threshold of detection except for 2 targets: the vasopressin 1a receptor (pIC<sub>50</sub> = 4.9) and the norepinephrine transporter (pIC<sub>50</sub> = 6.4).

The central  $\alpha,\beta$ -unsaturated amide of this cinnamide series represented a potential reactive chemical functionality. Indeed,  $\alpha,\beta$ -unsaturated amides are preceded to act as the electrophilic partner in conjugate addition reactions.<sup>280,281</sup> This is a concern in terms of drug development as electrophilic species are susceptible to covalent binding with nucleophilic portions of proteins, deoxyribonucleic acid, and cellular glutathione. Such



reactions *in vivo* may lead, respectively, to enzyme deactivation, genotoxicity and to compromised cellular function due to glutathione depletion.<sup>282,283,284</sup> Furthermore, the double bond could be metabolically unstable, by being oxidised to the corresponding epoxide or to the corresponding diol analogues.<sup>285</sup> However, work performed by other members of our laboratories showed that saturating the double bond or replacing the double bond with a cyclopropyl group reduced mPTP potency dramatically.<sup>241</sup> Additionally, it was shown that the (*Z*)-regioisomer analogue of **3.14** was much less potent than the (*E*)-cinnamide **3.14**, suggesting that the (*E*)-configuration of the double bond was important in order to optimally fit the cinnamide compound into the binding receptor.<sup>241</sup> The electrophilic nature of the double bond of compound **3.14** was therefore assessed by carrying out stability studies in presence of *N*-acetyl cysteine<sup>252</sup> or glutathione,<sup>286</sup> and no direct adduct or Michael addition adduct of compound **3.14** was observed. It is worth mentioning that the replacement of the  $\alpha,\beta$ -unsaturated ketone with a 5-membered heteroaromatic ring could achieve mPTP potency, especially with an isoxazole (work which led to the discovery of compounds **3.16a** and **3.17b** discussed in **Section 3.3, p. 161**),<sup>241</sup> however, compounds with low aqueous solubility were mostly obtained. Finally, it was shown that the two hydrogen bond donor motifs of compound **3.14** (the indazole and the amide NH) were required for mPTP activity.<sup>241</sup>

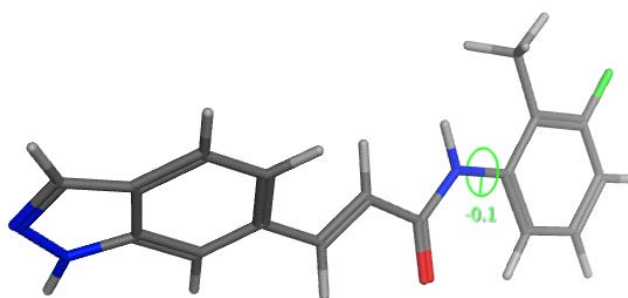
The initial SAR observations discussed above, made through use of the CRC assay and developed prior to the author commencing work on this area, are summarised in **Figure 74**.



**Figure 74: Summary of the previously established SAR of the cinnamide series**<sup>241</sup>

### 3.4.2. Previous attempts to increase the solubility of the cinnamide series

As mentioned when presenting the objectives for the cinnamide series (**Section 3.2.1.2, p. 156**), the lead 3-fluoro-2-methylbenzyl cinnamide **3.14** was a highly potent mPTP modulator (liver CRC  $pIC_{50} = 8.1$ ) with low aqueous solubility (FaSSIF solubility = 5  $\mu\text{g/mL}$ ). The combination of a high number of aromatic rings, the lack of polar functionalities and the overall flat nature of the molecule could contribute to the low aqueous solubility. Hence, the dihedral angle between the benzene and the amide moiety of the local low energy conformation of compound **3.14** was calculated to be around  $0^\circ$ , using the MOE® software (**Figure 75**).



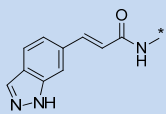
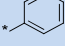
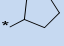
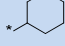
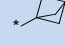
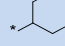
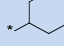
Compound **3.14**  
Dihedral angle =  $0.1^\circ$   
FaSSIF solubility =  $5 \mu\text{g/mL}$

**Figure 75: Low energy conformation of compound 3.14**

Prior to the author commencing work on this area, two separate work streams were investigated in an attempt to increase the aqueous solubility of the cinnamide series while maintaining its mPTP potency: replacement of the indazole ring with more polar heterocycles and replacement of the right-hand side benzene with either saturated or heteroaromatic rings.<sup>241</sup> However, these two strategies were unsuccessful in identifying cinnamides with a profile meeting the programme optimisation goals. For the first area of focus, it was determined that the indazole motif was difficult to be replaced with a suitable isostere without reducing mPTP potency.<sup>241</sup> Consequently, indazole was retained at the left hand-side of the cinnamide series.

Regarding the phenyl ring of the cinnamide template, the first attempts to increase the aqueous solubility were made by replacing the benzene with aliphatic rings. Hence, the cyclopentyl analogue **3.73**, the cyclohexyl analogue **3.74**, the bicyclo[1.1.1]pentanyl analogue **3.75** and aliphatic rings containing heteroatoms such as tetrahydropyran **3.76** and methylpiperidine **3.77** were prepared (**Table 33**).<sup>241</sup> As intended, all these compounds displayed a reduced PFI in comparison to the initial cinnamide hit compound **3.18** (PFI = 6.6). Consequently, the cyclopentyl analogue **3.73** displayed an increased CLND solubility ( $\geq 73 \mu\text{g/mL}$ ) compared to **3.18**. However, the other aliphatic

replacement compounds **3.74** and **3.75** displayed similar or lower CLND solubility. Regarding the compounds with an aliphatic rings containing heteroatoms, the aqueous solubility was largely improved, with a CLND solubility of  $\geq 115$   $\mu\text{g/mL}$  and  $\geq 104$   $\mu\text{g/mL}$  for tetrahydropyran **3.76** and methylpiperidine **3.77**, respectively. Nevertheless, all of the saturated ring analogues exhibited a reduced mPTP activity, with liver CRC  $\text{pIC}_{50}$  varying from less than 4 for tetrahydropyran **3.76** and methylpiperidine **3.77** to 6.1 for the bicyclo[1.1.1]pentanyl analogue **3.75**.<sup>241</sup> Based on this, none of the aliphatic ring cinnamide compounds were progressed further in our medicinal chemistry project.

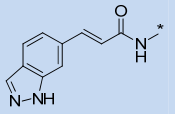
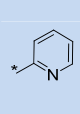
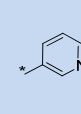
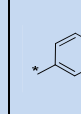

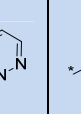
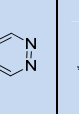
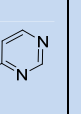
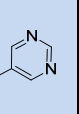
|  |  |  |  |  |  |  |
|---|---|---|---|---|---|---|
| <b>Compound</b>   | <b>3.18</b>   | <b>3.73</b>   | <b>3.74</b>   | <b>3.75</b>   | <b>3.76</b>   | <b>3.77</b>   |
| <b>Liver CRC <math>\text{pIC}_{50}</math></b>                                     | 6.5   | 5.7   | 5.6   | 6.1   | < 4   | < 4   |
| <b>MW</b>   | 263   | 255   | 269   | 253   | 271   | 284   |
| <b>clogP</b>  | 3.1   | 2.8   | 3.3   | 2   | 0.9   | 1.3   |
| <b>Chrom logD / PFI</b>   | 3.6 / 6.6   | 3.1 / 5.1   | 3.8 / 5.8   | 3.1 / 5.1   | 1.7 / 3.7   | 0.4 / 2.4   |
| <b>CLND (<math>\mu\text{g/mL}</math>)</b>   | 37  | $\geq 73$   | 10  | 41  | $\geq 115$  | $\geq 104$  |
| <b>FaSSIF (<math>\mu\text{g/mL}</math>)</b>                                       | ND  | 46  | 2   | 41  | 187   | > 1059 <sup>a</sup>   |

<sup>a</sup>This FaSSIF solubility was measured after a 24 h incubation period (instead of 4 h).

**Table 33: Saturation of the benzene in the cinnamide template<sup>241</sup>**

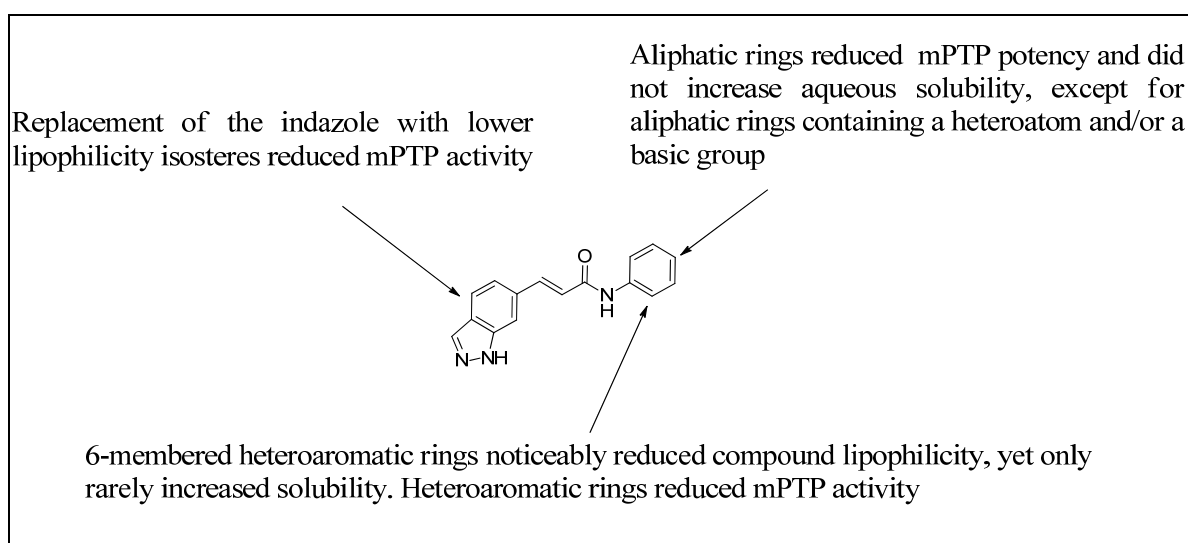
In summary, this set of compounds suggested that an aromatic group at the right-hand side part of the cinnamide series was preferred for mPTP activity. Additionally, it was noted, with methylpiperidine **3.77**, that introducing a basic amine seemed to be a good strategy for increasing significantly the aqueous solubility, albeit at the detriment of CRC potency.

Since it was found with the compounds in **Table 33** that an aromatic ring at the right-hand side position of the cinnamide series was preferred for mPTP potency, various 6-membered heteroaromatic rings were investigated as a less lipophilic alternative to benzene.<sup>241</sup> Thus, the benzene of the cinnamide hit **3.18** was replaced with pyridine (compounds **3.78**, **3.79** and **3.80**), pyridazine (compounds **3.81** and **3.82**), pyrimidine (compounds **3.83** and **3.84**) and pyrazine (compound **3.85**, **Table 34**).<sup>241</sup> The first observation from this set of analogues was that the primary mPTP potency was greatly reduced by the introduction of nitrogen atoms in the phenyl ring. Indeed, the liver CRC pIC<sub>50</sub> of the progenitor compound **3.18** was 6.5, whereas all the compounds from **Table 34** had a liver CRC pIC<sub>50</sub> less than 4, except for the 3- and 4-pyridyl analogues **3.79** and **3.80** (pIC<sub>50</sub> = 5.1 and 4.7, respectively). Additionally, the PFI values underlined the fact that this set of heteroaromatic compounds were markedly more polar than the starting phenyl ring-containing **3.18**, since the measured PFI varied between 4.4 for pyridazine **3.82** to 5.8 for 2-pyridine **3.78**, in comparison with the measured PFI of 6.6 for the benzyl cinnamide **3.18**. Despite this, this set of analogues did not achieve any noticeable improvement of the aqueous solubility since only the CLND solubility of pyrimidine **3.83** was higher than the one of the starting benzyl cinnamide **3.18** (CLND solubility = 53 µg/mL compared with 37 µg/mL). All the other analogues from **Table 34**, for which the solubility was measured, showed a lower aqueous solubility.

|   |   |   |   |   |   |   |   |   |
|---|---|---|---|---|---|---|---|---|
|  |  |  |  |  |  |  |  |  |
| <b>Compound</b>   | <b>3.78</b>   | <b>3.79</b>   | <b>3.80</b>   | <b>3.81</b>   | <b>3.82</b>   | <b>3.83</b>   | <b>3.84</b>   | <b>3.85</b>   |
| <b>Liver CRC pIC<sub>50</sub></b>   | < 4   | 5.1   | 4.7   | < 4   | < 4   | < 4   | < 4   | < 4   |
| <b>MW</b>   | 264   | 264   | 278   | 265   | 265   | 265   | 265   | 265   |
| <b>clogP</b>  | 2.5   | 2.5   | 3   | 1.7   | 1.7   | 1.8   | 1.8   | 1.8   |
| <b>PFI</b>  | 5.8   | 5.2   | ND  | 4.8   | 4.4   | 5.1   | 4.6   | 5.1   |
| <b>CLND (µg/mL)</b>   | 9   | 10  | ND  | 19  | 10  | 53  | 16  | 24  |

**Table 34: Replacement of the benzene with 6-membered heteroaromatic rings<sup>241</sup>**

The previous attempts to increase solubility of the cinnamide series are summarised in **Figure 76**.<sup>241</sup>



**Figure 76: Summary of the previous attempts to increase the solubility of the cinnamide series<sup>241</sup>**

### 3.5. Results and discussion: Optimisation of the cinnamide series

#### 3.5.1. Strategy to improve the profile of the cinnamide series

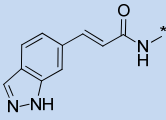
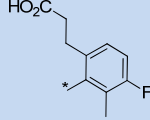
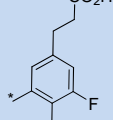
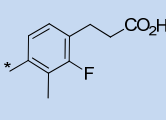
From the set of cinnamide indazoles discussed in the previous sections, only a handful of these molecules displayed the required solubility with regard to our optimisation goals, even for the analogues with PFI less than 6. This could imply that, for this specific class of compounds, only targeting the PFI might not be sufficient in order to achieve our desired solubility. Conversely, the high solubility of the piperidine analogue **3.77** (FaSSIF solubility > 1059 µg/mL, **Table 33, p. 203**) demonstrated the beneficial effect on aqueous solubility of introducing an ionisable centre on the cinnamide series. However, the introduction of the piperidinyl moiety had resulted in a loss of activity against mPTP. From consideration of this result, it was reasoned that the introduction of a basic group might be an attractive strategy to improve solubility, but that the challenge would be to balance this physicochemical improvement with mPTP activity. Therefore, the first strategy for the cinnamide series was to investigate whether a basic group could be introduced while retaining mPTP activity. Moreover, the introduction of this structural feature will have to deliver molecules with acceptable DMPK profile, for them to be considered for progression into *in vivo* PK/PD experiments.

#### 3.5.2. Introduction of a basic group in the cinnamide series

Taking into consideration the SAR features ascertained previously, it was considered that the highest probability of retaining activity while introducing an additional structural motif on the molecule was to substitute the right-hand side benzene. Additionally, three extended carboxylic acid molecules (compounds **3.86**, **3.87** and **3.88**, **Table 35**) were prepared by other members of our laboratories, as precursors of potential tool compounds for a biological target identification effort.<sup>241</sup> In relation to the current study, these compounds were relevant in suggesting that both the *ortho*- and the *meta*-position to the amide bond were tolerant to substitution with a polar group with regard to mPTP activity. Indeed, the *ortho*- and *meta*-propanoic acid derivatives **3.86**

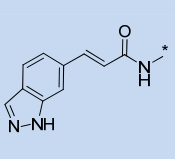
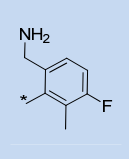
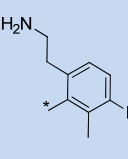
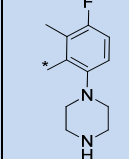
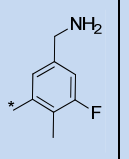
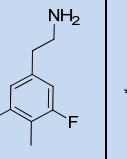
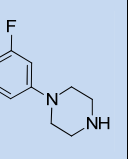
and **3.87** displayed a liver CRC pIC<sub>50</sub> of 7 and 6.6, respectively. Conversely, the *para*-propanoic acid derivative **3.88** was much less active, with a liver CRC pIC<sub>50</sub> of 4.8. Hence, these carboxylic acid compounds suggested that the *ortho*- and the *meta*-position to the amide bond were the most promising attachment points for introducing potential aqueous-solubilising groups. Analogue **3.86** was in fact an appealing molecule, since its high mPTP activity was combined with a good aqueous solubility (FaSSiF = 133 µg/mL), a low microsomal clearance (less than 0.7 mL/min/g for every species investigated) and a high free fraction in rat blood (Fu,bl = 5.3%). However, this cinnamide carboxylic acid analogue **3.86** also proved to have a low permeability (Madin-Darby canine kidney permeability = 41 nm/sec) which could potentially limit its oral absorption *in vivo*. As a probable consequence of this low permeability, compound **3.86** was characterised by a sub-optimal *in vivo* PK profile, since in a mouse SOA study at 5 mg/kg, the molecule displayed a limited systemic C<sub>max</sub> of 0.09 µM (T<sub>max</sub> = 30 min) and a low area under the curve (AUC) of 0.13 µM.h. This *in vivo* PK profile explained why the progression compound **3.86** was paused from the project.



|  |  |  |  |
|---|---|--|---|
| <b>Compound</b>   | <b>3.86</b>   | <b>3.87</b>  | <b>3.88</b>   |
| <b>Liver CRC pIC<sub>50</sub></b>   | 7   | 6.6  | 4.8   |
| <b>MW</b>   | 367   | 367  | 367   |
| <b>clogP</b>  | 2.3   | 3.2  | 3.2   |
| <b>Chrom logD / PFI</b>   | ND / ND   | 1.7 / 4.7  | 1.5 / 4.5   |
| <b>CLND (µg/mL)</b>   | ND  | ≥ 106  | ≥ 116   |
| <b>FaSSIF (µg/mL)</b>   | 133   | 42   | 114   |
| <b>h IVC (mL/min/g)</b>   | < 0.6   | < 0.6  | < 0.6   |
| <b>r IVC (mL/min/g)</b>   | < 0.7   | < 0.7  | < 0.7   |
| <b>m IVC (mL/min/g)</b>   | < 0.7   | < 0.7  | 0.7   |
| <b>Fu,bl</b>  | 5.3%  | 3.1%   | 3.3%  |

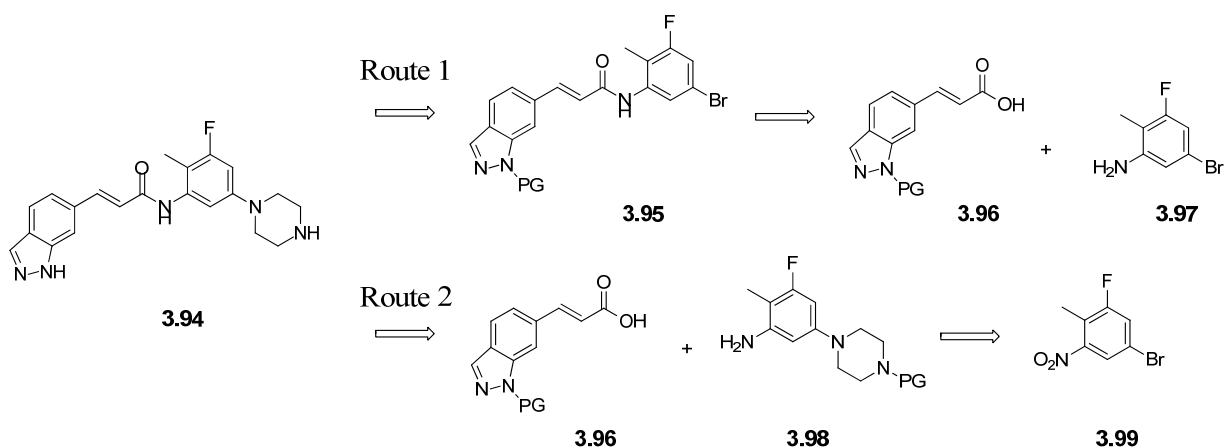
**Table 35: Profile of the carboxylic acids 3.86, 3.87 and 3.88<sup>241</sup>**

Prior to compound synthesis, several potential basic groups at the *ortho*- and the *meta*-position to the amide bond of the cinnamide series were considered. Additionally, the 3-fluoro-2-methyl functionalisation on the benzene was retained, since this had previously demonstrated to increase mPTP potency (see **Table 27, p. 157**). Three basic groups were envisaged: aminomethyl group (compounds **3.89** and **3.92**, **Table 36**), aminoethyl group (compounds **3.90** and **3.93**) and piperazine (**3.91** and **3.94**). However, the piperazinyl analogues **3.91** and **3.94** offered the advantage of not having an additional benzylic CH<sub>2</sub>, which is a potential metabolic liability,<sup>284</sup> with regard to oxidation of the benzylic CH<sub>2</sub> to the corresponding benzylic alcohol. Hence, the decision was taken to prioritise the synthesis of piperazines **3.91** and **3.94**.

|   |   |   |   |  |   |   |
|---|---|---|---|--|---|---|
|  |  |  |  |  |  |  |
| <b>Compound</b>   | <b>3.89</b>   | <b>3.90</b>   | <b>3.91</b>   | <b>3.92</b>  | <b>3.93</b>   | <b>3.94</b>   |
| <b>MW</b>   | 324   | 338   | 379   | 324  | 338   | 379   |
| <b>clogP</b>  | 1.7   | 1.8   | 2.9   | 2.3  | 2.7   | 2.9   |
| <b>Calculated PFI</b>   | 5.3   | 5.4   | 5   | 4.8  | 5.2   | 4.9   |

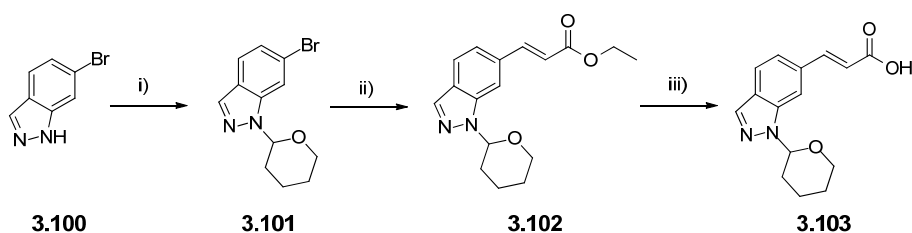
**Table 36: Amine-containing molecules envisaged to combine aqueous solubility with mPTP potency**

In order to synthesise the targeted compounds **3.91** and **3.94**, two retrosynthetic approaches were considered (**Figure 77**). It was reasoned that the key step towards the formation of the products would be the introduction of the piperazine onto the benzene for which a transition metal-catalysed cross-coupling Buchwald-Hartwig reaction was envisaged. The most attractive route would be introducing the piperazine towards the end of the synthesis, as this would allow us to efficiently investigate the formation of other amine-containing molecules in the event that analogues **3.91** and **3.94** revealed to be interesting. Accordingly, in the first retrosynthetic approach (Route 1), the piperazinyl derivative **3.94** would be obtained by a transition metal-catalysed cross-coupling of the bromobenzyl intermediate **3.95** with piperazine. The bromobenzyl analogue **3.95** would be the product of an amidation reaction between the indazole cinnamic acid **3.96** and the commercially available aniline **3.97**. It is worth noting that the THP-protected version of the indazole cinnamic acid **3.96** was available in bulk in our laboratories, since this intermediate was used to synthesise the compounds discussed previously. The alternative retrosynthetic approach (Route 2) relied on performing the Buchwald-Hartwig reaction with the commercial bromobenzyl analogue **3.99**, prior to forming the amide bond between the aniline derivative **3.98** and the cinnamic acid **3.96**. This second approach would be less convergent than the first route for the introduction of the amine onto the target, however, it offered the advantage on executing the Buchwald-Hartwig reaction on a less functionalised system.



**Figure 77: Retrosynthetic analysis of compound 3.94**

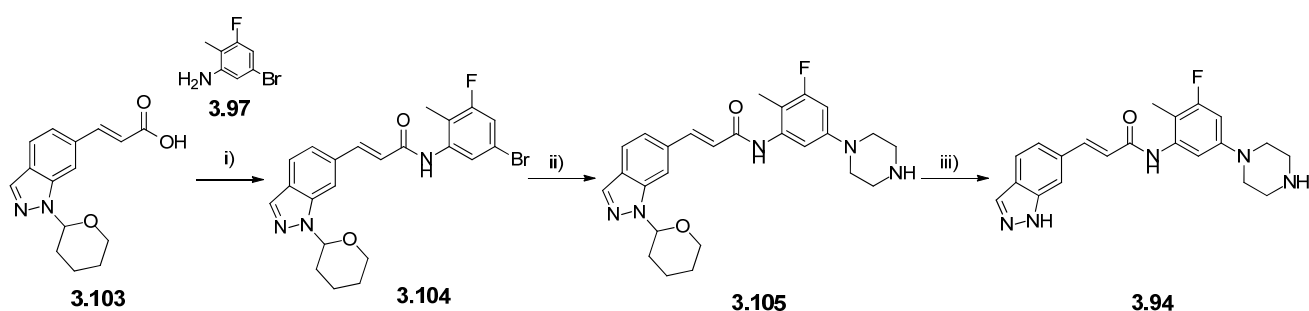
Due to the opportunity for late stage diversification, route 1 was examined as a priority for the preparation of compound **3.94**. As stated previously, the THP-protected indazole cinnamic acid **3.103** was synthesised previously by another member of our laboratories, following **Scheme 28**.<sup>287</sup> The commercially available 6-bromoindazole **3.100** was protected using 3,4-dihydro-2*H*-pyran. A Heck coupling with ethyl acrylate afforded the indazole cinnamate ester **3.102** in good yield, which was saponified under basic conditions to give the THP-protected indazole cinnamic acid **3.103**.



i) 3,4-dihydro-2*H*-pyran (2 eq), pyridinium *p*-toluenesulfonate (0.2 eq), THF, 70 °C, **quantitative**; ii) ethyl acrylate (1.2 eq), Pd(OAc)<sub>2</sub> (0.05 eq), tri-*o*-tolylphosphine (0.1 eq), NEt<sub>3</sub> (1.2 eq), DMF, 120 °C, **93%**; iii) 2 M NaOH aqueous solution (6 eq), THF:MeOH = 1:0.3, rt, **94%**.

**Scheme 28: Previous synthesis of THP-protected indazole cinnamic acid 3.103**<sup>287</sup>

The route employed to synthesise the targeted piperazine-containing cinnamide **3.94** is described in **Scheme 29**. An amidation reaction, mediated by HATU, was carried out with 5-bromo-3-fluoro-2-methylaniline **3.97** in order to afford the bromobenzyl analogue **3.104** in modest yields, probably due to the low nucleophilicity of the relatively electron-poor aniline. Several reaction conditions were investigated (**Table 37**) for the Buchwald-Hartwig coupling with piperazine to give the piperazinyl intermediate **3.105**. A final deprotection of the THP group under acidic conditions afforded compound **3.94**.

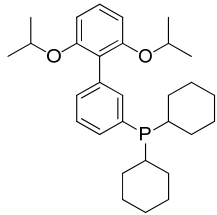
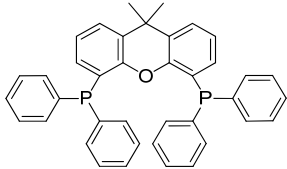


i) 5-bromo-3-fluoro-2-methylaniline **3.97** (1.5 eq), HATU (1.8 eq), *N,N*-diisopropylethylamine (3.1 eq), DMF, rt to 50 °C, **35%**; ii) piperazine (1.5 eq), Pd<sub>2</sub>(dba)<sub>3</sub> (0.1 eq), NaO<sup>t</sup>Bu (1.5 eq), toluene, **see Table 37** for ligand, temperature, mode of heating and **yields**; iii) 4 M HCl solution in dioxane (10 eq), EtOH, 50 °C, **56%**.

### Scheme 29: Synthesis of the piperazinyl analogue **3.94**

A range of reaction conditions and reagents were considered for the Buchwald-Hartwig coupling of the bromobenzyl derivative **3.104** with piperazine (**Table 37**). The palladium-catalysed carbon-nitrogen coupling has been reviewed on several occasions in the literature, especially from an industrial point view.<sup>288</sup> Of special interest for the current study is the review from Buchwald's group<sup>289</sup> which can be viewed as a user's guide in order to select reaction conditions for this type of coupling reaction. Indeed, it is well established that the outcome of the Buchwald reaction is highly substrate-specific and that yields heavily depend on reaction parameters, such as Pd source, base, solvent and temperature. In our specific case, the cross-coupling reaction of a secondary

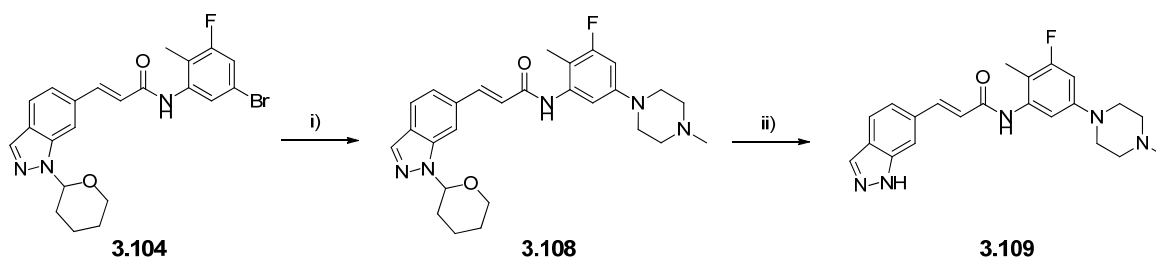
aliphatic amine (piperazine) was investigated, and for this system the recommendation<sup>289</sup> is to use RuPhos **3.106** (Table 37) as a ligand. Nevertheless, in order to have a point of comparison with this monodentate phosphine ligand presenting a biaryl backbone, the bisphosphine XantPhos **3.107** (Table 37) was also investigated. As a source of palladium for this reaction, the stable Pd(0) complex Pd<sub>2</sub>(dba)<sub>3</sub> was used as it obviated the need for a reduction step to form the Pd(0) species. Toluene and NaO<sup>t</sup>Bu were used, as solvent and base, respectively, as these tend to be the most common solvent and base for this type of reaction.<sup>289</sup>

|  |                   |  |           |       |
|---|-------------------|--|-----------|-------|
| <b>3.106, RuPhos</b>  |                   | <b>3.107, XantPhos</b>   |           |       |
| Entry   | Ligand            | Temperature  | Microwave | Yield |
| 1   | XantPhos (0.2 eq) | 80 °C to 110 °C  | no        | 0%    |
| 2   | RuPhos (0.2 eq)   | 80 °C to 110 °C  | no        | 43%   |
| 3   | RuPhos (0.2 eq)   | 80 °C  | yes       | 16%   |

**Table 37: Reaction conditions for the Buchwald-Hartwig coupling to synthesise the piperazinyl intermediate 3.105**

Based on the results shown in **Table 37**, it was established that the reaction did not proceed when using XantPhos as a ligand (entry **1**), that the reaction afforded the targeted intermediate **3.105** in a moderate yield when RuPhos was used thermally (entry **2**) and that only a poor yield was obtained when RuPhos was used under microwave irradiation (entry **3**). It was hypothesised that the high basicity of NaO<sup>t</sup>Bu ( $pK_a = 17$ ) compared to the calculated  $pK_a$  of the amide NH of **3.104** (calculated  $pK_a = 13.9$ ) might have hampered this reaction. If this reaction was to be repeated, it would be pertinent to investigate lower basicity bases, such as NaOMe ( $pK_a = 15.5$ ) as an organic base, or weak inorganic bases such as Cs<sub>2</sub>CO<sub>3</sub>, K<sub>3</sub>PO<sub>4</sub> and K<sub>2</sub>CO<sub>3</sub>, which have actually demonstrated to increase the functional group tolerance of palladium-catalysed amination reactions.<sup>290</sup>

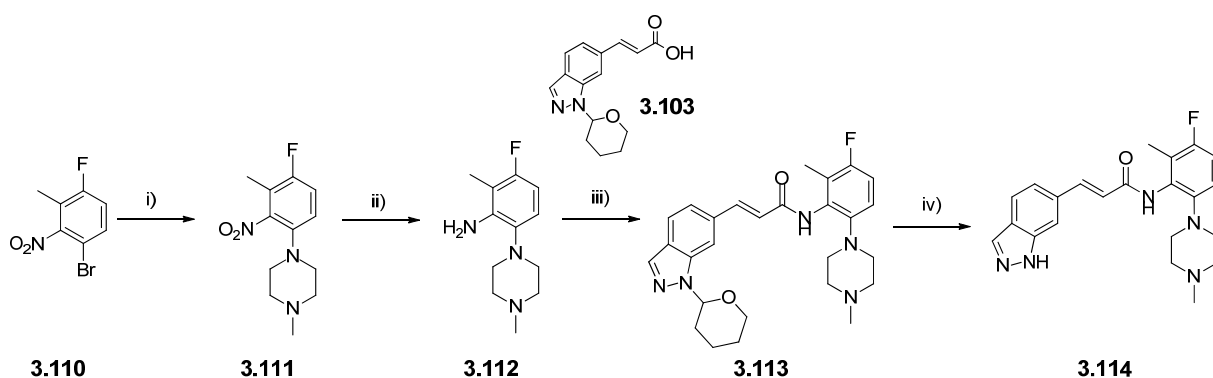
In an attempt to assess the versatility of the Buchwald chemistry devised for our template, and in order to deliver an additional potentially interesting final compound for testing, the route developed above was carried out with *N*-methylpiperazine to prepare compound **3.109** (**Scheme 30**). In this specific case, the THP-protected intermediate **3.108** was not purified by regular chromatography, but the basicity of the methylpiperazinyl group was utilised to purify the intermediate **3.108** by ion exchange chromatography. The product obtained was progressed directly to the acidic deprotection step without further purification, offering the final compound **3.109** in 21% yield over two steps, which was a comparable yield to that obtained previously for compound **3.94**.



i) *N*-methylpiperazine (1.5 eq), Pd<sub>2</sub>(dba)<sub>3</sub> (0.1 eq), RuPhos (0.2 eq), NaO<sup>t</sup>Bu (1.5 eq), toluene, 110 °C; ii) 4 M HCl solution in dioxane (10 eq), EtOH, 50 °C, **21% over 2 steps**.

### Scheme 30: Synthetic route to access the methylpiperazinyl analogue 3.109

For the analogues where the piperazinyl group was *ortho* to the amide bond, it was anticipated that the Buchwald chemistry would be more problematic, due to steric hindrance hampering the reaction. In order to address this potential limitation, the route to these compounds employed the Buchwald coupling as a first step (Route 2 from **Figure 77**, p. 210), starting with the commercially available bromo-nitrobenzyl derivative **3.110** (**Scheme 31**). In this case, two different sets of conditions were investigated for the Buchwald coupling. Firstly, RuPhos with Pd<sub>2</sub>(dba)<sub>3</sub> under microwave irradiation yielded the targeted piperazine intermediate **3.111** in 35% (**Table 38**, entry 1) and, interestingly, the use of BINAP **3.115** with Pd(OAc)<sub>2</sub> offered the product with an improved yield of 59% (**Table 38**, entry 2). After having introduced the piperazinyl group onto the phenyl ring, nitrobenzene **3.111** was reduced to its corresponding aniline equivalent **3.112** using tin chloride. An amide coupling with the THP-protected indazole cinnamic acid **3.103** afforded the indazole protected intermediate **3.113**, which was subsequently deprotected under acidic conditions to deliver the *ortho*-piperazinylbenzyl compound **3.114** (**Scheme 31**).



i) *N*-methylpiperazine (1.5 eq), NaO<sup>t</sup>Bu (1.5 eq), toluene, 120 °C, microwave, see Table 38 for catalyst, ligand and yields; ii) SnCl<sub>2</sub> (5 eq), EtOH, 70 °C to 80 °C, **66%**; iii) (*E*)-3-(1-(tetrahydro-2*H*-pyran-2-yl)-1*H*-indazol-6-yl)acrylic acid **3.103** (1.2 eq), HATU (2 eq), *N,N*-diisopropylethylamine (4 eq), DMF, rt, **46%**; iv) 3 M HCl solution in MeOH (5 eq), EtOH, 50 °C, **55%**.

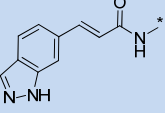
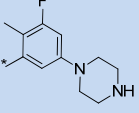
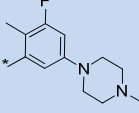
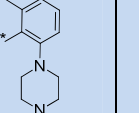
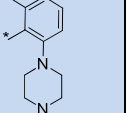
**Scheme 31: Synthetic route to prepare the *ortho*-piperazinybenzyl analogue 3.114**

| <br><b>BINAP, 3.115</b> |  |            |
|-------------------------|--|------------|
| Entry                   | Catalyst and ligand  | Yield      |
| 1                       | Pd <sub>2</sub> (dba) <sub>3</sub> (0.1 eq)<br>RuPhos (0.2 eq) | <b>35%</b> |
| 2                       | Pd(OAc) <sub>2</sub> (0.15 eq)<br>BINAP (0.2 eq)               | <b>59%</b> |

**Table 38: Reaction conditions for the Buchwald-Hartwig coupling to synthesise 3.111**



The *meta*-piperazinybenzyl compounds **3.94** and **3.109**, alongside with their *ortho*-substituted analogues **3.91** and **3.114**, respectively, were submitted to biological profiling (**Table 39**). It should be noted that compound **3.91** and its synthetic route was designed by the author, and that its synthesis was carried out by an external collaborator.<sup>154</sup>

|  |  |  |  |  |
|---|---|---|---|---|
| Compound  | <b>3.94</b>   | <b>3.109</b>  | <b>3.91</b> <sup>154</sup>  | <b>3.114</b>  |
| Liver CRC pIC <sub>50</sub>   | 4.3   | 4.7 <sup>a</sup>  | < 4   | 6.2   |
| Brain CRC pIC <sub>50</sub>   | ND  | < 4   | ND  | 5.5   |
| LE / LLE  | 0.21 / 0.18   | 0.22 / 0.17   | NA / NA   | 0.29 / 0.24   |
| MW  | 379   | 394   | 379   | 394   |
| clogP   | 2.9   | 3.5   | 2.9   | 3.5   |
| Chrom logD / PFI  | ND  | 3.1 / 6.1   | 2 / 5   | 2.7 / 5.7   |
| CLND (µg/mL)  | ND  | ≥ 148   | ≥ 133   | ≥ 154   |
| FaSSiF (µg/mL)  | 167   | 350   | > 1000  | 798   |
| h IVC (mL/min/g)  | ND  | ND  | < 0.6   | 3   |
| r IVC (mL/min/g)  | ND  | ND  | 1.8   | 5.4   |
| m IVC (mL/min/g)  | ND  | ND  | 1.5   | 8.1   |
| Fu,bl   | ND  | ND  | 8.1%  | 9.2%  |

<sup>a</sup>Compound was only reported active in 3 out of 6 test occasions.

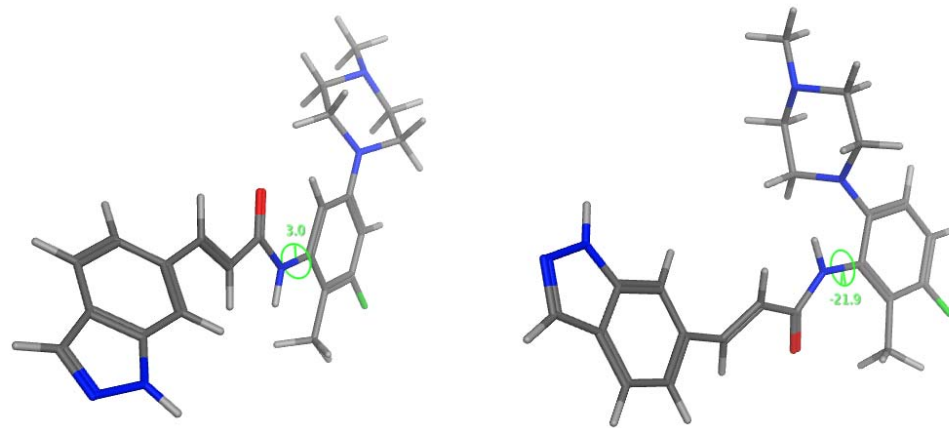
**Table 39: Profile of the piperazinybenzyl analogues 3.94, 3.109, 3.91 and 3.114**

The first observation was that these analogues were much less active against mPTP than the progenitor 3-fluoro-2-methylbenzyl cinnamide **3.14** (liver CRC pIC<sub>50</sub> = 8.1, **Table 27, p. 157**), particularly the two *meta*-piperazinybenzyl analogues **3.94** and **3.109** which

were only weakly active in our primary biological assay (liver CRC  $pIC_{50}$  = 4.3 and 4.7, respectively). Concerning the *ortho*-piperazinylbenzyl analogues, the unsubstituted piperazine **3.91** was below the threshold of activity for our biological assay, whereas *N*-methylpiperazine **3.114** displayed a modest biological potency (liver CRC  $pIC_{50}$  = 6.2). Despite the reduction in potency, all these four piperazinyl analogues met our solubility criteria of FaSSIF solubility greater than 100  $\mu\text{g/mL}$ , indicating that the strategy of introducing a basic group into the cinnamide chemical series was robust with regard to increasing the aqueous solubility.

Interestingly, the *ortho*-piperazinylbenzyl derivatives were more soluble than their corresponding *meta*-substituted analogues, despite having similar respective lipophilicity. Indeed, the FaSSIF solubilities of the *ortho*-substituted *NH*-piperazine **3.91** and *N*-methylpiperazine **3.114** (FaSSIF > 1000  $\mu\text{g/mL}$  and = 798  $\mu\text{g/mL}$ , respectively) were significantly higher compared to that of their corresponding *meta*-substituted analogues **3.94** and **3.109** (FaSSIF = 167  $\mu\text{g/mL}$  and = 350  $\mu\text{g/mL}$ , respectively). It was hypothesised that a greater steric hindrance encountered by the *ortho*-substituted analogues, leading to a larger dihedral angle between the phenyl ring and the amide bond, was driving the observed increase in FaSSIF solubility. Similar observations have been reported in the literature, and a recent review<sup>291</sup> highlights how disrupting molecular planarity by increasing the dihedral angle, which in turn leads to a decreased crystal packing energy, increases aqueous solubility. To support this theory in the current study, the dihedral angle between the phenyl ring and the amide moiety for the local low energy conformation was calculated for the *meta*-piperazinylbenzyl analogue **3.109** and its corresponding *ortho*-piperazinylbenzyl isomer **3.114** (**Figure 78**). The predicted dihedral angle of the *meta* analogue **3.109** was indeed much smaller than the one of the *ortho* compound **3.114**, with absolute values of  $3^\circ$  and  $21.9^\circ$ , respectively.

This finding could differentiate the cinnamide series over the isoxazole series, for which the high degree of planarity of the lead compound **3.16a**, evidenced by its crystal structure (**Figure 72** and **Figure 73**, p. 198), was hypothesised to contribute to its low aqueous solubility.

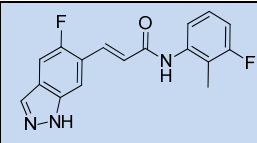


Compound **3.109**  
Dihedral angle = 3°  
FaSSIF solubility = 350 µg/mL

Compound **3.114**  
Dihedral angle = 21.9°  
FaSSIF solubility = 798 µg/mL

**Figure 78: Dihedral angles for the low local energy conformation of molecules 3.109 and 3.114**

Encouraged by the fact that compound **3.114** combined high aqueous solubility and moderate mPTP activity, approaches to further increase mPTP potency were explored. Prior to the author commencing work on this area, it was discovered that addition of a fluorine at the 5-position of the indazole increased mPTP inhibitory activity, but also that the concomitant increase in lipophilicity was detrimental for solubility.<sup>241</sup> As an example of this SAR observation, the 5-fluoroindazole **3.116** (Table 40), prepared previously by other members of our laboratories,<sup>241</sup> displayed an increased CRC potency (pIC<sub>50</sub> greater than 9) over the corresponding unsubstituted indazole **3.14** (liver CRC pIC<sub>50</sub> of 8.1), however, **3.116** exhibited a low FaSSIF solubility of 1 µg/mL.

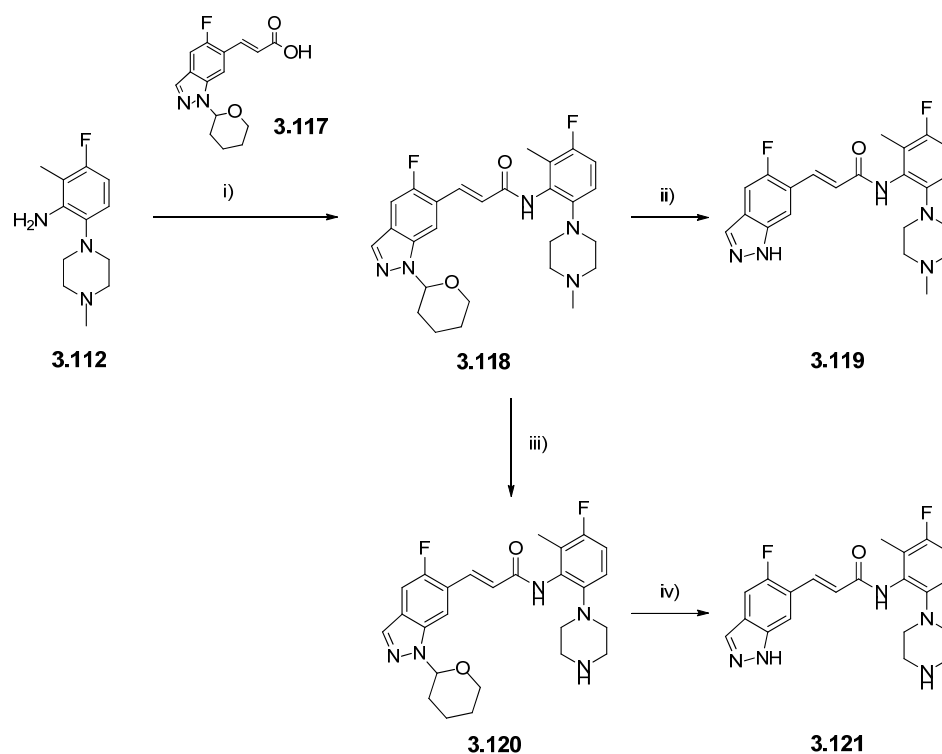
| Structure                   |  |
|-----------------------------|--|
| Compound                    | 3.116  |
| Liver CRC pIC <sub>50</sub> | > 9  |
| Brain CRC pIC <sub>50</sub> | 8.7 <sup>a</sup>   |
| LE / LLE                    | > 0.53 / > 0.42  |
| MW                          | 313  |
| clogP                       | 3.7  |
| Chrom logD / PFI            | 4.5 / 7.5  |
| CLND (µg/mL)                | 1  |
| FaSSIF (µg/mL)              | 1  |
| h IVC (mL/min/g)            | 1.8  |
| r IVC (mL/min/g)            | 10.9   |
| m IVC (mL/min/g)            | 18.1   |
| Fu,bl                       | 1.8%   |

<sup>a</sup>Compound was only reported with a measured pIC<sub>50</sub> value in 2 out of 6 test occasions and for the other 4 test occasions, pIC<sub>50</sub> was greater than 9.

**Table 40: Profile of the 5-fluoroindazole analogue 3.116, prepared previously in our laboratories<sup>241</sup>**

In relation to the current study, it was reasoned that the increase in lipophilicity resulting from the introduction of the fluorine could be offset by the presence of the basic piperazine. Accordingly, the relevant 5-fluoroindazole analogues were prepared. The amide intermediate **3.118** (Scheme 32) was obtained by reacting the aniline derivative **3.112**, made previously according to Scheme 31 (p. 215), with the 5-fluoroindazole cinnamic acid derivative **3.117**, which was synthesised elsewhere in our laboratories following a similar route to the one exemplified in Scheme 28 (p. 210).<sup>241</sup> The *N*-methylpiperazinyl **3.119** was then obtained after acidic deprotection of the THP protecting group. In an effort to expedite the synthesis of the corresponding

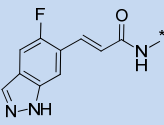
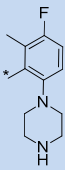
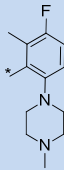
unsubstituted piperazine analogue **3.121** (Scheme 32), *N*-demethylation of the intermediate **3.118** was attempted. This was achieved *via* a two-step process involving the formation of the *N*-oxide version of the piperazine with a peroxy acid derivative, followed by a FeSO<sub>4</sub>•7H<sub>2</sub>O mediated Polonovski reaction<sup>292</sup> to afford the desired secondary amine **3.120**, in 20% yield. During the course of this reaction, the treatment of the crude residue obtained with an aqueous solution of the iron-chelating agent ethylenediaminetetraacetic acid (EDTA) was performed in order to help the separation of residual iron salts.<sup>293</sup> The final deprotection step under acidic conditions afforded the targeted unsubstituted piperazine compound **3.121**.



i) (*E*)-3-(5-fluoro-1-(tetrahydro-2*H*-pyran-2-yl)-1*H*-indazol-6-yl)acrylic acid **3.117** (1.2 eq), HATU (1.5 eq), *N,N*-diisopropylethylamine (2 eq), DMF, rt, **82%**; ii) 3 M HCl solution in MeOH (10 eq), EtOH, 50 °C, **95%**; iii) magnesium monoperoxyphthalate hexahydrate (80% by weight, 1.1 eq), then iron(II) sulfate heptahydrate (1.9 eq), then 0.4 M EDTA aqueous solution (excess), MeOH, rt, **20%**; iv) 3 M HCl solution in MeOH (10 eq), EtOH, 50 °C, **75%**.

**Scheme 32: Synthetic route to obtain the 5-fluoroindazole *ortho*-piperazinylbenzyl analogues **3.119** and **3.121****

The impact of the introduction of the 5-fluoroindazole in the unsubstituted piperazine compound **3.121** (**Table 41**) dramatically changed its biological profile in comparison to the 5-*H*-indazole progenitor compound **3.91** (**Table 39, p. 216**), since the liver CRC pIC<sub>50</sub> increased from below the threshold of the biological assay to 5.9. Additionally, the FaSSIF solubility dropped from over 1000 µg/mL to 70 µg/mL, an observation which was somewhat challenging to rationalise. However, for the *N*-methylpiperazine **3.119** (**Table 41**), our hypothesis of balancing the increased lipophilicity resulting from the 5-fluoroindazole with the presence of the piperazine was successful. Indeed, compound **3.119** displayed the combination of a promising mPTP potency (liver CRC pIC<sub>50</sub> of 6.9) and an excellent FaSSIF solubility (798 µg/mL), which was an unprecedented profile for the cinnamide chemical series. Despite this significant breakthrough, the *in vitro* microsomal clearance was sub-optimal, with, for instance, a high mouse IVC of 12.9 µg/mL, and it was therefore necessary to investigate further the DMPK profile of these novel basic group-containing molecules.

|   |   |   |
|---|---|---|
|  |  |  |
| <b>Compound</b>   | <b>3.121</b>  | <b>3.119</b>  |
| <b>Liver CRC pIC<sub>50</sub></b>   | 5.9   | 6.9   |
| <b>Brain CRC pIC<sub>50</sub></b>   | 5.4   | 6.8   |
| <b>LE / LLE</b>   | 0.28 / 0.24   | 0.31 / 0.25   |
| <b>MW</b>   | 397   | 411   |
| <b>clogP</b>  | 3.2   | 3.8   |
| <b>Chrom logD / PFI</b>   | 2.3 / 5.3   | 2.9 / 5.9   |
| <b>CLND (µg/mL)</b>   | ≥ 110   | ≥ 165   |
| <b>FaSSIF (µg/mL)</b>   | 70  | 798   |
| <b>h IVC (mL/min/g)</b>   | < 0.6   | 7.1   |
| <b>r IVC (mL/min/g)</b>   | 1.5   | 7.9   |
| <b>m IVC (mL/min/g)</b>   | 2.8   | 12.9  |
| <b>Fu,bl</b>  | 7.4%  | 7.9%  |

**Table 41: Profile of the 5-fluoroindazole piperazinyl derivatives 3.121 and 3.119**

### 3.5.3. Attempts to optimise the DMPK profile of the basic group-containing cinnamides

From the previous section, the two most promising compounds in terms of combining mPTP potency and aqueous solubility were the two *ortho*-piperazinylbenzyl cinnamides **3.114** and **3.119**. An additional benefit from the introduction of the basic piperazine was that the *in vitro* fraction unbound in rat blood increased significantly. Thus, the blood fraction unbound increased from to 2.6% for the progenitor compound **3.14** (Table 27, p. 157) to 9.2% in the piperazinyl molecule **3.114** (Table 39, p. 216) and to 7.9% in compound **3.119** (Table 41, p. 222). However, the *in vitro* microsomal clearance of the piperazine-containing cinnamides was sub-optimal, especially in mouse for which the microsomal clearance went from 5.9 mL/min/g for compound **3.14** to 8.1 mL/min/g and to 12.9 mL/min/g for analogues **3.114** and **3.119**, respectively. This could potentially be a critical limitation for this new class of basic group-containing compounds, since mouse was the animal species considered for potential PK/PD studies. With a view to benchmark the *in vivo* PK profile of these new piperazine-containing molecules, mouse SOA studies were carried out on compounds **3.114** (Figure 80) and **3.119** (Figure 81), and these data were compared with the SOA profile of the progenitor compound **3.14** (Figure 79).<sup>268</sup>

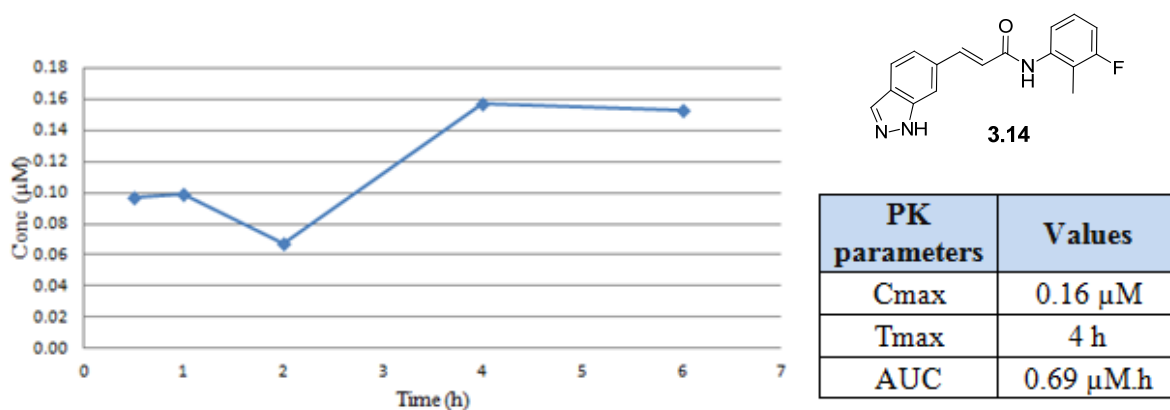


Figure 79: PK profile of the mouse SOA model of compound 3.14 at 5 mg/kg



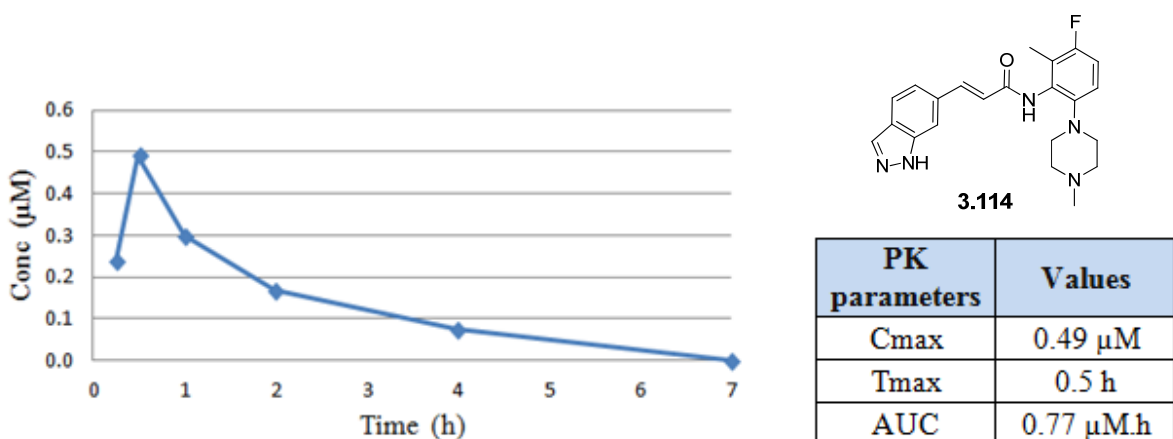


Figure 80: PK profile of the mouse SOA model of compound 3.114 at 5 mg/kg

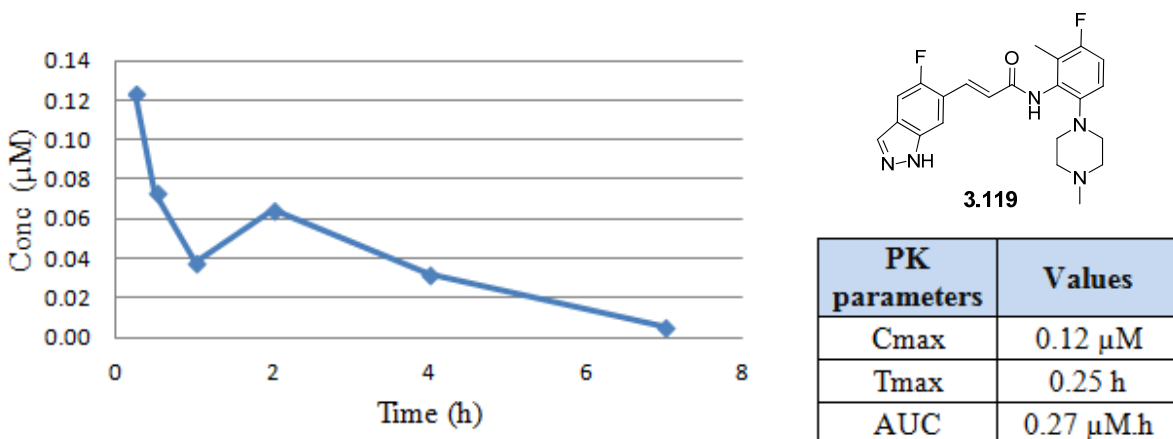


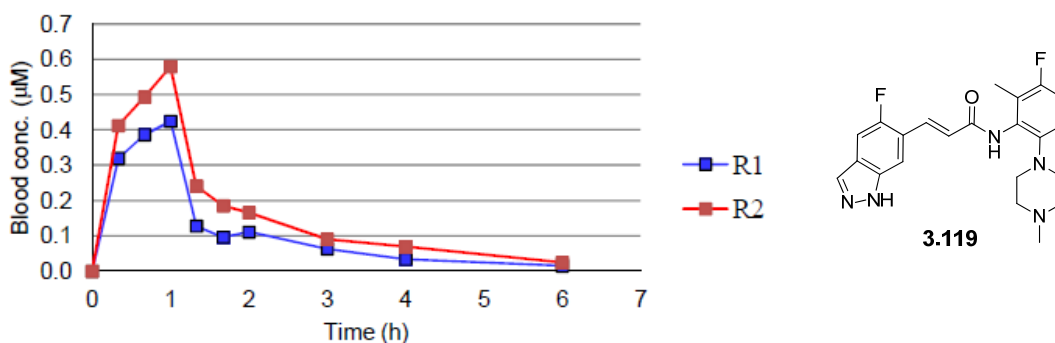
Figure 81: PK profile of the mouse SOA model of compound 3.119 at 5 mg/kg

The cinnamide analogues **3.14**, **3.114** and **3.119** displayed low systemic exposure in mouse after oral dosing. Indeed, these compounds exhibited an AUC of less than 1 µM.h, which was much lower than the AUC of 8.12 µM.h observed for the previously discussed compound **3.16a** from the isoxazole series (Figure 67, p. 184). For the recently identified compounds **3.114** and **3.119**, these sub-optimal *in vivo* PK profiles paused their progression within our medicinal chemistry programme.

In an attempt to rationalise the low *in vivo* exposures observed, it was reasoned that the profile obtained could either be limited by compound absorption or by rapid clearance (or by a combination of the two). These cinnamide compounds exhibited good membrane permeability, since the artificial membrane permeability was measured at 463 nm/sec, 290 nm/sec and 360 nm/sec for compounds **3.14**, **3.114** and **3.119**, respectively. Hence, the low systemic exposure of compound **3.14** could be attributed to a mixture of poor oral absorption driven by low aqueous solubility (FaSSIF = 5 µg/mL), and high clearance (m IVC = 5.9 mL/min/g). However, for the two piperazine-containing molecules **3.114** and **3.119**, it was hypothesised that the combination of good aqueous solubility and good membrane permeability would confer them an acceptable level of oral absorption. Consequently, rapid clearance could be the main contributor to their sub-optimal *in vivo* PK profiles.

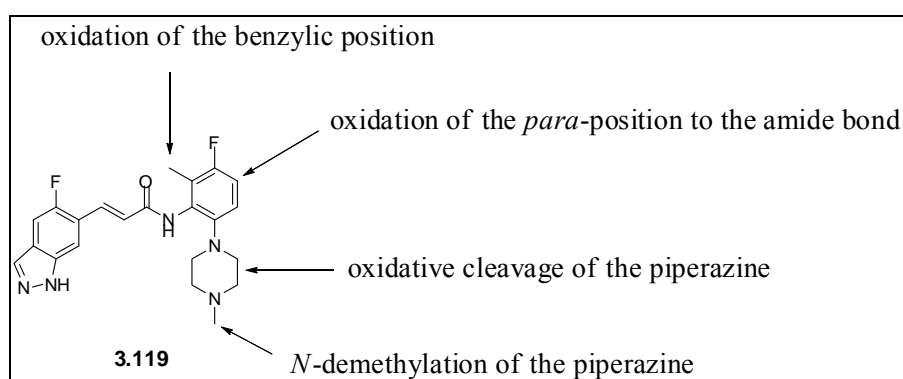
To verify this theory, compound **3.119** was administered intravenously (therefore bypassing absorption) to two rats, at a 1 mg/kg dose, and the compound blood concentration was measured at different time points (**Figure 82**).<sup>268</sup> Averaging the results obtained for the two rats, the C<sub>max</sub> observed was 0.50 µM, the half-life was 1.6 h and the *in vivo* clearance was measured at 65 mL/min/g. This rapid IV clearance (the average rat liver blood flow is estimated at 85 mL/min/g)<sup>294</sup> was therefore unambiguously a key parameter explaining the overall sub-optimal *in vivo* PK profile after oral administration.

Accordingly, modulating the *in vitro* clearance of the basic-containing cinnamides, in order to ultimately improve their *in vivo* clearance, was considered a new important optimisation goal.



**Figure 82: Rat PK profile of compound 3.119 after 1 mg/kg IV administration**

In order to help the design of molecules which would potentially overcome the clearance issue identified, an *in vitro* metabolite identification study was carried out on compound **3.119** by another member of our laboratories.<sup>171</sup> In this experiment, **3.119** was incubated at 10 µM in mouse microsomes and the major metabolites obtained were identified using a LC-QTOF-MS (quadrupole time-of-flight mass spectrometer). From this study, four major sites of metabolism were highlighted: the toluene methyl group of the benzene, the *para*-position to the amide bond, the *N*-methyl group of the piperazine and the piperazinyl ring itself (**Figure 83**).



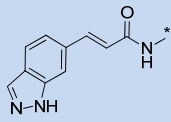
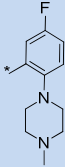
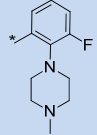
**Figure 83: Major metabolic soft spots of compound 3.119, observed after a metabolite identification study from incubation in mouse microsomes<sup>171</sup>**

Taking the above results into consideration, novel analogues were designed and synthesised to investigate these metabolic liabilities separately. For this study, the indazole was left unsubstituted and therefore compound **3.114** will be considered as the benchmark compound with regard to *in vitro* microsomal clearance (mouse IVC = 8.1 mL/min/g for **3.114**, **Table 39**, **p. 216**). It was envisaged that if optimised compounds were to be identified, the corresponding 5-fluoroindazole analogue could subsequently be synthesised.

### **3.5.3.1. Investigation of the 1<sup>st</sup> metabolic site: the toluene methyl group**

Firstly, the metabolic risk induced by the toluene methyl group *ortho* to the amide bond was assessed by considering analogues **3.122** and **3.123** (**Table 42**), which were designed by the author and synthesised by an external collaborator.<sup>154</sup> In compound **3.122**, the toluene methyl group was removed, since this was the simplest way to assess the impact on this group on microsomal clearance. The analogue obtained displayed a marginal reduction in the *in vitro* microsomal clearance across all species, as for instance, the mouse IVC was reduced from 8.1 mL/min/g for compound **3.114** (**Table 39**, **p. 216**) to 5.8 mL/min/g for the corresponding des-methyl analogue **3.122**. Nevertheless, this improvement was not significant and it was assumed that simply removing the toluene methyl metabolic liability would not be sufficient to address the overall *in vivo* metabolic clearance concern. Furthermore, the reduction in potency (liver CRC pIC<sub>50</sub> of **3.122** was 4.7) resulting from this structural modification highlighted again the importance of this methyl group for mPTP activity. Lastly, the drop in FaSSIF solubility experienced when removing the methyl group *ortho* to the amide bond (FaSSIF solubility went from 798 µg/mL for the progenitor compound **3.114** to 76 µg/mL for the des-methyl analogue **3.122**) was consistent with the molecular planarity disruption hypothesis illustrated in **Figure 78** (**p. 218**).

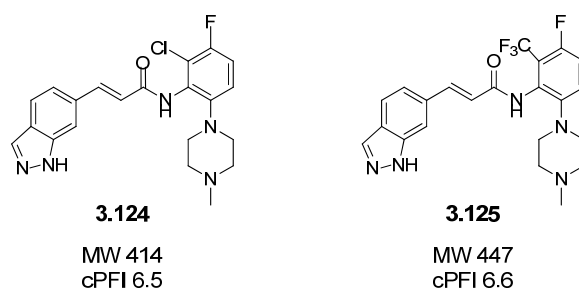
Regarding compound **3.123** (Table 42), the aim was to vary the substitution pattern of the phenyl ring and to rearrange the substituents while removing the toluene methyl group. However, not only did this alternative substitution pattern completely abolish mPTP activity, but no reduction in *in vitro* clearance was achieved in comparison to compound **3.114**.

|   |   |   |
|---|---|---|
|  |  |  |
| <b>Compound</b>   | <b>3.122</b> <sup>154</sup>   | <b>3.123</b> <sup>154</sup>   |
| <b>Liver CRC pIC<sub>50</sub></b>   | 4.7 <sup>a</sup>  | < 4   |
| <b>LE / LLE</b>   | 0.23 / 0.16   | NA  |
| <b>MW</b>   | 379   | 379   |
| <b>clogP</b>  | 3.6   | 3.6   |
| <b>Chrom logD / PFI</b>   | 3.6 / 6.6   | 3.5 / 6.5   |
| <b>CLND (µg/mL)</b>   | 18  | ≥ 145   |
| <b>FaSSIF (µg/mL)</b>   | 76  | 250   |
| <b>h IVC (mL/min/g)</b>   | 1.6   | 2.6   |
| <b>r IVC (mL/min/g)</b>   | 6.2   | 8.9   |
| <b>m IVC (mL/min/g)</b>   | 5.8   | 11.3  |
| <b>Fu,bl</b>  | 2.6%  | 5.5%  |

<sup>a</sup>Compound was only reported active in 1 out of 2 test occasions.

**Table 42: Profile of the compounds designed to remove the toluene methyl group**

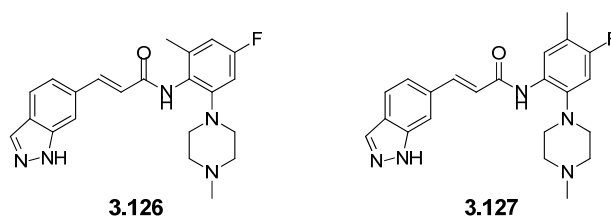
Two additional molecules were considered in order to prevent the metabolism induced by the toluene methyl group: the corresponding chlorobenzyl analogue **3.124** and the trifluoromethylbenzyl derivative **3.125** (**Figure 84**). However, these analogues were not synthesised in light of the combination of their high molecular weight and their moderately high calculated PFI.



**Figure 84: Potential compounds to prevent the metabolism induced by the toluene methyl group**

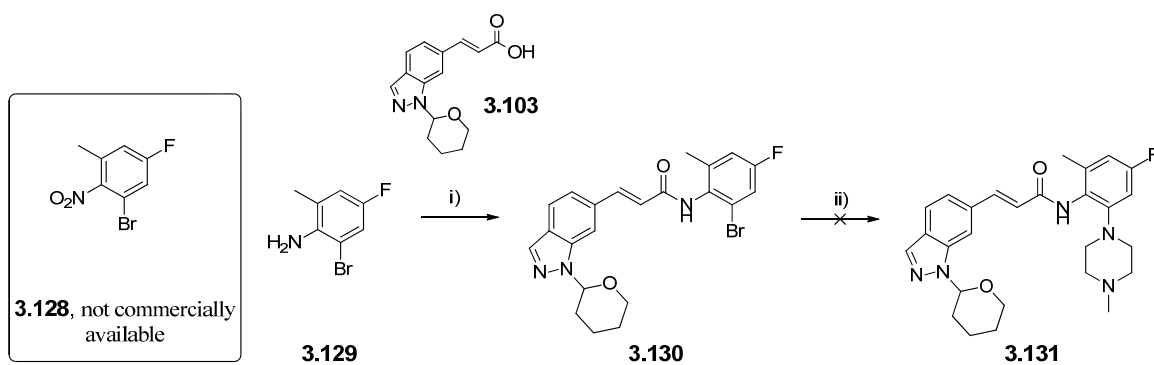
### 3.5.3.2. Investigation of the 2<sup>nd</sup> metabolic site: the *para*-position to the amide bond

The second metabolic liability investigated was the *para*-position to the amide bond, for which it was thought that introducing a fluorine atom could have the potential to block the metabolism.<sup>166,295,296</sup> It was hypothesised that retaining the three initial substituents of the benzene (methyl, fluoro and piperazinyl groups), but rearranging them in order to place the fluorine at the *para*-position to the amide bond would constitute a pragmatic approach in order to maintain mPTP potency during this exercise. Therefore, the 4-fluorobenzyl derivatives **3.126** and **3.127** were considered (**Figure 85**).



**Figure 85: Compounds designed to prevent the metabolism occurring at the *para*-position to the amide bond**

While compound **3.127** was synthesised by an external collaborator following a similar synthetic route than the one described previously in **Scheme 31** (p. 215),<sup>154</sup> the synthesis of compound **3.126** required additional investigation, since the relevant starting bromo-nitrobenzyl derivative **3.128** (**Scheme 33**), for which the chemistry was initially developed, was not commercially available. Nevertheless, 2-bromo-4-fluoro-6-methylaniline **3.129** was commercially accessible, hence it was coupled with the THP-protected indazole cinnamic acid **3.103** to afford the amide analogue **3.130** (**Scheme 33**). However, the different attempts to achieve the Buchwald coupling leading to the piperazinyl derivative **3.131** were unsuccessful.



i) (*E*)-3-(1-(tetrahydro-2*H*-pyran-2-yl)-1*H*-indazol-6-yl)acrylic acid **3.103** (1 eq), HATU (1.5 eq), *N,N*-diisopropylethylamine (1.5 eq), DMF, rt, **37%**; ii) piperazine (1.5 eq), NaO*t*Bu (1.5 eq), toluene, see **Table 43** for catalyst, ligand, temperature, mode of heating and **yields**.

**Scheme 33: Synthetic route attempted in order to obtain the piperazinyl analogue 3.131**

Three sets of conditions were attempted for the Pd-catalysed coupling of bromobenzene **3.130** with methylpiperazine: the system Pd(OAc)<sub>2</sub>/BINAP both under microwave irradiations (**Table 43**, entry **1**) and conventional heating (**Table 43**, entry **2**), and the system Pd<sub>2</sub>(dba)<sub>3</sub>/RuPhos under thermal conditions (**Table 43**, entry **3**). However, in the course of these three reactions, a mixture of unreacted starting material and the des-bromobenzyl version of **3.130** but no targeted product was observed by monitoring with LCMS. A different synthetic approach was therefore considered.

| Entry    | Catalyst and ligand  | Temperature | Microwave | Yield     |
|----------|--|-------------|-----------|-----------|
| <b>1</b> | Pd(OAc) <sub>2</sub> (0.15 eq)<br>BINAP (0.2 eq)               | 120 °C      | yes       | <b>0%</b> |
| <b>2</b> | Pd(OAc) <sub>2</sub> (0.15 eq)<br>BINAP (0.2 eq)               | 100 °C      | no        | <b>0%</b> |
| <b>3</b> | Pd <sub>2</sub> (dba) <sub>3</sub> (0.1 eq)<br>RuPhos (0.2 eq) | 80 °C       | no        | <b>0%</b> |

**Table 43: Attempted reaction conditions for the Buchwald-Hartwig coupling to form 3.131**

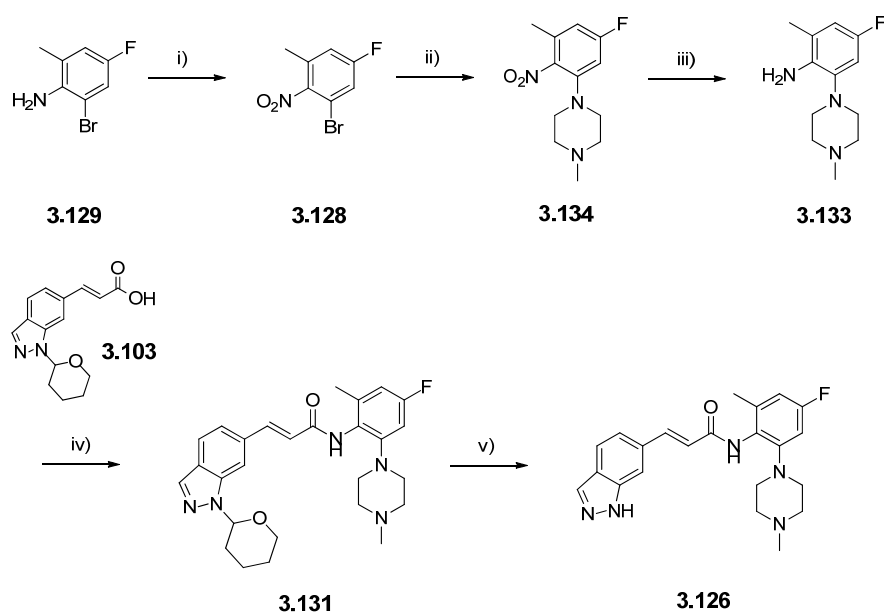
The alternative methodology explored was to perform the metal-catalysed cross coupling of aniline **3.129** with methylpiperazine **3.132** in order to deliver the piperazine intermediate **3.133** (**Table 44**) and two sets of conditions were attempted: the most efficient Buchwald conditions identified so far for our class of compounds, Pd(OAc)<sub>2</sub>/BINAP under microwave irradiations (entry **1**), and a Ullmann-type coupling with copper iodide and a bidentate diamine ligand (entry **2**). In these reactions again, no targeted coupling product was observed. In this specific case, it was hypothesised that the aniline nitrogen was able to chelate to the metal used (either Pd or Cu), preventing the reaction to occur.<sup>297</sup> In an effort to circumvent this issue, the Buchwald coupling was also attempted after protecting the aniline nitrogen with either a phthalimide protecting group or a benzyl protecting group, however, in these instances the des-bromobenzyl version of the starting material was mostly obtained upon attempting the aromatic amination reaction.



| Entry | Reagents   | Solvent | Temperature | Microwave | Yield |
|-------|--|---------|-------------|-----------|-------|
| 1     | <i>N</i> -methylpiperazine (1.5 eq)<br>Pd(OAc) <sub>2</sub> (0.15 eq)<br>BINAP (0.2 eq)<br>NaO <sup>t</sup> Bu (1.5 eq)                                      | toluene | 120 °C      | yes       | 0%    |
| 2     | <i>N</i> -methylpiperazine (1.2 eq)<br>CuI (0.1 eq)<br>trans- <i>N,N'</i> -dimethylcyclohexane-1,2-diamine (0.2 eq)<br>K <sub>3</sub> PO <sub>4</sub> (2 eq) | toluene | 110 °C      | yes       | 0%    |

**Table 44: Reaction conditions investigated to form the piperazinyl intermediate 3.133**

Based on our previous successes when carrying out Buchwald couplings on bromo-nitrobenzyl derivatives, the decision was made to attempt oxidising the commercially available aniline **3.129** to its corresponding nitrobenzyl analogue **3.128** and then to perform the palladium-catalysed cross-coupling on the subsequent bromo-nitrobenzyl derivative. Thus, treatment of aniline **3.129** with *meta*-chloroperbenzoic acid (*m*-CPBA) afforded the corresponding nitrobenzyl intermediate **3.128** in 61% yield (**Scheme 34**). The subsequent Buchwald coupling with methylpiperazine, followed by reduction of the nitro group afforded the aniline derivative **3.133**. The HATU-mediated amide coupling afforded intermediate **3.131** which was deprotected under acidic conditions to give the required 4-fluorobenzyl derivative **3.126**.

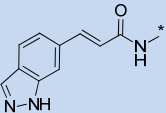
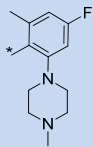
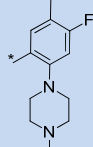


i) *m*-CPBA (70% by weight, 5 eq), DCM, 0 °C to rt, **61%**; ii) *N*-methylpiperazine (2.4 eq), Pd<sub>2</sub>(dba)<sub>3</sub> (0.2 eq), BINAP (0.4 eq), NaO<sup>t</sup>Bu (1.5 eq), toluene, 80 °C; iii) SnCl<sub>2</sub> (4 eq), EtOH, 70 °C, **16% over 2 steps**; iv) (*E*)-3-(1-(tetrahydro-2*H*-pyran-2-yl)-1*H*-indazol-6-yl)acrylic acid **3.103** (1.2 eq), HATU (1.5 eq), *N,N*-diisopropylethylamine (1.5 eq), DMF, rt, **61%**; v) 3 M HCl solution in MeOH (10 eq), EtOH, 50 °C, **83%**.

#### Scheme 34: Synthetic route to prepare the 4-fluorobenzyl analogue **3.126**

These two novel substitution patterns of the benzene afforded compounds which displayed a moderate mPTP potency (liver CRC pIC<sub>50</sub> of 6.3 for **3.126** and 6.5 for **3.127**, **Table 45**) combined with an aqueous solubility meeting our optimisation goals. However, the 4-fluorobenzyl derivative **3.127** did not offer any noticeable improvement over the progenitor molecule **3.114** regarding *in vitro* microsomal clearance, since for instance, the mouse microsomal clearance of analogue **3.127** was 7 mL/min/g compared to 8.1 mL/min/g for **3.114**. As for compound **3.126**, the reduction in microsomal clearance across all species was encouraging, but these clearance values were still above our optimisation goals of 2 mL/min/g. Additionally, the mPTP activity of **3.126** still had to be increased in order to meet the requirements of our targeted profile. Based upon previous SAR, introduction of the fluorine at the 5-position of the indazole could

increase its biological activity, however, this modification was also anticipated to be accompanied with an increase in the *in vitro* microsomal clearance. Indeed, the mouse microsomal clearance increased by 12.2 mL/min/g going from unsubstituted indazole **3.14** (Table 27, p. 157) to 5-fluoroindazole **3.116** (Table 40, p. 219) and increased by 4.8 mL/min/g going from unsubstituted indazole **3.114** (Table 39, p.216) to 5-fluoroindazole **3.119** (Table 41, p. 222). Consequently, even if the exercise of blocking the metabolic liability of the *para*-position to the amide bond was in part successful, the efforts in this area were halted at this stage.

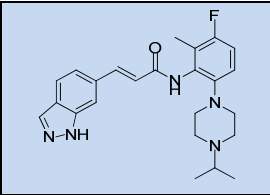
|  |  |  |
|---|---|---|
| <b>Compound</b>   | <b>3.126</b>  | <b>3.127</b> <sup>154</sup>   |
| <b>Liver CRC pIC<sub>50</sub></b>   | 6.3   | 6.5   |
| <b>Brain CRC pIC<sub>50</sub></b>   | 6.5   | 6.1   |
| <b>LE / LLE</b>   | 0.30 / 0.24   | 0.30 / 0.22   |
| <b>MW</b>   | 393   | 393   |
| <b>clogP</b>  | 3.5   | 4.1   |
| <b>Chrom logD / PFI</b>   | 2.8 / 5.8   | 3.8 / 6.8   |
| <b>CLND (µg/mL)</b>   | ≥ 198   | ≥ 162   |
| <b>FaSSIF (µg/mL)</b>   | 125   | 157   |
| <b>h IVC (mL/min/g)</b>   | 1.6   | 1.4   |
| <b>r IVC (mL/min/g)</b>   | 3.6   | 7.3   |
| <b>m IVC (mL/min/g)</b>   | 3.6   | 7   |
| <b>Fu,bl</b>  | 13.1%   | 2.6%  |

**Table 45: Profile of the compounds designed to circumvent the metabolic liability induced by the *para*-position to the amide bond**

### 3.5.3.3. Investigation of the 3<sup>rd</sup> metabolic site: *N*-demethylation of the piperazine

The next metabolic soft spot identified by the metabolism study on compound **3.119** was *N*-demethylation of the piperazine. A comparison of the microsomal clearance profile between the *N*-methylpiperazine **3.114** and its corresponding unsubstituted piperazinyl analogue **3.91** underlined the key role caused by this metabolic pathway. Indeed, the microsomal clearance of compound **3.91** was less than 2 mL/min/g in all species (**Table 39, p. 216**), matching our optimisation goals. At the same time, the lack of mPTP potency of compound **3.91** (liver CRC pIC<sub>50</sub> < 4) emphasised the importance for biological activity to substitute the piperazinyl nitrogen with an alkyl group. Taking into account these observations, *N*-isopropylpiperazine **3.135** (**Table 46**) was suggested by the author and prepared by an external collaborator,<sup>154</sup> since it was reasoned that the steric hindrance provided by the isopropyl group could potentially hamper the binding of the compound to the metabolising enzymes.<sup>283</sup>

The potency of **3.135** (CRC pIC<sub>50</sub> = 5.1) was reduced compared to the corresponding methylpiperazine cinnamide **3.114** (CRC pIC<sub>50</sub> of 6.2) and the microsomal clearance actually increased. This could indicate that the theory of increasing steric hindrance in the vicinity to the piperazinyl nitrogen in order to minimise metabolism was either incorrect or that the bulkiness of the isopropyl group was not sufficient to prevent binding to the metabolising enzymes. The *tert*-butylpiperazine version of this compound was therefore envisaged, however, the drop in mPTP activity already observed going from a methyl to an isopropyl group would suggest that increasing the size of the alkyl group would likely reduce further mPTP activity. Another possible explanation for the observed increase in microsomal clearance of compound **3.135** could be that the metabolism was shifted onto another metabolic soft spot of the molecule. In that case, this would mean that several concomitant structural modifications of the cinnamide series would be required in order to address the *in vitro* undesirable clearance. Based on the above observations, it was decided to deprioritise this area of work and to investigate the remaining metabolic soft spot that had been identified.

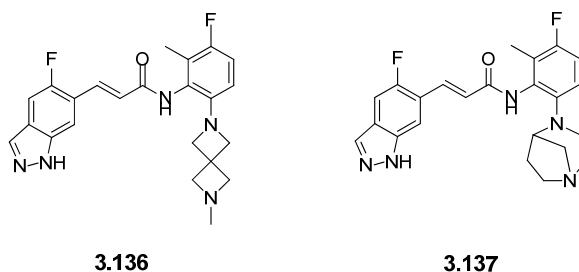
|                                   |  |
|-----------------------------------|--|
| <b>Structure</b>                  |  |
| <b>Compound</b>                   | <b>3.135</b> <sup>154</sup>  |
| <b>Liver CRC pIC<sub>50</sub></b> | 5.1  |
| <b>LE / LLE</b>                   | 0.22 / 0.15  |
| <b>MW</b>                         | 422  |
| <b>clogP</b>                      | 4.3  |
| <b>Chrom logD / PFI</b>           | 2.9 / 5.9  |
| <b>CLND (µg/mL)</b>               | 122  |
| <b>FaSSIF (µg/mL)</b>             | 497  |
| <b>h IVC (mL/min/g)</b>           | 2.9  |
| <b>r IVC (mL/min/g)</b>           | 16.2   |
| <b>m IVC (mL/min/g)</b>           | 13.2   |
| <b>Fu,bl</b>                      | 11.1%  |

**Table 46: Profile of the isopropyl-piperazinyl analogue 3.135**

#### 3.5.3.4. Investigation of the 4<sup>th</sup> metabolic site: the piperazinyl ring

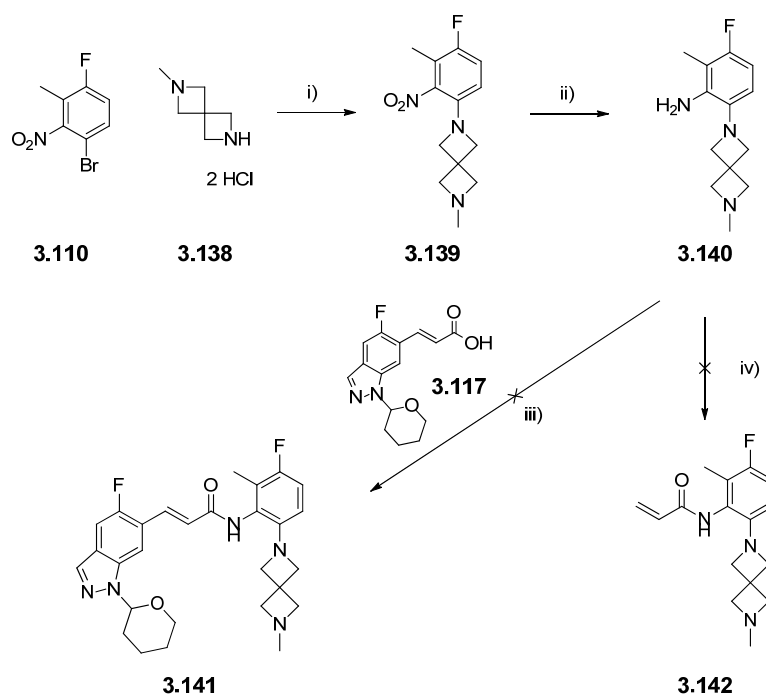
The final metabolism pathway detected during the course of the metabolite identification study of compound **3.119** lay in the metabolic instability of the piperazinyl ring. Two replacements of piperazine were considered: the corresponding spirocyclic analogue **3.136** and the bridged piperazine **3.137** (**Figure 86**). Spirocycles have recently witnessed an increased use within medicinal chemistry discovery programmes, mostly because they introduce a structural novelty, but also because they have shown to improve physicochemical and pharmacokinetic properties.<sup>298,299</sup> Of particular relevance for the current study, replacing a piperazinyl group with a diazaspino[3.3]heptanyl motif was precedent to reduce *in vitro* clearance.<sup>300</sup> Based on this, the spirocyclic analogue **3.136**

was envisaged. Regarding the bridged system **3.137**, it was expected that the increase in the steric hindrance of the piperazinyl ring would potentially reduce the binding of the compound to the metabolising enzymes, therefore reducing its microsomal clearance.



**Figure 86: Potential replacement compounds to address the metabolic liability induced by the piperazinyl ring**

The first step towards the synthesis of the spirocyclic analogue **3.136** involved a Buchwald cross-coupling using the commercially available 2-methyl-2,6-diazaspiro[3.3]heptane dihydrochloride **3.138** and this reaction proceeded in a 46% yield (Scheme 35). The nitrobenzyl intermediate **3.139** obtained was then reduced under a hydrogen atmosphere in the presence of a palladium catalyst to afford the aniline intermediate **3.140**. However, the subsequent step of amide formation using the 5-fluoroindazole cinnamic acid derivative **3.117** did not lead to the targeted amide **3.141**, but rather afforded mainly an undetermined by-product, for which NMR studies indicated that the spirocyclic group had opened. An alternative route attempted was to form the acrylamide analogue **3.142**, as a precursor for a subsequent Heck reaction, but again, treatment of aniline **3.140** with 3-chloropropanoyl chloride under basic conditions did not afford any targeted product. LCMS and NMR observations showed that the spirocyclic moiety of the starting material had again degraded and that the bicyclic ring had opened. Based on concerns of the chemical stability of the spirocyclic group within our system, the decision was made to discard this structural replacement within the current study.



i) 2-methyl-2,6-diazaspiro[3.3]heptane dihydrochloride **3.138** (1 eq), 1-bromo-4-fluoro-3-methyl-2-nitrobenzene **3.110** (1.2 eq), Pd<sub>2</sub>(dba)<sub>3</sub> (0.1 eq), RuPhos (0.2 eq), NaO<sup>t</sup>Bu (3.5 eq), toluene, 120 °C, microwave, **46%**; ii) H<sub>2</sub> atmosphere, Pd/C (10% by weight, 0.2 eq), EtOH, rt, **95%**; iii) ((*E*)-3-(5-fluoro-1-(tetrahydro-2*H*-pyran-2-yl)-1*H*-indazol-6-yl)acrylic acid **3.117** (1.2 eq), HATU (3 eq), *N,N*-diisopropylethylamine (3 eq), DMF, rt, **0%**; iv) 3-chloropropanoyl chloride (1.5 eq), *N,N*-diisopropylethylamine (5 eq), DCM, 0 °C to rt, **0%**.

**Scheme 35: The different synthetic routes attempted towards the synthesis of the spirocyclic compound 3.136**

Regarding the bridged piperazine compound **3.137**, it was reasoned that the most pragmatic way to access the desired compound would be to attempt a coupling between nitrobenzene **3.110** and the commercially available 1,4-diazabicyclo[3.2.1]octane dihydrochloride **3.143** (Table 47). However, despite repeated attempts, the resulting bridged piperazine intermediate **3.144** was not obtained and the reaction resulted essentially in the observation of the unreacted starting nitrobenzene **3.110**. Hence, our preferred Buchwald conditions using either Pd<sub>2</sub>(dba)<sub>3</sub>/RuPhos or Pd(OAc)<sub>2</sub>/BINAP left the starting material untouched (Table 47, entry 1 and 2, respectively). The alternative

phosphine ligand XPhos **3.145** (**Table 47**) was preceded in the literature to successfully undergo Buchwald coupling with the same bridged piperazine **3.143**,<sup>301</sup> albeit in low yields. Thus, this ligand was tested, in conjunction with a milder base, dipotassium phosphate (**Table 47**, entry **3**), but again, no conversion of the starting nitrobenzene **3.110** was observed, even when increasing the loading of catalyst and ligand (**Table 47**, entry **4**). Finally, two sets of conditions were tried to perform a direct nucleophilic aromatic displacement of the bromine by 1,4-diazabicyclo[3.2.1]octane **3.143** under conventional heating (**Table 47**, entry **5**)<sup>302</sup> and under microwave irradiation (**Table 47**, entry **6**),<sup>303</sup> yet these attempts left the starting bromobenzyl reagent **3.110** unreacted. It was speculated that the introduction of 1,4-diazabicyclo[3.2.1]octane on the benzene was precluded because of steric hindrance.

Since it was proven difficult to access relevant piperazine replacement molecules in an expedient fashion, a different strategy was adopted in order to identify alternative cinnamide compounds with an attractive profile. This strategy is discussed in the **Section 3.5.5 (p. 243)**.



| Entry | Reagents   | Solvent           | T °C                | Microwave | Yield     |
|-------|--|-------------------|---------------------|-----------|-----------|
| 1     | <b>3.143</b> (1.5 eq)<br>Pd <sub>2</sub> (dba) <sub>3</sub> (0.1 eq)<br>RuPhos (0.2 eq)<br>NaO <sup>t</sup> Bu (3.5 eq)          | toluene           | 120 °C              | yes       | <b>0%</b> |
| 2     | <b>3.143</b> (1.5 eq)<br>Pd(OAc) <sub>2</sub> (0.1 eq)<br>BINAP (0.2 eq)<br>NaO <sup>t</sup> Bu (3.5 eq)                         | toluene           | 120 °C              | yes       | <b>0%</b> |
| 3     | <b>3.143</b> (1.5 eq)<br>Pd <sub>2</sub> (dba) <sub>3</sub> (0.1 eq)<br>XPhos (0.2 eq)<br>K <sub>2</sub> HPO <sub>4</sub> (3 eq) | <sup>t</sup> BuOH | 120 °C to<br>150 °C | yes       | <b>0%</b> |
| 4     | <b>3.143</b> (1.5 eq)<br>Pd <sub>2</sub> (dba) <sub>3</sub> (1 eq)<br>XPhos (2 eq)<br>K <sub>3</sub> PO <sub>4</sub> (3 eq)      | <sup>t</sup> BuOH | 120 °C              | yes       | <b>0%</b> |
| 5     | <b>3.143</b> (1 eq)<br>K <sub>2</sub> CO <sub>3</sub> (3.5 eq)   | dioxane           | 110 °C              | no        | <b>0%</b> |
| 6     | <b>3.143</b> (1 eq)<br><i>N,N</i> -diisopropylethylamine<br>(3.5 eq)   | DMF               | 200 °C              | yes       | <b>0%</b> |

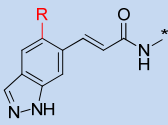
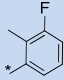
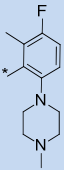
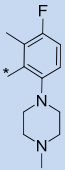
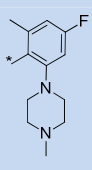
**Table 47: Reaction conditions attempted in order to deliver the bridged piperazine intermediate 3.144**

### 3.5.4. Conclusion of the work on the basic group-containing cinnamides

The exercise of introducing a basic group on the benzene in the cinnamide series highlighted that the *ortho*-position to the amide bond was the most appropriate attachment point. Even if tolerated by the biological target, the introduction of the piperazine motif on the benzene was accompanied with a noticeable reduction in mPTP activity, with about a 2 log units decrease in the liver CRC pIC<sub>50</sub> (**Table 48**). Nevertheless, this structural modification delivered compounds with an unprecedented profile, combining sub-micromolar mPTP potency with excellent aqueous solubility. The 5-fluoroindazole derivative **3.119** (**Table 48**) and the 4-fluorobenzene compound **3.126** (**Table 48**) were identified as the most desirable molecules from this set of basic group-containing analogues.

A key limitation of this class of compounds was their moderate to high microsomal clearance, which translated into sub-optimal *in vivo* mouse PK. The metabolite identification experiment carried out on compound **3.119** (**Figure 83**, **p. 226**) enabled us to identify the key metabolic soft spots and to focus on specific structural modifications in an attempt to reduce the metabolism of the cinnamide series. Even if some structural changes reduced the *in vitro* clearance to a certain extent (*e.g.* compound **3.126**, **Table 45**, **p. 234**), it was shown that removing or blocking one metabolic soft spot at a time was insufficient in reducing the microsomal clearance to levels which would be consistent with low *in vivo* clearance. Consequently, compounds exhibiting the overall profile required to meet our optimisation goals were not identified from the set of molecules described here.

**Table 48** summarises the key compounds identified in the piperazine-containing cinnamide series along with the initial lead cinnamide **3.14** and their most relevant biological data.

|   |   |   |   |   |
|---|---|---|---|---|
|  |  |  |  |  |
| <b>Structure, R =</b>   | H   | H   | F   | H   |
| <b>Compound</b>   | <b>3.14</b>   | <b>3.114</b>  | <b>3.119</b>  | <b>3.126</b>  |
| <b>Liver CRC pIC<sub>50</sub></b>   | 8.1 <sup>a</sup>  | 6.2   | 6.9   | 6.3   |
| <b>Chrom logD / PFI</b>   | 4.1 / 7.1   | 2.7 / 5.7   | 2.9 / 5.9   | 2.8 / 5.8   |
| <b>CLND (µg/mL)</b>   | 4   | ≥ 154   | ≥ 165   | ≥ 198   |
| <b>FaSSIF (µg/mL)</b>   | 5   | 798   | 798   | 125   |
| <b>m IVC (mL/min/g)</b>   | 5.9   | 8.1   | 12.9  | 3.6   |

<sup>a</sup>Compound was only reported with a measured pIC<sub>50</sub> value in 8 out of 13 test occasions and for the other 5 test occasions, pIC<sub>50</sub> was greater than 9.

**Table 48: Key compounds from the cinnamide series**

It would have been appropriate to investigate alternative basic groups in place of the piperazinyl group, which was in fact identified to be a metabolic soft spot. However, considering the amount of time it would take to identify basic group-containing cinnamides with a profile satisfying our optimisation goals, it was decided to reconsider a better starting point, especially with regard to *in vivo* PK. This effort is discussed in the subsequent section.

Furthermore, this work demonstrated that the phenotypic screening approach adopted during this optimisation campaign afforded highly robust SAR. This data has indeed enabled both decision-making and design of new mPTP modulators going forward.

Finally, the study carried out on the piperazine-containing cinnamides was critical in highlighting the positive impact of having a di-*ortho*-substitution pattern to the amide bond on increasing the molecular dihedral angle and on increasing aqueous solubility (**Figure 78, p. 218**). This new information was taken into account when re-investigating a better starting point for optimisation, and this is discussed in the next section.

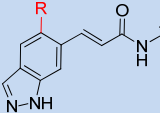
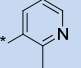
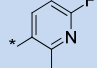
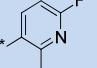
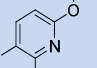
### 3.5.5. The pyridyl cinnamide series

#### 3.5.5.1. Previous work done on the pyridyl cinnamide series

While the level of interest of the basic group-containing cinnamides diminished due to sub-optimal DMPK profile, it was considered whether some of the lessons learned during this previous exercise could be applied to another sub-series of molecules. More specifically, it was questioned whether the increased aqueous solubility observed when having a di-*ortho*-substitution pattern to the amide bond could be applied elsewhere. Careful consideration of the previously synthesised compounds prompted us to focus on cinnamides with a pyridine instead of a benzene as being potential candidates for introducing the di-*ortho*-substitution motif. Indeed, a set of previously prepared pyridyl cinnamides by other members of the team<sup>241</sup> displayed moderate to high mPTP potency and acceptable *in vitro* and *in vivo* DMPK profiles. This sub-series of the cinnamide series was previously discontinued as it was proven difficult to increase mPTP potency without reducing aqueous solubility.<sup>241</sup>

As an illustration, the 2-methylpyridyl cinnamide **3.146** (**Table 49**) displayed moderate mPTP activity (liver CRC pIC<sub>50</sub> of 5.8), a low PFI of 4.9 and high aqueous solubility (FaSSIF = 137 µg/mL).<sup>241</sup> In an attempt to increase the biological activity of this sub-series of pyridyl compounds, it was previously discovered by other member of our laboratories that substitution of the *para*-position to the amide bond with fluorine or a methoxy group increased significantly the mPTP activity.<sup>241</sup> Indeed, the corresponding 6-fluoro-2-methylpyridyl analogue **3.147** and the 6-methoxy-2-methylpyridyl analogue **3.149** exhibited a liver CRC pIC<sub>50</sub> of 7.3 and 7.6, respectively (**Table 49**). Additionally, the 5-fluoroindazole **3.148** displayed a CRC pIC<sub>50</sub> close to 8. However, the introduction of the 6-fluoro and the 6-methoxy groups onto the pyridine was also accompanied with an increase in lipophilicity and accordingly, the PFI of compounds **3.147** and **3.149** (PFI = 5.7 and 5.9, respectively) were markedly higher than the PFI of the progenitor compound **3.146** (PFI = 4.9). As a result, the FaSSIF solubility of these more potent 6-substituted pyridyl analogues was low, with FaSSIF solubilities less than 20 µg/mL.

The 6-fluoro-2-methylpyridyl analogue **3.147** was remarkable as its CLND solubility was much higher (CLND solubility was tested four times, at 22,  $\geq 89$ ,  $\geq 97$  and  $\geq 112$   $\mu\text{g/mL}$ , respectively) than its FaSSIF solubility of 15  $\mu\text{g/mL}$ . For this compound, it was hypothesised that the marked difference between the kinetic and the thermodynamic solubilities could be driven by a tight crystal packing, which would mainly be reflected in the FaSSIF solubility measurement. This observation supported further the value of attempting to disrupt the molecular planarity of this sub-series of pyridyl cinnamides.

|  |  |  |  |  |
|---|---|---|---|---|
| <b>Structure, R =</b>   | H   | H   | F   | H   |
| <b>Compound</b>   | <b>3.146</b>  | <b>3.147</b>  | <b>3.148</b>  | <b>3.149</b>  |
| <b>Liver CRC pIC<sub>50</sub></b>   | 5.8   | 7.3   | 7.9 <sup>a</sup>  | 7.6   |
| <b>LE / LLE</b>   | 0.38 / 0.34   | 0.45 / 0.40   | 0.47 / 0.41   | 0.45 / 0.37   |
| <b>MW</b>   | 278   | 296   | 314   | 308   |
| <b>clogP</b>  | 2.3   | 2.6   | 2.9   | 3.2   |
| <b>Chrom logD / PFI</b>   | 1.9 / 4.9   | 2.7 / 5.7   | 3.2 / 6.2   | 2.9 / 5.9   |
| <b>CLND (<math>\mu\text{g/mL}</math>)</b>   | $\geq 73$   | 22 <sup>b</sup>   | 24  | 4   |
| <b>FaSSIF (<math>\mu\text{g/mL}</math>)</b>                                       | 137 <sup>c</sup>  | 15  | 3   | 4   |
| <b>h IVC (mL/min/g)</b>   | 1.6   | 1.1   | 1.3   | < 0.6   |
| <b>r IVC (mL/min/g)</b>   | 1.9   | 4.1   | 4.6   | 1.3   |
| <b>m IVC (mL/min/g)</b>   | 6.3   | 4.2   | 7.4   | 3.5   |
| <b>Fu,bl</b>  | 12.7%   | 8%  | 3.7%  | 3.2%  |

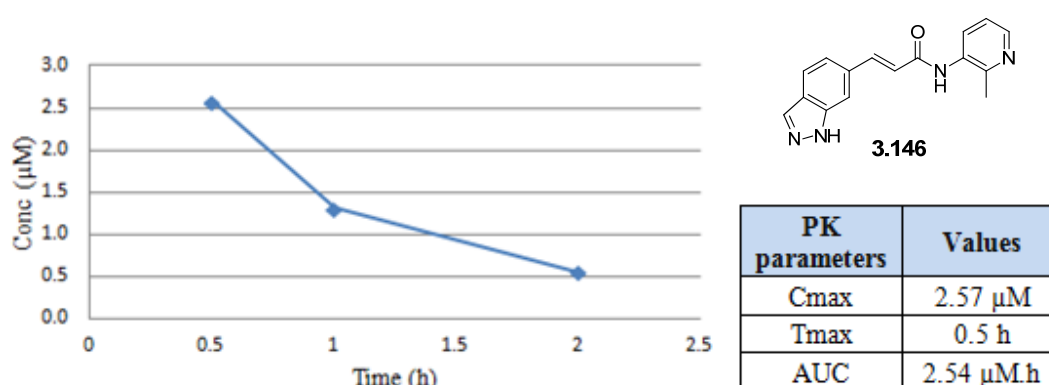
<sup>a</sup>Compound was only reported with a measured pIC<sub>50</sub> value in 7 out of 10 test occasions and for the other 3 test occasions, pIC<sub>50</sub> was greater than 9; <sup>b</sup>Compound was only reported with a measured CLND value in 1 out of 4 test occasions and for the other 3 occasions, CLND was  $\geq 89$ , 97 and 112  $\mu\text{g/mL}$ , respectively;

<sup>c</sup>This FaSSIF solubility was measured after a 24 h incubation period (instead of 4 h).

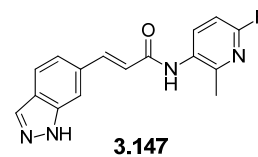
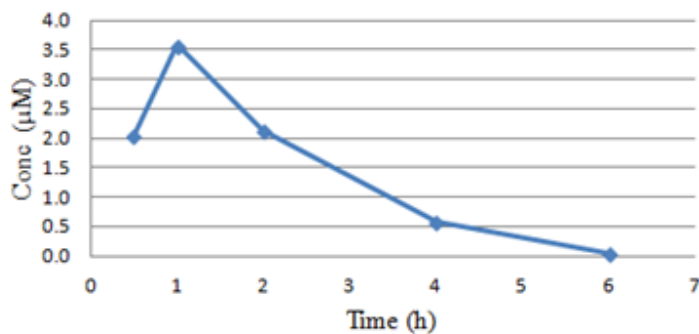
**Table 49: Profile of the previous pyridyl cinnamide derivatives<sup>241</sup>**

The additional piece of data that strengthens the proposal to re-evaluate the pyridyl cinnamide sub-series was the fact that their *in vivo* PK profiles were notably better than the previously studied benzene derived cinnamides. Thus, the four compounds from **Table 49** were tested in the mouse SOA model at 5 mg/kg (**Figure 87** to **Figure 90**).<sup>268</sup> Except for compound **3.148**, all these pyridyl derivatives displayed a C<sub>max</sub> greater than 1 μM and AUC comprised between 2.42 and 7.07 μM.h, which was a significant increase in the level of exposure than those observed for the benzyl cinnamides discussed previously, for which AUC was below 1 μM.h (**Figure 79** to **Figure 81**, p. **223**). These *in vivo* systemic exposures were still lower compared to our optimisation goals or to the levels achieved with isoxazole **3.16a** (C<sub>max</sub> = 5.05 μM and AUC = 8.12 μM.h, **Figure 67**, p. **184**), however, they constituted a reasonable starting point for a further optimisation effort.

Conversely, the 5-fluoroindazole pyridyl analogue **3.148** exhibited a very low *in vivo* blood exposure, with a C<sub>max</sub> of 0.08 μM and an AUC of 0.16 μM.h (**Figure 89**). In this specific case, it was hypothesised that the combination of high clearance (mouse IVC = 7.4 mL/min/g) and poor absorption, most likely as a result of low aqueous solubility (FaSSIF = 3 μg/mL), was limiting *in vivo* exposure.

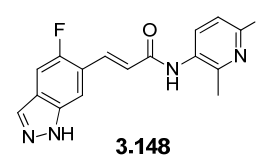
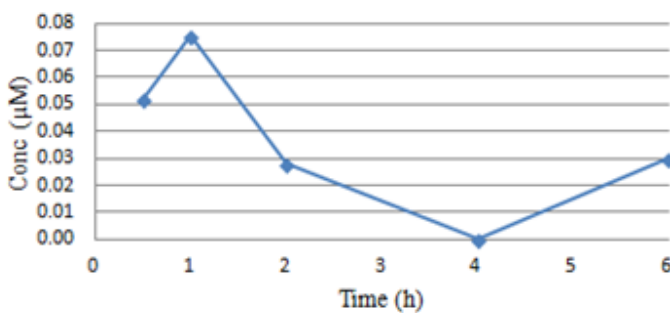


**Figure 87: PK profile of the mouse SOA model of compound 3.146 at 5 mg/kg**



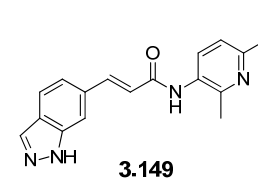
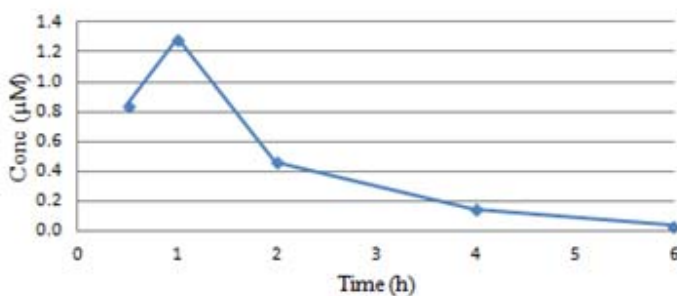
| PK parameters    | Values    |
|------------------|-----------|
| C <sub>max</sub> | 3.58 µM   |
| T <sub>max</sub> | 1 h       |
| AUC              | 7.07 µM.h |

**Figure 88: PK profile of the mouse SOA model of compound 3.147 at 5 mg/kg**



| PK parameters    | Values    |
|------------------|-----------|
| C <sub>max</sub> | 0.08 µM   |
| T <sub>max</sub> | 1 h       |
| AUC              | 0.16 µM.h |

**Figure 89: PK profile of the mouse SOA model of compound 3.148 at 5 mg/kg**



| PK parameters    | Values    |
|------------------|-----------|
| C <sub>max</sub> | 1.29 µM   |
| T <sub>max</sub> | 1 h       |
| AUC              | 2.42 µM.h |

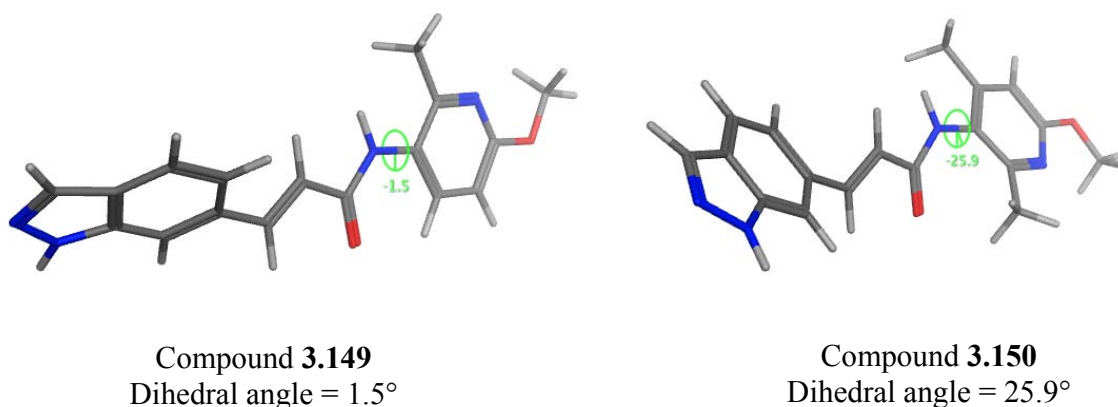
**Figure 90: PK profile of the mouse SOA model of compound 3.149 at 5 mg/kg**

### 3.5.5.2. Introduction of a di-*ortho*-substitution pattern to the amide bond on the pyridine

Taking into consideration the points discussed above, the pyridyl cinnamide sub-series was re-evaluated by considering a di-*ortho*-substitution pattern around the bond linking the amide and the pyridine. It was reasoned that the resulting disruption of molecular planarity, identified while working on the benzene derived cinnamide series, could increase aqueous solubility and, subsequently, could increase oral absorption.

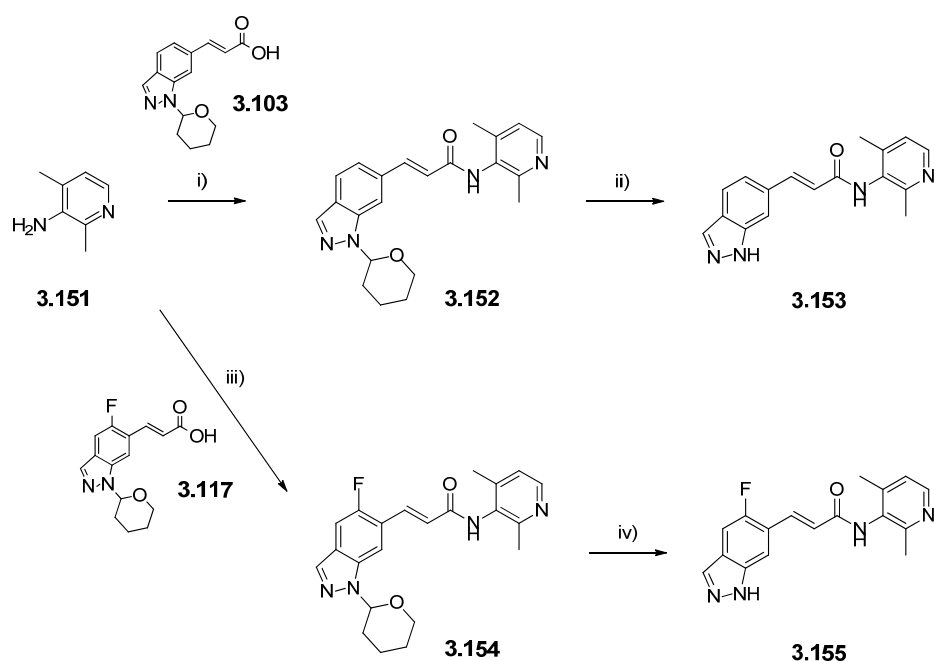
To assess this theory, an additional methyl group was chosen as a substituent to be introduced *ortho* to the amide bond. In an attempt to investigate the resulting conformational impact, the dihedral angle between the pyridyl ring and the amide bond was calculated for the low energy conformation of the 6-methoxy-2-methylpyridyl analogue **3.149** and the 6-methoxy-2,4-dimethylpyridyl derivative **3.150** (**Figure 91**). The absolute values of the dihedral angle for compound **3.149** and compound **3.150** were 1.5° and 25.9°, respectively. Thus, the increase in the dihedral angle resulting from the introduction of the extra methyl was predicted to be similar compared to the one resulting in the introduction of the *ortho*-piperidinyl group observed in the basic-containing cinnamide series (**Figure 78, p. 218**).





**Figure 91: Dihedral angles for the low local energy conformation of molecules 3.149 and 3.150**

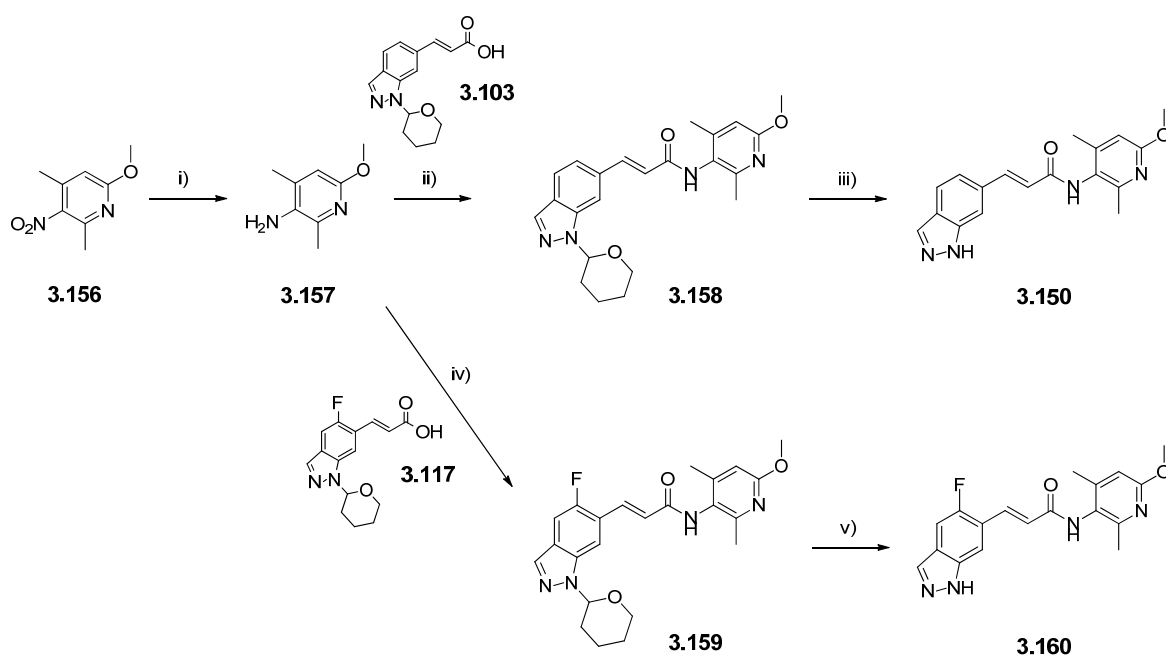
The first two 2,4-dimethylpyridyl analogues synthesised were the unsubstituted indazole **3.153** and the 5-fluoroindazole **3.155** (Scheme 36) in order to expediently assess our hypothesis. The two-step process involved a HATU-mediated amide formation between the commercially available aniline **3.151** and the relevant THP-protected cinnamic acid derivatives **3.103** and **3.117**, respectively, followed by the removal of the THP protecting group under acidic conditions.



i) (*E*)-3-(1-(tetrahydro-2*H*-pyran-2-yl)-1*H*-indazol-6-yl)acrylic acid **3.103** (1 eq), 2,4-dimethylpyridin-3-amine **3.151** (1.2 eq), HATU (1.2 eq), *N,N*-diisopropylethylamine (1.5 eq), DMF, 0 °C to 60 °C, **68%**; ii) 3 M HCl solution in MeOH (5 eq), MeOH, 60 °C, **33%**; iii) (*E*)-3-(5-fluoro-1-(tetrahydro-2*H*-pyran-2-yl)-1*H*-indazol-6-yl)acrylic acid **3.117** (1 eq), 2,4-dimethylpyridin-3-amine **3.151** (1.1 eq), HATU (1.5 eq), *N,N*-diisopropylethylamine (1.5 eq), DMF, rt, **55%**; iv) 3 M HCl solution in MeOH (10 eq), MeCN, 60 °C, **64%**.

### Scheme 36: Synthetic route to the 2,4-dimethylpyridyl analogues **3.153** and **3.155**

An additional pair of 2,4-dimethylpyridyl derivatives with a 6-methoxy substituent was also synthesised, motivated by the attractive mPTP potency and moderate mouse IVC of the previous 6-methoxy-2-methylpyridyl analogue **3.149** (Table 49, p. 244). Thus, the starting nitropyridyl intermediate **3.156** was reduced under a hydrogen atmosphere in the presence of a palladium catalyst and the aniline **3.157** obtained was coupled with the relevant cinnamic acid intermediates **3.103** and **3.117**, respectively (Scheme 37). The two resulting THP-protected indazoles **3.158** and **3.159** were deprotected with hydrochloric acid to afford the indazole pyridyl cinnamide **3.150** and the 5-fluoroindazole pyridyl cinnamide **3.160**, respectively.

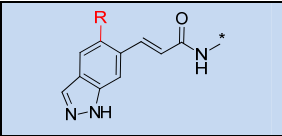
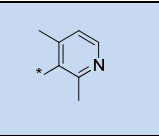
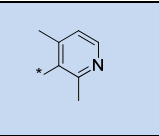
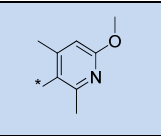
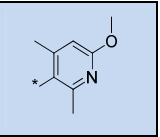


i) H<sub>2</sub> atmosphere, Pd/C (10% by weight, 0.2 eq), EtOH, rt, **99%**; ii) *(E)*-3-(1-(tetrahydro-2H-pyran-2-yl)-1H-indazol-6-yl)acrylic acid **3.103** (1.1 eq), HATU (1.5 eq), *N,N*-diisopropylethylamine (1.5 eq), DMF, rt, **88%**; iii) 3 M HCl solution in MeOH (10 eq), MeCN, 60 °C, **63%**; iv) *(E)*-3-(5-fluoro-1-(tetrahydro-2H-pyran-2-yl)-1H-indazol-6-yl)acrylic acid **3.117** (1.1 eq), HATU (1.5 eq), *N,N*-diisopropylethylamine (1.5 eq), DMF, rt, **90%**; v) 3 M HCl solution in MeOH (10 eq), MeCN, 60 °C, **35%**.

### Scheme 37: Synthetic route to the 2,4-dimethylpyridyl analogues **3.150** and **3.160**

When exploring the profiles of the pyridyl analogues **3.153** and **3.155** (Table 50), it was observed that the introduction of the 4-methyl group on the pyridine increased marginally mPTP activity. Indeed, the liver CRC pIC<sub>50</sub> of the progenitor derivative **3.146** was 5.8 (Table 49, p. 244), while the one of its corresponding 2,4-dimethylpyridyl analogue **3.153** was 6.2. The solubility of these compounds increased in comparison to their progenitor **3.146**, since the FaSSIF solubility raised from 137 µg/mL for compound **3.146** to 189 µg/mL and 368 µg/mL for the indazole **3.153** and the 5-fluoroindazole **3.155**, respectively. More interestingly, the introduction of the additional methyl group on the pyridine reduced microsomal clearance, since almost all the *in vitro* microsomal clearance values of **3.153** and **3.155** were below the threshold of detection of the assay.

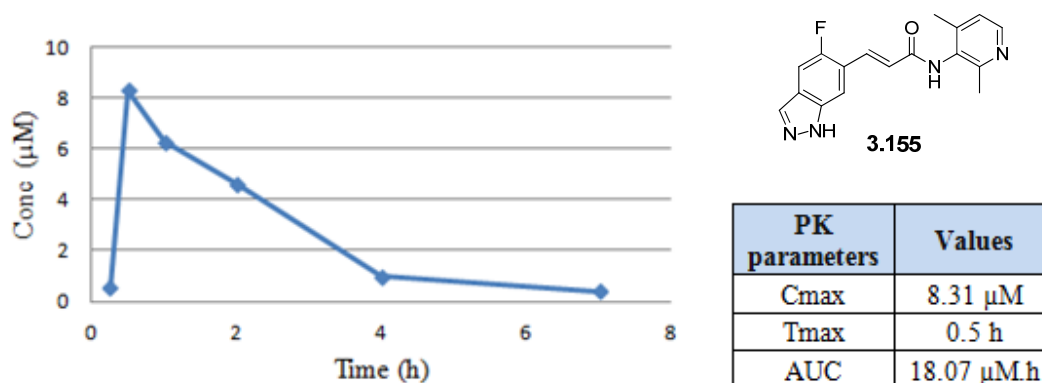
Regarding the two 6-methoxy-2,4-dimethylpyridyl analogues **3.150** and **3.160** (Table 50), the introduction of the methyl group at the 4-position of the pyridine reduced mPTP activity. Indeed, the 6-methoxy-2,4-dimethylpyridyl derivative **3.150** had a liver CRC pIC<sub>50</sub> of 6.7 compared with a liver CRC pIC<sub>50</sub> of 7.6 for its 6-methoxy-2-methylpyridyl progenitor **3.149** (Table 49, p. 244). Nevertheless, when combining the 2,4-dimethylpyridyl group with the 5-fluoroindazole in compound **3.160**, high mPTP potency was achieved (liver CRC pIC<sub>50</sub> = 7.8). Even if the FaSSIF solubilities of these two 6-methoxy-2,4-dimethylpyridyl compounds were below our initial optimisation goals (60 and 64 µg/mL for compounds **3.150** and **3.160**, respectively), these compounds were 15 times more soluble than their progenitor **3.149**, which was a significant achievement. Moreover, the *in vitro* microsomal clearance of **3.150** and **3.160** was below 1.5 mL/min/g in every species investigated. Lastly, these four 2,4-dimethylpyridyl compounds **3.153**, **3.155**, **3.150** and **3.160** exhibited high rat blood fraction unbound, greater than our optimisation goal of 2%.

|  |  |  |  |  |
|---|---|---|---|---|
| <b>Structure, R =</b>   | H   | F   | H   | F   |
| <b>Compound</b>   | <b>3.153</b>  | <b>3.155</b>  | <b>3.150</b>  | <b>3.160</b>  |
| <b>Liver CRC pIC<sub>50</sub></b>   | 6.2   | 6.5   | 6.7   | 7.8   |
| <b>LE / LLE</b>   | 0.38 / 0.36   | 0.38 / 0.35   | 0.38 / 0.32   | 0.42 / 0.35   |
| <b>MW</b>   | 292   | 310   | 322   | 340   |
| <b>clogP</b>  | 2.2   | 2.5   | 3   | 3.3   |
| <b>Chrom logD / PFI</b>   | 2 / 5   | 2.3 / 5.3   | 3 / 6   | 3.4 / 6.4   |
| <b>CLND (µg/mL)</b>   | ≥ 147   | ≥ 99  | ≥ 133   | 73 <sup>a</sup>   |
| <b>FaSSIF (µg/mL)</b>   | 189   | 368   | 60  | 64  |
| <b>h IVC (mL/min/g)</b>   | < 0.6   | 0.7   | < 0.6   | 0.8   |
| <b>r IVC (mL/min/g)</b>   | < 0.7   | < 0.7   | < 0.7   | < 0.7   |
| <b>m IVC (mL/min/g)</b>   | < 0.7   | 1.4   | < 0.7   | 1.5   |
| <b>Fu,bl</b>  | 11%   | 8.8%  | 6.4%  | 2.6%  |

<sup>a</sup>Compound was only reported with a measured CLND value in 1 out of 3 test occasions and for the other 2 occasions, CLND was ≥ 95 and 112 µg/mL, respectively.

**Table 50: Profile of the 2,4-dimethylpyridyl cinnamide derivatives**

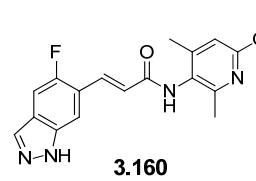
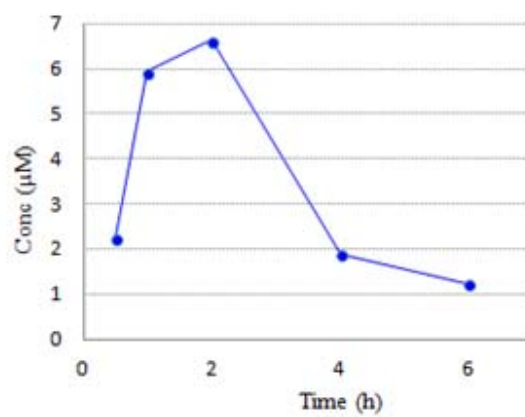
Encouraged by their *in vitro* profiles, two of the 2,4-dimethylpyridyl cinnamides, compounds **3.155** and **3.160**, were progressed to mouse SOA PK studies, at 5 mg/kg.<sup>268</sup> The 5-fluoroindazole **3.155** displayed an enhanced blood exposure in comparison to its progenitor compound **3.146**, since the C<sub>max</sub> and the AUC of the 2,4-dimethylpyridyl analogue **3.155** (8.31 µM and 18.07 µM.h, respectively, **Figure 92**) were significantly higher than the C<sub>max</sub> and the AUC of the 2-methylpyridyl derivative **3.146** (2.57 µM and 2.54 µM.h, respectively, **Figure 87, p. 245**). It was reasoned that the increase in aqueous solubility of **3.155** facilitated *in vivo* absorption and that the reduction in *in vitro* microsomal clearance translated into lower *in vivo* clearance.



**Figure 92: PK profile of the mouse SOA model of compound 3.155 at 5 mg/kg**

A consistent *in vivo* PK improvement was observed when comparing the *in vivo* systemic exposure of the 6-methoxy-2,4-dimethylpyridyl analogue **3.160** with the 6-methoxy-2-methylpyridyl analogue **3.149**. Indeed, the C<sub>max</sub> and the AUC of **3.160** (6.64 µM and 20.08 µM.h, respectively, **Figure 93**) were considerably higher than the C<sub>max</sub> and the AUC of its progenitor compound **3.149** (1.29 µM and 2.42 µM.h, respectively, **Figure 90, p. 246**). In fact, the mouse blood exposure of the 6-methoxy-2,4-dimethylpyridyl analogue **3.160** was also enhanced compared to the lead isoxazole **3.16a** (C<sub>max</sub> = 5.05 µM and AUC = 8.12 µM.h, **Figure 67, p. 184**), which was a significant breakthrough for the cinnamide series.

An additional benefit provided by the *in vivo* systemic profile of **3.160** was that the exposure was more prolonged than the previously investigated compounds. Indeed, at the 4 h time point, the systemic concentration was measured to be 1.91 µM, 1 µM and 0.59 µM for compounds **3.160**, **3.155** and **3.16a**, respectively. This could potentially confer a longer duration of action *in vivo* to cinnamide **3.160**.



| PK parameters    | Values     |
|------------------|------------|
| C <sub>max</sub> | 6.64 µM    |
| T <sub>max</sub> | 2 h        |
| AUC              | 20.08 µM.h |

**Figure 93: PK profile of the mouse SOA model of compound 3.160 at 5 mg/kg**

### 3.5.6. Conclusion on the work carried out on the cinnamide series

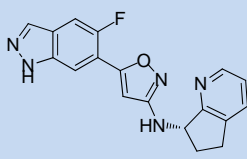
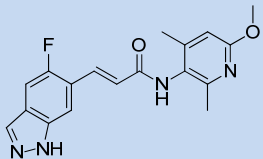
In an attempt to enhance the profile of the cinnamide series, for which the key limitations were determined to be sub-optimal aqueous solubility and DMPK profile, the introduction of a piperazinyl group on the benzene was investigated. This basic group was demonstrated to reduce the lipophilicity of compounds and to increase significantly their aqueous solubility. However, this structural modification proved to reduce the mPTP activity and did not improve the DMPK profile of the benzene derived cinnamide series. As a result, even if several interesting analogues were identified, none of them combined the overall profile required for progression to PK/PD animal studies. Nevertheless, during the course of this exercise, an attractive SAR finding arose, suggesting that a di-*ortho*-substitution pattern to the amide bond had the potential to increase aqueous solubility, while being tolerated for mPTP activity.

This structural innovation was investigated within a pyridyl cinnamide sub-series, which represented a better starting point with regard to *in vivo* PK. This effort led to the identification of the 6-methoxy-2,4-dimethylpyridyl analogue **3.160** which displayed a desirable overall profile. Indeed, **3.160** was a potent mPTP modulator (liver CRC pIC<sub>50</sub> = 7.8), with a reasonable level of lipophilicity and aqueous solubility (PFI = 6.4, CLND = 73 µg/mL and FaSSIF = 64 µg/mL) and with high level of *in vivo* systemic exposure.

When comparing the profile of the pyridyl cinnamide **3.160** with the lead isoxazole **3.16a** (Table 51), both compounds had similar mPTP activity, however, **3.160** displayed reduced lipophilicity (PFI of 6.4 for **3.160** compared with 7.6 for **3.16a**) and a considerably improved aqueous solubility. Moreover, cinnamide **3.160** displayed superior *in vitro* DMPK parameters and *in vivo* PK profile.

The initial objective for the cinnamide series was to identify analogues with a superior profile compared with the isoxazole series and compound **3.160** robustly achieved this goal. Consequently, **3.160** was submitted for several animal PK/PD experiments, in order to assess mPTP target engagement *in vivo* with a cinnamide compound. The results from these studies will be expected to further contribute towards target validation efforts in modulating mPTP in a variety of important disease states.



|                                   |                   | Targeted profile |  |  |
|-----------------------------------|-------------------|------------------|--|---|
| <b>Compound</b>                   |                   |                  | <b>3.16a</b>   | <b>3.160</b>  |
| <b>Liver CRC pIC<sub>50</sub></b> |                   | > 7              | 7.7 <sup>a</sup>   | 7.8   |
| <b>LE / LLE</b>                   |                   | > 0.3            | 0.42 / 0.38  | 0.42 / 0.35   |
| <b>MW</b>                         |                   | < 400            | 335  | 340   |
| <b>clogP</b>                      |                   | < 3              | 2.8  | 3.3   |
| <b>PFI</b>                        |                   | < 6              | 7.6  | 6.4   |
| <b>CLND (µg/mL)</b>               |                   | > 100            | 5 <sup>b</sup>   | 73 <sup>c</sup>   |
| <b>FaSSIF (µg/mL)</b>             |                   | > 100            | 6  | 64  |
| <b>h IVC (mL/min/g)</b>           |                   | < 2              | 1.2  | 0.8   |
| <b>r IVC (mL/min/g)</b>           |                   | < 2              | 1.6  | < 0.7   |
| <b>m IVC (mL/min/g)</b>           |                   | < 2              | 4.3  | 1.5   |
| <b>Fu,bl</b>                      |                   | > 2%             | 0.7%   | 2.6%  |
| <b>Mouse SOA (5 mg/kg)</b>        | <b>Cmax (µM)</b>  | > 3              | 5.05   | 6.64  |
|                                   | <b>AUC (µM.h)</b> | > 5              | 8.12   | 20.08   |

<sup>a</sup>Compound was only reported with a measured pIC<sub>50</sub> value in 43 out of 49 test occasions and for the other 6 test occasions, pIC<sub>50</sub> was greater than 9; <sup>b</sup>Compound was only reported with a measured CLND value in 5 out of 6 test occasions and for the other 1 test occasion, CLND was < 1 µg/mL; <sup>c</sup>Compound was only reported with a measured CLND value in 1 out of the 3 test occasions and for the other 2 occasions, CLND was ≥ 95 and 112 µg/mL, respectively.

**Table 51: Profile of the pyridyl cinnamide 3.160 vs. the targeted profile and the profile of isoxazole 3.16a**

### 3.6. Overall conclusions of the mPTP programme and future work

In the isoxazole series, optimisation of the previously developed synthetic route to compound **3.17b** allowed us to expediently synthesise enough material for a decision-enabling *in vivo* PK study and for its absolute configuration determination. The strategy of carrying out the chiral separation of the cyclopenta[*b*]pyridin-5-ol intermediate **3.20** prior to the Mitsunobu step, as opposed to chirally separate the racemic mixture **3.17**, provided a more efficient overall synthetic route. An interesting enantioselective synthetic approach, employing a CBS-reduction step, proved to afford high e.e., however, this alternative strategy was less efficient compared with the use of chiral chromatography. The comparison of the newly generated *in vivo* PK data of **3.17b** with that of the initial lead isoxazole **3.16a** allowed the decision to progress **3.16a** for PK/PD animal work. Subsequently, optimisation of the efficiency and of the practicality of the Mitsunobu step towards the synthesis of isoxazole **3.16a** was achieved by using ADDP as an alternative reducing agent to DIAD. The original route delivered isoxazole **3.16a** in 4% over 9 steps, while the new conditions afforded compound **3.16a** in an overall yield of 18%. This improvement had a dramatic impact when 100 g of isoxazole **3.16a** was synthesised *via* external collaboration.

Concerning the cinnamide series, a novel mPTP modulator **3.160** was identified with a physicochemical and DMPK profile enabling its progression to PK/PD animal studies. The optimisation process started from benzene derived cinnamide analogues with poor aqueous solubility and *in vivo* PK. The introduction of a basic group was investigated as a strategy to improve the overall profile of the molecules. This approach was proven to be successful for certain parameters, such as lipophilicity and aqueous solubility, however, the DMPK profile of the benzene derived cinnamide series remained sub-optimal. A novel di-*ortho*-substitution pattern to the amide bond was identified as a handle to increase solubility while retaining mPTP potency, and this finding was successfully transferred onto the pyridyl cinnamide series to ultimately deliver the 6-methoxy-2,4-dimethylpyridyl analogue **3.160**. The medicinal chemistry campaign for

the cinnamide series has therefore enabled the discovery of molecules with a significantly improved aqueous solubility and *in vivo* DMPK profile compared to the isoxazole lead compounds.

Furthermore, the data that will be generated from the animal PK/PD experiments with isoxazole **3.16a** and cinnamide **3.160** will be critical for understanding the level of mPTP inhibition required to see an *in vivo* physiological effect. The biological profile of the next generation of mPTP modulators will ultimately be refined based on these results.

Several future work streams from the current study could be investigated. For the isoxazole series, it would be pertinent to see whether a similar strategy of disrupting the molecular planarity of **3.16a**, evidenced by its X-ray generated during the course of this work, could successfully increase the aqueous solubility of the isoxazole series. For the cinnamide series, the next steps for the development of compound **3.160** as a drug candidate would be to generate a more extensive biological profile (*e.g. in vivo* toxicology studies). However, the early results from our internal cross-selectivity panel showed that **3.160** was at least 250 times more selective for mPTP compared to 53 biological targets which are known to potentially induce side-effects. Moreover, as a follow-up to the encouraging results obtained when introducing a methyl group *ortho* to the amide bond, it would be relevant to investigate further the modulation of the dihedral angle, for instance by adding bulkier groups than methyl. However, since the lipophilicity of **3.160** was already moderate (PFI of 6.4), these *ortho* groups would need to have little impact on lipophilicity, which could be challenging.

Revisiting the discussion on the two major types of pharmacological assays, target-based and phenotype-based assays, described in **Chapter 1.3 (p. 14)**, a major limitation of the use of phenotypic assays was identified to be the impossibility of doing structure-based drug discovery, rendering the molecular design of drugs more difficult. Nevertheless, the medicinal chemistry optimisation carried out on the cinnamide series in the course of this research project clearly demonstrated that even when the biological target is

unknown, SAR can be generated and molecules with an improved profile can be identified. This study has shown that combining the phenotypic approach together with modern concepts of oral drug likeness and emphasis on physicochemical properties can lead to the identification of high quality small molecule drugs. It is likely that this strategy could be of value for other biological targets associated with different diseases in the future.

Of course, it will now be interesting to elucidate the exact mechanism of action of the lead compounds from the isoxazole and the cinnamide series, and the molecules generated here could be useful assets in enabling this.

## 4. Experimental section

### 4.1. General Methods

All reaction solvents used were of analytical grade and purchased from Sigma-Aldrich or Merck. The solvents in anhydrous form were stored under nitrogen after each use. All reagents were purchased from standard suppliers such as Sigma-Aldrich, Lancaster, Fluorochem, TCI, Apollo and Combi-blocks, and were used without further purification. All air-sensitive reactions were conducted under an inert nitrogen atmosphere.

**Microwave reactions** were carried out in a Biotage or Anton-Parr initiator set to high absorption. Reactions were performed in single-use glass vessels (capacity = 0.2, 2, 5 or 20 mL).

**<sup>1</sup>H nuclear magnetic resonance (NMR)** spectra were recorded on a Bruker DPX (400 MHz) or a Bruker Advance (600 MHz) spectrometer. Chemical shifts ( $\delta_{\text{H}}$ ) were quoted in ppm, relative to tetramethylsilane and were internally referenced to the residual solvent peak. Coupling constants ( $J$ ) were given in Hz to the nearest 0.1 Hz. The following abbreviations were used: s, singlet; d, doublet; t, triplet; sxt, sextet; spt, septet; dd, double doublet; td, triplet of doublets; dt, double triplet; ddd, double doublet of doublets; m, multiplet; br., broad.

**<sup>13</sup>C nuclear magnetic resonance** spectra were recorded on a Bruker DPX (400 MHz) or a Bruker Advance (600 MHz) spectrometer. Chemical shifts ( $\delta_{\text{C}}$ ) were quoted in ppm, referenced relative to the residual solvent peak.

**High-resolution mass spectrometry (HRMS)** experiments were carried out using a Micromass QTOF Ultima hybrid quadrupole time-of-flight mass spectrometer equipped with a Z-spray (ESI) interface, over a mass range of 100-1100 Da, with a scan time of 0.9 s and an interscan delay of 0.1 s. Reserpine was used as the external mass calibrant

( $[M+H]^+ = 609.2812$  Da). The elemental composition was calculated using MassLynx® v4.1 for the  $[M+H]^+$ .

**All high-resolution mass spectra were recorded by Bill Leavens from GlaxoSmithKline, R&D Stevenage, UK.**<sup>304</sup>

**Melting points (mp)** were determined on a Stuart SMP3 or on a Stuart SMP40 melting point apparatus. Values are quoted in degrees centigrade.

**Infrared (IR) spectra** were recorded on a Perkin Elmer Spectrum One Fourier Transform or on a Bruker Alpha-p spectrometer, with samples loaded as solids. Only selected absorptions were reported and quoted in reciprocal centimeters ( $\text{cm}^{-1}$ ).

**Specific rotations  $[\alpha]_D$**  were measured on a Rudolph Research Analytical AUTOPOL V polarimeter, at 589 nm wavelength. Compounds were dissolved in DMSO- $d_6$  (concentration quoted when data are reported) and measurements were done at 25 °C. The specific rotation value quoted was the average of five measurements.

**All specific rotations were recorded by Douglas Minick from GlaxoSmithKline, R&D Durham, US.**<sup>242</sup>

**Dihedral angle calculations** were carried out using Molecular Operating Environment® (MOE®) version MOE2009.10 or MOE2014.09.<sup>143</sup> The dihedral angles quoted are for the local low energy conformations.

#### **Analytical liquid chromatography-mass spectrometry (LCMS)**

The analyses were carried out on a Waters Acquity ultra performance liquid chromatography BEH C<sub>18</sub> column (50 mm x 2.1 mm i.d., 1.7  $\mu\text{m}$  packing diameter) or on a Waters Acquity ultra performance liquid chromatography CSH C<sub>18</sub> column (50 mm x 2.1 mm i.d., 1.7  $\mu\text{m}$  packing diameter) at 40 °C or at 45 °C. The ultraviolet (UV) detection system was an averaged signal from wavelength of 210 nm to 350 nm or 210 nm to 450 nm. Mass spectra were recorded on a mass spectrometer using alternate scan

positive and negative mode electrospray ionisation. Two LCMS conditions were used and are quoted as either “**acidic conditions**” or “**basic conditions**”.

For the “**acidic conditions**”, the solvents employed were: A = 0.1% v/v formic acid in water; B = 0.1% v/v formic acid in acetonitrile. The flow rate was 1 mL/min and below is an example of a typical gradient system:

| Time (min) | %A | %B |
|------------|----|----|
| 0          | 97 | 3  |
| 1.5        | 5  | 95 |
| 1.9        | 5  | 95 |
| 2          | 97 | 3  |

For the “**basic conditions**”, the solvents employed were: A = 10 mM ammonium bicarbonate aqueous solution adjusted to pH 10 with an ammonium hydroxide aqueous solution; B = acetonitrile. The flow rate was 1 mL/min and below is an example of a typical gradient system:

| Time (min) | %A | %B  |
|------------|----|-----|
| 0          | 99 | 1   |
| 1.5        | 3  | 97  |
| 1.9        | 3  | 97  |
| 2          | 0  | 100 |

For the outsourcing partner LCMS conditions, the analyses were carried out on an Agilent ultra performance liquid chromatography Sunfire C<sub>18</sub> column (50 mm x 4.6 mm i.d., 3.5 µm packing diameter) or on an Agilent ultra performance liquid chromatography XBridge C<sub>18</sub> column (50 mm x 4.6 mm i.d., 3.5 µm packing diameter) at 40 °C or at 50 °C. The UV detection system was an averaged signal from wavelength of 190 nm to 400 nm. Mass spectra were recorded on a mass spectrometer using alternate scan positive and negative mode electrospray ionisation. Two LCMS conditions were used and are quoted as either “**outsourcing partner acidic conditions**” or “**outsourcing partner basic conditions**”.

For the “**outsourcing partner acidic conditions**”, the solvents employed were: A = 0.01% v/v trifluoroacetic acid in water; B = 0.01% v/v trifluoroacetic acid in acetonitrile. The flow rate was 1.5 mL/min and the gradient used was:

| Time (min) | %A | %B  |
|------------|----|-----|
| 0          | 95 | 5   |
| 0.8        | 0  | 100 |
| 1.9        | 0  | 100 |

For the “**outsourcing partner basic conditions**”, the solvents employed were: A = 10 mM ammonium bicarbonate aqueous solution; B = acetonitrile. The flow rate was 2 mL/min and the gradient used was:

| Time (min) | %A | %B |
|------------|----|----|
| 0          | 95 | 5  |
| 1.2        | 5  | 95 |
| 2.5        | 5  | 95 |
| 2.51       | 95 | 5  |

### **Mass directed auto-preparative (MDAP) chromatography**

The preparative separations were carried out on a X-select CSH C<sub>18</sub> column (150 mm x 30 mm i.d., 5 µm packing diameter) at ambient temperature. The UV detection system was an averaged signal from wavelength of 210 nm to 350 nm. Mass spectra were recorded on a mass spectrometer using alternate scan positive and negative mode electrospray ionisation. Two LCMS conditions were used and are quoted as either “**acidic conditions**” or “**basic conditions**”.

For the “**acidic conditions**”, the solvents employed were: A = 0.1% v/v formic acid in water; B = 0.1% v/v formic acid in acetonitrile. For the “**basic conditions**”, the solvents employed were A = 10 mM ammonium bicarbonate aqueous solution adjusted to pH 10 with an ammonium hydroxide aqueous solution; B = Acetonitrile. An appropriate elution gradient over 15 min at a flow rate of 40 mL/min was chosen for each compound



depending on their retention time on the analytical LCMS system, and below is an example of a regularly chosen gradient system:

| Time (min) | %A | %B |
|------------|----|----|
| 0          | 85 | 15 |
| 1          | 85 | 15 |
| 10         | 45 | 55 |
| 11         | 1  | 99 |
| 15         | 1  | 99 |

**Column chromatographies** were performed on a Flashmaster II system, which is an automated multiuser flash chromatography system, available from Argonaut Technologies Ltd, which utilises disposable, normal phase cartridges (from 2 to 330 g sizes).

#### **Analytical chiral high-performance liquid chromatography (HPLC) method 1**

Column: Daicel Chiralpak IA column, 4.6 mm i.d. x 250 mm, 5 µm particle size. Elution: isocratic mobile phase, isohexane:EtOH = 60:40, flow rate 1 mL/min, run time 30 min. A photodiode array detector was used to collect the spectra between 210 and 400 nm.

#### **Analytical chiral HPLC method 2**

Column: Daicel Chiralpak IA column, 4.6 mm i.d. x 250 mm, 5 µm particle size. Elution: isocratic mobile phase, isohexane:EtOH = 90:10, flow rate 1 mL/min, run time 60 min. A photodiode array detector was used to collect the spectra between 210 and 400 nm.

#### **Analytical chiral HPLC method 3**

Column: Daicel Chiralpak IA column, 4.6 mm i.d. x 250 mm, 5 µm particle size. Elution: isocratic mobile phase, isohexane:EtOH = 95:5, flow rate 1 mL/min, run time 60 min. A photodiode array detector was used to collect the spectra between 210 and 400 nm.

#### **Analytical chiral HPLC method 4**

Column: Daicel Chiralpak IB column, 4.6 mm i.d. x 250 mm, 5 µm particle size. Elution: isocratic mobile phase, isohexane:EtOH = 90:10, flow rate 1 mL/min, run time 30 min. A photodiode array detector was used to collect the spectra between 210 and 400 nm.

#### **Analytical chiral HPLC method 5**

Column: Daicel Chiralpak IA column, 4.6 mm i.d. x 250 mm, 3 µm particle size. Elution: mixture isohexane:EtOH with the gradient shown below, flow rate 1 mL/min, run time 60 min. A photodiode array detector was used to collect the spectra between 210 and 400 nm.

| <b>Time (min)</b> | <b>% isohexane</b> | <b>% EtOH</b> |
|-------------------|--------------------|---------------|
| 0                 | 60                 | 40            |
| 0.5               | 60                 | 40            |
| 30                | 20                 | 80            |
| 60                | 20                 | 80            |

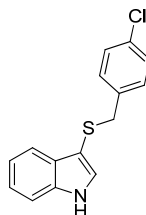
#### **Biological assays**

All the data from biological assays quoted in this thesis resulted from measurements carried out by members of the pharmacology group of GlaxoSmithKline. All pIC<sub>50</sub> quoted in this thesis are an average of at least two independent determinations.

#### **Assays using animals or animal tissues**

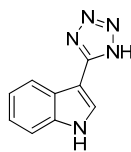
All animal studies were conducted in accordance with the GSK Policy on the Care, Welfare and Treatment of Laboratory Animals and were reviewed by the Institutional Animal Care and Use Committee either at GSK or by the ethical review process at the institution where the work was performed.

## 4.2. Experimental preparation of the indole analogues for the I<sub>CRAC</sub> programme



2.32

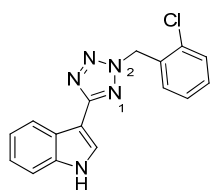
**3-((4-Chlorobenzyl)thio)-1H-indole (2.32)**; To a degassed solution of 1H-indole-3-thiol (150 mg, 1.01 mmol) in DMF (2 mL) was added 60% by weight sodium hydride (48.2 mg, 1.21 mmol) in portions. The resulting mixture was stirred under nitrogen at room temperature for 30 min. To this was added a solution of 1-(bromomethyl)-4-chlorobenzene (248 mg, 1.21 mmol) in DMF (1 mL) dropwise. The resulting mixture was then stirred at room temperature under nitrogen for 2 h and was carefully quenched with water (5 mL). The reaction mixture was extracted with DCM (2 x 5 mL). The organic extracts were combined, dried by filtration through a hydrophobic frit and concentrated *in vacuo*. The crude material was purified by MDAP (acidic conditions) to afford the title compound as a beige solid; yield 77% (212 mg); **LCMS** (acidic conditions) (ES +ve) *m/z* 274 (M+H)<sup>+</sup>, Rt = 1.30 min; **<sup>1</sup>H NMR** (400 MHz, DMSO-d<sub>6</sub>): δ = 11.29 (br. s, 1H), 7.51 (d, *J* = 7.8 Hz, 1H), 7.40 (d, *J* = 8.1 Hz, 1H), 7.29 - 7.22 (m, 3H), 7.18 - 7.02 (m, 4H), 3.86 ppm (s, 2H); **<sup>13</sup>C NMR** (101 MHz, DMSO-d<sub>6</sub>): δ = 138.0, 136.3, 131.1, 130.7, 130.5, 128.8, 128.0, 121.7, 119.5, 118.2, 112.0, 102.2, 39.5 ppm; **HRMS** (ES +ve) calcd for C<sub>15</sub>H<sub>13</sub>ClNS<sup>+</sup> (M+H)<sup>+</sup> 274.0452, found 274.0454; **IR** ν (cm<sup>-1</sup>) 3375, 740; **mp** 115.4 °C.



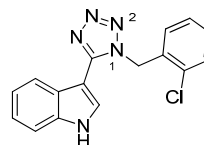
**2.34**

**3-(1H-Tetrazol-5-yl)-1H-indole (2.34)**; 1H-Indole-3-carbonitrile (1.00 g, 7.03 mmol), sodium azide (0.915 g, 14.07 mmol), triethylamine hydrochloride (2.90 g, 21.10 mmol) and toluene (5 mL) were charged to a reaction tube and the reaction mixture was stirred to 105 °C overnight. A 2 M HCl aqueous solution (3 mL) was carefully added and the solution was stirred vigorously for 15 min. The reaction mixture was partitioned between EtOAc (100 mL) and water (100 mL). The organic layer was dried by filtration through a hydrophobic frit and concentrated *in vacuo*. The crude mixture was loaded on an ion-exchange aminopropyl silica cartridge, eluted with MeOH (2 x column volumes (CV)) and with a 10% v/v AcOH in MeOH solution (2 x CV). The acidic fraction was concentrated *in vacuo* to afford the title compound; yield 71% (920 mg); **LCMS** (acidic conditions) (ES +ve) *m/z* 186 (M+H)<sup>+</sup>, Rt = 0.62 min; **<sup>1</sup>H NMR** (400 MHz, DMSO-d<sub>6</sub>): δ = 11.84 (br. s, 1H), 8.21 (d, *J* = 7.3 Hz, 1H), 8.07 (d, *J* = 3.0 Hz, 1H), 7.53 (d, *J* = 7.3 Hz, 1H), 7.30 - 7.14 ppm (m, 2H), *tetrazole NH was not observed*.

<sup>1</sup>H NMR data consistent with those reported in literature.<sup>305</sup>



**2.18**



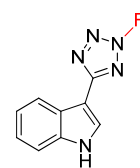
**2.35**

**3-(2-(2-Chlorobenzyl)-2H-tetrazol-5-yl)-1H-indole (2.18)** and **3-(1-(2-Chlorobenzyl)-1H-tetrazol-5-yl)-1H-indole (2.35)**; A suspension of 3-(1H-tetrazol-5-yl)-1H-indole (150 mg, 0.81 mmol) and K<sub>2</sub>CO<sub>3</sub> (168 mg, 1.22 mmol) in DMF (5 mL) was stirred at

room temperature for 20 min. A solution of 1-(bromomethyl)-2-chlorobenzene (183 mg, 0.89 mmol) in DMF (2 mL) was added dropwise and the resulting suspension was stirred for 15 h at room temperature. Water (5 mL), brine (2 mL) and DCM (5 mL) were added to the mixture and the organic phase was separated. The aqueous layer was further extracted with DCM (5 mL). The organic extracts were combined, dried by filtration through a hydrophobic frit and concentrated *in vacuo*. The residue obtained was purified by MDAP (acidic conditions) to afford the title *N*<sup>1</sup>- and *N*<sup>2</sup>-alkylated tetrazole regioisomers:

**3-(1-(2-Chlorobenzyl)-1*H*-tetrazol-5-yl)-1*H*-indole (2.35)**; yield 4% (11 mg); **LCMS** (acidic conditions) (ES +ve) *m/z* 310 (M+H)<sup>+</sup>, *Rt* = 1.02 min; **<sup>1</sup>H NMR** (600 MHz, DMSO-*d*<sub>6</sub>): δ = 12.07 (br. s, 1H), 8.18 (d, *J* = 7.7 Hz, 1H), 7.98 (s, 1H), 7.54 (t, *J* = 7.0 Hz, 2H), 7.40 (td, *J* = 7.7, 1.5 Hz, 1H), 7.34 (td, *J* = 7.3, 0.7 Hz, 1H), 7.27 (td, *J* = 7.7, 1.1 Hz, 1H), 7.22 (t, *J* = 7.0 Hz, 1H), 7.09 (dd, *J* = 8.0, 1.1 Hz, 1H), 5.92 ppm (s, 2H); **<sup>13</sup>C NMR** (101 MHz, DMSO-*d*<sub>6</sub>): δ = 150.7, 136.0, 132.6, 132.0, 130.2, 129.8, 129.7, 127.8, 127.3, 125.3, 122.9, 121.0, 120.6, 112.2, 98.0, 49.0 ppm.

**3-(2-(2-Chlorobenzyl)-2*H*-tetrazol-5-yl)-1*H*-indole (2.18)**, yield 60% (150 mg); **LCMS** (acidic conditions) (ES +ve) *m/z* 310 (M+H)<sup>+</sup>, *Rt* = 1.16 min; **<sup>1</sup>H NMR** (600 MHz, DMSO-*d*<sub>6</sub>): δ = 11.72 (br. s, 1H), 8.11 (d, *J* = 7.7 Hz, 1H), 8.08 (s, 1H), 7.56 (d, *J* = 7.3 Hz, 1H), 7.52 - 7.48 (m, 2H), 7.47 - 7.40 (m, 2H), 7.21 (t, *J* = 7.0 Hz, 1H), 7.17 (t, *J* = 7.0 Hz, 1H), 6.06 ppm (s, 2H); **<sup>13</sup>C NMR** (151 MHz, DMSO-*d*<sub>6</sub>): δ = 162.0, 136.4, 133.2, 131.7, 131.4, 130.7, 129.7, 127.8, 126.2, 124.6, 122.2, 120.4, 120.2, 112.1, 102.5, 53.6 ppm; **HRMS** (ES +ve) calcd for C<sub>16</sub>H<sub>13</sub>ClN<sub>5</sub><sup>+</sup> (M+H)<sup>+</sup> 310.0859, found 310.0858; **IR** ν (cm<sup>-1</sup>) 3305, 1588, 745; **mp** 187.2 °C.

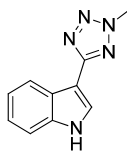


General procedure for the preparation of 2.36-2.42 and 2.45-2.46:

A suspension of 3-(1*H*-tetrazol-5-yl)-1*H*-indole (27 mg, 0.15 mmol), K<sub>2</sub>CO<sub>3</sub> (31 mg, 0.22 mmol) and the appropriate alkylating agents (either chloro-, bromo- or iodo-derivative, 0.18 mmol) in DMF (1 mL) were stirred at room temperature for 2 h. The reactions were then checked by LCMS and depending on the profiles observed, reactions were worked up or the following actions were taken before work up:

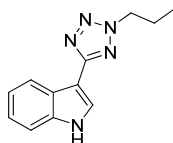
| Cmpd | Actions taken   |
|------|---|
| 2.39 | K <sub>2</sub> CO <sub>3</sub> (31 mg, 0.22 mmol) added and mixture stirred at room temperature overnight. K <sub>2</sub> CO <sub>3</sub> (31 mg, 0.22 mmol) added, reaction stirred at 60 °C for 2 h and at 110 °C for 2 h in a microwave. |
| 2.40 | K <sub>2</sub> CO <sub>3</sub> (31 mg, 0.22 mmol) added and mixture stirred at room temperature overnight. K <sub>2</sub> CO <sub>3</sub> (31 mg, 0.22 mmol) added and reaction stirred at 60 °C for 4 h.                                   |
| 2.41 | K <sub>2</sub> CO <sub>3</sub> (31 mg, 0.22 mmol) added and mixture stirred at room temperature overnight.  |
| 2.42 | K <sub>2</sub> CO <sub>3</sub> (31 mg, 0.22 mmol) added and mixture stirred at room temperature overnight.  |

The solvent was dried under a stream of nitrogen. The residue obtained was purified by MDAP (acidic conditions) to afford the expected *N*<sup>2</sup>-alkylated tetrazole regioisomer:



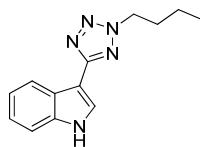
**2.36**

**3-(2-Methyl-2H-tetrazol-5-yl)-1H-indole (2.36);**<sup>148</sup> from iodomethane (25 mg, 0.18 mmol); yield 11% (4 mg); **LCMS** (acidic conditions) (ES +ve)  $m/z$  200 (M+H)<sup>+</sup>,  $R_t$  = 0.82 min; **<sup>1</sup>H NMR** (600 MHz, DMSO- $d_6$ ):  $\delta$  = 11.62 (br. s, 1H), 8.12 (d,  $J$  = 7.6 Hz, 1H), 8.03 (s, 1H), 7.50 (d,  $J$  = 7.9 Hz, 1H), 7.21 (t,  $J$  = 7.7 Hz, 1H), 7.17 (t,  $J$  = 7.6 Hz, 1H), 4.36 ppm (s, 3H).



**2.37**

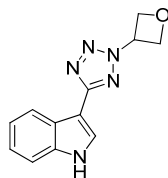
**3-(2-Propyl-2H-tetrazol-5-yl)-1H-indole (2.37);**<sup>148</sup> from 1-iodopropane (30 mg, 0.18 mmol); yield 8% (3 mg); **LCMS** (acidic conditions) (ES +ve)  $m/z$  228 (M+H)<sup>+</sup>,  $R_t$  = 1.00 min; **<sup>1</sup>H NMR** (600 MHz, DMSO- $d_6$ ):  $\delta$  = 11.72 (br. s, 1H), 8.17 (d,  $J$  = 7.9 Hz, 1H), 8.08 (s, 1H), 7.50 (d,  $J$  = 7.9 Hz, 1H), 7.27 - 7.15 (m, 2H), 4.67 (t,  $J$  = 6.8 Hz, 2H), 2.00 (sxt,  $J$  = 7.1 Hz, 2H), 0.91 ppm (t,  $J$  = 7.4 Hz, 3H).



**2.38**

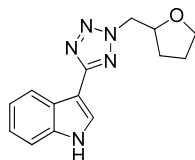
**3-(2-Butyl-2H-tetrazol-5-yl)-1H-indole (2.38);**<sup>148</sup> from 1-iodobutane (33 mg, 0.18 mmol); yield 10% (4 mg); **LCMS** (acidic conditions) (ES +ve)  $m/z$  242 (M+H)<sup>+</sup>,  $R_t$  =

1.10 min;  $^1\text{H NMR}$  (600 MHz, DMSO- $d_6$ ):  $\delta$  = 11.74 (br. s, 1H), 8.16 (d,  $J$  = 7.9 Hz, 1H), 8.08 (s, 1H), 7.50 (d,  $J$  = 7.9 Hz, 1H), 7.24 - 7.15 (m, 2H), 4.71 (t,  $J$  = 7.0 Hz, 2H), 1.96 (quin,  $J$  = 7.3 Hz, 2H), 1.32 (sxt,  $J$  = 7.5 Hz, 2H), 0.92 ppm (t,  $J$  = 7.4 Hz, 3H).



**2.39**

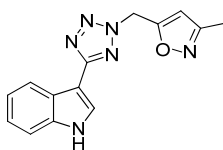
**3-(2-(Oxetan-3-yl)-2H-tetrazol-5-yl)-1H-indole (2.39)**,<sup>148</sup> from 3-iodooxetane (33 mg, 0.18 mmol); yield 10% (4 mg); **LCMS** (acidic conditions) (ES +ve)  $m/z$  242 (M+H)<sup>+</sup>,  $R_t$  = 0.81 min;  $^1\text{H NMR}$  (600 MHz, DMSO- $d_6$ ):  $\delta$  = 11.80 (br. s, 1H), 8.21 (d,  $J$  = 7.9 Hz, 1H), 8.15 (s, 1H), 7.52 (d,  $J$  = 7.6 Hz, 1H), 7.26 - 7.17 (m, 2H), 6.27 - 6.18 (m, 1H), 5.16 - 5.10 (m, 2H), 5.09 - 5.03 ppm (m, 2H).



**2.40**

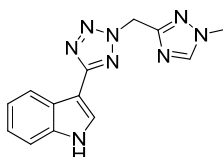
**3-(2-((Tetrahydrofuran-2-yl)methyl)-2H-tetrazol-5-yl)-1H-indole (2.40)**,<sup>148</sup> from 2-(bromomethyl)tetrahydrofuran (29 mg, 0.18 mmol); yield 3% (1.2 mg); **LCMS** (acidic conditions) (ES +ve)  $m/z$  270 (M+H)<sup>+</sup>,  $R_t$  = 0.92 min;  $^1\text{H NMR}$  (600 MHz, DMSO- $d_6$ ):  $\delta$  = 11.80 (br. s, 1H), 8.16 (d,  $J$  = 7.6 Hz, 1H), 8.08 (s, 1H), 7.50 (d,  $J$  = 7.9 Hz, 1H), 7.27 - 7.13 (m, 2H), 4.84 - 4.70 (m, 2H), 4.44 (dd,  $J$  = 6.4, 4.9 Hz, 1H), 3.79 - 3.71 (m, 1H), 3.69 - 3.62 (m, 1H), 2.12 - 2.04 (m, 1H), 1.88 - 1.80 (m, 2H), 1.80 - 1.72 ppm (m, 1H).





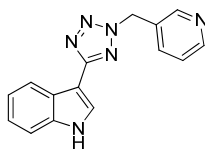
**2.41**

**5-((5-(1H-Indol-3-yl)-2H-tetrazol-2-yl)methyl)-3-methylisoxazole (2.41);**<sup>148</sup> from 5-(chloromethyl)-3-methylisoxazole (23 mg, 0.18 mmol); yield 12% (6 mg); **LCMS** (acidic conditions) (ES +ve)  $m/z$  281 (M+H)<sup>+</sup>,  $R_t$  = 0.92 min; **<sup>1</sup>H NMR** (600 MHz, DMSO- $d_6$ ):  $\delta$  = 11.80 (br. s, 1H), 8.17 - 8.09 (m, 2H), 7.51 (d,  $J$  = 7.9 Hz, 1H), 7.27 - 7.15 (m, 2H), 6.58 (s, 1H), 6.24 (s, 2H), 2.24 ppm (s, 3H).



**2.42**

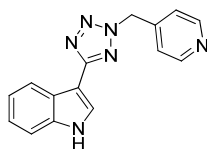
**3-(2-((1-Methyl-1H-1,2,4-triazol-3-yl)methyl)-2H-tetrazol-5-yl)-1H-indole (2.42);**<sup>148</sup> from 3-(chloromethyl)-1-methyl-1H-1,2,4-triazole (23 mg, 0.18 mmol); yield 4% (2 mg); **LCMS** (acidic conditions) (ES +ve)  $m/z$  281 (M+H)<sup>+</sup>,  $R_t$  = 0.73 min; **<sup>1</sup>H NMR** (600 MHz, DMSO- $d_6$ ):  $\delta$  = 11.77 (br. s, 1H), 8.48 (s, 1H), 8.12 (d,  $J$  = 7.9 Hz, 1H), 8.08 (s, 1H), 7.50 (d,  $J$  = 7.9 Hz, 1H), 7.25 - 7.14 (m, 2H), 6.00 (s, 2H), 3.86 ppm (s, 3H).



**2.45**

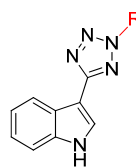
**3-(2-(Pyridin-3-ylmethyl)-2H-tetrazol-5-yl)-1H-indole (2.45);**<sup>148</sup> from 3-(bromomethyl)pyridine hydrobromide (45 mg, 0.18 mmol); yield 6% (3 mg); **LCMS**

(acidic conditions) (ES +ve)  $m/z$  277 (M+H)<sup>+</sup>, Rt = 0.72 min; <sup>1</sup>H NMR (600 MHz, DMSO-d<sub>6</sub>): δ = 11.78 (br. s, 1H), 8.74 (s, 1H), 8.59 (d,  $J$  = 4.5 Hz, 1H), 8.14 (d,  $J$  = 7.9 Hz, 1H), 8.10 (d,  $J$  = 2.6 Hz, 1H), 7.86 (d,  $J$  = 7.6 Hz, 1H), 7.51 (d,  $J$  = 7.9 Hz, 1H), 7.45 (dd,  $J$  = 7.6, 4.5 Hz, 1H), 7.25 - 7.13 (m, 2H), 6.06 ppm (s, 2H).



**2.46**

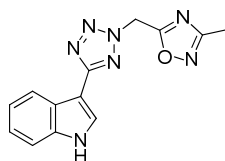
**3-(2-(Pyridin-4-ylmethyl)-2H-tetrazol-5-yl)-1H-indole (2.46)**;<sup>148</sup> from 4-(bromomethyl)pyridine hydrobromide (45 mg, 0.18 mmol); yield 9% (4 mg); LCMS (acidic conditions) (ES +ve)  $m/z$  277 (M+H)<sup>+</sup>, Rt = 0.66 min; <sup>1</sup>H NMR (600 MHz, DMSO-d<sub>6</sub>): δ = 11.77 (br. s, 1H), 8.63 - 8.57 (m, 2H), 8.16 - 8.09 (m, 2H), 7.55 - 7.47 (m, 1H), 7.37 - 7.31 (m, 2H), 7.25 - 7.15 (m, 2H), 6.09 ppm (s, 2H).



*General procedure for the preparation of 2.43-2.44:*

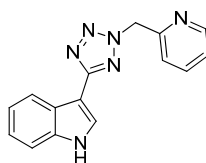
To a suspension of 3-(1H-tetrazol-5-yl)-1H-indole (50 mg, 0.27 mmol) and K<sub>2</sub>CO<sub>3</sub> (56 mg, 0.41 mmol) in DMF (2 mL) was added the appropriate alkylating agent (either chloro- or bromo-derivative, 0.32 mmol) in DMF (2 mL). The resulting suspension was stirred for 15 h at room temperature. The mixture was partitioned between water (5 mL), brine (2 mL) and DCM (5 mL). The aqueous layer was further extracted with DCM (5 mL). The organic extracts were combined, dried by filtration through a hydrophobic frit and solvents were removed under a stream of nitrogen. The residue obtained was

purified by MDAP (acidic or basic conditions) to afford the expected *N*<sup>2</sup>-alkylated tetrazole regioisomer:



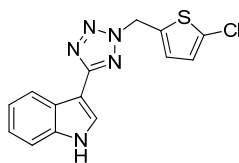
**2.43**

**5-((5-(1*H*-Indol-3-yl)-2*H*-tetrazol-2-yl)methyl)-3-methyl-1,2,4-oxadiazole (2.43);** from 5-(chloromethyl)-3-methyl-1,2,4-oxadiazole (43 mg, 0.32 mmol); yield 54% (41 mg); **LCMS** (acidic conditions) (ES +ve) *m/z* 282 (M+H)<sup>+</sup>, *Rt* = 0.89 min; **<sup>1</sup>H NMR** (400 MHz, DMSO-*d*<sub>6</sub>): δ = 11.78 (br. s, 1H), 8.15 - 8.10 (m, 2H), 7.51 (d, *J* = 7.6 Hz, 1H), 7.26 - 7.15 (m, 2H), 6.55 (s, 2H), 2.35 ppm (s, 3H); **<sup>13</sup>C NMR** (101 MHz, DMSO-*d*<sub>6</sub>): δ = 172.6, 167.5, 162.5, 136.5, 126.6, 124.5, 122.3, 120.5, 120.1, 112.2, 102.1, 47.5, 11.0 ppm; **HRMS** (ES +ve) calcd for C<sub>13</sub>H<sub>12</sub>N<sub>7</sub>O<sup>+</sup> (M+H)<sup>+</sup> 282.1098, found 282.1088; **IR** ν (cm<sup>-1</sup>) 3381, 1590, 742; **mp** 152.9 °C.



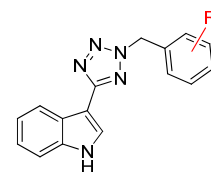
**2.44**

**3-(2-(Pyridin-2-ylmethyl)-2*H*-tetrazol-5-yl)-1*H*-indole (2.44);** from 2-(bromomethyl)pyridine hydrobromide (82 mg, 0.32 mmol); yield 43% (32 mg); **LCMS** (acidic conditions) (ES +ve) *m/z* 277 (M+H)<sup>+</sup>, *Rt* = 0.86 min; **<sup>1</sup>H NMR** (400 MHz, DMSO-*d*<sub>6</sub>): δ = 11.70 (br. s, 1H), 8.54 (d, *J* = 4.5 Hz, 1H), 8.12 (d, *J* = 7.3 Hz, 1H), 8.08 (s, 1H), 7.87 (td, *J* = 7.7, 1.8 Hz, 1H), 7.52 - 7.43 (m, 2H), 7.42 - 7.36 (m, 1H), 7.25 - 7.13 (m, 2H), 6.09 ppm (s, 2H).



**2.47**

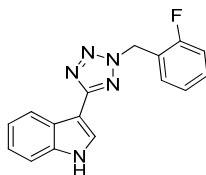
**3-(2-((5-Chlorothiophen-2-yl)methyl)-2H-tetrazol-5-yl)-1H-indole (2.47)**, To a suspension of 3-(2H-tetrazol-5-yl)-1H-indole (30 mg, 0.162 mmol) and  $K_2CO_3$  (33.6 mg, 0.243 mmol) in DMF (2 mL) was added 2-chloro-5-(chloromethyl)thiophene (32.5 mg, 0.194 mmol). The reaction mixture was stirred at room temperature overnight. Water (5 mL) and DCM (5 mL) were added. The organic layer was separated and the aqueous layer was further extracted with DCM (5 mL). The organic extracts were combined, dried by filtration through a hydrophobic frit and solvents were removed under a stream of nitrogen. The residue obtained was purified by MDAP (acidic conditions) to afford the title compound; yield 53% (27 mg); **LCMS** (acidic conditions) (ES +ve)  $m/z$  316 (M+H)<sup>+</sup>,  $R_t$  = 1.17 min; **<sup>1</sup>H NMR** (400 MHz, DMSO- $d_6$ ):  $\delta$  = 11.73 (br. s, 1H), 8.14 (d,  $J$  = 6.8 Hz, 1H), 8.09 (d,  $J$  = 2.5 Hz, 1H), 7.50 (d,  $J$  = 6.8 Hz, 1H), 7.26 - 7.15 (m, 3H), 7.08 (d,  $J$  = 4.0 Hz, 1H), 6.17 ppm (s, 2H); **<sup>13</sup>C NMR** (101 MHz, DMSO- $d_6$ ):  $\delta$  = 162.1, 136.4, 134.9, 129.6, 128.9, 126.9, 126.3, 124.6, 122.3, 120.5, 120.2, 112.1, 102.4, 50.5 ppm; **HRMS** (ES +ve) calcd for  $C_{14}H_{11}ClN_5S^+$  (M+H)<sup>+</sup> 316.0418, found 316.0414; **IR**  $\nu$  ( $cm^{-1}$ ) 3401, 1589, 748; **mp** 135.1°C.



*General procedure for the preparation of 2.49-2.51 and 2.54-2.56:*

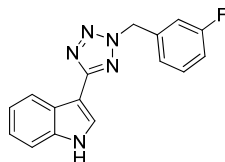
A suspension of 3-(1H-tetrazol-5-yl)-1H-indole (50 mg, 0.27 mmol),  $K_2CO_3$  (56 mg, 0.41 mmol) and the appropriate alkylating agent (0.32 mmol) in DMF (2 mL) was stirred at room temperature overnight. Water (5 mL) and DCM (5 mL) were added. The organic layer was separated and the aqueous layer was further extracted with DCM (5

mL). The organic extracts were combined, dried by filtration through a hydrophobic frit and solvents were removed under a stream of nitrogen. The residue obtained was purified by MDAP (acidic conditions) to afford the expected *N*<sup>2</sup>-alkylated tetrazole regioisomers:



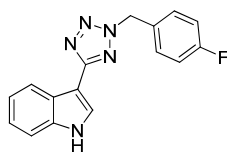
**2.49**

**3-(2-(2-Fluorobenzyl)-2H-tetrazol-5-yl)-1H-indole (2.49)**; from (bromomethyl)-2-fluorobenzene (61.2 mg, 0.32 mmol); yield; 36% (28.4 mg); **LCMS** (acidic conditions) (ES +ve) *m/z* 294 (M+H)<sup>+</sup>, *Rt* = 1.10 min; **<sup>1</sup>H NMR** (400 MHz, DMSO-*d*<sub>6</sub>): δ = 11.71 (br. s, 1H), 8.11 (d, *J* = 8.1 Hz, 1H), 8.07 (s, 1H), 7.56 - 7.43 (m, 3H), 7.33 - 7.24 (m, 2H), 7.24 - 7.13 (m, 2H), 6.02 ppm (s, 2H).



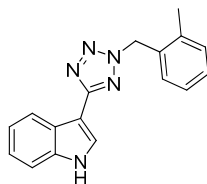
**2.50**

**3-(2-(3-Fluorobenzyl)-2H-tetrazol-5-yl)-1H-indole (2.50)**; from (bromomethyl)-3-fluorobenzene (61.2 mg, 0.32 mmol); yield 51% (40.4 mg); **LCMS** (acidic conditions) (ES +ve) *m/z* 294 (M+H)<sup>+</sup>, *Rt* = 1.10 min; **<sup>1</sup>H NMR** (400 MHz, DMSO-*d*<sub>6</sub>): δ = 11.72 (br. s, 1H), 8.13 (dd, *J* = 6.7, 1.1 Hz, 1H), 8.09 (s, 1H), 7.52 - 7.43 (m, 2H), 7.32 - 7.15 (m, 5H), 6.02 ppm (s, 2H).



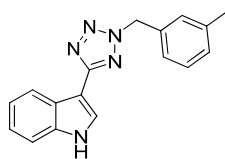
**2.51**

**3-(2-(4-Fluorobenzyl)-2H-tetrazol-5-yl)-1H-indole (2.51)**; from (bromomethyl)-4-fluorobenzene (61.2 mg, 0.32 mmol); yield 51% (40.7 mg); **LCMS** (acidic conditions) (ES +ve)  $m/z$  294 (M+H)<sup>+</sup>,  $R_t$  = 1.10 min; **<sup>1</sup>H NMR** (400 MHz, DMSO- $d_6$ ):  $\delta$  = 11.70 (br. s, 1H), 8.13 (dd,  $J$  = 7.1, 1.0 Hz, 1H), 8.07 (s, 1H), 7.55 - 7.46 (m, 3H), 7.29 - 7.14 (m, 4H), 5.97 ppm (s, 2H).



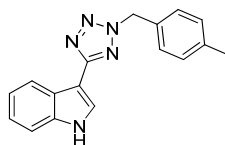
**2.54**

**3-(2-(2-Methylbenzyl)-2H-tetrazol-5-yl)-1H-indole (2.54)**; from (bromomethyl)-2-methylbenzene (60 mg, 0.32 mmol); yield 33% (25.4 mg); **LCMS** (acidic conditions) (ES +ve)  $m/z$  290 (M+H)<sup>+</sup>,  $R_t$  = 1.15 min; **<sup>1</sup>H NMR** (400 MHz, DMSO- $d_6$ ):  $\delta$  = 11.70 (br. s, 1H), 8.11 (d,  $J$  = 7.1 Hz, 1H), 8.06 (s, 1H), 7.49 (d,  $J$  = 7.6 Hz, 1H), 7.31 - 7.22 (m, 4H), 7.22 - 7.14 (m, 2H), 5.97 (s, 2H), 2.41 ppm (s, 3H).



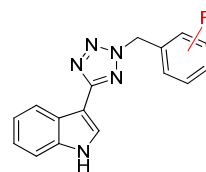
**2.55**

**3-(2-(3-Methylbenzyl)-2H-tetrazol-5-yl)-1H-indole (2.55)**; from (bromomethyl)-3-methylbenzene (60 mg, 0.32 mmol); yield 51% (40.1 mg); **LCMS** (acidic conditions) (ES +ve)  $m/z$  290 (M+H)<sup>+</sup>,  $R_t$  = 1.17 min; **<sup>1</sup>H NMR** (400 MHz, DMSO- $d_6$ ):  $\delta$  = 11.70 (br. s, 1H), 8.14 (d,  $J$  = 7.1 Hz, 1H), 8.07 (s, 1H), 7.49 (d,  $J$  = 7.6 Hz, 1H), 7.30 (t,  $J$  = 7.6 Hz, 1H), 7.25 - 7.14 (m, 5H), 5.92 (s, 2H), 2.30 ppm (s, 3H).



**2.56**

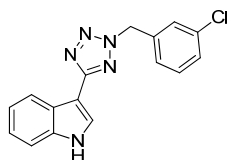
**3-(2-(4-Methylbenzyl)-2H-tetrazol-5-yl)-1H-indole (2.56)**; from (bromomethyl)-4-methylbenzene (60 mg, 0.32 mmol); yield 57% (44.1 mg); **LCMS** (acidic conditions) (ES +ve)  $m/z$  290 (M+H)<sup>+</sup>,  $R_t$  = 1.17 min; **<sup>1</sup>H NMR** (400 MHz, DMSO- $d_6$ ):  $\delta$  = 11.69 (br. s, 1H), 8.13 (d,  $J$  = 7.1 Hz, 1H), 8.06 (s, 1H), 7.49 (d,  $J$  = 7.6 Hz, 1H), 7.35 - 7.30 (m, 2H), 7.24 - 7.14 (m, 4H), 5.91 (s, 2H), 2.29 ppm (s, 3H).



*General procedure for the preparation of 2.52-2.53:*

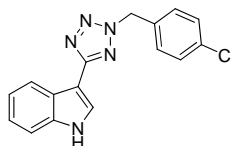
A suspension of 3-(1H-tetrazol-5-yl)-1H-indole (70 mg, 0.38 mmol),  $K_2CO_3$  (78 mg, 0.57 mmol) and the appropriate alkylating agent (93 mg, 0.45 mmol) in DMF (2 mL) was stirred at room temperature for 2 h. Water (5 mL) and DCM (5 mL) were added.

The organic layer was separated and the aqueous layer was further extracted with DCM (5 mL). The organic extracts were combined, dried by filtration through a hydrophobic frit and solvents were removed under a stream of nitrogen. The residue obtained was purified by MDAP (acidic conditions) to afford the expected *N*<sup>2</sup>-alkylated tetrazole regioisomers:



**2.52**

**3-(2-(3-Chlorobenzyl)-2H-tetrazol-5-yl)-1H-indole (2.52)**; from (bromomethyl)-3-chlorobenzene (93 mg, 0.45 mmol); yield 48% (55.8 mg); **LCMS** (acidic conditions) (ES +ve) *m/z* 310 (M+H)<sup>+</sup>, *Rt* = 1.17 min; **<sup>1</sup>H NMR** (400 MHz, DMSO-*d*<sub>6</sub>): δ = 11.72 (br. s, 1H), 8.13 (d, *J* = 7.3 Hz, 1H), 8.09 (d, *J* = 2.5 Hz, 1H), 7.53 (s, 1H), 7.49 (d, *J* = 7.6 Hz, 1H), 7.47 - 7.43 (m, 2H), 7.41 - 7.35 (m, 1H), 7.25 - 7.15 (m, 2H), 6.01 ppm (s, 2H).

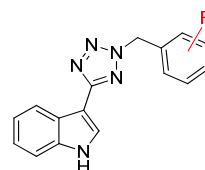


**2.53**

**3-(2-(4-Chlorobenzyl)-2H-tetrazol-5-yl)-1H-indole (2.53)**; from (bromomethyl)-4-chlorobenzene (93 mg, 0.45 mmol); yield 45% (52.6 mg); **LCMS** (acidic conditions) (ES +ve) *m/z* 310 (M+H)<sup>+</sup>, *Rt* = 1.17 min; **<sup>1</sup>H NMR** (400 MHz, DMSO-*d*<sub>6</sub>): δ = 11.71 (br. s, 1H), 8.13 (d, *J* = 7.1 Hz, 1H), 8.08 (d, *J* = 1.8 Hz, 1H), 7.52 - 7.43 (m, 5H), 7.24 - 7.14 (m, 2H), 5.99 ppm (s, 2H); **<sup>13</sup>C NMR** (101 MHz, DMSO-*d*<sub>6</sub>): δ = 162.1, 136.4, 133.4, 133.2, 130.2, 128.9, 126.2, 124.6, 122.2, 120.4, 120.2, 112.1, 102.5, 54.9 ppm;

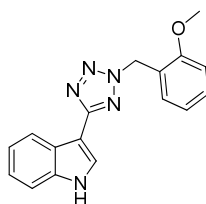


**HRMS** (ES +ve) calcd for  $C_{16}H_{13}ClN_5$  (M+H)<sup>+</sup> 310.0854, found 310.0854; **IR**  $\nu$  (cm<sup>-1</sup>) 3400, 1589, 744; **mp** 149.4 °C.



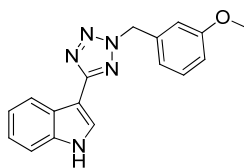
*General procedure for the preparation of 2.57-2.59:*

A suspension of 3-(1H-tetrazol-5-yl)-1H-indole (50 mg, 0.27 mmol), K<sub>2</sub>CO<sub>3</sub> (56 mg, 0.41 mmol) and the appropriate alkylating agent (either chloro- and bromo-derivative, 0.27 mmol) in DMF (2 mL) were stirred at room temperature overnight. The solvent was dried under a stream of nitrogen and the residue obtained was purified by MDAP (acidic conditions) to give the expected N<sup>2</sup>-alkylated tetrazole regioisomers:



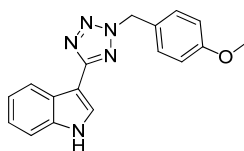
**2.57**

**3-(2-(2-Methoxybenzyl)-2H-tetrazol-5-yl)-1H-indole (2.57)**; from 1-(chloromethyl)-2-(methoxy)benzene (42.3 mg, 0.27 mmol); yield 31% (25.3 mg); **LCMS** (acidic conditions) (ES +ve)  $m/z$  306 (M+H)<sup>+</sup>, Rt = 1.12 min; **<sup>1</sup>H NMR** (400 MHz, DMSO-d<sub>6</sub>):  $\delta$  = 11.68 (br. s, 1H), 8.11 (d,  $J$  = 7.3 Hz, 1H), 8.05 (s, 1H), 7.48 (d,  $J$  = 7.6 Hz, 1H), 7.39 (td,  $J$  = 7.6, 1.5 Hz, 1H), 7.28 (dd,  $J$  = 7.6, 1.5 Hz, 1H), 7.23 - 7.13 (m, 2H), 7.09 (d,  $J$  = 8.1 Hz, 1H), 6.99 (t,  $J$  = 7.6 Hz, 1H), 5.88 (s, 2H), 3.81 ppm (s, 3H).



2.58

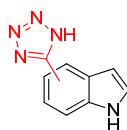
**3-(2-(3-Methoxybenzyl)-2H-tetrazol-5-yl)-1H-indole (2.58)**; from 1-(bromomethyl)-3-(methoxy)benzene (54.3 mg, 0.27 mmol); yield 59% (48.6 mg); **LCMS** (acidic conditions) (ES +ve)  $m/z$  306 (M+H)<sup>+</sup>, Rt = 1.09 min; **<sup>1</sup>H NMR** (400 MHz, DMSO-d<sub>6</sub>):  $\delta$  = 11.71 (br. s, 1H), 8.14 (d,  $J$  = 7.0 Hz, 1H), 8.08 (d,  $J$  = 2.8 Hz, 1H), 7.49 (d,  $J$  = 7.3 Hz, 1H), 7.32 (t,  $J$  = 7.9 Hz, 1H), 7.25 - 7.14 (m, 2H), 7.04 - 7.00 (m, 1H), 6.99 - 6.91 (m, 2H), 5.94 (s, 2H), 3.75 ppm (s, 3H).



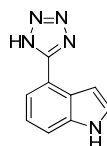
2.59

**3-(2-(4-Methoxybenzyl)-2H-tetrazol-5-yl)-1H-indole (2.59)**; from 1-(bromomethyl)-4-(methoxy)benzene (54.3 mg, 0.27 mmol); yield 38% (31.6 mg); **LCMS** (acidic conditions) (ES +ve)  $m/z$  306 (M+H)<sup>+</sup>, Rt = 1.09 min; **<sup>1</sup>H NMR** (400 MHz, DMSO-d<sub>6</sub>):  $\delta$  = 11.69 (br. s, 1H), 8.13 (d,  $J$  = 7.3 Hz, 1H), 8.06 (d,  $J$  = 2.5 Hz, 1H), 7.49 (d,  $J$  = 7.3 Hz, 1H), 7.41 (d,  $J$  = 8.8 Hz, 2H), 7.24 - 7.14 (m, 2H), 6.97 (d,  $J$  = 8.8 Hz, 2H), 5.88 (s, 2H), 3.74 ppm (s, 3H); **<sup>13</sup>C NMR** (101 MHz, DMSO-d<sub>6</sub>):  $\delta$  = 162.0, 159.4, 136.4, 129.9, 126.4, 126.1, 124.6, 122.2, 120.4, 120.2, 114.2, 112.1, 102.6, 55.4, 55.2 ppm; **HRMS** (ES +ve) calcd for C<sub>17</sub>H<sub>16</sub>N<sub>5</sub>O (M+H)<sup>+</sup> 306.1349, found 306.1344; **IR**  $\nu$  (cm<sup>-1</sup>) 3403, 1588, 747; **mp** 134.7 °C.

General procedure for the preparation of the (1H-tetrazol-5-yl)-1H-indole analogues (2.64-2.67):

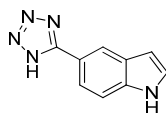


The appropriate 1H-indole-carbonitrile derivative (4-, 5-, 6- or 7-carbonitrile analogues, 1.00 g, 7.03 mmol), sodium azide (0.55 g, 8.44 mmol) and triethylamine hydrochloride (1.94 g, 14.07 mmol) in toluene (15 mL) were stirred at 100 °C for 10 h. The reaction mixture was cooled to room temperature and a 2 M HCl aqueous solution (5 mL) was carefully added and the resulting solution was stirred vigorously for 15 minutes. The reaction mixture was partitioned between EtOAc (50 mL) and water (50 mL). The organic layer was dried by filtration through a hydrophobic frit and concentrated *in vacuo*. The crude mixture was loaded on an ion-exchange aminopropyl silica cartridge, eluted with MeOH (2 x CV) and with a 10% v/v AcOH in MeOH solution (2 x CV). The acidic fraction was concentrated *in vacuo* to afford the (1H-tetrazol-5-yl)-1H-indole analogues:



2.64

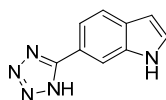
**4-(1H-Tetrazol-5-yl)-1H-indole (2.64)**; yield 20% (258 mg); LCMS (acidic conditions) (ES +ve)  $m/z$  186 (M+H)<sup>+</sup>, Rt = 0.55 min; <sup>1</sup>H NMR (400 MHz, DMSO-d<sub>6</sub>): δ = 11.46 (br. s, 1H), 7.69 (d,  $J$  = 6.8 Hz, 1H), 7.61 (d,  $J$  = 8.3 Hz, 1H), 7.54 (t,  $J$  = 2.6 Hz, 1H), 7.27 (t,  $J$  = 7.7 Hz, 1H), 7.14 ppm (t,  $J$  = 2.1 Hz, 1H), tetrazole NH was not observed.



**2.65**

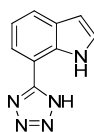
**5-(1H-Tetrazol-5-yl)-1H-indole (2.65)**; yield 63% (822 mg); LCMS (acidic conditions) (ES +ve)  $m/z$  186 (M+H)<sup>+</sup>, Rt = 0.56 min; <sup>1</sup>H NMR (400 MHz, DMSO-d<sub>6</sub>):  $\delta$  = 11.45 (br. s, 1H), 8.27 (s, 1H), 7.77 (dd,  $J$  = 8.4, 1.6 Hz, 1H), 7.58 (d,  $J$  = 8.4 Hz, 1H), 7.49 (t,  $J$  = 2.6 Hz, 1H), 6.60 ppm (t,  $J$  = 2.1 Hz, 1H), *tetrazole NH was not observed*.

<sup>1</sup>H NMR data consistent with those reported in literature.<sup>306</sup>



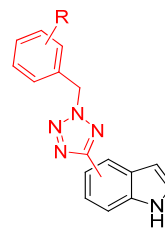
**2.66**

**6-(1H-Tetrazol-5-yl)-1H-indole (2.66)**; yield 61% (796 mg); LCMS (acidic conditions) (ES +ve)  $m/z$  186 (M+H)<sup>+</sup>, Rt = 0.64 min; <sup>1</sup>H NMR (400 MHz, DMSO-d<sub>6</sub>):  $\delta$  = 11.52 (br. s, 1H), 8.13 (s, 1H), 7.73 (d,  $J$  = 8.2 Hz, 1H), 7.67 (dd,  $J$  = 8.2, 1.5 Hz, 1H), 7.55 (t,  $J$  = 2.8 Hz, 1H), 6.57 - 6.51 ppm (m, 1H), *tetrazole NH was not observed*.



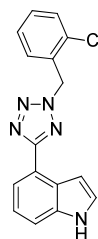
**2.67**

**7-(1H-Tetrazol-5-yl)-1H-indole (2.67)**; quantitative yield (1.63 g); LCMS (acidic conditions) (ES +ve)  $m/z$  186 (M+H)<sup>+</sup>, Rt = 0.78 min; <sup>1</sup>H NMR (400 MHz, DMSO-d<sub>6</sub>):  $\delta$  = 11.22 (br. s, 1H), 7.81 (dd,  $J$  = 7.7, 2.6 Hz, 2H), 7.47 (t,  $J$  = 2.8 Hz, 1H), 7.23 (t,  $J$  = 7.7 Hz, 1H), 6.60 ppm (dd,  $J$  = 3.0, 2.0 Hz, 1H), *tetrazole NH was not observed*.



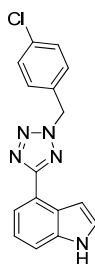
General procedure for the preparation of **2.68-2.75**:

A suspension of the appropriate (1*H*-tetrazol-5-yl)-1*H*-indole analogue (27 mg, 0.15 mmol) (either 4-, 5-, 6- or 7-(1*H*-tetrazol-5-yl)-1*H*-indole), K<sub>2</sub>CO<sub>3</sub> (31 mg, 0.23 mmol) and the appropriate alkylating agent (17 mg, 0.18 mmol) (either 1-(bromomethyl)-2-chlorobenzene or 1-(bromomethyl)-4-chlorobenzene) in DMF (1 mL) were stirred at room temperature for 2 h (at that stage for compound **2.71**, K<sub>2</sub>CO<sub>3</sub> (31 mg, 0.23 mmol) was added and the reaction mixture was stirred for an additional 1 h). The solvent was dried under a stream of nitrogen and the residue obtained was purified by MDAP (acidic conditions) to afford the expected *N*<sup>2</sup>-alkylated tetrazole regioisomers:



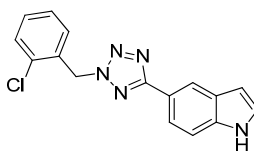
**2.68**

**4-(2-(2-Chlorobenzyl)-2*H*-tetrazol-5-yl)-1*H*-indole (2.68)**; yield 25% (11.1 mg); LCMS (acidic conditions) (ES +ve) *m/z* 310 (M+H)<sup>+</sup>, Rt = 1.15 min; <sup>1</sup>H NMR (600 MHz, DMSO-*d*<sub>6</sub>): δ = 11.43 (br. s, 1H), 7.83 (d, *J* = 7.2 Hz, 1H), 7.62 - 7.53 (m, 3H), 7.53 - 7.48 (m, 1H), 7.48 - 7.41 (m, 2H), 7.24 (t, *J* = 7.7 Hz, 1H), 7.08 - 7.01 (m, 1H), 6.12 ppm (s, 2H).



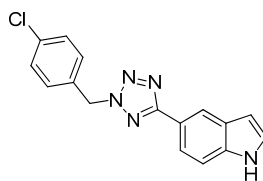
**2.69**

**4-(2-(4-Chlorobenzyl)-2H-tetrazol-5-yl)-1H-indole (2.69)**; yield 47% (21.1 mg); **LCMS** (acidic conditions) (ES +ve)  $m/z$  310 (M+H)<sup>+</sup>, Rt = 1.17 min; **<sup>1</sup>H NMR** (600 MHz, DMSO- $d_6$ ):  $\delta$  = 11.44 (br. s, 1H), 7.84 (d,  $J$  = 7.7 Hz, 1H), 7.58 (d,  $J$  = 7.9 Hz, 1H), 7.54 - 7.46 (m, 5H), 7.24 (t,  $J$  = 7.7 Hz, 1H), 7.11 - 7.06 (m, 1H), 6.05 ppm (s, 2H).



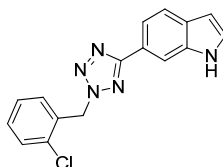
**2.70**

**5-(2-(2-Chlorobenzyl)-2H-tetrazol-5-yl)-1H-indole (2.70)**<sup>148</sup>; yield 40% (18.2 mg); **LCMS** (acidic conditions) (ES +ve)  $m/z$  310 (M+H)<sup>+</sup>, Rt = 1.14 min; **<sup>1</sup>H NMR** (600 MHz, DMSO- $d_6$ ):  $\delta$  = 11.38 (br. s, 1H), 8.26 (s, 1H), 7.77 (d,  $J$  = 8.7 Hz, 1H), 7.56 (d,  $J$  = 7.9 Hz, 1H), 7.54 - 7.49 (m, 2H), 7.49 - 7.41 (m, 3H), 6.58 - 6.54 (m, 1H), 6.06 ppm (s, 2H).



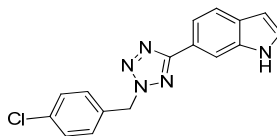
**2.71**

**5-(2-(4-Chlorobenzyl)-2H-tetrazol-5-yl)-1H-indole (2.71);**<sup>148</sup> yield 40% (18 mg);  
**LCMS** (acidic conditions) (ES +ve)  $m/z$  310 (M+H)<sup>+</sup>, Rt = 1.16 min; **<sup>1</sup>H NMR** (600 MHz, DMSO-d<sub>6</sub>):  $\delta$  = 11.38 (br. s, 1H), 8.28 (s, 1H), 7.79 (d,  $J$  = 8.7 Hz, 1H), 7.53 (d,  $J$  = 8.7 Hz, 1H), 7.51 - 7.42 (m, 5H), 6.58- 6.54 (m, 1H), 5.99 ppm (s, 2H).



**2.72**

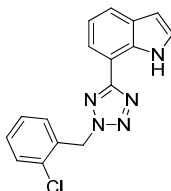
**6-(2-(2-Chlorobenzyl)-2H-tetrazol-5-yl)-1H-indole (2.72);**<sup>148</sup> yield 21% (9.7 mg);  
**LCMS** (acidic conditions) (ES +ve)  $m/z$  310 (M+H)<sup>+</sup>, Rt = 1.18 min; **<sup>1</sup>H NMR** (600 MHz, DMSO-d<sub>6</sub>):  $\delta$  = 11.37 (br. s, 1H), 8.10 (s, 1H), 7.70 - 7.64 (m, 2H), 7.56 (d,  $J$  = 7.9 Hz, 1H), 7.52 (d,  $J$  = 7.2 Hz, 1H), 7.51 - 7.48 (m, 1H), 7.48 - 7.40 (m, 2H), 6.53 - 6.48 (m, 1H), 6.06 ppm (s, 2H).



**2.73**

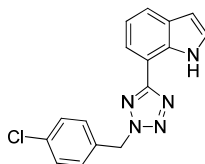
**6-(2-(4-Chlorobenzyl)-2H-tetrazol-5-yl)-1H-indole (2.73);**<sup>148</sup> yield 8% (3.6 mg);  
**LCMS** (acidic conditions) (ES +ve)  $m/z$  310 (M+H)<sup>+</sup>, Rt = 1.20 min; **<sup>1</sup>H NMR** (600

MHz, DMSO-d<sub>6</sub>):  $\delta$  = 11.40 (br. s, 1H), 8.11 (s, 1H), 7.71 - 7.65 (m, 2H), 7.52 - 7.44 (m, 5H), 6.53 - 6.48 (m, 1H), 5.99 ppm (s, 2H).



**2.74**

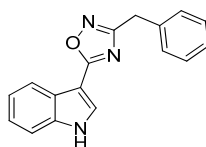
**7-(2-(2-Chlorobenzyl)-2H-tetrazol-5-yl)-1H-indole (2.74)**;<sup>148</sup> yield 59% (26.5 mg); **LCMS** (acidic conditions) (ES +ve) *m/z* compound did not show relevant ionisation, *Rt* = 1.29 min; **<sup>1</sup>H NMR** (600 MHz, DMSO-d<sub>6</sub>):  $\delta$  = 11.03 (br. s, 1H), 7.86 (d, *J* = 7.6 Hz, 1H), 7.76 (d, *J* = 7.6 Hz, 1H), 7.57 (d, *J* = 7.9 Hz, 1H), 7.52 (d, *J* = 7.2 Hz, 1H), 7.49 - 7.40 (m, 3H), 7.18 (t, *J* = 7.6 Hz, 1H), 6.63 - 6.57 (m, 1H), 6.16 ppm (s, 2H); **<sup>13</sup>C NMR** (101 MHz, DMSO-d<sub>6</sub>):  $\delta$  = 163.6, 133.1, 132.1, 131.5, 131.4, 130.8, 129.8, 129.2, 127.8, 127.0, 123.0, 119.7, 119.1, 109.7, 101.8, 54.1 ppm; **HRMS** (ES +ve) calcd for C<sub>16</sub>H<sub>13</sub>ClN<sub>5</sub> (M+H)<sup>+</sup> 310.0848, found 310.0854; **IR**  $\nu$  (cm<sup>-1</sup>) 3427, 1336, 747; **mp** 120.4 °C.



**2.75**

**7-(2-(4-Chlorobenzyl)-2H-tetrazol-5-yl)-1H-indole (2.75)**;<sup>148</sup> yield 47% (21.3 mg); **LCMS** (acidic conditions) (ES +ve) *m/z* compound did not show relevant ionisation, *Rt* = 1.31 min; **<sup>1</sup>H NMR** (600 MHz, DMSO-d<sub>6</sub>):  $\delta$  = 11.05 (br. s, 1H), 7.88 (d, *J* = 7.6 Hz, 1H), 7.76 (d, *J* = 7.6 Hz, 1H), 7.56 - 7.44 (m, 5H), 7.18 (t, *J* = 7.6 Hz, 1H), 6.63 - 6.57 (m, 1H), 6.08 ppm (s, 2H).

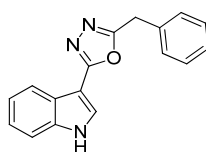




**2.79**

**3-Benzyl-5-(1*H*-indol-3-yl)-1,2,4-oxadiazole (2.79)**; A mixture of ethyl 1*H*-indole-3-carboxylate (150 mg, 0.79 mmol), *N*-hydroxy-2-phenylacetimidamide (143 mg, 0.95 mmol) and NaOMe (64.2 mg, 1.19 mmol) in THF (2 mL) was heated in a microwave at 150 °C for 45 min. The mixture was partitioned between water (5 mL) and DCM (5 mL). The organic layer was dried by filtration through a hydrophobic frit and solvents were removed under a stream of nitrogen. The residue obtained was purified by MDAP (acidic conditions) to afford the title compound as a pale yellow solid; yield 74% (161 mg); **LCMS** (acidic conditions) (ES +ve)  $m/z$  276 (M+H)<sup>+</sup>,  $R_t$  = 1.13 min; **<sup>1</sup>H NMR** (400 MHz, DMSO-*d*<sub>6</sub>):  $\delta$  = 12.21 (br. s, 1H), 8.33 (s, 1H), 8.12 - 8.04 (m, 1H), 7.59 - 7.51 (m, 1H), 7.42 - 7.31 (m, 4H), 7.31 - 7.22 (m, 3H), 4.14 ppm (s, 2H); **<sup>13</sup>C NMR** (101 MHz, DMSO-*d*<sub>6</sub>):  $\delta$  = 172.9, 169.1, 136.4, 136.2, 130.6, 128.9, 128.5, 126.7, 124.3, 122.9, 121.6, 119.9, 112.6, 99.9, 31.5 ppm; **HRMS** (ES +ve) calcd for C<sub>17</sub>H<sub>14</sub>N<sub>3</sub>O (M+H)<sup>+</sup> 276.1131, found 276.1129; **IR**  $\nu$  (cm<sup>-1</sup>) 3194, 1593, 718; **mp** 193.4 °C.

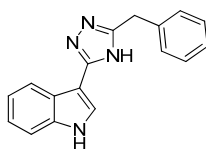
<sup>1</sup>H NMR and mp data consistent with those reported in literature.<sup>307</sup>



**2.81**

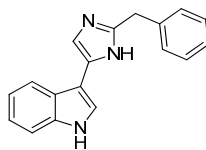
**2-Benzyl-5-(1*H*-indol-3-yl)-1,3,4-oxadiazole (2.81)**; A mixture of 2-phenylacetohydrazide (50 mg, 0.33 mmol), 1*H*-indole-3-carboxylic acid (64 mg, 0.4 mmol) in POCl<sub>3</sub> (1 mL) was heated in a microwave at 140 °C for 30 min. The reaction mixture was carefully poured onto ice and partitioned with CHCl<sub>3</sub> (5 mL). The organic

layer was dried by filtration through a hydrophobic frit and solvents were removed under a stream of nitrogen. The residue obtained was purified by MDAP (acidic conditions) to afford the title compound as a white solid; yield 16% (15 mg); **LCMS** (acidic conditions) (ES +ve)  $m/z$  276 (M+H)<sup>+</sup>,  $R_t$  = 0.98 min; **<sup>1</sup>H NMR** (400 MHz, DMSO- $d_6$ ):  $\delta$  = 11.96 (br. s, 1H), 8.10 (d,  $J$  = 1.8 Hz, 1H), 8.07 - 8.03 (m, 1H), 7.51 (d,  $J$  = 7.3 Hz, 1H), 7.40 - 7.37 (m, 4H), 7.33 - 7.26 (m, 1H), 7.23 (td,  $J$  = 1.4, 7.5 Hz, 2H), 4.34 ppm (s, 2H).



**2.82**

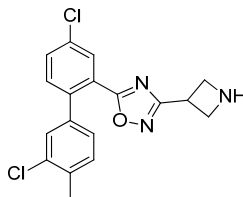
**3-(5-Benzyl-4H-1,2,4-triazol-3-yl)-1H-indole (2.82)**; A mixture of ethyl 1H-indole-3-carbimide (50 mg, 0.27 mmol), 2-phenylacetohydrazide (43.9 mg, 0.29 mmol) and triethylamine (0.11 mL, 0.8 mmol) in DMF (1.5 mL) was heated in a microwave at 120 °C for 20 min and then to 160 °C for 60 min. The mixture was partitioned between water (5 mL) and DCM (5 mL). The aqueous layer was further extracted with DCM (5 mL). The organic extracts were combined, dried by filtration through a hydrophobic frit and solvents were removed under a stream of nitrogen. The residue obtained was purified by MDAP (acidic condition) to afford the title compound; yield 6% (4.5 mg); **LCMS** (basic conditions) (ES +ve)  $m/z$  275 (M+H)<sup>+</sup>,  $R_t$  = 0.90 min; **<sup>1</sup>H NMR** (400 MHz, DMSO- $d_6$ ):  $\delta$  = 13.59 (br. s, 1H), 11.46 (br. s, 1H), 8.20 (d,  $J$  = 7.6 Hz, 1H), 7.95 - 7.76 (m, 1H), 7.47 - 7.39 (m, 1H), 7.37 - 7.27 (m, 4H), 7.23 (d,  $J$  = 6.5 Hz, 1H), 7.19 - 7.05 (m, 2H), 4.07 ppm (s, 2H).



**2.83**

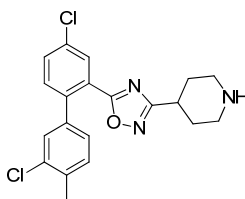
**3-(2-Benzyl-1H-imidazol-5-yl)-1H-indole (2.83)**,<sup>154</sup> LCMS (ES +ve)  $m/z$  274 (M+H)<sup>+</sup>, Rt = 1.01 min; **<sup>1</sup>H NMR** (400 MHz, DMSO- $d_6$ ):  $\delta$  = 11.83 (br. s, 1H), 11.07 (br. s, 1H), 7.86 (d,  $J$  = 7.8 Hz, 1H), 7.56 (d,  $J$  = 2.5 Hz, 1H), 7.39 (d,  $J$  = 7.8 Hz, 1H), 7.34 - 7.27 (m, 4H), 7.25 - 7.18 (m, 2H), 7.15 - 7.08 (m, 1H), 7.08 - 7.02 (m, 1H), 4.02 ppm (s, 2H); **<sup>13</sup>C NMR** (101 MHz, DMSO- $d_6$ ):  $\delta$  = 145.5, 138.8, 136.4, 130.6, 129.5, 128.4, 128.3, 126.1, 124.6, 121.5, 121.2, 119.8, 119.0, 111.5, 96.1, 34.2 ppm; **HRMS** (ES +ve) calcd for C<sub>18</sub>H<sub>16</sub>N<sub>3</sub> (M+H)<sup>+</sup> 274.1339, found 274.1339; **IR**  $\nu$  (cm<sup>-1</sup>) 3403, 2923, 1455, 743; **mp** 187.6 °C.

### 4.3. Experimental preparation of the oxadiazole analogues for the $I_{CRAC}$ programme



2.30

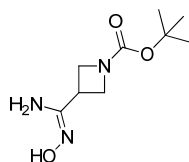
**3-(Azetidin-3-yl)-5-(3',4-dichloro-4'-methyl-[1,1'-biphenyl]-2-yl)-1,2,4-oxadiazole (2.30)**; Compound **2.30** was already available in the GSK internal compound library and the solid sample was analysed by LCMS before testing in the  $I_{CRAC}$  Jurkat assay; **LCMS** (acidic conditions) (ES +ve)  $m/z$  360 (M+H)<sup>+</sup>,  $R_t$  = 0.96 min.



2.91

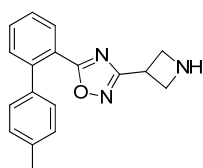
**5-(3',4-Dichloro-4'-methyl-[1,1'-biphenyl]-2-yl)-3-(piperidin-4-yl)-1,2,4-oxadiazole (2.91)**; Compound **2.91** was already available in the GSK internal compound library and the solid material was purified by MDAP (acidic conditions) to afford the title compound as a gum (as TFA salt); **LCMS** (acidic conditions) (ES +ve)  $m/z$  388 (M+H)<sup>+</sup>,  $R_t$  = 1.00 min; **<sup>1</sup>H NMR** (400 MHz, DMSO- $d_6$ ):  $\delta$  = 8.83 (br. s, 1H, *one proton of the piperidine NH<sub>2</sub><sup>+</sup>*), 8.56 (br. s, 1H, *one proton of the piperidine NH<sub>2</sub><sup>+</sup>*), 8.04 (d,  $J$  = 2.3 Hz, 1H), 7.83 (dd,  $J$  = 8.2, 2.3 Hz, 1H), 7.60 (d,  $J$  = 8.2 Hz, 1H), 7.37 (d,  $J$  = 8.2 Hz, 1H), 7.33 - 7.28 (m, 1H), 7.11 (dd,  $J$  = 7.8, 1.8 Hz, 1H), 3.36 - 3.26 (m, 2H), 3.25 - 3.16 (m, 1H), 3.13 - 3.00 (m, 2H), 2.37 (s, 3H), 2.13 - 2.04 (m, 2H), 1.89 - 1.76 ppm (m, 2H); **<sup>13</sup>C NMR** (101 MHz, DMSO- $d_6$ ):  $\delta$  = 174.5, 171.8, 139.1, 137.8, 135.2, 133.1, 133.0, 132.9, 132.3, 131.0, 129.8, 128.7, 127.4, 124.2, 42.2, 30.5, 25.8, 19.2 ppm; **HRMS** (ES

+ve) calcd for C<sub>20</sub>H<sub>20</sub>Cl<sub>2</sub>N<sub>3</sub>O (M+H)<sup>+</sup> 388.0978, found 388.0975; **IR** v (cm<sup>-1</sup>) 2822, 1659, 1131.



**2.116**

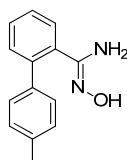
**tert-Butyl 3-(N-hydroxycarbamimidoyl)azetidine-1-carboxylate (2.116)**; A mixture of *tert*-butyl 3-cyanoazetidine-1-carboxylate (2.00 g, 10.98 mmol), hydroxylamine hydrochloride (1.53 g, 21.95 mmol) and NaOMe (1.19 g, 21.95 mmol) in anhydrous methanol (50 mL) was heated at reflux for 20 h. After cooling to room temperature, the mixture was filtered and the filtrate was concentrated *in vacuo*. The resulting white solid was triturated with EtOAc and filtered. The filtrate was concentrated to afford the title compound as a white solid; yield 95% (2.25 g); **LCMS** (acidic conditions) (ES +ve) *m/z* 160 ([M-<sup>t</sup>Bu]+H)<sup>+</sup>, Rt = 0.45 min; **<sup>1</sup>H NMR** (400 MHz, DMSO-d<sub>6</sub>): δ = 9.09 (br. s, 1H), 5.47 (br. s, 2H), 3.98 - 3.77 (m, 2H), 3.42 - 3.24 (m, 2H), 3.22 - 3.12 (m, 1H), 1.38 ppm (s, 9H).



**2.118**

**3-(Azetidin-3-yl)-5-(4'-methyl-[1,1'-biphenyl]-2-yl)-1,2,4-oxadiazole (2.118)**; A mixture of 4'-methyl-[1,1'-biphenyl]-2-carboxylic acid (70.5 mg, 0.332 mmol) and CDI (53.9 mg, 0.332 mmol) in DMF (2 mL) was stirred at room temperature for 30 min. *tert*-

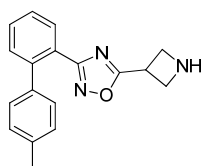
Butyl 3-(*N*-hydroxycarbamimidoyl)azetidine-1-carboxylate (65 mg, 0.302 mmol) and  $K_2CO_3$  (45.9 mg, 0.332 mmol) were added and the resulting mixture was heated in a microwave at 140 °C for 1 h. The mixture was partitioned between water (6 mL), a 2 M HCl aqueous solution (2 mL) and  $CHCl_3$  (6 mL). The organic layer was dried by filtration through a hydrophobic frit and solvents were removed under a stream of nitrogen. The residue obtained was purified by MDAP (acidic conditions) and the resulting material was dissolved in DCM (1.6 mL) and treated with TFA (1 mL, 12.98 mmol) at room temperature for 1 h. The mixture was concentrated under a stream of nitrogen to afford the title compound as a clear oil (as a TFA salt); yield 52% (63 mg); **LCMS** (acidic conditions) (ES +ve)  $m/z$  292 (M+H)<sup>+</sup>,  $R_t$  = 0.82 min; **<sup>1</sup>H NMR** (400 MHz, DMSO- $d_6$ ):  $\delta$  = 9.19 - 8.77 (m, 2H, *azetidine NH\_2*<sup>+</sup>), 8.00 (dd,  $J$  = 7.7, 1.1 Hz, 1H), 7.76 (td,  $J$  = 7.6, 1.3 Hz, 1H), 7.62 (td,  $J$  = 7.7, 1.3 Hz, 1H), 7.55 (dd,  $J$  = 7.8, 0.8 Hz, 1H), 7.21 (d,  $J$  = 8.1 Hz, 2H), 7.13 (d,  $J$  = 8.1 Hz, 2H), 4.44 - 4.21 (m, 3H), 4.21 - 4.07 (m, 2H), 2.34 ppm (s, 3H), **<sup>13</sup>C NMR** (101 MHz, DMSO- $d_6$ ):  $\delta$  = 177.0, 168.9, 142.0, 137.2, 136.6, 132.9, 131.3, 130.8, 129.0, 128.5, 127.9, 122.2, 49.0, 27.4, 20.6 ppm; **HRMS** (ES +ve) calcd for  $C_{18}H_{18}N_3O$  (M+H)<sup>+</sup> 292.1444, found 292.1445; **IR**  $\nu$  ( $cm^{-1}$ ) 2922, 1712, 1128.



**2.120**

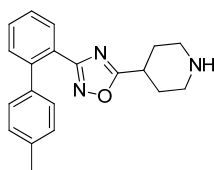
***N*-Hydroxy-4'-methyl-[1,1'-biphenyl]-2-carboximidamide (2.120)**; A mixture of 4'-methyl-[1,1'-biphenyl]-2-carbonitrile (3.00 g, 15.52 mmol), hydroxylamine hydrochloride (2.16 g, 31 mmol) and NaOMe (1.68 g, 31 mmol) in anhydrous methanol (40 mL) was heated at reflux for 50 h. After cooling to room temperature, the mixture was filtered and the filtrate was concentrated *in vacuo*. The resulting white solid was triturated with EtOAc and filtered. The filtrate was concentrated *in vacuo* and the

residue was purified on silica using a 0-100% EtOAc-cyclohexane gradient to afford the title compound as a white solid; yield 17% (580 mg); LCMS (acidic conditions) (ES +ve)  $m/z$  227 (M+H)<sup>+</sup>, Rt = 0.58 min; <sup>1</sup>H NMR (400 MHz, DMSO-d<sub>6</sub>): δ = 9.17 (s, 1H), 7.44 (dd,  $J$  = 7.3, 1.8 Hz, 1H), 7.42 - 7.30 (m, 5H), 7.17 (d,  $J$  = 7.8 Hz, 2H), 5.51 (br. s, 2H), 2.32 ppm (s, 3H).



**2.122**

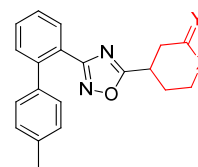
**5-(Azetidin-3-yl)-3-(4'-methyl-[1,1'-biphenyl]-2-yl)-1,2,4-oxadiazole (2.122);** A mixture of 1-(*tert*-butoxycarbonyl)azetidine-3-carboxylic acid (48.9 mg, 0.243 mmol) and CDI (39.4 mg, 0.243 mmol) in DMF (1 mL) was stirred at room temperature for 8 h. *N*-Hydroxy-4'-methyl-[1,1'-biphenyl]-2-carboximidamide (50 mg, 0.221 mmol) and K<sub>2</sub>CO<sub>3</sub> (33.6 mg, 0.243 mmol) were added and the resulting mixture was heated in a microwave at 140 °C for 1 h and at 160 °C for 1 h. The mixture was partitioned between water (5 mL), a 2 M HCl aqueous solution (2 mL) and DCM (5 mL). The organic layer was dried by filtration through a hydrophobic frit and solvents were removed under a stream of nitrogen. The residue obtained was purified by MDAP (acidic conditions) and the resulting material was dissolved in DCM (1 mL) and treated with TFA (0.5 mL, 6.49 mmol) at room temperature for 2 h. The mixture was concentrated under a stream of nitrogen to afford the title compound as a clear oil (as a TFA salt); yield 7% (6 mg); LCMS (acidic conditions) (ES +ve)  $m/z$  292 (M+H)<sup>+</sup>, Rt = 0.82 min; <sup>1</sup>H NMR (400 MHz, DMSO-d<sub>6</sub>): δ = 9.00 (br. s, 2H, *azetidine* NH<sub>2</sub><sup>+</sup>), 7.79 (dd,  $J$  = 7.7, 1.1 Hz, 1H), 7.66 (td,  $J$  = 7.6, 1.5 Hz, 1H), 7.56 (td,  $J$  = 7.6, 1.3 Hz, 1H), 7.48 (dd,  $J$  = 7.6, 1.0 Hz, 1H), 7.16 (d,  $J$  = 8.1 Hz, 2H), 7.11 (d,  $J$  = 8.1 Hz, 2H), 4.48 - 4.37 (m, 1H), 4.37 - 4.29 (m, 2H), 4.21 - 4.12 (m, 2H), 2.32 ppm (s, 3H).



#### 2.124

**3-(4'-Methyl-[1,1'-biphenyl]-2-yl)-5-(piperidin-4-yl)-1,2,4-oxadiazole (2.124);** A mixture of 1-(*tert*-butoxycarbonyl)piperidine-4-carboxylic acid (50.7 mg, 0.221 mmol) and CDI (39.4 mg, 0.243 mmol) in DMF (1 mL) was stirred at room temperature for 8 h. *N*-Hydroxy-4'-methyl-[1,1'-biphenyl]-2-carboximidamide (50 mg, 0.221 mmol) and K<sub>2</sub>CO<sub>3</sub> (33.6 mg, 0.243 mmol) were added and the resulting mixture was heated in a microwave at 140 °C for 1 h. The mixture was partitioned between water (5 mL), a 2 M HCl aqueous solution (2 mL) and DCM (5 mL). The organic layer was dried by filtration through a hydrophobic frit and solvents were removed under a stream of nitrogen. The residue obtained was purified by MDAP (acidic conditions) and the resulting material was dissolved in DCM (1 mL) and treated with TFA (0.5 mL, 6.49 mmol) at room temperature for 2 h. The mixture was concentrated under a stream of nitrogen to afford the title compound as a clear oil (as a TFA salt); yield 89% (85 mg); **LCMS** (acidic conditions) (ES +ve) *m/z* 320 (M+H)<sup>+</sup>, Rt = 0.82 min; **<sup>1</sup>H NMR** (400 MHz, DMSO-*d*<sub>6</sub>): δ = 8.65 (br. s, 1H, *one proton of the piperidine NH<sub>2</sub><sup>+</sup>*), 8.40 (br. s, 1H, *one proton of the piperidine NH<sub>2</sub><sup>+</sup>*), 7.74 (dd, *J* = 7.7, 1.1 Hz, 1H), 7.65 (td, *J* = 7.6, 1.3 Hz, 1H), 7.53 (td, *J* = 7.6, 1.3 Hz, 1H), 7.48 (dd, *J* = 7.7, 0.9 Hz, 1H), 7.14 (d, *J* = 8.2 Hz, 2H), 7.08 (d, *J* = 8.2 Hz, 2H), 3.48 - 3.34 (m, 1H), 3.32 - 3.18 (m, 2H), 3.11 - 2.92 (m, 2H), 2.32 (s, 3H), 2.11 (dd, *J* = 14.1, 3.5 Hz, 2H), 1.90 - 1.73 ppm (m, 2H); **<sup>13</sup>C NMR** (101 MHz, DMSO-*d*<sub>6</sub>): δ = 179.2, 168.4, 141.6, 137.1, 136.5, 130.9, 130.6, 130.2, 128.6, 128.6, 127.4, 124.9, 41.9, 30.5, 25.5, 20.6 ppm; **HRMS** (ES +ve) calcd for C<sub>20</sub>H<sub>22</sub>N<sub>3</sub>O (M+H)<sup>+</sup> 320.1757, found 320.1755; **IR** ν (cm<sup>-1</sup>) 2825, 1665, 1128.

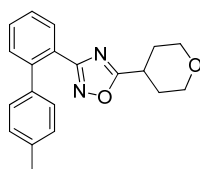




**2.128** : Y=H<sub>2</sub>, X=O  
**2.129** : Y=O, X=NH  
**2.130** : Y=O, X=NMe

*General procedure for the preparation of 2.128-2.130:*

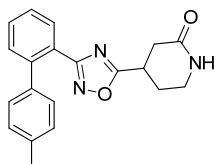
A mixture of the appropriate carboxylic acid derivative (0.243 mmol) and CDI (39.4 mg, 0.243 mmol) in DMF (1 mL) was stirred at room temperature for 90 min. *N*-Hydroxy-4'-methyl-[1,1'-biphenyl]-2-carboximidamide (50 mg, 0.221 mmol) and K<sub>2</sub>CO<sub>3</sub> (33.6 mg, 0.243 mmol) were added and the resulting mixture was heated in a microwave at 140 °C for 1 h. The mixture was partitioned between water (5 mL), a 2 M HCl aqueous solution (2 mL) and DCM (5 mL). The organic layer was dried by filtration through a hydrophobic frit and solvents were removed under a stream of nitrogen. The residue obtained was purified by MDAP (acidic conditions) to afford the expected 1,2,4-oxadiazoles:



**2.128**

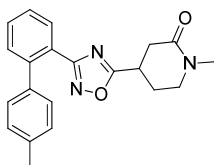
**3-(4'-Methyl-[1,1'-biphenyl]-2-yl)-5-(tetrahydro-2*H*-pyran-4-yl)-1,2,4-oxadiazole (2.128)**; from tetrahydro-2*H*-pyran-4-carboxylic acid (31.6 mg, 0.243 mmol); pale yellow oil; yield 86% (61 mg); LCMS (acidic conditions) (ES +ve) *m/z* 321 (M+H)<sup>+</sup>, Rt = 1.25 min; <sup>1</sup>H NMR (400 MHz, DMSO-*d*<sub>6</sub>): δ = 7.74 (dd, *J* = 7.7, 1.1 Hz, 1H), 7.63 (td, *J* = 7.6, 1.3 Hz, 1H), 7.52 (td, *J* = 7.6, 1.3 Hz, 1H), 7.47 (dd, *J* = 7.7, 1.3 Hz, 1H), 7.14 (d, *J* = 8.1 Hz, 2H), 7.06 (d, *J* = 8.1 Hz, 2H), 3.83 - 3.70 (m, 2H), 3.50 - 3.38 (m, 2H), 3.35 - 3.22 (m, 1H), 2.31 (s, 3H), 1.92 - 1.83 (m, 2H), 1.73 - 1.59 ppm (m, 2H); <sup>13</sup>C

**NMR** (101 MHz, DMSO- $d_6$ ):  $\delta$  = 180.7, 168.4, 141.6, 137.2, 136.4, 130.8, 130.5, 130.1, 128.6, 128.5, 127.4, 125.3, 65.5, 32.0, 29.2, 20.6 ppm; **HRMS** (ES +ve) calcd for  $C_{20}H_{21}N_2O_2$  (M+H)<sup>+</sup> 321.1598, found 321.1601; **IR**  $\nu$  ( $cm^{-1}$ ) 2955, 1565, 1347.



**2.129**

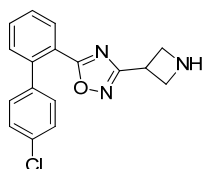
**4-(3-(4'-Methyl-[1,1'-biphenyl]-2-yl)-1,2,4-oxadiazol-5-yl)piperidin-2-one (2.129)**; from 2-oxopiperidine-4-carboxylic acid (34.8 mg, 0.243 mmol); white solid; yield 80% (59 mg); **LCMS** (acidic conditions) (ES +ve)  $m/z$  334 (M+H)<sup>+</sup>,  $R_t$  = 1.00 min; **<sup>1</sup>H NMR** (400 MHz, DMSO- $d_6$ ):  $\delta$  = 7.74 (dd,  $J$  = 7.7, 1.1 Hz, 1H), 7.64 (td,  $J$  = 7.6, 1.3 Hz, 1H), 7.57 (br. s, 1H), 7.53 (td,  $J$  = 7.6, 1.3 Hz, 1H), 7.47 (dd,  $J$  = 7.6, 1.0 Hz, 1H), 7.13 (d,  $J$  = 8.1 Hz, 2H), 7.07 (d,  $J$  = 8.1 Hz, 2H), 3.65 - 3.51 (m, 1H), 3.25 - 3.15 (m, 1H), 3.10 - 3.00 (m, 1H), 2.57 - 2.53 (m, 1H), 2.42 - 2.33 (m, 1H), 2.31 (s, 3H), 2.15 - 2.04 (m, 1H), 1.89 - 1.75 ppm (m, 1H).



**2.130**

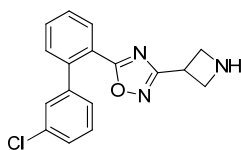
**1-Methyl-4-(3-(4'-methyl-[1,1'-biphenyl]-2-yl)-1,2,4-oxadiazol-5-yl)piperidin-2-one (2.130)**; from 1-methyl-2-oxopiperidine-4-carboxylic acid (38.2 mg, 0.243 mmol); pale yellow oil; yield 78% (60 mg); **LCMS** (acidic conditions) (ES +ve)  $m/z$  348 (M+H)<sup>+</sup>,  $R_t$  = 1.06 min; **<sup>1</sup>H NMR** (400 MHz, DMSO- $d_6$ ):  $\delta$  = 7.72 (dd,  $J$  = 7.7, 1.1 Hz, 1H), 7.64 (td,  $J$  = 7.6, 1.5 Hz, 1H), 7.52 (td,  $J$  = 7.6, 1.3 Hz, 1H), 7.47 (dd,  $J$  = 7.7, 0.9 Hz, 1H),

7.14 (d,  $J = 8.1$  Hz, 2H), 7.07 (d,  $J = 8.1$  Hz, 2H), 3.69 - 3.54 (m, 1H), 3.16 - 3.03 (m, 1H), 2.77 (s, 3H), 2.64 - 2.54 (m, 1H), 2.52 - 2.48 (m, 1H), 2.48 - 2.38 (m, 1H), 2.31 (s, 3H), 2.16 (m, 1H), 2.00 - 1.84 ppm (m, 1H).



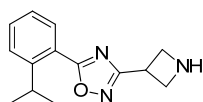
**2.132**

**3-(Azetidin-3-yl)-5-(4'-chloro-[1,1'-biphenyl]-2-yl)-1,2,4-oxadiazole (2.132);** A mixture of *tert*-butyl 3-(*N*-hydroxycarbamimidoyl)azetidine-1-carboxylate (43 mg, 0.2 mmol), 4'-chloro-[1,1'-biphenyl]-2-carboxylic acid (55.8 mg, 0.24 mmol) and PyBOP (125 mg, 0.24 mmol) were dissolved in DMF (0.4 mL). DIPEA (105  $\mu$ L, 0.6 mmol) was added and the resulting mixture was stirred at room temperature for 18 h. Pyridine (81  $\mu$ L, 1 mmol) was added and the mixture was heated in a microwave at 110  $^{\circ}$ C for 60 min. The reaction mixture was purified by MDAP (basic conditions). The material obtained was dissolved in DCM (0.2 mL) and TFA (0.2 mL, 2.6 mmol) and stirred at room temperature for 2 h. Solvents were removed under a stream of nitrogen to afford the title product (as TFA salt); yield 18% (15.5 mg); **LCMS** (acidic conditions) (ES +ve)  $m/z$  312 (M+H) $^{+}$ ,  $R_t = 0.83$  min;  **$^1$ H NMR** (600 MHz, DMSO- $d_6$ ):  $\delta = 9.23$  (br. s, 1H, *one proton of the azetidine NH $_2^+$* ), 9.07 (br. s, 1H, *one proton of the azetidine NH $_2^+$* ), 8.05 (dd,  $J = 7.7, 0.9$  Hz, 1H), 7.78 (td,  $J = 7.6, 1.1$  Hz, 1H), 7.67 (td,  $J = 7.6, 0.9$  Hz, 1H), 7.57 (d,  $J = 7.2$  Hz, 1H), 7.46 (d,  $J = 8.3$  Hz, 2H), 7.29 (d,  $J = 8.3$  Hz, 2H), 4.37 - 4.22 (m, 3H), 4.18 - 4.08 ppm (m, 2H).



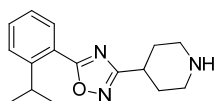
2.134

**3-(Azetidin-3-yl)-5-(3'-chloro-[1,1'-biphenyl]-2-yl)-1,2,4-oxadiazole (2.134);** A mixture of 3'-chloro-[1,1'-biphenyl]-2-carboxylic acid (77 mg, 0.332 mmol) and CDI (53.9 mg, 0.332 mmol) in DMF (2 mL) was stirred at room temperature for 30 min. *tert*-Butyl 3-(*N*-hydroxycarbamimidoyl)azetidine-1-carboxylate (65 mg, 0.302 mmol) and K<sub>2</sub>CO<sub>3</sub> (45.9 mg, 0.332 mmol) were added and the resulting mixture was heated in a microwave at 140 °C for 1 h. The mixture was partitioned between water (6 mL), a 2 M HCl aqueous solution (2 mL) and CHCl<sub>3</sub> (6 mL). The organic layer was dried by filtration through a hydrophobic frit and solvents were removed under a stream of nitrogen. The residue obtained was purified by MDAP (acidic conditions) and the resulting material was dissolved in DCM (1.6 mL) and treated with TFA (1 mL, 12.98 mmol) at room temperature for 1 h. The mixture was concentrated under a stream of nitrogen to afford the title compound as a clear oil (as a TFA salt); yield 34% (44 mg); **LCMS** (acidic conditions) (ES +ve) *m/z* 312 (M+H)<sup>+</sup>, Rt = 0.81 min; **<sup>1</sup>H NMR** (400 MHz, DMSO-d<sub>6</sub>): δ = 9.12 (br. s, 1H, *one proton of the azetidine NH<sub>2</sub><sup>+</sup>*), 8.92 (br. s, 1H, *one proton of the azetidine NH<sub>2</sub><sup>+</sup>*), 8.08 (dd, *J* = 7.8, 1.0 Hz, 1H), 7.79 (td, *J* = 7.6, 1.3 Hz, 1H), 7.69 (td, *J* = 7.6, 1.0 Hz, 1H), 7.60 (d, *J* = 7.8 Hz, 1H), 7.50 - 7.45 (m, 1H), 7.43 (d, *J* = 7.6 Hz, 1H), 7.41 - 7.37 (m, 1H), 7.22 - 7.17 (m, 1H), 4.41 - 4.21 (m, 4H), 4.20 - 4.06 ppm (m, 1H).



**2.137**

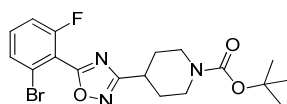
**3-(Azetidin-3-yl)-5-(2-isopropylphenyl)-1,2,4-oxadiazole (2.137)**; A mixture of *tert*-butyl 3-(*N*-hydroxycarbamimidoyl)azetidine-1-carboxylate (43 mg, 0.2 mmol), 2-isopropylbenzoic acid (39.4 mg, 0.24 mmol) and PyBOP (125 mg, 0.24 mmol) were dissolved in DMF (0.4 mL). DIPEA (105  $\mu$ L, 0.6 mmol) was added and the resulting mixture was stirred at room temperature for 18 h. Pyridine (81  $\mu$ L, 1 mmol) was added and the mixture was heated in a microwave at 110  $^{\circ}$ C for 30 min. The reaction mixture was purified by MDAP (basic conditions) and the resulting material was dissolved in DCM (0.2 mL) and TFA (0.2 mL, 2.6 mmol) and stirred at room temperature for 2 h. Solvents were removed under a stream of nitrogen to afford the title product as a gum (as TFA salt); yield 12% (8.4 mg); **LCMS** (acidic conditions) (ES +ve) *m/z* 244 ( $M+H$ )<sup>+</sup>, *Rt* = 0.74 min; **<sup>1</sup>H NMR** (600 MHz, DMSO-*d*<sub>6</sub>):  $\delta$  = 9.28 (br. s, 2H, *azetidine NH*<sub>2</sub><sup>+</sup>), 7.89 (d, *J* = 7.9 Hz, 1H), 7.72 - 7.59 (m, 2H), 7.43 (t, *J* = 6.8 Hz, 1H), 4.47 - 4.32 (m, 3H), 4.32 - 4.22 (m, 2H), 3.74 (spt, *J* = 6.8 Hz, 1H), 1.24 ppm (d, *J* = 6.8 Hz, 6H).



**2.138**

**5-(2-Isopropylphenyl)-3-(piperidin-4-yl)-1,2,4-oxadiazole (2.138)**; A mixture of *tert*-butyl 4-(*N*-hydroxycarbamimidoyl)piperidine-1-carboxylate (49 mg, 0.2 mmol), 2-isopropylbenzoic acid (39.4 mg, 0.24 mmol) and PyBOP (125 mg, 0.24 mmol) were dissolved in DMF (0.4 mL). DIPEA (105  $\mu$ L, 0.6 mmol) was added and the resulting mixture was stirred at room temperature for 18 h. Pyridine (81  $\mu$ L, 1 mmol) was added and the mixture was heated in a microwave at 110  $^{\circ}$ C for 30 min. The reaction mixture

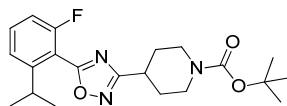
was purified by MDAP (basic conditions) and the resulting material was dissolved in DCM (0.2 mL) and TFA (0.2 mL, 2.6 mmol) and stirred at room temperature for 2 h. Solvents were removed under a stream of nitrogen to afford the title product as a gum (as TFA salt); yield 18% (14.2 mg); **LCMS** (acidic conditions) (ES +ve)  $m/z$  272 (M+H)<sup>+</sup>, Rt = 0.79 min; **<sup>1</sup>H NMR** (600 MHz, DMSO-d<sub>6</sub>): δ = 8.85 (br. s, 1H, *one proton of the piperidine NH<sub>2</sub><sup>+</sup>*), 8.61 (br. s, 1H, *one proton of the piperidine NH<sub>2</sub><sup>+</sup>*), 7.86 (d,  $J = 6.8$  Hz, 1H), 7.67 - 7.59 (m, 2H), 7.41 (t,  $J = 6.8$  Hz, 1H), 3.74 (spt,  $J = 6.8$  Hz, 1H), 3.52 - 3.33 (m, 2H), 3.33 - 3.26 (m, 1H), 3.14 - 3.04 (m, 1H), 2.52 - 2.48 (m, 1H), 2.24 - 2.15 (m, 2H), 1.99 - 1.88 (m, 2H), 1.23 ppm (d,  $J = 6.8$  Hz, 6H); **<sup>13</sup>C NMR** (101 MHz, DMSO-d<sub>6</sub>): δ = 175.6, 172.0, 148.8, 132.8, 130.0, 126.8, 126.4, 121.9, 48.5, 30.7, 29.2, 26.0, 23.5 ppm; **HRMS** (ES +ve) calcd for C<sub>16</sub>H<sub>22</sub>N<sub>3</sub>O (M+H)<sup>+</sup> 272.1757, found 272.1756; **IR** ν (cm<sup>-1</sup>) 2963, 1674, 1126.



**2.144**

**tert-Butyl 4-(5-(2-bromo-6-fluorophenyl)-1,2,4-oxadiazol-3-yl)piperidine-1-carboxylate (2.144)**; A mixture of 2-bromo-6-fluorobenzoic acid (495 mg, 2.26 mmol), HATU (1.52 g, 2.47 mmol) and DIPEA (895 μL, 5.14 mmol) in DMF (10 mL) was stirred at room temperature for 10 min. *tert*-Butyl 4-(*N*-hydroxycarbamimidoyl)piperidine-1-carboxylate (500 mg, 2.06 mmol) was added and the resulting mixture was stirred for 2 h. The reaction mixture was partitioned between water (25 mL) and DCM (25 mL). The aqueous phase was further extracted with DCM (25 mL). The organic extracts were combined, dried by filtration through a hydrophobic frit and the solvents were evaporated *in vacuo*. The resulting residue was dissolved in DMF (10 mL) and K<sub>2</sub>CO<sub>3</sub> (284 mg, 2.06 mmol) was added. The reaction mixture was heated in a microwave at 140 °C for 1 h. The mixture was partitioned between water (25

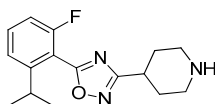
mL), and DCM (25 mL). The aqueous phase was further extracted with DCM (25 mL). The organic extracts were combined, washed with water (3 x 25 mL) and concentrated *in vacuo*. The resulting residue was purified on silica using a 0-50% EtOAc-cyclohexane gradient to afford the title compound as a colourless gum; yield 20% (178 mg); **LCMS** (acidic conditions) (ES +ve) *m/z* 370 and 372 ( $[M-tBu]+H$ )<sup>+</sup>, *Rt* = 1.34 min; **<sup>1</sup>H NMR** (400 MHz, DMSO-*d*<sub>6</sub>):  $\delta$  = 7.77 (d, *J* = 8.1 Hz, 1H), 7.70 (td, *J* = 8.2, 5.9 Hz, 1H), 7.57 (td, *J* = 9.0, 1.1 Hz, 1H), 4.02 - 3.89 (m, 2H), 3.25 - 3.14 (m, 1H), 3.05 - 2.91 (m, 2H), 2.08 - 1.96 (m, 2H), 1.68 - 1.55 (m, 2H), 1.41 ppm (s, 9H).



**2.145**

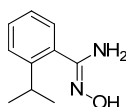
***tert*-Butyl 4-(5-(2-fluoro-6-isopropylphenyl)-1,2,4-oxadiazol-3-yl)piperidine-1-carboxylate (2.145)**; A flask charged with *tert*-butyl 4-(5-(2-bromo-6-fluorophenyl)-1,2,4-oxadiazol-3-yl)piperidine-1-carboxylate (62 mg, 0.145 mmol), dicyclohexyl(2',6'-dimethoxy-[1,1'-biphenyl]-2-yl)phosphine (4 mg, 9.74  $\mu$ mol) and Pd(OAc)<sub>2</sub> (4 mg, 0.018 mmol) was placed under vacuum and backfilled with nitrogen. THF (262  $\mu$ L) was added and the resulting mixture was stirred at room temperature for 5 min. A 0.5 M solution of isopropylzinc bromide in THF (320  $\mu$ L, 0.16 mmol) was added dropwise and the resulting mixture was stirred at room temperature for 16 h. A dilute solution of HCl was added (1 mL) and the mixture was partitioned between water (5 mL) and DCM (5 mL). The aqueous layer was further extracted with DCM (5 mL). The organic extracts were combined and solvents were removed under a stream of nitrogen. The residue obtained was purified by MDAP (acidic conditions) to afford the title product as a white solid; yield 14% (8 mg) (NB: the corresponding *n*-propyl regioisomer was obtained as a yellow gum in 19% yield, (11 mg)); **LCMS** (acidic conditions) (ES +ve) *m/z* 334 ( $[M-tBu]+H$ )<sup>+</sup>, *Rt* = 1.44 min; **<sup>1</sup>H NMR** (400 MHz, DMSO-*d*<sub>6</sub>):  $\delta$  = 7.74 - 7.65 (m, 1H), 7.48 - 7.41 (m, 1H), 7.35 - 7.27 (m, 1H), 4.04 - 3.91 (m, 2H), 3.23 - 3.12 (m, 1H), 3.05 - 2.88

(m, 3H), 2.08 - 1.98 (m, 2H), 1.68 - 1.55 (m, 2H), 1.42 (s, 9H), 1.18 ppm (d,  $J = 6.8$  Hz, 6H).



**2.141**

**5-(2-Fluoro-6-isopropylphenyl)-3-(piperidin-4-yl)-1,2,4-oxadiazole (2.141);** A solution of *tert*-butyl 4-(5-(2-fluoro-6-isopropylphenyl)-1,2,4-oxadiazol-3-yl)piperidine-1-carboxylate (8 mg, 0.021 mmol) in DCM (0.5 mL) was treated at room temperature with TFA (0.5 mL, 6.49 mmol) for 2 h. The solvent was evaporated under a stream of nitrogen to afford the titled product (as TFA salt); 94% (7.8 mg); **LCMS** (acidic conditions) (ES +ve)  $m/z$  290 (M+H)<sup>+</sup>, Rt = 0.80 min; **<sup>1</sup>H NMR** (400 MHz, DMSO- $d_6$ ):  $\delta = 8.60$  (br. s, 1H, *one proton of the piperidine NH<sub>2</sub><sup>+</sup>*), 8.36 (br. s, 1H, *one proton of the piperidine NH<sub>2</sub><sup>+</sup>*), 7.76 - 7.66 (m, 1H), 7.49 - 7.43 (m, 1H), 7.36 - 7.27 ppm (m, 1H), 3.46 - 3.21 (m, 3H), 3.17 - 3.02 (m, 2H), 2.95 (spt,  $J = 6.8$  Hz, 1H), 2.29 - 2.15 (m, 2H), 2.02 - 1.82 (m, 2H), 1.18 ppm (d,  $J = 6.8$  Hz, 6H).

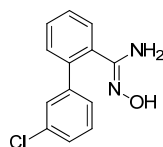


**2.170**

**N-Hydroxy-2-isopropylbenzimidamide (2.170);** A mixture of 2-isopropylbenzimidamide (2.84 g, 19.56 mmol), hydroxylamine hydrochloride (2.72 g, 39.1 mmol) and NaOMe (2.11 g, 39.1 mmol) in anhydrous methanol (25 mL) was heated in a microwave at 150 °C for 3 h. Reaction mixture was diluted with MeOH (75 mL) and the reaction mixture was heated at reflux for 18 h. NaOMe (2.11 g, 39.1 mmol) and hydroxylamine hydrochloride (2.72 g, 39.1 mmol) were added and the reaction mixture was stirred at

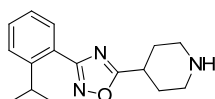


reflux for 120 h. The reaction mixture was partitioned between water (50 mL) and EtOAc (50 mL) and the aqueous layer was further extracted with EtOAc (50 mL). The organic extracts were combined and concentrated *in vacuo*. The resulting residue was purified on silica using a 0-50% EtOAc-cyclohexane gradient to afford the title product as a brown solid; yield 21% (730 mg); LCMS (acidic conditions) (ES +ve)  $m/z$  179 (M+H)<sup>+</sup>, Rt = 0.44 min; <sup>1</sup>H NMR (400 MHz, DMSO-d<sub>6</sub>):  $\delta$  = 9.24 (br. s, 1H), 7.38 - 7.31 (m, 2H), 7.23 - 7.15 (m, 2H), 5.70 (br. s, 2H), 3.31 (spt,  $J$  = 6.8 Hz, 1H), 1.18 ppm (d,  $J$  = 6.8 Hz, 6H).



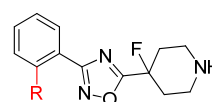
2.171

**3'-Chloro-N-hydroxy-[1,1'-biphenyl]-2-carboximidamide (2.171)**; A mixture of 3'-chloro-[1,1'-biphenyl]-2-carbonitrile (1.12 g, 5.24 mmol), hydroxylamine hydrochloride (0.73 g, 10.48 mmol) and NaOMe (0.57 g, 10.48 mmol) in anhydrous methanol (30 mL) was heated at reflux for 66 h. The reaction mixture was concentrated *in vacuo* and the residue was partitioned between water (50 mL) and DCM (50 mL) and the aqueous layer was further extracted with DCM (50 mL). The organic extracts were combined and concentrated *in vacuo*. The resulting residue was purified on silica using a 0-100% EtOAc-cyclohexane gradient to afford the title product as a colourless gum; yield 42% (543 mg); LCMS (acidic conditions) (ES +ve)  $m/z$  247 (M+H)<sup>+</sup>, Rt = 0.60 min; <sup>1</sup>H NMR (400 MHz, DMSO-d<sub>6</sub>):  $\delta$  = 9.23 (br. s, 1H), 7.52 - 7.33 (m, 8H), 5.65 ppm (br. s, 2H).



**2.152**

**3-(2-Isopropylphenyl)-5-(piperidin-4-yl)-1,2,4-oxadiazole (2.152)**; A mixture of 1-(*tert*-butoxycarbonyl)piperidine-4-carboxylic acid (100 mg, 0.436 mmol) and CDI (78 mg, 0.48 mmol) in DMF (2 mL) was stirred at room temperature for 30 min. *N*-Hydroxy-2-isopropylbenzimidamide (78 mg, 0.436 mmol) and K<sub>2</sub>CO<sub>3</sub> (66.3 mg, 0.48 mmol) were added and the resulting mixture was heated in a microwave at 140 °C for 1 h. The mixture was partitioned between water (10 mL), a 2 M HCl aqueous solution (2 mL) and CHCl<sub>3</sub> (10 mL). The organic layer was dried by filtration through a hydrophobic frit and solvents were removed under a stream of nitrogen. The resulting oil was dissolved in DCM (1.6 mL) and treated with TFA (1 mL) at room temperature for 1.5 h. The mixture was concentrated and purified by MDAP (basic conditions) to afford the title compound as a yellow oil (as the free base); yield 39% (46 mg); **LCMS** (basic conditions) (ES +ve) *m/z* 272 (M+H)<sup>+</sup>, Rt = 1.14 min; **<sup>1</sup>H NMR** (400 MHz, DMSO-*d*<sub>6</sub>): δ = 7.71 (d, *J* = 7.8 Hz, 1H), 7.58 - 7.50 (m, 2H), 7.39 - 7.30 (m, 1H), 3.56 (spt, *J* = 6.8 Hz, 1H), 3.29 - 3.16 (m, 1H), 3.07 - 2.96 (m, 2H), 2.73 - 2.60 (m, 2H), 2.06 - 1.96 (m, 2H), 1.79 - 1.64 (m, 2H), 1.21 ppm (d, *J* = 6.8 Hz, 6H), *piperidine NH was not observed*.

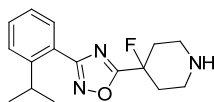


**2.153** : R=*i*Pr  
**2.173** : R=3-Cl-phenyl

*General procedure for the preparation of 2.153 and 2.173:*

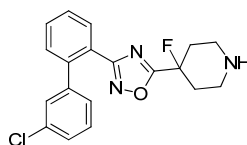
A mixture of the appropriate amidoxime derivative (0.365 mmol), 1-*tert*-butyl 4-ethyl 4-fluoropiperidine-1,4-dicarboxylate (121 mg, 0.438 mmol) and NaOMe (29.6 mg, 0.547 mmol) in THF (1 mL) was heated in a microwave at 150 °C for 45 min. 1-*tert*-butyl 4-ethyl 4-fluoropiperidine-1,4-dicarboxylate (121 mg, 0.438 mmol) and NaOMe (29.6 mg,

0.547 mmol) were added and the reaction mixture was heated in a microwave at 150 °C for 45 min. The mixture was partitioned between water (5 mL) and DCM (5 mL) and the aqueous layer was further extracted with DCM (5 mL). The organic extracts were combined, dried by filtration through a hydrophobic frit and solvents were removed under a stream of nitrogen. The residue obtained was purified by MDAP (acidic conditions) the resulting intermediate was dissolved in DCM (1 mL) and treated with TFA (0.5 mL, 6.49 mmol) at room temperature for 1 h. The mixture was concentrated under a stream of nitrogen to afford the expected oxadiazoles (as TFA salt):



**2.153**

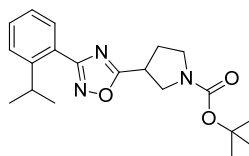
**5-(4-Fluoropiperidin-4-yl)-3-(2-isopropylphenyl)-1,2,4-oxadiazole (2.153)**; from *N*-hydroxy-2-isopropylbenzimidamide (65 mg, 0.365 mmol); white solid; yield 36% (52.4 mg); **LCMS** (basic conditions) (ES +ve)  $m/z$  290 (M+H)<sup>+</sup>,  $R_t$  = 1.20 min; **<sup>1</sup>H NMR** (400 MHz, DMSO- $d_6$ ):  $\delta$  = 8.91 (br. s, 1H, *one proton of the piperidine NH<sub>2</sub><sup>+</sup>*), 8.71 (br. s, 1H, *one proton of the piperidine NH<sub>2</sub><sup>+</sup>*), 7.75 (d,  $J$  = 7.6 Hz, 1H), 7.59 (d,  $J$  = 3.5 Hz, 2H), 7.43 - 7.35 (m, 1H), 3.56 (spt,  $J$  = 6.8 Hz, 1H), 3.49 - 3.38 (m, 2H), 3.34 - 3.20 (m, 2H), 2.62 - 2.52 (m, 2H), 2.50 - 2.38 (m, 2H), 1.23 ppm (d,  $J$  = 6.8 Hz, 6H); **<sup>13</sup>C NMR** (101 MHz, DMSO- $d_6$ ):  $\delta$  = 175.6 (d,  $J$  = 25.2 Hz), 168.3, 148.2, 131.7, 130.1, 126.4, 126.2, 124.0, 87.9 (d,  $J$  = 179.4 Hz), 48.6, 30.0 (d,  $J$  = 23.5 Hz), 29.5, 23.7 ppm; **HRMS** (ES +ve) calcd for C<sub>16</sub>H<sub>21</sub>FN<sub>3</sub>O (M+H)<sup>+</sup> 290.1663, found 290.1663; **IR**  $\nu$  (cm<sup>-1</sup>) 2961, 1671, 1142; **mp** 184.9 - 185.7 °C.



2.173

**3-(3'-Chloro-[1,1'-biphenyl]-2-yl)-5-(4-fluoropiperidin-4-yl)-1,2,4-oxadiazole**

(2.173); from 3'-chloro-*N*-hydroxy-[1,1'-biphenyl]-2-carboximidamide (90 mg, 0.365 mmol); white solid; yield 17% (29.6 mg); LCMS (basic conditions) (ES +ve)  $m/z$  358 (M+H)<sup>+</sup>, Rt = 1.22 min; <sup>1</sup>H NMR (400 MHz, DMSO-*d*<sub>6</sub>): δ = 8.83 (br. s, 1H, *one proton of the piperidine NH<sub>2</sub><sup>+</sup>*), 8.63 (br. s, 1H, *one proton of the piperidine NH<sub>2</sub><sup>+</sup>*), 7.88 (dd, *J* = 7.7, 1.1 Hz, 1H), 7.72 (td, *J* = 7.6, 1.3 Hz, 1H), 7.63 (td, *J* = 7.6, 1.3 Hz, 1H), 7.56 (dd, *J* = 7.6, 1.0 Hz, 1H), 7.44 - 7.35 (m, 2H), 7.29 (s, 1H), 7.16 (d, *J* = 7.3 Hz, 1H), 3.37 - 3.26 (m, 2H), 3.25 - 3.13 (m, 2H), 2.45 - 2.18 (m, 4H).

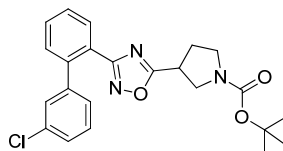


2.175

**tert-Butyl 3-(3-(2-isopropylphenyl)-1,2,4-oxadiazol-5-yl)pyrrolidine-1-carboxylate**

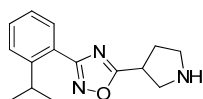
(2.175); A mixture of 1-(*tert*-butoxycarbonyl)pyrrolidine-3-carboxylic acid (580 mg, 2.69 mmol) and CDI (437 mg, 2.69 mmol) in DMF (2 mL) was stirred at room temperature for 30 min. *N*-Hydroxy-2-isopropylbenzimidamide (400 mg, 2.244 mmol) and K<sub>2</sub>CO<sub>3</sub> (372 mg, 2.69 mmol) were added and the resulting mixture was heated in a microwave at 140 °C for 1 h. The mixture was partitioned between water (20 mL) and DCM (20 mL) and the aqueous layer was further extracted with DCM (20 mL). The organic extracts were combined, dried by filtration through a hydrophobic frit and concentrated *in vacuo*. The resulting residue was purified on silica using a 0-25% EtOAc-cyclohexane gradient to afford the title product as a colourless oil; yield 92% (741 mg); LCMS (acidic conditions) (ES +ve)  $m/z$  302 ([M-<sup>*t*</sup>Bu]+H)<sup>+</sup>, Rt = 1.40 min; <sup>1</sup>H

**NMR** (400 MHz, DMSO- $d_6$ ):  $\delta$  = 7.70 (d,  $J$  = 7.6 Hz, 1H), 7.57 - 7.52 (m, 2H), 7.39 - 7.30 (m, 1H), 3.97 - 3.85 (m, 1H), 3.80 - 3.69 (m, 1H), 3.66 - 3.59 (m, 1H), 3.54 (spt,  $J$  = 6.8 Hz, 1H), 3.48 - 3.33 (m, 2H), 2.44 - 2.30 (m, 1H), 2.28 - 2.15 (m, 1H), 1.41 (s, 9H), 1.20 ppm (d,  $J$  = 6.8 Hz, 6H).



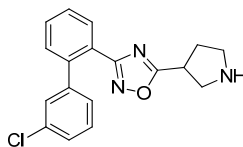
**2.176**

**tert-Butyl 3-(3-(3'-chloro-[1,1'-biphenyl]-2-yl)-1,2,4-oxadiazol-5-yl)pyrrolidine-1-carboxylate (2.176)**; A mixture of 1-(*tert*-butoxycarbonyl)pyrrolidine-3-carboxylic acid (371 mg, 1.726 mmol) and CDI (280 mg, 1.726 mmol) in DMF (2 mL) was stirred at room temperature for 30 min. 3'-chloro-*N*-hydroxy-[1,1'-biphenyl]-2-carboximidamide (355 mg, 1.439 mmol) and  $K_2CO_3$  (239 mg, 1.726 mmol) were added and the resulting mixture was heated in a microwave at 140 °C for 1 h. The mixture was partitioned between water (20 mL) and DCM (20 mL) and the aqueous layer was further extracted with DCM (20 mL). The organic extracts were combined, dried by filtration through a hydrophobic frit and concentrated *in vacuo*. The resulting residue was purified on silica using a 0-25% EtOAc-cyclohexane gradient to afford the title product as a colourless oil; yield 99% (602 mg); **LCMS** (acidic conditions) (ES +ve)  $m/z$  370 ( $[M-tBu+H]^+$ ),  $R_t$  = 1.43 min;  **$^1H$  NMR** (400 MHz, DMSO- $d_6$ ):  $\delta$  = 7.82 (dd,  $J$  = 7.8, 1.0 Hz, 1H), 7.68 (td,  $J$  = 7.6, 1.3 Hz, 1H), 7.59 (td,  $J$  = 7.6, 1.3 Hz, 1H), 7.53 (dd,  $J$  = 7.7, 0.9 Hz, 1H), 7.41 - 7.33 (m, 2H), 7.26 - 7.22 (m, 1H), 7.14 (dt,  $J$  = 6.9, 1.6 Hz, 1H), 3.85 - 3.73 (m, 1H), 3.68 - 3.57 (m, 1H), 3.46 - 3.36 (m, 1H), 3.35 - 3.31 (m, 1H), 3.28 - 3.22 (m, 1H), 2.31 - 2.19 (m, 1H), 2.06 - 1.93 (m, 1H), 1.40 ppm (s, 9H).



**2.161**

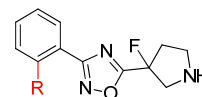
**3-(2-Isopropylphenyl)-5-(pyrrolidin-3-yl)-1,2,4-oxadiazole (2.161)**; *tert*-Butyl 3-(3-(2-isopropylphenyl)-1,2,4-oxadiazol-5-yl)pyrrolidine-1-carboxylate (80 mg, 0.224 mmol) was dissolved in DCM and treated with TFA (0.5 mL, 6.49 mmol) at room temperature for 1 h. The mixture was concentrated under a stream of nitrogen to afford the title compound as a colourless oil (as TFA salt); yield 100% (82.7 mg); **LCMS** (basic conditions) (ES +ve)  $m/z$  258 (M+H)<sup>+</sup>,  $R_t$  = 1.04 min; **<sup>1</sup>H NMR** (400 MHz, DMSO- $d_6$ ):  $\delta$  = 9.12 (br. s, 2H, *pyrrolidine NH*<sub>2</sub><sup>+</sup>), 7.72 (d,  $J$  = 7.6 Hz, 1H), 7.58 - 7.54 (m, 2H), 7.40 - 7.33 (m, 1H), 4.11 - 4.02 (m, 1H), 3.78 - 3.68 (m, 1H), 3.65 - 3.51 (m, 2H), 3.44 - 3.30 (m, 2H), 2.56 - 2.43 (m, 1H), 2.39 - 2.25 (m, 1H), 1.22 ppm (d,  $J$  = 6.8 Hz, 6H); **<sup>13</sup>C NMR** (101 MHz, DMSO- $d_6$ ):  $\delta$  = 178.7, 168.6, 148.5, 131.8, 130.4, 126.8, 126.5, 124.9, 49.0, 48.2, 45.5, 35.3, 29.6, 24.2 ppm; **HRMS** (ES +ve) calcd for C<sub>15</sub>H<sub>20</sub>N<sub>3</sub>O (M+H)<sup>+</sup> 258.1601, found 258.1604; **IR**  $\nu$  (cm<sup>-1</sup>) 2968, 1670, 1133.



**2.177**

**3-(3'-Chloro-[1,1'-biphenyl]-2-yl)-5-(pyrrolidin-3-yl)-1,2,4-oxadiazole (2.177)**; *tert*-Butyl 3-(3-(3'-chloro-[1,1'-biphenyl]-2-yl)-1,2,4-oxadiazol-5-yl)pyrrolidine-1-carboxylate (70 mg, 0.164 mmol) was dissolved in DCM and treated with TFA (0.5 mL, 6.49 mmol) at room temperature for 1 h. The mixture was concentrated under a stream of nitrogen to afford the title compound as a colourless oil (as TFA salt); yield 99% (71.3 mg); **LCMS** (basic conditions) (ES +ve)  $m/z$  326 (M+H)<sup>+</sup>,  $R_t$  = 1.11 min; **<sup>1</sup>H NMR** (400 MHz, DMSO- $d_6$ ):  $\delta$  = 9.11 (br. s, 2H, *pyrrolidine NH*<sub>2</sub><sup>+</sup>), 7.87 (dd,  $J$  = 7.6, 1.3 Hz, 1H), 7.69 (td,  $J$  = 7.6, 1.5 Hz, 1H), 7.61 (td,  $J$  = 7.6, 1.3 Hz, 1H), 7.53 (dd,  $J$  =

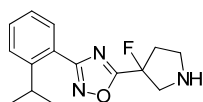
7.6, 1.0 Hz, 1H), 7.44 - 7.34 (m, 2H), 7.31 - 7.27 (m, 1H), 7.15 (dt,  $J = 7.3, 1.5$  Hz, 1H), 3.95 (quin,  $J = 7.8$  Hz, 1H), 3.69 - 3.58 (m, 1H), 3.44 - 3.34 (m, 1H), 3.34 - 3.17 (m, 2H), 2.45 - 2.31 (m, 1H), 2.15 - 2.03 ppm (m, 1H).



*General procedure for the preparation of 2.162 and 2.178:*

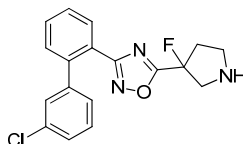
**2.162** : R=*i*Pr  
**2.178** : R=3-Cl-phenyl

To a solution of LDA (0.084 mL, 2 M solution in THF, 0.168 mmol) in THF (1 mL) cooled to  $-78$  °C was added dropwise a solution of the appropriate *tert*-butyl carbonate protected oxadiazole (0.14 mmol) in THF (1 mL). The resulting mixture was stirred at  $-78$  °C for 10 min and a solution of *N*-fluoro-*N*-(phenylsulfonyl)benzenesulfonamide (52.9 mg, 0.168 mmol) in THF (0.5 mL) was added dropwise. The reaction mixture was stirred at  $-78$  °C for 10 min and then at room temperature for 30 min. The reaction mixture was partitioned between water (5 mL) and DCM (5 mL) and the aqueous layer was further extracted with DCM (5 mL). The organic extracts were combined and concentrated under a stream of nitrogen. The residue obtained was purified by MDAP (acidic conditions) and the resulting intermediate was dissolved in DCM (1 mL) and treated with TFA (0.5 mL, 6.49 mmol) at room temperature for 1 h. The mixture was concentrated under a stream of nitrogen to afford the expected fluoro-oxadiazole analogues (as TFA salt):



**2.162**

**5-(3-Fluoropyrrolidin-3-yl)-3-(2-isopropylphenyl)-1,2,4-oxadiazole (2.162)**; from *tert*-butyl 3-(3-(2-isopropylphenyl)-1,2,4-oxadiazol-5-yl)pyrrolidine-1-carboxylate (50 mg, 0.14 mmol); yellow oil; yield 21% (11.3 mg); **LCMS** (basic conditions) (ES +ve)  $m/z$  276 (M+H)<sup>+</sup>,  $R_t$  = 1.12 min; **<sup>1</sup>H NMR** (600 MHz, DMSO-*d*<sub>6</sub>):  $\delta$  = 9.68 (br. s, 2H, *pyrrolidine NH*<sub>2</sub><sup>+</sup>), 7.75 (d,  $J$  = 7.7 Hz, 1H), 7.63 - 7.59 (m, 2H), 7.43 - 7.38 (m, 1H), 4.16 - 4.06 (m, 1H), 4.06 - 3.94 (m, 1H), 3.70 - 3.64 (m, 1H), 3.60 - 3.50 (m, 2H), 2.91 - 2.72 (m, 2H), 1.24 ppm (d,  $J$  = 6.8 Hz, 6H); **<sup>13</sup>C NMR** (151 MHz, DMSO-*d*<sub>6</sub>):  $\delta$  = 172.9 (d,  $J$  = 27.1 Hz), 168.5, 148.2, 131.6, 130.0, 126.4, 126.2, 123.8, 96.4 (d,  $J$  = 183.5 Hz), 53.4 (d,  $J$  = 24.3 Hz), 44.1, 35.5 (d,  $J$  = 23.2 Hz), 29.4, 23.6 ppm; **HRMS** (ES +ve) calcd for C<sub>15</sub>H<sub>19</sub>FN<sub>3</sub>O (M+H)<sup>+</sup> 276.1507, found 276.1506; **IR**  $\nu$  (cm<sup>-1</sup>) 2968, 1673, 1129.



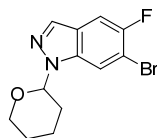
**2.178**

**3-(3'-Chloro-[1,1'-biphenyl]-2-yl)-5-(3-fluoropyrrolidin-3-yl)-1,2,4-oxadiazole (2.178)**; from *tert*-butyl 3-(3-(3'-chloro-[1,1'-biphenyl]-2-yl)-1,2,4-oxadiazol-5-yl)pyrrolidine-1-carboxylate (59.6 mg, 0.14 mmol); yellow oil; yield 17% (11.1 mg); **LCMS** (basic conditions) (ES +ve)  $m/z$  344 (M+H)<sup>+</sup>,  $R_t$  = 1.18 min; **<sup>1</sup>H NMR** (400 MHz, DMSO-*d*<sub>6</sub>):  $\delta$  = 9.61 (br. s, 2H, *pyrrolidine NH*<sub>2</sub><sup>+</sup>), 7.91 (dd,  $J$  = 7.6, 1.3 Hz, 1H), 7.73 (td,  $J$  = 7.6, 1.3 Hz, 1H), 7.65 (td,  $J$  = 7.6, 1.3 Hz, 1H), 7.56 (dd,  $J$  = 7.7, 1.1 Hz, 1H), 7.46 - 7.36 (m, 2H), 7.35 - 7.31 (m, 1H), 7.17 (dt,  $J$  = 7.4, 1.3 Hz, 1H), 4.07 - 3.92 (m, 1H), 3.89 - 3.70 (m, 1H), 3.66 - 3.54 (m, 1H), 3.53 - 3.42 (m, 1H), 2.82 - 2.66 (m,



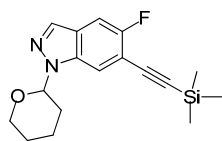
1H), 2.66 - 2.53 ppm (m, 1H); <sup>13</sup>C NMR (151 MHz, DMSO-d<sub>6</sub>): δ = 172.8 (d, *J* = 27.1 Hz), 168.4, 141.9, 140.1, 132.7, 131.6, 131.0, 130.3, 129.9, 128.6, 128.5, 127.7, 127.4, 123.9, 96.2 (d, *J* = 184.1 Hz), 53.2 (d, *J* = 25.4 Hz), 44.0, 35.4 (d, *J* = 22.7 Hz) ppm.

#### 4.4. Experimental preparation of the isoxazole analogues for the mPTP programme



3.33

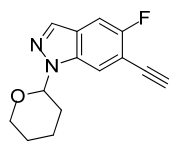
**6-Bromo-5-fluoro-1-(tetrahydro-2H-pyran-2-yl)-1H-indazole (3.33)**; To a stirred suspension of 6-bromo-5-fluoro-1H-indazole (15.50 g, 72.1 mmol) in 2-MeTHF (300 mL) was added 3,4-dihydro-2H-pyran (16.48 mL, 180 mmol) and pyridinium *p*-toluenesulfonate (1.81 g, 7.21 mmol). The resulting reaction mixture was stirred at 85 °C for 12 h. The above step was run on two duplicates and the reaction mixtures were combined for the work up. The reaction mixture obtained was concentrated *in vacuo*. The residue obtained was taken up in Et<sub>2</sub>O (220 mL) and EtOAc (5 mL). The suspension obtained was stirred at 40 °C for 10 min until it became a solution. The solution obtained was left to stand at room temperature for 2 h and a solid precipitated. The solid obtained was recovered by filtration to afford the title compound as pale yellow needles; yield 67% (28.76 g). The filtrate was concentrated *in vacuo* and the residue obtained was taken up Et<sub>2</sub>O (80 mL). The suspension obtained was stirred at 40 °C for 10 min until it became a solution. The solution was then left to stand at room temperature for 12 h and a solid precipitated. The solid obtained was recovered by filtration to afford the title compound as pale yellow needles; yield 8% (3.51 g). The filtrate was concentrated *in vacuo* and the residue obtained was purified on silica using a 0-100% EtOAc-cyclohexane gradient to afford the title compound as a pale yellow solid; yield 18% (7.91 g). Combined yield: 93% (combined mass: 40.18 g); **LCMS** (acidic conditions) (ES +ve) *m/z* 299 (M+H)<sup>+</sup>, Rt = 1.28 min; **<sup>1</sup>H NMR** (400 MHz, DMSO-d<sub>6</sub>): δ = 8.21 (d, *J* = 5.9 Hz, 1H), 8.14 (s, 1H), 7.77 (d, *J* = 8.8 Hz, 1H), 5.89 (dd, *J* = 9.7, 2.6 Hz, 1H), 3.91 - 3.83 (m, 1H), 3.81 - 3.73 (m, 1H), 2.44 - 2.30 (m, 1H), 2.09 - 1.90 (m, 2H), 1.80 - 1.65 (m, 1H), 1.63 - 1.52 ppm (m, 2H).



3.34

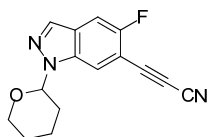
**5-Fluoro-1-(tetrahydro-2H-pyran-2-yl)-6-((trimethylsilyl)ethynyl)-1H-indazole**

(3.34); To a stirred solution of 6-bromo-5-fluoro-1-(tetrahydro-2H-pyran-2-yl)-1H-indazole (20.09 g, 67.2 mmol) in triethylamine (187 mL, 1343 mmol) was added copper(I) iodide (1.92 g, 10.07 mmol), bis(triphenylphosphine)palladium(II) chloride (7.07 g, 10.07 mmol) and ethynyltrimethylsilane (18.61 mL, 134 mmol). The resulting reaction mixture was heated at 75 °C for 4 h. The above step was run on two duplicates and the reaction mixtures were combined for the work up. The mixture obtained was filtered through a pad of celite and washed with EtOAc (2 L). The filtrate was concentrated *in vacuo* and the residue obtained was redissolved in EtOAc (300 mL) and water (300 mL). The organic layer was separated and the aqueous layer was further extracted with EtOAc (100 mL). The organic extracts were combined, washed with brine (100 mL), dried by filtration through a hydrophobic frit and solvents were removed *in vacuo*. The black oil obtained was purified on silica using a 0-10% EtOAc-cyclohexane gradient to afford the title compound as a pale yellow solid; yield 98% (42.62 g); LCMS (acidic conditions) (ES +ve)  $m/z$  317 (M+H)<sup>+</sup>, Rt = 1.52 min; <sup>1</sup>H NMR (400 MHz, DMSO-d<sub>6</sub>): δ = 8.13 (s, 1H), 8.01 (d, *J* = 5.9 Hz, 1H), 7.66 (d, *J* = 9.5 Hz, 1H), 5.92 (dd, *J* = 9.7, 2.3 Hz, 1H), 3.91 - 3.83 (m, 1H), 3.83 - 3.74 (m, 1H), 2.43 - 2.30 (m, 1H), 2.08 - 1.91 (m, 2H), 1.81 - 1.65 (m, 1H), 1.63 - 1.51 (m, 2H), 0.28 ppm (s, 9H).



3.35

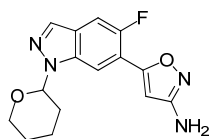
**6-Ethynyl-5-fluoro-1-(tetrahydro-2H-pyran-2-yl)-1H-indazole (3.35)**; To a solution of 5-fluoro-1-(tetrahydro-2H-pyran-2-yl)-6-((trimethylsilyl)ethynyl)-1H-indazole (17.86 g, 56.4 mmol) in anhydrous THF (200 mL) cooled in an ice bath was added 1 M TBAF in THF (59.3 mL, 59.3 mmol) *via* a dropping funnel over 20 min. The reaction mixture was left to stir in the ice bath for 40 min. The above step was run on two duplicates and the reaction mixtures were combined for the work up. The mixture obtained was concentrated *in vacuo*. The residue obtained was purified on silica using a 0-20% EtOAc-cyclohexane gradient to afford the title compound as a white solid; yield 89% (24.48 g); LCMS (acidic conditions) (ES +ve)  $m/z$  245 (M+H)<sup>+</sup>, Rt = 1.20 min; <sup>1</sup>H NMR (400 MHz, DMSO-d<sub>6</sub>):  $\delta$  = 8.14 (s, 1H), 8.03 (d,  $J$  = 5.6 Hz, 1H), 7.67 (d,  $J$  = 9.3 Hz, 1H), 5.89 (dd,  $J$  = 9.7, 2.3 Hz, 1H), 4.56 (s, 1H), 3.91 - 3.83 (m, 1H), 3.82 - 3.72 (m, 1H), 2.44 - 2.29 (m, 1H), 2.09 - 1.92 (m, 2H), 1.80 - 1.65 (m, 1H), 1.64 - 1.52 ppm (m, 2H).



3.36

**3-(5-Fluoro-1-(tetrahydro-2H-pyran-2-yl)-1H-indazol-6-yl)propiolonitrile (3.36)**; To a solution of 6-ethynyl-5-fluoro-1-(tetrahydro-2H-pyran-2-yl)-1H-indazole (13.13 g, 53.8 mmol) in THF (175 mL) cooled at -78 °C was added a solution of 1.6 M *n*-butyllithium in hexane (47 mL, 75.5 mmol) *via* a dropping funnel over 30 min. The resulting reaction mixture was stirred at -78 °C for 1 h. *p*-Toluenesulfonyl cyanide

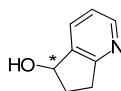
(10.70 g, 59 mmol) suspended in THF (30 mL) was added at -78 °C *via* a dropping funnel over 20 min. The resulting reaction mixture was stirred at -78 °C for 30 min and then at room temperature for 4 h. The reaction mixture was quenched with a saturated NH<sub>4</sub>Cl aqueous solution (150 mL), the organic layer was separated and the aqueous layer was extracted with EtOAc (2 x 100 mL). The organic extracts were combined, dried by filtration through a hydrophobic frit and solvents were removed *in vacuo*. The residue obtained was purified on silica using a 0-30% EtOAc-cyclohexane gradient to afford the title compound as a pale yellow solid; yield 70% (10.2 g); **LCMS** (acidic conditions) (ES +ve) *m/z* 186 ([M-THP]+H)<sup>+</sup>, Rt = 1.27 min; **<sup>1</sup>H NMR** (400 MHz, DMSO-d<sub>6</sub>): δ = 8.48 (d, *J* = 5.6 Hz, 1H), 8.24 (s, 1H), 7.84 (d, *J* = 9.3 Hz, 1H), 5.91 (dd, *J* = 9.7, 2.3 Hz, 1H), 3.93 - 3.84 (m, 1H), 3.83 - 3.71 (m, 1H), 2.44 - 2.30 (m, 1H), 2.12 - 1.92 (m, 2H), 1.81 - 1.67 (m, 1H), 1.65 - 1.54 ppm (m, 2H).



**3.37**

**5-(5-Fluoro-1-(tetrahydro-2H-pyran-2-yl)-1H-indazol-6-yl)isoxazol-3-amine (3.37);** To a stirred solution of 3-(5-fluoro-1-(tetrahydro-2H-pyran-2-yl)-1H-indazol-6-yl)propiolonitrile (1.00 g, 3.71 mmol) in THF (12 mL) and ethanol (3 mL) was added a solution of hydroxylamine hydrochloride (0.39 g, 5.57 mmol) in 1 M aqueous sodium hydroxide (9.28 mL, 9.28 mmol) *via* a dropping funnel over 15 min. The reaction mixture was stirred at room temperature for 1 h, diluted with water (30 mL) and extracted with EtOAc (2 x 30 mL). The organic extracts were combined, washed with brine (20 mL), dried by filtration through a hydrophobic frit and solvents were removed *in vacuo*. The residue obtained was suspended in water (40 mL) and the solid was filtered and rinsed with water (10 mL). The solid was then triturated with TBME (40 mL) to afford the title compound as an off-white solid; yield 60% (672 mg). The filtrate

obtained was concentrated *in vacuo* and purified on silica using a 0-50% EtOAc-cyclohexane gradient to afford the title compound as an off-white solid; yield 11% (122 mg). Combined yield: 71% (combined mass: 794 mg); **LCMS** (acidic conditions) (ES +ve)  $m/z$  303 (M+H)<sup>+</sup>, Rt = 1.02 min; **<sup>1</sup>H NMR** (400 MHz, DMSO-d<sub>6</sub>): δ = 8.21 (d,  $J$  = 5.9 Hz, 1H), 8.18 (s, 1H), 7.78 (d,  $J$  = 11.0 Hz, 1H), 6.33 (d,  $J$  = 4.6 Hz, 1H), 6.03 (dd,  $J$  = 9.5, 2.2 Hz, 1H), 5.79 (s, 2H), 3.94 - 3.74 (m, 2H), 2.47 - 2.31 (m, 1H), 2.11 - 1.93 (m, 2H), 1.85 - 1.69 (m, 1H), 1.67 - 1.50 ppm (m, 2H); **<sup>13</sup>C NMR** (101 MHz, DMSO-d<sub>6</sub>): δ = 165.3, 161.8 (d,  $J$  = 9.3 Hz), 154.1 (d,  $J$  = 242.8 Hz), 136.4, 134.1, 124.6 (d,  $J$  = 11.0 Hz), 115.8 (d,  $J$  = 17.6 Hz), 109.2 (d,  $J$  = 3.7 Hz), 106.9 (d,  $J$  = 24.2 Hz), 97.5, 84.4, 66.9, 29.4, 25.3, 22.5 ppm.



**3.20a and 3.20b**  
(single enantiomers)

**6,7-Dihydro-5H-cyclopenta[*b*]pyridin-5-ol (3.20a and 3.20b, single enantiomers);**<sup>252</sup>

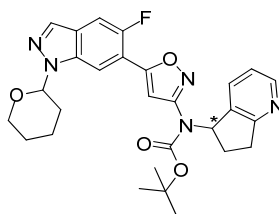
The commercial racemic 6,7-dihydro-5H-cyclopenta[*b*]pyridin-5-ol (1.10 g) was purified by chiral preparative HPLC, using a Daicel Chiralpak IA column (20 mm i.d. x 250 mm, 10 μm particle size). 12 injections of 900 μL were carried out, using an isocratic mobile phase isohexane:EtOH = 95:5, flow rate 18 mL/min, run time 60 min. A photodiode array detector was used to collect the spectra between 190 and 450 nm.

Fractions containing the two different enantiomers were combined separately and solvents were removed *in vacuo* to afford the two title single enantiomers:

- First eluting enantiomer **3.20a**, 31% (337 mg); **LCMS** (basic conditions) (ES +ve)  $m/z$  136 (M+H)<sup>+</sup>, Rt = 0.51 min; **chiral HPLC** (see Analytical chiral HPLC method 2) Rt = 9.9 min, e.e. > 99.9%; **<sup>1</sup>H NMR** (400 MHz, DMSO-d<sub>6</sub>): δ = 8.37 (dd,  $J$  = 4.8, 1.1 Hz, 1H), 7.69 (d,  $J$  = 7.3 Hz, 1H), 7.19 (dd,  $J$  = 7.3, 4.8 Hz, 1H),

5.40 (d,  $J = 5.6$  Hz, 1H), 5.11 - 5.07 (m, 1H), 3.01 - 2.90 (m, 1H), 2.85 - 2.73 (m, 1H), 2.44 - 2.33 (m, 1H), 1.87 - 1.75 ppm (m, 1H).

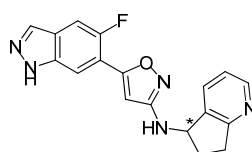
- Second eluting enantiomer **3.20b**, 20% (223 mg); **LCMS** (basic conditions) (ES +ve)  $m/z$  136 (M+H)<sup>+</sup>,  $R_t = 0.54$  min; **chiral HPLC** (see Analytical chiral HPLC method 2)  $R_t = 17.4$  min, e.e. = 99.8%; **<sup>1</sup>H NMR** (400 MHz, DMSO- $d_6$ ):  $\delta = 8.37$  (dd,  $J = 4.9, 1.0$  Hz, 1H), 7.69 (d,  $J = 7.6$  Hz, 1H), 7.19 (dd,  $J = 7.6, 4.9$  Hz, 1H), 5.39 (d,  $J = 5.6$  Hz, 1H), 5.11 - 5.07 (m, 1H), 3.01 - 2.90 (m, 1H), 2.85 - 2.73 (m, 1H), 2.44 - 2.34 (m, 1H), 1.86 - 1.75 ppm (m, 1H).



**3.40 (from 3.20a)**

***tert*-Butyl (6,7-dihydro-5H-cyclopenta[*b*]pyridin-5-yl)(5-(5-fluoro-1-(tetrahydro-2H-pyran-2-yl)-1H-indazol-6-yl)isoxazol-3-yl)carbamate (3.40, from Scheme 19);** To a stirred solution of *tert*-butyl (5-(5-fluoro-1-(tetrahydro-2H-pyran-2-yl)-1H-indazol-6-yl)isoxazol-3-yl)carbamate (300 mg, 0.745 mmol), 6,7-dihydro-5H-cyclopenta[*b*]pyridin-5-ol (121 mg, 0.895 mmol, **3.20a**, e.e. > 99.9%) and triphenylphosphine (391 mg, 1.491 mmol) in THF (5 mL) was added DIAD (0.293 mL, 1.491 mmol) dropwise at room temperature. The resulting reaction mixture was stirred at room temperature for 1 h and then diluted with EtOAc (15 mL), water (15 mL) and brine (15 mL). The organic phase was separated and the aqueous layer was further extracted with EtOAc (15 mL). The organic extracts were combined, washed with water (10 mL), washed with brine (5 mL), dried by filtration through a hydrophobic frit and concentrated *in vacuo*. The residue obtained was purified on silica using a 0-100%

EtOAc-cyclohexane gradient to afford the title compound as a white solid; yield 67% (261 mg); LCMS (acidic conditions) (ES +ve)  $m/z$  520 (M+H)<sup>+</sup>, Rt = 1.26 min; <sup>1</sup>H NMR (400 MHz, DMSO-d<sub>6</sub>):  $\delta$  = 8.39 (d,  $J$  = 4.9 Hz, 1H), 8.30 (d,  $J$  = 5.9 Hz, 1H), 8.21 (s, 1H), 7.84 (d,  $J$  = 11.0 Hz, 1H), 7.60 (d,  $J$  = 7.3 Hz, 1H), 7.22 - 7.13 (m, 2H), 6.11 - 6.00 (m, 2H), 3.93 - 3.74 (m, 2H), 3.14 - 2.92 (m, 2H), 2.69 - 2.56 (m, 1H), 2.45 - 2.26 (m, 2H), 2.11 - 1.92 (m, 2H), 1.83 - 1.68 (m, 1H), 1.65 - 1.52 (m, 2H), 1.33 ppm (s, 9H).

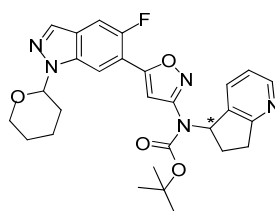


**3.17b**  
(single enantiomer)

***N*-(6,7-Dihydro-5*H*-cyclopenta[*b*]pyridin-5-yl)-5-(5-fluoro-1*H*-indazol-6-yl)isoxazol-3-amine (3.17b, single enantiomer, from Scheme 19)**; To a solution of *tert*-butyl (6,7-dihydro-5*H*-cyclopenta[*b*]pyridin-5-yl)(5-(5-fluoro-1-(tetrahydro-2*H*-pyran-2-yl)-1*H*-indazol-6-yl)isoxazol-3-yl)carbamate (255 mg, 0.491 mmol, **obtained in the experiment described just above**) in EtOH (5 mL) was added a 3 M HCl solution in MeOH (0.818 mL, 2.454 mmol). The reaction mixture was stirred at 50 °C for 16 h. The reaction mixture was cooled to room temperature, a 3 M HCl solution in MeOH (0.818 mL, 2.454 mmol) was added and the resulting mixture was stirred at 50 °C for 12 h. The reaction mixture was cooled to room temperature, a 3 M HCl solution in MeOH (0.818 mL, 2.454 mmol) was added and the resulting mixture was stirred at 60 °C for 12 h. The reaction mixture was concentrated *in vacuo* and the residue was taken up in 10 mL of a saturated NaHCO<sub>3</sub> aqueous solution (10 mL), water (10 mL) and EtOAc (30 mL). The organic layer was separated and the aqueous layer was further extracted with EtOAc (2 x 10 mL). The organic extracts were combined, washed with water (10 mL), washed with brine (10 mL), dried by filtration through a hydrophobic frit and concentrated *in vacuo*. The residue obtained was purified on silica using a 0-5% MeOH (+0.1% NEt<sub>3</sub>)-TBME



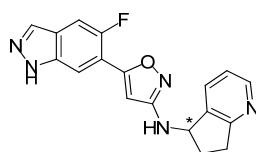
gradient to afford the title compound as a white solid; yield 75% (123.4 mg); **LCMS** (acidic conditions) (ES +ve)  $m/z$  336 (M+H)<sup>+</sup>, Rt = 0.69 min; **chiral HPLC** (see Analytical chiral HPLC method 1) Rt = 16.3 min, e.e. = 99.2%; **<sup>1</sup>H NMR** (400 MHz, DMSO-d<sub>6</sub>): δ = 13.43 (br. s, 1H), 8.41 (dd,  $J$  = 4.9, 1.0 Hz, 1H), 8.16 (s, 1H), 7.98 (d,  $J$  = 5.9 Hz, 1H), 7.82 - 7.70 (m, 2H), 7.20 (dd,  $J$  = 7.6, 4.9 Hz, 1H), 6.79 (d,  $J$  = 8.1 Hz, 1H), 6.38 (d,  $J$  = 4.4 Hz, 1H), 5.11 - 5.07 (m, 1H), 3.08 - 2.98 (m, 1H), 2.97 - 2.87 (m, 1H), 2.64 - 2.54 (m, 1H), 2.01 - 1.88 ppm (m, 1H); **<sup>13</sup>C NMR** (101 MHz, DMSO-d<sub>6</sub>): δ = 165.0, 164.4, 162.1, 153.7 (d,  $J$  = 241.1 Hz), 149.3, 137.8, 136.8, 134.2, 132.8, 123.4 (d,  $J$  = 10.3 Hz), 122.0, 115.3 (d,  $J$  = 17.6 Hz), 109.0, 106.5 (d,  $J$  = 24.0 Hz), 96.6 (d,  $J$  = 11.3 Hz), 56.5, 32.0, 31.8 ppm; **HRMS** (ES +ve) calcd for C<sub>18</sub>H<sub>15</sub>FN<sub>5</sub>O (M+H)<sup>+</sup> 336.1255, found 336.1266; **IR** ν (cm<sup>-1</sup>) 3168, 1559; **mp** 233.5 - 234.9 °C; **[α]<sub>D</sub><sup>25</sup>** = -79.5° (c 12.1 g/L, DMSO-d<sub>6</sub>).



**3.40 (from 3.20b)**

**tert-Butyl (6,7-dihydro-5H-cyclopenta[b]pyridin-5-yl)(5-(5-fluoro-1-(tetrahydro-2H-pyran-2-yl)-1H-indazol-6-yl)isoxazol-3-yl)carbamate (3.40, from Scheme 20);** To a stirred solution of *tert*-butyl (5-(5-fluoro-1-(tetrahydro-2H-pyran-2-yl)-1H-indazol-6-yl)isoxazol-3-yl)carbamate (200 mg, 0.497 mmol), 6,7-dihydro-5H-cyclopenta[b]pyridin-5-ol (81 mg, 0.596 mmol, **3.20b**, e.e. = **99.8%**) and triphenylphosphine (261 mg, 0.994 mmol) in THF (10 mL) was added DIAD (0.195 mL, 0.994 mmol) dropwise at room temperature. The resulting reaction mixture was stirred at room temperature for 1 h and then diluted with EtOAc (15 mL), water (15 mL) and brine (15 mL). The organic phase was separated and the aqueous layer was further extracted with EtOAc (15 mL). The organic extracts were combined, washed with water

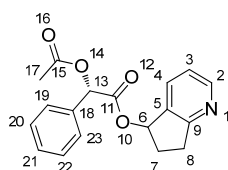
(10 mL), washed with brine (5 mL), dried by filtration through a hydrophobic frit and concentrated *in vacuo*. The residue obtained was purified on silica using a 0-100% EtOAc-cyclohexane gradient to afford the title compound as a white solid; yield 55% (143 mg); LCMS (acidic conditions) (ES +ve)  $m/z$  520 (M+H)<sup>+</sup>, Rt = 1.29 min; <sup>1</sup>H NMR (400 MHz, DMSO-d<sub>6</sub>): δ = 8.39 (d,  $J$  = 4.9 Hz, 1H), 8.30 (d,  $J$  = 5.6 Hz, 1H), 8.21 (s, 1H), 7.84 (d,  $J$  = 11.0 Hz, 1H), 7.60 (dd,  $J$  = 7.6, 1.2 Hz, 1H), 7.21 - 7.15 (m, 2H), 6.11 - 5.99 (m, 2H), 3.93 - 3.76 (m, 2H), 3.14 - 2.92 (m, 2H), 2.69 - 2.56 (m, 1H), 2.46 - 2.26 (m, 2H), 2.10 - 1.95 (m, 2H), 1.83 - 1.68 (m, 1H), 1.65 - 1.53 (m, 2H), 1.33 ppm (s, 9H).



**3.17a**  
(single enantiomer)

***N*-(6,7-Dihydro-5*H*-cyclopenta[*b*]pyridin-5-yl)-5-(5-fluoro-1*H*-indazol-6-yl)isoxazol-3-amine (3.17a, single enantiomer, from Scheme 20)**; To a solution of *tert*-butyl (6,7-dihydro-5*H*-cyclopenta[*b*]pyridin-5-yl)(5-(5-fluoro-1-(tetrahydro-2*H*-pyran-2-yl)-1*H*-indazol-6-yl)isoxazol-3-yl)carbamate (143 mg, 0.275 mmol, **obtained in the experiment described just above**) in EtOH (5 mL) was added a 3 M HCl solution in MeOH (0.917 mL, 2.75 mmol). The reaction mixture was stirred at 50 °C for 10 h. The reaction mixture was cooled to room temperature, a 3 M HCl solution in MeOH (0.917 mL, 2.75 mmol) was added and the resulting mixture was stirred at 70 °C for 6 h. The reaction mixture was concentrated *in vacuo* and the residue was taken up in 10 mL of a saturated NaHCO<sub>3</sub> aqueous solution (10 mL), water (10 mL) and EtOAc (30 mL). The organic layer was separated and the aqueous layer was further extracted with EtOAc (2 x 10 mL). The organic extracts were combined, washed with water (10 mL), washed with brine (10 mL), dried by filtration through a hydrophobic frit and concentrated *in vacuo*.

The residue obtained was purified on silica using a 0-5% MeOH (+0.1% NEt<sub>3</sub>)-TBME gradient to afford the title compound as a white solid; yield 78% (72 mg); **LCMS** (acidic conditions) (ES +ve) *m/z* 336 (M+H)<sup>+</sup>, Rt = 0.69 min; **chiral HPLC** (see Analytical chiral HPLC method 1) Rt = 10.3 min, e.e. = 99.0%; **<sup>1</sup>H NMR** (400 MHz, DMSO-d<sub>6</sub>): δ = 13.41 (br. s, 1H), 8.41 (dd, *J* = 4.9, 0.7 Hz, 1H), 8.16 (s, 1H), 7.98 (d, *J* = 5.6 Hz, 1H), 7.82 - 7.70 (m, 2H), 7.20 (dd, *J* = 7.6, 4.9 Hz, 1H), 6.79 (d, *J* = 8.1 Hz, 1H), 6.38 (d, *J* = 4.4 Hz, 1H), 5.11 - 5.07 (m, 1H), 3.08 - 2.98 (m, 1H), 2.97 - 2.86 (m, 1H), 2.64 - 2.53 (m, 1H), 2.02 - 1.86 ppm (m, 1H); **<sup>13</sup>C NMR** (101 MHz, DMSO-d<sub>6</sub>): δ = 165.0, 164.4, 162.1, 153.7 (d, *J* = 241.3 Hz), 149.3, 137.8, 136.9, 134.3, 132.7, 123.5 (d, *J* = 10.3 Hz), 122.0, 115.3 (d, *J* = 17.6 Hz), 108.8, 106.5 (d, *J* = 24.2 Hz), 96.6 (d, *J* = 11.0 Hz), 56.5, 32.0, 31.8 ppm; **HRMS** (ES +ve) calcd for C<sub>18</sub>H<sub>15</sub>FN<sub>5</sub>O (M+H)<sup>+</sup> 336.1255, found 336.1266; **IR** ν (cm<sup>-1</sup>) 3169, 1559; **mp** 213.6 - 215.2 °C; **[α]<sub>D</sub><sup>25</sup>** = +75.3° (c 15.2 g/L, DMSO-d<sub>6</sub>).

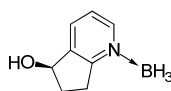


**3.41**

**(2*S*)-6,7-Dihydro-5*H*-cyclopenta[*b*]pyridin-5-yl 2-acetoxy-2-phenylacetate (3.41; 1:1 mixture of the two diastereoisomers A and B)**; To a stirred mixture of 6,7-dihydro-5*H*-cyclopenta[*b*]pyridin-5-ol (500 mg, 3.70 mmol, **commercial racemic**), (*S*)-(+)-2-acetoxy-2-phenylacetic acid (862 mg, 4.44 mmol) and DMAP (45.2 mg, 0.370 mmol) in DCM (20 mL) was added *N,N'*-dicyclohexylcarbodiimide (1.53 g, 7.40 mmol). The resulting reaction mixture was stirred at room temperature for 1 h and a solid precipitated. The reaction mixture was filtered and the cake was rinsed with TBME (30 mL). The filtrate obtained was concentrated *in vacuo* and the residue obtained was purified on silica using a 0-100% TBME-cyclohexane gradient to afford the title

compound as an orange oil; yield 89% (1.02 g); LCMS (acidic conditions) (ES +ve)  $m/z$  312 (M+H)<sup>+</sup>, Rt = 0.92 min; <sup>1</sup>H NMR (400 MHz, DMSO-d<sub>6</sub>): δ = 8.50 (dd,  $J$  = 4.9, 1.5 Hz, 1H,  $H_2$  for A), 8.45 (dd,  $J$  = 4.9, 1.5 Hz, 1H,  $H_2$  for B), 7.69 (dd,  $J$  = 7.8, 1.5 Hz, 1H,  $H_4$  for A), 7.50 - 7.37 (m, 11H,  $H_4$  for B and  $H_{19, 20, 21, 22, 23}$  for A and B), 7.26 (dd,  $J$  = 7.8, 4.9 Hz, 1H,  $H_3$  for A), 7.16 (dd,  $J$  = 7.6, 4.9 Hz, 1H,  $H_3$  for B), 6.21 (td,  $J$  = 7.7, 4.2 Hz, 2H,  $H_6$  for A and B), 5.93 (s, 1H,  $H_{13}$  for A), 5.92 (s, 1H,  $H_{13}$  for B), 3.09 - 2.99 (m, 1H,  $H_{8a}$  for A), 2.99 - 2.81 (m, 3H,  $H_{8b}$  for A and  $H_{8a, 8b}$  for B), 2.60 - 2.53 (m, 1H,  $H_{7a}$  for A), 2.49 - 2.38 (m, 1H,  $H_{7a}$  for B), 2.15 (s, 3H,  $H_{17}$  for A), 2.14 (s, 3H,  $H_{17}$  for B), 2.10 - 1.96 (m, 1H,  $H_{7b}$  for A), 1.88 - 1.77 ppm (m, 1H,  $H_{7b}$  for B).

**Optimisation of the CBS-mediated reduction: Investigation of the amount of *N,N*-diethylaniline-borane and CBS used (Table 28):**

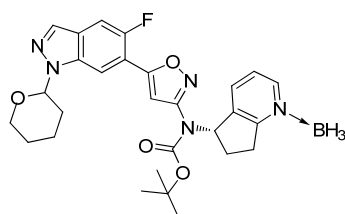


**3.20**  
**(R)-enantiomer**

**(R)-6,7-Dihydro-5H-cyclopenta[*b*]pyridin-5-ol, complexed with borane (3.20, Table 28);** (*S*)-*B*-Me-CBS, 1 M solution in toluene (various number of eq, see table below) and *N,N*-diethylaniline-borane complex (various number of eq, see table below) were dissolved in toluene (1 mL) under a nitrogen atmosphere. To this solution was added a solution of 6,7-dihydro-5H-cyclopenta[*b*]pyridin-5-one (various number of eq, see table below) in 1 mL of toluene dropwise over 5 min. The resulting reaction mixture was stirred at room temperature for 2 h. MeOH (1 mL) and a 1 N HCl aqueous solution (1 mL) were added. The resulting reaction mixture was stirred at room temperature for 30 min. EtOAc (5 mL) and water (5 mL) were added. The organic layer was partitioned and the aqueous layer was further extracted with EtOAc (5 mL). The organic extracts were combined, dried by filtration through a hydrophobic frit and concentrated *in vacuo*. The residue obtained was purified on silica using a 0-100% EtOAc-cyclohexane gradient to

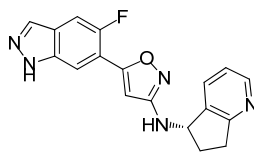
afford the title compound as a yellow oil; see **table below** for yield; LCMS (acidic conditions) (ES +ve)  $m/z$  136 ( $[M-BH_3]+H$ )<sup>+</sup>,  $R_t$  = 0.70 min; **chiral HPLC** (see Analytical chiral HPLC method 3)  $R_t$  = 31.2 min, e.e. = **see table below** (the other enantiomer had a  $R_t$  of 37.8 min); **<sup>1</sup>H NMR** (400 MHz, DMSO- $d_6$ ):  $\delta$  = 8.47 (d,  $J$  = 5.6 Hz, 1H), 8.05 (d,  $J$  = 7.6 Hz, 1H), 7.52 (dd,  $J$  = 7.6, 5.6 Hz, 1H), 5.67 (d,  $J$  = 6.4 Hz, 1H), 5.19 - 5.15 (m, 1H), 3.25 - 3.14 (m, 1H), 3.04 - 2.91 (m, 1H), 2.54 - 2.05 (br. s, 3H), 2.49 - 2.41 (m, 1H), 1.94 - 1.81 ppm (m, 1H).

| <b>Entry</b> | <b>6,7-Dihydro-5H-cyclopenta[<i>b</i>]pyridin-5-one</b> | <b><i>N,N</i>-Diethylaniline-borane</b> | <b>(<i>S</i>)-<i>B</i>-Me-CBS</b>        | <b>Yield</b>   | <b>e.e.</b> |
|--------------|---|---|--|----------------|-------------|
| <b>1</b>     | 300 mg<br>2.253 mmol                                    | <b>2 eq</b><br>0.801 mL<br>4.51 mmol    | <b>0.06 eq</b><br>0.135 mL<br>0.135 mmol | 64%<br>215 mg  | 74%         |
| <b>2</b>     | 100 mg<br>0.751 mmol                                    | <b>1.1 eq</b><br>0.147 mL<br>0.826 mmol | <b>1.1 eq</b><br>0.826 mL<br>0.826 mmol  | 31%<br>35 mg   | 96.4%       |
| <b>3</b>     | 100 mg<br>0.751 mmol                                    | <b>2 eq</b><br>0.267 mL<br>1.502 mmol   | <b>2 eq</b><br>1.502 mL<br>1.502 mmol    | 66%<br>73.5 mg | 96.4%       |



3.40

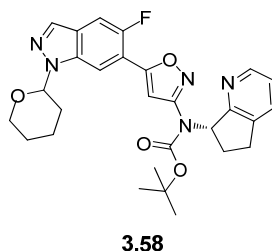
*tert*-Butyl ((*S*)-6,7-dihydro-5*H*-cyclopenta[*b*]pyridin-5-yl)(5-(5-fluoro-1-(tetrahydro-2*H*-pyran-2-yl)-1*H*-indazol-6-yl)isoxazol-3-yl)carbamate, complexed with borane (3.40, from Scheme 24); To a stirred solution of *tert*-butyl (5-(5-fluoro-1-(tetrahydro-2*H*-pyran-2-yl)-1*H*-indazol-6-yl)isoxazol-3-yl)carbamate (54.7 mg, 0.136 mmol), 6,7-dihydro-5*H*-cyclopenta[*b*]pyridin-5-ol, complexed with borane (17.5 mg, 0.117 mmol, (*R*)-enantiomer 3.20 from Table 28, entry 2, e.e. = 96.4%) and triphenylphosphine (67.9 mg, 0.259 mmol) in THF (2 mL) was added DIAD (0.051 mL, 0.259 mmol) dropwise at room temperature. The resulting reaction mixture was stirred at room temperature for 1 h and diluted with EtOAc (4 mL), water (4 mL) and brine. The organic phase was separated and the aqueous layer was further extracted with EtOAc (4 mL). The organic extracts were combined, dried by filtration through a hydrophobic frit and concentrated *in vacuo*. The residue obtained was purified on silica using a 0-60% TBME-cyclohexane to afford the title compound as a white solid; compound was progressed without further purification in the next synthetic step (46 mg); LCMS (acidic conditions) (ES +ve) *m/z* 520 ([M-BH<sub>3</sub>]+H)<sup>+</sup>, Rt = 1.49 min.



**3.17b,**  
**(S)-enantiomer**

**(S)-N-(6,7-Dihydro-5H-cyclopenta[*b*]pyridin-5-yl)-5-(5-fluoro-1H-indazol-6-yl)isoxazol-3-amine (3.17b, (S)-enantiomer, from Scheme 24);** To a solution of *tert*-butyl (6,7-dihydro-5H-cyclopenta[*b*]pyridin-5-yl)(5-(5-fluoro-1-(tetrahydro-2H-pyran-2-yl)-1H-indazol-6-yl)isoxazol-3-yl)carbamate, complexed with borane (45 mg, 0.084 mmol, **3.40, obtained in the experiment described just above**) in EtOH (4 mL) was added a 3 M HCl solution in MeOH (0.144 mL, 0.433 mmol). The resulting reaction mixture was stirred at 50 °C for 16 h. The reaction mixture was cooled to room temperature, a 3 M HCl solution in MeOH (0.144 mL, 0.433 mmol) was added and the resulting mixture was stirred at 70 °C for 12 h. The reaction mixture was concentrated *in vacuo* and the residue was purified by MDAP (acidic conditions), to afford the title compound as a white solid; yield over 2 steps 14% (5.3 mg); **LCMS** (acidic conditions) (ES +ve) *m/z* 336 (M+H)<sup>+</sup>, Rt = 0.70 min; **chiral HPLC** (see Analytical chiral HPLC method 1) Rt = 16.8 min, e.e. = 95.7%; **<sup>1</sup>H NMR** (400 MHz, DMSO-*d*<sub>6</sub>): δ = 13.42 (br. s, 1H), 8.41 (d, *J* = 4.9 Hz, 1H), 8.16 (s, 1H), 7.99 (d, *J* = 5.9 Hz, 1H), 7.80 - 7.72 (m, 2H), 7.20 (dd, *J* = 7.5, 4.9 Hz, 1H), 6.80 (d, *J* = 8.1 Hz, 1H), 6.38 (d, *J* = 4.4 Hz, 1H), 5.11 - 5.07 (m, 1H), 3.08 - 2.98 (m, 1H), 2.97 - 2.87 (m, 1H), 2.63 - 2.53 (m, 1H), 2.01 - 1.89 ppm (m, 1H); **<sup>13</sup>C NMR** (101 MHz, DMSO-*d*<sub>6</sub>): δ = 165.0, 164.4, 162.1, 153.7 (d, *J* = 241.3 Hz), 149.3, 137.8, 137.0, 134.2, 132.7, 123.5 (d, *J* = 10.3 Hz), 122.0, 115.4 (d, *J* = 17.6 Hz), 108.9, 106.5 (d, *J* = 24.2 Hz), 96.6 (d, *J* = 11.0 Hz), 56.5, 32.0, 31.8 ppm; **HRMS** (ES +ve) calcd for C<sub>18</sub>H<sub>15</sub>FN<sub>5</sub>O (M+H)<sup>+</sup> 336.1255, found 336.1257; **IR** ν (cm<sup>-1</sup>) 3172, 1561; **mp** 210.6 - 212.4 °C.

**Optimisation of the Mitsunobu reaction: Investigation of the amount of triphenylphosphine and DIAD (Table 29):**



***tert*-Butyl** ((*S*)-6,7-dihydro-5*H*-cyclopenta[*b*]pyridin-7-yl)(5-(5-fluoro-1-(tetrahydro-2*H*-pyran-2-yl)-1*H*-indazol-6-yl)isoxazol-3-yl)carbamate (**3.58**); To a stirred solution of *tert*-butyl (5-(5-fluoro-1-(tetrahydro-2*H*-pyran-2-yl)-1*H*-indazol-6-yl)isoxazol-3-yl)carbamate **3.39** (100 mg, 0.248 mmol), (*R*)-6,7-dihydro-5*H*-cyclopenta[*b*]pyridin-7-ol (33.6 mg, 0.248 mmol, **e.e.** > **99.9%**) and triphenylphosphine (various number of eq, **see table below**) in THF (5 mL) was added a solution of DIAD (various number of eq, **see table below**) in THF (3 mL) dropwise at room temperature. The resulting reaction mixture was stirred at room temperature for 18 h. The reaction mixture was diluted with EtOAc (4 mL), water (4 mL) and brine (2 mL). The organic layer was separated and the aqueous layer was further extracted with EtOAc (4 mL). The organic extracts were combined, dried by filtration through a hydrophobic frit and concentrated *in vacuo*. The residue obtained was purified on silica using a 0-60% TBME-cyclohexane gradient to afford two fractions: the recovered starting *tert*-butyl (5-(5-fluoro-1-(tetrahydro-2*H*-pyran-2-yl)-1*H*-indazol-6-yl)isoxazol-3-yl)carbamate **3.39**, **see table below** for yield; and the title compound contaminated with various amounts of diisopropyl hydrazine-1,2-dicarboxylate **3.59**, **see table below** for estimated yield of **3.58** from NMR ratio.



| Entry | PPh <sub>3</sub> used         | DIAD used                     | Yield of 3.39 recovered | Amount and molar ratio of product 3.58:by-product 3.59 (determined by <sup>1</sup> H NMR) | Estimated yield of 3.58 |
|-------|-------------------------------|-------------------------------|-------------------------|---|-------------------------|
| 1     | 2 eq<br>0.497 mmol<br>130 mg  | 2 eq<br>0.497 mmol<br>98 μL   | 56%<br>56 mg            | 93 mg<br>ratio = 1:4  | 28%                     |
| 2     | 3 eq<br>0.745 mmol<br>196 mg  | 3 eq<br>0.745 mmol<br>146 μL  | 50%<br>50 mg            | 153 mg<br>ratio = 1:7   | 32%                     |
| 3     | 10 eq<br>2.485 mmol<br>652 mg | 10 eq<br>2.485 mmol<br>488 μL | 56%<br>56 mg            | 443 mg<br>ratio = 1:31  | 28%                     |

- *tert*-Butyl (5-(5-fluoro-1-(tetrahydro-2*H*-pyran-2-yl)-1*H*-indazol-6-yl)isoxazol-3-yl)carbamate **3.39** recovered; LCMS (acidic conditions) (ES +ve) *m/z* 403 (M+H)<sup>+</sup>, Rt = 1.32 min; <sup>1</sup>H NMR (400 MHz, DMSO-*d*<sub>6</sub>): δ = 10.51 (br. s, 1H), 8.32 (d, *J* = 5.9 Hz, 1H), 8.21 (s, 1H), 7.83 (d, *J* = 11.0 Hz, 1H), 7.16 (d, *J* = 4.2 Hz, 1H), 6.07 (dd, *J* = 9.5, 2.2 Hz, 1H), 3.93 - 3.78 (m, 2H), 2.47 - 2.32 (m, 1H), 2.10 - 1.95 (m, 2H), 1.84 - 1.71 (m, 1H), 1.65 - 1.56 (m, 2H), 1.50 ppm (s, 9H).

#### Entry 1:

- The title compound **3.58** contaminated with diisopropyl hydrazine-1,2-dicarboxylate **3.59**; 93 mg; LCMS (acidic conditions) (ES +ve) *m/z* 520 (M+H)<sup>+</sup>, Rt = 1.42 min; <sup>1</sup>H NMR (400 MHz, DMSO-*d*<sub>6</sub>): δ = 8.87 (br. s, 8H, **by-product 3.59**), 8.37 - 8.29 (m, 2H), 8.22 (s, 1H), 7.84 (d, *J* = 11.0 Hz, 1H), 7.67 (d, *J* = 7.1 Hz, 1H), 7.29 - 7.17 (m, 2H), 5.99 (m, 2H), 4.85 - 4.71 (m, 8H, **by-product 3.59**), 3.92 - 3.76 (m, 2H), 3.07 - 2.90 (m, 2H), 2.69 - 2.57 (m, 1H), 2.46 - 2.30 (m, 2H), 2.10 - 1.96 (m, 2H), 1.87 - 1.70 (m, 1H), 1.64 - 1.54 (m, 2H), 1.25 (d, *J* = 3.4 Hz, 9H), 1.22 - 1.14 ppm (m, 48H, **by-product 3.59**).

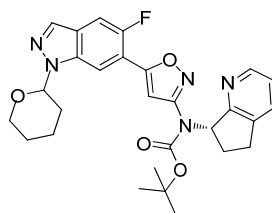
**Entry 2:**

- The title compound **3.58** contaminated with diisopropyl hydrazine-1,2-dicarboxylate **3.59**; 153 mg; LCMS (acidic conditions) (ES +ve)  $m/z$  520 (M+H)<sup>+</sup>, Rt = 1.42 min; <sup>1</sup>H NMR (400 MHz, DMSO-d<sub>6</sub>): δ = 8.87 (br. s, 14H, **by-product 3.59**), 8.37 - 8.29 (m, 2H), 8.22 (s, 1H), 7.84 (d,  $J$  = 11.2 Hz, 1H), 7.67 (d,  $J$  = 7.3 Hz, 1H), 7.27 - 7.18 (m, 2H), 6.08 - 5.95 (m, 2H), 4.85 - 4.71 (m, 14H, **by-product 3.59**), 3.92 - 3.77 (m, 2H), 3.07 - 2.90 (m, 2H), 2.70 - 2.56 (m, 1H), 2.47 - 2.31 (m, 2H), 2.09 - 1.96 (m, 2H), 1.87 - 1.70 (m, 1H), 1.64 - 1.54 (m, 2H), 1.25 (d,  $J$  = 3.2 Hz, 9H), 1.22 - 1.12 ppm (m, 84H, **by-product 3.59**).

**Entry 3:**

- The title compound **3.58** contaminated with diisopropyl hydrazine-1,2-dicarboxylate **3.59**; 443 mg; LCMS (acidic conditions) (ES +ve)  $m/z$  520 (M+H)<sup>+</sup>, Rt = 1.42 min; <sup>1</sup>H NMR (400 MHz, DMSO-d<sub>6</sub>): δ = 8.86 (br. s, 62H, **by-product 3.59**), 8.37 - 8.28 (m, 2H), 8.21 (s, 1H), 7.84 (d,  $J$  = 11.0 Hz, 1H), 7.67 (d,  $J$  = 7.6 Hz, 1H), 7.27 - 7.17 (m, 2H), 6.09 - 5.94 (m, 2H), 4.85 - 4.71 (m, 62H, **by-product 3.59**), 3.93 - 3.76 (m, 2H), 3.11 - 2.89 (m, 2H), 2.65 - 2.58 (m, 1H), 2.45 - 2.31 (m, 2H), 2.10 - 1.90 (m, 2H), 1.88 - 1.69 (m, 1H), 1.66 - 1.54 (m, 2H), 1.25 (d,  $J$  = 3.2 Hz, 9H), 1.19 ppm (d,  $J$  = 6.4 Hz, 372H, **by-product 3.59**).

**Optimisation of the Mitsunobu reaction: Investigation of the amount of triphenylphosphine and azodicarboxylic dipiperidide (ADDP, Table 31):**

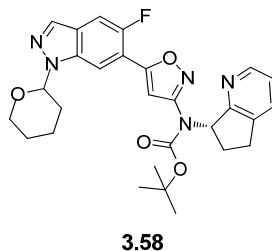


**3.58**

**tert-Butyl ((S)-6,7-dihydro-5H-cyclopenta[b]pyridin-7-yl)(5-(5-fluoro-1-(tetrahydro-2H-pyran-2-yl)-1H-indazol-6-yl)isoxazol-3-yl)carbamate (3.58);** To a stirred solution of *tert*-butyl (5-(5-fluoro-1-(tetrahydro-2H-pyran-2-yl)-1H-indazol-6-yl)isoxazol-3-yl)carbamate (100 mg, 0.248 mmol), (*R*)-6,7-dihydro-5H-cyclopenta[b]pyridin-7-ol (33.6 mg, 0.248 mmol, **e.e.** > **99.9%**) and triphenylphosphine (various number of eq, **see table below**) in THF (5 mL) was added a solution of azodicarboxylic dipiperidide (various number of eq, **see table below**) in THF (3 mL) dropwise at room temperature. The resulting reaction mixture was stirred at room temperature for 18 h. The reaction mixture was diluted with EtOAc (4 mL), water (4 mL) and brine (2 mL). The organic layer was separated and the aqueous layer was further extracted with EtOAc (4 mL). The organic extracts were combined, dried by filtration through a hydrophobic frit and concentrated *in vacuo*. The residue obtained was purified on silica using a 0-60% TBME-cyclohexane gradient to the title compound **3.58**, **see table below** for yield; **LCMS** (acidic conditions) (ES +ve) *m/z* 520 (M+H)<sup>+</sup>, *Rt* = 1.42 min; **chiral HPLC** (see Analytical chiral HPLC method 4) *Rt* = 11.0 min (one peak for the 2 wanted diastereoisomers; the two diastereoisomers which contained the unwanted indoline stereogenic centre were observed as two peaks, eluting at 15.7 and 16.6 min, respectively), **d.e.** = **see table below**; **<sup>1</sup>H NMR** (400 MHz, DMSO-*d*<sub>6</sub>): δ = 8.38 - 8.28 (m, 2H), 8.22 (s, 1H), 7.84 (d, *J* = 11.0 Hz, 1H), 7.67 (d, *J* = 7.3 Hz, 1H), 7.29 - 7.18 (m, 2H), 6.10 - 5.95 (m, 2H), 3.93 - 3.75 (m, 2H), 3.11 - 2.90 (m, 2H), 2.70 - 2.57 (m, 1H), 2.47 - 2.31 (m, 2H), 2.11 - 1.95 (m, 2H), 1.86 - 1.69 (m, 1H), 1.65 - 1.54 (m, 2H), 1.25 ppm (d, *J* = 3.4 Hz, 9H).

| Entry | PPh <sub>3</sub> used         | ADDP used                     | Yield of 3.58  | d.e. of 3.58 |
|-------|-------------------------------|-------------------------------|----------------|--------------|
| 1     | 2 eq<br>0.497 mmol<br>130 mg  | 2 eq<br>0.497 mmol<br>125 mg  | 0%             | NA           |
| 2     | 3 eq<br>0.745 mmol<br>196 mg  | 3 eq<br>0.745 mmol<br>188 mg  | 29%<br>37.8 mg | 98.9%        |
| 3     | 10 eq<br>2.485 mmol<br>652 mg | 10 eq<br>2.485 mmol<br>627 mg | 57%<br>74 mg   | 98.6%        |

**Optimisation of the Mitsunobu reaction: Investigation of the solvent (Table 32):**

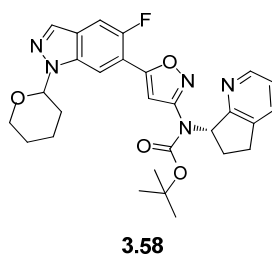


**tert-Butyl ((S)-6,7-dihydro-5H-cyclopenta[b]pyridin-7-yl)(5-(5-fluoro-1-(tetrahydro-2H-pyran-2-yl)-1H-indazol-6-yl)isoxazol-3-yl)carbamate (3.58);** To a stirred solution of *tert*-butyl (5-(5-fluoro-1-(tetrahydro-2H-pyran-2-yl)-1H-indazol-6-yl)isoxazol-3-yl)carbamate (100 mg, 0.248 mmol), (*R*)-6,7-dihydro-5H-cyclopenta[b]pyridin-7-ol (33.6 mg, 0.248 mmol, **e.e.** > **99.9%**) and triphenylphosphine (391 mg, 1.491 mmol) in solvent (5 mL, **see table below**) was added a solution of azodicarboxylic dipiperidide (376 mg, 1.491 mmol) in solvent (3 mL, **see table below**) dropwise at room temperature. The resulting reaction mixture was stirred at room temperature for 18 h. The reaction mixture was diluted with EtOAc (4 mL), water (4 mL) and brine (2 mL). The organic layer was separated and the aqueous layer was further extracted with EtOAc (4 mL). The organic extracts were combined, dried by filtration through a hydrophobic frit and concentrated *in vacuo*. The residue obtained

was purified on silica using a 0-60% TBME-cyclohexane gradient to afford the title compound **3.58**, see table below for yield; see p. 330 for the analytical description of the compound; d.e. = see table below.

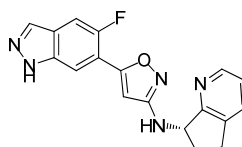
| Entry | Solvent used | Yield of 3.58  | d.e. of 3.58 |
|-------|--------------|----------------|--------------|
| 1     | 2-MeTHF      | 59%<br>76.6 mg | 98.9%        |
| 2     | Toluene      | 70%<br>90.7 mg | 99.1%        |
| 3     | DCM          | 0%             | NA           |

**Scale-up of the Mitsunobu reaction, with the optimised conditions (Scheme 27):**



***tert*-Butyl ((S)-6,7-dihydro-5H-cyclopenta[b]pyridin-7-yl)(5-(5-fluoro-1-(tetrahydro-2H-pyran-2-yl)-1H-indazol-6-yl)isoxazol-3-yl)carbamate (3.58)** (from Scheme 27); To a stirred solution of *tert*-butyl (5-(5-fluoro-1-(tetrahydro-2H-pyran-2-yl)-1H-indazol-6-yl)isoxazol-3-yl)carbamate (5.00 g, 12.42 mmol), (*R*)-6,7-dihydro-5H-cyclopenta[b]pyridin-7-ol (1.68 g, 12.42 mmol, e.e. > 99.9%) and triphenylphosphine (19.55 g, 74.5 mmol) in THF (150 mL) was added a solution of azodicarboxylic dipiperidide (18.81 g, 74.5 mmol) in THF (100 mL) dropwise at 0 °C. The resulting reaction mixture was stirred at room temperature for 21 h. The reaction mixture was diluted with EtOAc (200 mL), water (200 mL) and brine (50 mL). The organic layer was separated and the aqueous layer was further extracted with EtOAc (2 x 200 mL). The organic extracts were combined, washed with water (100 mL), washed with brine, dried by filtration through a hydrophobic frit and concentrated *in vacuo*. The residue obtained

was taken up in DCM (70 mL) and a solid precipitated. The mixture was filtered and the cake rinsed with DCM (20 mL). The filtrate obtained was purified on silica using a 0-60% TBME-cyclohexane gradient to afford the title compound **3.58**, yield 58% (3.71 g); see p. 330 for the analytical description of the compound; d.e. = 99.0%.

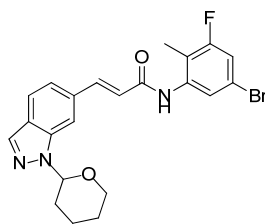


**3.16a,**  
**(S)-enantiomer**  
e.e. = 99.3%

**(S)-N-(6,7-Dihydro-5H-cyclopenta[b]pyridin-7-yl)-5-(5-fluoro-1H-indazol-6-yl)isoxazol-3-amine (3.16a, (S)-enantiomer)**; To a stirred solution of *tert*-butyl ((S)-6,7-dihydro-5H-cyclopenta[b]pyridin-7-yl)(5-(5-fluoro-1-(tetrahydro-2H-pyran-2-yl)-1H-indazol-6-yl)isoxazol-3-yl)carbamate (3.71 g, 7.14 mmol, d.e. = 99.0%, obtained in the experiment described just above) in EtOH (50 mL) was added a 3 M HCl solution in MeOH (23.80 mL, 71.4 mmol) at room temperature. The reaction mixture was then stirred at 75 °C for 7 h. The reaction mixture was concentrated *in vacuo*. The residue was diluted with 2-MeTHF (100 mL), water (100 mL) and a saturated NaHCO<sub>3</sub> aqueous solution (100 mL). The organic layer was separated and the aqueous layer was further extracted with 2-MeTHF (3 x 80 mL). The organic extracts were combined, washed with water (100 mL), brine (100 mL), dried by filtration through a hydrophobic frit and concentrated *in vacuo*. The residue obtained was dissolved in DMSO (40 mL) and to this solution was added water (100 mL). Upon the water addition, a white solid precipitated out of solution. The solid was recovered by filtration, washed with water (60 mL) and with TBME (60 mL) to afford the title compound as a white solid; yield 88% (2.10 g); **LCMS** (acidic conditions) (ES +ve) *m/z* 336 (M+H)<sup>+</sup>, Rt = 0.76 min; **chiral HPLC** (see Analytical chiral HPLC method 5) Rt = 16.0 min, e.e. = 99.3% (the other enantiomer

had a Rt of 34.7 min); **<sup>1</sup>H NMR** (400 MHz, DMSO-d<sub>6</sub>): δ = 13.41 (br. s, 1H), 8.40 (d, *J* = 4.9 Hz, 1H), 8.15 (s, 1H), 7.97 (d, *J* = 5.6 Hz, 1H), 7.76 (d, *J* = 11.2 Hz, 1H), 7.70 (dd, *J* = 7.6, 1.0 Hz, 1H), 7.25 (dd, *J* = 7.6, 4.9 Hz, 1H), 6.71 (d, *J* = 7.1 Hz, 1H), 6.46 (d, *J* = 4.4 Hz, 1H), 4.98 - 4.93 (m, 1H), 3.04 - 2.93 (m, 1H), 2.92 - 2.81 (m, 1H), 2.69 - 2.56 (m, 1H), 2.01 - 1.86 ppm (m, 1H); **<sup>13</sup>C NMR** (101 MHz, DMSO-d<sub>6</sub>): δ = 165.2, 163.7, 161.7, 153.8 (d, *J* = 241.3 Hz), 148.2, 136.9, 136.8, 134.3, 133.2, 123.4 (d, *J* = 10.3 Hz), 123.0, 115.5 (d, *J* = 18.3 Hz), 108.8, 106.4 (d, *J* = 24.2 Hz), 96.9 (d, *J* = 11.0 Hz), 58.5, 32.3, 27.7 ppm; **HRMS** (ES +ve) calcd for C<sub>18</sub>H<sub>15</sub>FN<sub>5</sub>O (M+H)<sup>+</sup> 336.1255, found 336.1266; **IR** ν (cm<sup>-1</sup>) 3170, 1543; **mp** 235.2 - 237.1 °C.

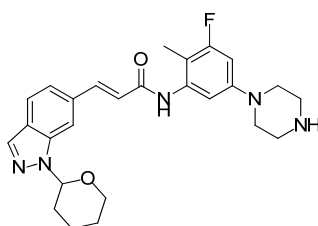
#### 4.5. Experimental preparation of the cinnamide analogues for the mPTP programme



3.104

**(E)-N-(5-Bromo-3-fluoro-2-methylphenyl)-3-(1-(tetrahydro-2H-pyran-2-yl)-1H-indazol-6-yl)acrylamide (3.104)**; To a stirred solution of (*E*)-3-(1-(tetrahydro-2H-pyran-2-yl)-1H-indazol-6-yl)acrylic acid (500 mg, 1.836 mmol) in DMF (10 mL) was added HATU (838 mg, 2.203 mmol) and *N,N*-diisopropylethylamine (0.8 mL, 4.59 mmol) at room temperature. The resulting solution was stirred for 10 min at room temperature and 5-bromo-3-fluoro-2-methylaniline (0.497 mL, 2.75 mmol) pre-dissolved in DMF (2 mL) was added dropwise. The resulting reaction mixture was stirred at room temperature for 18 h. HATU (400 mg, 1.05 mmol) and *N,N*-diisopropylethylamine (0.4 mL, 2.29 mmol) were added and the resulting solution was stirred at 50 °C for 24 h. The reaction mixture was diluted with water (20 mL) and EtOAc (20 mL). The organic layer was separated and the aqueous layer was further extracted with EtOAc (2 x 20 mL). The organic extracts were combined, washed with brine (20 mL), dried by filtration through a hydrophobic frit and concentrated *in vacuo*. The residue obtained was purified on silica using a 0-50% EtOAc-cyclohexane gradient to afford the title compound as a white solid; yield 35% (842 mg); LCMS (acidic conditions) (ES +ve) *m/z* 458, 460 (M+H)<sup>+</sup>, Rt = 1.36 min; <sup>1</sup>H NMR (400 MHz, DMSO-d<sub>6</sub>): δ = 9.75 (br. s, 1H), 8.15 (s, 1H), 8.04 (s, 1H), 7.89 - 7.82 (m, 2H), 7.78 (d, *J* = 15.7 Hz, 1H), 7.49 (dd, *J* = 8.3, 0.7 Hz, 1H), 7.33 (dd, *J* = 9.2, 1.8 Hz, 1H), 7.12 (d, *J* = 15.7 Hz, 1H), 5.91 (dd, *J* = 9.5, 2.2 Hz, 1H), 3.96 - 3.87 (m, 1H), 3.84 - 3.73 (m, 1H), 2.48 - 2.39 (m, 1H), 2.16 (d, *J* = 2.0 Hz, 3H), 2.12 - 2.03 (m, 1H), 2.03 - 1.95 (m, 1H), 1.83 - 1.70 (m, 1H), 1.67 - 1.57 ppm (m, 2H).





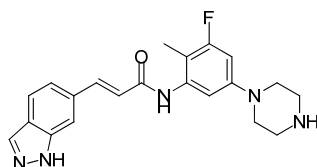
3.105

**(E)-N-(3-Fluoro-2-methyl-5-(piperazin-1-yl)phenyl)-3-(1-(tetrahydro-2H-pyran-2-yl)-1H-indazol-6-yl)acrylamide (3.105)**; Three reaction conditions investigated (**Table 37**):

- i) *(E)-N*-(5-Bromo-3-fluoro-2-methylphenyl)-3-(1-(tetrahydro-2H-pyran-2-yl)-1H-indazol-6-yl)acrylamide (30 mg, 0.065 mmol), Pd<sub>2</sub>(dba)<sub>3</sub> (6 mg, 6.55 μmol), XantPhos (7.6 mg, 0.013 mmol), piperazine (8.5 mg, 0.098 mmol) and NaO<sup>t</sup>Bu (9.4 mg, 0.098 mmol) were added to a reaction tube. The tube was sealed, degassed and back-filled with nitrogen. This operation was repeated 3 times. Toluene (2 mL) was added to the mixture under nitrogen. The reaction mixture was stirred at 80 °C for 5 hr. LCMS showed no trace of targeted product. The reaction mixture was then stirred at 110 °C for 12 h. LCMS showed no trace of targeted product and reaction was abandoned.
- ii) *(E)-N*-(5-Bromo-3-fluoro-2-methylphenyl)-3-(1-(tetrahydro-2H-pyran-2-yl)-1H-indazol-6-yl)acrylamide (30 mg, 0.065 mmol), Pd<sub>2</sub>(dba)<sub>3</sub> (6 mg, 6.55 μmol), RuPhos (6.1 mg, 0.013 mmol), piperazine (8.5 mg, 0.098 mmol) and NaO<sup>t</sup>Bu (9.4 mg, 0.098 mmol) were added to a reaction tube. The tube was sealed, degassed and back-filled with nitrogen. This operation was repeated 3 times. Toluene (2 mL) was added to the mixture under nitrogen. The reaction mixture was stirred at 80 °C for 5 hr, and then stirred at 110 °C for 12 h. The reaction mixture was cooled to room temperature and filtered through celite, washing with excess MeOH. The filtrate obtained was concentrated *in vacuo* and the residue was purified by MDAP (acidic conditions), to afford the title compound as a yellow gum; yield 43% (13 mg).

iii) (*E*)-*N*-(5-Bromo-3-fluoro-2-methylphenyl)-3-(1-(tetrahydro-2*H*-pyran-2-yl)-1*H*-indazol-6-yl)acrylamide (50 mg, 0.109 mmol), Pd<sub>2</sub>(dba)<sub>3</sub> (10 mg, 10.91 μmol), RuPhos (10.2 mg, 0.022 mmol), piperazine (14.1 mg, 0.164 mmol) and NaO<sup>t</sup>Bu (15.7 mg, 0.164 mmol) were added to a microwave vial. The tube was sealed, degassed and back-filled with nitrogen. This operation was repeated 3 times. Toluene (2 mL) was added to the mixture under nitrogen. The reaction mixture was heated in a microwave at 80 °C for 10 min. The reaction mixture was cooled to room temperature and diluted with water (2 mL) and EtOAc (2 mL). The organic layer was separated and the aqueous layer was further extracted with EtOAc (2 mL). The organic extracts were combined, concentrated *in vacuo* and the residue obtained was purified by MDAP (acidic conditions), to afford the title compound as a yellow gum; yield 16% (8 mg).

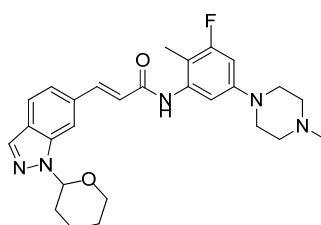
**LCMS** (acidic conditions) (ES +ve) *m/z* 464 (M+H)<sup>+</sup>, Rt = 0.86 min; **<sup>1</sup>H NMR** (400 MHz, DMSO-*d*<sub>6</sub>): δ = 9.58 (br. s, 1H), 8.32 (s, 1H), 8.15 (s, 1H), 8.00 (s, 1H), 7.84 (d, *J* = 8.3 Hz, 1H), 7.73 (d, *J* = 15.7 Hz, 1H), 7.48 (d, *J* = 8.3 Hz, 1H), 7.11 - 7.03 (m, 2H), 6.61 (dd, *J* = 13.2, 2.2 Hz, 1H), 5.90 (dd, *J* = 9.5, 2.4 Hz, 1H), 3.95 - 3.88 (m, 1H), 3.82 - 3.73 (m, 1H), 3.08 - 3.02 (m, 4H), 2.90 - 2.83 (m, 4H), 2.48 - 2.39 (m, 1H), 2.10 - 2.03 (m, 4H), 2.03 - 1.96 (m, 1H), 1.84 - 1.70 (m, 1H), 1.67 - 1.57 ppm (m, 2H).



**3.94**

**(*E*)-*N*-(3-Fluoro-2-methyl-5-(piperazin-1-yl)phenyl)-3-(1*H*-indazol-6-yl)acrylamide (3.94)**; To a suspension of (*E*)-*N*-(3-fluoro-2-methyl-5-(piperazin-1-yl)phenyl)-3-(1-(tetrahydro-2*H*-pyran-2-yl)-1*H*-indazol-6-yl)acrylamide (20 mg, 0.043 mmol) in EtOH (2 mL) was added a 4 M HCl solution in dioxane (0.108 mL, 0.431 mmol). The resulting reaction mixture was stirred at 50 °C for 4 h and then at room temperature for 16 h. The

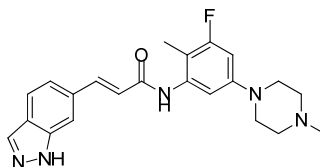
reaction mixture was concentrated *in vacuo* and the residue obtained was triturated with Et<sub>2</sub>O, filtered and the solid was purified by MDAP (acidic conditions), to afford the title compound as a pale orange solid, as the free base; yield 56% (9 mg); **LCMS** (acidic conditions) (ES +ve) *m/z* 380 (M+H)<sup>+</sup>, Rt = 0.72 min; **<sup>1</sup>H NMR** (400 MHz, DMSO-d<sub>6</sub>): δ = 13.21 (br. s, 1H), 9.55 (br. s, 1H), 8.30 (s, 1H), 8.11 (d, *J* = 0.7 Hz, 1H), 7.83 (d, *J* = 8.3 Hz, 1H), 7.77 (s, 1H), 7.72 (d, *J* = 15.7 Hz, 1H), 7.42 (d, *J* = 8.3 Hz, 1H), 7.10 (s, 1H), 7.06 (d, *J* = 15.7 Hz, 1H), 6.63 (dd, *J* = 13.2, 2.2 Hz, 1H), 3.16 - 3.08 (m, 4H), 2.98 - 2.90 (m, 4H), 2.06 ppm (d, *J* = 1.5 Hz, 3H).



**3.108**

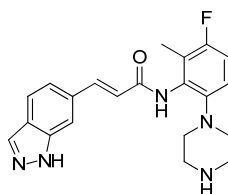
**(E)-N-(3-Fluoro-2-methyl-5-(4-methylpiperazin-1-yl)phenyl)-3-(1-(tetrahydro-2H-pyran-2-yl)-1H-indazol-6-yl)acrylamide (3.108);** (E)-N-(5-Bromo-3-fluoro-2-methylphenyl)-3-(1-(tetrahydro-2H-pyran-2-yl)-1H-indazol-6-yl)acrylamide (100 mg, 0.218 mmol), Pd<sub>2</sub>(dba)<sub>3</sub> (20 mg, 0.022 mmol), RuPhos (20.4 mg, 0.044 mmol), *N*-methylpiperazine (0.036 mL, 0.327 mmol) and NaO<sup>t</sup>Bu (31.5 mg, 0.327 mmol) were added to a reaction tube. The tube was sealed, degassed and back-filled with nitrogen. This operation was repeated 3 times. Toluene (2 mL) was added to the mixture under nitrogen. The reaction mixture was stirred at 110 °C under nitrogen for 3 h. The reaction mixture was cooled to room temperature and filtered through celite, washing with excess MeOH. The filtrate obtained was concentrated *in vacuo* and the residue was loaded with MeOH:DCM (1:1) on a strong cation exchange (SCX) cartridge, eluted with MeOH (3 x CV) and with a 2 M ammonia solution in MeOH (3 x CV). The basic methanolic fraction was concentrated *in vacuo* to afford the title compound as a brown gum;

compound was progressed without further purification in the next synthetic step (102 mg); **LCMS** (acidic conditions) (ES +ve)  $m/z$  478 (M+H)<sup>+</sup>, Rt = 0.85 min.



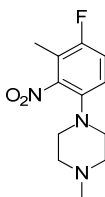
**3.109**

**(E)-N-(3-Fluoro-2-methyl-5-(4-methylpiperazin-1-yl)phenyl)-3-(1H-indazol-6-yl)acrylamide (3.109)**; To a suspension of (*E*)-*N*-(3-fluoro-2-methyl-5-(4-methylpiperazin-1-yl)phenyl)-3-(1-(tetrahydro-2*H*-pyran-2-yl)-1*H*-indazol-6-yl)acrylamide (102 mg, 0.214 mmol) in EtOH (2 mL) was added a 4 M HCl solution in dioxane (0.534 mL, 2.136 mmol). The resulting reaction mixture was stirred at 50 °C for 4 h. The reaction mixture was cooled to room temperature and filtered to remove the solid. The filtrate was concentrated *in vacuo* and the residue was purified by MDAP (acidic conditions), to afford the title compound as an off-white solid, as the formate salt; yield over 2 steps 21% (19.9 mg); **LCMS** (acidic conditions) (ES +ve)  $m/z$  394 (M+H)<sup>+</sup>, Rt = 0.72 min; **<sup>1</sup>H NMR** (400 MHz, DMSO-*d*<sub>6</sub>): δ = 13.24 (br. s, 1H), 9.52 (br. s, 1H), 8.24 (s, 1H, *formic acid*), 8.11 (d, *J* = 0.7 Hz, 1H), 7.82 (d, *J* = 8.6 Hz, 1H), 7.76 (s, 1H), 7.73 (d, *J* = 15.7 Hz, 1H), 7.42 (d, *J* = 8.6 Hz, 1H), 7.09 (s, 1H), 7.05 (d, *J* = 15.7 Hz, 1H), 6.62 (dd, *J* = 13.1, 2.3 Hz, 1H), 3.16 - 3.06 (m, 4H), 2.48 - 2.41 (m, 4H), 2.22 (s, 3H), 2.05 ppm (d, *J* = 1.7 Hz, 3H).



**3.91**

**(E)-N-(3-Fluoro-2-methyl-6-(piperazin-1-yl)phenyl)-3-(1H-indazol-6-yl)acrylamide (3.91)**;<sup>154</sup> as the hydrochloride salt; LCMS (outsourcing partner basic conditions) (ES +ve)  $m/z$  380 (M+H)<sup>+</sup>, Rt = 1.07 min; <sup>1</sup>H NMR (400 MHz, DMSO-d<sub>6</sub>): δ = 9.69 (br. s, 1H), 9.34 (br. s, 2H, piperazine NH<sub>2</sub><sup>+</sup>), 8.11 (s, 1H), 7.82 (d, *J* = 8.3 Hz, 1H), 7.80 (s, 1H), 7.74 (d, *J* = 15.7 Hz, 1H), 7.45 (d, *J* = 8.3 Hz, 1H), 7.28 (d, *J* = 15.7 Hz, 1H), 7.15 - 7.06 (m, 1H), 7.04 - 6.97 (m, 1H), 3.28 - 3.12 (m, 4H), 3.05 - 2.92 (m, 4H), 2.03 ppm (s, 3H), indazole NH was not observed.



**3.111**

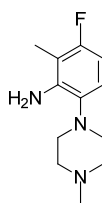
**1-(4-Fluoro-3-methyl-2-nitrophenyl)-4-methylpiperazine (3.111)**; Two reaction conditions investigated (**Table 38**):

i) 1-Bromo-4-fluoro-3-methyl-2-nitrobenzene (1.50 g, 6.41 mmol), Pd<sub>2</sub>(dba)<sub>3</sub> (0.59 g, 0.641 mmol), RuPhos (0.60 g, 1.282 mmol) and NaO<sup>t</sup>Bu (0.92 g, 9.61 mmol) were added to a microwave vial. Toluene (15 mL) and *N*-methylpiperazine (1.07 mL, 9.61 mmol) were added to the reaction mixture. The reaction mixture was heated in a microwave at 120 °C for 20 min. The reaction mixture was cooled to room temperature and filtered through celite, washing with excess MeOH. The filtrate obtained was concentrated *in vacuo* and the residue was loaded with MeOH on an ion-exchange SCX

cartridge, eluted with MeOH (3 x CV) and with a 2 M ammonia solution in MeOH (3 x CV). The basic methanolic fraction was concentrated *in vacuo* and the residue obtained was purified on silica using a 0-50% MeOH-TBME gradient to afford the title compound as a brown solid; yield 35% (565 mg).

ii) 1-Bromo-4-fluoro-3-methyl-2-nitrobenzene (1.84 g, 7.86 mmol), Pd(OAc)<sub>2</sub> (0.27 g, 1.179 mmol), BINAP (0.98 g, 1.572 mmol), and NaO<sup>t</sup>Bu (1.13 g, 11.79 mmol) were added to a microwave vial. Toluene (15 mL) and *N*-methylpiperazine (1.31 mL, 11.79 mmol) were added to the reaction mixture. The reaction mixture was heated in a microwave at 120 °C for 60 min. The reaction mixture was cooled to room temperature and loaded with MeOH on an ion-exchange SCX cartridge, eluted with MeOH (3 x CV) and with a 2 M ammonia solution in MeOH (3 x CV). The basic methanolic fraction was concentrated *in vacuo* and the residue obtained was purified on silica using a 0-25% MeOH (+1% triethylamine)-TBME gradient to afford the title compound as a brown solid; yield 59% (1.18 g).

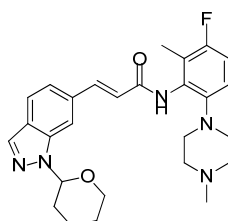
LCMS (acidic conditions) (ES +ve)  $m/z$  254 (M+H)<sup>+</sup>, Rt = 0.69 min; <sup>1</sup>H NMR (400 MHz, DMSO-d<sub>6</sub>): δ = 7.48 - 7.40 (m, 2H), 2.91 - 2.79 (m, 4H), 2.43 - 2.30 (m, 4H), 2.19 (s, 3H), 2.12 ppm (d, *J* = 2.0 Hz, 3H).



**3.112**

**3-Fluoro-2-methyl-6-(4-methylpiperazin-1-yl)aniline (3.112);** 1-(4-Fluoro-3-methyl-2-nitrophenyl)-4-methylpiperazine (1.75 g, 6.91 mmol) was dissolved in EtOH (50 mL) and tin(II) chloride dihydrate (6.24 g, 27.6 mmol) was added. The resulting reaction mixture was stirred at 70 °C for 12 h. Tin(II) chloride dihydrate (1.56 g, 6.91 mmol) was

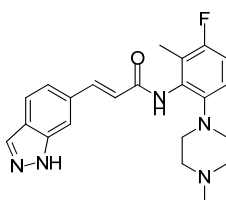
added and the resulting reaction mixture was stirred at 70 °C for 6 h. The reaction mixture was cooled to room temperature and solvents were evaporated *in vacuo*. The residue was taken up in EtOAc (100 mL), water (50 mL) and a saturated NaHCO<sub>3</sub> aqueous solution (20 mL). The insoluble materials were filtered and the solid was rinsed with excess EtOAc. The filtrate was concentrated *in vacuo* and the residue was purified on silica using a 0-50% MeOH-TBME gradient to afford the title compound as a brown solid; yield 66% (1.03 g); **LCMS** (acidic conditions) (ES +ve) *m/z* 224 (M+H)<sup>+</sup>, Rt = 0.55 min; **<sup>1</sup>H NMR** (400 MHz, DMSO-d<sub>6</sub>): δ = 6.82 (dd, *J* = 8.6, 5.9 Hz, 1H), 6.38 - 6.28 (m, 1H), 4.81 (br. s, 2H), 2.80 - 2.68 (m, 4H), 2.56 - 2.48 (m, 4H), 2.23 (s, 3H), 2.00 ppm (d, *J* = 1.5 Hz, 3H).



**3.113**

**(E)-N-(3-Fluoro-2-methyl-6-(4-methylpiperazin-1-yl)phenyl)-3-(1-(tetrahydro-2H-pyran-2-yl)-1H-indazol-6-yl)acrylamide (3.113)**; To a stirred solution of (E)-3-(1-(tetrahydro-2H-pyran-2-yl)-1H-indazol-6-yl)acrylic acid (113 mg, 0.416 mmol) in DMF (2 mL) was added HATU (263 mg, 0.693 mmol) and *N,N*-diisopropylethylamine (0.242 mL, 1.386 mmol) at room temperature. The resulting solution was stirred for 1 min and 3-fluoro-2-methyl-6-(4-methylpiperazin-1-yl)aniline (90 mg, 0.346 mmol) was added. The resulting reaction mixture was stirred at room temperature for 12 h. Water (5 mL) and EtOAc (5 mL) were added to the reaction mixture and the organic layer was separated. The aqueous layer was further extracted with EtOAc (5 mL). The organic extracts were combined, washed with brine (5 mL), dried by filtration through a hydrophobic frit and concentrated *in vacuo*. The residue was loaded with MeOH on an ion-exchange SCX cartridge, eluted with MeOH (3 x CV) and with a 2 M ammonia

solution in MeOH (3 x CV). The basic methanolic fraction was concentrated *in vacuo* and the residue obtained was purified on silica using a 0-50% MeOH-TBME gradient to afford the title compound as a yellow oil; yield 46% (76 mg); **LCMS** (acidic conditions) (ES +ve)  $m/z$  478 (M+H)<sup>+</sup>, Rt = 0.87 min; **<sup>1</sup>H NMR** (400 MHz, DMSO-d<sub>6</sub>): δ = 9.40 (br. s, 1H), 8.15 (s, 1H), 8.01 (s, 1H), 7.84 (d,  $J$  = 8.3 Hz, 1H), 7.75 (d,  $J$  = 15.7 Hz, 1H), 7.48 (d,  $J$  = 8.3 Hz, 1H), 7.20 - 7.03 (m, 2H), 7.02 - 6.94 (m, 1H), 5.89 (dd,  $J$  = 9.5, 2.2 Hz, 1H), 3.96 - 3.86 (m, 1H), 3.83 - 3.71 (m, 1H), 2.79 (br. s, 4H), 2.49 - 2.41 (m, 5H), 2.19 (s, 3H), 2.08 - 2.01 (m, 4H), 2.00 - 1.96 (m, 1H), 1.81 - 1.72 (m, 1H), 1.66 - 1.58 ppm (m, 2H).

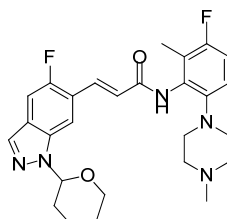


**3.114**

**(*E*)-*N*-(3-Fluoro-2-methyl-6-(4-methylpiperazin-1-yl)phenyl)-3-(1*H*-indazol-6-yl)acrylamide (3.114)**; To a suspension of (*E*)-*N*-(3-fluoro-2-methyl-6-(4-methylpiperazin-1-yl)phenyl)-3-(1-(tetrahydro-2*H*-pyran-2-yl)-1*H*-indazol-6-yl)acrylamide (74 mg, 0.155 mmol) in EtOH (2 mL) was added a 3 M HCl solution in MeOH (0.26 mL, 0.775 mmol). The resulting reaction mixture was stirred at 50 °C for 12 h. The reaction mixture was cooled to room temperature and solvents were evaporated *in vacuo*. The residue obtained was purified by MDAP (acidic conditions), to afford the title compound as an off-white solid, as the formate salt; yield 55% (37.3 mg); **LCMS** (acidic conditions) (ES +ve)  $m/z$  394 (M+H)<sup>+</sup>, Rt = 0.73 min; **<sup>1</sup>H NMR** (400 MHz, DMSO-d<sub>6</sub>): δ = 13.24 (br. s, 1H), 9.36 (br. s, 1H), 8.16 (s, 1H, *formic acid*), 8.11 (s, 1H), 7.83 (d,  $J$  = 8.3 Hz, 1H), 7.77 (s, 1H), 7.74 (d,  $J$  = 15.7 Hz, 1H), 7.43 (d,  $J$  = 8.3 Hz, 1H), 7.18 - 7.03 (m, 2H), 7.02 - 6.93 (m, 1H), 2.79 (br. s, 4H), 2.49 (br. s, 4H), 2.21 (s, 3H), 2.04 ppm (s, 3H); **<sup>13</sup>C NMR** (101 MHz, DMSO-d<sub>6</sub>): δ = 164.8, 163.6 (*formic acid*), 157.3 (d,  $J$  = 237.7 Hz), 145.5, 141.4, 140.7, 134.0, 133.1, 132.6 (d,  $J$  = 6.6 Hz),

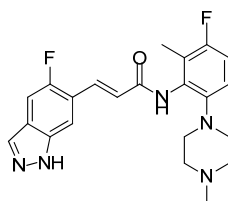


124.0 (d,  $J = 16.9$  Hz), 123.9, 121.9, 121.6, 119.4, 117.7 (d,  $J = 9.5$  Hz), 113.3 (d,  $J = 25.7$  Hz), 111.2, 55.2, 51.6, 46.1, 11.2 ppm (d,  $J = 3.7$  Hz); **HRMS** (ES +ve) calcd for  $C_{22}H_{25}FN_5O$  (M+H)<sup>+</sup> 394.2038, found 394.2043; **IR**  $\nu$  (cm<sup>-1</sup>) 3211, 2929, 1620, 1477; **mp** 185.6 - 187.4 °C.



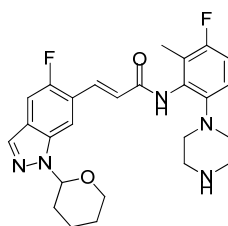
**3.118**

**(E)-3-(5-Fluoro-1-(tetrahydro-2H-pyran-2-yl)-1H-indazol-6-yl)-N-(3-fluoro-2-methyl-6-(4-methylpiperazin-1-yl)phenyl)acrylamide (3.118)**; To a stirred solution of (E)-3-(5-fluoro-1-(tetrahydro-2H-pyran-2-yl)-1H-indazol-6-yl)acrylic acid (201 mg, 0.693 mmol) in DMF (2 mL) was added 3-fluoro-2-methyl-6-(4-methylpiperazin-1-yl)aniline (150 mg, 0.577 mmol), HATU (329 mg, 0.866 mmol) and *N,N*-diisopropylethylamine (0.202 mL, 1.155 mmol) at room temperature. The resulting reaction mixture was stirred at room temperature for 48 h. Water (10 mL) and EtOAc (10 mL) were added to the reaction mixture and the organic layer was separated. The aqueous layer was further extracted with EtOAc (10 mL). The organic extracts were combined, washed with brine (10 mL), dried by filtration through a hydrophobic frit and concentrated *in vacuo*. The residue was purified on silica using a 0-50% MeOH-TBME gradient to afford the title compound as a yellow solid; yield 82% (235 mg); **LCMS** (acidic conditions) (ES +ve)  $m/z$  496 (M+H)<sup>+</sup>,  $R_t = 0.91$  min; **<sup>1</sup>H NMR** (400 MHz, DMSO-*d*<sub>6</sub>):  $\delta = 9.59$  (br. s, 1H), 8.15 (s, 2H), 7.76 (d,  $J = 15.7$  Hz, 1H), 7.69 (d,  $J = 11.0$  Hz, 1H), 7.24 (d,  $J = 15.7$  Hz, 1H), 7.12 - 7.04 (m, 1H), 7.03 - 6.93 (m, 1H), 5.93 (d,  $J = 8.3$  Hz, 1H), 3.98 - 3.86 (m, 1H), 3.85 - 3.71 (m, 1H), 2.76 (br. s, 4H), 2.48 - 2.34 (m, 5H), 2.18 (s, 3H), 2.11 - 1.96 (m, 5H), 1.82 - 1.69 (m, 1H), 1.66 - 1.56 ppm (m, 2H).



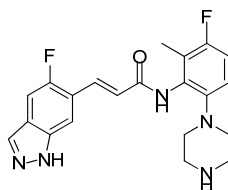
3.119

**(E)-3-(5-Fluoro-1H-indazol-6-yl)-N-(3-fluoro-2-methyl-6-(4-methylpiperazin-1-yl)phenyl)acrylamide (3.119)**; To a suspension of (E)-3-(5-fluoro-1-(tetrahydro-2H-pyran-2-yl)-1H-indazol-6-yl)-N-(3-fluoro-2-methyl-6-(4-methylpiperazin-1-yl)phenyl)acrylamide (100 mg, 0.202 mmol) in EtOH (2 mL) was added a 3 M HCl solution in MeOH (0.673 mL, 2.018 mmol). The resulting reaction mixture was stirred at 50 °C for 12 h. The reaction mixture was cooled to room temperature and solvents were evaporated *in vacuo*. The residue obtained was purified by MDAP (basic conditions), to afford the title compound as an off-white solid; yield 95% (79 mg); **LCMS** (acidic conditions) (ES +ve) *m/z* 412 (M+H)<sup>+</sup>, Rt = 0.75 min; **<sup>1</sup>H NMR** (400 MHz, DMSO-d<sub>6</sub>): δ = 13.29 (br. s, 1H), 9.51 (br. s, 1H), 8.11 (s, 1H), 7.88 (d, *J* = 4.4 Hz, 1H), 7.74 (d, *J* = 15.7 Hz, 1H), 7.66 (d, *J* = 11.2 Hz, 1H), 7.21 (d, *J* = 15.7 Hz, 1H), 7.12 - 7.03 (m, 1H), 7.01 - 6.94 (m, 1H), 2.78 (br. s, 4H), 2.45 (br. s, 4H), 2.19 (s, 3H), 2.04 ppm (s, 3H); **<sup>13</sup>C NMR** (101 MHz, DMSO-d<sub>6</sub>): δ = 164.5, 157.2 (d, *J* = 237.7 Hz), 155.9 (d, *J* = 241.4 Hz), 145.7, 137.4, 134.5, 134.0, 132.6 (d, *J* = 6.6 Hz), 124.8, 124.0 (d, *J* = 21.3 Hz), 123.4 (d, *J* = 11.0 Hz), 122.7 (d, *J* = 16.9 Hz), 117.6 (d, *J* = 8.1 Hz), 113.4 (d, *J* = 19.8 Hz), 111.2, 105.9 (d, *J* = 24.9 Hz), 55.3, 51.8, 46.2, 11.2 (d, *J* = 3.7 Hz) ppm; **HRMS** (ES +ve) calcd for C<sub>22</sub>H<sub>24</sub>F<sub>2</sub>N<sub>5</sub>O (M+H)<sup>+</sup> 412.1943, found 412.1944; **IR** ν (cm<sup>-1</sup>) 3208, 2936, 1620, 1479; **mp** 182.7 - 184.1 °C.



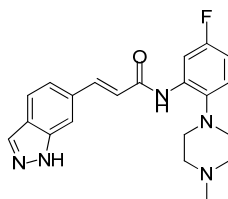
3.120

**(E)-3-(5-Fluoro-1-(tetrahydro-2H-pyran-2-yl)-1H-indazol-6-yl)-N-(3-fluoro-2-methyl-6-(piperazin-1-yl)phenyl)acrylamide (3.120)**; To a stirred solution of (E)-3-(5-fluoro-1-(tetrahydro-2H-pyran-2-yl)-1H-indazol-6-yl)-N-(3-fluoro-2-methyl-6-(4-methylpiperazin-1-yl)phenyl)acrylamide (148 mg, 0.299 mmol) in MeOH (3 mL) was added magnesium monoperoxyphthalate hexahydrate 80% by weight (203 mg, 0.329 mmol). The resulting reaction mixture was stirred at room temperature under nitrogen for 2 h. The reaction mixture was filtered and the solid was washed with MeOH (3 mL). Iron(II) sulfate heptahydrate (100 mg, 0.358 mmol) was added to the obtained filtrate and the reaction mixture was stirred at room temperature under nitrogen for 12 h. Iron(II) sulfate heptahydrate (60 mg, 0.215 mmol) was added and the reaction mixture was stirred at room temperature under nitrogen for 6 h. The reaction mixture was concentrated *in vacuo* and the residue was suspended in a 0.4 M EDTA aqueous solution (10 mL, 4.00 mmol) and EtOAc (10 mL). The organic layer was separated and the aqueous layer was further extracted with EtOAc (10 mL). The organic extracts were combined, dried by filtration through a hydrophobic frit and concentrated *in vacuo*. The residue was purified by MDAP (basic conditions), to afford the title compound as a yellow solid; yield 20% (29 mg); **LCMS** (basic conditions) (ES +ve)  $m/z$  482 (M+H)<sup>+</sup>,  $R_t = 1.13$  min; **<sup>1</sup>H NMR** (400 MHz, DMSO- $d_6$ ):  $\delta = 9.55$  (br. s, 1H), 8.15 (s, 2H), 7.76 (d,  $J = 15.9$  Hz, 1H), 7.69 (d,  $J = 11.0$  Hz, 1H), 7.23 (d,  $J = 15.9$  Hz, 1H), 7.08 (t,  $J = 9.0$  Hz, 1H), 6.95 (dd,  $J = 9.0, 5.6$  Hz, 1H), 5.92 (d,  $J = 7.8$  Hz, 1H), 3.96 - 3.86 (m, 1H), 3.84 - 3.71 (m, 1H), 2.80 (br. s, 4H), 2.69 (br. s, 4H), 2.48 - 2.34 (m, 1H), 2.11 - 1.95 (m, 5H), 1.83 - 1.69 (m, 1H), 1.66 - 1.55 ppm (m, 2H), *piperazine NH was not observed*.



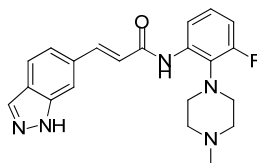
3.121

**(E)-3-(5-Fluoro-1H-indazol-6-yl)-N-(3-fluoro-2-methyl-6-(piperazin-1-yl)phenyl)acrylamide (3.121)**; To a suspension of (*E*)-3-(5-fluoro-1-(tetrahydro-2H-pyran-2-yl)-1H-indazol-6-yl)-N-(3-fluoro-2-methyl-6-(piperazin-1-yl)phenyl)acrylamide (29 mg, 0.060 mmol) in EtOH (2 mL) was added a 3 M HCl solution in MeOH (0.201 mL, 0.602 mmol). The resulting reaction mixture was stirred at 50 °C for 48 h. The reaction mixture was cooled to room temperature and solvents were evaporated *in vacuo*. The residue was loaded with MeOH on an ion-exchange SCX cartridge, eluted with MeOH (2 x CV) and with a 2 M ammonia solution in MeOH (2 x CV). The basic methanolic fraction was concentrated *in vacuo* to afford the title compound as an off-white solid; yield 75% (18 mg); **LCMS** (acidic conditions) (ES +ve) *m/z* 398 (M+H)<sup>+</sup>, *Rt* = 0.79 min; **<sup>1</sup>H NMR** (400 MHz, DMSO-*d*<sub>6</sub>): δ = 13.37 (br. s, 1H), 9.50 (br. s, 1H), 8.11 (s, 1H), 7.88 (d, *J* = 4.2 Hz, 1H), 7.74 (d, *J* = 15.9 Hz, 1H), 7.66 (d, *J* = 11.2 Hz, 1H), 7.23 (d, *J* = 15.9 Hz, 1H), 7.12 - 7.04 (m, 1H), 6.98 - 6.91 (m, 1H), 2.79 (br. s, 4H), 2.70 (br. s, 4H), 2.04 ppm (s, 3H), *piperazine NH was not observed*; **<sup>13</sup>C NMR** (101 MHz, DMSO-*d*<sub>6</sub>): δ = 164.7, 157.3 (d, *J* = 237.3 Hz), 156.0 (d, *J* = 237.7 Hz), 145.9, 137.4, 134.5, 134.1, 132.6 (d, *J* = 6.6 Hz), 124.6, 123.9 (d, *J* = 19.1 Hz), 123.5 (d, *J* = 11.4 Hz), 122.7 (d, *J* = 16.9 Hz), 118.0 (d, *J* = 7.3 Hz), 113.7 (d, *J* = 23.5 Hz), 111.1, 105.9 (d, *J* = 24.9 Hz), 52.6, 45.9, 11.2 ppm; **HRMS** (ES +ve) calcd for C<sub>21</sub>H<sub>22</sub>F<sub>2</sub>N<sub>5</sub>O (M+H)<sup>+</sup> 398.1787, found 398.1804; **IR** *v* (cm<sup>-1</sup>) 3254, 2923, 1613, 1475; **mp** 216.1 - 218.3 °C.



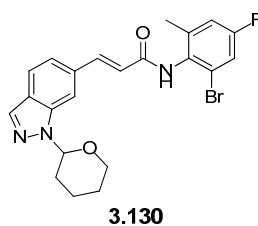
3.122

**(E)-N-(5-Fluoro-2-(4-methylpiperazin-1-yl)phenyl)-3-(1H-indazol-6-yl)acrylamide (3.122)**;<sup>154</sup> as the hydrochloride salt; LCMS (outsourcing partner acidic conditions) (ES +ve)  $m/z$  380 (M+H)<sup>+</sup>, Rt = 0.78 min; <sup>1</sup>H NMR (400 MHz, DMSO-d<sub>6</sub>):  $\delta$  = 13.33 (br. s, 1H), 10.39 (br. s, 1H, NH<sup>+</sup> piperazine), 9.25 (br. s, 1H), 8.19 (dd,  $J$  = 11.3, 3.0 Hz, 1H), 8.12 (s, 1H), 7.87 - 7.82 (m, 2H), 7.80 (d,  $J$  = 15.6 Hz, 1H), 7.53 (d,  $J$  = 8.3 Hz, 1H), 7.35 (d,  $J$  = 15.6 Hz, 1H), 7.30 (dd,  $J$  = 8.8, 5.8 Hz, 1H), 7.00 - 6.93 (m, 1H), 3.51 - 3.36 (m, 4H), 3.19 - 3.00 (m, 4H), 2.88 ppm (d,  $J$  = 4.5 Hz, 3H).

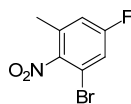


3.123

**(E)-N-(3-Fluoro-2-(4-methylpiperazin-1-yl)phenyl)-3-(1H-indazol-6-yl)acrylamide (3.123)**;<sup>154</sup> LCMS (outsourcing partner basic conditions) (ES +ve)  $m/z$  380 (M+H)<sup>+</sup>, Rt = 1.33 min; <sup>1</sup>H NMR (400 MHz, DMSO-d<sub>6</sub>):  $\delta$  = 13.29 (br. s, 1H), 9.28 (br. s, 1H), 8.16 (d,  $J$  = 8.2 Hz, 1H), 8.12 (s, 1H), 7.87 - 7.82 (m, 2H), 7.78 (d,  $J$  = 15.7 Hz, 1H), 7.56 (d,  $J$  = 8.3 Hz, 1H), 7.22 (td,  $J$  = 8.2, 6.0 Hz, 1H), 7.15 (d,  $J$  = 15.7 Hz, 1H), 6.94 (ddd,  $J$  = 12.3, 8.2, 1.0 Hz, 1H), 3.02 (br. s, 4H), 2.57 (br. s, 4H), 2.29 ppm (s, 3H).

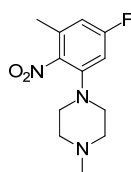


**(E)-N-(2-Bromo-4-fluoro-6-methylphenyl)-3-(1-(tetrahydro-2H-pyran-2-yl)-1H-indazol-6-yl)acrylamide (3.130)**; 2-Bromo-4-fluoro-6-methylaniline (0.75 g, 3.67 mmol), (E)-3-(1-(tetrahydro-2H-pyran-2-yl)-1H-indazol-6-yl)acrylic acid (1.00 g, 3.67 mmol), *N,N*-diisopropylethylamine (0.96 mL, 5.51 mmol) and HATU (2.10 g, 5.51 mmol) were dissolved in DMF (10 mL). The reaction mixture was stirred under nitrogen at room temperature for 96 h. The solvents were removed *in vacuo* and the residue was dissolved in water (20 mL) and EtOAc (15 mL). The organic layer was separated and the aqueous layer was further extracted with EtOAc (3 x 15 mL). The organic extracts were combined, dried by filtration through a hydrophobic frit and concentrated *in vacuo*. The residue was purified on silica using a 0-50% EtOAc-cyclohexane gradient to afford an impure material. The product was dissolved in a minimum volume of refluxing MeOH and left to stand for 12 h. The solid obtained was filtered to afford the title compound; yield 28% (465 mg). The filtrate was concentrated *in vacuo* and the residue was dissolved in a minimum volume of refluxing MeOH and left to stand for 12 h. The solid obtained was filtered to afford the title compound; yield 3% (44 mg). The filtrate was concentrated *in vacuo* and the residue was dissolved in a minimum volume of refluxing MeOH and left to stand for 12 h. The solid obtained was filtered to afford the title compound; yield 7% (117 mg); combined yield 37%; **LCMS** (acidic conditions) (ES +ve) *m/z* 458, 460 (M+H)<sup>+</sup>, Rt = 1.20 min; **<sup>1</sup>H NMR** (400 MHz, DMSO-*d*<sub>6</sub>): δ = 9.80 (br. s, 1H), 8.15 (s, 1H), 8.04 (s, 1H), 7.84 (d, *J* = 8.3 Hz, 1H), 7.75 (d, *J* = 15.7 Hz, 1H), 7.55 - 7.45 (m, 2H), 7.26 (dd, *J* = 9.3, 2.4 Hz, 1H), 6.99 (d, *J* = 15.7 Hz, 1H), 5.91 (dd, *J* = 9.7, 2.1 Hz, 1H), 3.96 - 3.88 (m, 1H), 3.83 - 3.73 (m, 1H), 2.48 - 2.39 (m, 1H), 2.24 (s, 3H), 2.11 - 1.96 (m, 2H), 1.83 - 1.70 (m, 1H), 1.68 - 1.56 ppm (m, 2H).



**3.128**

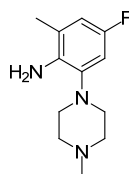
**1-Bromo-5-fluoro-3-methyl-2-nitrobenzene (3.128)**; 70% by weight *m*-CPBA (9.06 g, 36.8 mmol) was added in portions to a stirred solution of 2-bromo-4-fluoro-6-methylaniline (1.50 g, 7.35 mmol) in DCM (75 mL) at 0 °C. The above procedure was repeated once to obtain a second batch. After the addition was complete, the reaction mixture was warmed to and stirred at room temperature for 90 h. The reaction was quenched by cautious addition of a saturated sodium thiosulfate aqueous solution (50 mL). The resulting reaction mixture was left to stir at room temperature for 1 h. Both batches were combined and the resulting reaction mixture was stirred at room temperature for 20 h. The reaction mixture was filtered and the filtrate was extracted with EtOAc (3 x 100 mL). The organic extracts were combined, dried by filtration through a hydrophobic frit and concentrated *in vacuo*. The residue was purified on silica using a 0-10% MeOH-EtOAc gradient to afford the title compound as a white solid; yield 61% (2.08 g); **LCMS** (basic conditions) (ES +ve) *m/z* compound did not show relevant ionisation, *R*<sub>t</sub> = 1.23 min; **<sup>1</sup>H NMR** (400 MHz, DMSO-*d*<sub>6</sub>): δ = 7.78 (dd, *J* = 8.1, 2.6 Hz, 1H), 7.49 (dd, *J* = 9.2, 2.6 Hz, 1H), 2.32 ppm (s, 3H).



**3.134**

**1-(5-Fluoro-3-methyl-2-nitrophenyl)-4-methylpiperazine (3.134)**; 1-Bromo-5-fluoro-3-methyl-2-nitrobenzene (375 mg, 1.602 mmol), *N*-methylpiperazine (0.213 mL, 1.923 mmol), BINAP (200 mg, 0.320 mmol) and toluene (8 mL) were added to a reaction tube.

Nitrogen was bubbled through the resulting suspension for 5 min. NaO<sup>t</sup>Bu (231 mg, 2.404 mmol) and Pd<sub>2</sub>(dba)<sub>3</sub> (147 mg, 0.160 mmol) were subsequently added to the mixture. The tube was sealed, degassed and back filled with nitrogen. The reaction mixture was stirred at 80 °C under nitrogen for 20 h. Pd<sub>2</sub>(dba)<sub>3</sub> (147 mg, 0.160 mmol), *N*-methylpiperazine (0.213 mL, 1.923 mmol) and BINAP (200 mg, 0.320 mmol) were added and the resulting reaction mixture was stirred at 80 °C under nitrogen for 26 h. The reaction mixture was cooled to room temperature and filtered through celite, rinsing with water (30 mL) and EtOAc (30 mL). A 1 M HCl aqueous solution (30 mL) was added to the filtrate. The organic layer was separated, washed with a 1 M HCl aqueous solution (2 x 10 mL) and discarded. The aqueous layers were combined, diluted with a saturated NaHCO<sub>3</sub> aqueous solution (100 mL) and extracted with EtOAc (3 x 40 mL). The organic extracts were combined, dried by filtration through a hydrophobic frit and concentrated *in vacuo* to afford the title compound as a brown gum; the compound was progressed without further purification in the next synthetic step (226 mg); **LCMS** (basic conditions) (ES +ve) *m/z* 254, Rt = 1.13 min; **<sup>1</sup>H NMR** (400 MHz, DMSO-d<sub>6</sub>): δ = 7.15 (dd, *J* = 10.5, 2.4 Hz, 1H), 7.04 (dd, *J* = 9.0, 2.4 Hz, 1H), 2.93 - 2.88 (m, 4H), 2.39 - 2.32 (m, 4H), 2.22 (s, 3H), 2.19 ppm (s, 3H).

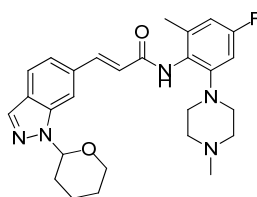


**3.133**

**4-Fluoro-2-methyl-6-(4-methylpiperazin-1-yl)aniline (3.133)**; 1-(5-Fluoro-3-methyl-2-nitrophenyl)-4-methylpiperazine (218 mg, 0.861 mmol) was dissolved in EtOH (5 ml) and tin(II) chloride dihydrate (777 mg, 3.44 mmol) was added. The reaction mixture was stirred under nitrogen at 70 °C for 26 h. The reaction mixture was cooled to room temperature and loaded on an ion-exchange SCX cartridge, eluted with MeOH (4 x CV)



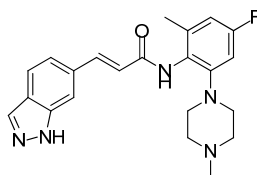
and with a 2 M ammonia solution in MeOH (4 x CV). The basic methanolic fraction was concentrated *in vacuo* and the residue was purified on silica using a 0-20% 10:1 MeOH:NH<sub>4</sub>OH-TBME gradient to afford the title compound as a white solid; yield over 2 steps 16% (58 mg); **LCMS** (basic conditions) (ES +ve) *m/z* 224, *Rt* = 0.97 min; **<sup>1</sup>H NMR** (400 MHz, DMSO-*d*<sub>6</sub>): δ = 6.66 (dd, *J* = 10.5, 2.7 Hz, 1H), 6.61 (dd, *J* = 9.3, 2.7 Hz, 1H), 4.29 (br. s, 2H), 2.82 - 2.71 (m, 4H), 2.50 - 2.45 (m, 4H), 2.23 (s, 3H), 2.10 ppm (s, 3H).



**3.131**

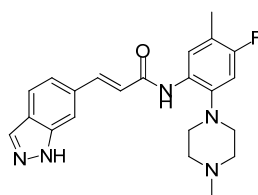
**(*E*)-*N*-(4-Fluoro-2-methyl-6-(4-methylpiperazin-1-yl)phenyl)-3-(1-(tetrahydro-2*H*-pyran-2-yl)-1*H*-indazol-6-yl)acrylamide (3.131);** 4-Fluoro-2-methyl-6-(4-methylpiperazin-1-yl)aniline (58 mg, 0.260 mmol), (*E*)-3-(1-(tetrahydro-2*H*-pyran-2-yl)-1*H*-indazol-6-yl)acrylic acid (85 mg, 0.312 mmol), *N,N*-diisopropylethylamine (0.068 mL, 0.390 mmol) and HATU (148 mg, 0.390 mmol) were dissolved in DMF (3 mL). The reaction mixture was stirred at room temperature for 68 h. The reaction mixture was diluted with water (5 mL) and extracted with EtOAc (3 x 5 mL). The organic extracts were combined, dried by filtration through a hydrophobic frit and concentrated *in vacuo*. The residue obtained was purified by MDAP (basic conditions), to afford the title compound as an off-white solid; yield 61% (75 mg); **LCMS** (basic conditions) (ES +ve) *m/z* 478, *Rt* = 1.18 min; **<sup>1</sup>H NMR** (400 MHz, DMSO-*d*<sub>6</sub>): δ = 9.28 (br. s, 1H), 8.14 (s, 1H), 8.00 (s, 1H), 7.84 (d, *J* = 8.3 Hz, 1H), 7.72 (d, *J* = 15.7 Hz, 1H), 7.48 (d, *J* = 8.3 Hz, 1H), 7.08 (d, *J* = 15.7 Hz, 1H), 6.80 (dd, *J* = 9.2, 2.7 Hz, 1H), 6.75 (dd, *J* = 10.8, 2.7 Hz, 1H), 5.90 (dd, *J* = 9.4, 2.1 Hz, 1H), 3.96 - 3.88 (m, 1H), 3.83 - 3.72 (m, 1H), 2.91 -

2.77 (m, 4H), 2.47 - 2.38 (m, 5H), 2.18 (s, 3H), 2.13 (s, 3H), 2.10 - 1.96 (m, 2H), 1.83 - 1.70 (m, 1H), 1.67 - 1.55 ppm (m, 2H).



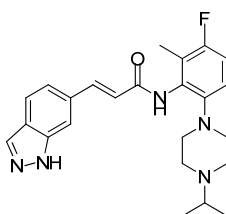
3.126

**(E)-N-(4-Fluoro-2-methyl-6-(4-methylpiperazin-1-yl)phenyl)-3-(1H-indazol-6-yl)acrylamide (3.126)**; To a suspension of (E)-N-(4-fluoro-2-methyl-6-(4-methylpiperazin-1-yl)phenyl)-3-(1-(tetrahydro-2H-pyran-2-yl)-1H-indazol-6-yl)acrylamide (74 mg, 0.155 mmol) in EtOH (2 mL) was added a 3 M HCl solution in MeOH (0.516 mL, 1.549 mmol). The resulting reaction mixture was stirred at 50 °C for 5 h. The reaction mixture was cooled to room temperature and diluted with EtOAc (10 mL), water (5 mL) and a saturated NaHCO<sub>3</sub> aqueous solution (10 mL). The organic layer was separated and the aqueous layer was further extracted with EtOAc (2 x 10 mL). The organic extracts were combined, dried by filtration through a hydrophobic frit and concentrated *in vacuo* to afford the title compound as a white solid; yield 83% (50.8 mg); **LCMS** (basic conditions) (ES +ve) *m/z* 394, *R<sub>t</sub>* = 0.98 min; **<sup>1</sup>H NMR** (400 MHz, DMSO-d<sub>6</sub>): δ = 13.26 (br. s, 1H), 9.25 (br. s, 1H), 8.11 (s, 1H), 7.82 (d, *J* = 8.3 Hz, 1H), 7.76 (s, 1H), 7.71 (d, *J* = 15.7 Hz, 1H), 7.42 (d, *J* = 8.3 Hz, 1H), 7.06 (d, *J* = 15.7 Hz, 1H), 6.80 (dd, *J* = 9.2, 2.7 Hz, 1H), 6.74 (dd, *J* = 10.6, 2.7 Hz, 1H), 2.90 - 2.79 (m, 4H), 2.47 - 2.38 (m, 4H), 2.18 (s, 3H), 2.13 ppm (s, 3H); **<sup>13</sup>C NMR** (101 MHz, DMSO-d<sub>6</sub>): δ = 164.7, 161.2 (d, *J* = 242.1 Hz), 151.3 (d, *J* = 9.5 Hz), 141.0, 140.7, 139.2, 134.1, 133.2, 126.8, 123.9, 122.0, 121.6, 119.4, 111.2, 110.7 (d, *J* = 22.0 Hz), 104.4 (d, *J* = 23.5 Hz), 55.2, 51.3, 46.2, 19.0 ppm; **HRMS** (ES +ve) calcd for C<sub>22</sub>H<sub>25</sub>FN<sub>5</sub>O (M+H)<sup>+</sup> 394.2038, found 394.2049; **IR** ν (cm<sup>-1</sup>) 3211, 2926, 1614, 1520; **mp** 237.7 - 238.2 °C.



3.127

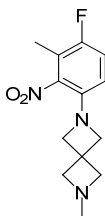
**(E)-N-(4-Fluoro-5-methyl-2-(4-methylpiperazin-1-yl)phenyl)-3-(1H-indazol-6-yl)acrylamide (3.127)**;<sup>154</sup> as the hydrochloride salt; LCMS (basic conditions) (ES +ve)  $m/z$  394 (M+H)<sup>+</sup>, Rt = 1.09 min; <sup>1</sup>H NMR (400 MHz, DMSO-d<sub>6</sub>): δ = 13.30 (br. s, 1H), 10.51 (br. s, 1H, *piperazine NH*<sup>+</sup>), 9.12 (br. s, 1H), 8.11 (s, 1H), 8.03 (d,  $J = 8.3$  Hz, 1H), 7.83 (d,  $J = 8.3$  Hz, 1H), 7.81 (s, 1H), 7.74 (d,  $J = 15.7$  Hz, 1H), 7.49 (d,  $J = 8.3$  Hz, 1H), 7.29 (d,  $J = 15.7$  Hz, 1H), 7.05 (d,  $J = 10.8$  Hz, 1H), 3.58 - 3.46 (m, 2H), 3.46 - 3.36 (m, 2H), 3.24 - 3.13 (m, 2H), 3.12 - 2.99 (m, 2H), 2.85 (s, 3H), 2.22 ppm (d,  $J = 1.2$  Hz, 3H).



3.135

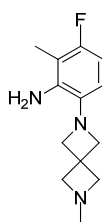
**(E)-N-(3-Fluoro-6-(4-isopropylpiperazin-1-yl)-2-methylphenyl)-3-(1H-indazol-6-yl)acrylamide (3.135)**;<sup>154</sup> as the hydrochloride salt; LCMS (outsourcing partner basic conditions) (ES +ve)  $m/z$  422 (M+H)<sup>+</sup>, Rt = 1.53 min; <sup>1</sup>H NMR (400 MHz, DMSO-d<sub>6</sub>): δ = 10.56 (br. s, 1H, *piperazine NH*<sup>+</sup>), 9.61 (br. s, 1H), 8.11 (s, 1H), 7.83 (d,  $J = 8.3$  Hz, 1H), 7.79 (s, 1H), 7.76 (d,  $J = 15.7$  Hz, 1H), 7.45 (d,  $J = 8.3$  Hz, 1H), 7.32 - 7.19 (m, 1H), 7.16 - 7.08 (m, 1H), 7.07 - 6.99 (m, 1H), 3.50 - 3.39 (m, 3H), 3.26 - 3.06 (m, 6H), 2.06 (s, 3H), 1.29 ppm (d,  $J = 6.6$  Hz, 6H), *indazole NH was not observed*; <sup>13</sup>C NMR (101 MHz, DMSO-d<sub>6</sub>): δ = 164.9, 157.8 (d,  $J = 239.1$  Hz), 143.7, 141.6, 140.8, 134.1,

134.0, 133.2, 124.1 (d,  $J = 20.5$  Hz), 124.0, 122.0, 121.5, 119.6, 118.3 (d,  $J = 8.8$  Hz), 113.4 (d,  $J = 23.5$  Hz), 111.3, 57.4, 48.6, 48.2, 16.9, 11.3 ppm (d,  $J = 4.5$  Hz).



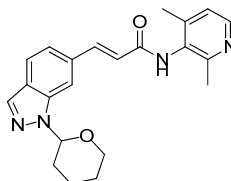
**3.139**

**2-(4-Fluoro-3-methyl-2-nitrophenyl)-6-methyl-2,6-diazaspiro[3.3]heptane (3.139);** 1-bromo-4-fluoro-3-methyl-2-nitrobenzene (759 mg, 3.24 mmol), 2-methyl-2,6-diazaspiro[3.3]heptane dihydrochloride (500 mg, 2.70 mmol), RuPhos (252 mg, 0.540 mmol), Pd<sub>2</sub>dba<sub>3</sub> (247 mg, 0.270 mmol) and NaO<sup>t</sup>Bu (909 mg, 9.45 mmol) were added to a microwave vial. To this was added toluene (18 mL). The reaction vessel was sealed, purged several times with vacuum and nitrogen, and heated in a microwave at 120 °C for 60 min. The reaction mixture was cooled to room temperature, filtered through a pad of celite, washing with EtOAc (30 mL). The filtrate was concentrated *in vacuo*. The residue was loaded on an ion-exchange SCX cartridge, eluted with MeOH (3 x CV) and with a 2 M ammonia solution in MeOH (3 x CV). The basic methanolic fraction was concentrated *in vacuo* and the residue was purified on reverse phase (C<sub>18</sub>) using a 0-100% MeCN (+0.2% ammonium hydroxide) in water (+0.2% ammonium hydroxide) gradient to afford the title compound as an orange solid; yield 46% (331 mg); **LCMS** (basic conditions) (ES +ve)  $m/z$  266, Rt = 1.16 min; **<sup>1</sup>H NMR** (400 MHz, DMSO-d<sub>6</sub>):  $\delta$  = 7.34 - 7.25 (m, 1H), 6.62 - 6.53 (m, 1H), 3.84 (s, 4H), 3.22 (s, 4H), 2.15 (s, 3H), 2.09 ppm (d,  $J = 2.2$  Hz, 3H).



**3.140**

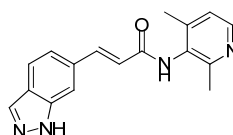
**3-Fluoro-2-methyl-6-(6-methyl-2,6-diazaspiro[3.3]heptan-2-yl)aniline (3.140)**; To a stirred solution of 2-(4-fluoro-3-methyl-2-nitrophenyl)-6-methyl-2,6-diazaspiro[3.3]heptane (328 mg, 1.236 mmol) in EtOH (10 mL) was added 10% by weight Pd/C (263 mg, 0.247 mmol). The resulting mixture was stirred under H<sub>2</sub> atmosphere (atmospheric pressure) for 2 h. The reaction mixture was filtered through celite, washing with EtOH (20 mL). The filtrate was concentrated *in vacuo* to afford the title compound as a brown sticky solid; yield 95% (275 mg); **LCMS** (basic conditions) (ES +ve) *m/z* 236, Rt = 0.96 min; **<sup>1</sup>H NMR** (400 MHz, DMSO-d<sub>6</sub>): δ = 6.41 - 6.34 (m, 1H), 6.29 (t, *J* = 9.3 Hz, 1H), 4.44 (br. s, 2H), 3.71 (s, 4H), 3.24 (s, 4H), 2.19 (s, 3H), 1.97 ppm (d, *J* = 1.6 Hz, 3H).



**3.152**

**(*E*)-N-(2,4-Dimethylpyridin-3-yl)-3-(1-(tetrahydro-2*H*-pyran-2-yl)-1*H*-indazol-6-yl)acrylamide (3.152)**; To a stirred solution of (*E*)-3-(1-(tetrahydro-2*H*-pyran-2-yl)-1*H*-indazol-6-yl)acrylic acid (150 mg, 0.551 mmol) in DMF (3 mL) at room temperature was added 2,4-dimethylpyridin-3-amine (81 mg, 0.661 mmol), *N,N*-diisopropylethylamine (0.144 mL, 0.826 mmol). The resulting reaction mixture was cooled to 0 °C and HATU (251 mg, 0.661 mmol) was added. The reaction mixture was

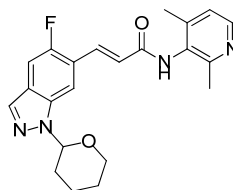
then stirred at 60 °C for 13 h. The reaction mixture was diluted with water (20 mL) extracted with EtOAc (2 x 20 mL). The organic extracts were combined, dried over MgSO<sub>4</sub> and concentrated *in vacuo*. The residue was purified on silica using a 0-10% MeOH-TBME gradient to afford the title compound as an off-white solid; yield 68% (140 mg); **LCMS** (acidic conditions) (ES +ve) *m/z* 377 (M+H)<sup>+</sup>, Rt = 0.80 min; **<sup>1</sup>H NMR** (400 MHz, DMSO-d<sub>6</sub>): δ = 9.76 (br. s, 1H), 8.24 (d, *J* = 4.9 Hz, 1H), 8.15 (s, 1H), 8.05 (s, 1H), 7.84 (d, *J* = 8.3 Hz, 1H), 7.75 (d, *J* = 15.7 Hz, 1H), 7.50 (d, *J* = 8.3 Hz, 1H), 7.17 (d, *J* = 4.9 Hz, 1H), 7.01 (d, *J* = 15.7 Hz, 1H), 5.91 (dd, *J* = 9.7, 2.3 Hz, 1H), 3.96 - 3.87 (m, 1H), 3.84 - 3.73 (m, 1H), 2.48 - 2.42 (m, 1H), 2.39 (s, 3H), 2.21 (s, 3H), 2.09 - 1.96 (m, 2H), 1.83 - 1.69 (m, 1H), 1.68 - 1.56 ppm (m, 2H).



**3.153**

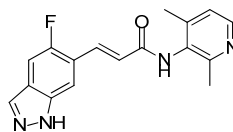
**(*E*)-*N*-(2,4-Dimethylpyridin-3-yl)-3-(1*H*-indazol-6-yl)acrylamide (3.153)**; To a suspension of (*E*)-*N*-(2,4-dimethylpyridin-3-yl)-3-(1-(tetrahydro-2*H*-pyran-2-yl)-1*H*-indazol-6-yl)acrylamide (135 mg, 0.359 mmol) in MeOH (3 mL) was added a 3 M HCl solution in MeOH (0.598 mL, 1.793 mmol). The resulting reaction mixture was stirred at 60 °C for 4 h. The reaction mixture was cooled to room temperature and solvents were evaporated *in vacuo*. The residue obtained was purified by MDAP (acidic conditions), to afford the title compound as a gum, as the formate salt; yield 33% (42 mg); **LCMS** (acidic conditions) (ES +ve) *m/z* 293, Rt = 0.59 min; **<sup>1</sup>H NMR** (400 MHz, DMSO-d<sub>6</sub>): δ = 13.25 (br. s, 1H), 9.73 (br. s, 1H), 8.24 (d, *J* = 4.9 Hz, 1H), 8.15 (s, 1H, *formic acid*), 8.11 (d, *J* = 0.7 Hz, 1H), 7.83 (d, *J* = 8.4 Hz, 1H), 7.79 (s, 1H), 7.75 (d, *J* = 15.7 Hz, 1H), 7.45 (dd, *J* = 8.4, 0.7 Hz, 1H), 7.17 (d, *J* = 4.9 Hz, 1H), 6.98 (d, *J* = 15.7 Hz, 1H), 2.39 (s, 3H), 2.21 ppm (s, 3H); **<sup>13</sup>C NMR** (101 MHz, DMSO-d<sub>6</sub>): δ = 164.1, 163.5 (*formic acid*), 155.6, 146.9, 144.6, 141.4, 140.7, 134.0, 133.0, 131.9, 123.9, 123.7,

121.8, 121.6, 119.3, 111.4, 21.7, 18.1 ppm; **HRMS** (ES +ve) calcd for C<sub>17</sub>H<sub>17</sub>N<sub>4</sub>O (M+H)<sup>+</sup> 293.1397, found 293.1403; **IR** v (cm<sup>-1</sup>) 3179, 2928, 1620, 1524.



**3.154**

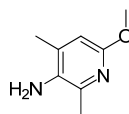
**(E)-N-(2,4-Dimethylpyridin-3-yl)-3-(5-fluoro-1-(tetrahydro-2H-pyran-2-yl)-1H-indazol-6-yl)acrylamide (3.154)**; (*E*)-3-(5-Fluoro-1-(tetrahydro-2H-pyran-2-yl)-1H-indazol-6-yl)acrylic acid (200 mg, 0.689 mmol), 2,4-dimethylpyridin-3-amine (93 mg, 0.758 mmol), HATU (393 mg, 1.033 mmol) and *N,N*-diisopropylethylamine (0.180 mL, 1.033 mmol) were dissolved in DMF (10 mL). The reaction mixture was stirred under nitrogen at room temperature for 80 h and then purified by MDAP (basic conditions), to afford the title compound as a white solid; yield 55% (149.8 mg); **LCMS** (acidic conditions) (ES +ve) *m/z* 395 (M+H)<sup>+</sup>, Rt = 1.08 min; **<sup>1</sup>H NMR** (400 MHz, DMSO-d<sub>6</sub>): δ = 9.88 (br. s, 1H), 8.24 (d, *J* = 4.9 Hz, 1H), 8.20 (d, *J* = 5.9 Hz, 1H), 8.15 (s, 1H), 7.78 (d, *J* = 15.7 Hz, 1H), 7.70 (d, *J* = 11.0 Hz, 1H), 7.17 (d, *J* = 4.9 Hz, 1H), 7.13 (d, *J* = 15.7 Hz, 1H), 5.94 (dd, *J* = 9.5, 2.4 Hz, 1H), 3.97 - 3.86 (m, 1H), 3.85 - 3.73 (m, 1H), 2.48 - 2.41 (m, 1H), 2.39 (s, 3H), 2.21 (s, 3H), 2.12 - 1.95 (m, 2H), 1.82 - 1.69 (m, 1H), 1.67 - 1.55 ppm (m, 2H).



3.155

**(E)-N-(2,4-Dimethylpyridin-3-yl)-3-(5-fluoro-1H-indazol-6-yl)acrylamide (3.155);**

To a solution of (E)-N-(2,4-dimethylpyridin-3-yl)-3-(5-fluoro-1-(tetrahydro-2H-pyran-2-yl)-1H-indazol-6-yl)acrylamide (146 mg, 0.370 mmol) in MeCN (5 mL) was added a 3 M HCl solution in MeOH (1.23 mL, 3.70 mmol). The resulting reaction mixture was stirred at 60 °C for 16 h. The reaction mixture was concentrated *in vacuo*. The residue obtained was purified by MDAP (basic conditions), to afford the title compound as a white solid; yield 64% (73.4 mg); **LCMS** (acidic conditions) (ES +ve) *m/z* 311, *Rt* = 0.49 min; **<sup>1</sup>H NMR** (400 MHz, DMSO-*d*<sub>6</sub>): δ = 13.39 (br. s, 1H), 9.89 (br. s, 1H), 8.27 (d, *J* = 4.9 Hz, 1H), 8.11 (s, 1H), 7.91 (d, *J* = 5.9 Hz, 1H), 7.76 (d, *J* = 15.7 Hz, 1H), 7.67 (d, *J* = 11.5 Hz, 1H), 7.23 (d, *J* = 4.9 Hz, 1H), 7.11 (d, *J* = 15.7 Hz, 1H), 2.40 (s, 3H), 2.23 ppm (s, 3H); **<sup>13</sup>C NMR** (101 MHz, DMSO-*d*<sub>6</sub>): δ = 164.0, 155.6, 156.1 (d, *J* = 241.3 Hz), 147.0, 144.6, 137.3, 134.8, 134.2, 131.8, 124.6, 123.7, 123.5 (d, *J* = 9.5 Hz), 122.6 (d, *J* = 16.9 Hz), 111.5, 105.9 (d, *J* = 24.6 Hz), 21.6, 18.1 ppm; **HRMS** (ES +ve) calcd for C<sub>17</sub>H<sub>16</sub>FN<sub>4</sub>O (M+H)<sup>+</sup> 311.1303, found 311.1304; **IR** *v* (cm<sup>-1</sup>) 3218, 2945, 1622, 1532; **mp** 243.9 - 244.5 °C.

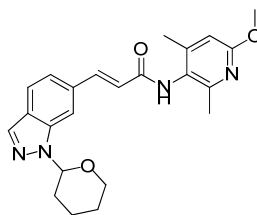


3.157

**6-Methoxy-2,4-dimethylpyridin-3-amine (3.157);** To a stirred solution of 6-methoxy-2,4-dimethyl-3-nitropyridine (300 mg, 1.647 mmol) in EtOH (10 mL) was added 10% by weight Pd/C (350 mg, 0.329 mmol). The resulting reaction mixture was stirred under H<sub>2</sub> atmosphere (atmospheric pressure) for 12 h. The reaction mixture was filtered

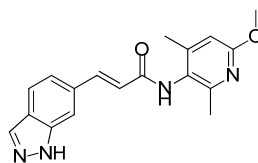


through celite, washing with EtOH (20 mL). The filtrate was concentrated *in vacuo* to afford the title compound as a brown oil; yield 99% (249 mg); LCMS (basic conditions) (ES +ve)  $m/z$  153 (M+H)<sup>+</sup>, Rt = 0.67 min; <sup>1</sup>H NMR (400 MHz, DMSO-d<sub>6</sub>): δ = 6.33 (s, 1H), 4.21 (br. s, 2H), 3.69 (s, 3H), 2.23 (s, 3H), 2.08 ppm (s, 3H).



3.158

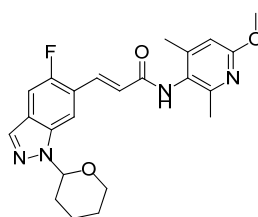
**(E)-N-(6-Methoxy-2,4-dimethylpyridin-3-yl)-3-(1-(tetrahydro-2H-pyran-2-yl)-1H-indazol-6-yl)acrylamide (3.158)**; To a stirred solution of (*E*)-3-(1-(tetrahydro-2H-pyran-2-yl)-1H-indazol-6-yl)acrylic acid (138 mg, 0.506 mmol) in DMF (5 mL) was added 6-methoxy-2,4-dimethylpyridin-3-amine (70 mg, 0.460 mmol), HATU (262 mg, 0.690 mmol) and *N,N*-diisopropylethylamine (0.120 mL, 0.690 mmol). The reaction mixture was stirred under nitrogen at room temperature for 8 h. The reaction mixture was concentrated *in vacuo* and the residue was dissolved in water (30 mL) and EtOAc (30 mL). The organic phase was separated and the aqueous layer was further extracted with EtOAc (20 mL). The organic extracts were combined, washed with water (20 mL), washed with brine (20 mL), dried by filtration through a hydrophobic frit and concentrated *in vacuo*. The residue was purified on silica using a 0-100% EtOAc-cyclohexane gradient to afford the title compound as a white solid; yield 88% (165 mg); LCMS (acidic conditions) (ES +ve)  $m/z$  407 (M+H)<sup>+</sup>, Rt = 1.01 min; <sup>1</sup>H NMR (400 MHz, DMSO-d<sub>6</sub>): δ = 9.56 (br. s, 1H), 8.15 (s, 1H), 8.03 (s, 1H), 7.84 (d, *J* = 8.3 Hz, 1H), 7.73 (d, *J* = 15.7 Hz, 1H), 7.49 (d, *J* = 8.3 Hz, 1H), 6.98 (d, *J* = 15.7 Hz, 1H), 6.60 (s, 1H), 5.91 (dd, *J* = 9.7, 2.3 Hz, 1H), 3.95 - 3.88 (m, 1H), 3.83 (s, 3H), 3.81 - 3.74 (m, 1H), 2.48 - 2.39 (m, 1H), 2.30 (s, 3H), 2.15 (s, 3H), 2.11 - 1.96 (m, 2H), 1.83 - 1.70 (m, 1H), 1.69 - 1.56 ppm (m, 2H).



3.150

**(E)-3-(1H-Indazol-6-yl)-N-(6-methoxy-2,4-dimethylpyridin-3-yl)acrylamide (3.150);**

To a solution of (E)-N-(6-methoxy-2,4-dimethylpyridin-3-yl)-3-(1-(tetrahydro-2H-pyran-2-yl)-1H-indazol-6-yl)acrylamide (163 mg, 0.401 mmol) in MeCN (10 mL) was added a 3 M HCl solution in MeOH (1.337 mL, 4.01 mmol). The resulting reaction mixture was stirred at 60 °C for 4 h. The reaction mixture was concentrated *in vacuo*. The residue obtained was purified by MDAP (acidic conditions), to afford the title compound as a white solid; yield 63% (81 mg); **LCMS** (acidic conditions) (ES +ve) *m/z* 323, Rt = 0.75 min; **<sup>1</sup>H NMR** (400 MHz, DMSO-*d*<sub>6</sub>): δ = 13.26 (br. s, 1H), 9.53 (br. s, 1H), 8.11 (s, 1H), 7.82 (d, *J* = 8.3 Hz, 1H), 7.78 (s, 1H), 7.72 (d, *J* = 15.7 Hz, 1H), 7.43 (d, *J* = 8.3 Hz, 1H), 6.95 (d, *J* = 15.7 Hz, 1H), 6.60 (s, 1H), 3.83 (s, 3H), 2.29 (s, 3H), 2.15 ppm (s, 3H); **<sup>13</sup>C NMR** (101 MHz, DMSO-*d*<sub>6</sub>): δ = 164.4, 161.5, 152.9, 148.3, 141.1, 140.7, 134.1, 133.1, 125.8, 123.9, 121.9, 121.5, 119.3, 111.2, 108.8, 53.5, 21.4, 18.3 ppm; **HRMS** (ES +ve) calcd for C<sub>18</sub>H<sub>19</sub>N<sub>4</sub>O<sub>2</sub> (M+H)<sup>+</sup> 323.1503, found 323.1504; **IR** ν (cm<sup>-1</sup>) 3214, 2927, 1604, 1469; **mp** 254.7 - 255.3 °C.

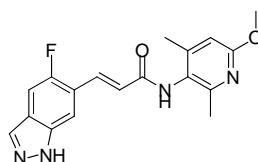


3.159

**(E)-3-(5-Fluoro-1-(tetrahydro-2H-pyran-2-yl)-1H-indazol-6-yl)-N-(6-methoxy-2,4-dimethylpyridin-3-yl)acrylamide (3.159);**

To a stirred solution of (E)-3-(5-fluoro-1-(tetrahydro-2H-pyran-2-yl)-1H-indazol-6-yl)acrylic acid (147 mg, 0.506 mmol) in DMF

(5 mL) was added 6-methoxy-2,4-dimethylpyridin-3-amine (70 mg, 0.460 mmol), HATU (262 mg, 0.690 mmol) and *N,N*-diisopropylethylamine (0.120 mL, 0.690 mmol). The reaction mixture was stirred under nitrogen at room temperature for 8 h. The reaction mixture was concentrated *in vacuo* and the residue was dissolved in water (30 mL) and EtOAc (30 mL). The organic phase was separated and the aqueous layer was further extracted with EtOAc (20 mL). The organic extracts were combined, washed with water (20 mL), washed with brine (20 mL), dried by filtration through a hydrophobic frit and concentrated *in vacuo*. The residue was purified on silica using a 0-100% EtOAc-cyclohexane gradient to afford the title compound as a white solid; yield 90% (175.2 mg); **LCMS** (acidic conditions) (ES +ve) *m/z* 425 (M+H)<sup>+</sup>, *Rt* = 1.08 min; **<sup>1</sup>H NMR** (400 MHz, DMSO-*d*<sub>6</sub>): δ = 9.67 (br. s, 1H), 8.19 (d, *J* = 5.9 Hz, 1H), 8.15 (s, 1H), 7.76 (d, *J* = 15.8 Hz, 1H), 7.69 (d, *J* = 11.0 Hz, 1H), 7.10 (d, *J* = 15.8 Hz, 1H), 6.60 (s, 1H), 5.94 (dd, *J* = 9.7, 2.3 Hz, 1H), 3.95 - 3.87 (m, 1H), 3.83 (s, 3H), 3.81 - 3.74 (m, 1H), 2.48 - 2.37 (m, 1H), 2.29 (s, 3H), 2.15 (s, 3H), 2.11 - 1.96 (m, 2H), 1.82 - 1.70 (m, 1H), 1.66 - 1.57 ppm (m, 2H).



**3.160**

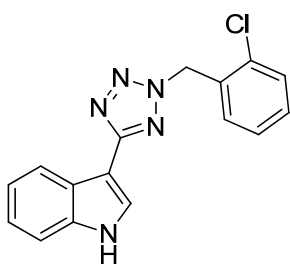
**(*E*)-3-(5-Fluoro-1*H*-indazol-6-yl)-*N*-(6-methoxy-2,4-dimethylpyridin-3-yl)acrylamide (3.160)**; To a solution of (*E*)-3-(5-fluoro-1-(tetrahydro-2*H*-pyran-2-yl)-1*H*-indazol-6-yl)-*N*-(6-methoxy-2,4-dimethylpyridin-3-yl)acrylamide (172 mg, 0.405 mmol) in MeCN (10 mL) was added a 3 M HCl solution in MeOH (1.337 mL, 4.01 mmol). The resulting reaction mixture was stirred at 60 °C for 4 h. The reaction mixture was concentrated *in vacuo*. The residue obtained was purified by MDAP (acidic conditions), to afford the title compound as a white solid; yield 35% (48 mg); **LCMS** (acidic conditions) (ES +ve) *m/z* 341, *Rt* = 0.82 min; **<sup>1</sup>H NMR** (400 MHz, DMSO-*d*<sub>6</sub>): δ

= 13.39 (br. s, 1H), 9.64 (br. s, 1H), 8.11 (s, 1H), 7.90 (d,  $J = 6.1$  Hz, 1H), 7.73 (d,  $J = 15.9$  Hz, 1H), 7.66 (d,  $J = 11.2$  Hz, 1H), 7.07 (d,  $J = 15.9$  Hz, 1H), 6.60 (s, 1H), 3.83 (s, 3H), 2.29 (s, 3H), 2.15 ppm (s, 3H);  $^{13}\text{C}$  NMR (101 MHz, DMSO- $d_6$ ):  $\delta = 164.3, 161.5, 156.1$  (d,  $J = 240.6$  Hz), 152.8, 148.3, 137.3, 134.5, 134.0, 125.7, 124.7, 123.3 (d,  $J = 8.8$  Hz), 122.6 (d,  $J = 16.9$  Hz), 111.4, 108.8, 105.8 (d,  $J = 24.9$  Hz), 53.5, 21.4, 18.3 ppm; HRMS (ES +ve) calcd for  $\text{C}_{18}\text{H}_{18}\text{FN}_4\text{O}_2$  (M+H) $^+$  341.1408, found 341.1412; IR  $\nu$  ( $\text{cm}^{-1}$ ) 3221, 2926, 1617, 1472; mp 237.4 - 238.1 °C.

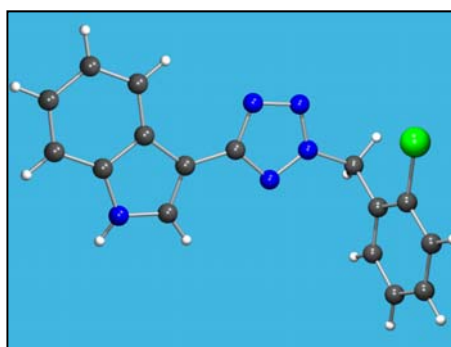
## 5. Appendices

### 5.1. Appendix 1: Single crystal X-ray diffraction crystallography of compound 2.18

#### Structure Report for 25709A1

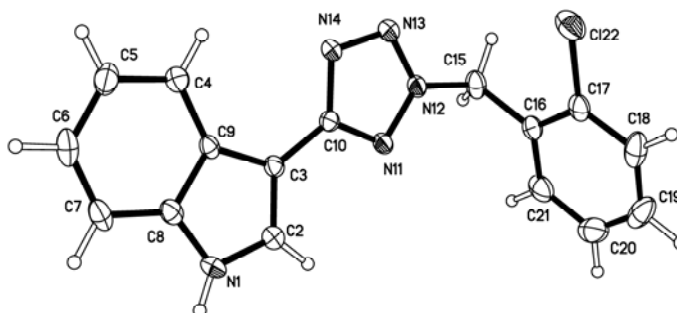


**2.18**



#### 3-{2-[(2-Chlorophenyl)methyl]-2H-tetrazol-5-yl}-1H-indole

The asymmetric unit contains a single, fully ordered molecule of compound **2.18** (Figure 1). The final R1 value [ $I > 2\sigma(I)$ ] was 3.91%. The structure confirms the atomic connectivity shown in the ISIS Draw sketch above, with bond lengths and angles being consistent with this.



**Figure 1.** A view of a molecule of compound **2.18** from the 25709A1 crystal structure, showing the numbering scheme employed. Anisotropic atomic displacement ellipsoids for the non-hydrogen atoms are shown at the 50% probability level. Hydrogen atoms are displayed with an arbitrarily small radius.

**Table 1. Sample and crystal data for 25709A1.**

---

|                          |   |
|--------------------------|---|
| Identification code      | 25709A1   |
| Compound number          | compound <b>2.18</b>  |
| Crystallization solvents | Acetonitrile, water and formic acid   |
| Crystallization method   | Evaporation of MDAP fraction  |
| Moiety formula           | C <sub>16</sub> H <sub>12</sub> ClN <sub>5</sub>  |
| Empirical formula        | C <sub>16</sub> H <sub>12</sub> ClN <sub>5</sub>  |
| Formula weight           | 309.76  |
| Temperature              | 150(2) K  |
| Wavelength               | 0.71073 Å   |
| Crystal size             | 0.23 x 0.12 x 0.09 mm   |
| Crystal habit            | Colourless block  |
| Crystal system           | Triclinic   |
| Space group              | P $\bar{1}$   |
| Unit cell dimensions     | a = 8.2444(4) Å $\alpha$ = 88.541(4)°<br>b = 8.5596(4) Å $\beta$ = 84.635(4)°<br>c = 10.3958(6) Å $\gamma$ = 73.812(4)° |
| Volume                   | 701.45(6) Å <sup>3</sup>  |
| Z                        | 2   |
| Density (calculated)     | 1.467 Mg/m <sup>3</sup>   |
| Absorption coefficient   | 0.276 mm <sup>-1</sup>  |
| F(000)                   | 320   |

---

**Table 2. Data collection and structure refinement for 25709A1.**

|                                     |   |
|-------------------------------------|---|
| Diffractometer                      | Oxford Diffraction Gemini A Ultra   |
| Radiation source                    | Enhance (Mo) X-ray Source, MoK $\alpha$   |
| Data collection method              | $\omega$ scans  |
| Theta range for data collection     | 3.04 to 28.44°  |
| Index ranges                        | -11 $\leq h \leq$ 10, -10 $\leq k \leq$ 9, -9 $\leq l \leq$ 13  |
| Reflections collected               | 5474  |
| Independent reflections             | 2882 [R(int) = 0.0229]  |
| Coverage of independent reflections | 96.6%   |
| Variation in check reflections      | N/A   |
| Absorption correction               | Gaussian  |
| Max. and min. transmission          | 0.980 and 0.954   |
| Structure solution technique        | Direct methods  |
| Structure solution program          | SHELXTL V2008/4 (Bruker, 2008)  |
| Refinement technique                | Full-matrix least-squares on F <sup>2</sup>   |
| Refinement program                  | SHELXTL V2008/4 (Bruker, 2008)  |
| Function minimized                  | $\Sigma w(F_o^2 - F_c^2)^2$   |
| Data / restraints / parameters      | 2882 / 0 / 204  |
| Goodness-of-fit on F <sup>2</sup>   | 1.045   |
| $\Delta/\sigma_{\max}$              | 0.000   |
| Final R indices                     |   |
| 2361 data; I > 2 $\sigma$ (I)       | R1 = 0.0391, wR2 = 0.0868   |
| all data                            | R1 = 0.0527, wR2 = 0.0934   |
| Weighting scheme                    | $w = 1/[\sigma^2(F_o^2) + (0.0362P)^2 + 0.2632P]$<br>where P = [MAX(F <sub>o</sub> <sup>2</sup> , 0) + 2F <sub>c</sub> <sup>2</sup> ]/3 |
| Extinction coefficient              | 0.0030(17)  |
| Largest diff. peak and hole         | 0.319 and -0.408 eÅ <sup>-3</sup>   |
| Refinement summary:                 |   |
| Ordered Non-H atoms, XYZ            | Freely refined  |
| Ordered Non-H atoms, U              | Freely refined - anisotropic  |
| H atoms (on carbon), XYZ            | Idealized positions riding on attached atoms  |
| H atoms (on carbon), U              | Appropriate multiple of U(eq) for bonded atom   |
| H atoms (on heteroatoms), XYZ       | Freely refined  |
| H atoms (on heteroatoms), U         | Freely refined - isotropic  |
| Disordered atoms                    | No disorder   |

**Table 3. Atomic coordinates and equivalent isotropic atomic displacement parameters ( $\text{\AA}^2$ ) for 25709A1.**

$U_{\text{eq}}$  is defined as one third of the trace of the orthogonalised  $U^{\text{ij}}$  tensor.

|      | x           | y           | z           | $U_{\text{eq}}$ |
|------|-------------|-------------|-------------|-----------------|
| N1   | 0.2851(2)   | 0.78349(19) | 0.50204(15) | 0.0246(3)       |
| C2   | 0.2111(2)   | 0.6788(2)   | 0.56860(17) | 0.0220(4)       |
| C3   | 0.2465(2)   | 0.53535(19) | 0.50253(16) | 0.0169(3)       |
| C4   | 0.4201(2)   | 0.4536(2)   | 0.27905(17) | 0.0225(4)       |
| C5   | 0.5098(2)   | 0.5138(2)   | 0.18084(18) | 0.0290(4)       |
| C6   | 0.5309(2)   | 0.6700(2)   | 0.18708(19) | 0.0303(4)       |
| C7   | 0.4620(2)   | 0.7702(2)   | 0.29102(18) | 0.0263(4)       |
| C8   | 0.3703(2)   | 0.7101(2)   | 0.38978(17) | 0.0205(4)       |
| C9   | 0.3483(2)   | 0.5530(2)   | 0.38640(16) | 0.0169(3)       |
| C10  | 0.1965(2)   | 0.3925(2)   | 0.54676(16) | 0.0169(3)       |
| N11  | 0.10114(17) | 0.38650(16) | 0.65652(13) | 0.0184(3)       |
| N12  | 0.09465(18) | 0.23359(17) | 0.65707(13) | 0.0194(3)       |
| N13  | 0.17772(19) | 0.14853(17) | 0.55553(14) | 0.0241(3)       |
| N14  | 0.24360(19) | 0.24796(17) | 0.48312(14) | 0.0223(3)       |
| C15  | -0.0035(2)  | 0.1671(2)   | 0.75805(17) | 0.0249(4)       |
| C16  | 0.0526(2)   | 0.1776(2)   | 0.88992(16) | 0.0203(4)       |
| C17  | 0.1949(2)   | 0.0679(2)   | 0.93297(17) | 0.0223(4)       |
| C18  | 0.2436(3)   | 0.0778(3)   | 1.05528(19) | 0.0338(5)       |
| C19  | 0.1490(3)   | 0.2027(3)   | 1.1362(2)   | 0.0437(6)       |
| C20  | 0.0081(3)   | 0.3143(3)   | 1.0951(2)   | 0.0444(6)       |
| C21  | -0.0402(3)  | 0.3010(2)   | 0.97331(19) | 0.0329(5)       |
| Cl22 | 0.31672(6)  | -0.08744(6) | 0.83164(5)  | 0.03467(16)     |



**Table 4. Selected bond lengths (Å) for 25709A1.**

|         |          |          |            |
|---------|----------|----------|------------|
| N1-C2   | 1.360(2) | N1-C8    | 1.374(2)   |
| C2-C3   | 1.367(2) | C3-C9    | 1.434(2)   |
| C3-C10  | 1.447(2) | C4-C5    | 1.378(3)   |
| C4-C9   | 1.401(2) | C5-C6    | 1.399(3)   |
| C6-C7   | 1.374(3) | C7-C8    | 1.391(2)   |
| C8-C9   | 1.408(2) | C10-N11  | 1.332(2)   |
| C10-N14 | 1.358(2) | N11-N12  | 1.3247(19) |
| N12-N13 | 1.319(2) | N12-C15  | 1.466(2)   |
| N13-N14 | 1.317(2) | C15-C16  | 1.500(2)   |
| C16-C17 | 1.386(3) | C16-C21  | 1.387(2)   |
| C17-C18 | 1.380(3) | C17-Cl22 | 1.7364(18) |
| C18-C19 | 1.385(3) | C19-C20  | 1.378(4)   |
| C20-C21 | 1.379(3) |          |            |

**Table 5. Selected bond angles (°) for 25709A1.**

|              |            |              |            |
|--------------|------------|--------------|------------|
| C2-N1-C8     | 109.19(14) | N1-C2-C3     | 109.97(16) |
| C2-C3-C9     | 106.68(15) | C2-C3-C10    | 125.63(15) |
| C9-C3-C10    | 127.62(14) | C5-C4-C9     | 118.56(16) |
| C4-C5-C6     | 121.43(18) | C7-C6-C5     | 121.37(17) |
| C6-C7-C8     | 117.26(17) | N1-C8-C7     | 129.88(16) |
| N1-C8-C9     | 107.58(15) | C7-C8-C9     | 122.53(16) |
| C4-C9-C8     | 118.84(15) | C4-C9-C3     | 134.56(15) |
| C8-C9-C3     | 106.58(14) | N11-C10-N14  | 111.97(14) |
| N11-C10-C3   | 123.76(14) | N14-C10-C3   | 124.26(15) |
| N12-N11-C10  | 101.73(13) | N13-N12-N11  | 114.05(13) |
| N13-N12-C15  | 122.88(14) | N11-N12-C15  | 122.99(14) |
| N14-N13-N12  | 106.34(13) | N13-N14-C10  | 105.91(14) |
| N12-C15-C16  | 112.59(13) | C17-C16-C21  | 117.96(17) |
| C17-C16-C15  | 122.53(16) | C21-C16-C15  | 119.51(17) |
| C18-C17-C16  | 121.86(18) | C18-C17-Cl22 | 118.39(15) |
| C16-C17-Cl22 | 119.75(14) | C17-C18-C19  | 118.9(2)   |
| C20-C19-C18  | 120.2(2)   | C19-C20-C21  | 120.0(2)   |
| C20-C21-C16  | 121.0(2)   |              |            |

**Table 6. Selected torsion angles (°) for 25709A1.**

|                 |             |                 |             |
|-----------------|-------------|-----------------|-------------|
| C8-N1-C2-C3     | 0.3(2)      | N1-C2-C3-C9     | -0.5(2)     |
| N1-C2-C3-C10    | 176.64(15)  | C9-C4-C5-C6     | 0.5(3)      |
| C4-C5-C6-C7     | -0.5(3)     | C5-C6-C7-C8     | -0.1(3)     |
| C2-N1-C8-C7     | 178.93(18)  | C2-N1-C8-C9     | 0.03(19)    |
| C6-C7-C8-N1     | -178.20(17) | C6-C7-C8-C9     | 0.6(3)      |
| C5-C4-C9-C8     | 0.0(2)      | C5-C4-C9-C3     | 178.42(18)  |
| N1-C8-C9-C4     | 178.46(15)  | C7-C8-C9-C4     | -0.5(2)     |
| N1-C8-C9-C3     | -0.35(18)   | C7-C8-C9-C3     | -179.35(16) |
| C2-C3-C9-C4     | -178.00(18) | C10-C3-C9-C4    | 4.9(3)      |
| C2-C3-C9-C8     | 0.54(18)    | C10-C3-C9-C8    | -176.56(16) |
| C2-C3-C10-N11   | 3.4(3)      | C9-C3-C10-N11   | -179.99(16) |
| C2-C3-C10-N14   | -175.17(17) | C9-C3-C10-N14   | 1.4(3)      |
| N14-C10-N11-N12 | 0.72(18)    | C3-C10-N11-N12  | -178.03(15) |
| C10-N11-N12-N13 | -0.51(18)   | C10-N11-N12-C15 | -177.45(15) |
| N11-N12-N13-N14 | 0.11(19)    | C15-N12-N13-N14 | 177.05(14)  |
| N12-N13-N14-C10 | 0.34(18)    | N11-C10-N14-N13 | -0.69(19)   |
| C3-C10-N14-N13  | 178.05(15)  | N13-N12-C15-C16 | 123.47(17)  |
| N11-N12-C15-C16 | -59.9(2)    | N12-C15-C16-C17 | -79.5(2)    |
| N12-C15-C16-C21 | 100.65(19)  | C21-C16-C17-C18 | 0.8(3)      |
| C15-C16-C17-C18 | -179.07(16) | C21-C16-C17-C12 | -179.30(13) |
| C15-C16-C17-C12 | 0.8(2)      | C16-C17-C18-C19 | -1.1(3)     |
| C12-C17-C18-C19 | 178.95(14)  | C17-C18-C19-C20 | 0.5(3)      |
| C18-C19-C20-C21 | 0.6(3)      | C19-C20-C21-C16 | -0.9(3)     |
| C17-C16-C21-C20 | 0.2(3)      | C15-C16-C21-C20 | -179.89(17) |

**Table 7. Anisotropic atomic displacement parameters (Å<sup>2</sup>) for 25709A1.**The anisotropic atomic displacement factor exponent takes the form:  $-2\pi^2 [h^2a^{*2} U^{11} + \dots + 2hka^* b^* U^{12}]$ .

|      | U <sup>11</sup> | U <sup>22</sup> | U <sup>33</sup> | U <sup>23</sup> | U <sup>13</sup> | U <sup>12</sup> |
|------|-----------------|-----------------|-----------------|-----------------|-----------------|-----------------|
| N1   | 0.0344(9)       | 0.0152(8)       | 0.0270(9)       | -0.0003(6)      | -0.0035(7)      | -0.0110(7)      |
| C2   | 0.0271(9)       | 0.0192(9)       | 0.0203(9)       | 0.0006(7)       | -0.0015(7)      | -0.0077(7)      |
| C3   | 0.0184(8)       | 0.0153(8)       | 0.0172(9)       | 0.0022(6)       | -0.0044(6)      | -0.0043(7)      |
| C4   | 0.0254(9)       | 0.0202(9)       | 0.0216(9)       | 0.0021(7)       | -0.0034(7)      | -0.0057(7)      |
| C5   | 0.0326(10)      | 0.0324(10)      | 0.0204(10)      | 0.0041(8)       | 0.0000(8)       | -0.0075(9)      |
| C6   | 0.0289(10)      | 0.0384(11)      | 0.0264(11)      | 0.0143(9)       | -0.0026(8)      | -0.0151(9)      |
| C7   | 0.0288(10)      | 0.0258(10)      | 0.0297(11)      | 0.0116(8)       | -0.0103(8)      | -0.0151(8)      |
| C8   | 0.0216(9)       | 0.0190(8)       | 0.0227(9)       | 0.0049(7)       | -0.0092(7)      | -0.0066(7)      |
| C9   | 0.0175(8)       | 0.0165(8)       | 0.0183(9)       | 0.0047(6)       | -0.0066(6)      | -0.0062(7)      |
| C10  | 0.0196(8)       | 0.0162(8)       | 0.0157(8)       | 0.0013(6)       | -0.0054(6)      | -0.0048(7)      |
| N11  | 0.0221(7)       | 0.0155(7)       | 0.0191(8)       | 0.0024(6)       | -0.0037(6)      | -0.0072(6)      |
| N12  | 0.0259(8)       | 0.0176(7)       | 0.0177(8)       | 0.0036(6)       | -0.0044(6)      | -0.0105(6)      |
| N13  | 0.0361(9)       | 0.0180(7)       | 0.0203(8)       | 0.0015(6)       | -0.0021(7)      | -0.0112(7)      |
| N14  | 0.0343(8)       | 0.0154(7)       | 0.0186(8)       | 0.0019(6)       | -0.0013(6)      | -0.0097(6)      |
| C15  | 0.0252(9)       | 0.0286(10)      | 0.0252(10)      | 0.0091(7)       | -0.0050(7)      | -0.0143(8)      |
| C16  | 0.0222(9)       | 0.0208(9)       | 0.0201(9)       | 0.0047(7)       | 0.0023(7)       | -0.0116(7)      |
| C17  | 0.0248(9)       | 0.0224(9)       | 0.0231(10)      | 0.0066(7)       | -0.0010(7)      | -0.0128(8)      |
| C18  | 0.0378(11)      | 0.0477(13)      | 0.0258(11)      | 0.0145(9)       | -0.0111(9)      | -0.0267(10)     |
| C19  | 0.0728(17)      | 0.0587(15)      | 0.0188(11)      | 0.0034(10)      | -0.0029(10)     | -0.0505(14)     |
| C20  | 0.0757(17)      | 0.0338(12)      | 0.0274(12)      | -0.0065(9)      | 0.0169(11)      | -0.0277(12)     |
| C21  | 0.0408(11)      | 0.0235(10)      | 0.0310(11)      | 0.0037(8)       | 0.0115(9)       | -0.0085(9)      |
| Cl22 | 0.0337(3)       | 0.0239(3)       | 0.0408(3)       | 0.0042(2)       | 0.0036(2)       | -0.0014(2)      |

**Table 8. Hydrogen atom coordinates and isotropic atomic displacement parameters (Å<sup>2</sup>) for 25709A1.**

|      | x        | y        | z        | U        |
|------|----------|----------|----------|----------|
| H1   | 0.270(3) | 0.884(3) | 0.522(2) | 0.041(6) |
| H2   | 0.1446   | 0.7018   | 0.6491   | 0.026    |
| H4   | 0.4073   | 0.3471   | 0.2741   | 0.027    |
| H5   | 0.5584   | 0.4478   | 0.1073   | 0.035    |
| H6   | 0.5942   | 0.7075   | 0.1180   | 0.036    |
| H7   | 0.4764   | 0.8762   | 0.2953   | 0.032    |
| H15A | 0.0083   | 0.0518   | 0.7381   | 0.030    |
| H15B | -0.1249  | 0.2274   | 0.7581   | 0.030    |
| H18  | 0.3404   | 0.0002   | 1.0835   | 0.041    |
| H19  | 0.1815   | 0.2115   | 1.2205   | 0.052    |
| H20  | -0.0559  | 0.4003   | 1.1506   | 0.053    |
| H21  | -0.1385  | 0.3774   | 0.9461   | 0.039    |

**Table 9. Selected hydrogen bond information for 25709A1 (Å and °).**

| D-H...A       | d(D-H)  | d(H...A) | d(D...A) | <(DHA) |
|---------------|---------|----------|----------|--------|
| N1-H1...N13#1 | 0.86(2) | 2.21(2)  | 3.051(2) | 168(2) |

#1 x,y+1,z

## 5.2. Appendix 2: VCD analysis of compounds 3.17a and 3.17b

### *Ab Initio* VCD Analysis of compounds 3.17a and 3.17b

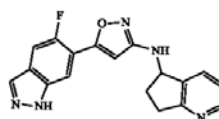
#### I. Sample Information:

- Date: March 27, 2014
- Submitter: Yannick Lacroix
- Analyst: Douglas Minick

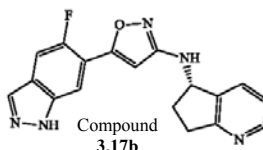
#### II. Technique: VCD

#### III. Experiment: Stereochemical analysis

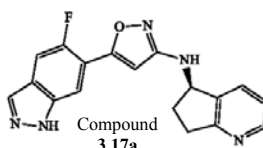
#### IV. Objective: Determine the absolute configuration of the unassigned chiral center:



#### V. Assigned Structures:



(*S*)-*N*-(6,7-dihydro-5*H*-cyclopenta[*b*]pyridin-5-yl)-5-(5-fluoro-1*H*-indazol-6-yl)isoxazol-3-amine



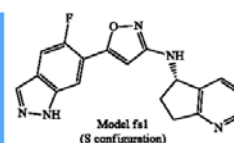
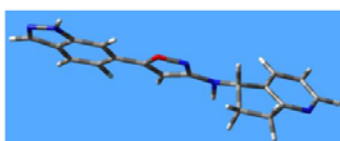
(*R*)-*N*-(6,7-dihydro-5*H*-cyclopenta[*b*]pyridin-5-yl)-5-(5-fluoro-1*H*-indazol-6-yl)isoxazol-3-amine

#### VI. Comments:

- Input as required.

#### VII. Theoretical Analysis:

- Model:



- Conformational Search: MOE systematic csearch (rmsd=0.25)/MMFF94x/ff/Born solv (e=80)
- Model Chemistry: # opt freq=(noraman,vcd) b3lyp/dgdzvp
- Conformational Analysis: Fractional populations estimated using Boltzmann statistics
- Lorentzian band width: 8 cm<sup>-1</sup>
- Frequency scale factor: 0.975
- Estimation of Confidence Limit: CompareVOA (BioTools, Inc.) analysis (Section X)

#### VIII. Experimental:

- Spectrometer: BioTools ChiralIR-2X FT-VCD spectrometer operated at 4 cm<sup>-1</sup>
- VCD Frequency Range: 2400-800 cm<sup>-1</sup>
- PEM Calibration: PEM calibrated at 1400 cm<sup>-1</sup>
- PEM Retardation Settings: PEM1 = 0.250\*λ; PEM2 = 0.245\*λ
- ChiralIR-2X Scan Method(s):
  - Compound **3.17b**: three 4 hr blocks (37440 total scans)
  - Compound **3.17a**: single 4 hr block scan (12480 total scans)
- Solvent: d<sub>6</sub>-DMSO
- Concentrations:
  - [Compound **3.17b**] ~ 12.6mg/135ul
  - [Compound **3.17a**] ~ 12.6mg/150ul
- Baseline Correction (Modified Half-Difference):
  - VCD<sub>67-1</sub> (corr'd) = VCD<sub>67-1</sub> minus VCD<sub>74-1</sub>
  - VCD<sub>74-1</sub> (corr'd) = VCD<sub>74-1</sub> minus VCD<sub>67-1</sub>
- Additional Processing: Savitsky-Golay 9-point smooth

#### IX. Results:

- Analysis of Experimental and Calculated Data:  
The VCD and IR spectra of compound **3.17b** and compound **3.17a** are compared with calculated data in Figures 1 and 2, respectively. The green box in each figure highlights the spectral range over which VCD data were used to assign stereochemistry and estimate the confidence limit (Section X).

Inspection of VCD data in the analysis range indicates that the VCD spectrum of compound **3.17b** is largely coincident with the model spectrum and compound **3.17a** largely its mirror image. These results are consistent with compound **3.17b** having the same absolute configuration as the model and compound **3.17a** having the opposite configuration of the model. Based on these findings, compound **3.17b** was assigned with S absolute configuration and compound **3.17a** with R absolute configuration.

The confidence limit (CL) for these assignments was estimated to be ≥97%, consistent with a moderate-to-high level of reliability (Section X).

While the CL estimated for this study is a bit lower than desired, the level of analysis was sufficient for making reliable assignments. Two major factors were responsible for lowering the CL: (a) use of a shorter scan time for **3.17a** (b) inaccuracy in the frequency calculated for the NH bending mode (see band assignments in figures). The shorter scan time for **3.17a** resulted in lower accuracy in the experimental VCD intensities used by CompareVOA (Section X) to estimate the CL. Furthermore, miss-alignment between calc'd and obs'd NH bands in the 1550-1500 cm<sup>-1</sup> region could not be corrected by CompareVOA (Section X), lowering the overall correlation between VCD data in the analysis range and in turn, the CL. As an afterword, if the analysis range is narrowed to 1490-1090 cm<sup>-1</sup> (still an acceptable window for VCD analysis), the CL approaches 100%.

With respect to the IR data included in the lower panel of each figure, the spectrum calculated for Model fs1m1 is in good qualitative agreement with the experimental IR spectra, disregarding the frequency offset in the 1550-1500  $\text{cm}^{-1}$ . Close agreement between these spectra provides an independent cross-check of the correctness of the two dimensional conformational space and also demonstrates proper computational analysis of the solution phase conformational space occupied by 3.17a and 3.17b under experimental conditions.

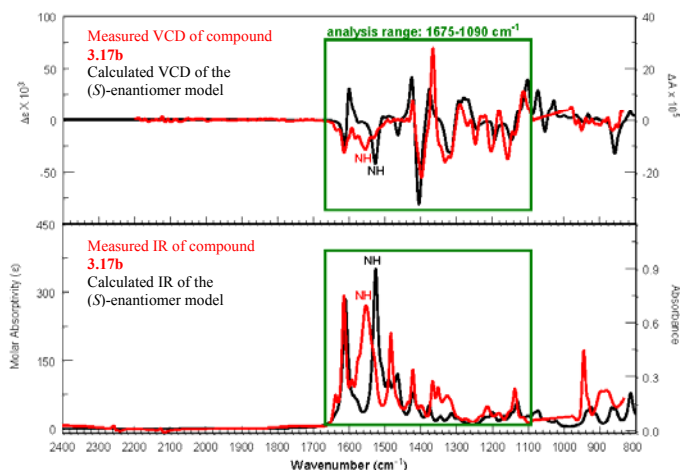


Figure 1: VCD spectra of compound 3.17b and Model fs1m1 (top); IR spectra of compound 3.17b and Model fs1m1 (bottom).

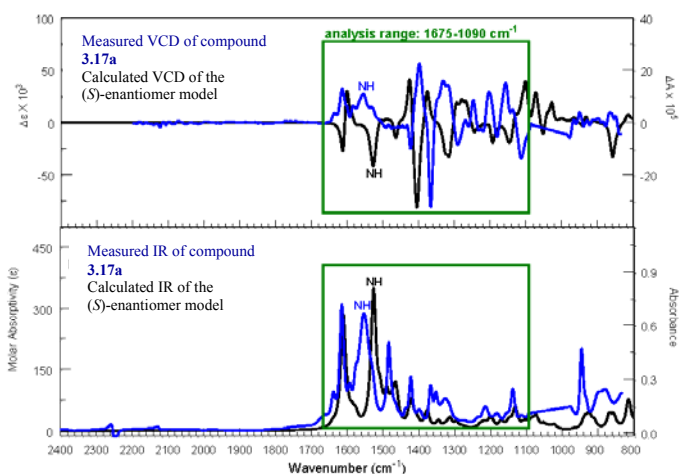


Figure 2: VCD spectra of compound 3.17a and Model fs1m1 (top); IR spectra of compound 3.17a and Model fs1m1 (bottom).

#### X. Estimated Level of Reliability

- The confidence limit in this study was estimated using CompareVOA™ (BioTools, Inc.), an automated tool for quantifying the level of agreement between calculated and observed VCD data.
- The confidence limit was determined from the absolute values of two parameters from CompareVOA™: total neighborhood similarity (TNS (VCD)) and the enantiomeric similarity index (ESI).
- The confidence limit was then determined by comparing these values to the ranges reported in the table:

| Reliability | *TNS (VCD)<br>(range) | *ESI<br>(range) | Confidence Limit (CL)<br>(range) |
|-------------|-----------------------|-----------------|----------------------------------|
| High        | ≥ 70                  | ≥ 60            | > 99 %                           |
| Medium      | 60 - 70               | 50 - 60         | 95 – 99 %                        |
| Low         | 50 - 60               | 40 – 50         | 90 – 95 %                        |
| Unreliable  | < 50                  | < 40            | < 90 %                           |

\*absolute value

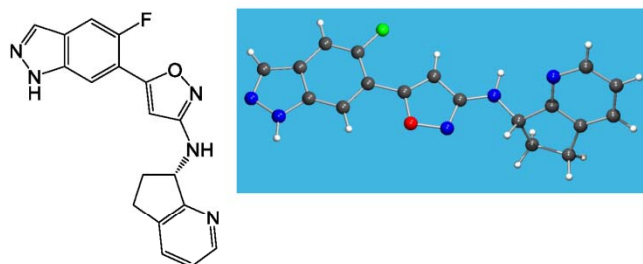
- CompareVOA results for the current study:
  - Analysis range: 1675-1090 cm<sup>-1</sup>
  - Region omitted: none
  - Range of statistical analysis (minimum 400 cm<sup>-1</sup>): 585 cm<sup>-1</sup>
  - Width of triangular weighting function: 20 cm<sup>-1</sup>
  - TNS (VCD): 63.0 (absolute value)
  - ESI: 62.7 (absolute value)
- *Estimated Confidence Limit:*     **≥97%**



### 5.3. Appendix 3: Single crystal X-ray diffraction crystallography of compound 3.16a

#### Crystal Structure Information for 57770C2

2-D ChemDraw and 3-D ball and stick representations



Compound 3.16a

(*S*)-*N*-(6,7-Dihydro-5*H*-cyclopenta[*b*]pyridin-7-yl)-5-(5-fluoro-1*H*-indazol-6-yl)isoxazol-3-amine

#### Points of note

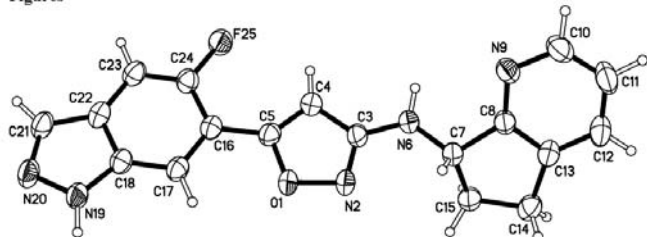
- The asymmetric unit contains four independent molecules of compound 3.16a, henceforth referred to as molecule **A** (Figure 1), molecule **B** (Figure 2, with ' added to the atom names), molecule **C** (Figure 3, with " added) and molecule **D** (Figure 4, with \* added). In the following discussion, molecule **A** is described in some detail, with corresponding findings for molecules **B**, **C** and **D** being presented in square brackets.
- Final R1 [ $I > 2\sigma(I)$ ] = 3.04 %.
- The absolute configuration has been unambiguously determined from anomalous scattering effects; the chiral centre C7 has the (*S*) configuration.
- The isoxazole ring is approximately coplanar with the indazole fused ring system, with a dihedral angle of 1.81(6)° [8.30(5)°, 5.40(6)°, 3.75(4)°].

- The cyclopentene ring has an envelope conformation, with C15 as the flap atom.
- The four molecules in the asymmetric unit (which is the complete unit cell) differ mainly in the orientation of the dihydrocyclopenta[*b*]pyridine fused ring system relative to the mean plane of the rest of the molecule, by rotation about the N6-C7 bond, as shown in the multiple overlay of the molecules in Figure 5.
- The dihydrocyclopenta[*b*]pyridine rings in molecule **C** appear to exhibit greater librational motion than other parts of the structure based on the somewhat elongated atomic displacement ellipsoids seen in Figure 3. This motion or dynamic disorder leads to some minor geometric artefacts in this region, such as slightly shortened bond lengths.
- The four independent molecules form a discrete tetrameric cluster held together by eight hydrogen bonds, as shown in Figure 6, with geometrical details of the hydrogen bonds in Table 9. Pairs of molecules (**A** with **B**, **C** with **D**) are connected by N19-H19...N2 hydrogen bonds, and these two pairs are linked by N6-H6...N9 hydrogen bonds (**A** with **C**, **B** with **D**) to give the complete tetramer, which has approximate  $D_2$  (222) symmetry.
- The tetrameric units are stacked on top of each other in the *a*-axis direction, with ring-stacking interactions both within and between tetramers, as shown in Figure 7. Ring-stacking interactions occur between isoxazole rings, and between indazole fused ring systems. A packing diagram is shown in Figure 8, the view being along the ring-stacking direction.
- After data collection at 150K, a unit cell determination at 295K was carried out on the same crystal. The two primitive triclinic unit cells are presented below (150K top and 295K bottom).

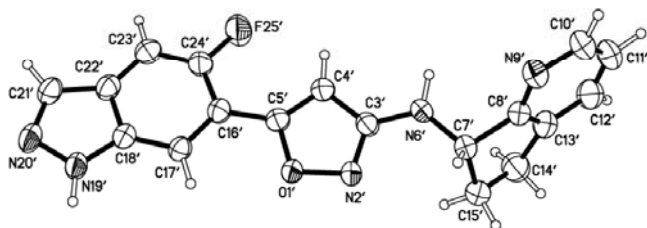
| <i>a</i> / Å | <i>b</i> / Å | <i>c</i> / Å | $\alpha$ / ° | $\beta$ / ° | $\gamma$ / ° | <i>V</i> / Å <sup>3</sup> |
|--------------|--------------|--------------|--------------|-------------|--------------|---------------------------|
| 7.25630(16)  | 13.3952(3)   | 16.8439(4)   | 100.4337(17) | 96.8289(18) | 91.4473(17)  | 1597.08(6)                |
| 7.3494(15)   | 13.434(4)    | 16.958(4)    | 100.079(18)  | 97.944(18)  | 90.876(17)   | 1631.3(6)                 |

The 295K cell was refined from 461 reflections, and the 150K cell from 20988 reflections in the complete data set. The unit cell volume at 295K is 2.1 % greater than at 150K.

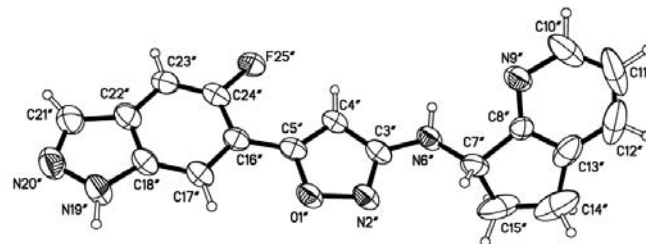
Figures



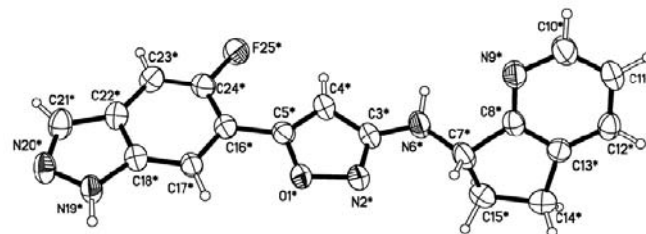
**Figure 1.** A view of molecule A of compound 3.16a from the 57770C2 crystal structure, showing the numbering scheme employed. Anisotropic atomic displacement ellipsoids for the non-hydrogen atoms are shown at the 50% probability level. Hydrogen atoms are displayed with an arbitrarily small radius.



**Figure 2.** A view of molecule B of compound 3.16a from the 57770C2 crystal structure, showing the numbering scheme employed. Anisotropic atomic displacement ellipsoids for the non-hydrogen atoms are shown at the 50% probability level. Hydrogen atoms are displayed with an arbitrarily small radius.



**Figure 3.** A view of molecule C of compound 3.16a from the 57770C2 crystal structure, showing the numbering scheme employed. Anisotropic atomic displacement ellipsoids for the non-hydrogen atoms are shown at the 50% probability level. Hydrogen atoms are displayed with an arbitrarily small radius.



**Figure 4.** A view of molecule D of compound 3.16a from the 57770C2 crystal structure, showing the numbering scheme employed. Anisotropic atomic displacement ellipsoids for the non-hydrogen atoms are shown at the 50% probability level. Hydrogen atoms are displayed with an arbitrarily small radius.

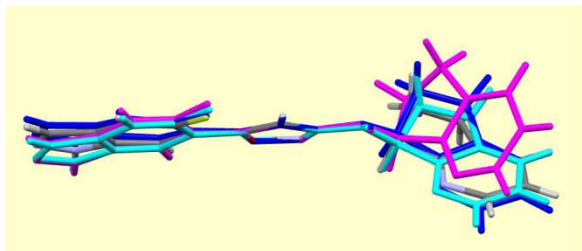


Figure 5. Least-squares fit for atoms O1 to C5 of molecule A (coloured by atom type) with the corresponding atoms of molecules B (coloured magenta, RMS = 0.010 Å), C (coloured cyan, RMS = 0.008 Å), and D (coloured blue, RMS = 0.010 Å).

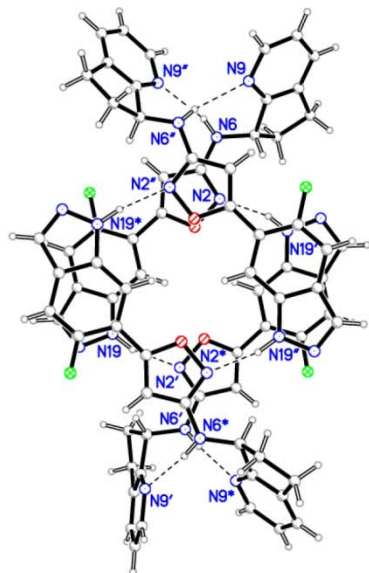


Figure 6. Hydrogen bonding in the 57770C2 crystal structure. Hydrogen bonds are displayed as dashed lines. Donor and acceptor atoms are labelled.

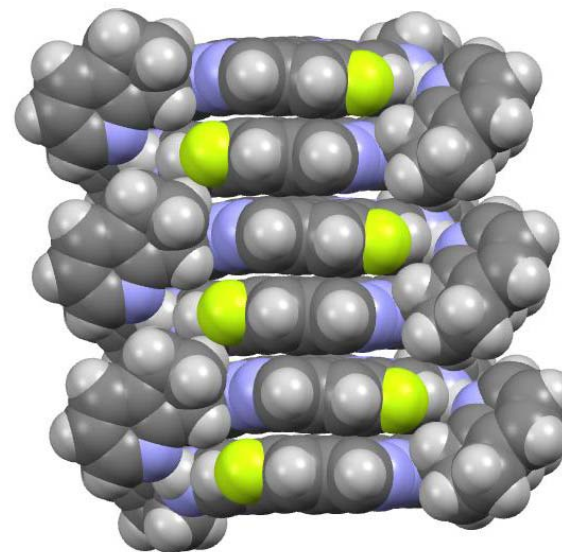
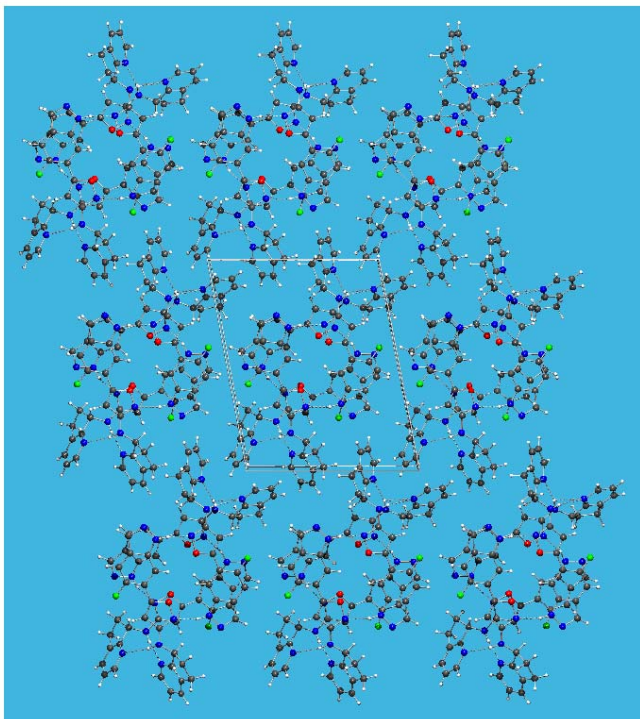


Figure 7. Space-filling model of three tetramer units, showing the ring-stacking interactions within and between tetramers.



**Figure 8.** Packing plot for the 57770C2 crystal structure viewed down the crystallographic  $\alpha$ -axis ( $b$ -axis horizontal). Hydrogen bonds are displayed as dashed lines.

**Table 1. Sample and crystal data for 57770C2.**

|                          |   |                          |
|--------------------------|---|--------------------------|
| Identification code      | 57770C2   |                          |
| Compound number          | Compound <b>3.16a</b>                             |                          |
| Proj                     |   |                          |
| Che                      |   |                          |
| X-r                      |   |                          |
| Cry                      |   |                          |
| Crystallization solvents | Methanol and toluene                              |                          |
| Crystallization method   | Slow evaporation                                  |                          |
| Moiety formula           | C <sub>13</sub> H <sub>14</sub> FN <sub>3</sub> O |                          |
| Empirical formula        | C <sub>13</sub> H <sub>14</sub> FN <sub>3</sub> O |                          |
| Formula weight           | 335.34  |                          |
| Temperature              | 150(2) K  |                          |
| Wavelength               | 1.54178 Å   |                          |
| Crystal size             | 0.18 x 0.15 x 0.12 mm                             |                          |
| Crystal habit            | Colourless block                                  |                          |
| Crystal system           | Triclinic   |                          |
| Space group              | P1  |                          |
| Unit cell dimensions     | a = 7.25630(16) Å                                 | $\alpha$ = 100.4337(17)° |
|                          | b = 13.3952(3) Å                                  | $\beta$ = 96.8289(18)°   |
|                          | c = 16.8459(4) Å                                  | $\gamma$ = 91.4473(17)°  |
| Volume                   | 1597.08(6) Å <sup>3</sup>                         |                          |
| Z                        | 4   |                          |
| Density (calculated)     | 1.395 Mg/m <sup>3</sup>                           |                          |
| Absorption coefficient   | 0.825 mm <sup>-1</sup>                            |                          |
| F(000)                   | 696   |                          |

**Table 2. Data collection and structure refinement for 57770C2.**

|                                     |  |
|-------------------------------------|--|
| Diffractometer                      | Oxford Diffraction Gemini A Ultra  |
| Radiation source                    | Enhance Ultra (Cu) X-ray Source, CuK $\alpha$  |
| Data collection method              | $\omega$ scans   |
| Theta range for data collection     | 2.69 to 66.34 $^\circ$   |
| Index ranges                        | $-8 \leq h \leq 8, -15 \leq k \leq 15, -19 \leq l \leq 19$                               |
| Reflections collected               | 43479  |
| Independent reflections             | 10842 [R(int) = 0.0287]  |
| Coverage of independent reflections | 99.5 %   |
| Variation in check reflections      | N/A  |
| Absorption correction               | Analytical   |
| Max. and min. transmission          | 0.916 and 0.901  |
| Structure solution technique        | Direct methods   |
| Structure solution program          | SHELXT (Sheldrick, 2014)   |
| Refinement technique                | Full-matrix least-squares on F <sup>2</sup>  |
| Refinement program                  | SHELXTL V2008/4 (Bruker, 2008)   |
| Function minimized                  | $\Sigma w(F_o^2 - F_c^2)^2$  |
| Data / restraints / parameters      | 10842 / 3 / 934  |
| Goodness-of-fit on F <sup>2</sup>   | 1.048  |
| $\Delta \sigma_{\max}$              | 0.001  |
| Final R indices                     |  |
| 10169 data; $F > 2\sigma(I)$        | R1 = 0.0304, wR2 = 0.0773  |
| all data                            | R1 = 0.0338, wR2 = 0.0802  |
| Weighting scheme                    | calc $w = 1/[\sigma^2(F_o^2) + (0.0469P)^2 + 0.1399P]$<br>where $P = (F_o^2 + 2F_c^2)/3$ |
| Absolute structure parameter        | 0.06(8)  |
| Extinction coefficient              | 0.00072(11)  |
| Largest diff. peak and hole         | 0.173 and -0.134 e $\text{\AA}^{-3}$   |

## Refinement summary:

|                               |   |
|-------------------------------|---|
| Ordered Non-H atoms, XYZ      | Freely refined                                |
| Ordered Non-H atoms, U        | Freely refined - anisotropic                  |
| H atoms (on carbon), XYZ      | Idealized positions riding on attached atoms  |
| H atoms (on carbon), U        | Appropriate multiple of U(eq) for bonded atom |
| H atoms (on heteroatoms), XYZ | Freely refined                                |
| H atoms (on heteroatoms), U   | Freely refined - isotropic                    |
| Disordered atoms              | No modelled disorder                          |

**Table 3. Atomic coordinates and equivalent isotropic atomic displacement parameters ( $\text{\AA}^2$ ) for 57770C2.**U<sub>eq</sub> is defined as one third of the trace of the orthogonalized U<sub>ij</sub> tensor.

|     | x           | y           | z           | U <sub>eq</sub> |
|-----|-------------|-------------|-------------|-----------------|
| O1  | 0.33043(18) | 0.56379(9)  | 0.63612(8)  | 0.0410(3)       |
| N2  | 0.3280(2)   | 0.66760(11) | 0.67313(10) | 0.0419(4)       |
| C3  | 0.4001(2)   | 0.67246(14) | 0.74851(12) | 0.0369(4)       |
| C4  | 0.4479(2)   | 0.57485(14) | 0.76528(12) | 0.0388(4)       |
| C5  | 0.4040(2)   | 0.51119(13) | 0.69295(11) | 0.0352(4)       |
| N6  | 0.4225(2)   | 0.76326(12) | 0.80202(11) | 0.0422(4)       |
| C7  | 0.4033(2)   | 0.85660(13) | 0.77015(12) | 0.0383(4)       |
| C8  | 0.5174(2)   | 0.94489(13) | 0.82290(11) | 0.0356(4)       |
| N9  | 0.6892(2)   | 0.93810(12) | 0.85897(10) | 0.0402(4)       |
| C10 | 0.7684(3)   | 1.02628(16) | 0.90187(13) | 0.0502(5)       |
| C11 | 0.6828(3)   | 1.11774(16) | 0.90917(14) | 0.0548(5)       |
| C12 | 0.5058(3)   | 1.12214(14) | 0.87080(13) | 0.0477(5)       |
| C13 | 0.4212(2)   | 1.03353(13) | 0.82586(11) | 0.0382(4)       |
| C14 | 0.2343(3)   | 1.01287(15) | 0.77589(13) | 0.0455(4)       |
| C15 | 0.2062(3)   | 0.89696(15) | 0.76510(13) | 0.0440(4)       |
| C16 | 0.4197(2)   | 0.40235(13) | 0.66317(11) | 0.0333(4)       |
| C17 | 0.3605(2)   | 0.36128(13) | 0.58256(11) | 0.0352(4)       |
| C18 | 0.3714(2)   | 0.25689(13) | 0.55772(11) | 0.0340(4)       |
| N19 | 0.3218(2)   | 0.19663(11) | 0.48375(10) | 0.0382(3)       |
| N20 | 0.3480(2)   | 0.09772(11) | 0.48614(10) | 0.0433(4)       |
| C21 | 0.4160(3)   | 0.09447(14) | 0.56181(12) | 0.0420(4)       |
| C22 | 0.4366(2)   | 0.19267(13) | 0.61083(11) | 0.0368(4)       |
| C23 | 0.5027(3)   | 0.23514(14) | 0.69195(12) | 0.0390(4)       |
| C24 | 0.4931(2)   | 0.33740(14) | 0.71502(11) | 0.0361(4)       |
| F25 | 0.55735(16) | 0.38046(8)  | 0.79376(6)  | 0.0468(3)       |

**Table 3 (continued). Atomic coordinates and equivalent isotropic atomic displacement parameters (Å<sup>2</sup>) for 57770C2.**

$U_{eq}$  is defined as one third of the trace of the orthogonalized  $U^j$  tensor.

|      | x           | y            | z           | $U_{eq}$  |
|------|-------------|--------------|-------------|-----------|
| O1'  | 0.18145(18) | 0.40119(9)   | 0.39405(7)  | 0.0390(3) |
| N2'  | 0.1993(2)   | 0.29915(11)  | 0.35444(9)  | 0.0381(3) |
| C3'  | 0.1665(2)   | 0.30116(14)  | 0.27637(11) | 0.0351(4) |
| C4'  | 0.1285(3)   | 0.39983(14)  | 0.26186(11) | 0.0375(4) |
| C5'  | 0.1399(2)   | 0.45854(14)  | 0.33615(11) | 0.0353(4) |
| N6'  | 0.1678(2)   | 0.21551(12)  | 0.21813(9)  | 0.0402(4) |
| C7'  | 0.2391(3)   | 0.12186(14)  | 0.24025(11) | 0.0385(4) |
| C8'  | 0.2686(3)   | 0.05332(14)  | 0.16125(11) | 0.0410(4) |
| N9'  | 0.4138(3)   | 0.06340(13)  | 0.12146(11) | 0.0518(4) |
| C10' | 0.4052(4)   | 0.00078(18)  | 0.04850(15) | 0.0659(7) |
| C11' | 0.2597(5)   | -0.06713(19) | 0.01604(15) | 0.0738(8) |
| C12' | 0.1099(4)   | -0.07585(17) | 0.05823(14) | 0.0673(7) |
| C13' | 0.1152(3)   | -0.01392(15) | 0.13376(13) | 0.0502(5) |
| C14' | -0.0214(3)  | -0.00222(18) | 0.19473(14) | 0.0581(6) |
| C15' | 0.0923(3)   | 0.05987(16)  | 0.27146(12) | 0.0476(5) |
| C16' | 0.1212(2)   | 0.56637(14)  | 0.36699(11) | 0.0372(4) |
| C17' | 0.1663(2)   | 0.60747(14)  | 0.44847(11) | 0.0349(4) |
| C18' | 0.1505(2)   | 0.71184(13)  | 0.47304(11) | 0.0350(4) |
| N19' | 0.1863(2)   | 0.77152(12)  | 0.54792(11) | 0.0398(4) |
| N20' | 0.1560(2)   | 0.87037(12)  | 0.54559(11) | 0.0447(4) |
| C21' | 0.0980(3)   | 0.87384(15)  | 0.46850(13) | 0.0461(5) |
| C22' | 0.0907(3)   | 0.77602(14)  | 0.41907(12) | 0.0404(4) |
| C23' | 0.0419(3)   | 0.73405(16)  | 0.33678(13) | 0.0532(5) |
| C24' | 0.0585(3)   | 0.63240(16)  | 0.31414(12) | 0.0501(5) |
| F25' | 0.0111(3)   | 0.58953(10)  | 0.23453(7)  | 0.0816(5) |

**Table 3 (continued). Atomic coordinates and equivalent isotropic atomic displacement parameters (Å<sup>2</sup>) for 57770C2.**

$U_{eq}$  is defined as one third of the trace of the orthogonalized  $U^j$  tensor.

|       | x           | y           | z           | $U_{eq}$   |
|-------|-------------|-------------|-------------|------------|
| O1''  | 0.81314(19) | 0.61533(10) | 0.60876(8)  | 0.0447(3)  |
| N2''  | 0.8676(2)   | 0.60891(13) | 0.69174(10) | 0.0442(4)  |
| C3''  | 0.8485(2)   | 0.70069(15) | 0.73247(11) | 0.0393(4)  |
| C4''  | 0.7885(2)   | 0.76843(14) | 0.68084(11) | 0.0378(4)  |
| C5''  | 0.7654(2)   | 0.71172(14) | 0.60508(12) | 0.0381(4)  |
| N6''  | 0.8842(2)   | 0.72435(13) | 0.81569(10) | 0.0422(4)  |
| C7''  | 0.9011(3)   | 0.64570(15) | 0.86470(13) | 0.0445(5)  |
| C8''  | 0.8270(3)   | 0.67794(13) | 0.94437(11) | 0.0372(4)  |
| N9''  | 0.6676(2)   | 0.72228(13) | 0.95163(10) | 0.0479(4)  |
| C10'' | 0.6254(4)   | 0.74569(19) | 1.02831(17) | 0.0744(9)  |
| C11'' | 0.7375(7)   | 0.7255(2)   | 1.09482(17) | 0.1040(14) |
| C12'' | 0.8993(7)   | 0.6810(2)   | 1.08490(17) | 0.1001(13) |
| C13'' | 0.9463(4)   | 0.65519(16) | 1.00780(15) | 0.0639(6)  |
| C14'' | 1.1095(5)   | 0.6028(3)   | 0.9770(2)   | 0.0986(12) |
| C15'' | 1.1032(4)   | 0.6224(2)   | 0.8927(2)   | 0.0847(9)  |
| C16'' | 0.6969(2)   | 0.73168(15) | 0.52482(12) | 0.0389(4)  |
| C17'' | 0.6710(3)   | 0.65347(15) | 0.45758(12) | 0.0421(5)  |
| C18'' | 0.6041(3)   | 0.67823(16) | 0.38292(12) | 0.0436(5)  |
| N19'' | 0.5672(3)   | 0.61804(16) | 0.30751(11) | 0.0528(5)  |
| N20'' | 0.5040(3)   | 0.67227(16) | 0.25023(11) | 0.0607(5)  |
| C21'' | 0.4981(4)   | 0.76666(19) | 0.28889(14) | 0.0593(6)  |
| C22'' | 0.5600(3)   | 0.77668(17) | 0.37323(12) | 0.0486(5)  |
| C23'' | 0.5847(3)   | 0.85606(17) | 0.44135(13) | 0.0503(5)  |
| C24'' | 0.6521(3)   | 0.83062(16) | 0.51334(13) | 0.0467(5)  |
| F25'' | 0.68081(18) | 0.90603(9)  | 0.58053(7)  | 0.0586(3)  |

**Table 3 (continued). Atomic coordinates and equivalent isotropic atomic displacement parameters (Å<sup>2</sup>) for 57770C2.**

U<sub>eq</sub> is defined as one third of the trace of the orthogonalized U<sup>ij</sup> tensor.

|      | x           | y           | z            | U <sub>eq</sub> |
|------|-------------|-------------|--------------|-----------------|
| O1*  | 0.70857(19) | 0.39791(10) | 0.37635(7)   | 0.0450(3)       |
| N2*  | 0.6532(2)   | 0.40667(13) | 0.29393(9)   | 0.0437(4)       |
| C3*  | 0.6458(2)   | 0.31328(15) | 0.25276(11)  | 0.0375(4)       |
| C4*  | 0.6931(2)   | 0.24228(15) | 0.30396(11)  | 0.0376(4)       |
| C5*  | 0.7311(2)   | 0.29880(14) | 0.37956(11)  | 0.0358(4)       |
| N6*  | 0.6015(2)   | 0.29193(14) | 0.17011(10)  | 0.0439(4)       |
| C7*  | 0.5423(3)   | 0.37139(15) | 0.12646(12)  | 0.0441(5)       |
| C8*  | 0.3882(2)   | 0.33680(14) | 0.05799(10)  | 0.0365(4)       |
| N9*  | 0.2475(2)   | 0.27386(14) | 0.06276(10)  | 0.0475(4)       |
| C10* | 0.1192(3)   | 0.2530(2)   | -0.00296(13) | 0.0561(6)       |
| C11* | 0.1255(3)   | 0.29498(16) | -0.07155(11) | 0.0467(5)       |
| C12* | 0.2729(3)   | 0.36065(14) | -0.07528(11) | 0.0414(4)       |
| C13* | 0.4091(3)   | 0.38140(14) | -0.00924(11) | 0.0393(4)       |
| C14* | 0.5842(3)   | 0.44767(19) | 0.00693(16)  | 0.0642(6)       |
| C15* | 0.6905(3)   | 0.41320(19) | 0.08196(15)  | 0.0637(6)       |
| C16* | 0.7930(2)   | 0.27777(15) | 0.46108(11)  | 0.0364(4)       |
| C17* | 0.8283(2)   | 0.35755(15) | 0.52691(11)  | 0.0361(4)       |
| C18* | 0.8914(2)   | 0.33361(14) | 0.60236(11)  | 0.0353(4)       |
| N19* | 0.9367(2)   | 0.39520(14) | 0.67660(9)   | 0.0398(4)       |
| N20* | 0.9978(2)   | 0.34121(14) | 0.73414(9)   | 0.0453(4)       |
| C21* | 0.9906(3)   | 0.24501(17) | 0.69701(12)  | 0.0474(5)       |
| C22* | 0.9235(2)   | 0.23413(15) | 0.61325(11)  | 0.0390(4)       |
| C23* | 0.8858(3)   | 0.15327(16) | 0.54640(12)  | 0.0431(4)       |
| C24* | 0.8208(3)   | 0.17780(15) | 0.47388(11)  | 0.0396(4)       |
| F25* | 0.78160(17) | 0.10092(8)  | 0.40832(7)   | 0.0507(3)       |

**Table 4. Selected bond lengths (Å) for 57770C2.**

|           |          |           |            |
|-----------|----------|-----------|------------|
| O1-C5     | 1.356(2) | O1-N2     | 1.4186(18) |
| N2-C3     | 1.304(3) | C3-N6     | 1.370(2)   |
| C3-C4     | 1.429(3) | C4-C5     | 1.353(3)   |
| C5-C16    | 1.465(2) | N6-C7     | 1.451(3)   |
| C7-C8     | 1.506(2) | C7-C15    | 1.540(3)   |
| C8-N9     | 1.333(2) | C8-C13    | 1.389(3)   |
| N9-C10    | 1.344(2) | C10-C11   | 1.380(3)   |
| C11-C12   | 1.375(3) | C12-C13   | 1.373(3)   |
| C13-C14   | 1.500(3) | C14-C15   | 1.536(3)   |
| C16-C17   | 1.382(3) | C16-C24   | 1.411(3)   |
| C17-C18   | 1.392(3) | C18-N19   | 1.360(2)   |
| C18-C22   | 1.401(3) | N19-N20   | 1.350(2)   |
| N20-C21   | 1.320(3) | C21-C22   | 1.415(3)   |
| C22-C23   | 1.404(3) | C23-C24   | 1.360(3)   |
| C24-F25   | 1.368(2) |           |            |
| O1'-C5'   | 1.359(2) | O1'-N2'   | 1.4246(18) |
| N2'-C3'   | 1.314(2) | C3'-N6'   | 1.369(2)   |
| C3'-C4'   | 1.415(3) | C4'-C5'   | 1.344(2)   |
| C5'-C16'  | 1.459(3) | N6'-C7'   | 1.462(3)   |
| C7'-C8'   | 1.515(2) | C7'-C15'  | 1.532(3)   |
| C8'-N9'   | 1.331(3) | C8'-C13'  | 1.393(3)   |
| N9'-C10'  | 1.351(3) | C10'-C11' | 1.370(4)   |
| C11'-C12' | 1.381(4) | C12'-C13' | 1.383(3)   |
| C13'-C14' | 1.501(3) | C14'-C15' | 1.538(3)   |
| C16'-C17' | 1.380(3) | C16'-C24' | 1.411(3)   |
| C17'-C18' | 1.396(2) | C18'-N19' | 1.358(2)   |
| C18'-C22' | 1.401(3) | N19'-N20' | 1.354(2)   |
| N20'-C21' | 1.326(3) | C21'-C22' | 1.416(3)   |
| C22'-C23' | 1.398(3) | C23'-C24' | 1.358(3)   |
| C24'-F25' | 1.359(2) |           |            |

**Table 4 (continued). Selected bond lengths (Å) for 57770C2.**

|           |          |           |          |
|-----------|----------|-----------|----------|
| O1"-C5"   | 1.356(2) | O1"-N2"   | 1.425(2) |
| N2"-C3"   | 1.314(2) | C3"-N6"   | 1.372(2) |
| C3"-C4"   | 1.409(3) | C4"-C5"   | 1.351(3) |
| C5"-C16"  | 1.457(3) | N6"-C7"   | 1.451(3) |
| C7"-C8"   | 1.500(3) | C7"-C15"  | 1.544(3) |
| C8"-N9"   | 1.322(3) | C8"-C13"  | 1.377(3) |
| N9"-C10"  | 1.347(3) | C10"-C11" | 1.376(5) |
| C11"-C12" | 1.344(6) | C12"-C13" | 1.368(4) |
| C13"-C14" | 1.490(4) | C14"-C15" | 1.486(5) |
| C16"-C17" | 1.388(3) | C16"-C24" | 1.414(3) |
| C17"-C18" | 1.393(3) | C18"-N19" | 1.368(3) |
| C18"-C22" | 1.398(3) | N19"-N20" | 1.355(3) |
| N20"-C21" | 1.317(3) | C21"-C22" | 1.419(3) |
| C22"-C23" | 1.407(3) | C23"-C24" | 1.357(3) |
| C24"-F25" | 1.365(2) |           |          |
| O1*-C5*   | 1.352(2) | O1*-N2*   | 1.426(2) |
| N2*-C3*   | 1.312(2) | C3*-N6*   | 1.367(2) |
| C3*-C4*   | 1.417(3) | C4*-C5*   | 1.352(3) |
| C5*-C16*  | 1.472(3) | N6*-C7*   | 1.445(3) |
| C7*-C8*   | 1.506(2) | C7*-C15*  | 1.532(3) |
| C8*-N9*   | 1.327(2) | C8*-C13*  | 1.394(3) |
| N9*-C10*  | 1.342(3) | C10*-C11* | 1.378(3) |
| C11*-C12* | 1.382(3) | C12*-C13* | 1.380(3) |
| C13*-C14* | 1.500(3) | C14*-C15* | 1.550(3) |
| C16*-C17* | 1.388(2) | C16*-C24* | 1.410(3) |
| C17*-C18* | 1.395(3) | C18*-N19* | 1.367(2) |
| C18*-C22* | 1.399(3) | N19*-N20* | 1.352(2) |
| N20*-C21* | 1.323(3) | C21*-C22* | 1.417(3) |
| C22*-C23* | 1.409(3) | C23*-C24* | 1.356(3) |
| C24*-F25* | 1.364(2) |           |          |

**Table 5. Selected bond angles (°) for 57770C2.**

|                |            |                |            |
|----------------|------------|----------------|------------|
| C5-O1-N2       | 108.50(13) | C3-N2-O1       | 105.41(14) |
| N2-C3-N6       | 121.05(17) | N2-C3-C4       | 112.03(16) |
| N6-C3-C4       | 126.92(18) | C5-C4-C3       | 104.17(17) |
| C4-C5-O1       | 109.87(16) | C4-C5-C16      | 135.22(18) |
| O1-C5-C16      | 114.91(15) | C3-N6-C7       | 118.65(17) |
| N6-C7-C8       | 112.77(15) | N6-C7-C15      | 115.07(16) |
| C8-C7-C15      | 102.41(14) | N9-C8-C13      | 125.45(16) |
| N9-C8-C7       | 123.98(16) | C13-C8-C7      | 110.54(15) |
| C8-N9-C10      | 114.61(16) | N9-C10-C11     | 124.02(19) |
| C12-C11-C10    | 119.86(18) | C13-C12-C11    | 117.65(18) |
| C12-C13-C8     | 118.40(17) | C12-C13-C14    | 130.98(18) |
| C8-C13-C14     | 110.62(15) | C13-C14-C15    | 102.78(15) |
| C14-C15-C7     | 105.31(14) | C17-C16-C24    | 118.62(16) |
| C17-C16-C5     | 119.75(16) | C24-C16-C5     | 121.63(16) |
| C16-C17-C18    | 117.74(17) | N19-C18-C17    | 130.43(18) |
| N19-C18-C22    | 106.60(16) | C17-C18-C22    | 122.95(17) |
| N20-N19-C18    | 111.72(16) | C21-N20-N19    | 106.11(15) |
| N20-C21-C22    | 111.52(17) | C18-C22-C23    | 119.11(17) |
| C18-C22-C21    | 104.05(16) | C23-C22-C21    | 136.83(19) |
| C24-C23-C22    | 117.14(18) | C23-C24-F25    | 118.14(17) |
| C23-C24-C16    | 124.32(17) | F25-C24-C16    | 117.54(15) |
| C5'-O1'-N2'    | 108.34(13) | C3'-N2'-O1'    | 104.88(14) |
| N2'-C3'-N6'    | 122.09(17) | N2'-C3'-C4'    | 112.02(16) |
| N6'-C3'-C4'    | 125.88(17) | C5'-C4'-C3'    | 104.99(16) |
| C4'-C5'-O1'    | 109.77(16) | C4'-C5'-C16'   | 135.04(18) |
| O1'-C5'-C16'   | 115.18(15) | C3'-N6'-C7'    | 120.25(16) |
| N6'-C7'-C8'    | 106.18(15) | N6'-C7'-C15'   | 112.40(16) |
| C8'-C7'-C15'   | 101.94(15) | N9'-C8'-C13'   | 125.82(17) |
| N9'-C8'-C7'    | 123.82(17) | C13'-C8'-C7'   | 110.12(17) |
| C8'-N9'-C10'   | 114.49(19) | N9'-C10'-C11'  | 123.9(2)   |
| C10'-C11'-C12' | 120.6(2)   | C11'-C12'-C13' | 117.1(2)   |
| C12'-C13'-C8'  | 118.1(2)   | C12'-C13'-C14' | 131.4(2)   |
| C8'-C13'-C14'  | 110.44(17) | C13'-C14'-C15' | 102.96(17) |
| C7'-C15'-C14'  | 105.32(16) | C17'-C16'-C24' | 117.77(17) |
| C17'-C16'-C5'  | 121.25(17) | C24'-C16'-C5'  | 120.97(17) |
| C16'-C17'-C18' | 117.98(17) | N19'-C18'-C17' | 130.37(18) |
| N19'-C18'-C22' | 106.52(16) | C17'-C18'-C22' | 123.10(17) |
| N20'-N19'-C18' | 111.86(17) | C21'-N20'-N19' | 106.01(16) |
| N20'-C21'-C22' | 111.17(18) | C23'-C22'-C18' | 118.89(18) |
| C23'-C22'-C21' | 136.7(2)   | C18'-C22'-C21' | 104.44(17) |
| C24'-C23'-C22' | 117.06(19) | C23'-C24'-F25' | 118.29(19) |
| C23'-C24'-C16' | 125.18(19) | F25'-C24'-C16' | 116.54(17) |



**Table 5 (continued). Selected bond angles (°) for 57770C2.**

|                |            |                |            |
|----------------|------------|----------------|------------|
| C5*-O1*-N2"    | 108.57(13) | C3*-N2*-O1"    | 104.73(16) |
| N2*-C3*-N6"    | 122.1(2)   | N2*-C3*-C4"    | 112.15(17) |
| N6*-C3*-C4"    | 125.71(17) | C5*-C4*-C3"    | 105.10(17) |
| C4*-C5*-O1"    | 109.41(18) | C4*-C5*-C16"   | 134.12(18) |
| O1*-C5*-C16"   | 116.43(15) | C3*-N6*-C7"    | 121.36(17) |
| N6*-C7*-C8"    | 111.46(16) | N6*-C7*-C15"   | 114.40(18) |
| C8*-C7*-C15"   | 101.9(2)   | N9*-C8*-C13"   | 125.14(19) |
| N9*-C8*-C7"    | 123.76(18) | C13*-C8*-C7"   | 111.10(19) |
| C8*-N9*-C10"   | 114.9(2)   | N9*-C10*-C11"  | 123.4(3)   |
| C12*-C11*-C10" | 119.9(2)   | C11*-C12*-C13" | 118.5(3)   |
| C12*-C13*-C8"  | 118.2(3)   | C12*-C13*-C14" | 131.2(3)   |
| C8*-C13*-C14"  | 110.5(2)   | C15*-C14*-C13" | 103.9(2)   |
| C14*-C15*-C7"  | 107.3(2)   | C17*-C16*-C24" | 118.07(19) |
| C17*-C16*-C5"  | 120.75(18) | C24*-C16*-C5"  | 121.17(17) |
| C16*-C17*-C18" | 117.51(19) | N19*-C18*-C17" | 130.2(2)   |
| N19*-C18*-C22" | 106.45(19) | C17*-C18*-C22" | 123.31(18) |
| N20*-N19*-C18" | 111.67(19) | C21*-N20*-N19" | 105.97(19) |
| N20*-C21*-C22" | 111.8(2)   | C18*-C22*-C23" | 119.4(2)   |
| C18*-C22*-C21" | 104.15(18) | C23*-C22*-C21" | 136.5(2)   |
| C24*-C23*-C22" | 116.4(2)   | C23*-C24*-F25" | 118.06(19) |
| C23*-C24*-C16" | 125.30(19) | F25*-C24*-C16" | 116.64(19) |
|                |            |                |            |
| C5*-O1*-N2*    | 108.64(13) | C3*-N2*-O1*    | 104.97(15) |
| N2*-C3*-N6*    | 121.72(19) | N2*-C3*-C4*    | 111.86(16) |
| N6*-C3*-C4*    | 126.40(18) | C5*-C4*-C3*    | 104.93(18) |
| O1*-C5*-C4*    | 109.59(17) | O1*-C5*-C16*   | 115.01(15) |
| C4*-C5*-C16*   | 135.38(19) | C3*-N6*-C7*    | 120.20(17) |
| N6*-C7*-C8*    | 113.38(16) | N6*-C7*-C15*   | 115.05(18) |
| C8*-C7*-C15*   | 101.68(16) | N9*-C8*-C13*   | 124.64(16) |
| N9*-C8*-C7*    | 123.57(17) | C13*-C8*-C7*   | 111.76(17) |
| C8*-N9*-C10*   | 115.97(17) | N9*-C10*-C11*  | 123.7(2)   |
| C10*-C11*-C12* | 119.47(18) | C13*-C12*-C11* | 117.96(18) |
| C12*-C13*-C8*  | 118.22(17) | C12*-C13*-C14* | 131.88(19) |
| C8*-C13*-C14*  | 109.88(17) | C13*-C14*-C15* | 102.81(18) |
| C7*-C15*-C14*  | 106.09(18) | C17*-C16*-C24* | 118.81(17) |
| C17*-C16*-C5*  | 119.82(17) | C24*-C16*-C5*  | 121.36(17) |
| C16*-C17*-C18* | 117.48(18) | N19*-C18*-C17* | 130.34(18) |
| N19*-C18*-C22* | 106.86(17) | C17*-C18*-C22* | 122.79(17) |
| N20*-N19*-C18* | 111.38(17) | C21*-N20*-N19* | 106.21(16) |
| N20*-C21*-C22* | 111.54(19) | C18*-C22*-C23* | 119.52(18) |
| C18*-C22*-C21* | 104.00(17) | C23*-C22*-C21* | 136.5(2)   |
| C24*-C23*-C22* | 116.84(19) | C23*-C24*-F25* | 118.05(18) |
| C23*-C24*-C16* | 124.52(18) | F25*-C24*-C16* | 117.42(17) |

**Table 6. Selected torsion angles (°) for 57770C2.**

|                 |             |                 |             |
|-----------------|-------------|-----------------|-------------|
| C5-O1-N2-C3     | 0.52(18)    | O1-N2-C3-N6     | 178.74(15)  |
| O1-N2-C3-C4     | -1.5(2)     | N2-C3-C4-C5     | 1.9(2)      |
| N6-C3-C4-C5     | -178.36(17) | C3-C4-C5-O1     | -1.5(2)     |
| C3-C4-C5-C16    | 177.68(19)  | N2-O1-C5-C4     | 0.66(19)    |
| N2-O1-C5-C16    | -178.67(13) | N2-C3-N6-C7     | -13.3(3)    |
| C4-C3-N6-C7     | 166.91(17)  | C3-N6-C7-C8     | -151.42(16) |
| C3-N6-C7-C15    | 91.6(2)     | N6-C7-C8-N9     | 40.3(3)     |
| C15-C7-C8-N9    | 164.53(18)  | N6-C7-C8-C13    | -141.86(17) |
| C15-C7-C8-C13   | -17.6(2)    | C13-C8-N9-C10   | 1.0(3)      |
| C7-C8-N9-C10    | 178.51(18)  | C8-N9-C10-C11   | 0.0(3)      |
| N9-C10-C11-C12  | -0.3(4)     | C10-C11-C12-C13 | -0.2(3)     |
| C11-C12-C13-C8  | 1.1(3)      | C11-C12-C13-C14 | -178.4(2)   |
| N9-C8-C13-C12   | -1.5(3)     | C7-C8-C13-C12   | -179.35(18) |
| N9-C8-C13-C14   | 178.08(18)  | C7-C8-C13-C14   | 0.2(2)      |
| C12-C13-C14-C15 | -163.2(2)   | C8-C13-C14-C15  | 17.3(2)     |
| C13-C14-C15-C14 | -27.5(2)    | N6-C7-C15-C14   | 150.30(17)  |
| C8-C7-C15-C14   | 27.6(2)     | C4-C5-C16-C17   | -179.34(19) |
| O1-C5-C16-C17   | -0.2(2)     | C4-C5-C16-C24   | 1.0(3)      |
| O1-C5-C16-C24   | -179.86(15) | C24-C16-C17-C18 | 2.1(2)      |
| C5-C16-C17-C18  | -177.57(15) | C16-C17-C18-N19 | 179.02(16)  |
| C16-C17-C18-C22 | 0.9(3)      | C17-C18-N19-N20 | -177.36(17) |
| C22-C18-N19-N20 | 0.98(19)    | C18-N19-N20-C21 | -0.4(2)     |
| N19-N20-C21-C22 | -0.3(2)     | N19-C18-C22-C23 | 178.30(16)  |
| C17-C18-C22-C23 | -3.2(3)     | N19-C18-C22-C21 | -1.07(18)   |
| C17-C18-C22-C21 | 177.42(16)  | N20-C21-C22-C18 | 0.9(2)      |
| N20-C21-C22-C23 | -178.3(2)   | C18-C22-C23-C24 | 2.3(3)      |
| C21-C22-C23-C24 | -178.6(2)   | C22-C23-C24-F25 | -179.81(15) |
| C22-C23-C24-C16 | 0.7(3)      | C17-C16-C24-C23 | -3.0(3)     |
| C5-C16-C24-C23  | 176.63(17)  | C17-C16-C24-F25 | 177.53(14)  |
| C5-C16-C24-F25  | -2.8(2)     |                 |             |

Table 6 (continued). Selected torsion angles (°) for 57770C2.

|                     |             |                     |             |
|---------------------|-------------|---------------------|-------------|
| C5'-O1'-N2'-C3'     | -0.48(18)   | O1'-N2'-C3'-N6'     | -178.79(15) |
| O1'-N2'-C3'-C4'     | 0.34(19)    | N2'-C3'-C4'-C5'     | -0.1(2)     |
| N6'-C3'-C4'-C5'     | 179.01(17)  | C3'-C4'-C5'-O1'     | -0.25(19)   |
| C3'-C4'-C5'-C16'    | 178.55(19)  | N2'-O1'-C5'-C4'     | 0.46(19)    |
| N2'-O1'-C5'-C16'    | -178.60(14) | N2'-C3'-N6'-C7'     | -11.2(3)    |
| C4'-C3'-N6'-C7'     | 169.75(17)  | C3'-N6'-C7'-C8'     | -165.16(16) |
| C3'-N6'-C7'-C15'    | 84.2(2)     | N6'-C7'-C8'-N9'     | 78.5(2)     |
| C15'-C7'-C8'-N9'    | -163.7(2)   | N6'-C7'-C8'-C13'    | -96.12(19)  |
| C15'-C7'-C8'-C13'   | 21.7(2)     | C13'-C8'-N9'-C10'   | -0.4(3)     |
| C7'-C8'-N9'-C10'    | -174.1(2)   | C8'-N9'-C10'-C11'   | 0.9(4)      |
| N9'-C10'-C11'-C12'  | -0.6(4)     | C10'-C11'-C12'-C13' | -0.4(4)     |
| C11'-C12'-C13'-C8'  | 0.9(4)      | C11'-C12'-C13'-C14' | 179.1(3)    |
| N9'-C8'-C13'-C12'   | -0.6(3)     | C7'-C8'-C13'-C12'   | 173.9(2)    |
| N9'-C8'-C13'-C14'   | -179.1(2)   | C7'-C8'-C13'-C14'   | -4.7(3)     |
| C12'-C13'-C14'-C15' | 167.3(3)    | C8'-C13'-C14'-C15'  | -14.4(3)    |
| N6'-C7'-C15'-C14'   | 83.4(2)     | C8'-C7'-C15'-C14'   | -29.8(2)    |
| C13'-C14'-C15'-C7'  | 27.5(2)     | C4'-C5'-C16'-C17'   | -170.89(19) |
| O1'-C5'-C16'-C17'   | 7.9(2)      | C4'-C5'-C16'-C24'   | 8.3(3)      |
| O1'-C5'-C16'-C24'   | -172.98(17) | C24'-C16'-C17'-C18' | -1.2(3)     |
| C5'-C16'-C17'-C18'  | 177.99(16)  | C16'-C17'-C18'-N19' | -179.46(17) |
| C16'-C17'-C18'-C22' | 0.2(3)      | C17'-C18'-N19'-N20' | 178.84(17)  |
| C22'-C18'-N19'-N20' | -0.9(2)     | C18'-N19'-N20'-C21' | 0.7(2)      |
| N19'-N20'-C21'-C22' | -0.3(2)     | N19'-C18'-C22'-C23' | -179.33(18) |
| C17'-C18'-C22'-C23' | 0.9(3)      | N19'-C18'-C22'-C21' | 0.62(19)    |
| C17'-C18'-C22'-C21' | -179.10(16) | N20'-C21'-C22'-C23' | 179.7(2)    |
| N20'-C21'-C22'-C18' | -0.2(2)     | C18'-C22'-C23'-C24' | -1.0(3)     |
| C21'-C22'-C23'-C24' | 179.1(2)    | C22'-C23'-C24'-F25' | 179.7(2)    |
| C22'-C23'-C24'-C16' | -0.1(4)     | C17'-C16'-C24'-C23' | 1.2(3)      |
| C5'-C16'-C24'-C23'  | -178.0(2)   | C17'-C16'-C24'-F25' | -178.58(18) |
| C5'-C16'-C24'-F25'  | 2.2(3)      |                     |             |

Table 6 (continued). Selected torsion angles (°) for 57770C2.

|                         |             |                         |             |
|-------------------------|-------------|-------------------------|-------------|
| C5'-O1'-N2'-C3''        | 0.31(17)    | O1''-N2''-C3''-N6''     | 178.52(15)  |
| O1''-N2''-C3''-C4''     | -1.43(19)   | N2''-C3''-C4''-C5''     | 2.0(2)      |
| N6''-C3''-C4''-C5''     | -177.93(16) | C3''-C4''-C5''-O1''     | -1.73(19)   |
| C3''-C4''-C5''-C16''    | 175.87(18)  | N2''-O1''-C5''-C4''     | 0.94(18)    |
| N2''-O1''-C5''-C16''    | -177.13(14) | N2''-C3''-N6''-C7''     | -15.1(3)    |
| C4''-C3''-N6''-C7''     | 164.80(17)  | C3''-N6''-C7''-C8''     | -145.64(17) |
| C3''-N6''-C7''-C15''    | 99.5(2)     | N6''-C7''-C8''-N9''     | 45.3(3)     |
| C15''-C7''-C8''-N9''    | 167.74(19)  | N6''-C7''-C8''-C13''    | -134.69(18) |
| C15''-C7''-C8''-C13''   | -12.3(2)    | C13''-C8''-N9''-C10''   | 0.2(3)      |
| C7''-C8''-N9''-C10''    | -179.84(18) | C8''-N9''-C10''-C11''   | -0.1(3)     |
| N9''-C10''-C11''-C12''  | 0.6(4)      | C10''-C11''-C12''-C13'' | -1.2(4)     |
| C11''-C12''-C13''-C8''  | 1.3(4)      | C11''-C12''-C13''-C14'' | -177.6(3)   |
| N9''-C8''-C13''-C12''   | -0.8(3)     | C7''-C8''-C13''-C12''   | 179.2(2)    |
| N9''-C8''-C13''-C14''   | 178.4(2)    | C7''-C8''-C13''-C14''   | -1.6(3)     |
| C12''-C13''-C14''-C15'' | -165.5(3)   | C8''-C13''-C14''-C15''  | 15.5(3)     |
| C13''-C14''-C15''-C7''  | -22.8(3)    | N6''-C7''-C15''-C14''   | 142.0(2)    |
| C8''-C7''-C15''-C14''   | 21.6(3)     | C4''-C5''-C16''-C17''   | -173.19(18) |
| O1''-C5''-C16''-C17''   | 4.3(2)      | C4''-C5''-C16''-C24''   | 5.8(3)      |
| O1''-C5''-C16''-C24''   | -176.73(16) | C24''-C16''-C17''-C18'' | 0.6(2)      |
| C5''-C16''-C17''-C18''  | 179.64(16)  | C16''-C17''-C18''-N19'' | 179.40(19)  |
| C16''-C17''-C18''-C22'' | -1.0(3)     | C17''-C18''-N19''-N20'' | -179.75(19) |
| C22''-C18''-N19''-N20'' | 0.6(2)      | C18''-N19''-N20''-C21'' | -0.8(2)     |
| N19''-N20''-C21''-C22'' | 0.6(3)      | N19''-C18''-C22''-C23'' | -179.78(18) |
| C17''-C18''-C22''-C23'' | 0.5(3)      | N19''-C18''-C22''-C21'' | -0.2(2)     |
| C17''-C18''-C22''-C21'' | -179.88(18) | N20''-C21''-C22''-C18'' | -0.3(3)     |
| N20''-C21''-C22''-C23'' | 179.2(2)    | C18''-C22''-C23''-C24'' | 0.3(3)      |
| C21''-C22''-C23''-C24'' | -179.1(2)   | C22''-C23''-C24''-F25'' | 178.94(17)  |
| C22''-C23''-C24''-C16'' | -0.6(3)     | C17''-C16''-C24''-C23'' | 0.2(3)      |
| C5''-C16''-C24''-C23''  | -178.83(19) | C17''-C16''-C24''-F25'' | -179.40(16) |
| C5''-C16''-C24''-F25''  | 1.6(3)      |                         |             |

**Table 6 (continued). Selected torsion angles (°) for 5770C2.**

|                     |             |                     |             |
|---------------------|-------------|---------------------|-------------|
| C5*-O1*-N2*-C3*     | -0.05(18)   | O1*-N2*-C3*-N6*     | -178.26(16) |
| O1*-N2*-C3*-C4*     | 0.24(19)    | N2*-C3*-C4*-C5*     | -0.3(2)     |
| N6*-C3*-C4*-C5*     | 178.07(17)  | N2*-O1*-C5*-C4*     | -0.16(19)   |
| N2*-O1*-C5*-C16*    | 178.60(13)  | C3*-C4*-C5*-O1*     | 0.3(2)      |
| C3*-C4*-C5*-C16*    | -178.11(18) | N2*-C3*-N6*-C7*     | -6.5(3)     |
| C4*-C3*-N6*-C7*     | 175.28(18)  | C3*-N6*-C7*-C8*     | -141.01(18) |
| C3*-N6*-C7*-C15*    | 102.5(2)    | N6*-C7*-C8*-N9*     | 39.4(3)     |
| C15*-C7*-C8*-N9*    | 163.48(19)  | N6*-C7*-C8*-C13*    | -142.47(17) |
| C15*-C7*-C8*-C13*   | -18.4(2)    | C13*-C8*-N9*-C10*   | 0.2(3)      |
| C7*-C8*-N9*-C10*    | 178.14(19)  | C8*-N9*-C10*-C11*   | -1.7(3)     |
| N9*-C10*-C11*-C12*  | 1.5(4)      | C10*-C11*-C12*-C13* | 0.1(3)      |
| C11*-C12*-C13*-C8*  | -1.4(3)     | C11*-C12*-C13*-C14* | -179.9(2)   |
| N9*-C8*-C13*-C12*   | 1.3(3)      | C7*-C8*-C13*-C12*   | -176.82(17) |
| N9*-C8*-C13*-C14*   | -179.9(2)   | C7*-C8*-C13*-C14*   | 2.0(2)      |
| C12*-C13*-C14*-C15* | -166.2(2)   | C8*-C13*-C14*-C15*  | 15.1(3)     |
| N6*-C7*-C15*-C14*   | 149.92(19)  | C8*-C7*-C15*-C14*   | 27.0(2)     |
| C13*-C14*-C15*-C7*  | -26.3(3)    | O1*-C5*-C16*-C17*   | -1.7(2)     |
| C4*-C5*-C16*-C17*   | 176.66(19)  | O1*-C5*-C16*-C24*   | 179.42(15)  |
| C4*-C5*-C16*-C24*   | -2.2(3)     | C24*-C16*-C17*-C18* | 0.6(2)      |
| C5*-C16*-C17*-C18*  | -178.32(15) | C16*-C17*-C18*-N19* | 180.00(17)  |
| C16*-C17*-C18*-C22* | 1.4(2)      | C17*-C18*-N19*-N20* | -178.11(17) |
| C22*-C18*-N19*-N20* | 0.7(2)      | C18*-N19*-N20*-C21* | -0.4(2)     |
| N19*-N20*-C21*-C22* | -0.1(2)     | N19*-C18*-C22*-C23* | 179.09(16)  |
| C17*-C18*-C22*-C23* | -2.0(3)     | N19*-C18*-C22*-C21* | -0.67(19)   |
| C17*-C18*-C22*-C21* | 178.22(16)  | N20*-C21*-C22*-C18* | 0.5(2)      |
| N20*-C21*-C22*-C23* | -179.2(2)   | C18*-C22*-C23*-C24* | 0.6(3)      |
| C21*-C22*-C23*-C24* | -179.8(2)   | C22*-C23*-C24*-F25* | -179.40(15) |
| C22*-C23*-C24*-C16* | 1.5(3)      | C17*-C16*-C24*-C23* | -2.1(3)     |
| C5*-C16*-C24*-C23*  | 176.78(17)  | C17*-C16*-C24*-F25* | 178.77(15)  |
| C5*-C16*-C24*-F25*  | -2.3(2)     |                     |             |

**Table 7. Anisotropic atomic displacement parameters (Å<sup>2</sup>) for 5770C2.**

The anisotropic atomic displacement factor exponent takes the form:  $-2\pi^2 [h^2 a^{*2} U^{11} + \dots + 2hka^* b^* U^{12}]$

|     | U <sup>11</sup> | U <sup>22</sup> | U <sup>33</sup> | U <sup>23</sup> | U <sup>13</sup> | U <sup>12</sup> |
|-----|-----------------|-----------------|-----------------|-----------------|-----------------|-----------------|
| O1  | 0.0521(7)       | 0.0231(6)       | 0.0442(7)       | 0.0015(5)       | -0.0016(6)      | 0.0031(5)       |
| N2  | 0.0481(9)       | 0.0225(8)       | 0.0510(10)      | 0.0016(7)       | -0.0023(7)      | 0.0017(6)       |
| C3  | 0.0320(8)       | 0.0270(9)       | 0.0483(11)      | 0.0027(8)       | -0.0019(8)      | -0.0006(7)      |
| C4  | 0.0407(9)       | 0.0309(10)      | 0.0423(10)      | 0.0045(8)       | -0.0018(8)      | 0.0032(7)       |
| C5  | 0.0326(8)       | 0.0299(9)       | 0.0432(10)      | 0.0089(8)       | 0.0023(7)       | 0.0007(7)       |
| N6  | 0.0444(8)       | 0.0275(8)       | 0.0489(9)       | 0.0015(7)       | -0.0093(7)      | 0.0004(6)       |
| C7  | 0.0373(9)       | 0.0274(9)       | 0.0464(10)      | 0.0020(8)       | -0.0030(8)      | 0.0016(7)       |
| C8  | 0.0339(8)       | 0.0287(9)       | 0.0423(10)      | 0.0027(7)       | 0.0031(7)       | 0.0000(7)       |
| N9  | 0.0346(8)       | 0.0360(8)       | 0.0459(9)       | 0.0003(7)       | -0.0004(6)      | -0.0015(6)      |
| C10 | 0.0375(10)      | 0.0488(12)      | 0.0572(12)      | -0.0020(10)     | -0.0038(9)      | -0.0043(9)      |
| C11 | 0.0556(12)      | 0.0347(11)      | 0.0659(14)      | -0.0082(10)     | 0.0035(10)      | -0.0088(9)      |
| C12 | 0.0536(11)      | 0.0273(10)      | 0.0608(12)      | 0.0015(9)       | 0.0119(10)      | 0.0021(8)       |
| C13 | 0.0398(9)       | 0.0296(9)       | 0.0461(10)      | 0.0071(8)       | 0.0088(8)       | 0.0026(7)       |
| C14 | 0.0412(10)      | 0.0368(10)      | 0.0582(12)      | 0.0088(9)       | 0.0033(9)       | 0.0091(8)       |
| C15 | 0.0349(9)       | 0.0361(10)      | 0.0575(12)      | 0.0059(9)       | -0.0041(8)      | 0.0031(7)       |
| C16 | 0.0328(8)       | 0.0291(9)       | 0.0387(9)       | 0.0070(7)       | 0.0071(7)       | 0.0021(7)       |
| C17 | 0.0370(9)       | 0.0277(9)       | 0.0421(10)      | 0.0098(8)       | 0.0054(7)       | 0.0017(7)       |
| C18 | 0.0348(9)       | 0.0296(9)       | 0.0393(10)      | 0.0085(8)       | 0.0082(7)       | 0.0020(7)       |
| N19 | 0.0504(9)       | 0.0248(8)       | 0.0397(9)       | 0.0073(7)       | 0.0046(7)       | 0.0025(6)       |
| N20 | 0.0567(9)       | 0.0241(8)       | 0.0495(10)      | 0.0063(7)       | 0.0088(8)       | 0.0049(7)       |
| C21 | 0.0552(11)      | 0.0274(9)       | 0.0463(11)      | 0.0112(8)       | 0.0100(9)       | 0.0086(8)       |
| C22 | 0.0397(9)       | 0.0285(9)       | 0.0451(10)      | 0.0097(8)       | 0.0123(8)       | 0.0055(7)       |
| C23 | 0.0472(10)      | 0.0338(10)      | 0.0399(10)      | 0.0131(8)       | 0.0098(8)       | 0.0099(8)       |
| C24 | 0.0390(9)       | 0.0344(10)      | 0.0352(9)       | 0.0043(8)       | 0.0084(7)       | 0.0054(7)       |
| F25 | 0.0645(7)       | 0.0406(6)       | 0.0345(6)       | 0.0060(5)       | 0.0032(5)       | 0.0102(5)       |

**Table 7 (continued). Anisotropic atomic displacement parameters (Å<sup>2</sup>) for 57770C2.**The anisotropic atomic displacement factor exponent takes the form:  $-2\pi^2 [h^2 a^{*2} U^{11} + \dots + 2hka^* b^* U^{12}]$ .

|      | U <sup>11</sup> | U <sup>22</sup> | U <sup>33</sup> | U <sup>23</sup> | U <sup>13</sup> | U <sup>12</sup> |
|------|-----------------|-----------------|-----------------|-----------------|-----------------|-----------------|
| O1'  | 0.0567(7)       | 0.0278(6)       | 0.0318(6)       | 0.0047(5)       | 0.0031(5)       | 0.0064(5)       |
| N2'  | 0.0531(9)       | 0.0272(8)       | 0.0329(8)       | 0.0022(6)       | 0.0059(7)       | 0.0051(6)       |
| C3'  | 0.0370(9)       | 0.0357(10)      | 0.0319(9)       | 0.0028(8)       | 0.0074(7)       | 0.0014(7)       |
| C4'  | 0.0441(9)       | 0.0362(10)      | 0.0335(9)       | 0.0084(8)       | 0.0058(7)       | 0.0057(8)       |
| C5'  | 0.0373(9)       | 0.0353(10)      | 0.0339(9)       | 0.0086(8)       | 0.0031(7)       | 0.0038(7)       |
| N6'  | 0.0570(9)       | 0.0354(9)       | 0.0284(8)       | 0.0029(7)       | 0.0095(7)       | 0.0064(7)       |
| C7'  | 0.0494(10)      | 0.0329(10)      | 0.0333(9)       | 0.0036(7)       | 0.0089(8)       | 0.0055(8)       |
| C8'  | 0.0569(11)      | 0.0319(9)       | 0.0356(9)       | 0.0063(8)       | 0.0106(8)       | 0.0063(8)       |
| N9'  | 0.0663(11)      | 0.0435(9)       | 0.0489(10)      | 0.0058(8)       | 0.0231(8)       | 0.0109(8)       |
| C10' | 0.1001(18)      | 0.0495(13)      | 0.0543(13)      | 0.0052(11)      | 0.0395(13)      | 0.0166(13)      |
| C11' | 0.129(2)        | 0.0449(13)      | 0.0456(13)      | -0.0075(10)     | 0.0269(14)      | 0.0031(14)      |
| C12' | 0.109(2)        | 0.0393(12)      | 0.0487(13)      | -0.0035(10)     | 0.0097(13)      | -0.0114(12)     |
| C13' | 0.0685(13)      | 0.0348(11)      | 0.0458(11)      | 0.0037(9)       | 0.0075(10)      | -0.0016(9)      |
| C14' | 0.0647(14)      | 0.0510(13)      | 0.0580(13)      | 0.0047(10)      | 0.0163(11)      | -0.0096(10)     |
| C15' | 0.0610(12)      | 0.0414(11)      | 0.0428(11)      | 0.0087(9)       | 0.0155(9)       | 0.0036(9)       |
| C16' | 0.0403(9)       | 0.0325(10)      | 0.0390(10)      | 0.0064(8)       | 0.0053(8)       | 0.0059(7)       |
| C17' | 0.0351(8)       | 0.0309(9)       | 0.0387(10)      | 0.0076(8)       | 0.0027(7)       | 0.0042(7)       |
| C18' | 0.0340(9)       | 0.0307(9)       | 0.0408(10)      | 0.0068(8)       | 0.0061(7)       | 0.0017(7)       |
| N19' | 0.0476(9)       | 0.0275(8)       | 0.0428(9)       | 0.0034(7)       | 0.0037(7)       | 0.0036(6)       |
| N20' | 0.0515(9)       | 0.0265(8)       | 0.0564(10)      | 0.0060(7)       | 0.0102(8)       | 0.0048(7)       |
| C21' | 0.0567(12)      | 0.0307(10)      | 0.0532(12)      | 0.0110(9)       | 0.0101(10)      | 0.0077(8)       |
| C22' | 0.0429(10)      | 0.0334(10)      | 0.0466(11)      | 0.0100(8)       | 0.0083(8)       | 0.0059(8)       |
| C23' | 0.0795(14)      | 0.0391(11)      | 0.0445(11)      | 0.0168(9)       | 0.0046(10)      | 0.0165(10)      |
| C24' | 0.0745(14)      | 0.0394(11)      | 0.0351(10)      | 0.0074(9)       | -0.0005(9)      | 0.0101(10)      |
| F25' | 0.1553(15)      | 0.0486(8)       | 0.0353(7)       | 0.0075(6)       | -0.0148(8)      | 0.0274(8)       |

**Table 7 (continued). Anisotropic atomic displacement parameters (Å<sup>2</sup>) for 57770C2.**The anisotropic atomic displacement factor exponent takes the form:  $-2\pi^2 [h^2 a^{*2} U^{11} + \dots + 2hka^* b^* U^{12}]$ .

|       | U <sup>11</sup> | U <sup>22</sup> | U <sup>33</sup> | U <sup>23</sup> | U <sup>13</sup> | U <sup>12</sup> |
|-------|-----------------|-----------------|-----------------|-----------------|-----------------|-----------------|
| O1''  | 0.0572(8)       | 0.0371(7)       | 0.0381(7)       | -0.0024(6)      | 0.0128(6)       | 0.0020(6)       |
| N2''  | 0.0551(9)       | 0.0389(9)       | 0.0373(8)       | -0.0022(7)      | 0.0148(7)       | 0.0005(7)       |
| C3''  | 0.0379(9)       | 0.0394(10)      | 0.0390(10)      | -0.0020(8)      | 0.0138(8)       | -0.0047(8)      |
| C4''  | 0.0370(9)       | 0.0337(10)      | 0.0412(10)      | -0.0016(8)      | 0.0128(8)       | -0.0024(7)      |
| C5''  | 0.0349(9)       | 0.0333(10)      | 0.0451(10)      | 0.0001(8)       | 0.0132(8)       | -0.0023(7)      |
| N6''  | 0.0547(9)       | 0.0340(9)       | 0.0375(9)       | -0.0001(7)      | 0.0145(7)       | 0.0009(7)       |
| C7''  | 0.0537(11)      | 0.0311(10)      | 0.0501(11)      | 0.0029(8)       | 0.0184(9)       | 0.0052(8)       |
| C8''  | 0.0482(10)      | 0.0256(8)       | 0.0366(9)       | 0.0044(7)       | 0.0020(8)       | 0.0030(7)       |
| N9''  | 0.0579(10)      | 0.0423(9)       | 0.0443(9)       | 0.0022(7)       | 0.0173(8)       | 0.0082(8)       |
| C10'' | 0.110(2)        | 0.0456(13)      | 0.0729(19)      | -0.0055(12)     | 0.0577(17)      | -0.0034(13)     |
| C11'' | 0.226(5)        | 0.0490(16)      | 0.0425(15)      | 0.0009(12)      | 0.056(2)        | -0.027(2)       |
| C12'' | 0.209(4)        | 0.0444(15)      | 0.0392(14)      | 0.0126(12)      | -0.020(2)       | -0.006(2)       |
| C13'' | 0.0918(17)      | 0.0327(11)      | 0.0595(14)      | 0.0094(10)      | -0.0223(12)     | 0.0021(11)      |
| C14'' | 0.0790(19)      | 0.0657(19)      | 0.140(3)        | 0.017(2)        | -0.032(2)       | 0.0239(15)      |
| C15'' | 0.0575(14)      | 0.0702(18)      | 0.142(3)        | 0.0424(19)      | 0.0366(17)      | 0.0317(13)      |
| C16'' | 0.0356(9)       | 0.0387(10)      | 0.0427(10)      | 0.0036(8)       | 0.0130(8)       | -0.0003(7)      |
| C17'' | 0.0453(10)      | 0.0392(11)      | 0.0411(11)      | 0.0008(9)       | 0.0139(8)       | -0.0045(8)      |
| C18'' | 0.0466(10)      | 0.0448(11)      | 0.0389(10)      | 0.0015(9)       | 0.0148(8)       | -0.0041(8)      |
| N19'' | 0.0714(12)      | 0.0478(11)      | 0.0381(9)       | 0.0017(8)       | 0.0132(8)       | -0.0026(9)      |
| N20'' | 0.0829(13)      | 0.0618(12)      | 0.0388(10)      | 0.0095(9)       | 0.0124(9)       | 0.0066(10)      |
| C21'' | 0.0779(15)      | 0.0570(14)      | 0.0463(12)      | 0.0125(11)      | 0.0142(11)      | 0.0132(11)      |
| C22'' | 0.0530(11)      | 0.0517(13)      | 0.0429(11)      | 0.0061(10)      | 0.0167(9)       | 0.0040(9)       |
| C23'' | 0.0577(12)      | 0.0447(12)      | 0.0490(12)      | 0.0041(9)       | 0.0137(9)       | 0.0134(9)       |
| C24'' | 0.0493(11)      | 0.0424(11)      | 0.0457(11)      | -0.0045(9)      | 0.0144(9)       | 0.0039(9)       |
| F25'' | 0.0787(8)       | 0.0419(7)       | 0.0496(7)       | -0.0056(5)      | 0.0038(6)       | 0.0176(6)       |

**Table 7 (continued). Anisotropic atomic displacement parameters (Å<sup>2</sup>) for 57770C2.**

The anisotropic atomic displacement factor exponent takes the form:  $-2\pi^2 [h^2 a^{*2} U^{11} + \dots + 2hka^* b^* U^{12}]$ .

|      | U <sup>11</sup> | U <sup>22</sup> | U <sup>33</sup> | U <sup>23</sup> | U <sup>13</sup> | U <sup>12</sup> |
|------|-----------------|-----------------|-----------------|-----------------|-----------------|-----------------|
| O1*  | 0.0644(8)       | 0.0405(8)       | 0.0272(6)       | 0.0038(6)       | -0.0007(6)      | -0.0059(6)      |
| N2*  | 0.0543(9)       | 0.0449(10)      | 0.0293(8)       | 0.0064(7)       | -0.0024(7)      | -0.0058(7)      |
| C3*  | 0.0316(8)       | 0.0462(11)      | 0.0314(9)       | 0.0013(8)       | 0.0002(7)       | 0.0017(7)       |
| C4*  | 0.0352(9)       | 0.0423(10)      | 0.0327(9)       | 0.0017(8)       | 0.0001(7)       | 0.0062(8)       |
| C5*  | 0.0339(9)       | 0.0388(10)      | 0.0334(9)       | 0.0044(8)       | 0.0034(7)       | -0.0018(7)      |
| N6*  | 0.0527(9)       | 0.0415(10)      | 0.0330(8)       | 0.0017(7)       | -0.0065(7)      | 0.0079(8)       |
| C7*  | 0.0496(10)      | 0.0399(11)      | 0.0359(10)      | -0.0026(8)      | -0.0088(8)      | 0.0047(8)       |
| C8*  | 0.0405(9)       | 0.0355(9)       | 0.0306(9)       | -0.0012(7)      | 0.0025(7)       | 0.0080(7)       |
| N9*  | 0.0436(9)       | 0.0607(11)      | 0.0388(9)       | 0.0143(8)       | 0.0002(7)       | -0.0016(8)      |
| C10* | 0.0444(11)      | 0.0744(15)      | 0.0484(12)      | 0.0173(11)      | -0.0052(9)      | -0.0113(10)     |
| C11* | 0.0455(10)      | 0.0558(12)      | 0.0341(10)      | 0.0029(9)       | -0.0061(8)      | 0.0051(9)       |
| C12* | 0.0540(11)      | 0.0390(10)      | 0.0301(9)       | 0.0045(8)       | 0.0020(8)       | 0.0115(8)       |
| C13* | 0.0465(10)      | 0.0327(9)       | 0.0371(10)      | 0.0026(8)       | 0.0042(8)       | 0.0030(8)       |
| C14* | 0.0676(14)      | 0.0564(14)      | 0.0667(15)      | 0.0223(12)      | -0.0112(11)     | -0.0190(11)     |
| C15* | 0.0567(13)      | 0.0587(14)      | 0.0703(15)      | 0.0186(12)      | -0.0190(11)     | -0.0201(11)     |
| C16* | 0.0320(8)       | 0.0433(11)      | 0.0339(9)       | 0.0054(8)       | 0.0068(7)       | 0.0013(7)       |
| C17* | 0.0359(9)       | 0.0397(10)      | 0.0316(9)       | 0.0048(8)       | 0.0031(7)       | 0.0000(8)       |
| C18* | 0.0309(8)       | 0.0423(11)      | 0.0326(9)       | 0.0050(8)       | 0.0053(7)       | 0.0056(7)       |
| N19* | 0.0457(9)       | 0.0435(10)      | 0.0292(8)       | 0.0068(7)       | -0.0012(6)      | 0.0073(7)       |
| N20* | 0.0501(9)       | 0.0527(11)      | 0.0330(9)       | 0.0095(8)       | -0.0002(7)      | 0.0163(8)       |
| C21* | 0.0550(12)      | 0.0508(12)      | 0.0391(10)      | 0.0132(9)       | 0.0057(9)       | 0.0182(9)       |
| C22* | 0.0368(9)       | 0.0451(11)      | 0.0364(10)      | 0.0081(9)       | 0.0076(8)       | 0.0093(8)       |
| C23* | 0.0501(11)      | 0.0400(11)      | 0.0419(11)      | 0.0078(9)       | 0.0145(9)       | 0.0098(8)       |
| C24* | 0.0420(10)      | 0.0407(11)      | 0.0352(10)      | 0.0009(8)       | 0.0110(8)       | 0.0027(8)       |
| F25* | 0.0730(8)       | 0.0404(6)       | 0.0370(6)       | -0.0016(5)      | 0.0135(5)       | 0.0013(5)       |

**Table 8. Hydrogen atom coordinates and isotropic atomic displacement parameters (Å<sup>2</sup>) for 57770C2.**

|       | x        | y          | z          | U        |
|-------|----------|------------|------------|----------|
| H4    | 0.4989   | 0.5584     | 0.8157     | 0.047    |
| H6    | 0.501(3) | 0.7653(18) | 0.8464(15) | 0.051(6) |
| H7    | 0.4437   | 0.8455     | 0.7146     | 0.046    |
| H10   | 0.8909   | 1.0256     | 0.9288     | 0.060    |
| H11   | 0.7459   | 1.1775     | 0.9406     | 0.066    |
| H12   | 0.4442   | 1.1843     | 0.8752     | 0.057    |
| H14A  | 0.2344   | 1.0345     | 0.7227     | 0.055    |
| H14B  | 0.1364   | 1.0480     | 0.8049     | 0.055    |
| H15A  | 0.1340   | 0.8687     | 0.7117     | 0.053    |
| H15B  | 0.1394   | 0.8784     | 0.8087     | 0.053    |
| H17   | 0.3140   | 0.4029     | 0.5454     | 0.042    |
| H19   | 0.276(3) | 0.2172(17) | 0.4338(14) | 0.044(6) |
| H21   | 0.4472   | 0.0338     | 0.5810     | 0.050    |
| H23   | 0.5521   | 0.1942     | 0.7292     | 0.047    |
| H4'   | 0.1010   | 0.4202     | 0.2107     | 0.045    |
| H6'   | 0.191(3) | 0.2272(15) | 0.1694(13) | 0.033(5) |
| H7'   | 0.3561   | 0.1351     | 0.2792     | 0.046    |
| H10'  | 0.5063   | 0.0040     | 0.0178     | 0.079    |
| H11'  | 0.2618   | -0.1086    | -0.0359    | 0.089    |
| H12'  | 0.0076   | -0.1223    | 0.0363     | 0.081    |
| H14C  | -0.0646  | -0.0692    | 0.2044     | 0.070    |
| H14D  | -0.1303  | 0.0347     | 0.1765     | 0.070    |
| H15C  | 0.0118   | 0.1053     | 0.3037     | 0.057    |
| H15D  | 0.1520   | 0.0144     | 0.3060     | 0.057    |
| H17'  | 0.2070   | 0.5660     | 0.4867     | 0.042    |
| H19'  | 0.225(3) | 0.7517(18) | 0.5959(15) | 0.048(6) |
| H21'  | 0.0656   | 0.9341     | 0.4490     | 0.055    |
| H23'  | -0.0011  | 0.7748     | 0.2984     | 0.064    |
| H4''  | 0.7687   | 0.8388     | 0.6960     | 0.045    |
| H6''  | 0.840(3) | 0.7789(19) | 0.8339(14) | 0.045(6) |
| H7''  | 0.8324   | 0.5820     | 0.8341     | 0.053    |
| H10'' | 0.5124   | 0.7778     | 1.0370     | 0.089    |
| H11'' | 0.7007   | 0.7430     | 1.1476     | 0.125    |
| H12'' | 0.9792   | 0.6678     | 1.1304     | 0.120    |
| H14E  | 1.2266   | 0.6315     | 1.0105     | 0.118    |
| H14F  | 1.0985   | 0.5290     | 0.9771     | 0.118    |
| H15E  | 1.1416   | 0.5620     | 0.8563     | 0.102    |
| H15F  | 1.1885   | 0.6808     | 0.8915     | 0.102    |
| H17'' | 0.6979   | 0.5856     | 0.4623     | 0.051    |
| H19'' | 0.587(4) | 0.549(2)   | 0.2937(17) | 0.077(9) |
| H21'' | 0.4575   | 0.8213     | 0.2634     | 0.071    |
| H23'' | 0.5557   | 0.9238     | 0.4372     | 0.060    |

**Table 8 (continued). Hydrogen atom coordinates and isotropic atomic displacement parameters (Å<sup>2</sup>) for 57770C2.**

|      | x        | y          | z          | U        |
|------|----------|------------|------------|----------|
| H4*  | 0.6972   | 0.1706     | 0.2885     | 0.045    |
| H6*  | 0.560(3) | 0.225(2)   | 0.1498(15) | 0.060(7) |
| H7*  | 0.4989   | 0.4287     | 0.1656     | 0.053    |
| H10* | 0.0183   | 0.2068     | -0.0022    | 0.067    |
| H11* | 0.0292   | 0.2789     | -0.1159    | 0.056    |
| H12* | 0.2802   | 0.3906     | -0.1219    | 0.050    |
| H14G | 0.5568   | 0.5205     | 0.0194     | 0.077    |
| H14H | 0.6558   | 0.4360     | -0.0401    | 0.077    |
| H15G | 0.7771   | 0.3599     | 0.0646     | 0.076    |
| H15H | 0.7627   | 0.4713     | 0.1179     | 0.076    |
| H17* | 0.8100   | 0.4259     | 0.5208     | 0.043    |
| H19* | 0.921(3) | 0.4662(19) | 0.6876(12) | 0.041(5) |
| H21* | 1.0261   | 0.1901     | 0.7232     | 0.057    |
| H23* | 0.9051   | 0.0848     | 0.5519     | 0.052    |

**Table 9. Selected hydrogen bond information for 57770C2 (Å and °).**

| D-H...A         | d(D-H)  | d(H...A) | d(D...A) | <(DHA)    |
|-----------------|---------|----------|----------|-----------|
| N6-H6...N9"     | 0.88(2) | 2.20(3)  | 3.050(3) | 163(2)    |
| N19-H19...N2'   | 0.96(2) | 1.92(2)  | 2.847(2) | 162.2(19) |
| N6'-H6'...N9*   | 0.90(2) | 2.09(2)  | 2.979(2) | 172.8(17) |
| N19'-H19'...N2  | 0.91(3) | 1.96(3)  | 2.840(3) | 160(2)    |
| N6"-H6"...N9    | 0.83(2) | 2.42(3)  | 3.229(2) | 169(2)    |
| N19"-H19"...N2* | 0.94(3) | 1.97(3)  | 2.889(3) | 166(3)    |
| N6*-H6*...N9'   | 0.93(3) | 2.33(3)  | 3.242(3) | 168(2)    |
| N19*-H19*...N2" | 0.95(2) | 1.95(3)  | 2.890(3) | 170.3(19) |

## 6. References

- 1 Scannell, J. W.; Blanckley, A.; Boldon, H.; Warrington, B. *Nat. Rev. Drug Discov.* **2012**, *11*, 191-200.
- 2 Pammolli, F.; Magazzini, L.; Riccaboni, M. *Nat. Rev. Drug Discov.* **2011**, *10*, 428-438.
- 3 Kola, I.; Landis, J. *Nat. Rev. Drug Discov.* **2004**, *3*, 711-715.
- 4 Unpublished results from Green, D. V. S. *GlaxoSmithKline*, R&D Stevenage, UK.
- 5 Cook, D.; Brown, D.; Alexander, R.; March, R.; Morgan, P.; Satterthwaite, G.; Pangalos, M. N. *Nat. Rev. Drug Discov.* **2014**, *13*, 419-431.
- 6 Leeson, P. D.; Empfield, J. R. *Ann. Reports Med. Chem.* **2010**, *45*, 393-407.
- 7 Lipinski, C. A.; Lombardo, F.; Dominy, B. W.; Feeney, P. J. *Adv. Drug Del. Rev.* **1997**, *23*, 3-25.
- 8 Meanwell, N. A. *Chem. Res. Toxicol.* **2011**, *24*, 1420-1456.
- 9 Young, R. J. *Physical Properties in Drug Design*, In *Tactics in Contemporary Drug Design*, edited by Meanwell, N. A.; Springer Inc. **2015**.
- 10 Waring, M. J. *Expert Opin. Drug Discov.* **2010**, *5*, 235-248.
- 11 Leeson, P. D.; Springthorpe, B. *Nat. Rev. Drug Discov.* **2007**, *6*, 881-890.
- 12 Keserü, G. M.; Makara, G. M. *Nat. Rev. Drug Discov.* **2009**, *8*, 203-212.
- 13 Hopkins, A. L.; Groom, C. R.; Alex, A. *Drug Discov. Today* **2004**, *9*, 430-431.
- 14 Mortenson, P. N.; Murray, C. W. *RSC - BMCS Fragment-Based Drug Discovery* **2009**.
- 15 Hughes, J. D.; Blagg, J.; Price, D. A.; Bailey, S.; DeCrescenzo, G. A.; Devraj, R. V.; Ellsworth, E.; Fobian, Y. M.; Gibbs, M. E.; Gilles, R. W.; Greene, N.; Huang, E.; Krieger-Burke, T.; Loesel, J.; Wager, T.; Whiteley, L.; Zhang, Y. *Bioorg. Med. Chem. Lett.* **2008**, *18*, 4872-4875.
- 16 Waring, M. J. *Bioorg. Med. Chem. Lett.* **2009**, *19*, 2844-2851.
- 17 Gleeson, M. P. *J. Med. Chem.* **2008**, *51*, 817-834.
- 18 Ritchie, T. J.; Macdonald, S. J. F. *Drug Discov. Today* **2009**, *14*, 1011-1020.
- 19 Hill, A. P.; Young, R. J. *Drug Discov. Today* **2010**, *15*, 648-655.
- 20 Young, R.; Green D. V. S.; Luscombe, C. N.; Hill, A. P. *Drug Discov. Today* **2011**, *16*, 822-830.
- 21 Pellegatti, M.; Pagliarusco, S.; Solazzo, L.; Colato, D. *Expert Opin. Drug Metab. Toxicol.* **2011**, *7*, 1009-1020.
- 22 Trainor, G. L. *Annu. Rep. Med. Chem.* **2007**, *42*, 489-502.
- 23 Raboisson, P.; Manthey, C. L.; Chaikin, M.; Lattanze, J.; Crystler, C.; Leonard, K.; Pan, W.; Tomczuck, B. E.; Marugán, J. J. *Eur. J. Med. Chem.* **2006**, *41*, 847-861.
- 24 Smith, D. A.; Di, L.; Kerns, E. H. *Nat. Rev. Drug Discov.* **2010**, *9*, 929-939.

- 
- 25 Liu, X.; Chen, C.; Hop, C. E. C. A. *Curr. Top. Med. Chem.* **2011**, *11*, 450-466.
  - 26 Schmidt, S.; Gonzalez, D.; Derendorf, H. *J. Pharm. Sciences* **2010**, *99*, 1107-1122.
  - 27 Emoto, C.; Murayama, N.; Rostami-Hodjegan, A.; Yamazaki, H. *Curr. Drug Met.* **2011**, *11*, 678-685.
  - 28 Obach, A. S. *Curr. Top. Med. Chem.* **2011**, *11*, 334-339.
  - 29 Jones, B. C.; Middleton, D. S.; Youdim, K. *Prog. Med. Chem.* **2009**, *47*, 239-263.
  - 30 Johnson, T. W.; Dress, K. R.; Edwards, M. *Bioorg. Med. Chem. Lett.* **2009**, *19*, 5560-5564.
  - 31 Roden, D. M. *N. Engl. J. Med.* **2004**, *350*, 1013-1022.
  - 32 Witchel, H. J. *Cardiovasc. Ther.* **2011**, *9*, 251-259.
  - 33 Raschi, E.; Ceccarini, L.; De Ponti, F.; Recanatini, M. *Expert Opin. Drug Metab. Toxicol.* **2009**, *5*, 1005-1021.
  - 34 Du-Cuny, L.; Chen, L.; Zhang, S. *J. Chem. Inf. Model* **2011**, *51*, 2948-2960.
  - 35 Durdagi, S.; Subbotina, J.; Lees-Miller, J.; Guo, J.; Duff, H. J.; Noskov, S. Y. *Curr. Med. Chem.* **2010**, *17*, 3514-3532.
  - 36 Aronov, A. M. *Curr. Top. Med. Chem.* **2008**, *8*, 1113-1127.
  - 37 Waring, M. J.; Johnstone, C. *Bioorg. Med. Chem. Lett.* **2007**, *17*, 1759-1764.
  - 38 Gleeson, M. P.; Hersey, A.; Montanari, D.; Overington, J. *Nat. Rev. Drug Discov.* **2011**, *10*, 197-208.
  - 39 Zheng, W.; Thorne, N.; McKew J. C. *Drug Discov. Today* **2013**, *18*, 1067-1073.
  - 40 Paul, S. M.; Mytelka, D. S.; Dunwiddie, C. T.; Persinger, C. C.; Munos, B. H.; Lindborg, S. R.; Schacht, A. L. *Nat. Rev. Drug Discov.* **2010**, *9*, 203-214.
  - 41 Fang, Y. *Comb. Chem. High Throughput Screen.* **2014**, *17*, 566-578.
  - 42 Prior, M.; Chiruta, C.; Currais, A.; Goldberg, J.; Ramsey, J.; Dargusch, R.; Maher, P. A.; Schubert, D. *ACS Chem. Neurosci.* **2014**, *5*, 503-513.
  - 43 Zhang, M.; Luo, G.; Zhou, Y.; Wang, S.; Zhong, Z. *J. Biomol. Screen.* **2014**, *19*, 1-16.
  - 44 Gilbert, I. H. *J. Med. Chem.* **2013**, *56*, 7719-7726.
  - 45 Peters, J.-U. *J. Med. Chem.* **2013**, *56*, 8955-8971.
  - 46 Anighoro, A.; Bajorath, J.; Rastelli, G. *J. Med. Chem.* **2014**, *57*, 7874-7887.
  - 47 Kotz, J. *Science-Business eXchange* **2012**, *5(15)*.
  - 48 Lee, J.; Bogyo, M. *Curr. Opin. Chem. Biol.* **2013**, *17*, 118-126.
  - 49 Hart, C. P. *Drug Discov. Today:Targets* **2005**, *10*, 513-519.
  - 50 Swinney, D. C. *Clin. Pharmacol. Ther.* **2013**, *93*, 299-301.
  - 51 Vane, J. R.; Botting, R. M. *Thromb. Res.* **2003**, *110*, 255-258.
  - 52 Swinney, D. C.; Anthony, J. *Nat. Rev. Drug Discov.* **2011**, *10*, 507-519.
  - 53 Eder, J.; Sedrani, R.; Wiesmann, C. *Nat. Rev. Drug Discov.* **2014**, *13*, 577-587.
  - 54 Wilson, I. *Molecular Recognition*, In *Handbook of Cell Signaling*, Second Edition, edited by Bradshaw, R. A.; Dennis, E. A.; Elsevier Inc. **2010**.
  - 55 Minor, D. L. *An Overview of Ion Channel Structure*, In *Functioning of Transmembrane Receptors in Cell Signalling*, edited by Bradshaw, R. A.; Dennis, E. A.; Elsevier Inc. **2011**.



- 
- 56 Alexander, S. P. H.; Mathie, A.; Peters, J. A. *Guide to Receptors and Channels (GRAC)*, Fourth Edition, *Br. J. Pharmacol.* **2009**, *158* (Suppl. 1), S124-S155.
- 57 Patrick, G. L. *Proteins as Drug Targets: Receptor Structure and Signal Transduction*, In *An Introduction to Medicinal Chemistry*; Oxford University Press Inc. **2005**.
- 58 Doyle, D. A.; Morais Cabral, J.; Pfuetzner, R. A.; Kuo, A.; Gulbis, J. M.; Cohen, S. L.; Chait, B. T.; MacKinnon, R. *Science* **1998**, *280*, 69-77.
- 59 De Groot, M. *Future Med. Chem.* **2010**, *2*, 697-701.
- 60 Bagal, S. K.; Brown, A. D.; Cox, P. J.; Omoto, K.; Owen, R. M.; Pryde, D. C.; Sidders, B.; Skerratt, S. E.; Stevens, E. B.; Storer, R. I.; Swain, N. A. *J. Med. Chem.* **2013**, *56*, 593-624.
- 61 Clapham, D. E. *Cell* **2007**, *131*, 1047-1058.
- 62 Hübner, C. A.; Jentsch, T. J. *Hum. Mol. Genet.* **2002**, *11*, 2435-2445.
- 63 Overington, J. P.; Al-Lazikani, B.; Hopkins, A. L. *Nat. Rev. Drug Discov.* **2006**, *5*, 326-327.
- 64 Steele, D. S.; Hwang, H.-S.; Knollmann, B. C. *Cardiovasc. Res.* **2013**, *98*, 326-327.
- 65 Kellinghaus, C. *Ther. Clin. Risk Manag.* **2009**, *5*, 757-766.
- 66 Cummins, T. R. *J. Physiol.* **2007**, *582*, 11.
- 67 Kaczorowski, G. J.; McManus, O. B.; Priest, B. T.; Garcia, M. L. *J. Gen. Physiol.* **2008**, *131*, 399-405.
- 68 Berridge, M. J.; Lipp, P.; Bootman, M. D. *Mol. Cell Biol.* **2000**, *1*, 11-21.
- 69 Crabtree, G. R. *Cell* **1999**, *96*, 611-614.
- 70 Feske, S. *Nat. Rev. Immunol.* **2007**, *7*, 690-702.
- 71 Ertel, E. A.; Campbell, K. P.; Harpold, M. M.; Hofmann, F.; Mori, Y.; Perez-Reyes, E.; Schwartz, A.; Snutch, T. P.; Tanabe, T.; Birnbaumer, L.; Tsien, R. W. *Neuron* **2000**, *25*, 533-535.
- 72 Lory, P.; Chemin, J. *Expert Opin. Ther. Targets* **2007**, *11*, 717-722.
- 73 Putney, J. W. *Cell Calcium* **1986**, *7*, 1-12.
- 74 Putney, J. W. *Mol. Interv.* **2010**, *4*, 209-218.
- 75 Hogan, P. G.; Lewis, R. S.; Rao, A. *Annu. Rev. Immunol.* **2010**, *28*, 491-533.
- 76 Feske, S.; Prakriya, M.; Rao, A.; Lewis, R. S. *J. Exp. Med.* **2005**, *202*, 651-662.
- 77 Parekh, A. B. *Nat. Rev. Drug Discov.* **2010**, *9*, 399-410.
- 78 Sweeney, Z. K.; Minatti, A.; Button, D. C.; Patrick, S. *ChemMedChem* **2009**, *4*, 706-718.
- 79 Derler, I.; Fritsch, R.; Schindl, R.; Romanin, C. *Expert Opin. Drug Discov.* **2008**, *3*, 787-800.
- 80 Yamashita, M.; Navarro-Borelly, L.; McNally, B. A.; Prakriya, M. *J. Gen. Physiol.* **2007**, *130*, 525-540.
- 81 Giachini, F. R.; Lima, V. V.; Hannan, J. L.; Carneiro, F. S.; Webb, R. C.; Tostes, R. C. *Braz. J. Med. Biol. Res.* **2011**, *44*, 1080-1087.
- 82 Carrasco, S.; Meyer, T. *Nat. Cell Biol.* **2010**, *12*, 416-418.
- 83 Hoth, M.; Penner, R. *Nature* **1992**, *355*, 353-355.

- 
- 84 Roos, J.; DiGregorio, P. J.; Yeromin, A. V.; Ohlsen, K.; Lioudyno, M.; Zhang, S.; Safrina, O.; Kozak, J. A.; Wagner, S. L.; Cahalan, M. D.; Veliçelebi, G.; Stauderman, K. A. *J. Cell. Biol.* **2005**, *169*, 435-445.
- 85 Liou, J.; Lyang Kim, M.; Do Heo, W.; Jones, J. T.; Myers, J. W.; Ferrell Jr., J. E.; Meyer, T. *Curr. Biol.* **2005**, *15*, 1235-1241.
- 86 Stathopoulos, P. B.; Zheng, L.; Li, G.-Y.; Plevin, M. J.; Ikura, M. *Cell* **2008**, *135*, 110-122.
- 87 Vig, M.; Peinelt, C.; Beck, A.; Koomoa, D. L.; Rabah, D.; Koblan-Huberson, M.; Kraft, S.; Turner, H.; Fleig, A.; Penner, R.; Kinet, J.-P. *Science* **2006**, *312*, 1220-1223.
- 88 Feske, S.; Gwack, Y.; Prakriya, M.; Srikanth, S.; Puppel, S.-H.; Tanasa, B.; Hogan, P. G.; Lewis, R. S.; Daly, M.; Rao, A. *Nature* **2006**, *441*, 179-185.
- 89 Zhang, S. L.; Yeromin, A. V.; Zhang, X. H.-F.; Yu, Y.; Safrina, O.; Penna, A.; Roos, J.; Stauderman, K. A.; Cahalan, M. D. *Proc. Natl. Acad. Sci. USA* **2006**, *103*, 9357-9362.
- 90 Yeromin, A. V.; Zhang, S. L.; Jiang, W.; Yu, Y.; Safrina, O.; Cahalan, M. D. *Nature* **2006**, *443*, 226-229.
- 91 Prakriya, M.; Feske, S.; Gwack, Y.; Srikanth, S.; Rao, A.; Hogan, P. G. *Nature* **2006**, *443*, 230-233.
- 92 Penna, A.; Demuro, A.; Yeromin, A. V.; Zhang, S. L.; Safrina, O.; Parker, I.; Cahalan, M. D. *Nature* **2008**, *456*, 116-122.
- 93 Ji, W.; Xu, P.; Li, Z.; Lu, J.; Liu, L.; Zhan, Y.; Chen, Y.; Hille, B.; Xu, T.; Chen, L. *Proc. Natl. Acad. Sci. USA* **2008**, *105*, 13668-13673.
- 94 Hou, X.; Pedi, L.; Diver, M. M.; Long, S. B. *Science* **2012**, *338*, 1308-1313.
- 95 Wu, M. M.; Luik, R. M.; Lewis, R. S. *Cell Calcium* **2007**, *42*, 163-172.
- 96 Wu, M. M.; Buchanan, J.; Luik, R. M.; Lewis, R. S. *J. Cell Biol.* **2006**, *174*, 803-813.
- 97 Peinelt, C.; Vig, M.; Koomoa, D. L.; Beck, A.; Nadler, M. J. S.; Koblan-Huberson, M.; Lis, A.; Fleig, A.; Penner, R.; Kinet, J. P. *Nat. Cell Biol.* **2006**, *8*, 771-773.
- 98 Soboloff, J.; Spassova, M. A.; Tang, X. D.; Hewavitharana, T.; Xu, W.; Gill, D. L. *J. Biol. Chem.* **2006**, *281*, 20661-20665.
- 99 Mercer, J. C.; Dehaven, W. I.; Smyth, J. T.; Wedel, B.; Boyles, R. R.; Bird, G. S.; Putney J. W. *J. Biol. Chem.* **2006**, *281*, 24979-24990.
- 100 Muik, M.; Frischauf, I.; Derler, I.; Fahrner, M.; Bergsmann, J.; Eder, P.; Schindl, R.; Hesch, C.; Polzinger, B.; Fritsch, R.; Kahr, H.; Madl, J.; Gruber, H.; Groschner, K.; Romanin, C. *J. Biol. Chem.* **2008**, *283*, 8014-8022.
- 101 Muik, M.; Fahrner, M.; Derler, I.; Schindl, R.; Bergsmann, J.; Frischauf, I.; Groschner, K.; Romanin, C. *J. Biol. Chem.* **2009**, *284*, 8421-8426.
- 102 Derler, I.; Schindl, R.; Fritsch, R.; Heftberger, P.; Riedl M. C.; Begg, M.; House, D.; Romanin, C. *Cell Calcium* **2013**, *53*, 139-151.
- 103 Partiseti, M.; Le Deist, F.; Hivroz, C.; Fischer, A.; Korn, H.; Choquet, D. *J. Biol. Chem.* **1994**, *269*, 32327-32335.

- 
- 104 Le Deist, F.; Hivroz, C.; Partiseti, M.; Thomas, C.; Buc, H. A.; Oleastro, M.; Belohradsky, B.; Choquet, D.; Fischer, A. *Blood* **1995**, *85*, 1053-1062.
- 105 Feske, S.; Giltnane, J.; Dolmetsch, R.; Staudt, L. M.; Rao, A. *Nat. Immunol.* **2001**, *2*, 316-324.
- 106 Picard, C.; McCarl, C.-A.; Papolos, A.; Khalil, S.; Lüthy, K.; Hivroz, C.; Le Deist, F.; Rieux-Laucat, F.; Rechavi, G.; Rao, A.; Fischer, A.; Feske, S. *N. Engl. J. Med.* **2009**, *360*, 1971-1980.
- 107 Baba, Y.; Nishida, K.; Fujii, Y.; Hirano, T.; Hikida, M.; Kurosaki, T. *Nat. Immunol.* **2008**, *9*, 81-88.
- 108 Vig, M.; DeHaven, W. I.; Bird, G. S.; Billingsley, J. M.; Wang, H.; Rao, P. E.; Hutchings, A. B.; Jouvin, M.-H.; Putney, J. W.; Kinnet, J.-P. *Nat. Immunol.* **2008**, *9*, 89-96.
- 109 All the Jurkat cell assays were performed by Begg, M.; Heathcote, M.; Hoslin, A.; Lucas, F. *GlaxoSmithKline*, R&D Stevenage, UK; unpublished results.
- 110 Treiman, M.; Caspersen, C.; Christensen, S. B. *Trends Pharmacol. Sci.* **1998**, *19*, 131-135.
- 111 Gee, K. R.; Brown, K. A.; Chen, W.-N. U.; Bishop-Stewart, J.; Gray, D.; Johnson, I. *Cell Calcium* **2000**, *27*, 97-106.
- 112 <http://www.rockefeller.edu/htsrc/pdf/EnVisionFeatures.pdf>;  
accessed 10/10/2012.
- 113 All the LAD2 mast cell assays were performed by Russell, L. *GlaxoSmithKline*, R&D Stevenage, UK; unpublished results.
- 114 All donors provided written informed consent for use of their samples, and the collection and use of the samples received Institutional Ethics Committee approval.
- 115 All the PBMCs assays were performed by Hoslin, A.; Wayne, G. *GlaxoSmithKline*, R&D Stevenage, UK; unpublished results.
- 116 Campbell, J. D. M.; Foerster, A.; Lasmanowicz, V.; Niemöller, M.; Scheffold, A.; Fahrendorff, M.; Rauser, G.; Assenmacher, M.; Richter, A. *Clin. Exp. Immunol.* **2011**, *163*, 1-10.
- 117 Huang, H.; Park, P.-H.; McMullen, M. R.; Nagy, L. E. *J Gastro. Hep.* **2008**, *23*, S50-S53.
- 118 Gessani, S.; Belardelli, F. *Cytokine Growth Factor Rev.* **1998**, *9*, 117-123.
- 119 Molleman, A. *Patch Clamping, An Introduction Guide to Patch Clamp Electrophysiology* **2003**, John Wiley & Sons, Ltd.
- 120 Dunlop, J.; Bowlby, M.; Peri, R.; Vasilyev, D.; Arias, R. *Nat. Rev. Drug Discov.* **2008**, *7*, 358-368.
- 121 <http://pcwww.liv.ac.uk/~petesmif/petesmif/research/electrophysiology.htm>;  
accessed on 26/06/2015.
- 122 All the electrophysiology assays were performed by Rumley, S. *GlaxoSmithKline*, R&D Stevenage, UK; unpublished results.
- 123 Bamaung, N. Y.; Basha, A.; Djuric, S. W.; Gubbins, E. J.; Luly, J. R.; Tu, N. P.; Madar, D. J.; Warrior, U.; Wiedeman, P. E.; Zhou, X. U. N.; Sciotti, R. J.; Wagenaar, F. L. (Abbott Laboratories), *US20010044445A1*, **2001**.

- 
- 124 Kubota, H.; Yonetoku, Y.; Sugasawa, K.; Funatsu, M.; Kawazoe, S.; Toyoshima, A.; Okamoto, Y.; Ishikawa, J.; Takeuchi, M. (Yamanouchi Pharmaceutical Co. Ltd.), *US6348480B1*, **2002**.
- 125 Betageri, R. (Boehringer Ingelheim Pharmaceuticals), *WO2001070703A2*, **2001**.
- 126 Xie, Y.; Holmqvist, M.; Mahiou, J.; Ono, M.; Sun, L.; Chen, S.; Zhang, S.; Jiang, J.; Chimmanamada, D.; Fleig, A.; Yu, C. Y. (Synta Pharmaceuticals), *WO2005009954A2*, **2005**.
- 127 Velcelebi, G.; Stauderman, K. A.; Pleyner, D. P. M.; Cheng, S.; Whitten, J. P. (Calcimedica, Inc.), *WO2009/035818A1*, **2009**.
- 128 [http://www.calcimedica.com/PR\\_08.html](http://www.calcimedica.com/PR_08.html); accessed on 26/06/2015.
- 129 Rice, L. V.; Bax, H. J.; Russell, L. J.; Barrett, V. J.; Walton, S. E.; Deakin, A. M.; Thomson, S. A.; Lucas, F.; Solari, R.; House, D.; Begg, M. *Eur. J. Pharmacol.* **2013**, *704*, 49-57.
- 130 Ashmole, I.; Duffy, S. M.; Leyland, M. L.; Morrison, V. S.; Begg, M.; Bradding, P. *J. Allergy Clin. Immunol.* **2012**, *129*, 1628-1635.
- 131 Hughes, A. D.; Jones, L. H. *Future Med. Chem.* **2011**, *3*, 1585-1605.
- 132 Ritchie, T. R.; Luscombe, C. N.; Macdonald, S. J. F. *J. Chem. Inf. Model.* **2009**, *49*, 1025-1032.
- 133 Jones, R. M.; Neef, N. *Xenobiotica* **2012**, *42*, 86-93.
- 134 Forbes, B.; O'Lone, R.; Pribul Allen, P.; Cahn, A.; Clarke, C.; Collinge, M.; Dailey, L. A.; Donnelly, L. E.; Dybowski, J.; Hassall, D.; Hildebrand, D.; Jones, R. M.; Kilgour, J.; Klapwijk, J.; Maier, C. C.; McGovern, T.; Nikula, K.; Parry, J. D.; Reed, M. D.; Robinson, I.; Tomlinson, L.; Wolfreys, A. *Adv. Drug Deliv. Rev.* **2014**, *71*, 15-33.
- 135 Coe, D. M.; Cooper, A. W. J.; Gore, P. M.; House, D.; Senger, S.; Vile, S. (GlaxoSmithKline), *WO2010122088A1*, **2010**.
- 136 Allen, D. G.; Coe, D. M.; Cooper, A. W. J.; Gore, P. M.; House, D.; Senger, S.; Sollis, S. L.; Vile, S.; Wilson, C. (GlaxoSmithKline), *WO2010122089A1*, **2010**.
- 137 Unpublished results from *GlaxoSmithKline*, R&D Stevenage, UK.
- 138 Unpublished results from Bravi, G.; Hatley, R.; House, D.; Lacroix, Y.; Le Gall, A. *GlaxoSmithKline*, R&D Stevenage, UK.
- 139 Guido, R. V. C.; Olivia, G.; Andricopulo, A. D. *Combin. Chem. High Through. Screen.* **2011**, *14*, 830-839.
- 140 Larsson, A.; Jansson, A.; Åberg, A.; Nordlund, P. *Curr. Opin. Chem. Biol.* **2011**, *15*, 482-488.
- 141 Unpublished results from Hatley, R.; Lacroix, Y. *GlaxoSmithKline*, R&D Stevenage, UK.
- 142 Steventon, G. B.; Mitchell, S. C. *Expert Opin. Drug Metab. Toxicol.* **2009**, *5*, 1213-1221.
- 143 Molecular operating environment®:  
<https://www.chemcomp.com/MOE2014.htm>; accessed on 28/06/2015.
- 144 Finnegan, W. G.; Henry, R. A.; Lofquist, R. *J. Am. Chem. Soc.* **1958**, *80*, 3908-3911.
- 145 Unpublished results from Copley, R. *GlaxoSmithKline*, R&D Stevenage, UK.

- 
- 146 Ritchie, T. J.; Macdonald, S. J. F.; Young, R. J.; Pickett, S. D. *Drug Discov. Today* **2011**, *16*, 164-171.
- 147 Ritchie, T. J.; Macdonald, S. J. F.; Peace, S.; Pickett, S. D.; Luscombe, C. N. *Med. Chem. Commun.* **2012**, *3*, 1062-1069.
- 148 Unpublished results from Maduli, E. *GlaxoSmithKline*, R&D Stevenage, UK.
- 149 Compound **2.48** was already present in the GlaxoSmithKline internal compound collection.
- 150 Unpublished results from Moriarty, M. *GlaxoSmithKline*, R&D Stevenage, UK.
- 151 Leach, A.; Bradshaw, J.; Green, D. V. S.; Hann, M. M. *J. Chem. Inf. Comput. Sci.* **1999**, *39*, 1161-1172.
- 152 Jug, K.; Chiodo, S. *J. Phys. Chem. A* **2003**, *107*, 4172-4183.
- 153 Boström, J.; Hogner, A.; Llinàs, A.; Wellner, E.; Plowright, A. T. *J. Med. Chem.* **2012**, *55*, 1817-1830.
- 154 This compound was synthesised by an external collaborator; *ChemPartner*, Shanghai, CHINA; unpublished results.
- 155 Unpublished results from Hatley, R.; Moriarty, M.; Wix, E. *GlaxoSmithKline*, R&D Stevenage, UK.
- 156 Unpublished results from Hatley, R.; House, D.; Lacroix, Y.; Maduli, E.; Moriarty, M.; Wix, E. *GlaxoSmithKline*, R&D Stevenage, UK.
- 157 Lin, Y.; Lang, Jr., S. A.; Lovell, M. F.; Perkinson, N. A. *J. Org. Chem.* **1979**, *44*, 4160-4164.
- 158 Nicolaides, D. N.; Fylaktakidou, K. C.; Litinas, K. E.; Papageorgio, G. K.; Hadjipavlou-Litina, D. J. *J. Heterocycl. Chem.* **1998**, *35*, 619-625.
- 159 Santilli, A. A.; Morris, R. L. *J. Heterocycl. Chem.* **1979**, *16*, 1197-1200.
- 160 Liang, G.-B.; Feng, D. D. *Tetrahedron Lett.* **1996**, *37*, 6627-6630.
- 161 Peters, J.-U.; Schnider, P.; Mattei, P.; Kansy, M. *ChemMedChem* **2009**, *4*, 680-686.
- 162 Jamieson, C.; Moir, E. M.; Rankovic, Z.; Wishart, G. *J. Med. Chem.* **2006**, *49*, 5029-5046.
- 163 Lin, J. H. *Drug Metab. Dispos.* **1995**, *23*, 1008-1021.
- 164 Bogaards, J. J. P.; Bertrand, M.; Jackson, P.; Oudshoorn, M. J.; Weaver, R. J.; van Bladeren, P. J.; Walther, B. *Xenobiotica* **2000**, *30*, 1131-1152.
- 165 Guengerich, F. P. *Chem. Biol. Interact.* **1997**, *106*, 161-182.
- 166 Stepan, A. F.; Mascitti, V.; Beaumont, K.; Kalgutkar, A. S. *Med. Chem. Commun.* **2013**, *4*, 631-652.
- 167 Smith, S. W.; Fu, G. C. *Angew. Chem. Int. Ed. Engl.* **2008**, *47*, 9334-9336.
- 168 Joshi-Pangu, A.; Ganesh, M.; Biscoe, M. R. *Org. Lett.* **2011**, *13*, 1218-1221.
- 169 Thaler, T.; Haag, B.; Gavryushin, A.; Schober, K.; Hartmann, E.; Gschwind, R. M.; Zipse, H.; Mayer, P.; Knochel, P. *Nat. Chem.* **2010**, *10*, 125-130.
- 170 Han, C.; Buchwald, S. L. *J. Am. Chem. Soc.* **2009**, *131*, 7532-7533.
- 171 Unpublished results from Pasikanti, K. *GlaxoSmithKline*, R&D Singapore, SINGAPORE.

- 
- 172 MetaSite® is a computational procedure that predicts metabolic transformations related to cytochrome- and flavin-containing monooxygenase-mediated reactions in phase I metabolism:  
<http://www.moldiscovery.com/software/metasite/>; accessed on 26/06/2015.
- 173 Unpublished results from Reid, I. *GlaxoSmithKline*, R&D Stevenage, UK.
- 174 Morgenthaler, M.; Schweizer, E.; Hoffmann-Röder, A.; Benini, F.; Martin, R. E.; Jaeschke, G.; Wagner, B.; Fischer, H.; Bendels, S.; Zimmerli, D.; Schneider, J.; Diederich, F.; Kansy, M.; Müller, K. *ChemMedChem* **2007**, *2*, 1100-1115.
- 175 Martin, R. E.; Plancq, B.; Gavelle, O.; Wagner, B.; Fischer, H.; Bendels, S.; Müller, K. *ChemMedChem* **2007**, *2*, 285-287.
- 176 Lovering, F.; Bikker, J.; Humblet, C. *J. Med. Chem.* **2009**, *52*, 6752-6756.
- 177 Smith, G. K.; Wood, E. R. *Drug Discov. Today: Technologies* **2010**, *7*, e13-e19.
- 178 Zorov, D. B.; Isaev, N. K.; Plotnikov, E. Y.; Zorova, L. D.; Stelmashook, E. V.; Vasileva, A. K.; Arkhangelskaya, A. A.; Khrjapenkova, T. G. *Biochemistry (Mosc.)* **2007**, *72*, 1115-1126.
- 179 Davis, R. E.; Williams, M. J. *Pharmacol. Exp. Ther.* **2012**, *342*, 598-607.
- 180 Kroemer, G.; Galluzzi, L.; Brenner, C. *Physiol. Rev.* **2007**, *87*, 99-163.
- 181 Martin, L. J. *Prog. Mol. Biol. Transl. Sci.* **2012**, *107*, 355-415.
- 182 Halestrap, A. P. *J. Mol. Cell. Cardiol.* **2009**, *46*, 821-831.
- 183 Leung, A. W. C.; Halestrap, A. P. *Biochim. Biophys. Acta* **2008**, *1777*, 946-952.
- 184 Zamzami, N.; Kroemer, G. *Nat. Rev. Cell Biol.* **2001**, *2*, 67-71.
- 185 Alam, M. R.; Baetz, D.; Ovize, M. *J. Mol. Cell. Cardiol.* **2015**, *78*, 80-89.
- 186 Javadoz, S.; Kuznetsov, A. *Front. Phys.* **2013**, *4*, 1-5.
- 187 Crompton, M.; Ellinger, H.; Costi, A. *Biochem. J.* **1988**, *255*, 357-360.
- 188 Tanveer, A.; Virji, S.; Andreeva, L.; Totty, N. F.; Hsuan, J. J.; Ward, J. M.; Crompton, M. *Eur. J. Biochem.* **1996**, *238*, 166-172.
- 189 Baines, C. P.; Kaiser, R. A.; Purcell, N. H.; Blair, N. S.; Osinska, H.; Hambleton, M. A.; Brunskill, E. W.; Sayen, M. R.; Gottlieb, R. A.; Dorn, G. W.; Robbins, J.; Molkentin, J. D. *Nature* **2005**, *434*, 658-662.
- 190 Elrod, J. W.; Molkentin, J. D. *Circ. J.* **2013**, *77*, 1111-1122.
- 191 Kokoszka, J. E.; Waymire, K. G.; Levy, S. E.; Sligh, J. E.; Cai, J.; Jones, D. P.; MacGregor, G. R.; Wallace, D. C. *Nature* **2004**, *427*, 461-465.
- 192 Crompton, M.; Virji, S.; Ward, J. M. *Eur. J. Biochem.* **1998**, *258*, 729-735.
- 193 Baines, C. P.; Kaiser, R. A.; Sheiko, T.; Craigen, W. J.; Molkentin, J. D. *Nat. Cell. Biol.* **2007**, *9*, 550-555.
- 194 Karch, J.; Molkentin, J. D. *Proc. Natl. Acad. Sci. USA* **2014**, *111*, 10396-10397.
- 195 Kwong, J. Q.; Davis, J.; Baines, C. P.; Sargent, M. A.; Karch, J.; Wang, X.; Huang, T.; Molkentin, J. D. *Cell Death Differ.* **2014**, *21*, 1209-1217.
- 196 Giorgio, V.; von Stockum, S.; Antoniel, M.; Fabbro, A.; Fogolari, F.; Forte, M.; Glick, G. D.; Petronilli, V.; Zoratti, M.; Szabó, I.; Lippe, G.; Bernardi, P. *Proc. Natl. Acad. Sci. USA* **2013**, *110*, 10580-10585.
- 197 Alavian, K. N.; Beutner, G.; Lazrove, E.; Sacchetti, S.; Park, H.-A.; Licznerski, P.; Li, H.; Nabili, P.; Hockensmith, K.; Graham, M.; Porter Jr., G. A.; Jonas, E. A. *Proc. Natl. Acad. Sci. USA* **2014**, *111*, 5887-5892.
- 198 Bonora, M.; Bravo-San Pedro, J. M.; Kroemer, G.; Galluzzi, L.; Pinton, P. *Cell Cycle* **2014**, *13*, 2666-2670.

- 
- 199 Bonora, M.; Wieckowski, M. R.; Chinopoulos, C.; Kepp, O.; Kroemer, G.; Galluzzi, L.; Pinton, P. *Oncogene* **2014**, *33*, 1-12.
- 200 Laslett, L. J.; Alagona, P.; Clark, B. A.; Drozda, J. P.; Saldivar, F.; Wilson, S. R.; Poe, C.; Hart, M. *J. Am. Coll. Cardiol.* **2012**, *60*, S1-S49.
- 201 Halestrap, A. P.; Clarke, S. J.; Javadov, S. A. *Cardiovasc. Res.* **2004**, *61*, 372-385.
- 202 Halestrap, A. P.; Richardson, A. P. *J. Mol. Cell. Cardiol.* **2015**, *78*, 129-141.
- 203 Morciano, G.; Giorgi, C.; Bonora, M.; Punzetti, S.; Pavasini, R.; Wieckowski, M. R.; Campo, G.; Pinton, P. *J. Mol. Cell. Cardiol.* **2015**, *78*, 142-153.
- 204 Griffiths, E. J.; Halestrap, A. P. *J. Mol. Cell. Cardiol.* **1993**, *25*, 1461-1469.
- 205 Piot, C.; Croisille, P.; Staat, P.; Thibault, H.; Rioufol, G.; Mewton, N.; Elbelghiti, R.; Cung, T. T.; Bonnefoy, E.; Angoulvant, D.; Macia, C.; Raczka, F.; Sportouch, C.; Gahide, G.; Finet, G.; André-Fouët, X.; Revel, D.; Kirkorian, G.; Monassier, J.-P.; Derumeaux, G.; Ovize, M. *N. Eng. J. Med.* **2008**, *359*, 473-481.
- 206 Hausenloy, D. J.; Kunst, G.; Boston-Griffiths, E.; Kolvekar, S.; Chaubey, S.; John, L.; Desai, J.; Yellon, D. M. *Heart* **2014**, *100*, 544-549.
- 207 Chiari, P.; Angoulvant, D.; Mewton, N.; Desebbe, O.; Obadia, J.-F.; Robin, J.; Farhat, F.; Jegaden, O.; Bastien, O.; Lehot, J.-J.; Ovize, M. *Anesthesiology* **2014**, *21*, 232-238.
- 208 Norenberg, M. D.; Rao, K. V. R. *Neurochem. Intern.* **2007**, *50*, 983-997.
- 209 Paradies, G.; Paradies, V.; Ruggiero, F. M.; Petrosillo, G. *Mech. Ageing Dev.* **2013**, *134*, 1-9.
- 210 Morota, S.; Månsson, R.; Hansson, M. J.; Kasuya, K.; Shimazu, M.; Hasegawa, E.; Yanagi, S.; Omi, A.; Uchino, H.; Elmér, E. *Exp. Neurol.* **2009**, *218*, 353-362.
- 211 Picone, P.; Nuzzo, D.; Caruana, L.; Scafidi, V.; Di Carlo, M. *Oxid. Med. Cell. Longev.* **2014**, Article ID 780179.
- 212 Du, H.; Guo, L.; Fang, F.; Chen, D.; Sosunov, A. A.; McKhann, G. M.; Yan, Y.; Wang, C.; Zhang, H.; Molkentin, J. D.; Gunn-Moore, F. J.; Vonsattel, J. P.; Arancio, O.; Chen, J. X.; Yan, S. D. *Nat. Med.* **2008**, *14*, 1097-1105.
- 213 Muyderman, H.; Chen, T. *Br. J. Pharmacol.* **2014**, *171*, 2191-2205.
- 214 Keep, M.; Elmér, E.; Fong, K. S. K.; Csiszar, K. *Brain Res.* **2001**, *894*, 327-331.
- 215 Martin, L. J.; Gertz, B.; Pan, Y.; Price, A. C.; Molkentin, J. D.; Chang, Q. *Exp. Neurol.* **2009**, *218*, 333-346.
- 216 Irwin, W. A.; Bergamin, N.; Sabatelli, P.; Reggiani, C.; Megighian, A.; Merlini, L.; Braghetta, P.; Columbaro, M.; Volpin, D.; Bressan, G. M.; Bernardi, P.; Bonaldo, P. *Nat. Genet.* **2003**, *35*, 367-371.
- 217 Palma, E.; Tiepolo, T.; Angelin, A.; Sabatelli, P.; Maraldi, N. M.; Basso, E.; Forte, M. A.; Bernardi, P.; Bonaldo, P. *Hum. Mol. Gen.* **2009**, *18*, 2024-2031.
- 218 Mazzeo, A. T.; Beat, A.; Singh, A.; Bullock, M. R. *Exp. Neurol.* **2009**, *218*, 363-370.
- 219 Korde, A. S.; Pettigrew, L. C.; Craddock, S. D.; Pocernich, C. B.; Waldmeier, P. C.; Maragos, W. F. *J. Neurotrauma* **2007**, *24*, 895-908.
- 220 Sweeney, Z. K.; Fu, J.; Wiedmann, B. *J. Med. Chem.* **2014**, *57*, 7145-7159.
- 221 Waldmeier, P. C.; Feldtrauer, J.-J.; Qian, T.; Lemasters, J. J. *Mol. Pharmacol.* **2002**, *62*, 22-29.

- 
- 222 Hansson, M. J.; Mattiasson, G.; Månsson, R.; Karlsson, J.; Keep, M. F.; Waldmeier, P. C.; Ruegg, U. T.; Dumont, J. M.; Besseghir, K.; Elmér, E. *J. Bioenerg. Biomembr.* **2004**, *36*, 407-413.
- 223 Reutenauer, J.; Dorchies, O. M.; Patthey-Vuadens, O.; Vuagniaux, G.; Ruegg, U. T. *Br. J. Pharmacol.* **2008**, *155*, 574-584.
- 224 Rao, K. V. R.; Carlson, E. A.; Yan, S. S. *Biochim. Biophys. Acta* **2014**, *1842*, 1267-1272.
- 225 Vuagniaux, G.; Gavillet, B.; Crabbé, R. (Debio Recherche Pharmaceutique SA), *WO2011/141891A1*, **2011**.
- 226 Fu, J.; Karur, S.; Li, X.; Lu, P.; Mergo, W.; Rivkin, A.; Sweeney, Z. K.; Tjandra, M.; Weiss, A.; Yifru, A. (Novartis AG), *WO2014/049540*, **2014**.
- 227 Fancelli, D.; Abate, A.; Amici, R.; Bernardi, P.; Ballarini, M.; Cappa, A.; Carezzi, G.; Colombo, A.; Contursi, C.; Di Lisa, F.; Dondio, G.; Gagliardi, S.; Milanese, E.; Minucci, S.; Pain, G.; Pelicci, P. G.; Saccani, A.; Storto, M.; Thaler, F.; Varasi, M.; Villa, M.; Plyte, S. *J. Med. Chem.* **2014**, *57*, 5333-5347.
- 228 Fancelli, D.; Varasi, M.; Plyte, S.; Ballarini, M.; Cappa, A.; Carezzi, G.; Minucci, S.; Pain, G.; Villa, M. (Congenia SRL), *WO2010/049768A1*, **2010**.
- 229 Phase 1 clinical study of GNX-5086:  
<http://www.congenia.it/docs/Congenias%20Announces%20Initiation%20of%20Phase%20I%20Enrollment.pdf>; accessed on 21/07/2015.
- 230 Martin, L. J.; Fancelli, D.; Wong, M.; Niedzwiecki, M.; Ballarini, M.; Plyte, S.; Chang, Q. *Front. Cell. Neurosci.* **2014**, *8*, No. 433.
- 231 Bordet, T.; Buisson, B.; Michaud, M.; Drouot, C.; Galéa, P.; Delaage, P.; Akentieva, N. P.; Evers, A. S.; Covey, D. F.; Ostuni, M. A.; Lacapère, J.-J.; Massaad, C.; Schumacher, M.; Steidl, E.-M.; Maux, D.; Delaage, M.; Handerson, C. E.; Pruss, R. M. *J. Pharmacol. Exp. Ther.* **2007**, *322*, 709-720.
- 232 Ricchelli, F.; Šileikytė, J.; Bernardi, P. *Biochim. Biophys. Acta* **2011**, *1807*, 482-490.
- 233 Bordet, T.; Berna, P.; Abitbol, J.-L.; Pruss, R. M. *Pharmaceuticals* **2010**, *3*, 345-368.
- 234 Martin, L. J. *IDrugs* **2010**, *13*, 568-580.
- 235 Lenglet, T.; Lacomblez, L.; Abitbol, J.-L.; Ludolph, A.; Mora, J. S.; Robberecht, W.; Shaw, P. J.; Pruss, R. M.; Cuvier, V.; Meininger, V. *Eur. J. Neurol.* **2014**, *21*, 529-536.
- 236 Kim, Y. S.; Jung, S. H.; Park, B.-G.; Ko, M. K.; Jang, H.-S.; Choi, K.; Baik, J.-H.; Lee, J. K.; Pae, A. N.; Cho, Y. S.; Min, S.-J. *Eur. J. Med. Chem.* **2013**, *62*, 71-83.
- 237 Jung, S. H.; Choi, K.; Pae, A. N.; Lee, J. K.; Choo, H.; Keum, G.; Cho, Y. S.; Min, S.-J. *Org. Biomol. Chem.* **2014**, *12*, 9674-9682.
- 238 Shevtsova, E. F.; Vinogradova, D. V.; Kireeva, E. G.; Reddy, V. P.; Aliev, G.; Bachurin, S. O. *Curr. Alzheimer Res.* **2014**, *11*, 422-429.
- 239 All the CRC assays were performed by Chueng, A.; Ramachandran, S.; Rozier, C.; Searle, K.; Tan, Y.-M. *GlaxoSmithKline*, R&D Singapore, SINGAPORE; unpublished results.
- 240 Fontaine, E.; Ichas, F.; Bernardi, P. *J. Biol. Chem.* **1998**, *273*, 25734-25740.
- 241 Unpublished results from Ahmed, M.; Chan, D.; Duncan, S.; Lee, K. C.; Oon, P.; Rivers, E.; Tan, E. *GlaxoSmithKline*, R&D Singapore, SINGAPORE.



- 
- 242 Unpublished results from Minick, D. *GlaxoSmithKline*, R&D Durham, US.
- 243 Walsh, J. S.; Miwa, G. T. *Annu. Rev. Pharmacol. Toxicol.* **2011**, *51*, 145-167.
- 244 Kalgutkar, A. S.; Driscoll, J.; Zhao, S. X.; Walker, G. S.; Shepard, R. M.; Soglia, J. R.; Atherton, J.; Yu, L.; Mutlib, A. E.; Munchhof, M. J.; Reiter, L. A.; Jones, C. S.; Doty, J. L.; Trevena, K. A.; Shaffer, C. L.; Ripp, S. *Chem. Res. Toxicol.* **2007**, *20*, 1954-1965.
- 245 Zeng, Q.; Zhang, D.; Yao, G.; Wohlhieter, G. E.; Wang, X.; Rider, J.; Reichelt, A.; Monenschein, H.; Hong, F.-T.; Falsey, J.; Dominguez, C.; Bourbeau, M. P.; Allen, J. G. (Amgen Inc.), *WO2009/011880A2*, **2009**.
- 246 Wu, Y.-Q.; Limburg, D. C.; Wilkinson, D. E.; Hamilton, G. S. *Org. Lett.* **2000**, *2*, 795-797.
- 247 Akula, R.; Yan, X.; Ibrahim, H. *RSC Adv.* **2013**, *3*, 10731-10735.
- 248 Rutan, K. J.; Heldrich, F. J.; Borges, L. F. *J. Org. Chem.* **1995**, *60*, 2948-2950.
- 249 Klement, I.; Lennick, K.; Tucker, C. E.; Knochel, P. *Tetrahedron Lett.* **1993**, *34*, 4623-4626.
- 250 Unpublished results from Lee, K. C. *GlaxoSmithKline*, R&D Singapore, SINGAPORE.
- 251 Unpublished results from Duncan, S. *GlaxoSmithKline*, R&D Singapore, SINGAPORE.
- 252 Unpublished results from Graham, S. *GlaxoSmithKline*, R&D Singapore, SINGAPORE.
- 253 He, Y.; Wang, B.; Dukor, R. K.; Nafie, L. A. *Applied Spectroscopy* **2011**, *65*, 699-723.
- 254 Golkiewicz, W.; Polak, B. *Indirect Methods for the Chromatographic Resolution of Drug Enantiomers*, In *Drug Stereochemistry, Analytical Methods and Pharmacology*, edited by Józwiak, K.; Lough, W. J.; Wainer, I. W.; Informa Healthcare **2012**, 69-94.
- 255 Ilisz, I.; Berkecz, R.; Péter, A. *J. Pharm. Bio. Anal.* **2008**, *47*, 1-15.
- 256 Bhushan, R.; Brückner, H. *Amino Acids* **2004**, *27*, 231-247.
- 257 Daverio, P.; Zanda, M. *Tetrahedron: Asymmetry* **2001**, *12*, 2225-2259.
- 258 Galatsis, P. *CBS Reduction*, In *Name Reactions for Functional Group Transformations*, edited by Li, J. J.; Corey, E. J.; Wiley-Interscience Eds. **2007**, 2-21.
- 259 Glushkov, V. A.; Tolstikov, A. G. *Russ. Chem. Rev.* **2004**, *73*, 581-608.
- 260 Cho, B. T. *Chem. Soc. Rev.* **2009**, *38*, 443-452.
- 261 Cho, B. T. *Tetrahedron* **2006**, *62*, 7621-7643.
- 262 Duquette, J.; Zhang, M.; Zhu, L.; Reeves, R. S. *Org. Process Res. Dev.* **2003**, *7*, 285-288.
- 263 Zajac, M. A. *J. Org. Chem.* **2008**, *73*, 6899-6901.
- 264 Quallich, G. J.; Woodall, T. M. *Tetrahedron Lett.* **1993**, *34*, 785-788.
- 265 Lynch, J. E.; Choi, W.-B.; Churchill, H. R. O.; Volante, R. P.; Reamer, R. A.; Ball, R. G. *J. Org. Chem.* **1997**, *62*, 9223-9228.
- 266 D'Elia, V.; Liu, Y.; Zipse, H. *Eur. J. Org. Chem.* **2011**, *8*, 1527-1533.
- 267 Matsumoto, Y.; Tsuzuki, R.; Matsuhisa, A.; Masuda, N.; Yamagiwa, Y.; Yanagisawa, I.; Shibanuma, T.; Nohira, H. *Chem. Pharm. Bull.* **1999**, *47*, 971-979.

- 
- 268 The *in vivo* PK work of the mPTP research programme was performed by Aw, C. C.; Browne, E.; Lim, J.; Mettu, V.; Pasikanti, K.; Su, Z. *GlaxoSmithKline*, R&D Singapore, SINGAPORE; unpublished results.
- 269 Reynolds, A. J.; Kassiou, M. *Curr. Org. Chem.* **2009**, *13*, 1610-1632.
- 270 Kumara Swamy, K. C.; Bhuvan Kumar, N. N.; Balaraman, E.; Pavan Kumar, K. V. P. *Chem. Rev.* **2009**, *109*, 2551-2651.
- 271 Tsunoda, T.; Yamamiya, Y.; Itô, S. *Tetrahedron Lett.* **1993**, *10*, 1639-1642.
- 272 Tsunoda, T.; Otsuka, J.; Yamamiya, Y.; Itô, S. *Chem. Lett.* **1994**, *23*, 539-542.
- 273 Humphries, P. S.; Do, Q.-Q. T.; Wilhite, D. M. *Beilstein J. Org. Chem.* **2006**, *2*, No. 21.
- 274 Itô, S.; Tsunoda, T. *Pure Appl. Chem.* **1999**, *71*, 1053-1057.
- 275 Saeed, A.; Mahesar, P. A.; Zaib, S.; Khan, M. S.; Matin, A.; Shahid, M.; Iqbal, J. *Eur. J. Med. Chem.* **2014**, *78*, 43-53.
- 276 Germain, A. R.; Carmody, L. C.; Nag, P. P.; Morgan, B.; VerPlank, L.; Fernandez, C.; Donckele, E.; Feng, Y.; Perez, J. R.; Dandapani, S.; Palmer, M.; Lander, E. S.; Gupta, P. B.; Schreiber, S. L.; Munoz, B. *Bioorg. Med. Chem. Lett.* **2013**, *23*, 1834-1838.
- 277 Yoya, G. K.; Bedos-Belval, F.; Constant, P.; Duran, H.; Daffé, M.; Baltas, M. *Bioorg. Med. Chem. Lett.* **2009**, *19*, 341-343.
- 278 Doherty, E. M.; Fotsch, C.; Bo, Y.; Chakrabarti, P. P.; Chen, N.; Gavva, N.; Han, N.; Kelly, M. G.; Kincaid, J.; Klionsky, L.; Liu, Q.; Ognyanov, V. I.; Tamir, R.; Wang, X.; Zhu, J.; Norman, M. H.; Treanor, J. J. S. *J. Med. Chem.* **2005**, *48*, 71-90.
- 279 Nardi, A.; Olesen, S.-P. *Expert Opin. Ther. Patents* **2007**, *17*, 1215-1226.
- 280 Rossiter, B. E.; Swingle, N. M. *Chem. Rev.* **1992**, *92*, 771-806.
- 281 Hayashi, T.; Yamasaki, K. *Chem. Rev.* **2003**, *103*, 2829-2844.
- 282 Park, B. K.; Kitteringham, N. R.; Maggs, J. L.; Pirmohamed, M.; Williams, D. P. *Annu. Rev. Pharmacol. Toxicol.* **2005**, *45*, 177-202.
- 283 Kalgutkar, A. S. *Role of Bioactivation in Idiosyncratic Drug Toxicity: Structure-Toxicity Relationships*, In *Advances in Bioactivation Research*, edited by Elfarra, A.; Springer **2008**, 27-55.
- 284 Kalgutkar, A. S.; Gardner, I.; Obach, R. S.; Shaffer, C. L.; Callegari, E.; Henne, K. R.; Mutlib, A. E.; Dalvie, D. K.; Lee, J. S.; Nakai, Y.; O'Donnell, J. P.; Boer, J.; Harriman, S. P. *Curr. Drug Metab.* **2005**, *6*, 161-225.
- 285 Penner, N.; Woodward, C.; Prakash, C. *Drug Metabolizing Enzymes and Biotransformations Reactions*, In *ADME-Enabling Technologies in Drug Design and Development*, edited by Zhang, D.; Surapaneni, S.; John Wiley & Sons, Inc. **2012**, 545-565.
- 286 Unpublished results from Su, Z. *GlaxoSmithKline*, R&D Singapore, SINGAPORE.
- 287 Unpublished results from Chan, D. *GlaxoSmithKline*, R&D Singapore, SINGAPORE.
- 288 Schlummer, B.; Scholz, U. *Adv. Synth. Catal.* **2004**, *346*, 1599-1626.
- 289 Surry, D. S.; Buchwald, S. L. *Chem. Sci.* **2011**, *2*, 27-50.
- 290 Wolfe, J. P.; Buchwald, S. L. *Tetrahedron Lett.* **1997**, *38*, 6359-6362.
- 291 Ishikawa, M.; Hashimoto, Y. *J. Med. Chem.* **2011**, *54*, 1539-1554.

- 
- 292 Thavaneswaran, S.; Scammells, P. J. *Bioorg. Med. Chem. Lett.* **2006**, *16*, 2868-2871.
- 293 McCamley, K.; Ripper, J. A.; Singer, R. D.; Scammells, P. J. *J. Org. Chem.* **2003**, *68*, 9847-9850.
- 294 Kuwahira, I.; Gonzalez, N. C.; Heisler, N.; Piiper, J. *J. Appl. Physiol.* **1993**, *74*, 203-210.
- 295 Meanwell, N. A. *J. Med. Chem.* **2011**, *54*, 2529-2591.
- 296 Wu, Y.-J.; Davis, C. D.; Dworetzky, S.; Fitzpatrick, W. C.; Harden, D.; He, H.; Knox, R. J.; Newton, A. E.; Philip, T.; Polson, C.; Sivarao, D. V.; Sun, L.-Q.; Tertysnikova, S.; Weaver, D.; Yeola, S.; Zoeckler, M.; Sinz, M. W. *J. Med. Chem.* **2003**, *46*, 3778-3781.
- 297 Shen, Q.; Shekhar, S.; Stambuli, J. P.; Hartwig, J. F. *Angew. Chem. Int. Ed.* **2005**, *44*, 1371-1375.
- 298 Carreira, E. M.; Fessard, T. C. *Chem. Rev.* **2014**, *114*, 8257-8322.
- 299 Stocks, M. J.; Wilden, G. R. H.; Pairaudeau, G.; Perry, M. W. D.; Steele, J.; Stonehouse, J. P. *ChemMedChem* **2009**, *4*, 800-808.
- 300 Burkhard, J. A.; Wagner, B.; Fisher, H.; Schuler, F.; Müller, K.; Carreira, E. M. *Angew. Chem. Int. Ed.* **2010**, *49*, 3524-3527.
- 301 Ratcliffe, P. D.; Clarkson, T. R.; Jeremiah, F.; Maclean, J. K. F. (N. V. Organon), *WO2011/045258A1*, **2011**.
- 302 Marzabadi, M. R.; Wetzell, J.; DeLeon, J. E.; Lagu, B.; Gluchowski, C.; Noble, S.; Nagarathnam, D. (Cooper & Dunham LLP), *US2003/0069261A1*, **2003**.
- 303 Cheng, C. C.; Huang, X.; Shipps, Jr. G. W.; Wang, Y.-S.; Wyss, D. F.; Soucy, K. A.; Jiang, C.-K.; Agrawal, S.; Ferrari, E.; He, Z.; Huang, H.-C. *ACS Med. Chem. Lett.* **2010**, *1*, 466-471.
- 304 All high-resolution mass spectrometry experiments were performed by Leavens, B. *GlaxoSmithKline*, R&D Stevenage, UK; unpublished results.
- 305 Dolušić, E.; Larrieu, P.; Moineaux, L.; Stroobant, V.; Pilotte, L.; Colau, D.; Pochet, L.; Van den Eynde, B.; Masereel, B.; Wouters, J.; Frédérick, R. *J. Med. Chem.* **2011**, *54*, 5320-5334.
- 306 Amantini, D.; Beleggia, R.; Fringuelli, F.; Pizzo, F.; Vaccaro, L. *J. Org. Chem.* **2004**, *69*, 2896-2898.
- 307 Moloney, G. P.; Angus, J. A.; Robertson, A. D.; Stoermer, M. J.; Robinsom, M.; Wright, C. E.; McRae, K.; Christopoulos, A. *Eur. J. Med. Chem.* **2008**, *43*, 513-539.